https://doi.org/10.35662/unine-thesis-3119

University of Neuchâtel, Switzerland

Faculty of Sciences

Centre for Hydrogeology and Geothermics (CHYN)

Data integration and automated geological modeling of Quaternary aquifers

Thesis presented for the degree of

DOCTEUR ÈS SCIENCES

by

Ludovic Schorpp

Thesis advisor:	Philippe Renard, Université de Neuchâtel, CH
Examiners:	Luca Colombera, Università di Pavia, I
	Marijke Huysmans, Vrije Universiteit Brussel, B
	Dany Lauzon, Polytechnique Montréal, CA
	Julien Straubhaar, Université de Neuchâtel, CH
	Philip Wehrens, Swisstopo, CH

Defended on the 30th of May 2024

unine
Université de Neuchâtel
Faculté des sciences

Rue Emile-Argand 11
CH-2000 Neuchâtel
doctorat.sciences@unine.ch

IMPRIMATUR POUR THESE DE DOCTORAT

La Faculté des sciences de l'Université de Neuchâtel autorise l'impression de la présente thèse soutenue par

Monsieur Ludovic SCHORPP

Titre :

"Data integration and automated stochastic geological modeling of Quaternary aquifers"

sur le rapport des membres du jury composé comme suit :

- **Prof. tit. Philippe Renard,** directeur de thèse, UniNE
- **Prof. Marijke Huysmans,** Vrije Universiteit Brussel, Belgique
- **Prof. Ass. Dany Lauzon,** Ecole Polytechnique de Montréal, Canada
- **Prof. Ass. Luca Colombera,** Università di Pavia, Italie
- **Dr Julien Straubhaar,** UniNE
- **Dr Philip Wehrens,** Swisstopo, Suisse

Neuchâtel, le 10 juillet 2024 Le Doyen, Prof. R. Bshary

The sediments are a sort of epic poem of the Earth

Rachel Carson, 1951

Remerciements

Tout travail, scientifique ou non, ne peut aboutir sans la participation d'un grand nombre de soutiens, qu'ils soient moraux ou techniques, à la personne (ou aux personnes) effectuant ledit travail. Ces aides sont nécessaires et permettent, à plus d'un titre, de progresser, peu importe les difficultés et embûches rencontrées. Bien évidemment, cette thèse ne fait pas figure d'exception et n'aurait jamais pu être complétée sans l'aide de mes artisan.ne.x.s et scientifique.x.s de l'ombre.

Parce que sans argent, ni ressources, il est difficile d'aller très loin, il faut mentionner que ce travail a été financé par le Fonds national suisse (FNS), ainsi que par l'Université de Neuchâtel (UNINE) et réalisé au sein du centre d'hydrogéologie et de géothermie (CHYN). Le travail concernant la vallée du Rhin a été financé par l'Office Fédéral de la Topographie (SWISSTOPO). Je remercie toutes ces institutions de m'avoir fait confiance durant ces années. Je remercie également tous les membres du jury de mon comité de thèse, Marijke Huysmans, Dany Lauzon, Luca Colombera et Philip Wehrens, pour avoir accepté d'évaluer cette thèse ainsi que pour leurs remarques et commentaires très pertinents et avisés.

Il est impossible de ne pas remercier celui qui a initié en moi la passion de la recherche et m'a soutenu et supervisé durant ces longues années, j'ai nommé **Philippe Renard**. Merci de m'avoir fait confiance pour cette thèse et d'avoir toujours su trouver les mots pour me guider, me réorienter dans le bon chemin (plus d'une fois), tes patientes (et longues) relectures avisées de mes manuscrits qui ont probablement dû provoquer quelques arrachages de cheveux ou encore les discussions passionnantes autour des cafés quotidiens, ... Les mots me manquent pour décrire à quel point tu as été un superviseur exemplaire. Il me faut également que je remercie grandement **Julien Straubhaar** pour être le développeur de *geone* sur lequel repose pratiquement l'entièreté de ma thèse. Merci pour ton temps, tes conseils avisés, ta rapidité à corriger les, pas si nombreux, bugs de *geone* et tes relectures précises et enrichissantes des articles que l'on a écrits en commun. Tu as été la clé de voûte de ce travail.

Une thèse sans collègue avec qui la partager serait bien terne et triste. C'est pour cela qu'il me faut absolument remercier tous les membres du Randlab avec qui j'ai eu la chance de partager ces moments particuliers de la thèse merci à **Ana**, **Robin**, **Tanguy**, **Célia** et **Nina**. Vous avez tous et toutes contribuées d'une façon ou d'une autre à ma bonne santé mentale. Que ce soit en me demandant régulièrement comment j'allais, comment avançait mes projets ou bien les innombrables pauses café qui ont ponctué ces quatre années. Merci également à **Valentin** de m'avoir si bien supervisé au master au point que j'en veuille faire un doctorat (sans une once d'ironie), échanger et discuter avec toi a toujours été enrichissant et source d'inspiration. Merci aussi à mon illustre collègue de bureau **Alexis** qui m'a initié à la vie de doctorant et qui m'a servi, à son grand dam, de bêta-testeur d'ArchPy.

Mais le CHYN ne s'arrête pas au Randlab et aussi rempli d'autres gens super. Merci à mes collègues, **Éléonore**, **Théo**, **Kalliopi**, **Thanushika**, **Léa**, **Saeed**, **Hugo**, **Morgane**, **Gaëlle**, **Ronny**, **François**, **Ronan**, **Ernesto** sans qui l'aventure doctorale aurait quand même été beaucoup moins marrante. Nos discussions et plaintes respectives ont toujours su me rappeler qu'on est beaucoup à être (ou a l'avoir été.e) dans cette galère du monde académique. Merci également aux stagiaires **Solène**, **Margot** et **Chloé** venues pour des périodes de temps certes courtes mais riches en échanges et en rires.

Mais que serait une thèse sans ami.e.x.s vers qui se plaindre quand plus rien ne fonctionne ou que tu dois préparer tes slides pour deux conférences qui ont lieu le surlendemain et qui ne comprennent pas vraiment ce que tu fais mais te soutiennes quoiqu'il arrive. Tout d'abord un immense merci à **Florent**, vers qui j'ai toujours pu me plaindre de tout et rien, tout en recevant des commentaires éclairés. Merci pour les séances de courses quasi hebdomadaires (et les discussions qui vont avec) qui m'ont permis de maintenir un équilibre entre thèse, vie sociale et santé. Merci beaucoup à **Giulia** pour nos échanges sur nos passions communes telle que Pokémon (mais pas que !) ainsi que nos ateliers cuisine (pas toujours réussis). Merci au camarade **François** pour les discussions passionnées sur notre système économique et politique ainsi que les parties de mtg avec Valentin à pas d'heures dans les bâtiments de l'université. Un merci tout particulier à **Mylène** pour avoir été à l'écoute des mes divers problèmes et une source de distraction (dans le bon sens du terme !). Énorme merci à mes ami.e.x.s et camarades de la Grève du Climat Neuchâtel avec qui j'ai pu partager de très chouettes moments d'actions militantes. Merci à **Maxime** pour ta présence et ta bonne humeur qui a toujours su me motiver. **Jonathan**, bien que tu n'aies pas été autant présent que pour le travail de master, tu m'as tout de même accompagné un bon bout de temps en début de thèse et tu as toujours été là quand j'en ai eu besoin, merci infiniment.

Je remercie aussi mes parents qui ont fait plus que de m'accompagner durant cette période, longue mais nécessaire, que fut mon parcours scolaire et académique. Merci à mes mes frères et soeurs qui ont toujours eu du mal à

comprendre ce que faisait leur grand frère mais qui m'ont toujours soutenu à leur manière. Sans vous, cela n'aurait pas été possible. Finalement, je remercie aussi toutes ces personnes que j'ai certainement oublié.e.x.s ou que je n'ai pas pu explicitement cité.e.x.s ici.

Mais les plus grands remerciements vont bien évidemment à celle qui, depuis quelques temps déjà, partage ma vie. **Aurélie**, vivre avec un doctorant n'est pas toujours facile, particulièrement en fin de thèse. Mais malgré tout, tu as toujours été là pour moi, en toutes circonstances, du début jusqu'à la fin. Merci d'avoir été ma grande conseillère qui m'a incité à prendre des pauses et à savoir lâcher prise quand il le fallait. Tu as été ma plus grande confidente et d'un grand secours car il est certain que sans toi, je n'aurais pas pu aller au bout de ce travail qui m'a toujours paru plus simple et abordable grâce à toi. Merci.

Abstract

The subject of this thesis is the modeling of heterogeneity in Quaternary aquifers and geological formations. More specifically, it seeks to integrate existing geological data into modeling procedures and find ways of automating them as far as possible. Various lines of research are being investigated to address these challenges. First, a literature review of facies modeling methods, characterizing the heterogeneity of the subsurface, is carried out in order to gain an overview as complete as possible of existing algorithms and methods. The aim was also to propose a recent and up-to-date classification of these methods, to help in the selection of a method according to the situation. Potential research gaps in this field are also identified. Second, an approach and module is developed to tackle the challenges of the thesis. The result is the proposal of a hierarchical, semi-automatic and stochastic approach, called ArchPy, which makes it easy to combine geological expertise, represented in the form of a stratigraphic pile, and various geological data. This hierarchical approach operates in three stages: stratigraphic unit, facies and petrophysical properties. These represent different scales of geological complexity, and enable a high degree of heterogeneity to be achieved. In order to demonstrate ArchPy's usefulness, it is then applied to different geological sites and improved at several points depending on the situation. However, ArchPy faces some issues that limits its automation. In particular, the difficulty associated with the construction of the stratigraphic pile led to the proposition of a new algorithm to automatically determine the stratigraphic pile based on borehole records. A method is also proposed to solve the recurrent problem of missing stratigraphic information in drilling data. Once ArchPy approach is set up, it is necessary to refine its second step - facies modeling - which is particularly to accurately model depending on the geological context. To this aim, a novel facies modeling methods, called EROSim, to better represent sedimentary structures is proposed. This method is distinctive because it employs surfaces to represent various geological events that can impact the heterogeneity of a sedimentary formation. The presented tools and methods showcase the advantages and usefulness of stochastic, automated, and open-access methods for geological modeling. Specifically, ArchPy establishes the groundwork for a stochastic geological modeling toolbox with a broad range of applications, including the creation of intricate geological models or coupling in inversion processes. This thesis contributes to the development

of geological modeling, which is becoming more accessible and available to the geoscientific community and beyond.

Keywords

uncertainty; geological modeling; geostatistics; Quaternary modeling, automated workflow, data integration, open science

Résumé

Cette thèse a pour sujet d'étude la modélisation de l'hétérogénéité des aquifères et formations géologiques du Quaternaire. Plus particulièrement, elle cherche à intégrer au mieux les données géologiques existantes au sein des procédures de modélisation et à trouver des façons de les automatiser au maximum. Différents axes de recherches sont investigués afin de répondre à ces problématiques. Dans un premier temps, une revue littéraire des méthodes de modélisation de faciès, caractérisant largement l'hétérogénéité du sous-sol, est réalisée afin d'avoir une vue aussi complète que possible sur les algorithmes et méthodes existantes. Le but était aussi de proposer une classification récente et actualisée de ces méthodes dans le but d'aider à la sélection d'une méthode en fonction des situations. Les potentielles lacunes en matière de recherche dans ce domaine sont également identifiées. A la suite de cela, une proposition d'une approche hiérarchique, semi-automatique et stochastique, appelée ArchPy est proposée. Elle permet de facilement combiner l'expertise géologique, représentée sous la forme d'une pile stratigraphique, et les différentes données géologiques. Cette approche hiérarchique opère en trois étapes: unité stratigraphique, faciès et propriétés pétrophysiques. Elles représentent différentes échelles de complexité géologique et permettent d'atteindre une grande complexité en terme d'hétérogénéité. ArchPy a ensuite été utilisé sur différents sites géologiques afin de démontrer ses capacités de modélisation. Cependant, ArchPy est confronté à certains problèmes qui limitent son automatisation. En particulier, la difficulté associée à la construction de la pile stratigraphique a conduit à la proposition d'un nouvel algorithme pour déterminer automatiquement la pile stratigraphique sur la base des données lithologiques des forages. Une méthode est également proposée afin de résoudre le problème récurrent des informations stratigraphiques manquantes dans les données de forages. Une fois l'approche ArchPy mise en place, il est nécessaire d'affiner sa deuxième étape - la modélisation des faciès - qui est particulièrement délicate à modéliser en fonction du contexte géologique. Dans ce but, une nouvelle méthode de modélisation des faciès, appelée EROSim, permet de mieux représenter les structures sédimentaires. Cette méthode a la particularité qu'elle utilise des surfaces pour représenter les différents évènements géologiques pouvant affecter l'hétérogénéité d'une formation sédimentaire. Les outils et méthodes présentées montrent l'intérêt et le bénéfice des méthodes stochastiques, automatisées et en

accès libre pour la modélisation géologique. ArchPy pose notamment les bases d'une boite à outils de modélisation géologique stochastique ayant un large panel d'utilisations, tel que la réalisation de modèles géologiques complexes ou le couplage dans des processus d'inversion. Cette thèse participe ainsi au développement d'une modélisation géologique devenant de plus en plus accessible et libre d'accès, pour le bien commun de la communauté géoscientifique, et au-delà.

Mots-clés

incertitude ; modélisation géologique ; géostatistique ; modélisation du Quaternaire, automatisation, intégration de données; science ouverte

Contents

Chapter 1

Introduction

1.1 Context and problematic

The geology of Switzerland is rich and varied. Many different geological formations and units have been conscientiously described and mapped over the last centuries. However, of all the types of rock that cover Switzerland, the great majority of the population is concentrated on a very specific and restricted geological unit, Quaternary. Quaternary deposits, which have been deposited in the past 2.58 million years, cover a large portion of geological deposits in Switzerland (Fig. 1.1). This geological period is marked by repetitive glacial cycles, which, in combination with alluvial and lacustrine processes, have led to complex, diverse and intertwined sedimentary deposits. A notable characteristic of Quaternary deposits is their unconsolidated nature, comprising a spectrum of granulometric classes ranging from clays to boulders. Consequently, these deposits exhibit pronounced heterogeneity, which poses challenges in their characterization and interaction. Despite these complexities, Quaternary formations play an essential role in Swiss society, serving as primary groundwater reservoirs, geothermal energy sources, and repository of construction materials, such as gravel and sand. In addition, they serve as important sites for civil engineering projects, including tunnels, building foundations, and nuclear waste repositories. Furthermore, the flat terrain associated with Quaternary deposits provides favorable conditions for agricultural activities and building construction. In particular, substantial underground utilization 90% in Switzerland is concentrated within Quaternary and unconsolidated deposits (Volken et al. 2016).

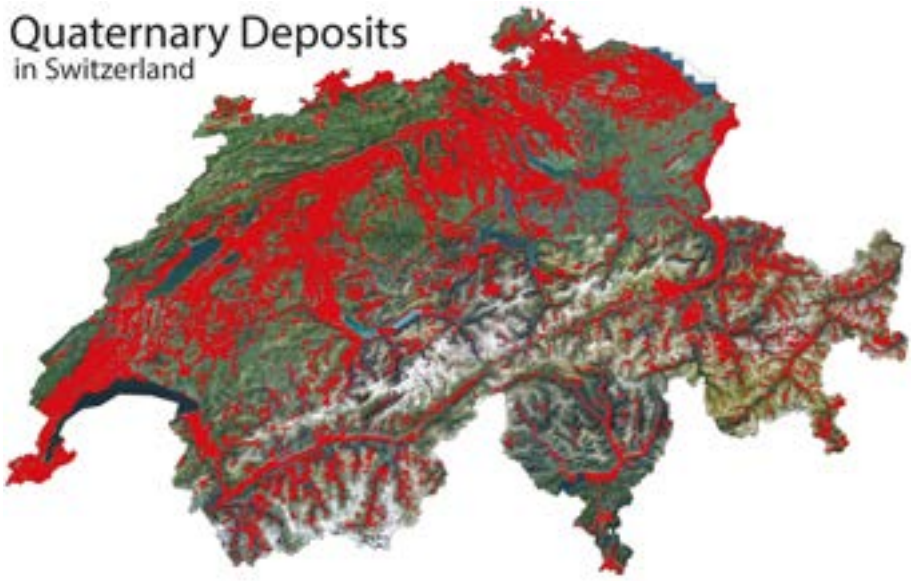

Figure 1.1: *Location in red of the Quaternary deposits in Switzerland, modified from Volken et al. 2016.*

For these reasons, it is important to correctly characterize the heterogeneity of the subsurface. This makes it easier to plan the dimensions of underground structures, to react to accidental pollution events and to reduce or even avoid accidents (e.g. collapses, internal erosion, etc.) which can occur more easily within unconsolidated deposits. To achieve this, geological and hydrogeological models must be developed, integrating diverse datasets to accurately represent the geological and hydrogeological conditions of an area. The aim of the geological model is to give a representation of the subsurface physical properties that then serve as input for the hydrogeological model. The groundwater model is then used to reproduce the complex hydrodynamics of the underground relying on physical equations and boundary conditions that represent the state of the problem to be solved. Several different variables can be simulated (water level, chemical species, heat, etc.) depending on the problem. Once a model has been built and calibrated, it can be used to test different scenarios and simulate what can be expected in reality. Notably, it can be used to make predictions according to the evolution of certain parameters, such as climate or anthropogenic activity, which is particularly useful in the context of climate change. Nevertheless, constructing reliable models is intricate and requires a comprehensive understanding of the involved processes and geological-hydrogeological contexts. Moreover, ensuring data quantity **and** quality is essential to model realism and to account for local and regional characteristics.

However, data collection is often undertaken by a large number of different actors (companies, local authorities, and individuals), on decadal time scales, which makes it very difficult to have standardized and homogenized data that can be easily and automatically integrated into modeling workflows. In this spirit, the Swiss Geological Survey (Swisstopo) launched the *GeoQuat* project a few years ago, to collect, harmonize, and centralize existing Quaternary data, as well as build 3D geological models. For this project, several pilot sites were selected to demonstrate the advantages and benefits of the approach: Lucerne Lake, Rhone Valley (Visp), Birrfeld area, and Upper Aare Valley. These four areas contain Quaternary valleys that have been shaped by glaciers and filled with Quaternary deposits. However, modeling of these areas has shown limitations in terms of quality, respect for the geological context and sedimentological rules, and the tools available for producing models of this scale. All this makes geological modeling difficult, complicated, slow, and difficult to reproduce in other locations. Furthermore, stochastic approaches (multiple different models) are often neglected compared to deterministic approaches (one unique model), which means that uncertainty is not considered in the final models. These uncertainties are then ignored and do not affect flow and transport models, which can have important consequences in terms of water resource management and remediation. It is therefore clear that there is a lack of research into the creation of stochastic Quaternary geological models integrating several different types of data at the same time and doing so in an automatic and reproducible way.

1.2 Current methods and limitations

The standard hydrogeological modeling approach is decomposed into several steps that are generally done separately. It begins with data collection (geological, geophysical, hydrogeological, etc.) and drawing up a geological and hydrogeological conceptual model of the area (conceptual step). If available, geophysical data are analyzed and inverted (geophysical inversion step). They are used in combination with geological data to construct a geological model with the desired modeling approach (geological modeling step). A groundwater model is then constructed and calibrated, based on the geological model and conceptual model, and finally used to make predictions (hydrogeological modeling step). Each step of this workflow involves an important amount of manual work that is operated using different tools and software, generally proprietary and expensive. Moreover, it is generally not possible to interface easily these software, making it difficult to have a completely integrated and holistic workflow where each step can be influenced by the others. In the standard approach, once the geophysical inversion has been done, it is not touched anymore, and so is the interpreted geological model. It is then very likely that errors and inconsistencies can arise between each model. The classical example is the groundwater model that has been calibrated on hydrogeological data (e.g. discharge measurements, hydraulic heads), does not respect the geophysical data. Additionally, the final models are not geologically realistic, although they are based on geological models. There is hence a lack of openly accessible tools and software that would leverage the development of more integrated approaches that can easily integrate different kinds of data while preserving geologically realistic models.

Each of the aforementioned steps is important, but the geological modeling step is of particular importance. The problem is not as clear-cut as for a hydrogeological or geophysical model. The physical processes behind a geological site are poorly and incompletely understood. It is therefore difficult to use physically-based methods that can consider all the geological processes (hydrodynamics, sediment erosion and transport, diagenesis, crystallization, tectonics, geodynamics, dissolution, etc.) directly to geological modeling. Therefore, alternative approaches have been used throughout the history of geological modeling, mainly based on interpolation methods (e.g., Matheron 1963; Journel et al. 1990; Pyrcz et al. 2014; Wellmann et al. 2018). They seek to determine statistically at any point in a simulation domain the geology, mainly based on geological data (e.g. boreholes, dips). In addition, geological processes act on different spatial scales, leading to heterogeneity that can be characterized hierarchically. For this reason, the traditional approach to geological modeling is actually hierarchical and consists of three steps (Pyrcz et al. 2014): stratigraphical unit model, facies model, and petrophysical (or property) model, as illustrated in Figure 1.2.

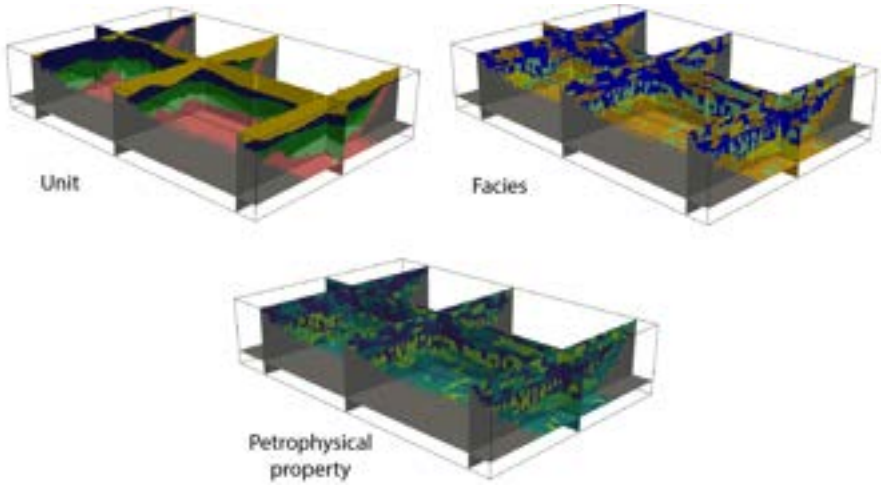

Figure 1.2: *Hierarchical geological modeling principle. Unit and facies models are categorical fields and property model is a continuous model.*

The purpose of the unit model is to delineate stratigraphic units, which represent different geological time periods, with generally different geological settings. The units are then filled with facies, or lithologies, to build the facies model. Facies models reproduce the internal heterogeneity of a particular unit which is assumed to be determined by the spatial distribution of facies (e.g. gravel, sand, clay, silt). Finally, the petrophysical models are obtained by simulating or attributing continuous values inside the previously obtained facies. With this approach, complex and heterogeneous models can be obtained. However, some limitations and issues restrain the applicability of this approach. First, there is currently a lack of free and open-source software that can perform all these steps in a reproducible, stochastic way, while allowing great flexibility in the choice of methods employed at each stage. Second, existing software do not allow for simulating units hierarchy which is a common concept in sedimentology where units contain subunits which themselves contain subsubunits and so on. Failure to take this hierarchy into account can make it difficult to simulate certain simple geological situations (Zuffetti et al. 2020). Third, facies modeling can be undertaken using a number of different methods, but due to the lack of systematic comparative studies, it is not always easy to choose the most appropriate one. It is also not uncommon to be unaware of the existence of certain methods. Finally, the integration of geological and expert knowledge in the modeling process remains difficult. Therefore, there is a lack of open tools and integrative solutions, as well as general and precise guidelines for all the steps in stochastic geological modeling.

1.3 The PheniX project

To address existing limitations in the geological and hydrogeological modeling of Quaternary formations, the PheniX project was started in 2019. It has been funded by the Swiss National Foundation (SNF) and this thesis has been partly done in the framework of this project. Engaging various stakeholders from the private sector, public authorities, and academic institutions, the project aimed to rethink methodologies and philosophies around groundwater and geological modeling. Aligned with its objectives, the SNF-funded PheniX project aims to develop a comprehensive suite of tools aimed at assessing uncertainty and integrating data in groundwater modeling, with a specific emphasis on Quaternary aquifers, the main and widely used groundwater reservoirs. The project is decomposed into four pivotal tasks (Fig. 1.3): data acquisition and model benchmarking on synthetic and real data, the development of new random function models (notably substition random function models Lantuéjoul 2001; Straubhaar et al. 2024), automated creation of consistent geological models, and finally the integration of data through joint inverse conditioning techniques.

The PheniX project aimed to improve the understanding and modeling of Quaternary aquifers by combining advanced geostatistical and inverse methodologies with extensive data acquisition efforts. The idea was to enhance the reliability and applicability of groundwater assessments within these critical geological settings. To validate the methodologies and tools developed within the project framework, a test site has been selected. The Upper Aare Valley was chosen because a large amount of geological data had already been harmonized as part of the Geoquat project. The Upper Aare Valley is an alpine glacial valley located between the cities of Bern and Thun. The interplay of Quaternary processes has led to an intricate geology and complex heterogeneity. From a hydrogeological perspective, there are two aquifers: an upper aquifer, which is between 5 and 50 meters thick and is extensively used by local communities, industry, and the private sector, and a lower aquifer, whose extent and geometry are largely unknown. The subsurface of this region is therefore very important both for the protection and sustainability of existing resources (upper aquifer) and for the discovery and characterization of potential new resources (e.g. lower aquifer).

The project involved two PhD students, Alexis Neven and Ludovic Schorpp, as well as the collaboration of many other Masters and PhD students. The aim of the Alexis's thesis was to gather an important geophysical data set over the whole study area, as well as to develop new methodologies to invert and integrate both geophysical and groundwater data into consistent geological models. In particular, he used some of the tools and algorithms developed in this study, showing the first concrete applications of the present thesis. He was able to demonstrate various semiautomatic methodologies for assimilating geophysical, geological, and hydrogeological data, requiring little additional effort for each new data acquisition (Neven et al. 2022a,b, 2023).

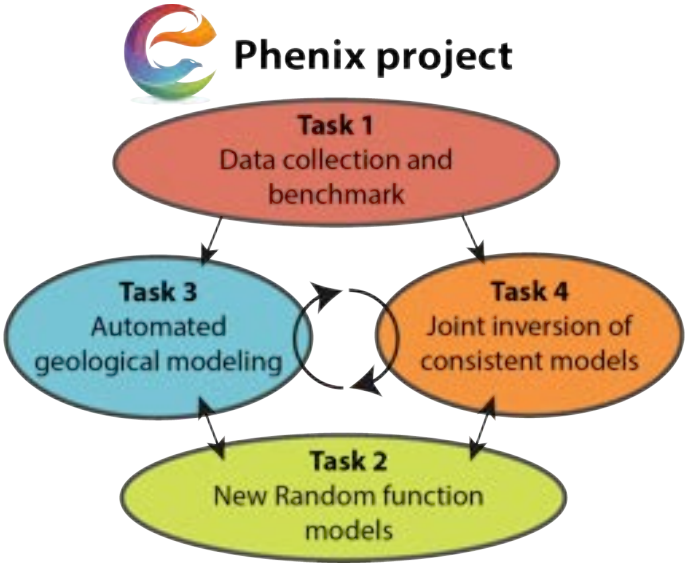

Figure 1.3: *Overall structure of the PheniX project, decomposed into four tasks.*

1.4 Thesis objectives and structure

The purpose of this thesis is to develop new tools and algorithms to facilitate the integration of geological data and knowledge into the modeling process. A particular focus is to make geological modeling more automatic and easily reproducible, to facilitate its application to different cases. To this end, in this thesis several aspects of Quaternary geological modeling are carried out. They are represented by 8 chapters, including the present introduction.

Chapter 2: This thesis begins with an overview chapter which presents and discusses the existing facies modeling methods and how they can be used more effectively. It is planned to adapt this chapter in the future to propose it as a review article.

Chapter 3: This chapter is the center of the thesis and presents a novel methodology and tool to setup hierarchical models, the ArchPy approach. All other chapters deal with parts or particularities of this approach to make it more effective. This chapter has been published in Frontiers and Earth sciences (Schorpp et al. 2022).

Chapter 4: In this chapter, an algorithm is presented to automatically reconstruct the unit orders in the stratigraphic pile, the main concept of ArchPy, solely based on borehole data. It is also shown how the algorithm can be used to find errors in the data and to help refine the geological concept.

Chapter 5: This chapter presents a concrete application of ArchPy and the automatic pile tool to model the stratigraphical units of the Rhine Valley. Other important aspects are also addressed, such as the choice of a hypothetical best single model from a set of stochastic realizations.

Chapter 6: This chapter covers a machine learning method to automatically determine the stratigraphical unit of boreholes, based on lithological description. To illustrate the methodology, a geological model of the Upper Aare Valley is also constructed using ArchPy.

Chapter 7: This thesis concludes with a chapter that introduces a new facies modeling method, EROSim, which uses surfaces as a means of better characterizing and modeling the structures and patterns that can be observed in glaciofluvial deposits.

And finally, the main contributions of the present work and potential perspectives on the future of Quaternary modeling are given in *Chapter 8*.

Chapter 2

Subsurface heterogeneity with facies modeling: methods, applications and perspectives

Abstract

The subsurface serves as a critical arena for various anthropogenic activities and incidents, encompassing endeavors such as drinking water collection, geotechnical structures, geothermal installations, and management of contaminant pollutions. To effectively investigate and dimension such facilities, physical forward models are indispensable, necessitating a thorough consideration of the subsurface's heterogeneous nature, strongly linked to its sedimentological context. Over the past four decades, significant strides have been made in geostatistics and numerical facies modeling to capture this heterogeneity. However, the range of available methods, ranging from simplistic nearest neighbor approaches to highly complex, physically-based sediment transport models, often represents a major challenge for practitioners. The selection of appropriate methods is of paramount importance, as each produces distinct results and requires different data, conceptualizations, and parameterizations. In response to this challenge, this research offers an exhaustive overview and classification of over fifteen diverse methodologies. Each method is accompanied by a historical background, detailed description, and assessment across multiple criteria such as conditioning, realism, and grid-free capabilities. Advantages and disadvantages are presented and compared, providing invaluable insights and decision-making tools for modelers. Finally, a list of guidelines and recommendations are proposed, as well as a list of potential research gaps that should be filled to help the discipline move towards better modeling practices and make it more accessible to a wider audience.

2.1 Introduction

Subsurface heterogeneity of hydraulic parameters and transport properties (hydraulic conductivity, porosity, dispersivity) is one of the main sources of uncertainty when it comes to solving groundwater flow and transport problems, with large implications and consequences if not adequately estimated (De Marsily et al. 2005; Anderson et al. 2015). While it is tempting to consider an equivalent homogeneous medium following the Occham razor principle, this approach is quite limited and it does not reflect the reality, as the underground is heterogeneous whether we like it or not (De Marsily et al. 2005).

The manifestation of subsurface heterogeneity can vary considerably. Sedimentological processes involve a multitude of factors, including water, air, and ice, driven by forces such as gravity, earth rotation, and tectonics. These processes erode existing rocks and transport the resulting sediments to various environments. Consequently, the interplay of these complex processes results in deposits comprising a wide range of sediments, varying in origin and grain size. These sediment variations, in turn, significantly influence the physical properties of the underground.

In the first place, continuous, but heterogeneous, stochastic models were developed to represent heterogeneity, assuming that the parameters were log-normally distributed using the convenient mathematical framework of Gaussian Random Fields (Matheron 1963, GRF). Example of applications of these GRFs has since been numerous and continues until recently (e.g., Dagan 1989; Geng et al. 2020; Severino et al. 2024). However, such models produce images of the subsurface that do not make much sense, geologically speaking. It has long been recognized that the distribution of heterogeneity in the subsurface was not smooth, nor Gaussian, and to correctly capture it, abrupt and discrete facies models were preferred, particularly when high contrasts are present (De Marsily et al. 1998; Journel et al. 1998; De Marsily et al. 2005). Indeed, it has been demonstrated that the spatial distribution of facies in the subsurface has a great impact on flow simulations, but especially on transport simulations (e.g., Gómez-Hernández et al. (1998), Comunian et al. (2011b), and Bennett et al. (2017)). For this reason, the concept of hydrofacies, which relates to the groundwater properties of the facies, is critical (Anderson 1989; Klingbeil et al. 1999). To this task, facies models are well dedicated, as they integer geological data and knowledge in order to improve our understanding of the subsurface heterogeneity.

One common approach to model heterogeneity is to use hierarchical models. Three levels of hierarchy are generally considered: the stratigraphical unit level, the facies level, and the property level (Pyrcz et al. 2014; Ringrose et al. 2016). The first level represents the domain of large and extensive stratigraphic units distinguished by their sedimentological age, such as the Holocene unit or the late Pleistocene unit. This unit model can be refined by considering sublevels of hierarchy, assuming that units comprise subunits (Zuffetti et al. 2020). The second level aims to capture heterogeneity at a finer scale through facies models. These models seek to simulate the distribution of lithofacies or hydrofacies within each previously simulated unit. The method of defining facies may vary between units depending on the geological context and/or available data. Additionally, further hierarchical levels can be incorporated at this stage, where smaller-scale facies are simulated within larger-scale ones (e.g., Bennett et al. 2019). Finally, the last step involves populating the facies models with continuous values to replicate fine-scale heterogeneity within the facies.

Obviously, the higher up we go in the hierarchy, the greater the impact on final heterogeneity, indicating that unit models hold significant importance. However, it is worth noting that unit models are generally better constrained and more thoroughly understood compared to facies models. This is because units can be delineated by surfaces that span the entire simulation domain, resulting in a strong spatial correlation of the units. Consequently, the second level, the facies model, assumes primary importance. Heterogeneity is predominantly governed by facies (lithologies); yet, the associated uncertainties are considerable, underscoring the critical nature of selecting an appropriate facies model.

There are a large number of facies methods and classifying them is not a straightforward task. Several authors (e.g., Koltermann et al. 1996; Falivene et al. 2007b; Pyrcz et al. 2014, 2015) have proposed different classifications, but for some methods, the class boundaries are quite blurred, easily falling into two or more classes. In reality, these methods can be defined using different criteria: numerical nature of the facies (pixel, patch, object, surface, etc.), grid-dependent or grid-free, Gaussian or not, deterministic vs. stochastic, conditionability (ability to respect field data, hard or soft), training-image based, geological realism, or even applicability (can the method be generalized to different depositional environments?). Note that these criteria are not exhaustive and that the list could be extended significantly without difficulty. All the methods presented here perform differently on these different criteria, making rigorous classification difficult, if not impossible. This begs the question: what is the objective of classifying the methods? The answer to this question is that classification, though imperfect, remains essential for several reasons: (1) it is easier to draw parallels and correspondences between methods with similar characteristics; (2) grouping a set of similar methods under the same name is very practical and makes it easier for users to understand each other; (3) to prevent the use of several different names to refer to methods that are ultimately very similar, if not identical. But for such a classification to work and be effective, it needs to be adopted by all people who use these methods. However, this has not always been the case, and the methods presented here have had different names throughout their history and use.

Ultimately, each method has its advantages and disadvantages, and their uses depend on the context (objectives, prior knowledge of the site, available data, etc.). Hence, the aims of this paper are multiples: presenting the state of the art in terms of facies modeling; proposing a classification of the methods with their current limitations and possible improvements; identifying possible research gaps and guide future researches; to help any geoscientist, depending on her or his situation (level of geological knowledge, geostatistical background, number and quality of data, etc.), to choose an appropriate facies modeling method and finally to give insights about the applications and limitations of such methods. To help in this task, a summary of all the methods and their advantages and limitations, as well as classifications based on different criteria are proposed in the section of the perspectives for facies modeling.

Many reviews have already been published on the modeling of subsurface heterogeneity (Koltermann et al. 1996; De Marsily et al. 1998; De Marsily et al. 2005; Falivene et al. 2007a; Pyrcz et al. 2014). However, they do not cover the most recent developments. Consequently, there is a significant gap in the literature regarding a comprehensive overview of contemporary facies modeling techniques, which we aim to fill in this review paper. Given the complexity of the task and the multitude of existing methods to model geological heterogeneity, our overview will be specifically focused on facies modeling techniques. We will not address the modeling of continuous values or inverse and optimization

methods, which are also pertinent to facies modeling. We also focus on sedimentary environments, as heterogeneity holds particular importance in porous environments. However, it should be noted that the methodologies discussed herein can also be applied in other geological settings, such as fracture, volcanic or karst environments.

The chapter is organized as follows: section 2 defines the terminology and introduces briefly common geostatistical concepts and how facies can be numerically represented. Sections 3 to 9 present and detail the existing facies modeling methods by category. In the footsteps of Falivene et al. (2007a) and Pyrcz et al. (2014), we recognize the following major categories: deterministic, variogram-based, multiple-point statistics (MPS), object-based, and process-based. To these, we also propose to add the deformation-based and machine learning-based methods. Section 10 propose a synthesis and a classification of all the presented methods. Section 11 discuss the potential perspectives for the future of facies modeling and section 12 concludes this overview.

2.2 Definitions

Before describing the methods, it is necessary to define certain terms and provide some basic definitions.

2.2.1 Terminology

Facies

In geology, the term "facies" is used to define a geological deposit according to its deposition environment and sedimentological setting. For example, a rock described as a beach facies indicates that it has been deposited in a tidal environment submitted to the related processes (e.g., tides, longshore drift, storms). There is a sedimentological logic behind this term, which is very convenient, as it becomes possible to determine a part of the geological properties of the deposits (lithologies and their spatial structures) based on their facies name.

However, in a broader sense, 'facies' can also refer to deposits of similar lithology, known as 'lithofacies', or deposits with similar fossil assemblages, known as 'biofacies'. Additionally, 'facies' can be used to describe deposits with similar hydraulic properties, such as hydraulic conductivity and porosity, which are referred to as 'hydrofacies' (Anderson 1989). It is important to note that the distinction between lithofacies and hydrofacies is critical. Although links can be made between lithofacies and hydrofacies, it is important to recognize that the connection is not always straightforward, especially due to diagenesis (Slatt et al. 1990). Diagenetic processes such as cementation or compaction can alter the physical properties of lithofacies. As a result, lithofacies that are traditionally classified as permeable (e.g., sand) may be classified as imperme-

able when considered as hydrofacies. The decision to model either lithofacies or hydrofacies can then be critical and depends on the objectives and problems to be solved, but also on the sedimentological processes.

In final, the goal is to categorize geological deposits with *similar* characteristics under the same facies names, based on the interests of the geologist and what is deemed *similar* (Koltermann et al. 1996). The similarity between geological features is mainly a consequence of the scale. At the basin level ($\sim$ 100-10'000 m), heterogeneity is expressed through geological strata, tectonism, and regional trends in lithologies (Koltermann et al. 1996). On the valley scale ($\sim$ 1-100 m), heterogeneity is characterized mainly by channels, point bars, and other architectural elements (Miall 2013). On a smaller scale, features such as flow regime features ($\sim$ 0.01-1 m) are represented by various geological formations such as ripples, cross-bedding, and lamination.

In the end, we propose to consider all these facies concepts under the simple term 'facies' for the remainder of this study. The reason for this is to maintain generality. A wide variety of methods have been developed to model facies, and some of them can be adapted to several different scales and geological settings, while others are only designed to model specific situations. The goal is to present the list of algorithms to model geological features that are similar (i.e., to make spatial categorical models). The methods are general, while the definition of similarities is context dependent.

Facies model

The term, facies model, can describe two different things depending on the context and must not be confused.

For sedimentologists, a facies model is a simplified and *conceptual* description of a particular sedimentological record and environment (Miall 2013). Such models elucidate the depositional setting, facies associations, and aim to extract the general features while omitting local sedimentological variations. The aim is to have a kind of general template to interpret similar sedimentological deposits. A classical facies model is the sequence of Bouma (1962) which describes the typical sedimentological sequence of turbidites. However, it is important to note that not all turbidites will exhibit this sequence because of various factors such as the content of sand and mud, the local bathymetry, etc. Rather, it serves as a guiding framework for interpretation under standard conditions.

But it can also mean a numerical facies model. These are digital representations of the spatial distribution of the facies and serve other purposes than conceptual facies models. Generally, they serve to feed physical forward models such as groundwater, geophysical, or geotechnical models. Because the facies represent part of the underground that are "similar", it means that petrophys-

ical properties that are intrinsic are likely to be close within the same facies. As such, numerical facies models manifest as categorical fields assigning each cell of a simulation domain to a specific facies. They constitute the subject of the present study.

Conditioning data

In most practical situations, facies models need to respect certain kind of field observations or data. These data are named conditioning data. We recognize two types: hard and soft conditioning data.

Hard data consist of direct observations of subsurface facies and can be seen as a kind of peephole to the truth that is the immensity of the underground heterogeneity. These data points, such as those obtained from wells, are generally considered unquestionable and must be honored.

Soft data is a more ambiguous term as it can indicate any type of data that is not hard data. But generally, soft data means data that are related to the variable of interest but are not the variable in itself. In case of a facies, these include indirect measurements such as some geophysical data (seismic reflection, electromagnetic, gravity, etc.) and direct measurements (other than facies) such as groundwater levels, geophysical logs, chemical composition, etc. Soft data can also mean interpreted data (derived from previous measurements) such as facies proportions maps and curves or even geological knowledge of the area (geometries of facies bodies, orientations, etc.). Soft information can be used to constrain facies models to some extent, depending on the methods utilized.

Not all facies methods are equal when it comes to using data. While some can easily integrate hard and soft data, others may face challenges. Moreover, soft data itself is not equal. Some methods can easily incorporate geometry and orientation information while maintaining control over local facies proportions. Conversely, some methods do not provide these capabilities.

The conditioning data are important in facies modeling because they tend to control which methods are used, since it is generally desirable to obtain models that respect the data as closely as possible.

Expert and geological knowledge

Geological knowledge, mentioned in the previous definition, refers to an expert's knowledge of a geological site. Depending on the situation, the amount and type of this knowledge can be extremely different, ranging from general elements, such as the sedimentological context, to more precise elements such as a preferential direction of anisotropy or the size and shape of certain geological features. It is how the geologist and modeler imagine a certain geological

site and can be viewed as a kind of mental image of the geology. It is often the result of a combination of factors that influence the geologist's thinking. Such as previous knowledge of other sites analogous to the one being studied, the analysis of old data from similar sites, the education, and experience of the geologist. All factors that can influence the geological knowledge of a geologist of a particular area.

Geological knowledge is essential in facies modeling, as it is the base to fill gap between data. For example, knowing that we are in a fluvial environment already enables us to make choices about the methods we will use, the geometries and processes we are trying to reproduce (channel shapes, flood plains, meander migration, etc.).

2.2.2 Facies representation methods

This subsection details the different numerical methods that can be used to represent facies. Facies are categorical values and cannot be interpolated or modeled simply with the existing methods for continuous variables. Therefore, several approaches have been developed to circumvent this issue. Actually, four different approaches exist: indicator approach, truncated approach, tessellation of the domain, and facies proportions. The first three are the most common and seek to create a categorical field of a modeling domain, while the last one is continuous and seek to predict in each location the facies proportions. These approaches are now briefly presented.

Indicator functions

In this approach, categorical values and therefore facies are represented using an indicator function (Journel 1983b; Journel et al. 1990). One indicator function $I_i(x)$ is defined for each facies i. It takes the value $I_i(x) = 1$ if facies i is present at location x in the simulation domain, and it takes the value 0 otherwise. To represent n facies, the method considers n indicator functions that are correlated since only one can be equal to 1 at a certain location and all the others are equal to zero. Following this principle, there are different techniques to predict the value of the indicator functions in the domain and simulate them. In many geostatistical approaches designed to simulated categories, the indicator is not forecast directly but, instead, the probability $P[I_i(X) = 1]$ of the indicator function being equal to one (probability of observing the facies i) is the quantity that is estimated (Alabert 1989; Fogg et al. 1998; Strebelle 2002; Allard et al. 2021). The same approach is used in Machine Learning approaches (Breiman 2001). Note, however, that some methods simulate the indicator directly and bypass the probability calculation such as the Direct Sampling MPS method (Mariethoz et al. 2010a) for example or Generative Adversarial neural Networks (Laloy et al. 2018).

Truncation of a continuous field

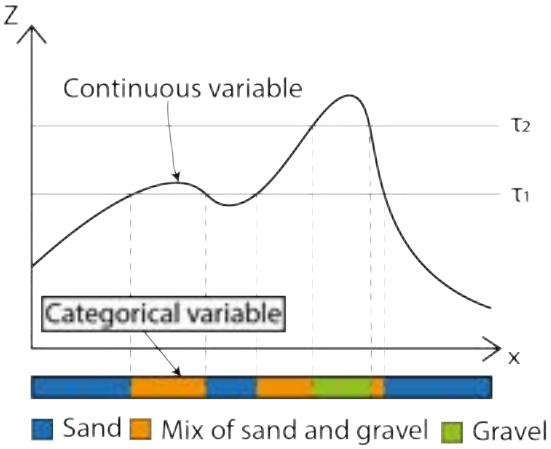

Figure 2.1: *One-dimensional principle of truncation to generate categorical variable from a continuous variable. Modified from Pyrcz et al. (2014). Note that here thresholds are constant through space (straight lines).*

This approach proposes transforming one (or more) continuous latent field(s) into a categorical field by truncating it with one or several thresholds. The application of these thresholds separates the continuous variable in different regions, each corresponding to one category. This method has been introduced by Matheron et al. (1987) in spatial statistics for geological applications and called the truncated Gaussian method (Galli et al. 1994; Mariethoz et al. 2009; Armstrong et al. 2011) and a similar idea was introduced by Osher et al. (1988) in physics and called the level-set method (Osher et al. 1988; Allaire et al. 2002; Dervieux et al. 2006; Cardiff et al. 2009). The ways to construct the underlying continuous field(s) differ in these approaches, but the principle is always the same: truncating the continuous values. Figure 2.1, shows an example of the truncation of a continuous variable. The two thresholds are represented by the horizontal lines. When the continuous values are above τ_1 and below τ_2, the category, or attributed facies, is the orange one (mix of sand and gravel). When the continuous value is lower than τ_1, the facies is sand, and when it is above τ_2 the facies is gravel. The choice of the thresholds is generally made with the aim of respecting the proportions of each facies, depending on the distribution of the latent variables, often considered as normally distributed (Falivene et al. 2007b; Armstrong et al. 2011). Thresholds can vary spatially to take into account varying proportions, both horizontally and vertically (Beucher et al. 2016).

Tessellation of the domain

This approach aims to define regions in the modeling domain to delineate the facies boundaries. This can be done using many different techniques. One can for example model the spatial boundaries between the facies as surfaces in 3D or lines in 2D. The boundaries can have specific geological constrained geometries or they can simply be defined to split the domain into regions that are the closest to certain observations (nearest neighbor). Another method, often employed since the early work on boolean simulations (Haldorsen et al. 1984; Begg et al. 1985), is to use numerical objects with a predefined geometry and place these objects in the domain. The boundaries between objects define the tessellation of the domain. The objects often have a geological significance (e.g., meanders, lobes, stratigraphic surfaces, etc.). Compared to the truncation approach, the tessellation one alleviates the need to construct a continuous latent field and can provide more control over the generated geometries. By adding sophisticated rules on the relation between the objects and their probability of occurrence one can generate extremely realistic spatial distributions of facies with these approaches (Lopez et al. 2009; Pyrcz et al. 2009).

Facies proportions

Finally, some methods do not use directly categorical values but they predict the proportions of the different grain classes in each part of the modeling domain directly (Granjeon 1996; Koltermann et al. 1996; Lesser et al. 2004). The resulting models are continuous rather than categorical. While this may seem like a more natural way to model the subsurface, it is no less challenging to do correctly. To achieve this, one must be able to predict or estimate the movement of the different grain classes throughout the sedimentological history of the modeling site. This can imply considering hydrodynamics, bedload and suspended transport, sediment supply or tectonic factors (e.g., uplift, subsidence). This approach is primarily used by process-based methods that are physically based and capable of modeling sediment transport, deposition, compaction, fluid movement, and diagenesis.

2.3 Deterministic methods

We start this overview by the simplest facies modeling methods: the deterministic ones. They are defined as methods that produce a single unique subsurface model of the distribution of the facies, underground without uncertainty quantification.

Often they need little or no parameterization. In these cases, they are simple to use and produce results in an instant, provided that parameters (if required) have been defined. But they can also involve a significant degree of manual interpretation and then take much longer time and effort (Cowan et al. 2002).

We divide the most commonly used deterministic methods in hydrogeology in three categories: manual interpretation, nearest neighbor interpolation, and continuous interpolation methods.

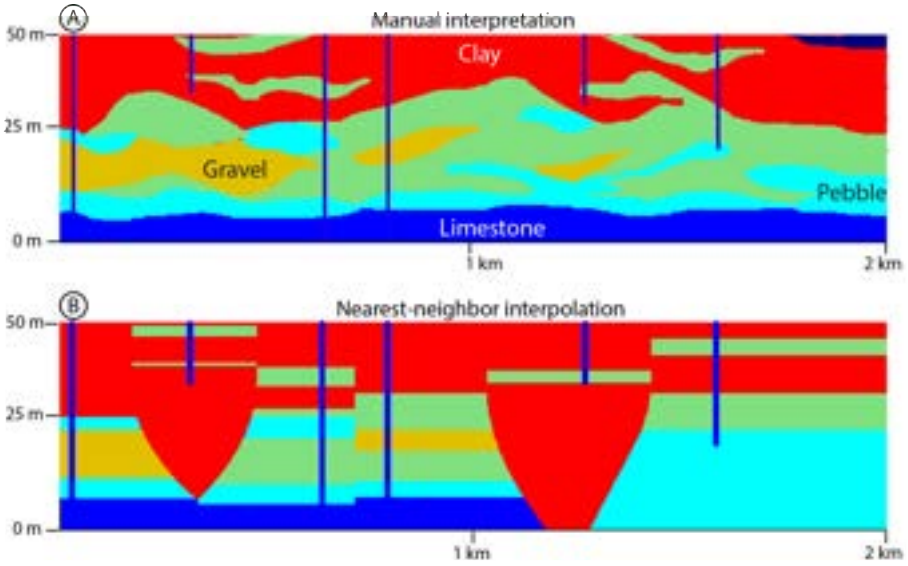

Figure 2.2: *Examples of a vertical cross-section facies model for a fluvioglacial deposit around Copenhagen in Denmark.* ***A****) manual interpretation taken from Imbeaux (1930).* ***B****) nearest neighbor interpolation without anisotropy. The conditioning data (boreholes) are represented by the dark blue vertical lines. Note that the vertical scale is exaggerated as compared to the horizontal scale.*

2.3.1 Manual interpretation

One of the most natural and traditional ways to characterize heterogeneity is to rely on expert knowledge and let the geologist manually delineates the boundaries between the facies (Houlding et al. 1994; Bosch et al. 2009; Sech et al. 2009). The geologist builds what Jørgensen et al. (2015) call a *cognitive 3D geological model*. This approach appears to be convenient as, on the one hand, it does not necessarily require any computational resources but, on the other hand, it needs expert information and sufficient time. The main advantage of the method is that it allows geologists to construct models with reasonable structures even when the data set is extremely scarce. By relying on general geological concepts and analogy with other sites, most geologists can construct such cognitive models. We believe that this is the reason why most models are made using this approach.

However, the quality of the model depends strongly on the experience of the person making the model. His interpretation of the local geology can be biased, influenced by many factors such as his background and expertise. Estimating

the uncertainty of such models is difficult. Replicating the results is another major difficulty. Moreover, while it is simple to draw in 2D, the task is much more complex in 3D. Therefore, in these situations a common approach is to draw several vertical cross-sections on the simulation domain, to extract control points, and to interpolate the interfaces between the sections (Jørgensen et al. 2015). This approach works well for geological layers that can be tracked through the whole domain such as stratigraphical units, but is more difficult when it comes to smaller geological features such as facies.

Figure 2.2A shows an example of a geological manual interpretation on a 2D cross-section. The structures appear realistic with elongated shapes and respect the data at the wells. However, this is only one possibility of the subsurface, and other interpretations could have been drawn. This highlights a significant issue with the manual interpretation method, which is highly dependent on the user. This means that the features depicted in the drawing can vary significantly depending on the person creating it. When a geologist draws an interpretation, he relies on his knowledge of the site and experience. Therefore, even though the method allows for flexibility in drawing, it has poor reproducibility, making updating the model a cumbersome and time-consuming task. It is possible that over time, different geologists may work on the same manually interpreted models with varying perspectives, without fully comprehending how the model was initially constructed. Moreover, when the data sets are dense, it may become extremely cumbersome to integrate all the data manually (Cowan et al. 2002).

2.3.2 Nearest neighbor interpolation

Nearest Neighbor (NN) interpolation is one of the simplest algorithms to interpolate facies. At location x, the algorithm assigns the facies observed at the closest data point (Wilkinson et al. 1983; Tartakovsky et al. 2007). It is one of the most commonly used and available deterministic methods in classical geomodeling software (Babak 2014). But it has received little enthusiasm from the scientific community because it does not generate realistic geological features. The boundaries between the facies are straight and the resulting geometries depend heavily on the available data. Figure 2.2B shows, for example, that NN generates modeling artifacts (e.g., the two clay cone shapes below the shallowest boreholes) and unrealistic facies boundaries. However, note that it is our geological common sense that indicates that Figure 2.2B is less realistic than Figure 2.2A. But, there is a possibility that the NN is closer to the truth than the manual interpretation. For this example, we know that this is not the case as the cross-section shown in Figure 2.2A has been drawn using more than 30 boreholes by an experienced geologist. For this reason, the manual interpretation can be considered as much more reliable than the nearest-neighbor interpolation (Fig. 2.2B) based only on 6 boreholes. But in general, it is difficult to be certain about which model predicts better the reality. This is a general

question for all the methods presented in this review, and this is why cross-validation techniques have been developed (Deutsch 1998; Juda et al. 2020). When the data set is large, NN can provide good results when compared to more advanced methods (Tartakovsky et al. 2007).

The basic method described in the previous paragraph can be improved in several manners. One can for example use the k closest neighbors (kNN) and take the most frequent in this ensemble (Hastie et al. 2009). This is a classical method in machine learning. One can also perturb the distance computation to select the closest neighbor but account for geological anisotropy (Volken et al. 2016). This can be done by transforming the data coordinates using anisotropy factors (in the x, y and/or z direction) before applying the nearest-neighbor algorithm. Retaking the example of Figure 2.2B, this would help the limestone layer at the bottom of the model extend through the whole domain as in the manual interpretation.

2.3.3 Continuous interpolation approaches

Another deterministic approach to estimate the spatial facies distribution is to rely on well-known continuous interpolation methods such as inverse distance weighting (Shepard 1968, IDW) and to combine them with the indicator or truncation representation methods presented previously (section 2.2.2).

Note here that stochastic interpolation methods such as kriging are not considered as they can provide an estimate of uncertainty on the interpolation. Kriging and related methods combined with indicator and truncated approaches are covered in the dedicated section on variogram-based methods (section 2.4).

Truncation of one latent variable

The truncation approach considers one latent variable $Z(x)$ and several thresholds. All the facies are placed on one scale for the latent variable and an order needs to be defined. The choice of the thresholds is not restricted, but they are typically determined to respect the target facies proportions. A common practice is to define intervals for each facies such that their lengths (range of values) are proportional to the facies proportion. Then, it is necessary to convert the conditioning facies data into continuous data. It can be done by choosing the average value of each intervals (Falivene et al. 2007b, e.g., if the facies sand has the lower and upper limits of -1 and 0 respectively, all sand data points will be set to -0.5). Once the thresholds have been defined and data transformed to continuous values, any interpolation method can be applied. A common algorithm used for this purpose is Inverse Distance Weighting interpolation (IDW) (Falivene et al. 2007b; Babak 2014), but any interpolation technique can be used, as long as it can handle irregularly spaced data. IDW estimates $Z(x)$ by computing a weighted average of the neighboring data points. The weights

are inversely proportional to the distance between x and the data raised to a user-defined power. Closer data have greater weights than distant ones. One advantage of IDW is that it requires only two parameters (the power and the number of maximum neighbors), while still providing some flexibility. Note that if anisotropy is considered, then three parameters are required where the anisotropic factor must be defined.

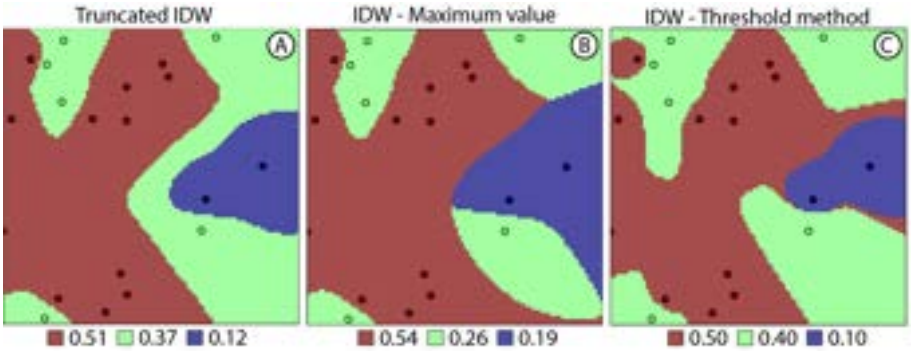

Figure 2.3: *Results of three deterministic methods on a 2D synthetic case. Circled data are hard data.* ***A****) facies model using the truncated approach where IDW was used as the interpolator.* ***B****) Model showing the facies with the maximum value of the indicator (explained below) at each pixel of the simulation grid where the indicator functions were interpolated with IDW.* ***C****) facies model where thresholds were used and adjusted to match a certain facies proportion and using IDW. For threshold methods and truncated approaches, identical target facies proportions were used.*

Figure 2.3A shows an application of this method. 20 points with three different facies constitute the data set and are shown on the map. The facies at these locations have been transformed in continuous latent values, that were interpolated and truncated. The resulting map shows a systematic ordering of the facies (red, green, and blue). The green facies surrounds the blue facies. With this approach, it is not possible to have the red and blue facies side by side. Another coding of the facies with a different order (e.g., red, blue, and green) will lead to a completely different result. The boundaries between the facies are rather straight.

Despite the appeal of estimating a categorical model directly using one single interpolation, this method suffers from several problems. First, it requires an ordering of the facies. In Figure 2.1, the sand and gravel facies can never be touched because the mix of sand and gravel will always be between the two. This is a strong assumption about the spatial distribution of the facies that works well if the facies are ordered, but which may prove difficult to apply in many cases. Second, as the distribution of the latent variable is not known, the choice of the thresholds is not straightforward and it can be difficult to respect the target facies proportions. One way to circumvent this issue would be to perform the interpolation first and determine the thresholds in a second step

to respect proportions. But, as the interpolation relies on the conditioning data, which themselves depend on the thresholds, the problem is not easily solved.

According to Falivene et al. (2007b) the deterministic truncation of one single latent variable methods generally perform poorly as compared to the indicator approaches. They recommend using truncation approaches only if there is a clear ordering of the facies observed in the data.

Indicator approaches

Indicator approaches involve converting facies data into indicator values and interpolating them to obtain a continuous value $Z_i(x)$ (between 0 and 1) for each location in the simulation domain. This process is repeated for each facies, resulting in a series of interpolated values $Z_i(x)$ between 0 and 1 (2D or 3D), one for each facies. The values $Z_i(x)$ are sometimes interpreted as a probability, but one must be very careful with this interpretation because $Z_i(x)$ are not defined on any well-defined probabilistic space and are not proper probabilities.

In the second step, the resulting $Z_i(x)$ maps must combined to obtain a single categorical map. Two methods are employed: (1) the *Maximum value* and (2) the *Multi-Thresholds* approach.

For the *Maximum value* method, at any location x the values $\{Z_i(x), i = 1, \ldots, n\}$ are compared and the facies k corresponding to the highest value $Z_k(x), k \in [1, \ldots, n]$ is selected. This method is often described as the *Most probable value* but to be rigorous it should be only employed when the values $Z_i(x)$ represent a proper probability.

For the *Multi-Thresholds* approach, an ensemble of thresholds is computed to truncate $Z_i(x)$ and to ensure that the final categorical map will respect the proportions of the facies (Ritzi Jr et al. 1994; Guadagnini et al. 2004). Practically, we define an empty resulting grid and we choose a facies i and adjust a threshold τ so that the mean of the boolean map $Z_i(x) > \tau$ is closest to the proportions of the target facies p_i that can be input by the user or inferred from the data. When τ has been found, the true cells of $Z_i(x) > \tau$ are assigned to the final grid as belonging to facies i. Then another facies is chosen and we repeat the above instructions. Two important things to note, primarily, once the cells have been assigned to the final grid, they cannot be changed, secondly, it is essential to begin the facies assignment by the rarest facies to ensure to respect the target proportions p_i.

The first option is straightforward and simple to understand, but it can lead to artifacts or errors because it does not consider the adjacency of the facies. Moreover, the rarest facies, which can sometimes have a significant impact on groundwater flows by acting as preferential paths or hydraulic barriers, are less

likely to appear than others and there is a risk that they will be underrepresented. The second option, on the other hand, ensures that the proportions and continuity of the facies over the simulation domain are respected.

An example of these two methods using IDW is shown in Figures 2.3B and 2.3C. The target facies proportions are 10% for blue facies, 50% for red facies, and 40% for green facies. These two cases show the differences between choosing between the maximum value facies and the threshold method with IDW. Globally, both maps share some similarities, but the facies proportions and the exact locations of the boundaries are different. Notably, the maximum value method overrepresents the blue facies and underrepresents the green facies. This issue is not present in the other methods, which have greater control over the final proportions.

The Figure 2.4 presents another example of the indicator approach using IDW with the data from Figure 2.2. The IDW method produces smoother interfaces and more realistic features compared to the nearest-neighbor interpolation method (Fig. 2.2B). However, a lot of artifacts and unrealistic structures remain such as the deep clay cones (red facies) under two boreholes or the non continuity of the limestone layer (dark blue facies) at the bottom. Probably the use of an anisotropy would help to partly solve this issue.

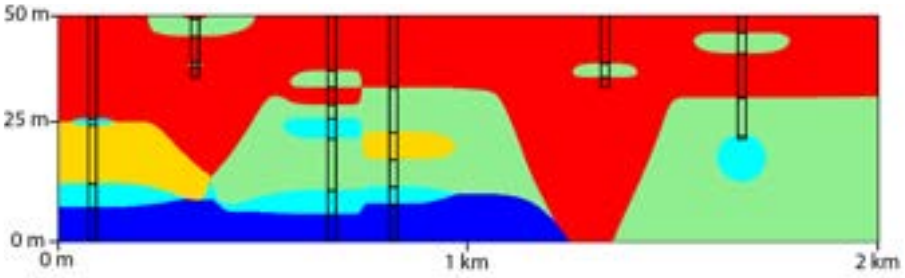

Figure 2.4: *Maximum value method with IDW using same data of the cross-section shown in Figure 2.2. For corresponding reference colors of the facies see the original Figure.*

2.3.4 Machine learning approaches

A class of algorithms that is well known for their classification abilities is the machine learning algorithms. We have already seen that nearest neighbors methods are frequently employed to interpolate facies. The k-Nearest Neighbors algorithm is slightly more advanced (Hastie et al. 2009) and can also be used to map lithologies or facies. For example, Martín-Martín et al. (2023) used it to map the 3D stratigraphic architecture of the Llobregat River Delta in Spain. Other machine algorithms such as support vector machines have also been used to delineate facies (Tartakovsky et al. 2004; Wohlberg et al. 2005; Smirnoff et al. 2008). As for the previous methods in this section, often the

results can be accurate when large data sets are available, but when the data sets are too sparse the methods contain little geological information and the resulting geometries are often not plausible from a geological perspective.

2.3.5 Summary

To conclude, deterministic methods provide images of the subsurface quickly and easily, but, by definition, are unique. As a result, there is no direct estimate of uncertainty. Moreover, these methods are highly data-driven. Integration of hard-conditioning data is not a problem as they are generally mandatory. Soft data can also be integrated in the form of probability maps by simple combination with indicator approaches and spatially varying thresholds for truncated approaches. An important advantage, however, is that none of them is grid-dependent, so it is possible to estimate the facies at any point in the domain. Finally, these methods are far less popular than stochastic methods, which are more flexible, realistic, and provide a measure of uncertainty.

2.4 Variogram-based methods

These methods use two-point spatial statistics to model the spatial distribution of categorical variables and produce equiprobable realizations of the subsurface. The measure of these two-point spatial statistics is the variogram, which has been a major foundation for a large number of spatial statistics studies since it was proposed by Matheron (1963). First, the notions of variogram and kriging are briefly presented.

2.4.1 Basic geostatistical concepts

The variogram

The variogram is a measure of the spatial statistics of a continuous variable that is expressed in terms of variance against distance. It can be computed using the following formula:

$$\gamma(h) = \frac{1}{2N(h)} \sum_{i=1}^{N(h)} (z(x_i + h) - z(x_i))^2 \tag{2.1}$$

Where h is the lag distance between pair of points, $\gamma(h)$ is the variogram for a specific lag distance h, $N(h)$ denotes the number of pairs of points separated by lag distance h, $z(x_i)$ represents the variable of interest at location x_i and $z(x_i + h)$ represents the variable of interest at location h units away from x_i. As this expression divides the total by two, the variogram is also called semivariogram. Mathematically, the variogram represents the expected semi

variance of a variable at a given distance. Naturally, we expect it to be close to 0 at the origin and to increase with distance (closer data points are more similar than farther ones).

The given expression assumes perfect computation of the variogram for each lag distance h, which is not realistic. In practice, a discrete approach is used where pairs of points are grouped into lag distance categories, and the mean value of the variogram is computed for each category. The computed variogram on a set of data points is commonly referred to as an experimental variogram. Once the experimental variogram is obtained, predefined variogram models, which are equations with parameters, are typically fitted to it. The parameters of these models generally include the range, which is associated with the spatial correlation of the variable, and the contribution, which corresponds to the variance of the variable. The most widely used variogram models are the spherical, exponential, Matérn, gaussian, and cubic models. Variogram models can be combined to create more intricate variogram structures, allowing for the replication of a diverse range of experimental variogram curves.

When the variable of interest is an indicator function ($z(x_i)$ becomes $I(x_i)$ in eq. 2.1), the variogram is then referred as the indicator variogram (IV). IVs are frequently utilized in facies modeling as an input by various methods, and also to ensure that the models accurately reproduce the expected two-point statistics.

When a variogram is used to describe the correlation between different variables, it is called a cross-variogram. Practically, in equation 2.1 the two compared z will be two different variables, for example temperature and elevation. The idea is to see how these two variables changes with respect to their lag distance. Similarly, cross-indicator variograms are indicator variograms that compare two different indicator functions (two different facies).

Kriging

Kriging is a class of interpolators, introduced by Matheron (1963), inspired from the work of Krige (1951), which are based on a weighted linear combination of the neighboring values. The weights are determined in order to minimize the kriging variance (or the error). In its simplest form, for any location where the variable is unknown, the kriging estimation can be written as:

$$Z_0^* = \sum_i \lambda_i Z_i \tag{2.2}$$

where Z_0^* is the estimated value at unknown location, λ_i the weight associated to data point i and Z_i is the value of the variable of interest at data point i.

The difficulty relies in determining the weights. Fortunately, Matheron (1963) demonstrated the relationship between the variograms and the weights (λ), allowing them to be easily determined based solely on the constraint to determine a variogram model. Kriging provides not only an estimate of the value, but also a variance (or error) on the estimates, making it practical to combine with stochastic approaches.

There is no single kriging method, but a whole range based on different assumptions. The most commonly used in facies modeling are simple kriging, which assumes that the mean of the variable is known, and cokriging, which takes advantage of the cross-variogram to provide more accurate estimates. Of particular interest for facies modeling, when kriging is used to interpolate an indicator function, it is called Indicator Kriging (IK). Interested readers are encouraged to consult Chiles et al. (2012) for more information on kriging and related methods.

2.4.2 Sequential Indicator Simulation

Sequential Indicator Simulation (Alabert 1989; Journel 1989; Journel et al. 1990; Gómez-Hernández et al. 2021, SIS) is an algorithm that was developed to generate discrete stochastic realizations using the indicator formalism developed by Journel (1983b).

The basic idea of SIS is to fill the simulation grid node by node, conditionally to hard data and previously simulated nodes. SIS relies on IK which assumes that IVs are known for each facies. In detail, the basic algorithm consists of the following steps:

1. Create an empty simulation grid and add the conditioning data to it
2. Randomly select an empty cell c_j
3. Estimate facies probabilities p_i at the empty cell location with IK based on already assigned cells (both hard data and previously simulated cells)
4. Draw a facies according to p_i and assign it to c_j
5. Go to step 2 until no empty cell are remaining

Figures 2.5A-D show SIS realizations based on the conceptual model drawn in Figure 2.2A. The hard data and proportions are respected, the strong global anisotropy is reproduced, and we also have an estimate of the uncertainty with the set of stochastic realizations. But while SIS generates images that appear more realistic than the NN (Fig. 2.2B), it is difficult to regard them as plausible subsurface realities. Limitations are due to the building brick behind the

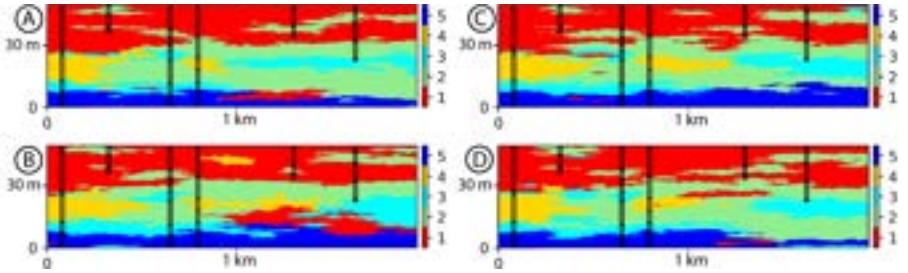

Figure 2.5: *Four equiprobable SIS realizations performed using same data as Fig. 2.2. Only borehole data have been considered in this example (no locally varying probabilities).*

methodology, the variogram. The variogram is a spatial measure of the **point-to-point** spatial correlation of a variable with respect to itself or between two variables, it is a two-point spatial statistic measure. These two-point statistics have been shown to have difficulties to capture the spatial statistics of complex geometries such as meandering channels (Guardiano et al. 1993; Dell'Arciprete et al. 2012). A problem that can be partly solved by considering cokriging at step 3 of the algorithm by integrating cross-variogram between each facies (see section 2.4.4) (Carle et al. 1996) or by considering the statistics of a higher number of points (see section 2.5).

The simplicity and flexibility of this algorithm makes it easy to integrate conditioning data, as well as expert knowledge. Integration of soft data (e.g., geophysical measurements) can be done in several ways: using facies probabilities derived from these soft data, or directly integrated in the modeling process with cokriging algorithms (Deutsch 2006). The latter is known to be difficult because it requires to estimate the cross-variograms between facies data and secondary data (Deutsch 2006; Pyrcz et al. 2014). Generally, if facies probabilities can be derived from soft data, the first option is preferred and can be integrated in two different manners: assuming locally variable mean during IK estimation (step 3) or by Bayesian update (Doyen et al. 1994). Bayesian update proposes to combine indicator probabilities (derived from IK) with soft facies probabilities (derived from facies data) using the Bayes equation. Orientation data can also be integrated by modifying the anisotropy (angle(s)) of the variogram model used during step 3, an example is shown in Figure 2.7 where the dip angle varies locally. It shows that SIS is able to generate (or at least approaching) elongated and semi-continuous features despite the limitations of two-point statistics (variogram). This methodology has been used, for example, by Thomas et al. (2019) to generate stochastic facies models of a continental shelf to study the fate of fresh groundwater on a decamillennial time scale.

Let us finally mention the nested (or hierarchical) version of SIS as proposed by Journel et al. (1998) and formalized by Zappa et al. (2006) as HSSIM for Hierarchical Sequential Simulation (Fig. 2.6). The goal is to simulate facies

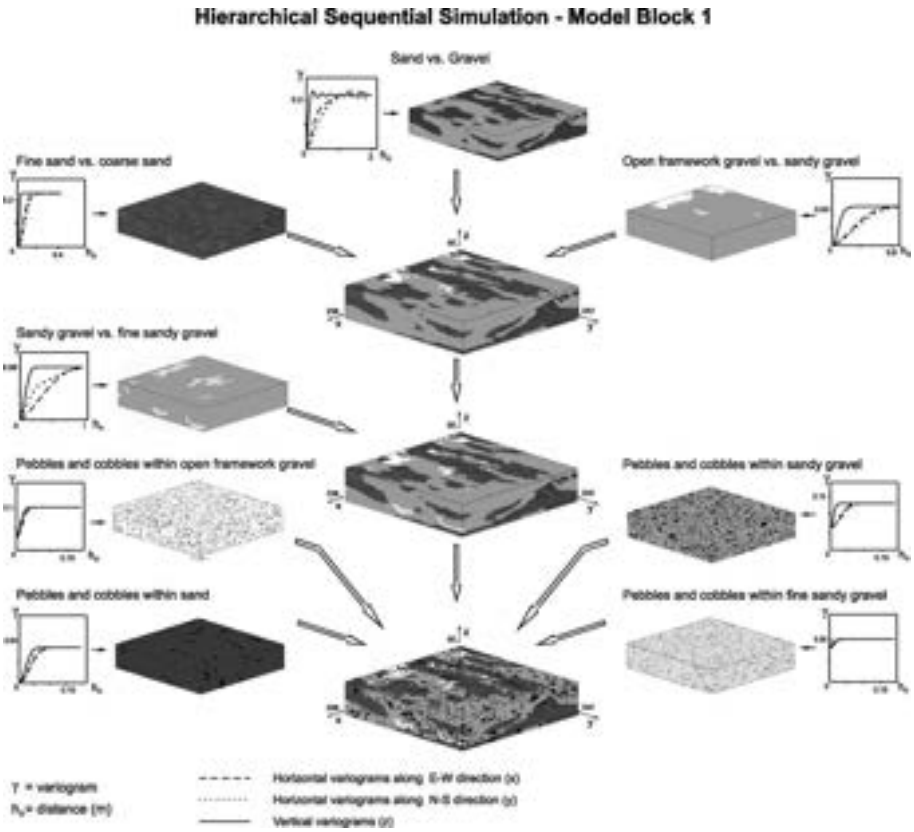

Figure 2.6: *HSSIM worklfow. First step consists in simulating sand facies all together against gravel facies. In the second step the different sand facies (fine sand, coarse sand) are simulated inside the global sand facies (from step 1) and the same applies for gravel facies. Finally all pebbles and cobbles are simulated in each previously simulated facies. Taken from Zappa et al. (2006).*

only in pairs, assuming that hierarchical relations exist within similar facies. For example, in the example shown in Figure 2.6, the sand facies are grouped together as well as the gravel facies, and a simulation of sand vs. gravel (first step) is performed to delineate the separations between the sand and the gravel facies. Then, the two gravel facies (open framework and sandy gravel) are simulated together exclusively where the gravel facies were simulated in the first step. The exact same procedure is applied for sand facies, and finally pebbles and cobbles are simulated inside each other's facies. This methodology gives greater control over the spatial distribution of facies and allows variograms to be defined for each binary simulation of facies. It generally reproduces subsurface heterogeneity and connectivity better than SIS alone, while reducing uncertainty (Comunian et al. 2016b).

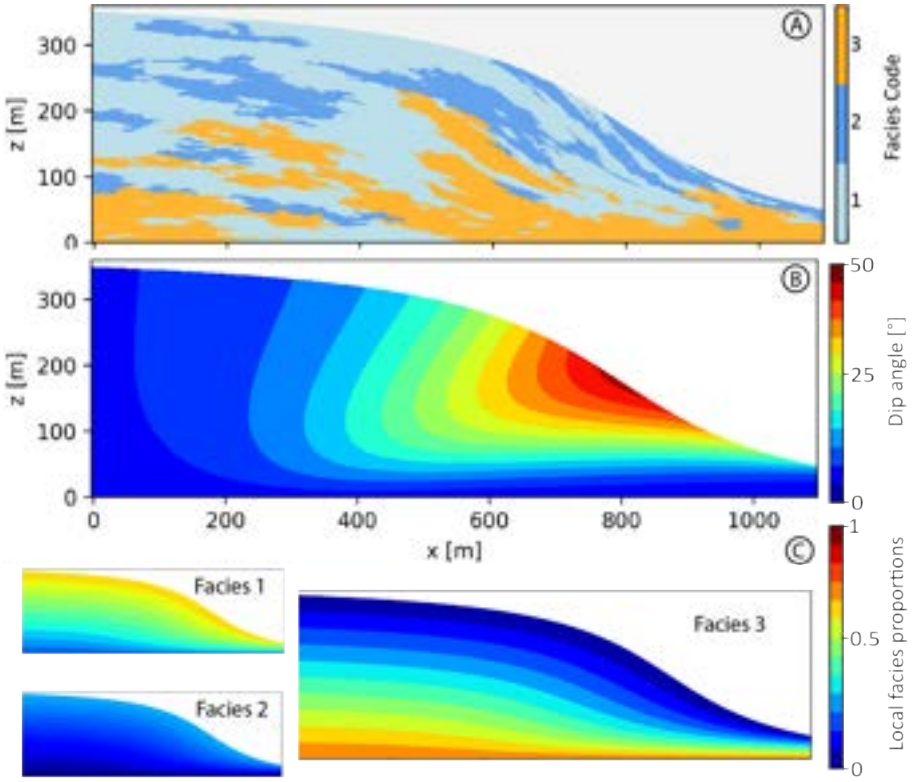

Figure 2.7: ***A****: Example of an SIS realization with locally varying angle anisotropy and facies proportions.* ***B****: Corresponding anisotropy (or dip) angle to horizontal.* ***C****: Corresponding local facies proportions. No hard data have been taken into account in this example.*

SIS is a well-known algorithm for geostatisticians and hydrogeologists, as can be seen from its various applications to facies modeling in a large number of geological settings such as glacial (e.g., Salsabili et al. 2021), alluvial (e.g., Huggenberger et al. 2006; Zappa et al. 2006; Dell'Arciprete et al. 2012), deltaic (e.g., Jorreto-Zaguirre et al. 2020), turbidite reservoirs (e.g., Alabert et al. 1990), clastic reservoirs (e.g., Journel et al. 1993), soil mapping (e.g., He et al. 2010) with large number of applications to hydrogeology (e.g., De Marsily et al. 1998; Huggenberger et al. 2006; Quental et al. 2012; Xue et al. 2022). The widespread popularity of SIS is mainly due to its simple parameterization, computational efficiency, and seamless data integration.

However, in addition to simulating unrealistic geological structures, as previously explained, SIS has been shown to suffer from several conceptual limitations (Emery 2004). These include imperfect respect for IVs, a limited number of possible variogram models (e.g. gaussian and cubic models unusable) or simulations significantly dependent on edge effects or number of nodes simulated.

This can lead to artifacts and is one of the reasons why some authors suggest using a simulation grid larger than the area of interest and then cutting it off (Falivene et al. 2007a). Finally, it has also been shown that SIS suffers from several issues when it comes to flow simulations based on SIS models. This is of primary concern given that, in the majority cases, the purpose of a facies model is to be applied to flow and transport models (De Marsily et al. 2005; Manzocchi et al. 2023).

2.4.3 Indicator Kriging

Alternatively, IK can also be used directly to interpolate the indicator functions and combined them in the same way as presented in the section on deterministic methods with the indicator approach (section 2.3.3). Note that the resulting model is in this case deterministic, despite that kriging is a stochastic method. Kriging uncertainty quantification could be used to produce several facies probability maps but is generally neglected. Again two approaches can be used to transform indicator functions to categorical fields, the maximum value facies method and the threshold method. The main difference with what have been presented in deterministic methods section is that the interpolation of the indicator function is performed with the kriging equations. This means that variograms have to be provided which allow to consider the spatial correlation of each facies. Examples of IK are shown in Figure 2.8A and Figure 2.8B. The target facies proportions are 10% for blue facies, 50% for red facies, and 40% for green facies. Again the threshold method allows to have a greater control on the facies proportions compared to the maximum value method. In this simple case, the results are similar to the one obtained with IDW, suggesting that both methods can be used interchangeably. For example, Falivene et al. (2007b) and Babak (2014) observe very similar results between both methods. IDW has even been shown to perform better than kriging for continuous variables if the data do not show a strong anisotropy and if they are relatively well dispersed and not clustered (Weber et al. 1992). Concerning NN, Babak (2014) have shown that NN models perform worse than IK and indicator IDW. However, all of these comparisons need to be tempered, as few studies to date have compared these methods with each other, and a greater number of different geological settings and case studies should be considered before drawing general conclusions. Results can highly depend on the parameters chosen.

Another example of IK is shown in Figure 2.9. Results are better than the ones obtained using IDW (Fig. 2.4) as a spatial model can be more easily considered with IK. This allows to have a continuity of the facies through the domain such as the limestone layer. Compared to results obtained with IDW and NN, structures are smoother and appear more realistic and closer to the reference (manual interpretation, Fig. 2.2A). This demonstrates the utility of IK over other interpolation methods such as IDW. However, there are still significant differences between the two models. The IK model exhibits greater

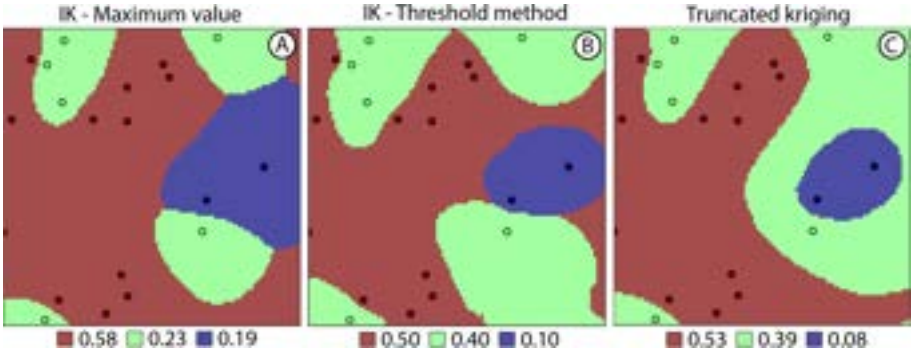

Figure 2.8: *Results of three deterministic methods on the same 2D synthetic case as shown in Figure 2.3. Circled data are hard data.* ***A****: model showing the facies with the maximum value at each pixel of the simulation grid using IK as interpolator.* ***B****: facies model where thresholds were used and adjusted to match a certain facies proportion and using IK.* ***C****: facies model using a truncated approach where kriging was used as the interpolator (see section 2.4.6). For threshold methods and truncated approaches, identical target facies proportions were used.*

homogeneity and less variability in the facies compared to the reference model. This is because kriging is an estimation method that smooths the results. The differences between the IK model and the simulations with SIS (Fig. 2.5) are evident, as the latter presents a variability similar to that of the reference model.

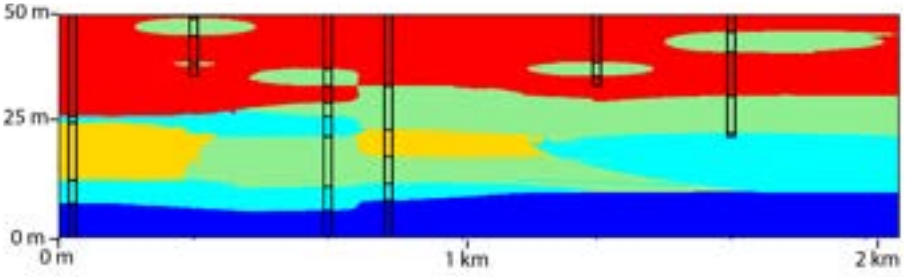

Figure 2.9: *IK using same data of the cross-section shown in Figure 2.2. The facies code were obtained by using the indicator value facies method. IV of each facies have been inferred on the borehole data. No locally varying probabilities have been considered. For corresponding reference colors of the facies see the original Figure*

Compared to IDW and other linear interpolator, kriging algorithms (simple or ordinary) are generally preferred, as they are well known to be optimal linear unbiased estimators that minimize variance assuming known two-point spatial correlation (variogram) and stationarity (no variation of the mean and variance over the simulation domain) (Matheron 1963; Chiles et al. 2012). IDW does not have these advantages, but, on the other hand, it requires little parameterization as only two parameters need to be adjusted (power and number

of neighbors) and can be used more "directly" than kriging, which requires the estimation of variograms, one for each facies (or only one in binary cases).

2.4.4 Transiogram based

TPROGS

A specific constraint of variogram-based techniques, notably with SIS, is their inherent difficulty to replicate asymmetrical structures, such as cyclicity or fining-upward sequences, which are common observed geological phenomena. Sequential methods, when viewed through the prism of variograms (or covariances), struggle to achieve similar outcomes. This challenge was among the motivations for the introduction of transiograms as an interesting alternative to variograms in stochastic facies modeling, as proposed by Carle et al. (1996).

A transiogram, as well as the indicator variogram, is a spatial measure of the difference of an indicator function (or categorical variable) with respect to a particular lag distance ($\mathbf{h}$). The distinctive feature of the transiogram lies in its intuitive nature, as it is rooted in the transition probabilities between the same facies, simple transiogram (ST), or between two distinct facies, cross-transiogram (CT). Its mathematical derivation is simple.

First, p_i is defined as the probability of observing facies i across the domain under stationarity assumptions and $p_{ij}(\mathbf{h})$ as the probability of observing facies j at a specific lag distance $\mathbf{h}$ from facies i. The cross-transiogram $t_{ij}(\mathbf{h})$ is thus conceived as the conditional probability of observing facies j at a lag distance ($\mathbf{h}$) from an arbitrary location $\mathbf{x}$, provided that facies i is observed at this location:

$$t_{ij}(\mathbf{h}) = \frac{p_{ij}(\mathbf{h})}{p_i} \tag{2.3}$$

Or, using indicator functions:

$$t_{ij}(\mathbf{h}) = \frac{\Pr\{I_i(\mathbf{x}) = 1 \text{ and } I_j(\mathbf{x}+\mathbf{h}) = 1\}}{\Pr\{I_i(\mathbf{x}) = 1\}} \tag{2.4}$$

where $\Pr\{...\}$ denotes a probability and $\mathbf{x}$, is an arbitrary location of the simulation domain. ST can be easily derived from equation 2.4 using the same facies index (replacing j by i). Equations 2.3 and 2.4 indicate that $t_{ij}(\mathbf{h})$ is a function of the proportion of the first facies (in this case p_i) and this is natural. Consider a prevalent facies with a high proportion; this facies is likely to occupy more significant space than the others, subsequently diminishing transitional probabilities. Consequently, there is a greater likelihood of encountering this

dominant facies at larger distances from any arbitrary location compared to any other facies.

One of the most important property of transiograms is that generally:

$$p_{ji}(\mathbf{h}) \neq p_{ij}(\mathbf{h}) \tag{2.5}$$

or equivalently,

$$p_{ji}(\mathbf{h}) \neq p_{ji}(-\mathbf{h}) \tag{2.6}$$

which is the definition of asymmetry. On the contrary, indicator variograms do not allow such relations and imply symmetry because variograms only consider the direction of the distance vector ($\mathbf{h}$), not its sense (Carle et al. 1996). This means, for example, that for a given direction and lag distance (e.g., 5 m in the positive direction z, $\mathbf{h} = (0, 0, 5)$ m), the probability of finding facies j 5 m above an occurrence of facies i ($p_{ij}(0, 0, 5)$) is not identical to the probability of finding facies i 5 m above an occurrence of facies j ($p_{ji}(0, 0, 5)$).

In addition, transiograms are more intuitive than variograms. They express probabilities of transition instead of variance, making them easier to understand and interpret. Transiograms also provide valuable insights into the average length of modeled facies bodies and their overall proportions. For a deeper understanding, the interested readers are encouraged to refer to Carle et al. (1996). Experimental transiograms are typically represented as a set of $k \times k$ transiograms, where k denotes the total number of facies, as exemplified in Figure 2.10. These have been computed on a synthetic data set. Diagonal graphs (Fig. 2.10A, F, K, P) show the spatial variability of a facies with itself (ST), while the others represent transitions from one facies to another (CT). They exhibit opposite behavior: ST decreases with distance, while CT increases. This is logical, as there is a spatial correlation between the facies, and two points close together are more likely to belong to the same facies than two further apart. However, we can observe an irregularity when observing the transition from facies 0 to facies 1 (Fig. 2.10B), where a decrease of the transition probabilities is observed after an initial increase. This decrease indicates that facies 1 often tends to overlap facies 0 more than in reverse. This phenomenon is not visible on the transiogram from facies 1 to facies 0 (Figure 2.10E), showing evidence of asymmetry. Facies 1 often overlaps Facies 0, but the reverse is not true. An important aspect of experimental transiograms is that the plateaus they reach correspond to the proportions of the target facies (column facies). For example, all transiograms in the second column (Figures 2.10B, F, J, N) converge to around 0.25, which corresponds to the proportion of facies 1 in the data.

Once the experimental transiograms have been computed, a spatial model can be fitted to them. Carle et al. (1997) have shown that this is achievable using a 1D continuous Markov Chain Model (MCM) that is defined as:

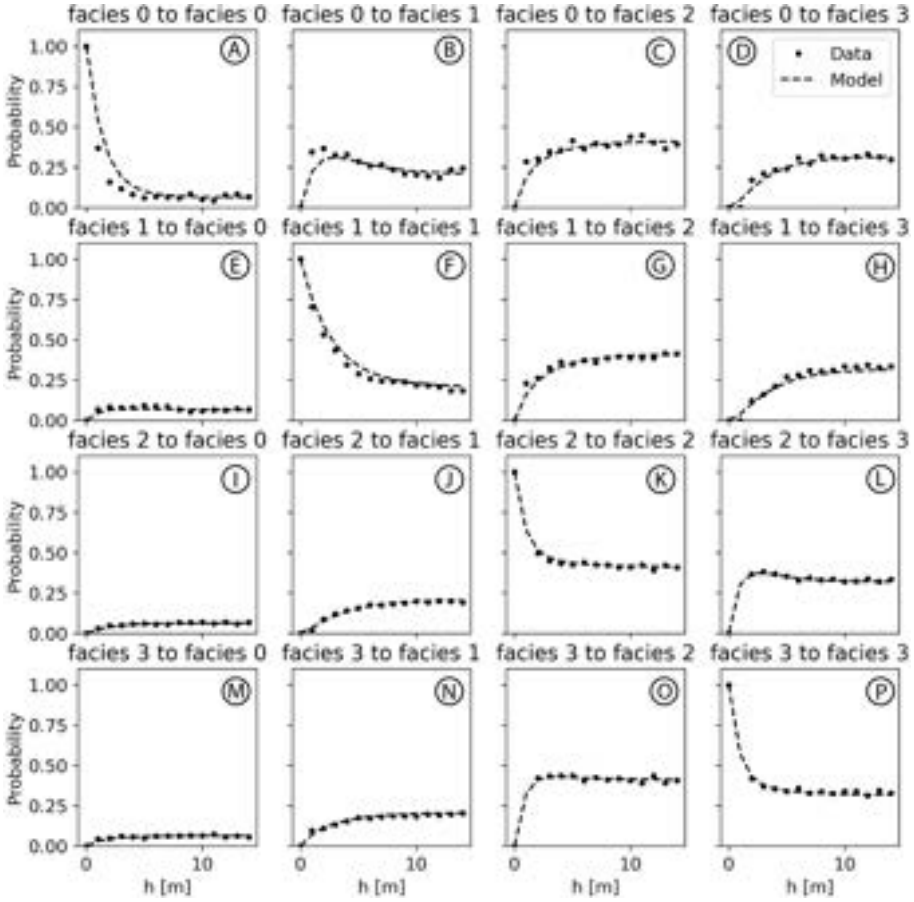

Figure 2.10: *Example of 16 experimental transiograms computed on a synthetic datset comprising four facies in z-direction. Each subplot represents the probability of observing facies j (column) at a certain distance in the z direction of facies i (row). Dashed lines represent the fitted 1D Markov Chain Model.*

$$\mathbf{T}(h_*) = \exp(\mathbf{R}_* h_*) \tag{2.7}$$

where $\mathbf{T}(h_*)$ denotes the MCM which is a matrix $k \times k$ (e.g., Fig. 2.10), $*$ represents an arbitrary direction (generally x, y, z), h_* is the distance lag in the $*$ direction and $\mathbf{R}_*$ is the transition rate matrix

$$\mathbf{R}_* = \begin{bmatrix} r_{11,*} & \dots & r_{1k,*} \\ \dots & \ddots & \dots \\ r_{k1,*} & \dots & r_{kk,*} \end{bmatrix} \tag{2.8}$$

where entries $r_{ij,*}$ represent the rate of change from category i to j per unit length in the $*$ direction. It can be shown that the rates of changes can be computed from the experimental transiograms by differentiation at the origin (i.e. the slope):

$$r_{ij,*} = \frac{\partial t_{ij}(0)}{\partial h_*} \tag{2.9}$$

Taking into account the transiograms from Figure 2.10 (that are in the z direction) and applying equation 2.9 to find the entries in R_z, the resulting MCM is shown as dashed lines in Figure 2.10. Assuming that similar MCM have been defined for the x and y directions, it is possible to combine these MCMs to develop a 3D MCM by interpolation (Carle et al. 1997; Carle et al. 1998). The final 3D MCM can be directly used to construct the indicator co-kriging equations (Carle et al. 1997) instead of using standard (cross)-variograms. This also means that stochastic simulations that reproduce the spatial statistics of the transiograms can be straightforwardly generated with the Sequential Indicator Simulation (SIS) algorithm.

All these components constitute the main building blocks of the Transition PRObability Geostatistics Software (TPROGS) method (Carle et al. 1996, 1997; Carle 2007). TPROGS can be thought of as a modified and improved version of the SIS algorithm. In TPROGS, the third step (see Section 2.4.2) involves transition probability-based cokriging that takes into account the spatial 3D Markov chain model. After a simulation is obtained, a final cleaning step is generally performed using simulated annealing. This step aims to enhance the agreement between the measured and modeled transition probabilities by minimizing an objective function (Carle et al. 1998). In this iterative algorithm, each node in the simulation is considered and modifications to the category are proposed to minimize the objective function. This process continues until a satisfactory criterion is met.

Figure 2.11 shows an example of a TPROGS simulation in which four fluvial facies are modeled. Note how the levees are often in contact and on top of the channels. This is expected as levees are generally located on the sides of a river (Miall 2013). Despite noisy realizations and improper placement of levees in some cases, it is important to note that such a result would not have been achievable with the SIS algorithm, demonstrating the added value of TPROGS in facies modeling.

TPROGS and transition probabilities-based cokriging have been widely used by the scientific community, particularly in hydrogeology, to characterize subsurface heterogeneity (e.g., Fogg et al. 1998; Weissmann et al. 1999, 2002; Green et al. 2014; Bianchi et al. 2015; Moreno et al. 2017; Guo et al. 2019). In particular we can mention Weissmann et al. (1999) who have constructed a complex and

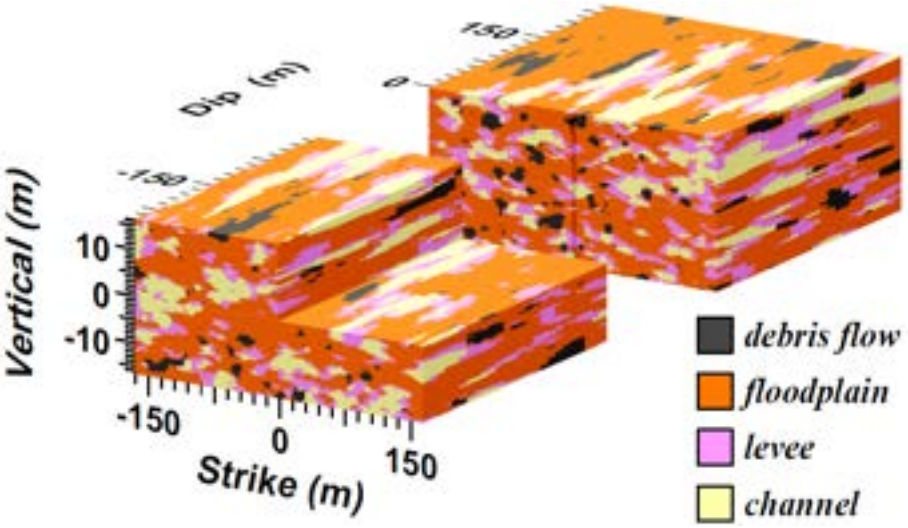

Figure 2.11: *Example of a 3D TPROGS model representing a fluvial environment with typical fluvial facies (floodplain, levee, channel and debris flow). Image taken from Carle (2007).*

plausible 3D model aquifer composed of different stratigraphical units. Each unit has been modeled separately with a different MCM; geological expert knowledge was also considered by imposing mean lengths in horizontal directions and by varying their orientations. The observed fining-upward sequence could be reproduced thanks to the asymmetry of the transiograms. Similarly, Bianchi et al. (2015) have integrated stratigraphical data as soft information to generate more realistic subsurface facies models with TPROGS. They have computed the proportion of each facies in each unit and use it as soft data constraint for the geostatistical simulations, providing an efficient way to combine a deterministic stratigraphic model with stochastic facies models. They observed a general reduction in the uncertainty of the prediction of groundwater heads and flux when soft data were considered. Weissmann et al. (2002) have investigated the effect of heterogeneity, modeled with TPROGS, on the age of groundwater and the transport of chlorofluorocarbon in a alluvial aquifer. They have notably found a wide distribution of groundwater ages due to the heterogeneity and outlined the problem to represent groundwater age by a single date. In the context of inverse modeling, Duan et al. (2022) have used TPROGS in combination of a discrete cosine transform to generate an ensemble of initial models in a data assimilation procedure with an ensemble data method.

This widespread use of TPROGS in hydrogeology is probably due to the fact that it is intuitive to understand and is frequently presented as a method that requires expert knowledge. Indeed, while it is simple to construct a transiogram (or a variogram) in the vertical direction, it is much more complicated in the horizontal direction because of a lack of data. Consequently, expert knowledge

is required, and the intuitive and straightforward workflow of transiograms makes it easy to add this kind of knowledge (e.g., Carle et al. 1996; Carle et al. 1998; Weissmann et al. 1999). While it is more difficult and less intuitive to do so with indicator variograms, although possible (Ritzi Jr 2000). Moreover, the possibility to consider asymmetric relations, which are frequently observed, is a significant advantage of TPROGS over standard SIS.

Furthermore, since SIS forms the foundation of TPROGS, they share certain advantages and limitations. For instance, TPROGS can also easily incorporate soft data information in the form of local probabilities, which can enhance geological realism and accommodate nonstationarity (He et al. 2014; Bianchi et al. 2015; He et al. 2015). Additionally, TPROGS can be applied across a wide range of geological environments, particularly in porous media, and can handle various complex situations. However, TPROGS also inherits many of the disadvantages associated with SIS. These include issues with sequential simulations (Emery 2004). Additionally, the simulation of noisy and unrealistic geological structures can affect the appearance of the simulation, although asymmetry helps is used to improve this aspect of the simulation. The use of simulated annealing also improves this aspect, but can generate artifacts when conditioning data are located close to the boundaries of the simulated area (Deutsch et al. 1994; Carle 1997). Another limitation is the requirement for a sufficient amount of horizontal data to infer a coherent geological model. A limitation that can be viewed as an opportunity to instill greater control over simulated geometries. For readers interested in deepening their understanding of TPROGS and related techniques, we recommend referring to the comprehensive review by Langousis et al. (2018).

In summary, TPROGs is a versatile method suitable for modeling subsurface heterogeneity across different spatial scales, from local to regional relying on transition probabilities. Like SIS, it benefits from a substantial amount of data, although data deficiencies can be mitigated with the incorporation of geological expert knowledge, facilitated by the intuitive transiogram framework. However, it should be mentioned that the facies produced by TPROGs may not exhibit highly realistic features and that simulated models depend on the questions that need to be addressed (Langousis et al. 2018). To achieve greater geological realism, more advanced modeling methods are necessary.

BME and MCP

The Bayesian Maximum Entropy (BME) approach, along with its simplified version, Markovian-type Categorical Prediction (MCP), is another method that leverages transiograms for spatial modeling prediction. The BME principle, originally introduced by Christakos (1990), serves as an interpolator (as kriging) and has been extended to predict categorical variables as well (Bogaert 2002). Its core objective is to identify a probability distribution that maximizes

entropy while still adhering to spatial statistics, univariate (simple transiogram) and bivariate (cross-transiograms) distributions. Maximization of entropy is a fundamental concept in probability theory and information theory (Jaynes 1957). It suggests that, when you have limited information about a system or process, the most unbiased or maximally uncertain probability distribution should be chosen as the best representation of your knowledge. In other words, the higher the entropy, the better the prediction. Unfortunately, BME has certain limitations due to memory constraints and computational requirements. As a result, it is generally suitable for a limited number of categories and a relatively small number of neighboring samples (Allard et al. 2011).

To address the limitations of BME, an alternative approach called Markovian-type Categorical Prediction (MCP) was introduced by Allard et al. (2011). MCP aims to approximate certain aspects of the BME method while overcoming its computational challenges. The fundamental concept of MCP revolves around estimating the conditional probability of observing a particular facies i at location $\mathbf{x}_0$ (i_0) given n neighbors data $i_1, \ldots, i_n$ at locations $\mathbf{x}_1, \ldots, \mathbf{x}_n$. The facies data $(i_1, \ldots, i_n)$ are categorical variables that can obtain values from 1 to k, the total number of categories (number of facies). The conditional probability is represented as $p_{i_0|i_1,\ldots,i_k}$. Allard et al. (2011) have shown that it can be approximated with the following relation:

$$p_{i_0|i_1,\ldots,i_n} = \frac{p_{i_0}^{1-n} \prod_{j=1}^{n} t_{i_j i_0}(\mathbf{h}_{0j})}{\sum_{i_0=1}^{k} p_{i_0}^{1-n} \prod_{j=1}^{n} t_{i_j i_0}(\mathbf{h}_{0j})} \tag{2.10}$$

where p_{i_0} is the probability of observing facies i at location $\mathbf{x}_0$, $t_{i_j i_0}(\mathbf{h})$ is the bivariate distribution (transiogram) between observed facies data i_j and facies i_0 at a $\mathbf{h}$ lag distance and $\mathbf{h}_{0j}$ is the lag distance between the location of the data $\mathbf{x}_j$ and the location where the estimation is done $\mathbf{x}_0$.

Equation 2.10 may seem complex at first, but it involves calculating the numerator for each possible facies by changing i_0 from 1 to k. The conditional probability can then be obtained by dividing the numerator for a given facies by the sum of all numerators for all facies.

The essential distinction between MCP and BME is seen in Equation 2.10. MCP focuses solely on transiograms between points of interest and data points (i_0 vs $i_1, \ldots, i_n$), neglecting the spatial statistics between data points themselves. This simplification significantly streamlines the computation of $p_{i_0|i_1,\ldots,i_k}$ and results in faster estimations and simulations compared to the BME method (Allard et al. 2011). A simplification that is generally acceptable, but can lead to erroneous predictions when data are tightly clustered (Allard et al. 2011).

An essential parameter in MCP is the number of neighbors considered (denoted as n in Equation 2.10), which primarily controls its computational cost. It is crucial to use an adequate number of neighbors to accurately reproduce the proportions of facies and transiograms. This balance results in a trade-off between achieving precise simulations and managing the computational cost.

MCP and especially BME were originally developed for soil science applications, where the number of samples is typically low and irregular. This presents a considerable challenge when estimating transiograms. To address these issues, the estimation of transiograms with MCP and BME often involves kernel smoothing techniques (D'Or et al. 2004; Allard et al. 2011) and the use of a training image (TI) assumed to represent the spatial statistics of the variable under study (Allard et al. 2011; Benoit et al. 2018). In the case of the TI, transiograms are inferred directly from the features and patterns within the TI. Figure 2.12A represents a three-facies classification sand dunes in the Gobi desert and is used to make MCP and BME estimations (Fig. 2.12C-F).

Once the transiograms are defined, estimates can be obtained using a weighted draw based on Equation 2.10. In the images presented in Figures 2.12C, E, we can see the MCP estimation maps, where in each location of the simulation domain the most probable facies is shown. The transiograms inferred from a TI (Figure 2.12A) and the conditioning data (Figure 2.12B). The corresponding results using BME are also shown in Figures 2.12D, F.

Figures 2.12C and 2.12D were created using omnidirectional transiograms (no anisotropy), while Figures 2.12E and 2.12F consider a preferential direction. It is noticeable that MCP shows similar results to those of BME, but MCP seems to produce smoother structures compared to BME. Furthermore, MCP outperformed BME in terms of computational speed, with MCP being 20 times faster (Allard et al. 2011). In a study by Sartore et al. (2016), various stochastic algorithms, including IK, SIS, and MCP, were compared, and it was found that MCP is the fastest method when a limited number of neighbors is used. This highlights the computational efficiency of MCP. Both methods reproduce the patterns and juxtaposition observed in the TI, such as the white facies, often located to the upper right of the black facies. The observed smoother structures are mainly due to the fact that only estimation maps are shown, not actual simulations. They can be easily obtained using the sequential algorithm in a similar way as in SIS, but by replacing indicator cokriging with MCP estimation.

Compared to BME, the simpler formulation and shorter calculation times of MCP have made it more accessible for applications in hydrogeology. Researchers like Benoit et al. (2018) and Fabbri et al. (2020) have employed MCP to simulate the spatial distributions and uncertainties of hydrostratigraphic units and hydrofacies. In particular, the ability to reproduce stratigraphic sequences, thanks to transiograms, is a valuable feature of MCP, as shown in

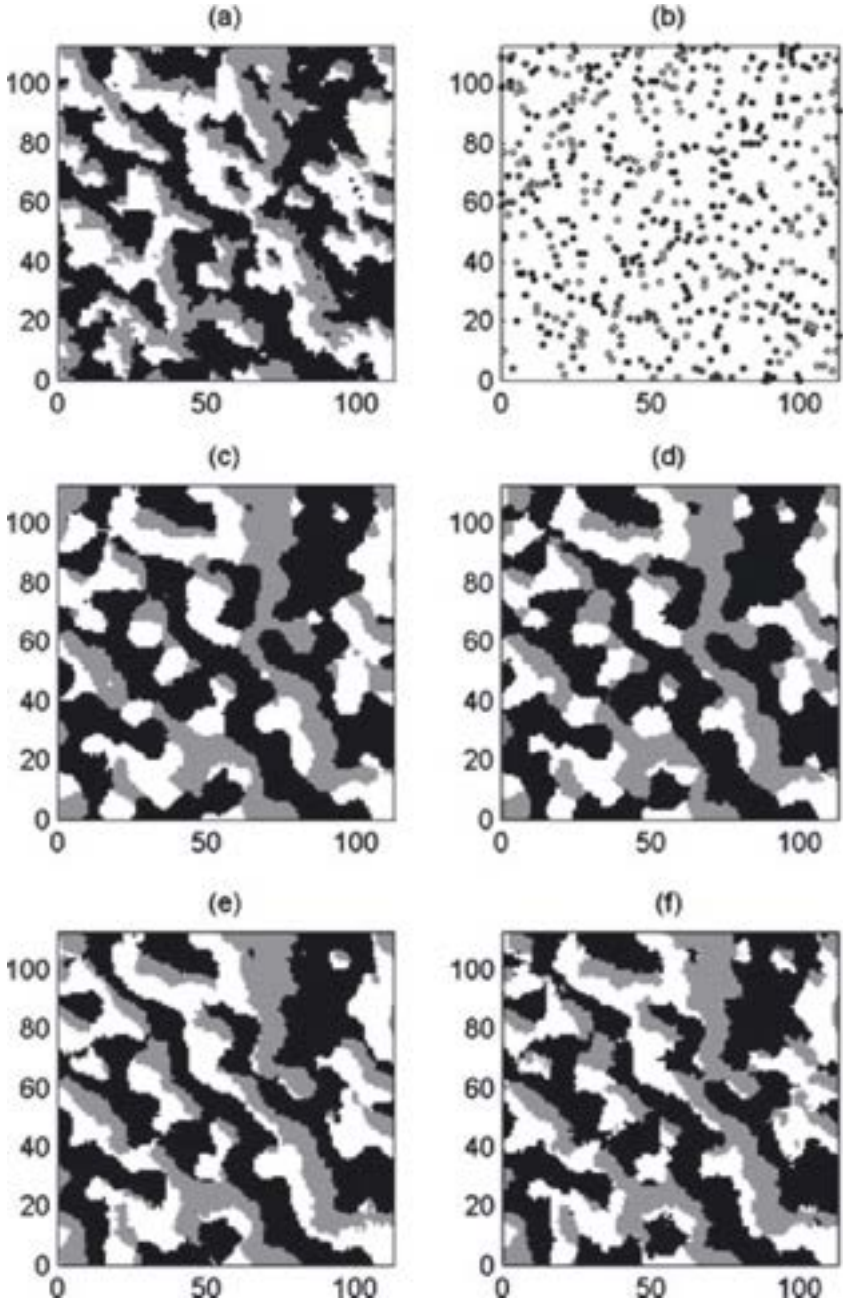

Figure 2.12: *Estimations example with MCP and BME with three facies, each colour represents a distinct facies. Figure taken from Allard et al. (2011).* ***A****: TI used to infer transiograms.* ***B****: Conditioning data point used to realize the estimations with MCP* ***C****,* ***E*** *and BME* ***D****,* ***F****. Estimations in* ***C*** *and* ***D*** *have been made using omni-directional transiograms while* ***E*** *and* ***F*** *have been made with a directional one.*

Benoit et al. (2018). Despite these applications, the use of MCP in hydrogeology remains relatively rare, opening the door to further studies to explore its potential and limitations in this field. The development of recent open-source packages such as the R package spMC (Sartore et al. 2016) can notably help to widespread the MCP methdology.

Essentially, MCP proposes the similar results as TPROGS by reproducing the asymmetry of transiograms but under the mathematical framework of maximization of the entropy rather than minimizing variance (i.e. kriging paradigm). Simulations are fast, but they lack of realism and are not able to produce curvilinear geological features such as channels. They heavily rely on data, and the use of a TI is often necessary to infer correctly the transiograms. Soft data can be easily integrated into the workflow through locally varying facies proportions. MCP may be faster than conventional geostatistical methods, but it lacks a number of essential features, such as nonstationarity and the ability to correlate simulations with secondary variables (as with cokriging). However, it is important to note that MCP is a relatively new method that may gain importance in the future. It is possible that these limitations will be addressed and resolved in the coming years.

2.4.5 Truncated (Pluri)-Gaussian

Originally, Truncated Gaussian Simulations (TGS) have been proposed by Matheron et al. (1987) to simulate a group of sediments (sandstone, shale, and shale deposits) that presented a significant ordering. The idea is the same as depicted in Figure 2.1, but this time considering the underlying (or latent) continuous variable as a Gaussian Random Function (Chiles et al. 2012, GRF). The use of GRF eliminates most of the shortcomings of deterministic truncation methods. Thresholds can easily be defined according to the proportions of each facies (the distribution of the simulation is known), and mathematical relationships exist between indicator variograms (IV) (as well as cross indicator variograms) and the variogram of the underlying Gaussian field (e.g., Galli et al. 1994; Emery 2007). But a major problem remains, the ordering of the facies. For these reasons, Le Loc'h et al. (1997) proposed to go beyond a single underlying (or latent) Gaussian field, the Truncated PluriGaussian Simulation Method (TPGS). The idea is to extend the number of GRFs and to truncate them with more advanced truncation rules. Any number of latent fields can be used, but common practice is generally two. In this case, thresholds are often visually represented by a square (often called "partition rule" or "flag") where each axis represents the values of a GRF and in which the associated facies are defined for each combination of values (Fig. 2.13). Consider the example in Figure 2.13. To determine the facies at a specific location (x, y), the two latent fields (G1 and G2) are evaluated at this location and the values are reported on the flag that maps the Gaussian values to the facies values. Note how the anisotropy of both fields is reflected in the facies simulation. The principle

can be generalized to more than two latent fields by defining the flag as an hypercube of n dimensional where n is the number of fields used.

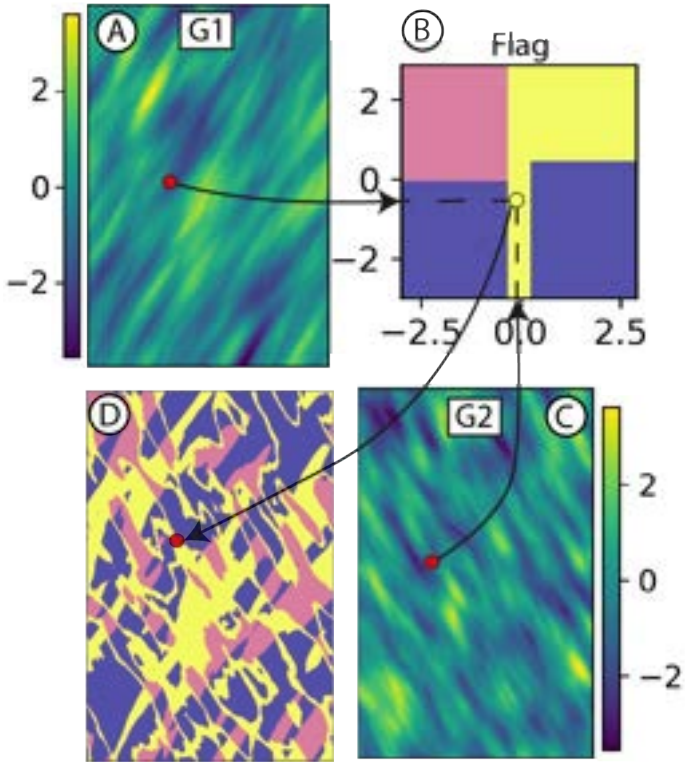

Figure 2.13: *Truncated PluriGaussian principle with two latent GRFs (**A**:G1, **C**:G2). **B** is the flag or partition rule apply on G1 and G2 and **D** is the resulting categorical simulation. To know the facies at a specific location (red circle), G1 and G2 are evaluated at this position and reported on the flag that maps the latent continuous gaussian values to categorical facies values (simulation).*

When working with a minimum of two latent fields, the necessity for facies to follow a strict order is eliminated, opening the door to a multitude of configurations. These configurations encompass various combinations of flags and latent fields, thereby affording a wide array of possibilities. The resultant proportions, general patterns, and spatial arrangement of the facies within TPGS are consequently governed by two key factors: latent fields and threshold flag (Armstrong et al. 2011). To go deeper, the influence of the flag is particularly pronounced in controlling not only the facies proportions and transitions, but also their connectivity (Beucher et al. 2016). Although latent fields have more pronounce impacts on the general shapes of the facies (size, orientations) and their boundaries with each other (smooth or erratic). Figure 2.14 presents a collection of simulations that utilize four markedly different flags and latent fields, effectively showcasing their impact on the facies models. There are two

sets of simulations: one using the latent fields in Figures 2.14A, B and another using those in Figures 2.14K, L, resulting in a total of eight simulations. The first thing to notice is the influence of the flag on the simulations, where the simulations of the first set are very different (Fig. 2.14D-2.14J), even using the same latent fields. Two different sets of latent fields were used (Fig. 2.14A, B vs. Fig. 2.14K, L) to show their influence on the simulations. Simulations shown in Figures 2.14D, M that use the simple flag shown in Figure 2.14C, exhibit patterns of both latent fields. The white facies, which is only influenced by G1, seems to cut the two green facies. A cut which may be related to an erosion process for example. This type of contact is frequently used in TPGS to represent the order of facies resulting from diverse geological processes (Armstrong et al. 2011). However, the structures generated appear only slightly convincing from a geological point of view, but are capable of smoother transitions between facies than SIS. By increasing the complexity of the flag (Fig. 2.14E), more interesting structures can be obtained with particularly well connected facies (dark green facies, Fig. 2.14F, N)) on two different scales (depending on G1 and G2). Such structures could be of particular interest, for example, in searching preferential paths in a soil or in a karst system. The last two flag examples (Fig. 2.14G, I) and simulations (Fig. 2.14H, O and Fig. 2.14J, P) are shown to demonstrate that there are no limitations in the definition of the flag and that acceptable simulations can still be obtained. However, in such situations, a certain number of problems and limitations arise and are discussed below.

Therefore, the selection of the flag becomes a crucial factor, typically achieved through a combination of borehole analysis within the region to establish facies transition probabilities. This process is further enriched by the incorporation of geological expertise, with the aim of simulating anticipated geological characteristics (Mariethoz et al. 2009). Unconditional simulations must always be performed before conditional ones to ensure expected geological features are simulated. Moreover, the flag is often modified spatially to match with local facies proportions because the spatial areas of each facies domain on the flag directly dictate its expected proportions. However, this fine-tuning presents challenges, particularly in cases involving complex flags such as the one illustrated in Figure 2.13B. This tuning becomes infeasible with irregular boundaries (such as the flags in Figures 2.14G, I). This complexity has prompted a prevalent approach in numerous TPGS studies, where the flag configuration is defined as an assemblage of rectangles (e.g., Mariethoz et al. 2009; Lauzon et al. 2023), with each facies corresponding to a distinct rectangle, as advocated by Armstrong et al. (2011). Following this, the adjustment of thresholds (boundaries) of the flag becomes trivial. As an example, the flag in Figure 2.13B would not be acceptable but the one in Figure 2.14C would.

Another important consideration within the realm of TPGS are the underlying Gaussian Random Functions (GRFs), as they exert a notable influence on the simulated facies (Fig. 2.14D-J vs. Fig. 2.14M-P). The standard approach involves initially defining a flag and subsequently employing diverse methodolo-

gies to align them with the IVs derived from the available data. Mathematical relations between facies IVs and latent field variograms have been established (Matheron et al. 1987; Le Loc'h et al. 1997; Emery 2007). With this foundation, it becomes feasible to make numerical predictions concerning the forthcoming IVs in a given simulation setting (with a specific flag and latent field configurations). The estimation of latent variograms transforms into an optimization challenge, necessitating the trial and adjustment of multiple variograms until the desired IVs are reproduced. However, it is important to acknowledge that this approach places significant computational demands and faces inherent optimization problems. Moreover, the more complex the flags are, the more the optimization is difficult because of the high number of thresholds. However, relations can be greatly simplified if the boundaries on the flag are parallel to the axis (Lantuéjoul 2001). For these practical reasons (facies proportions and variogram inference), in the vast majority of situations, simplified flags are used to reproduce facies spatial statistics more reliably (Armstrong et al. 2011; Madani et al. 2019).

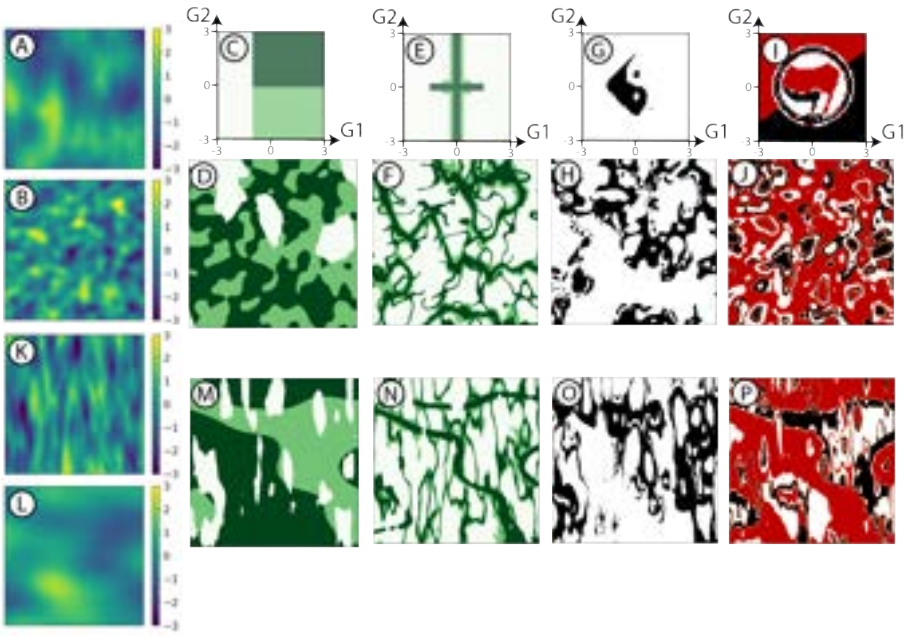

Figure 2.14: *Examples of TPGS simulations using four different flags (**C**, **E**, **G**, **I**) and their respective simulations (**D**, **F**, **H**, **J**) using Gaussian fields G1 (**A**) and G2 (**B**) and another set of simulations (**M**, **N**, **O**, **P**) using Gaussian fields G1 (**K**) and G2 (**L**). Flag in **E** is modified from Biver et al. (2015) and Oliver et al. (2018).*

Once the flag and Gaussian field parameters have been defined, it is easy to obtain unconditional simulations. Conditional simulations, on the other hand, first require transforming the (categorical) facies data into continuous values for each latent field. However, this transformation must be made with the under-

standing that a wide combination of values is possible (Emery 2007; Armstrong et al. 2011). For example, the yellow facies in Figure 2.13B can be found both in the right corner (where G2 is approximately greater than 0 and G1 approximately greater than 0) and in the bottom center (G1 around 0). As for the blue facies, it can be either in left or right rectangles. Moreover, it is necessary to ensure spatial continuity of the Gaussian values (i.e., that close data points have similar values to avoid artifact generation). This is generally done by applying sampling methods such as the Gibbs sampling algorithm, which is a Markov Chain Monte Carlo algorithm (MCMC) (Geman et al. 1984; Gelfand et al. 1990). Applied to TPGS, the algorithm consists first in assigning plausible but random values of each Gaussian field to each facies. Values are sequentially updated, one by one, by drawing from a Gaussian distribution conditioned by kriging using neighboring data. This operation is generally repeated several times until convergence is reached. For more details, the readers are invited to consult Armstrong et al. (2011). An alternative option is to use the sequential spectral turning band algorithm proposed by Lauzon et al. (2020a,b) which minimizes an objective function based on inequality constraints. This algorithm takes advantage of the 1D problem of the turning bands and uses constraints derived from data values and truncation flags to ensure that facies are respected at data locations.

In order to improve TPGS on its limitations, namely the definition of the flag, latent fields, and the efficient integration of more than four facies, several authors have proposed different approaches.

Allard et al. (2012a) have proposed an innovative approach to automatically determine the flag based on available bivariate data that can be measurements (geophysical measurements) or synthetic. This methodology can also take into account varying facies proportions. The idea is to build an estimation of the conditional probabilities of each facies with respect to the bivariate data and to combine these probabilities with target proportions (locally varying) to define the adapted local flag. The main drawback with this method is that it requires two geophysical measurements at every point in the simulation domain, or else has a decent geological concept in order to determine an initial flag. As a result, flag determination is no longer completely automatic.

Madani et al. (2015) and Madani et al. (2019) have proposed a hierarchical approach in which a large number of Gaussian latent fields are used (> 2). The particularity of the method is that only one threshold is applied per latent field, and the domains of each facies can lie between each of these thresholds. This can be seen as a generalization of simple flags mentioned earlier, where each facies is now defined by a hypercube of dimension n, where n is the number of latent fields simulated. Thresholds are easily adjusted to facies proportions, and, once thresholds are fixed, the estimation of latent variogram parameters is simple and fast to perform. One limitation of this approach is that it is

computationally demanding to increase the number of latent fields, especially in 3D.

Silva et al. (2019) went even further and proposed the hierarchical truncated plurigaussian (HTPG) approach, which is a generalization of the approach of Madani et al. (2015). The flag is resumed in a truncation tree that defines which latent fields separate which facies and by which thresholds. Each subsequent latent field separates facies in two or more groups (depending on the number of thresholds). If a group contains more than one facies, one or more additional truncations are necessary. In total, the number of thresholds is equal to the number of facies - 1. Figure 2.15 shows a realization using the HTPG method with four latent fields. The truncation tree indicates, for example, that Facies 1 is defined by the values of g1 that are below a certain threshold. Similarly, latent field g2 creates three groups: facies 2, 3, 4, facies 5 and facies 6, 7. Latent field g3 separates facies 2, facies 3 and facies 4. And finally, the latent field g4 separates facies 6 and facies 7. The resulting simulations can exhibit relatively complex patterns thanks to the hierarchical approach.

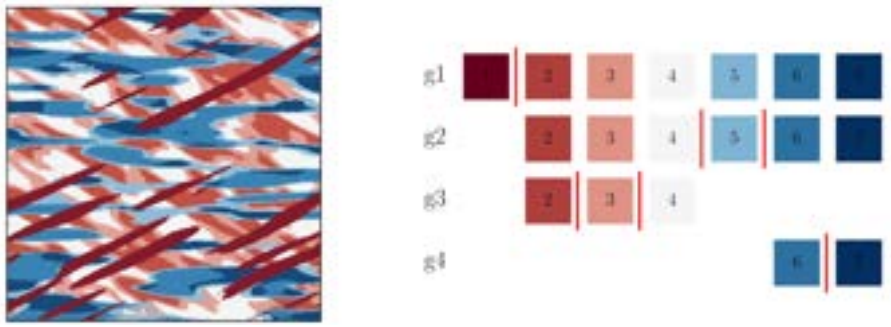

Figure 2.15: *One HTPG simulation using the truncation tree to the right. Thresholds are indicated by the vertical red lines. Image taken from the master thesis of Velasquez Sanchez (2023).*

Le Blévec et al. (2018, 2020) have detailed a workflow to simulate cyclic and rythmic deposits using TPGS. To this end, they have proposed to use correlated and spatially shifted latent fields (Le Blévec et al. 2018). Shift can be vertical only, horizontal only, or a combination of both allowing one to reproduce a large variety of depositional settings (tidal, continental shelf, abyssal, etc.). They also have proposed to integrate the diagenesis component as a third Gaussian latent field (Le Blévec et al. 2020).

Despite the substantial adoption of TPGS in industries such as mining and oil (e.g., Emery 2007; Madani et al. 2015; Caers et al. 2022), it has received relatively limited attention from hydrogeologists over its nearly three decades of existence. Hydrogeologists typically prefer other classical geostatistical methods (SIS or transiogram-based methods) or even TGS, as the definition of the flag

and latent Gaussian field is considerably more straightforward with TGS than with TPGS (Pyrcz et al. 2014).

Notable applications of TPGS in hydrogeology include the work of Mariethoz et al. (2009), who used it to characterize the heterogeneity of a polluted site and predict the evolution of the contaminated plume. Their pioneering study demonstrated the feasibility of constructing stochastic facies models based on a simple geological concept (flag). Similarly, Cherubini et al. (2009) employed TPGS to simulate hydrofacies within different stratigraphical units of a contaminated area. Furthermore, Modis et al. (2013) successfully developed a stochastic hydrofacies model for an aquifer using TPGS, highlighting its superior reliability compared to a standard SIS model. However, aside from the work of Mariethoz et al. (2009), there has been a scarcity of studies that integrate TPGS with an examination of its implications for fluid flows and transport processes. However, we can note the work of Pescimoro et al. (2022) who have shown the impact that TPGS can have on transport simulations. Their study delved into the influence of TPGS on non-Fickian transport, shedding light on how permeability contrast can exert control over these distinctive flow behaviors.

Recently, TPGS has seen interest in inverse methods. Thanks to its continuous latent fields, TPGS offers the advantage of being amenable to standard inversion tools. Various calibration methods have emerged, including gradient descent and optimization techniques (e.g., Liu et al. 2004; Lauzon et al. 2023), as well as ensemble data assimilation methods (e.g., Astrakova et al. 2015; Sebacher et al. 2017; Oliver et al. 2018; Todaro et al. 2023), which have achieved success in numerous cases. However, the choice of the flag is important and can lead to highly variable results if it is too complex (Oliver et al. 2018).

To conclude, these examples of the inverse and history matching problems underscore the potential of TPGS to improve hydrogeological modeling and aquifer characterization compared to SIS and deterministic methods. TPGS can easily integrate soft data in the form of local facies probabilities by adapting the flag locally, and secondary auxiliary data (geophysical, hydrological) can be integrated through data assimilation methods in an inverse procedure or can be used to automatically construct the flag and infer latent fields (Allard et al. 2012a). Hence, TPGS are highly flexible and have a solid mathematical background. Moreover, they can be grid-free depending on the GRF generation method. However, inference of latent GRFs is the main drawback of the method, and simplification of the geological concept (flag) is required to obtain desirable results, reducing the range of structures that can be generated.

2.4.6 Truncated Kriging

In extension of the TGS method, the truncated approach can also be used directly on a kriging interpolation of a latent variable. This is very similar to the deterministic method presented in the continuous interpolation methods section (section 2.3.3). A simple example is shown in Figure 2.8C. Truncated kriging (TK) imposes an ordering of the facies, unlike the IK models, as previously discussed with IDW equivalent methods.

However, this method has several issues in addition to the one mentioned previously (see section 2.3.3). As the kriging is chosen as the interpolation method, a variogram model has to be defined. The first idea to do this is to use the continuous values attributed to the facies data, but in doing so, it is not guaranteed that the final facies model respects the indicator variograms (IV). Although the relations between the continuous variogram and the IV can be computed for simulations (Armstrong et al. 2011), this is not the case for estimation (kriging). It is also unlikely that the final models follow a Gaussian distribution like with TGS or TPGS. This makes the determination of thresholds more complicated, as it is not possible to assume that the continuous variable will be normally distributed. Therefore, TK is not simple to apply and does not produce interesting results which limits its application. For this reason, it is generally not recommended for facies modeling (Falivene et al. 2007b).

2.4.7 Summary

To conclude the large chapter of variogram-based and related methods, they are practical and easy-to-use algorithms. They find widespread application across diverse geological contexts, as evidenced by their continued use today (e.g., Thomas et al. 2019; Xue et al. 2022). However, their reliance on data is a defining characteristic, which can be viewed as both an asset and a limitation. This inherent data dependence simplifies their integration, both of hard and soft data. Nevertheless, the challenge lies in the often insufficient quantity of data, particularly for estimating accurate horizontal and cross-variograms. This necessitates the infusion of conceptual knowledge into the modeling process, often by imposing spatial correlation lengths.

These methods excel in reproducing one- and two-point statistics, fostering a sense of assurance in their capacity to reproduce, statistically, the spatial arrangement of facies. This reassurance is valuable as it signifies that the model is not completely wrong and is less subject to the modeler's subjectivity. However, this advantage comes at the cost of trying to reproduce complex geological structures. Even if complex structures can technically be obtained with TPGS, the choice of the flag and latent fields is difficult, leading to poor control on the modeled shapes. Consequently, even if the models align with the available data, they may not align with the nuanced insights of domain experts. This

raises a critical question: Can a model lacking expert validation still be deemed valid?

2.5 Multiple Point Statistics

2.5.1 The concept

All the previously mentioned methods have one particular thing in common: they reproduce the spatial statistics of pairs of points, also called two-point statistics (variograms, transiograms). However, while these spatial measures are technically able to capture any complexity assuming that the exact experimental variogram is known (Srivastava 2018), it is more complicated in practical cases. Therefore, these methods usually cannot reproduce the complexity of the real world, as it has been shown by Strebelle (2000). It is possible to have subsurface models that have similar first- and second-order spatial statistics (proportions, variograms) but that exhibit completely different patterns. With the current geostatistical tools, the statistics of two points alone are not sufficient to simulate complex and realistic geological features.

A logical and natural evolution of this paradigm is to reproduce spatial statistics with more than two points; this is exactly for what Multiple Point Statistics (MPS) have been developed. MPS proposes to use high-order statistics (HOS) (groups of more than two points) to reproduce complex geological features that are impossible to get with other pixel-based methods (e.g., SIS, TPGS, MPC).

Considering HOS is not straightforward. Unlike variograms, graphically representing HOS is impractical due to the considerable number of lags in each group, which makes the interpretation of HOS more challenging. Moreover, the number of data required to estimate HOS and fine-tune geostatistical models is significantly higher compared to variograms. It therefore seems impossible to envisage HOS of order 10, 5 or even 3.

To address these challenges, Guardiano et al. (1993) introduced an innovative solution employing a conceptual representation of the variable of interest, the so-called Training Image (TI). Simply, a TI is an image, a concept, a visual representation of what is expected to be modeled. It can be obtained in various ways, such as manual interpretation and drawing, object-based methods or process-based methods. The TI is the main force of the MPS with the capacity to integrate geological knowledge into the modeling process and have important control over the shapes that are generated. Note that we will prefer here the term of Training Data Set (TD) rather than simply TI, considering that the TD is restricted not only to images, but also to time series, auxiliary variables, Karst networks, etc.

Using the TD, Guardiano et al. (1993) proposed the first MPS algorithm, ENESIM which uses the sequential algorithm (the same as for the SIS) but where

all necessary conditional probabilities are identified and inferred from the TD. However, their algorithm required a complete scan of the TD at each point of simulation, which was too computationally expensive for practical applications.

Viable alternatives were only proposed less than 10 years later, starting with the SNESIM algorithm (Strebelle 2000; Strebelle 2002). Since then, numerous alternative algorithms have been developed. The main MPS algorithms can be broadly categorized into four groups depending on whether they are pixel-based or patch-based and whether they compute conditional probabilities or directly sample the data. Although presenting all of these algorithms is beyond the scope of this paper, our aim is to provide an overview by presenting one algorithm per category. To have a detailed description of the different existing MPS algorithms, the reader can refer to the book of Mariethoz et al. (2014).

2.5.2 Basic algorithms

SNESIM

SNESIM is a pixel-based algorithm that estimates the conditional probabilities of TD and stores them in a search tree database prior to simulation (Strebelle 2002). These conditional probabilities are the probabilities of assigning a particular facies to an unattributed cell based on surrounding conditioning data. They are obtained using the singe-normal equation (SNE, Strebelle 2002), which involves analyzing the occurrences of facies data events. Once the probabilities are known, the sequential algorithm can be used (Journel 1989). Unlike ENESIM, SNESIM is less computationally demanding, but highly effective. It has found applications in a wide range of groundwater problems (e.g., Huysmans et al. 2009; Zhou et al. 2018; Kawo et al. 2023) and has contributed significantly to the diffusion and success of MPS techniques.

However, the original SNESIM had several limitations. One of the main limitations was its high memory usage when analyzing patterns in the training data that require a large number of neighbor higher-order statistics (HOS). Additionally, SNESIM is not capable of directly simulating continuous variables. While this is not an issue for facies modeling, it does limit its applicability in certain contexts, such as the simulation of petrophysical properties or auxiliary variables. Fortunately, SNESIM has also been improved on several of these issues (Strebelle et al. 2004, 2014) and more computationally efficient algorithmic approaches have been proposed (Straubhaar et al. 2011).

FILTERSIM

FILTERSIM (Zhang 2006; Wu et al. 2008) operates differently compared to SNESIM. Unlike SNESIM, which deals with values on a pixel-by-pixel basis, FILTERSIM is categorized as a patch-based MPS algorithm. The aim is to

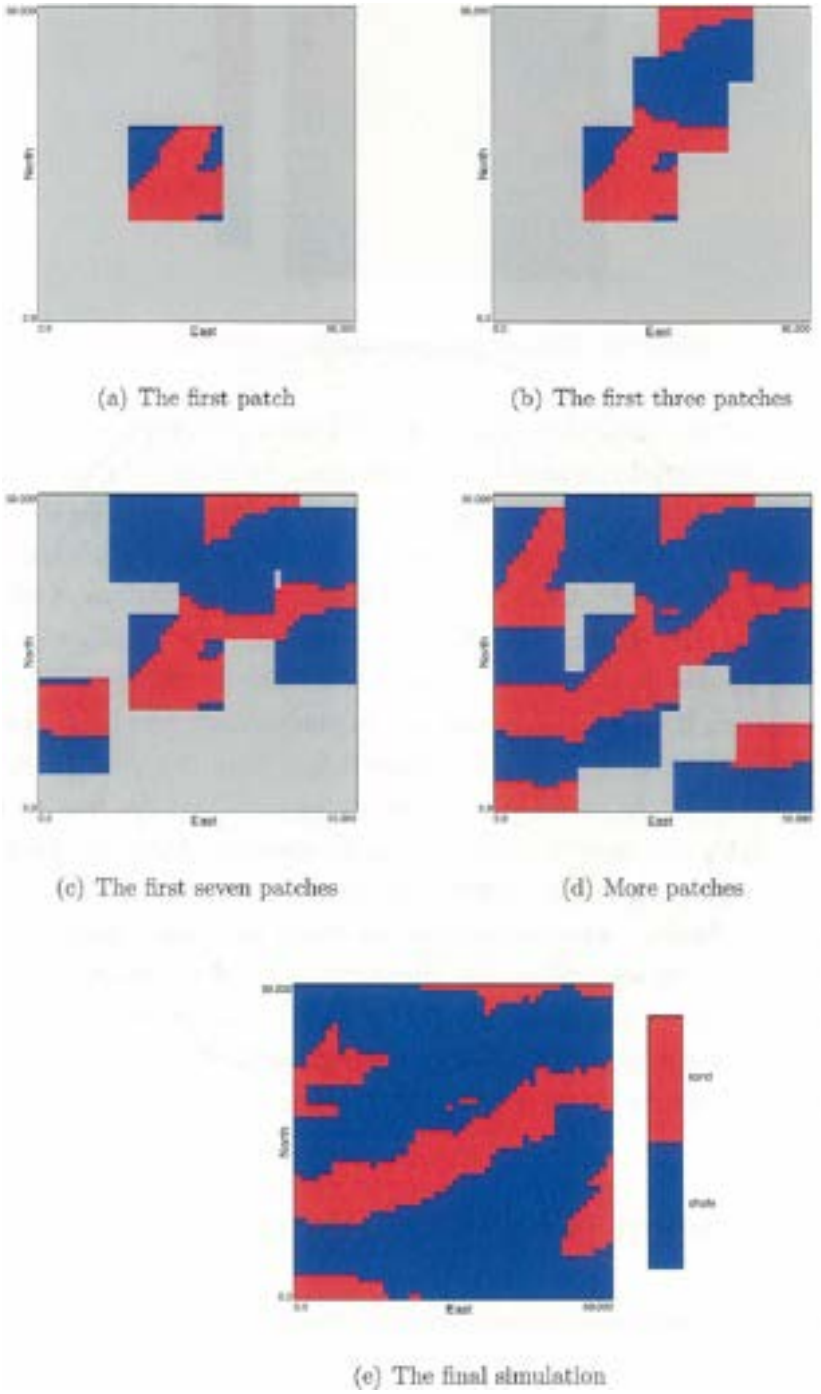

(a) The first patch

(b) The first three patches

(c) The first seven patches

(d) More patches

(e) The final simulation

Figure 2.16: *Different steps of a simple FILTERSIM simulation. Image taken from Zhang (2006).*

directly assign a patch (or pattern) of values (or facies) on the simulation grid. To do so, FILTERSIM relies on the use of filters to determine conditional probabilities. The filters also allow us to reduce the complexity of the patterns to reproduce. The filters are applied to the TD to obtain filter scores. These are then used to cluster the patterns based on similarities, and an average prototype pattern is computed for each cluster. As the simulation progresses, the grid is progressively filled with patches. (Fig. 2.16). One notable aspect of patch-based methods like FILTERSIM is that patches often overlap previously simulated ones, resulting in some cells being overwritten, as can be seen in Figure 2.16B.

Although this approach can better reproduce the patterns in the training image, it also presents challenges for conditioning, as the algorithm is less flexible. Additionally, selecting the most appropriate filters for a given training image is not a straightforward task.

DS

Direct Sampling (DS) has been proposed by Mariethoz et al. (2010b) in order to avoid computationally intensive calculation of conditional probabilities of SNESIM and FILTERSIM. DS is a pixel-based algorithm whose key innovation is its elimination of preprocessing steps on the TD before the simulation. This is achieved by directly sampling the value of interest (categorical or continuous) in the TD based on surrounding conditioning data (data event), as illustrated in Figure 2.17. Given a certain data event, the algorithm scans the TD until it finds a matching data, which is then assigned to the simulated node. In practice, and when the number of neighboring data considered is large (high HOS), it is not possible to find an exact match. In such cases, the DS algorithm computes the difference between the sampled-data event from the TD and the one in the simulation grid. If this difference is below a specified threshold t, it is accepted as a matching data point. Setting a very low threshold may result in the rejection of numerous candidates and slowing down the computation speed. To address this, another parameter, the max scan fraction f, limits the scanning of the TD to a certain percentage. The balance between t and f reflects a trade-off between achieving simulations that closely resemble the TD and computational efficiency. Additionally, considering the number of neighbors n as another parameter, DS requires the definition of three parameters, each dependent on specific cases and available computational resources.

DS is a flexible algorithm that allows for the simulation of categorical and continuous values without the need to compute any probabilities. This flexible approach makes the integration of auxiliary variables more straightforward than for other MPS algorithms and allows the simulation of nonstationary images (Mariethoz et al. 2010b). Moreover, DS is particularly well suited for handling multivariate problems involving multiple categorical, continuous, or

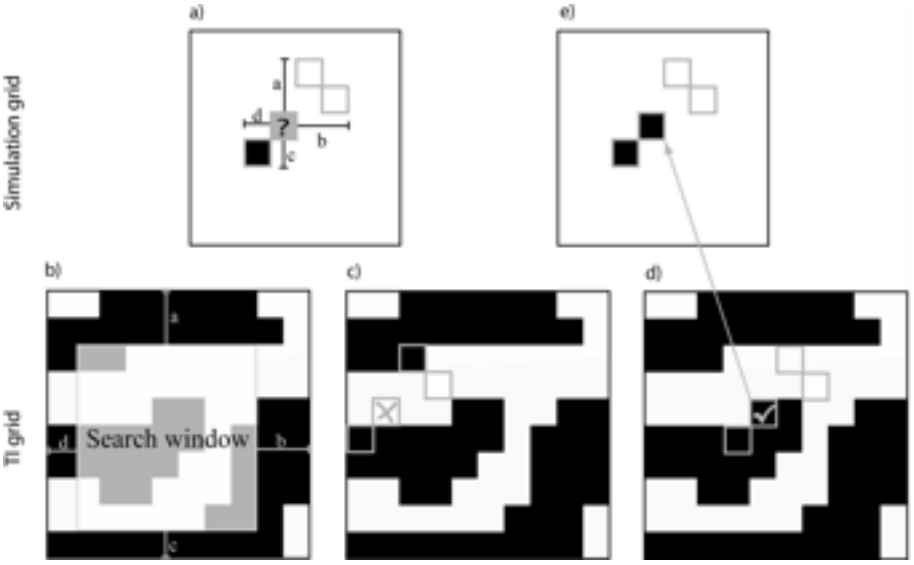

Figure 2.17: *DS principle on a binary case (2 facies). (a) The data event, where "?" node indicates the node to simulate. Black and white cells indicate already filled nodes (hard data or previously simulated nodes). (b) Search window used on the TI (or TD). (c) A random node is selected and a first scan of the TI is operated. It is not satisfactory because the upper node is black instead of white. (d) Another random node is selected, where the conditioning data are matched this time. (e) Assignment of the facies value to simulated node. Image taken from Mariethoz et al. (2010b).*

mixed variables. Soft conditioning data, such as orientations or facies proportions, can also be integrated through the use of auxiliary variables (Figure 2.18).

CCSIM

Cross-correlation-based simulation (Tahmasebi et al. 2012, CCSIM) is a patch-based algorithm which relies on the cross-correlation function to estimate the conditional probabilities. This function can be seen as a measure of similarity between two images and allows one to determine which patch in the TD is the most similar to a certain data event in the simulation grid. The pattern is then sampled directly from the TD and pasted onto the simulation grid. Additional care is also taken to ensure continuity between patches using a particular raster path.

Thanks to its patch-based approach and fast estimation of the best patch candidate with the cross-covariance function, CCSIM is a fast and efficient MPS algorithm that produces images very similar to TD (Figure 2.19). The method is also able to consider hard conditioning data with some limitations as well as

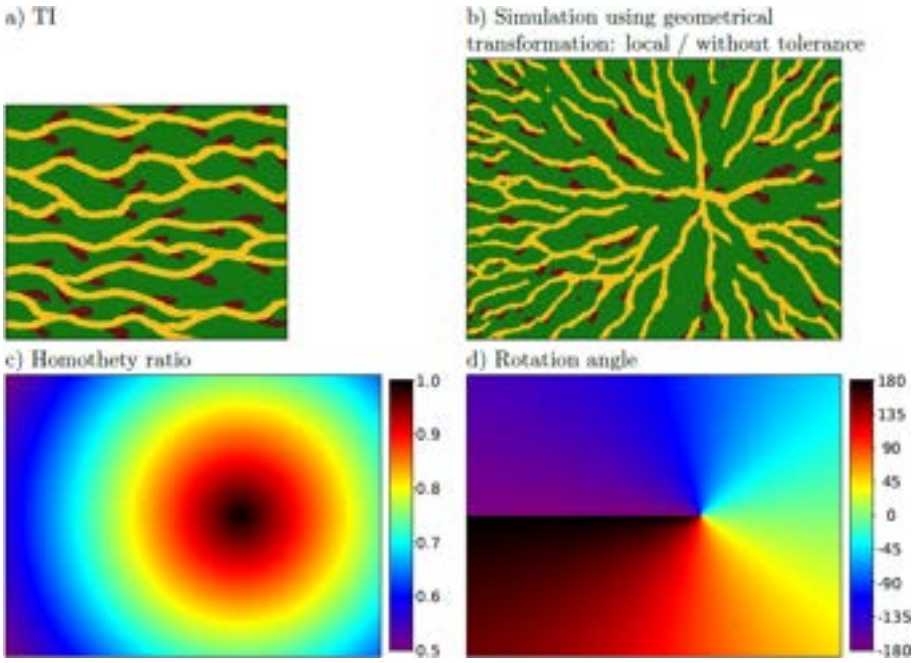

Figure 2.18: *Non-stationary simulation using the DS algorithm with its DeeSse implementation. Image taken from the DeeSse user's Guide (Straubhaar 2019). (a): Training Image. (c) and (d): Homothety and rotation to apply to the TI. (b): Resulting simulation.*

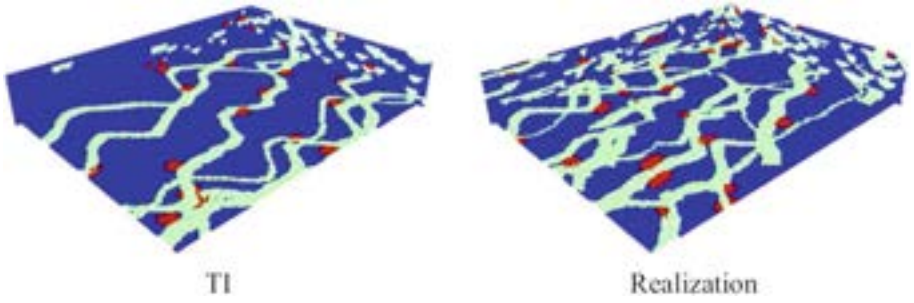

Figure 2.19: *Example of a 3D CCSIM realization using a fluvial TI. Image modified from Tahmasebi (2018).*

data are not ensured to be respected and artifacts may appear around conditioning data. This is particularly true when the number of data is dense.

Algorithms summary

The algorithms presented here, although not exhaustive, give an overview of the existing possibilities in terms of MPS. However, a systematic and complete comparison of the different methods is difficult due to the absence of a systematic comparative study in the literature. The problem is not simple, as it implies choosing representative test cases that are fair for each method. Moreover, each method must be optimized similarly in having comparable computing time. The choice of comparison criteria is also not obvious and very often relies on dimensionality reduction between a certain distance measure between the simulations and the reference, as well as on visual appreciation, which is inevitably subject to numerous biases. A systematic review of MPS algorithms would be very beneficial to MPS users.

But in general, what must be retained is that older methods, relying on the computation of conditional probabilities (e.g., SNESIM or FILTERSIM), are inferior to more recent algorithms based on sampling the data (e.g., DS and CCSIM). These methods are faster and more memory-efficient. Pixel-based methods provide greater flexibility and facilitate direct conditioning. In contrast, patch-based methods may pose challenges in this aspect. However, it should be noted that pixel-based methods often require more computational time to generate highly realistic simulations.

2.5.3 Auxiliary variables

The simulation of nonstationary images is a long-standing problem in geostatistics, where the assumption of stationarity is generally necessary to infer the statistics (Chiles et al. 2012). This is also the case for MPS. Most of the algorithms presented above require a stationary TD or at least a way to describe the non-stationarity of the TD using auxiliary variables.

Non-stationary simulation can also be obtained owing to the use of auxiliary variables. These variables, which generally cover the entire simulation grid, can be categorical or continuous, and provide information on various properties such as the local proportions of facies, the reference orientation of the TD, the deformation to be applied to the TD, and so on. Furthermore, it is possible to consider TDs that are themselves non-stationary, where the auxiliary variables describe the non-stationarity both on the TD and the simulation grid. Several MPS algorithms can consider this kind of additional data, but DS, thanks to its very simple formalism, is the one that offers the greatest freedom to date. Figure 2.18 is an example of a non-stationary MPS simulation with DS. In this case, two geometric transformations, homothety and rotation, are applied to

a stationary training image to obtain a simulation where channels follow the orientations and are rescaled given the auxiliary images provided. The channels are smaller near the edge of the domain compared to the right center of the image. Note the channel continuity that is preserved near the center of rotation, despite the abrupt changes of rotations. This flexibility is one of the reasons why MPS are so powerful in simulating a wide variety of settings using only one reference image. Such non-stationary simulations are harder to obtain with machine learning methods and require a large training data set (see section 2.8).

2.5.4 General applications

In terms of use and applications, MPS stands out as one of the most widely employed geostatistical modeling techniques and remains an active research area. Its ability to relatively easily integrate a geological concept through the TD is probably what makes these methods popular. In combination with easy conditioning to both hard and soft data and a reasonable computing time. For example, MPS have been widely used in hydrogeology (e.g., Huysmans et al. 2009; Zhou et al. 2018; Dall'Alba et al. 2020; Kawo et al. 2023). However, its versatility extends beyond facies modeling, covering a broad range of applications across various domains such as fracture models (Bruna et al. 2019), remote sensing gap filling (Mariethoz et al. 2012), or rainfall series prediction (Oriani et al. 2014).

One notable utility of MPS is to perform conditional simulations of methods that are difficult to condition, such as object-based methods or process-based methods (section 2.6 and section 2.9). These methods produce very detailed and more accurate representations of sedimentological processes than variogram-based methods but are generally harder to constrain to data. The outputs of these methods can then serve as TD for MPS. In this case, we can cite the study of Montero et al. (2021) who have used a rule-based model (section 2.6.5) to generate realistic TD of alluvial point bars, or Hoffimann et al. (2017) who have used FLUMY simulations (FLUMY™ 2022), a process-based channel migration model (section 2.9.4), in combination with a new patch-based MPS algorithm, IQSIM (Fig. 2.20).

However, we note that the simulations are not perfect. This is evidenced by connectivity analysis, which indicates that the connectivity of channel bodies is lower in simulations compared to the reference model (Hoffimann et al. 2017). This underscores the inherent limitations of MPS methods in reproducing intricate geological shapes generated by process-based models.

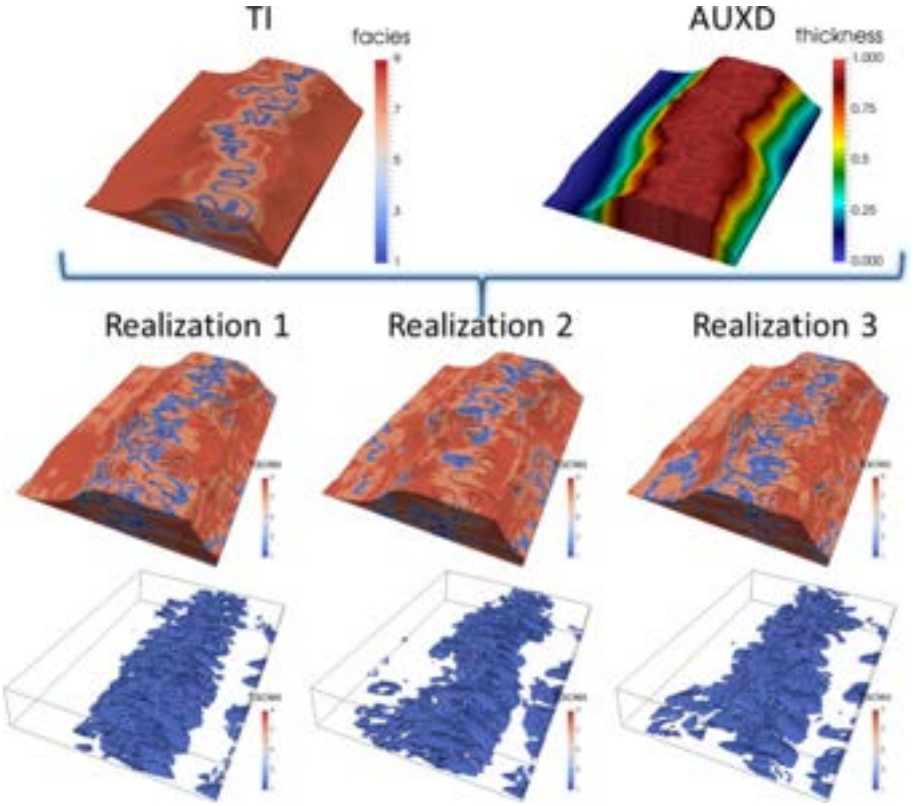

Figure 2.20: *MPS simulations using a FLUMY simulation as Training image. An auxiliary variable (thickness) is also defined to overcome the non-stationarity of the TI.*

2.5.5 Limitations

Apart from the difficulty to replicate highly complex geological structures, MPS is subject to several other limitations. One common drawback is the difficulty in parameterizing MPS for inverse problems. In contrast, TPGS, for instance, can be easily constrained due to their latent continuous Gaussian fields. Additionally, data assimilation techniques such as Ensemble Smoother and related methods (Emerick et al. 2013) cannot be applied to non-Gaussian variables. To address this challenge, Lam et al. (2020) capitalized on the Gaussian pyramid feature of DeeSse (an implementation of the DS algorithm in C, Straubhaar 2019) to condition MPS simulations to groundwater levels. The Gaussian pyramid, an image processing algorithm, allows one to work on different scales of the same image. Specifically, the reduced-scale images are continuous, enabling direct conditioning of these coarse levels to modify the finest and categorical levels based on available data.

Another limitation is the difficulty of making estimations with MPS, similarly to the case where kriging can be used to obtain estimations of GRFs. Typically, making estimations with MPS requires a large number of simulations, which can be both time- and memory-intensive. However, a recent advance by Jóhannsson et al. (2021) proposed a simple solution to directly compute the expected value as well as the variance (and other univariate statistics) without the need for simulations. To achieve this, they propose to modify the sequential algorithm used in many MPS algorithm (e.g., ENESIM, SNESIM). Instead of simulating a facies value in an empty cell, the conditional distribution is simply stored and can be used directly to obtain the estimation.

When the target properties differ significantly from the TD, the outcome of MPS simulations becomes blurry. Artifacts may be introduced to meet facies proportions, making it challenging to reproduce the TD features accurately. To solve this issue, Straubhaar et al. (2019) have proposed a deformation-based algorithm to create more TD without touching the general shapes and patterns (section 2.7)

But the greatest disadvantage of MPS, ironically also its greatest advantage, is the need and choice of the TD. Many questions naturally arise when it comes to choosing a TD for MPS. Should the TD be exactly similar to what we want to model, even if it is too complex? Or should it be considered more as a concept from which the MPS extracts its "essence" (Strebelle 2002)? Or said otherwise "What degree of complexity is ultimately required and necessary?". If too simple, the patterns will not be representative, but if too complex, they will not be reproduced and will greatly differ from the TD. How to select a particular TD when the geological concept is uncertain? The answer to these questions remains open as few studies have tried to test the impact of radically different TD on simulations and inversion problems (Juda et al. 2023).

Finally, most geological and facies models are done in 3D, which requires at least one 3D training image (without considering other auxiliary variables), which is not easy to obtain. A 2D image is simpler to obtain as it can be drawn and easily updated according to the modeling purposes. To this aim, other more complex facies modeling methods can prove to be useful (object-based, rule-based, process-based).

2.5.6 Summary

Although there are numerous additional aspects and challenges associated with MPS that could be explored further, we have resisted going deeper for the sake of conciseness. Over the past 20-25 years, MPS has garnered significant attention as a valuable tool in geostatistical modeling. Its ability to accurately replicate curvilinear features and a variety of geological structures, coupled with its ease of conditioning, especially in pixel-based algorithms, makes it

a more compelling option compared to traditional methods. Furthermore, the straightforward integration of auxiliary variables enables the generation of non-stationary images, expanding its applicability in diverse geological settings. The method is, however, not perfect as it still struggles of reproducing very complex geological structures at a reasonable computing cost. Given the current popularity of MPS, the shortcomings and limitations mentioned above of MPS are likely to be (and are) the subject of more comprehensive studies.

2.6 Object-based

2.6.1 Basic concepts and classification

Object-Based Methods (OBM), in their most general sense, are geostatistical and/or sedimentological techniques used to characterize subsurface heterogeneity by distributing spatial objects within a 2D or 3D simulation domain (e.g., Matheron 1967; Serra 1981; Haldorsen et al. 1984; Lantuéjoul 2001; Bennett et al. 2019). Each object within this approach is assumed to represent a geological facies or a group of related facies. OBM incorporates two key components:

1. **The objects:** Highly different depending on needs, they can exhibit variations in terms of quantity, shape, size, and hierarchy. This hierarchy allows for the modeling of geological structures at different scales and complexities. The choice of objects, along with their associated geometrical parameters, is often dependent on the specific geological context to be replicated. Objects can range from standard geometric shapes like circles, surfaces, lines (e.g., for representing faults and fractures) or rectangular cuboids. In addition, more complex objects can be employed to simulate specific sedimentological features such as channels, point bars, compound bars, levees, etc.
2. **Objects Placement:** Objects placement can follow various patterns, including randomness, repulsion, and attraction (where objects are positioned away, or close, from others), or more complex user-defined rules. These rules are generally formulated to adhere to specific geological principles and logic, ensuring that the placement of objects reflects or mimics real-world geological features and spatial relationships. Moreover, an appropriate placement also allows to respect conditioning data such as boreholes or facies proportions.

By playing with these two components, it is possible to obtain a wide range of different methods that are detailed below.

One particularity of OBM over most previously presented methods and process-based methods is its grid independence. Each object is created and stored independently from a simulation grid. This offers several advantages, including the ability to effortlessly create multiresolution models and efficient memory management and storage of the models. Using an analogy with Geographical Information System (GIS), OBM can be regarded as the vector format version of the facies model, while variogram-based or MPS methods are similar to the raster format.

Due to their definition, OBM can produce more realistic geological features than standard methods (SIS, TPGS, or MPS). OBM also provides a more precise characterization and representation of connectivity, particularly in the context of static connectivity, in the sense of Renard et al. (2013). This is a critical aspect, as it has been shown to have great control over flow and transport simulations (Renard et al. 2013). For example, when aiming to create a highly connected aquifer, OBM enables the utilization of elongated sand shapes to populate the simulation domain. This approach allows for the connection of any two sand points, even when they are distant from each other. In contrast, achieving such connectivity can be challenging with SIS (e.g., Dell'Arciprete et al. 2012) and may present difficulties with TPGS. It is worth mentioning that in this context, MPS performs reasonably well, but the generated geological features, due to their pixel-based nature, are still noisy and exhibit less straight boundaries in comparison to what can be achieved with OBM. However, the question of what is more realistic between smooth and noisy structures is open to debate.

Generally speaking, OBM is an interesting alternative to pixel-based methods, but it is not without its shortcomings, which largely depend on the specific OBM submethod used. OBM can be distinguished into five categories, based on the type of object or their placement.

- **Boolean models and standard object models:** These models propose placing a wide variety of objects, ranging from simple geometrical forms to more realistic ones (channels) with the particularity of the assumption that the placement of these objects follows a point process.
- **Geometric models:** Geometric models combine simple mathematical objects (e.g., planes, lines, cosine functions) to generate highly detailed and complex sedimentary structures.
- **Surface-based models:** In surface-based models, objects are represented as surfaces that are stacked on top of each other. Each surface delimits a geological event.
- **Rule-based models:** Rule-based models use complex placement rules that seek to mimic geological and sedimentological processes. They can be seen as an advanced version of the OBM.

- **Grammar-based models:** Grammar-based models employ formal language to generate geologically realistic objects and place them in space.

It is important to note that these methods are not mutually exclusive, and it is not uncommon to combine them to produce the desired sedimentological features.

2.6.2 Boolean Models and standard object models

Boolean models trace their roots to the 1960s (Matheron 1967) but where more actively developed and formalized the following decades (Matheron 1972; Delhomme et al. 1979; Serra 1981; Haldorsen et al. 1984; Begg et al. 1985; Haldorsen et al. 1986). In these illustrative cases, simple forms, such as disks or rectangles, are distributed. The term "boolean" originates from the function of these shapes in defining a specific facies of interest (e.g., sand), in contrast to a background facies, delineating the domain into two distinct subdomains: one for objects and the other for non-objects. The sizes of the objects (attributes) are determined by predefined probability distributions, and their spatial positioning (object placement) follows a Poisson point process (PPP). This combination of attributes and placement is often referred to as a Marked Point Process (Clemetsen et al. 1990; Tyler et al. 1992). Two realizations of a Boolean model are shown in Figures 2.21 A, B, where an ellipse form has been used to populate the domain. The ellipses are defined by three attributes, width, length, and orientations, which are drawn from given probability density functions (normal and uniform in this case).

Within a PPP, the count of points (that is, the number of objects to generate) follows a Poisson distribution, and their locations can be random (Figures 2.21A, B) or follow a locally variable density of points (Daley et al. 2003). This feature enables the method to be conditioned on locally variable proportions, as depicted in Figure 2.21C where objects are restricted by the probability map in Figure 2.21D.

Overlapping objects pose a conceptual problem since it is not natural to have two or more objects in the same place. This problem is generally solved by considering that younger objects "erode" the older ones if they overlap, but different rules can be used. This phenomenon is clearly depicted in examples from Figures 2.21. As an extreme example, placing a smaller object entirely covered by a larger one has no impact on the simulation; the small object "disappears" into the large one. This characteristic makes it challenging to establish a direct link between facies proportions and the number of objects to generate. For this reason, it is sometimes more advantageous to place objects until the desired fraction of the facies represented by the objects is achieved (Haldorsen et al. 1984). Alternatively, stochastic optimization algorithms, such

as simulated annealing, can also be used to address this problem (Tyler et al. 1992).

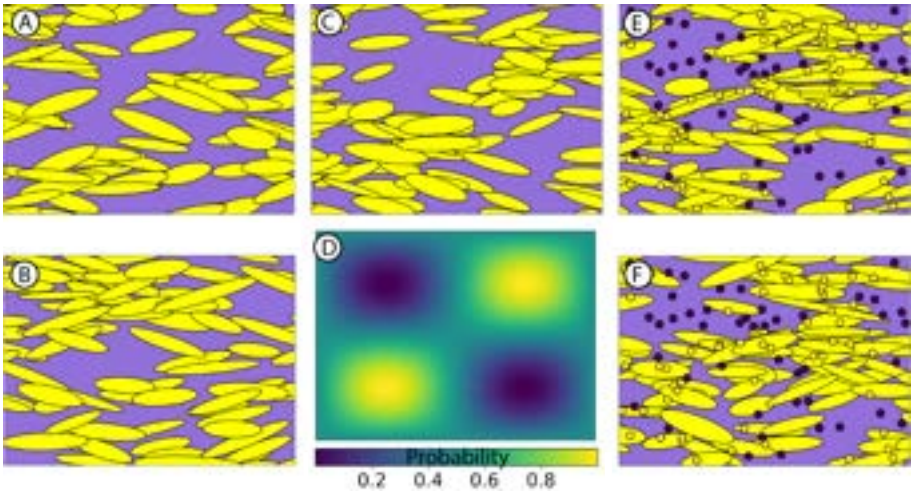

Figure 2.21: *Example of boolean model simulations using an ellipse to represent yellow facies that lay in a background purple facies. For each model, the number of generated ellipses follows a Poisson distribution with mean = 100.* ***A, B*** *are unconditional simulations with homogeneous density,* ***C*** *is an unconditional simulation with variable density shown in* ***D****. This density map represents the probability of an object to be kept during the simulation.* ***E, F*** *are two conditional simulations realized using a BaD process, where data points to respect are shown as purple and yellow dots.*

Conditioning a simple Boolean model can be accomplished through a birth-and-death (BaD) process (Lantuéjoul 2001). When starting from an already conditioned simulation, objects are iteratively created (birth) or removed (death) while ensuring that the conditioning data are constantly honored. The decision of whether to perform a birth or death action is determined by a probability that is contingent on the existing number of objects. If an excess of objects is present, the likelihood of implementing a death action increases, and conversely. That way, the simulations become a Markov chain where each state represents a conditional simulation. Care must be taken to sample simulations sufficiently different, as they are correlated with each other (Lantuéjoul 2001). Concerning the starting conditional simulation, it can be obtained in various ways such as covering the whole domain with a very large number of objects. More details on this step and conditional simulations of Boolean methods can be found in Lantuéjoul (2001). Example of conditional simulations are shown in Figures 2.21E, F.

Although easy to work with, models such as the one in Figure 2.21 are hard to apply to real-world problems and have been rapidly improved. In the 90s, significant attention was directed toward oil exploration in the North Sea, where numerous reservoirs of various sedimentological origins were investigated

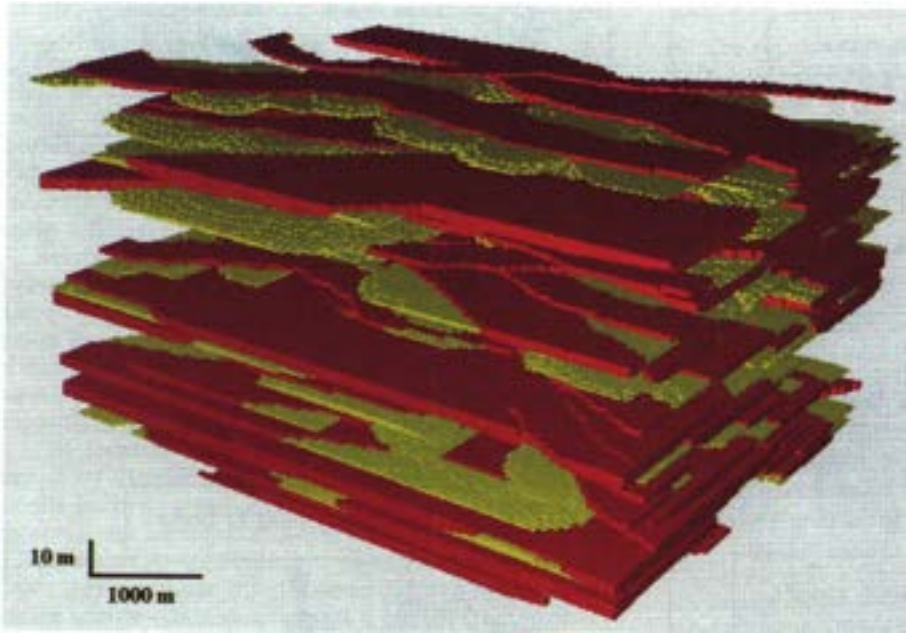

Figure 2.22: *3D object-based simulation realized with the software SESIMIRA (Gundesø et al. 1990) where channel belts are shown in red and crevasse splays in yellow. The background facies (shale) is not shown. The image is taken from Hatloy (1994).*

(e.g.,Damsleth et al. 1992; Tyler et al. 1992; Hatloy 1994). This required more flexible approaches. To address this need, Norwegian teams developed and applied various approaches and software tools (Clemetsen et al. 1990; Gundesø et al. 1990; Henriquez et al. 1990; Damsleth et al. 1992; Tyler et al. 1992; Hatloy 1994). These models enable the handling of a diverse range of objects (e.g., channels, simple forms, lobes, drawn by the user), the possibility to model more than two facies, and offer considerable flexibility in their placement. Placement possible schemes include attraction and/or repulsion of objects using user-defined functions, as well as considering geological rules, such as erosion between specific types of facies.

To distinguish these more practical models from Boolean ones, we propose referring to them as "standard OBM" because of their widespread use to the point of becoming a standard in the oil industry. Figure 2.22 illustrates one possible outcome of these methods, where channel belts are simulated using sinusoidal lines, and attributes are drawn from density functions based on existing data. It should be noted that the crevasse splays are correctly positioned along the channels, as expected in a fluvial environment. These models exhibit better reproduction of geological features, enhancing, at least visually, the geological realism of the simulations.

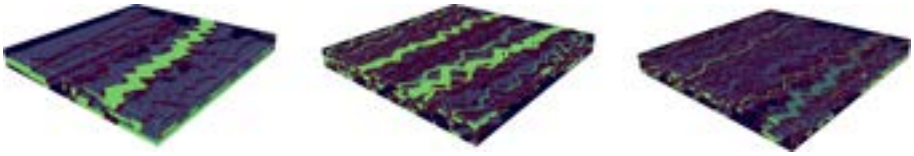

Figure 2.23: *Three example of FLUVSIM simulations where channels objects, with identical orientation, are placed inside a floodplain facies. Image taken from Colombera et al. (2012).*

Numerous OBM software and approaches have been developed over the years, but we will only present two open source and free options that may be of interest for hydrogeological problems.

FLUVSIM (Deutsch et al. 1996; Deutsch et al. 2002) is a standard OBM that is an open-source, free-to-use code that uses a hierarchical method of local coordinate transforms to simulate braided river systems. These transformations allow us to adapt the coordinate system to the principal direction of geological continuity. FLUVSIM operates at different hierarchical levels; it starts with the stratigraphical units which are bounded by 2D surfaces, populates them with a channel complex, and within each is placed a certain number of channels, levees, and crevasse splays. A background facies (floodplain) is also considered, resulting in a total of four facies: channel, levees, crevasses, and floodplain.

FLUVSIM defines channel objects through parameters such as orientation angle, sinuosity, and geostatistical measures (variograms) for width and thickness. These parameters are derived from user-defined density probability functions. The actual dimensions of the meander (width, thickness, and centerline of the channel) are modeled stochastically using 1D GRFs along the channel. Levees, placed along channels whose dimensions are positively correlated with channel dimensions. Meanwhile, the crevasses are shaped by a random-walk procedure. It occurs randomly along the channel according to facies proportions with a higher probability where the curvature of the channel is high. FLUVSIM proposes decent realizations of fluvial environments (Fig. 2.23) and offers the option of conditioning to both hard (boreholes) and soft (local proportions) data. However, flexibility comes with a price. A large number (16) of parameters are required to characterize the different objects, not to mention the proportions of facies that can vary in space. For each of the parameters, a probability distribution has to be provided. These can be inferred or deduced from previous geological studies or from sedimentological record databases (e.g., Colombera et al. 2012). We must also note that the conditioning process is not straightforward and depends on the number of data to be matched.

Recently, the python package HyVR (Bennett et al. 2019) proposes a hierarchical approach to model subsurface properties with objects. This hierarchy is based on five levels: stratigraphic units, architectural elements (Miall 2013,

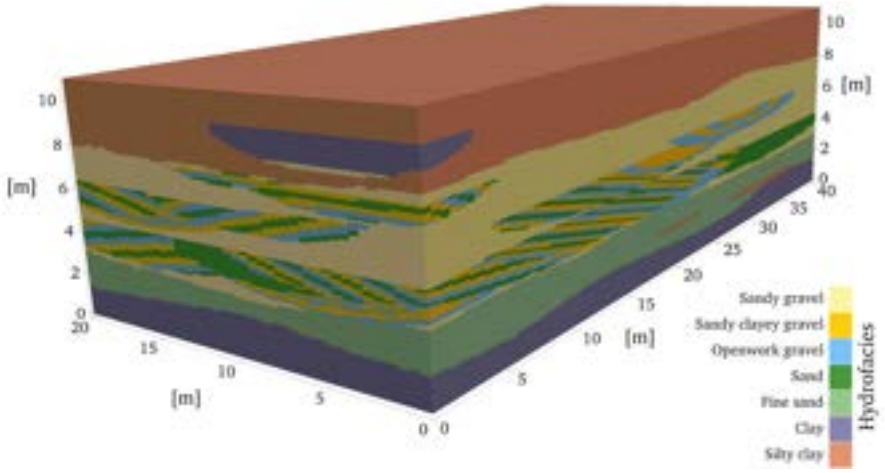

Figure 2.24: *Example of an HyVR hydrofacies simulation of the MADE site. Image taken from Bennett et al. (2019).*

channels, scours, sand bars, etc.), hydrofacies assemblages, hydrofacies (gravel, silt, sand) and microstructure (properties). Each of these levels can be refined as desired given the available data and information. HyVR is restricted to three object shapes but is able to generate a large panel of architectural elements and their internal variability. All of the object geometries are defined by user-defined density functions, and channel centerlines are computed using the model developed by Ferguson (1976).

Figure 2.24 shows a realization made on the MADE site, based on the geological interpretation of Bowling et al. (2005). In this figure, stratigraphic units are represented by the four extensive horizons (red, yellow, green, and purple), and architectural elements (a channel and multiple scours) are present in the red and yellow units. The scours are themselves filled with laminated hydrofacies. HyVR is capable to produce interesting and realistic images of the subsurface, but, as all other OBM, requires important work in parameterization of the model. Moreover, it does not support conditioning data.

These two last aspects are the main drawbacks of OBM (all kinds of OBM, not just standard OBM) and have been greatly discussed and investigated during the last decades.

First, the geometry and shape of objects are not obvious to determine, even if the conceptual model (e.g., the river regime) is assumed to be known, which is highly questionable (Miall 2014). A common approach is to derive object attributes (channel width, depth, width/depth ratio, sinuosity, length and width of compound bars, etc.) from modern sedimentological bodies, still in formation today, or from preserved sedimentological records (e.g., Tye 2004; Colombera

et al. 2012; Villamizar et al. 2015; Colombera et al. 2019). In this case, natural difficulties and questions arise such as the representativity of the past records compared to the modeling site, or the correspondence between modern observations and past records. All this is a source of great uncertainty, which is difficult to quantify but should be quantified one way or another. The size of objects can also be limited by measurements on site, such as well and wireline logs, but it is generally acknowledged that they cannot accurately capture the complexity of geological shapes, particularly in a fluvial setting (Miall 2014).

Second, standard OBM, while highly flexible for simulating diverse environments, comes with the notable drawback of conditioning, especially in the case of a large number of closely spaced data (Marini et al. 2018). The complexity of conditioning OBM poses a long-standing challenge and remains an active area of research (e.g., Wang et al. 2018). Various approaches have been suggested, such as simulated annealing (Deutsch et al. 1996), a fusion of BaD and simulated annealing (Tyler et al. 1992), direct conditioning (Viseur et al. 1998; Shmaryan et al. 1999), Metropolis-Hasting (Holden et al. 1998; Hauge et al. 2017), local object deformation (Holden et al. 1998; Henrion et al. 2010; Hauge et al. 2017), OBM simulation as a TD for MPS (Caers et al. 2004) or machine learning (ML, for example Song et al. 2021) and optimization of parametric models (Boisvert et al. 2014; Wang et al. 2018).

Going in-depth into these different conditioning approaches would be beyond the scope of this paper. Therefore, we will confine ourselves to a short explanation of each. The BaD, Metropolis-Hasting and simulated annealing methods place objects randomly in space and accept (or reject) given conditions. The major problem with these methods is that the acceptance rate tends to be very low when the number of data is high (Holden et al. 1998), drastically reducing their capacity to generate rapidly reliable conditional simulations.

Direct conditioning aims to place objects directly on the data. For example, forcing the channel centerline through well data (Viseur et al. 1998; Shmaryan et al. 1999). This ensures that data are respected, but these methods are difficult to implement and highly dependent on the objects to be used and the data to be conditioned.

Local deformation slightly modify geometries of existing objects. It can be done with the GRF (Holden et al. 1998; Hauge et al. 2017) or the object distance method (Henrion et al. 2010). Deformation is often used in conjunction with other methods to speed up and improve conditioning. Local deformation is not difficult to apply but does not ensure that data are respected.

Machine Learning (ML) algorithms and MPS can use OBM simulations as a training data set to perform conditional simulations. It has the advantage of being simple to apply and producing perfectly conditioned simulations. But they will suffer from the limitations of the chosen MPS or ML methods, as

well as not being perfectly capable of preserving the shapes of the OBM. More details on the applications of ML to facies modeling are given in the machine learning section (section 2.8).

Optimization combined with parameterized objects has shown promising results by accurately constraining an OBM in a dense well data set (Boisvert et al. 2014; Wang et al. 2018). In this method, objects geometries, orientations and locations are defined by parameters which are optimized in order to reduce an objective function based on hard and soft data. What is important in this approach is that each object is optimized separately, giving in the end a database of objects that respect the data. Conditional simulations are obtained by sampling random objects in this database and ensuring that all data are respected. The main difficulty of this approach is the parameterization of the objects, which also poses several limitations on the objects that can be used.

In summary, what must be retained is that conditioning with OBM is feasible but not straightforward and poses a number of problems, regardless of the technique used.

In terms of applications, standard OBM have been developed mainly for the characterization of oil reservoirs, and their use in hydrogeology or other geoscience fields has remained limited, particularly in the last 20-25 years (Bennett et al. 2019). The reasons for this difference in use are not clear, but can probably be attributed to budget differences between the oil and gas industries vs. groundwater exploration and exploitation. It is evident that OBMs necessitate a greater investment of time and energy to conceptualize, in addition to access to extensive geological databases to estimate object dimensions. Consequently, smaller hydrogeology companies, in comparison to oil industry giants, are considerably less able to utilize these methods. However, it is also crucial to consider the historical factor and to acknowledge that these methods were initially developed by oil and gas companies, and have predominantly remained within this domain, without significant crossover into other fields.

However, we can note Jussel et al. (1994) and Rauber et al. (1998) who have used simple OBM to characterize heterogeneity in fluvioglacial gravel aquifers and observe the impact on flow and transport. To this aim, they placed lenses of facies (open-framework gravel, sand, silt) in a gravel matrix based on detailed statistical description of these facies lenses. Another example is the work of Miller et al. (2000) who have used stochastic OBM lithofacies models to condition gamma-ray models to identify preferential groundwater pathways for downward migration of contaminants. More recently, Bennett et al. (2017) have used OBM realizations to investigate the effect of anisotropy on transport simulations. They have shown strong control of the variation of orientation of the anisotropy on the appearance of a twisting flow, enhancing transverse mixing.

As already explained, another major application of OBM is to construct more realistic TIs for use as TD in MPS or ML generative algorithms. Some object-based softwares have even been created with this aim, such as TiGenerator (Maharaja 2008) or Tetris (Boucher et al. 2010). For example, Comunian et al. (2011b) used TIs generated through a simple OBM to simulate the bedding structures observed in a fluvio-glacial aquifer outcrop. There are numerous other examples of similar applications (Falivene et al. 2007a; Bastante et al. 2008; Michael et al. 2010; Schorpp et al. 2022). The ease with which conditional simulations can be performed, coupled with the inherent need for a geological concept (TI), positions MPS as a natural and excellent complement to standard OBM.

2.6.3 Geometric models

An extension of standard OBM came with the use of mathematical and geometrical functions to parameterize small individual mathematical objects that are eventually combined in a complex manner to produce highly detailed sedimentological structures (Scheibe et al. 1995; Guin et al. 2010; Ramanathan et al. 2010a). These methods are actually very similar to standard OBM and it is debatable whether they should be separated. The major difference rely on the use of small and geometrical objects to create more complex and detailed structures at different hierarchical scales (from kilometer scale to centimeter scale). Where standard OBM generally does not seek to reproduce the internal structures of the objects, restraining its focus to a larger scale of heterogeneity.

To exemplify this approach, we highlight the work of Ramanathan et al. (2010a), who used geometric models to portray the heterogeneity of braided systems. To effectively capture the diverse heterogeneity scales inherent in such systems, they implemented a four-level hierarchy. Level 4 encompasses the abandoned channel belt, representing the entire modeling area. Level 3 is characterized by compound bars and large channel fills. Level 2 is defined by unit bars (constituting the compound bars) and crossbars. Lastly, Level 1 is marked by cross-strata sets composed of various lithofacies (sand, sandy gravel, and open-framework gravel). Additional information can be found in Bridge et al. (2006) and Ramanathan et al. (2010a).

Figure 2.25 shows how level 2 objects (unit bars) are created and assembled to form compound bars (level 3). Compound bars themselves are bounded by a geometric hull whose geometry is controlled by density functions. Channels are placed around the sides of the compound bars. Finally, the unit bars are filled by cross-strata polyhedra (level 1). Each of these objects is fully defined by an assemblage of geometrical planes. Similarly with Deutsch et al. (1996), each of these objects possesses its own coordinate system, allowing the placement of lower-level objects relative to them, without relying on absolute coordinates.

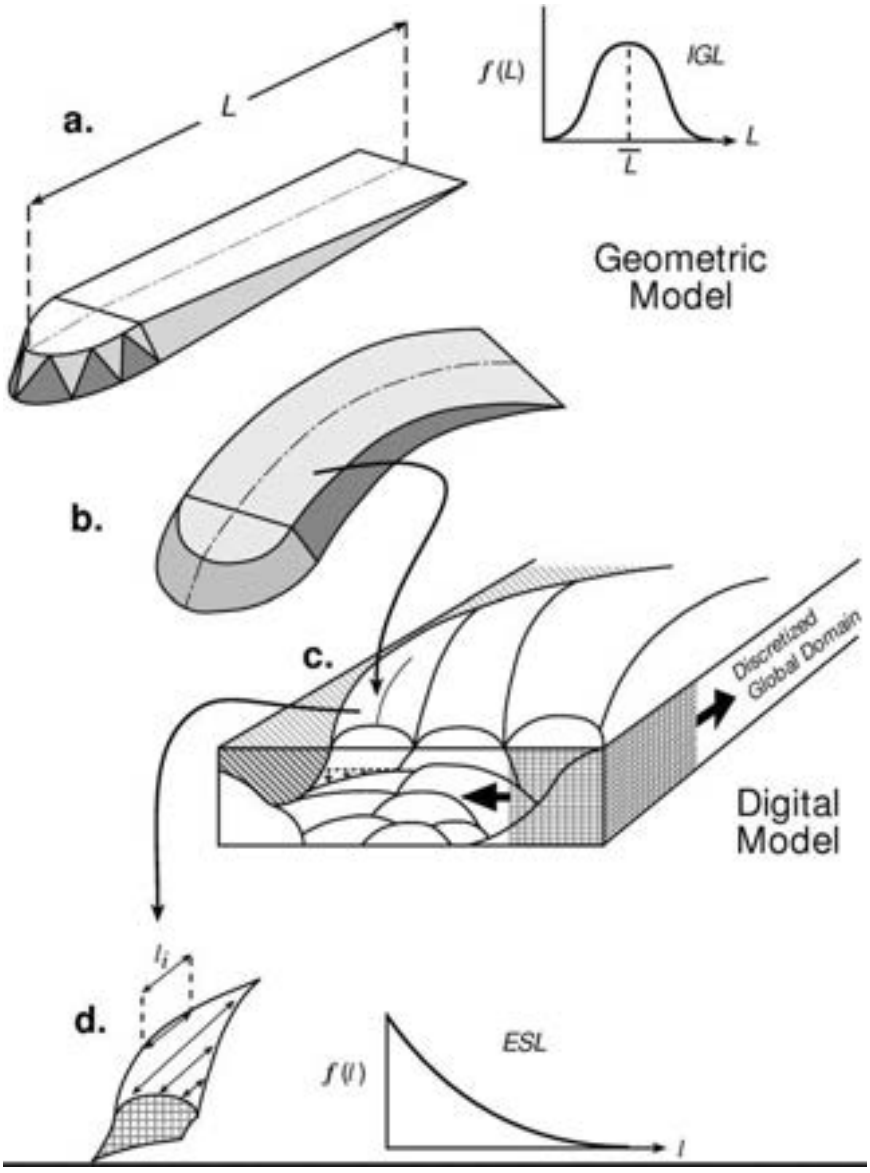

Figure 2.25: *Illustration of the workflow used by Ramanathan et al. (2010a) to create compound bars (level 3 of hierarchy) using unit bar objects (level 2).* ***a****: Creation of a polyhedron which is defined by a set of lengths that are drawn from user defined density functions (input geometric lengths, IGL).* ***b****: Curvature is added to the polyhedron.* ***c****: Polyhedrons are merged together to form the compound bars.* ***d****: Not all the polyhedron is kept in the final model. Length kept is sampled from a density function (exhaustively sampled lengths, ESL). Image taken from Ramanathan et al. (2010a).*

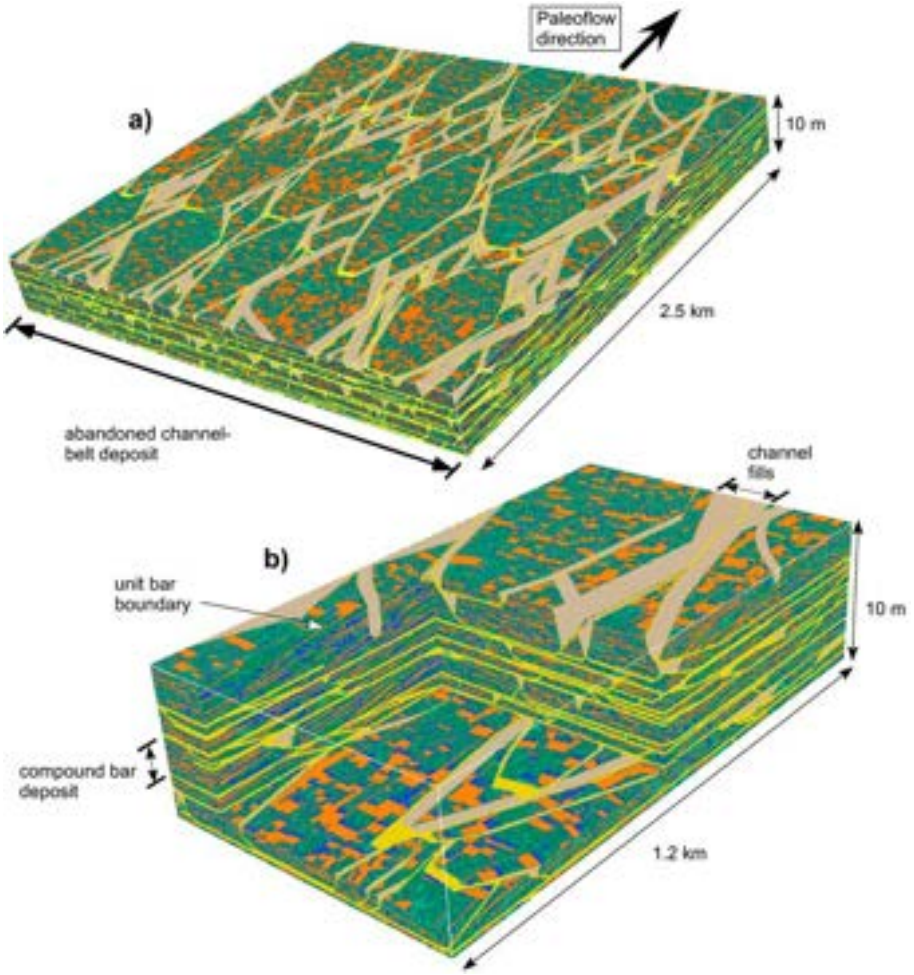

Figure 2.26: *3D images of the final models that can be obtained with the geometric approach. Yellow surfaces represents boundaries of compound bars and orange one the boundaries of unit bars. Blue color represents sand facies and green a gravelly sand facies. Image taken from Ramanathan et al. (2010a).*

This proves especially beneficial when dealing with deformed and rotated objects, as is the case with unit bars.

To build complete models (Fig. 2.26), level 3 objects are assembled and randomly placed in the simulation domain. The idea is not to reproduce the processes that have led to such facies assemblages, but to directly generate a complex set of geometric forms that are similar to conceptual models (Guin et al. 2010). Geometrical models can be seen as OBM methods that use more complex objects but with very simple placement. However, the approach developed by Ramanathan et al. (2010a) does not consider conditioning, which limits its use to practical cases. In fact, detailed geometric models have been poorly used to determine subsurface heterogeneity. Few examples addressed the effect of heterogeneity on CO_2 sequestration (Gershenzon et al. 2015; Ershadnia et al. 2021).

Geometric models offer the ability to represent heterogeneity on multiple scales. Furthermore, they are efficient in terms of storage, demanding only the parameters of the mathematical objects (e.g., coefficients of geometric planes). While these methods are interesting, there is ample room for advancement, both in terms of refining algorithms and addressing conditional cases involving boreholes, proportions, etc. The conditioning approach of Wang et al. (2018) (optimization of parameterized objects) could work well with geometric models since the objects are already parameterized. Additionally, there is potential to broaden the scope of applications. However, it is important to note that the creation of models using these methods requires substantial effort, involving tasks such as object parameterization and the selection of suitable probability densities.

2.6.4 Surface-based

The idea behind Surface-Based Models (SBM) is to consider that all or part of the geological features (layers, architectural elements, lithofacies, etc.) can be delineated by surfaces. SBM is a common method in structural and geological modeling where stratigraphic units are commonly separated by surfaces (Lajaunie et al. 1997; Wellmann et al. 2018). Here, we will focus on the use of these methods to delineate different kinds of facies rather than stratigraphical units.

SBM can be viewed as an OBM where objects are only surfaces. These surfaces can take explicit or implicit forms and be deterministic or stochastic, depending on the specific case. Notably, SBM frequently integrates the temporal dimension of geological deposition, with the stacking of various surfaces serving to delineate the desired geological structure and reproduce the associated processes. This aspect makes SBM very close to rule-based models, often confounding. However, it should be noted that there are examples of SBM

that do not rely on strong rules that govern surface placement. Due to this distinction, we propose differentiating these two methods.

The typical SBM workflow starts with an initial topography and progressively adds surfaces. The "volume" generated between each new surface and all preceding surfaces contributes to the creation of a distinct geological entity. It is possible to delineate each of these entities in greater detail using other facies methods, which will allow us to characterize their internal structures more accurately. Therefore, SBM are generally not used alone but in combination with different facies techniques (e.g., Zhang et al. 2009). Based on the geometry of the entity and the geological processes influencing its formation, various trends (i.e. facies proportions) can be employed to guide lithofacies modeling. A common illustration involves the utilization of a fining-upward sequence, where coarse lithofacies are represented at the base and progressively transition to finer lithofacies towards the top of the entity.

SBM made its debut more than 20 years ago (Wen et al. 1998; Xie et al. 1999; Xie et al. 2000, 2001). Wen et al. (1998) combined cosine functions with 2D GRFs to generate bedforms to model the structures of the tidal bed. They also considered different stages of deposition and erosion to mimic the tidal environment in a realistic way. Independently, Xie et al. (2000) used a similar approach by developing SURFSIM, an SBM software that can honor local well data and integrate basic rules to restrict the location of surfaces.

An important application of SBM occurred through the research conducted by Pyrcz et al. (2005), particularly in the development of a surface-based stochastic lobe model tailored for turbidite deposits. Their methodology consists in defining a lobe element with an initial bathymetry in which multiple flow events are simulated (Fig. 2.27A). Each of these events is represented by a stochastic surface, and the volume of the event is defined by this surface at the top and the current bathymetry (previously stacked simulated surfaces) at the bottom. The geometry of these surfaces is constrained by density functions and deformed to follow a flow path. The choice of the flow path aligns with physical reasoning, as it is more likely for flow events to traverse lower elevations. This way of positioning a specific feature (here the flow path) to previous features is symptomatic for rule-based models, which are presented below. To introduce irregularity and facilitate conditioning, the surfaces are further modified by adding stochastic residuals with GRF. A typical resulting model of these stacking surfaces is shown in Figure 2.27B. Finally, Pyrcz et al. (2005) used inferred trends from geological data to condition the modeling of properties, such as porosity and permeability. This strategic approach facilitated the seamless integration of soft data into the overall modeling process.

Representing various lithofacies using surfaces is a common practice. However, a significant challenge associated with this approach lies in the inherent difficulty of determining whether a specific lithofacies observation can be correlated with

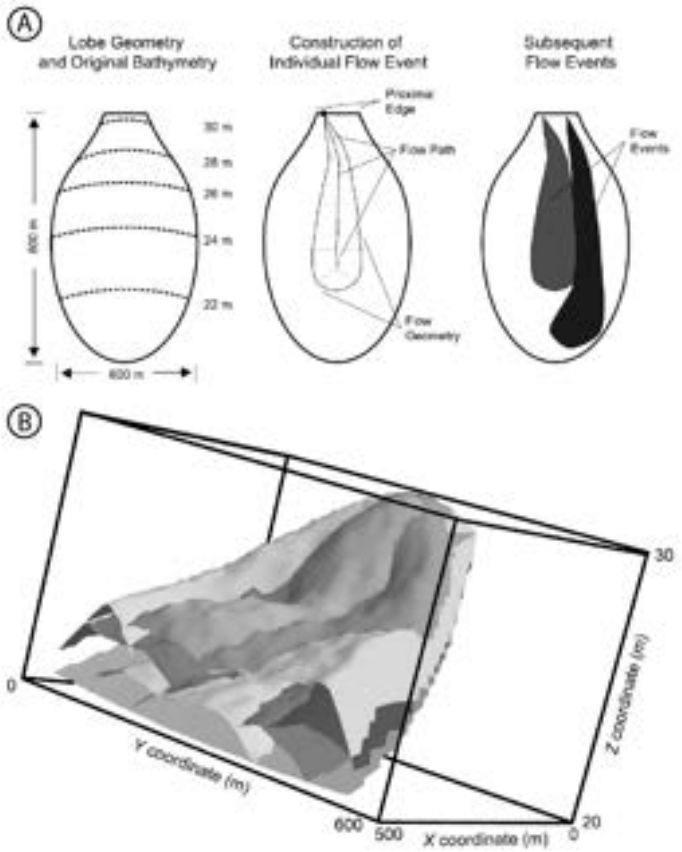

Figure 2.27: ***A****: Schematic representation of the methodology used by Pyrcz et al. (2005) to model flow events. A lobe is firstly defined, flow paths are calculated based on actual bathymetry and a deformed surface is added to it to represent the flow event.* ***B****: resulting 3D model after stacking multiple events. Images modified from Pyrcz et al. (2005).*

surrounding well observations, especially when that facies has been deposited multiple times. One cannot, or hardly, know whether two sand observations of two adjacent wells resulted from the exact same depositional event.

To answer this problem, Allard et al. (2021) recently introduced a method that involves stacking of stochastic surfaces that represent the depositional events, the thickness modeled using latent GRF. Their approach, applied to a known stratigraphic pile that delineates the history of depositional events (lithofacies), systematically explores possible configurations within wells. The method evaluates the likelihood of each configuration, a crucial aspect considering that the borehole information is often incomplete. This incompleteness arises from the fact that the borehole data often lacks direct information about the specific

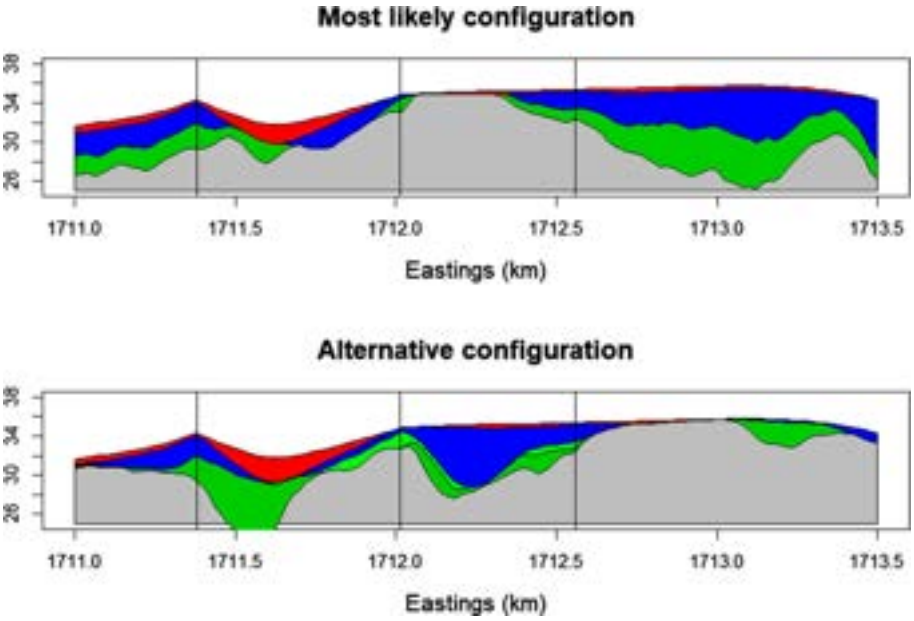

Figure 2.28: *Cross-section of 3D models made with the method developed by Allard et al. (2021) using real data. Four different facies are modeled: red, blue, green, and gray; tone variations of these colors indicate identical lithofacies but from distinct events. Image taken from Allard et al. (2021).*

layer to which a given observed thickness belongs. Employing a Markov Chain Monte Carlo (MCMC) algorithm, the researchers were successful in sampling model parameters, such as variograms, and exploring lithofacies configurations that maximize the likelihood within a Bayesian framework.

An applied example of this method is shown in Figure 2.28. Note the two different green facies in the alternative configuration, indicating two distinct depositional events of the same lithofacies. The method can propose different possible facies configurations (lightgreen facies, darkgreen facies, or a combination of both) and sort them by likelihood. This way of integrating likelihood into facies models is particularly innovative and could represent a new way of modeling facies, not only with SBM. However, their method still has some limitations: the method works better with few wells (< 20), no consideration of erosion (only deposition), and the necessity to provide a parent sequence (stratigraphic pile), which is not straightforward.

The SBM presented here focuses on stochastic approaches. However, it is important to note that SBM using deterministic surfaces is just as widespread, if not more so, than stochastic approaches (e.g., Sech et al. 2009; Niu et al. 2021; Alpak et al. 2022). Recently, Nonuniform Rational B-splines (NURBS) have recently gained interest in the modeling of different sedimentological objects

(Ruiu et al. 2016; Jacquemyn et al. 2019; Moulaeifard et al. 2023). Although interesting and capable of reproducing a wide range of structures, these methods require a great deal of manual work to create the control points needed to reproduce realistic geological objects. In addition, its deterministic nature makes uncertainty quantification difficult. However, deterministic methods, and particularly, are still useful for parameterizing complex geological objects to be used with other OBM or to build TI for MPS.

The effectiveness of conditioning SBM realizations is highly dependent on the rules employed to constrain surface positions. For example, local conditioning of surfaces in the turbidite model by Pyrcz et al. (2005) revealed computational limitations, particularly in terms of computation time, due to the low acceptance rates of surfaces, especially when dealing with a large number of data. An optimization approach was presented by Bertoncello et al. (2013), where the sensitivity analysis precedes the optimization of the surface parameters based on their sensitivity order (in mismatch). However, a drawback of this method is its difficulty in capturing the full variability of posterior models, since only a restricted number of parameters are sequentially optimized. Wingate et al. (2016) proposed the use of variational inference, a Bayesian method, aiming to replace the challenging-to-sample posterior distribution of the model (surface geometries, positioning, etc.) with easily manageable distributions (e.g., Gaussian) that are optimized, often through gradient descent. Although its method may not match the performance of a standard MCMC approach, it demonstrated significantly faster computation times, 240 hours for MCMC versus 10 minutes for its method for the same number of posterior samples. Note that variational inference is very general and can be applied to any method requiring sample distributions. It is not restricted to SBM.

Although quite recent, SBM have been applied in several different settings: deep marine deposits (Pyrcz et al. 2005; Zhang et al. 2009), rock outcrop (Xie et al. 2000), shoreface (Sech et al. 2009), tidal deposits (Wen et al. 1998; Nordahl et al. 2008), point bars (Niu et al. 2021), and even volcanic aquifer (Koneshloo et al. 2018). This is largely due to the flexibility of the method and also to the surfaces themselves, which may be conceptual, but are natural and familiar to the geologist as a means of delimiting distinct geological features. Or, as stated by Moulaeifard et al. (2023): "Surface representation is one of the common concepts between geology and computer graphics"(Moulaeifard et al. 2023, p. 82).

In contrast to pixel-based methods, such as SIS, TPGS, and MPS, SBM stands out for its ability to maintain distinct intricate geometries throughout the modeling process, similar to other OBM. In summary, SBM serves as a crucial tool, demonstrating its efficacy in various scenarios and providing interpretable information to geologists. Although not universally applicable, SBM proves particularly valuable for delineating larger sedimentological structures (e.g., surfaces of order 3 to 5 according to Miall classification (Miall 2013)). However, the chal-

lenge of conditioning remains, prompting ongoing research efforts, especially in applied cases.

2.6.5 Rule-based

Rule-based models (RBM) are an "evolution" of the OBM that is based on how to spatially place objects (Hassanpour et al. 2013). This placement is controlled by user-defined rules that are supposed to mimic the results of realistic geological processes, similar to process-based models, but without considering the complex physical processes and equations behind it (Pyrcz et al. 2014, 2015). They are consequently faster and generally require fewer parameters. Over time, RBM has been referred to as event-based or process-mimicking. The use of the term 'process-based' should be avoided as it is more commonly associated with methods that incorporate physical equations in their modeling process (e.g., Pyrcz et al. 2014). An important difference of RBM compared to standard OBM is the consideration of time (Pyrcz et al. 2015). Objects are spatially and temporally placed in the simulation domain given some rules that can be different given the time of the simulation or the actual state of the domain. By integrating this new dimension, the models get closer to the real processes of deposition and erosion that characterize geological features. But, on the other hand, the difficulty of conditioning the OBM, already not straightforward, increases significantly.

RBMs are site-specific by nature, and the rules used heavily rely on the processes they are meant to mimic. As a result, it is impossible to provide broad guidelines, and every RBM technique differs greatly from the others. In order to demonstrate the potential and challenges of RBM, we will present various approaches and applications of RBM in various sedimentological contexts, beginning with alluvial deposits.

Much like standard OBM, RBM has found application in modeling fluvial settings, driven by its importance as a hydrocarbon reservoir and major groundwater aquifers. This preference is underpinned by two primary reasons: first, the well-established and extensively studied nature of fluvial processes, as sedimentologists and geomorphologists have delved deeply into their dynamics; second, the ease with which the evolution of these systems can be observed over time at a human scale. From these previous studies, field observations, empirical data, and physical equations can help select the rules to be used in RBM in fluvial settings.

Ironically enough, RBM was one of the first numerical facies modeling methods, with the two independent works of Allen (1978) and Bridge et al. (1979). They pioneered the construction of 2D cross-section numerical models that relied on predefined rules to replicate the heterogeneity of an alluvial setting, taking into account factors such as avulsion (when a river abandons its bed for a new one),

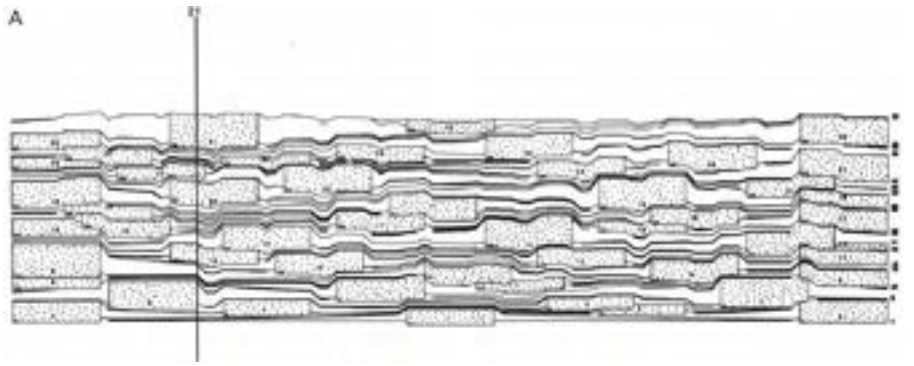

Figure 2.29: *One realization of the model developed by Bridge et al. (1993). The rectangles containing dots represents channel deposits (presumably sand-gravel) while lines delimit the different levels of floodplain aggradation. Compaction is also visible where channels are smaller ad lines less thick in the deepest part of the model. Model dimension are 10 km by 0.25 km (vertical exaggeration 10x).*

tectonic influences, compaction, and aggradation. For example, in the model of Bridge et al. (1979), the new position of the channel is controlled by a rule that states that when an avulsion occurs, the new channel is always placed at the lowest elevation of the floodplain. Later, an updated version of this model was proposed by Bridge et al. (1993) and Mackey et al. (1995), relating processes with more accurate empirical relations (Fig. 2.29) and extending it to 3D to realistically model the effect of avulsion on the spatial distribution of sand bodies.

Although these models are relatively simple, deterministic and do not incorporate conditioning to well data, their primary purpose is to evaluate the relationships between different factors and the connectivity of channel bodies.

Created in the footstep of FLUVSIM, ALLUVSIM (Pyrcz et al. 2009) has brought a significant improvement in alluvial RBM. While some features from FLUVSIM are inheriting, such as geometries, levees, and crevasse splays, the key distinction lies in the treatment of channel centerlines. Unlike random placement, ALLUVSIM introduces an evolution model for channel centerlines that reflects simplified, yet realistic meander dynamics (Fig. 2.30C). This results in more authentic patterns, allowing for channel rollbacks, which can lead to cutoffs and the formation of oxbow lakes. Although channel migration is deterministic, other parameters, including channel, levee, and crevasse geometries, are stochastic and derived from density functions. The model also incorporates stochastic avulsions, simulating instances where a portion of the centerline is abandoned and subsequently resimulated. All objects interact with each other through rules that are controlled by user inputs.

The resulting ALLUVSIM models show complex heterogeneity (Fig. 2.30), demonstrating its ability to realistically mimic a meandering system setting. In terms of conditioning, ALLUVSIM is able to respect global and local facies proportions, but has more difficulty with hard data. To simplify the conditioning of hard data, the fluvial facies are grouped into two facies: "net" (channel, levees, and crevasses) and "non-net" (overbank fines and channel abandonment). Conditioning is performed by an iterative procedure to adjust the position of the channel centerlines and by an image cleaning procedure. For more information, see Pyrcz et al. (2009). In the end, the conditioning is only an approximation and, if the number of boreholes is too high, it is unable to provide correct simulations. ALLUVSIM perfectly demonstrates the essence of RBM with their ability to produce realistic models, but a very poor conditioning which limits its applicability to real cases.

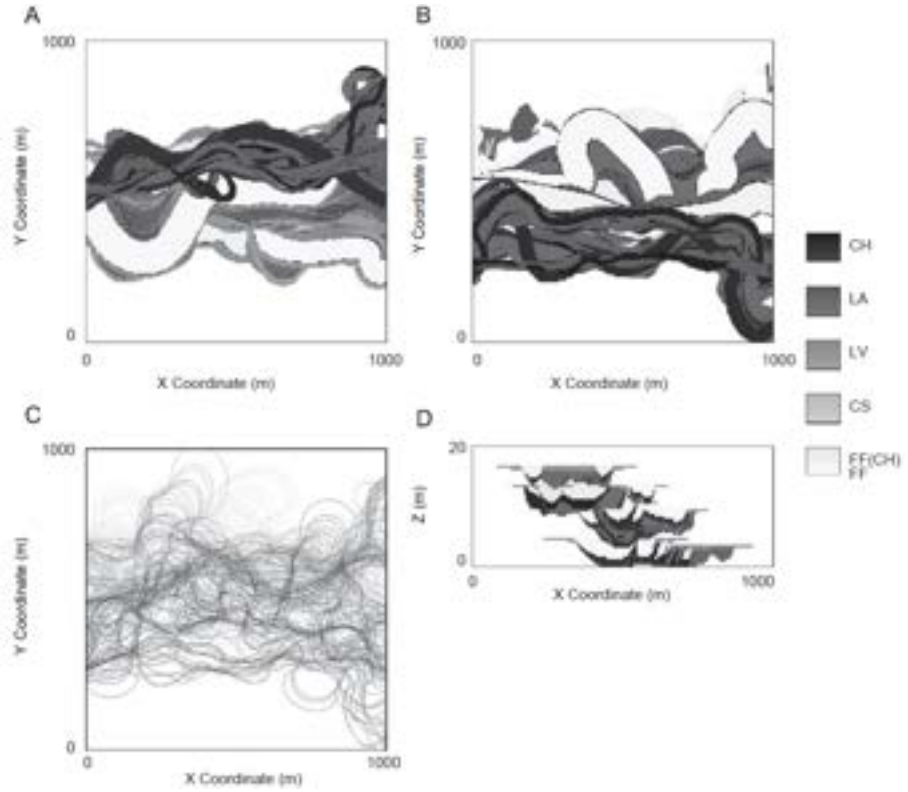

Figure 2.30: *Example of a 3D alluvsim model.* ***A****: horizontal cross-section at elevation z=5m.* ***B****: horizontal cross-section at elevation z=10m.* ***C****: all centerlines generated and migrated during the simulation, grey scale indicates relative age of the centerline (white: old, dark:young).* ***D****: vertical cross-section at position x=10m. Facies code: CH (channel), LA (lateral accretion elements), LV (levees), CS (crevasse splay), FF (overbank fines). Figure taken from Pyrcz et al. (2009).*

Parquer et al. (2017) also proposed a method to reproduce realistic channel migrations without using physically based models. Their innovative approach is to literally see things in a different way. Beginning with an initial channel position, they decompose the channel into half-meanders (river loops, separated by inflection points) and systematically move them backward using simple geometrical relations. The method is stochastic, with the amplitude of migration for each half-meander drawn from user-defined density functions. Another distinctive feature of this method is the decomposition of the channel migration vector into two components: lateral and downstream. This dual-component representation provides a high degree of flexibility in meander migration. The model also incorporates vertical channel migration, allowing the creation of 3D models.

Although the method was not explicitly designed to accommodate well conditioning data, it does consider abandoned river meanders and past oxbow lakes during the simulation (Fig. 2.31). To incorporate realistic timelines for meander abandonments, a time window is assigned to each oxbow lake. However, a challenge lies in the algorithm's inability to guarantee the integration of all oxbow lakes during the simulation.

The methodology presented is intriguing and demonstrates that realistic channel migration patterns can be achieved through simple rules and empirical relations. However, for seamless integration with stochastic algorithms like ALLUVSIM, there is room for improvement, particularly in the realm of conditioning, both soft and hard data. Although there are challenges, these improvements are likely feasible. In conjunction with empirical measurements of river migration with respect to curvature (Sylvester et al. 2019; Donovan et al. 2021) one could also consider improving the realism and imposing constraints on such models.

Another approach to fluvial deposits is the approach of Hassanpour et al. (2013), where the emphasis is on the definition of the objects rather than their placement. Detailed and complex objects (inclined heterolic strata (IHS), complex channel patterns) are modeled, but channel migration is not explicitly considered, but integrated with IHS. Channel centerlines are randomly positioned in the simulation domain and various fluvial objects are attached to it. Objects whose geometries are stochastically parameterized with density functions. The "rules" prioritize the spatial distribution of objects relative to each other rather than attempting to mimic specific processes that are supposed to reproduce the expected spatial distribution of the objects. In this sense, the method is not very far from standard OBM, prompting a question about its classification within RBM. According to Pyrcz et al. (2015), this method falls into the category of *draft geometric rules* methods where heterogeneity is directly imposed rather than explicitly modeled through specific processes. Nevertheless, the approach offers a reasonable conditioning algorithm to the well data, with limitations when the number of wells is high. It maintains a certain level of heterogeneity and realism while at the same time streamlining

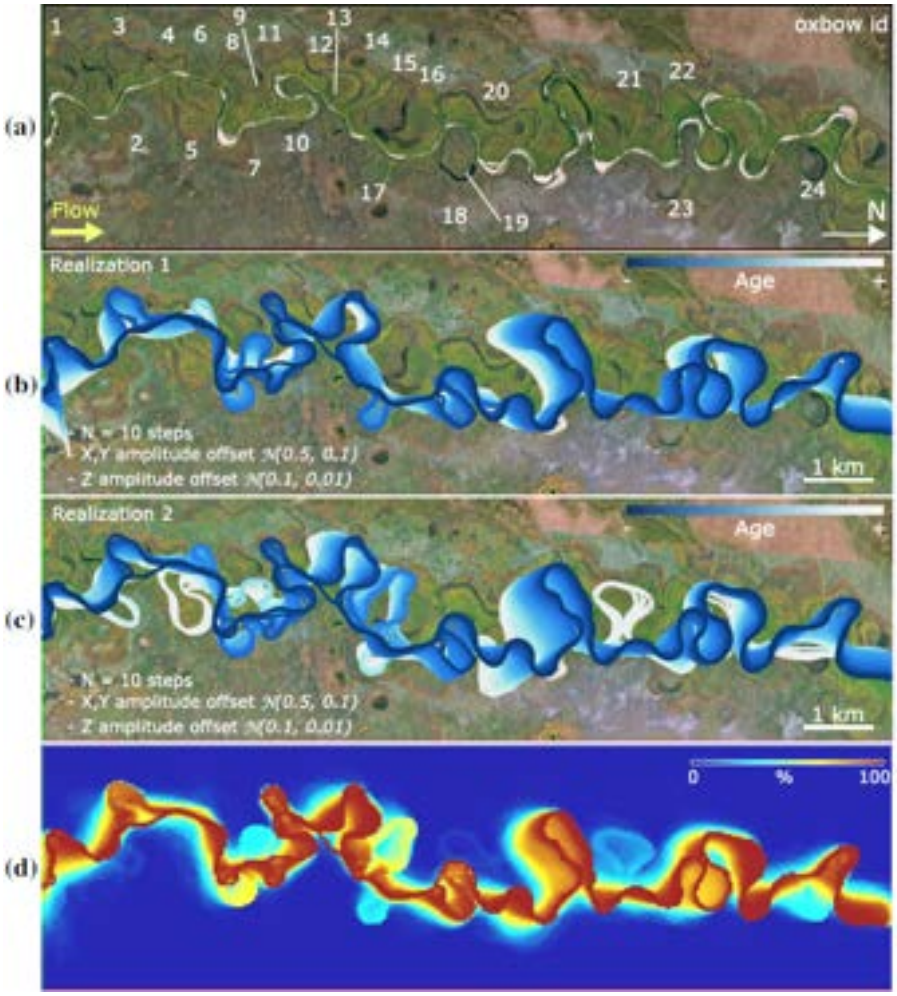

Figure 2.31: *Application of the algorithm of Parquer et al. (2017) to satellite data (**a**). 24 oxbow lakes have been mapped. (**b**) and (**c**): two stochastic simulations, see how oxbow lakes are not all considered in the these two examples. (**d**): Probability of channel occurrences on 100 simulations.*

the conditioning process, providing a pragmatic compromise between speed and geological fidelity.

The PB-SAND algorithm of Yan et al. (2017) further pushes the heterogeneity modeling of fluvial deposits by focusing on the internal straigraphy and lithofacies associations in the point bars. PB-SAND begins by predicting the evolution of the channel centerline given channel positions at three key times that are supposed to represent the initial, middle, and late life of the meander. Migration times between each of these times also need to be provided. Figure 2.32A shows an example of channel migration. Subsequently, PB-SAND continues to model the internal stratigraphy of point bars by using half-cosine functions to represent accretion surfaces. These accretion surfaces represent the deposition events of the river and are primarily influenced by the migration rate of the river. The unit sedimentary volumes, delineated by the accretion surfaces, are then populated with lithofacies. This is achieved through the application of five rules that govern the spatiotemporal occurrence, proportion, and distribution of lithofacies within the modeled point bar elements. These sets of rules can be applied individually or in combination, offering flexibility in determining the association of lithofacies of the modeled sedimentary structures. For example, in Figure 2.32B, the complex evolution of the proportions of lithofacies in the cross section f is depicted. This dynamic representation reflects the intricate rules applied by PB-SAND to emulate the complex depositional processes of sandy point bars and counterpoint bars (Yan et al. 2017). PB-SAND accounts for the temporal evolution of the deposits, in which, as the simulation progresses, older deposits may be eroded. Consequently, only a small fraction of the facies originates from the initial time, as indicated by the blue lines in Figure 2.32A, with these deposits observable in cross-section f (Fig. 2.32B).

It should be added that PB-SAND is a combination of deterministic (channel migration, point bar shapes) and stochastic (mud drapes) features that are all determined by a large number of parameters (more than 50). Most of these parameters are deterministic (one value), but we can imagine that probabilistic distributions could also be used to increase the variability in the models. Models are not conditioned on hard data but a partial soft conditioning can be obtained on facies proportions.

To bypass the main issue of PB-SAND, which requires a provision of channel position at three distinct times as well as migration times, PB-SAND have been combined with the backward meander migration algorithm (Parquer et al. 2020). The study highlighted the importance of synergizing different modeling approaches with similar objectives. This integration not only aids in overcoming specific limitations of individual methods, but also contributes to a more comprehensive exploration of uncertainty in subsurface heterogeneity modeling.

To approach the complexity of braided systems, Webb (1994) have proposed a stochastic RBM. The general idea is to stack the topographic surfaces of

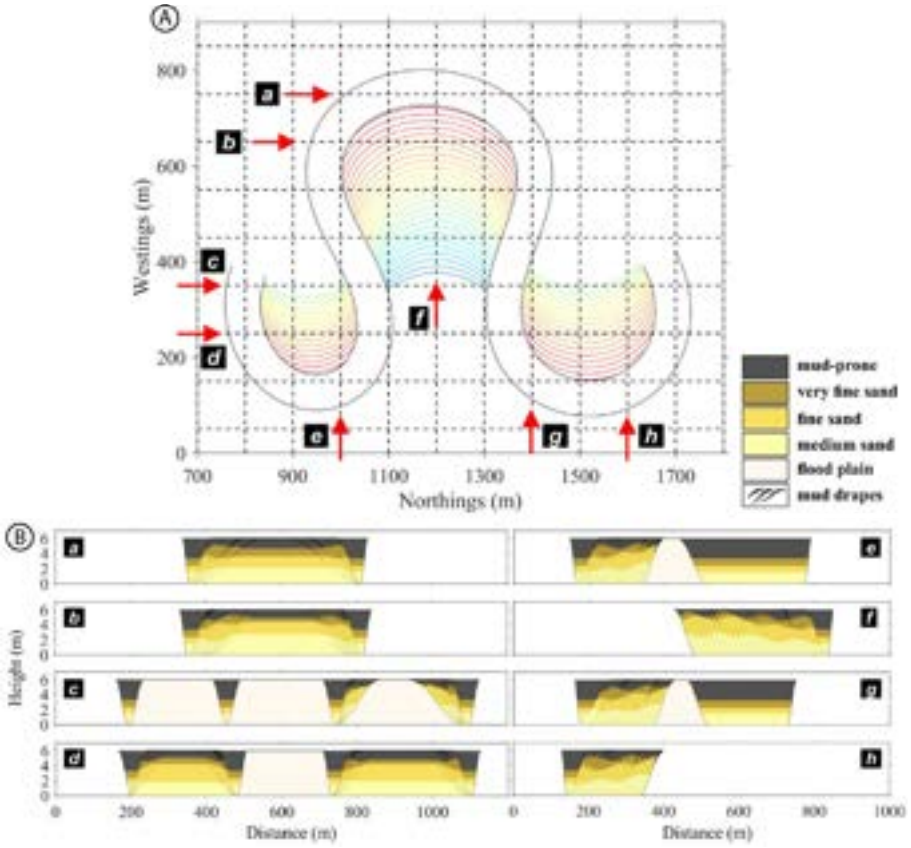

Figure 2.32: *Example of an application of PB-SAND to real field data (Yan et al. 2017).* ***A****: Channel migration steps from the oldest (blue) to the youngest (red) channel centerlines. letters (a - h) indicate the position of cross sections shown in* ***B****. Figure modified from Yan et al. (2017).*

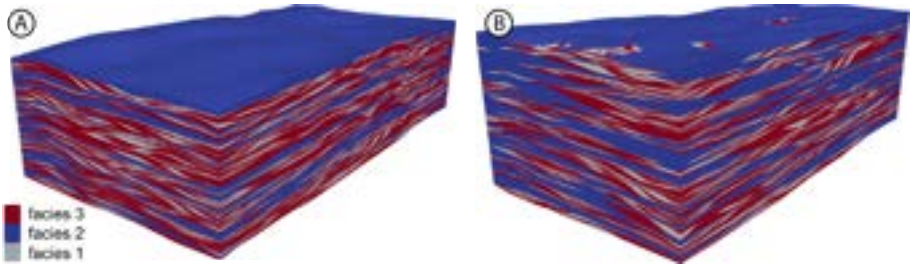

Figure 2.33: *3D realization of the approach developed by Pirot et al. (2015) with different aggradation rate. Model* ***A*** *has an aggradation rate 30x lower than model* ***B****. Images taken and modified from Pirot et al. (2015).*

the braided rivers that define individual regions (facies). The method begins by producing channel networks using a random walk approach to mimic the distribution of the channel flow paths. For each network, a topography surface is generated assuming the geometry parameters of the channel (drawn from density functions). The channels are also assigned a flow velocity according to user input and empirical data. The different surfaces are stacked on each other to delimit distinct geometrical elements. Finally, facies are attributed to elements on the basis of different criteria, such as the probability of transition and the Froude number, which is an indicator of flow energy. The idea of using this number is to correlate the presence of certain facies according to the hydraulic regime (e.g., more coarse facies when the Froude number is high). This approach generates realistic sedimentary characteristics similar to those seen in the field. Anderson et al. (1999) used it to create facies models of a Quaternary aquifer, which were then used as input for groundwater flow simulations to determine preferential flow paths in the aquifer.

Pirot et al. (2015) proposed a similar method, but in which topographic surfaces were generated using MPS, using real topographic measurements of braided rivers as TD. This approach included aggradation by shifting the surfaces upward according to a specified aggradation rate, as well as geological rules to simulate erosional and depositional processes. It also refined the facies distribution within each element by taking into account an estimate of surface flow to guide an iterative deformation scheme. The resulting models showed cross-stratified sediments that resembled outcrops of braided systems (Fig. 2.33). Although this method produces visually realistic results, it does not consider conditioning on hard data.

Due to their great importance for hydrocarbon reservoirs, RBM have also been developed for abyssal deposits (3000-6000 m deep) (Pyrcz et al. 2005; McHargue et al. 2011; Sylvester et al. 2011). Main processes include lobe models (already discussed in the SBM section) and deep channels (turbidites). One practical aspect is that the latter sedimentological process is common to fluvial processes. This implies that similar methods can be used for both environments.

Sylvester et al. (2011) have combined a 2D RBM turbidite model with a meander evolution model to generate 3D realizations of the abyssal subsurface in a deep-sea channel environment. They were able to produce realistic models that are similar to interpreted seismic cross-section of such environments.

McHargue et al. (2011) have proposed a complete and detailed RBM, integrating various processes such as erosion-depositional cycles, cycle hierarchies, avulsion, and dynamic positioning of the flow events. All of these were considered using the rules and empirical relations that are the building blocks of their approach. A typical turbidite cycle consists of an early erosive phase, where the equilibrium profile is lowered, followed by a gradual increase of the profile, which increases the aggradation of the system. Their model helped them

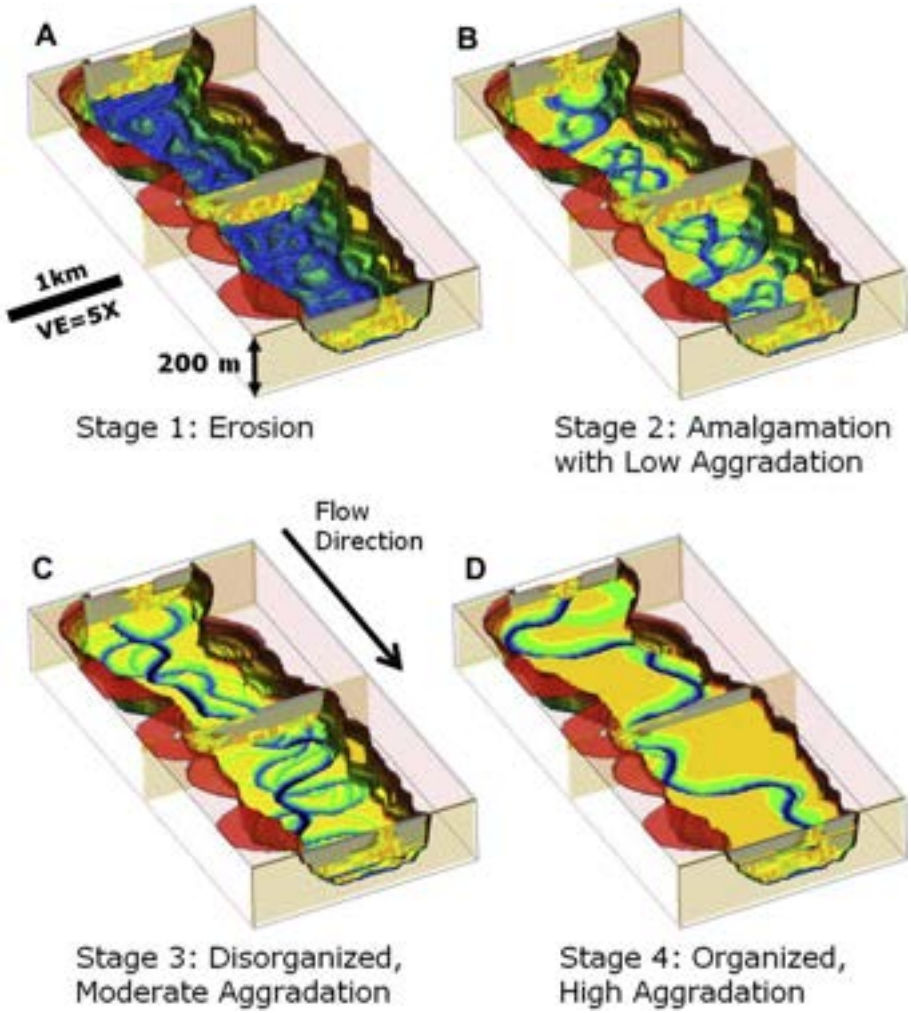

Figure 2.34: *Fours stages in the model developed by McHargue et al. (2011).* ***A****: Erosion phase, no or little deposition occurs during this phase.* ***B****: Sand-rich flows with the beginning of the aggradation phase.* ***C****: Mixed sand-mud flows, increase in aggradation, and disorganized channels.* ***D****: Mud-rich flows with high aggradation rate with organized channels. The model is 2 km × 10 km × 200 m. The colors of the 3D model indicate the depth of erosion with red (shallowest), yellow, green, and blue (deepest). Orange corresponds to the aggradation deposits. The facies in the cross sections are represented by orange (axis), yellow (off-axis), green (margin) and gray (abandonment), see McHargue et al. (2011) for complete description of these facies. Vertical exaggeration = 5 m. Figure taken from McHargue et al. (2011).*

to demonstrate their suggestion of the influence of sediment nature of flows on stacking patterns of channels. Where mud-rich flows favor the development of organized channels, while sand-rich flows favor disorganized channels. In total, four different stages are recognized during a cycle (Fig. 2.34), where the equilibrium profile gradually increases and the flows become muddier.

Their study exemplifies RBM, taking advantage of a significant amount of geological information to establish rules that are stochastically combined to generate an ensemble of plausible models that respect geological concepts. The absence of mention of conditioning in their paper suggests that addressing conditioning in such a complex model may present challenges, further emphasizing the trade-offs involved in modeling complex geological processes.

To finish this long, but not exhaustive list of RBM, we would like to present the genetic approach (Teles et al. 2001, 2004, 2006). It is technically not a method in itself, but rather a way of combining existing OBM with paleoclimatic data and past geological settings to reproduce the geological history of a specific site. The genetic approach differs from other methods in that it breaks down the problem into different periods that make sense from a geological point of view.

Their method involves reconstructing the geological history of an alluvial valley and estimating for each period (referred to genetic period): the time interval, the fluvial regime (meandering or braided), and the thickness of sediment deposited or eroded. The approach employs different methods to reproduce the effects of each regime on sediment, specifically focusing on the spatial distribution and thickness of erosion and/or deposition. For example, Teles et al. (2001) have modeled braided systems with a standard OBM where compound bars of varying shapes and sizes are randomly positioned in the domain. And, depending on the genetic period, deposits or erodes a certain amount of sediment. In contrast, meandering systems are modeled by connecting multiple sinusoidal sections to construct the channel path. Along this path, erosion and deposition processes occur, with magnitude influenced by the genetic period and available data. Multiple channels are generated until the end of the period, achieving the desired elevation. Note that any method can be used to model each genetic period. For example, they suggested using empirical rules to constrain the meander evolution to have more realistic simulations.

This method has been compared with other geostatistical methods (Teles et al. 2004, 2006, SIS) and has shown more realistic results in terms of flow and transport results. Notably, the ability to have preferential paths with channel deposits, as with OBM.

The main difficulty of the method is to correctly define these genetic periods, as paleoclimatic data are often incomplete, past fluvial regimes are difficult to define (Miall 2013), and absolute measures of time are not always available.

Furthermore, the intensity of each period (amount of sediment deposited or eroded) is not straightforward to obtain. Additionally, conditioning the model to hard data poses a significant challenge and is not addressed in the current model. The authors acknowledge the need for further studies to investigate and address these conditioning challenges. Despite challenges, the fundamental idea of the genetic approach is intriguing. With modern geological data and computational resources, there is potential for interesting results.

As we have seen with the multiple examples of RBM, conditioning is generally the major drawback of all methods. Direct conditioning is a complex process due to the evolving nature of the model over time. RBMs are models that often consider the notion of time, where the sedimentological state is evolving through time. However, predicting the state of the model at a future time point (e.g., at time $t + 10$) is challenging, making it difficult to ensure accurate positioning of different objects without important deformations that may compromise realism. Furthermore, the more complex and restrictive the rules, the more difficult it is to condition the final model, but greater geological realism is achieved. This can be viewed as a trade-off between the presence of interesting and realistic features and the necessity of perfect and strict conditioning on hard and soft data. This trade-off is in contrast to simpler methods such as SIS, where conditioning is straightforward.

However, conditioning is not completely impossible, as seen with different examples (Pyrcz et al. 2009; Hassanpour et al. 2013; Parquer et al. 2017), but it is only partial and largely dependent on the phenomena simulated and the level of complexity considered. Some conditioning methods, as discussed in the SBM section (section 2.6.4), could potentially be applied to RBM. Examples include variational inference (Wingate et al. 2016) or sequential optimization of the most influential parameters (Bertoncello et al. 2013). However, these are still research gaps that need to be addressed in future studies. For simplicity, RBM conditioning is obtained through MPS (see section 2.5) or machine learning algorithms (see section 2.8).

There has been a definite craze for RBM over the last 15 years, with numerous approaches developed and investigated. It is worth noting that the presented list of approaches is not exhaustive and that there are other RBM for similar environments, as well as in different settings such as deltaic (Cazanacli 2021) or aeolian (Yan et al. 2024) environments. For the sake of consistency, these are not detailed here as the main objective was mainly to give an overview of how RBM works.

Because of their difficulty in conditioning and the need to build more complex conceptual models than the other OBM, RBM have mainly remained research tools. Improvements could be realized if more open source solutions and software were made available to ease their spreading. Moreover, a very large number of parameters are required, not only for the geometries of the objects but

also for the rules that need to be consistent with the specific features of the modeling site. It is also important to note that most RBM have been developed for fluvial or abyssal environments. Pointing out a significant research gap in the application of RBM in other sedimentological contexts, such as glacial environments.

Assuming large efforts into the building of the geological concept, RBM are, in the end, able to produce very realistic models that are computationally reasonable, which is a major advantage over process-based methods. As they are still quite recent, a significant amount of research is expected in this field, which will surely improve the approaches and ease their use to a larger audience.

2.6.6 Grammar-based

We finish the OBM section with the grammar-based models (GBM) which have received little attention in geosciences despite interesting results in other fields (e.g., Prusinkiewicz et al. 1996).

GBM relies on formal language theory, an applied mathematics discipline that involves constructing words composed of letters from an alphabet, following specific rules, both outlined in a formal grammar. Despite appearing disconnected from geological modeling, the concept involves treating geological objects as if they are composed of basis geometrical elements, where each of these elements is represented as letters.These letters are combined into series, akin to how basic geometries form geological shapes such as channels. With this assumption, it becomes possible to use the formal grammar theory to generate and manipulate geological models. The complex task now is to define the grammar (i.e. the rules) to generate series of letters that are consistent geologically. Multiple algorithms and grammars can be used, depending on the complexity desired, but few of them have been applied to geological studies so far.

Hill et al. (2007) introduced a grammar called Geosyntax, which has been applied to address various challenges of geological modeling. This includes simulating 1D sedimentary sequences (Hill et al. 2007), creating 2D cross sections of sedimentary successions (Hill et al. 2008), and channel-related deposits (Hill et al. 2009, Fig. 2.35). The fundamental concept involves manipulating basic shapes, referred to as terminal symbols, which are organized into more intricate forms known as parent symbols. These parent symbols are then arranged according to the grammar's rules, facilitating the creation of the desired geometries. In the context of channel simulations (Hill et al. 2009; Hill 2009), terminal symbols mainly encompass tight and gentle bends parameterized by bezier curves. Parent symbols, representing bends, consist of three terminal bend symbols, one for the channel and two for overbank deposits. Each symbol is endowed with attributes governing its geometry, such as width, length, depth, etc., which are drawn from user-defined density distributions.

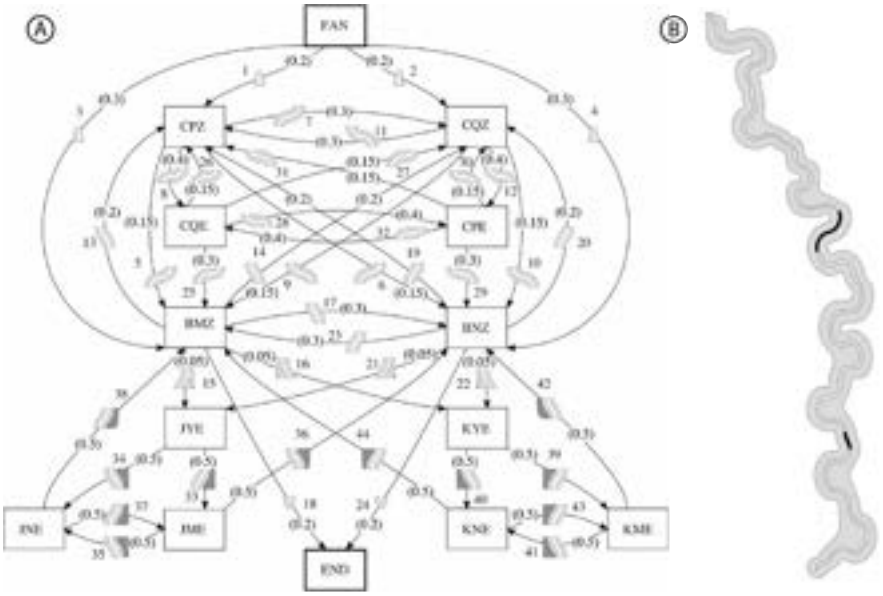

Figure 2.35: *Key-features of the Geosyntax grammar for channels simulation. Three facies are considered: channel (white), overbank (lightgrey) and crevasse splay (darkgrey).* ***A****: Finite-state diagram used to generate the channels. State are indicated in squares and rules by arrows. Each rule has a number, a probability and a schematic representation of the parent symbol used by the rule. Note the complexity of diagram considering that only twelve states are represented.* ***B****: A conditional simulation of a channel, conditioning "symbols" are shown in black.*

They use two types of rules: parent-generating rules, which specify the permissible use of parent symbols (the complex ones) based on a given state, and terminal-generating rules, which detail how to construct parent symbols using terminal symbols. In the case of Hill et al. (2009), the parent-generating rules are represented by a finite-state diagram (Fig. 2.35A), which undergoes evolution from one state to another with associated probabilities. Here, a state denotes a specific configuration of the system at a given time, generally determined by the last symbol added. The finite-state diagram directs the evolution of the state in a predefined manner, restricting certain combinations of parent symbols, such as merging two successive S-bend shapes. Diagrams and rules are typically constructed on the basis of geological knowledge and analog data, but involve significant challenges.

The method can handle sparse conditioning data, but requires that these be first transformed into symbols (Fig. 2.35B). The conditioning process involves backtracking the finite-state diagram to find a suitable rule to generate the matching symbol and deformation of the symbols to match the exact position of the conditioning data.

The Geosyntax approach is interesting and offers numerous advantages. It exhibits versatility, demonstrating adaptability to various settings, even in cases where the grammar was not explicitly designed for the specific application (Hill 2009). The generated models are compact and can be succinctly represented as lists of strings and attributes. Furthermore, the method can produce a large amount of conceptual information through its grammar, and it boasts computational efficiency. However, several problems remain. The manual determination of rules and their corresponding transition probabilities poses a difficulty. The conditioning is also notably limited, requiring explicit definition of conditioning symbols, thereby reducing the method's flexibility. Furthermore, the independent simulation of objects hinders the ability to model their interdependence, rendering it impossible to simulate channel migration, for example.

The approach used by Rongier et al. (2017) is somewhat different as it relies on a simpler grammar, L-systems, originally developed to simulate the growth of trees and roots. L-systems combines segments based on a set of user-defined parameters and rules, where the segments form the root network or tree skeleton. The growth of the network can be notably influenced by a set of attractive or repulsive constraints to control the direction and length of segments. For plants, these constraints can be interpreted as the environment in which the plant growth (amount of light, other plants, etc.) affects the plant evolution and its final shape. As in the case of other GBM, the resulting network is a list of letters with geometrical attributes.

In their work, Rongier et al. (2017) adapted L-systems to model channelized systems within a valley, incorporating various constraints to consider borehole data and local proportions (Fig. 2.36). The stochastic model extends into 3D, allowing for a progressive aggradation of the system.

Although the method is interesting and delivers promising results, it is essential to note that it involves a substantial number of parameters that pose challenges in terms of determination (Rongier et al. 2017). Although default values may offer practical solutions in certain scenarios, their universal applicability is not guaranteed. Moreover, L-systems are also mainly used to generate line networks, which are not easily transposable to all geological settings. Further research is warranted to comprehensively explore the issues and challenges of applying L-systems to facies modeling.

To summarize, GBM is an interesting alternative to other modeling approaches but that have been poorly investigated. The flexibility and the compactness of using formal grammar allow us to generate relatively complex geological shapes while considering conditioning data. The major difficulty lies in defining the rules that control the construction of the shapes. This is particularly the case with the Geosyntax grammar (Hill et al. 2009). To overcome this limitation, advanced algorithms need to be developed to transfer the geological information (analogs, sedimentological rules, well data, etc.) into these rules. Various

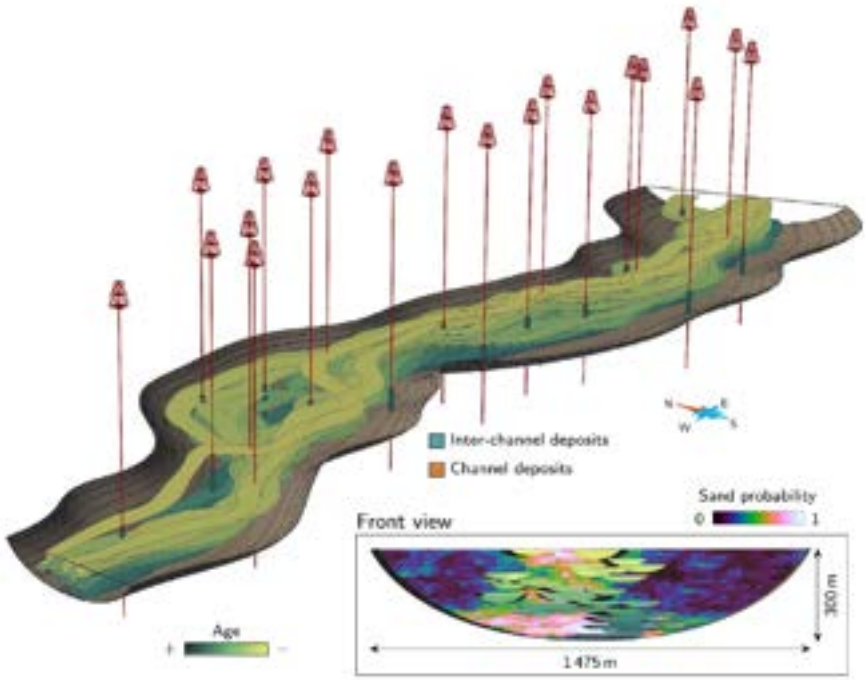

Figure 2.36: *3D conditional simulation of the channel model using L-systems (Rongier et al. 2017). Boreholes are represented and are encoded with two facies: channel or inter-channel deposits. Front view shows the evolution of the channel according to time. Image modified from Rongier et al. (2017).*

approaches can be envisaged, such as automatic image analysis, but the problem is not straightforward. Additionally, leveraging recent advances in machine learning, particularly deep learning, where language models based on transformers proven effective in various contexts (Vaswani et al. 2017), could provide valuable assistance. Given that GBM operates with strings, language models could seamlessly integrate with the methodology and contribute to improved conditioning, for example.

In conclusion, GBMs produce interesting and encouraging results which is possibly an important and potential area of future research regarding facies modeling.

2.6.7 Summary

OBMs are very diverse, versatile and efficient methods that can replicate intricate geologies at reasonable computing costs, as long as appropriate objects and rules are used. Considering the five different categories of OBMs presented in

this review, very different results are obtainable. They should not, however, be considered completely separate, as these methods are often combined in order to benefit from the advantages of each. In addition, other object approaches not covered in this study can be considered which are significantly different from the others. For example Erharter et al. (2021) proposed to generate point clouds with varying point densities to mimic direction and dimensions of geological bodies (or geobodies) for geotechnical applications. Point clouds are then clustered and meshed according to some criteria to delimit each geobody. Objects are then directly created using points.

However, while OBMs have many advantages, they also have limitations. One of the most significant challenges is conditioning, especially hard conditioning, which is still an active area of research. Additionally, parameterizing an OBM can be difficult due to the large number of parameters involved. Conceptualization can also be challenging, as it is not always easy to link geological processes with geological shapes or objects. When modeling in an alluvial setting, it is crucial to distinguish between braided and meandering systems, as the generated shapes and methods used are very different. However, distinguishing between the two based on borehole records is difficult, and river systems can change rapidly. Therefore, it is necessary to properly characterize and understand the geology of the modeling site to correctly conceptualize object-based models. This is especially true for RBMs.

2.7 Deformation-based

These methods are based on other facies models. They are modified and improved by deforming them according to certain criteria. These approaches differ from previously seen methods as they are not entirely self-sufficient and cannot produce a facies model without a preexisting model. MPS algorithms can also be considered as not self-sufficient methods. Within the deformation-based category, two discernible methods have been identified: compression-based models and pixel deformation models.

2.7.1 Compression-based

The compression-based approach, introduced by Manzocchi et al. (2007), offers a departure from the conventional treatment of connectivity as an indirect measure to respect and instead considers it directly as an input parameter. Specifically, they employ the amalgamation ratio (AR) as their connectivity measure, representing the proportion of a layer of a specific facies that is vertically connected to other layers of the same facies. In particular, they observed that Boolean models (see section 2.6.2) tend to exhibit a nearly 1:1 relationship between facies proportions (Net-to-Gross ratio, NTG) and AR. This alignment is expected under the assumption of random object placement, but it is not commonly observed in outcrops or in models based on processes and RBM.

They showed that AR is generally lower than NTG, or in other words that Boolean models are too connected for a given NTG. More information on the connectivity of facies modeling methods can be found in Walsh et al. (2021a). To address this issue, they proposed the compression-based models (CBM).

The idea is pretty simple and starts with a model, generated with the facies modeling method of choice, with the correct connectivity but incorrect proportions. Facies objects are then vertically deformed, compressed, or extended, in order to respect the facies proportions. The ratio between initial and final thicknesses is called the compression factor (c_F) and is defined as:

$$c_F = \frac{1 - \frac{1}{NTG}}{1 - \frac{1}{NTG_I}} \tag{2.11}$$

where NTG and NTG_I are the target and, respectively, the initial Net-to-Gross ratio (sand proportion over fines). This can be simply seen as a rescale of the facies layers according to their proportions. The great advantage of this method is that a wide variety of models can be obtained by playing with connectivity (AR) and proportions (NTG) as shown in Figure 2.37. On each column, the models are obtained by deformation of the corresponding OBM located on the ascending diagonal (col 1 - row 3, col 2 - row 2, col 3 - row 1). These compressed models are difficult, if not impossible, to obtain with classical methods (Walsh et al. 2021b).

CBM can produce different results depending on the initial model chosen. The major difficulty of this approach is to know the correct initial NTG to obtain the desired AR. Moreover, AR is not an applicable measure of connectivity for pixel-based method and, for these reasons, Walsh et al. (2021a) have proposed the following equation:

$$NTG_I = 1 - (1 - NTG_C)^{P+1} \tag{2.12}$$

This equation establishes a relationship between the initial NTG and the percolation threshold (P), which values range between 0 and 1. The percolation threshold serves as a more relevant measure of connectivity for pixel-based methods. Here, NTG_C represents the critical Net-to-Gross ratio, a variable that depends on the chosen method.(Walsh et al. 2021a).

The method has also been improved to consider more than two facies and different hierarchical levels, allowing to consider more complex situations. Conditional simulations can be achieved by transforming the borehole data into a nondeformed space, as outlined by Walsh et al. (2021b) and Manzocchi et al. (2023). The conditioning data, once transformed, are utilized for conditional

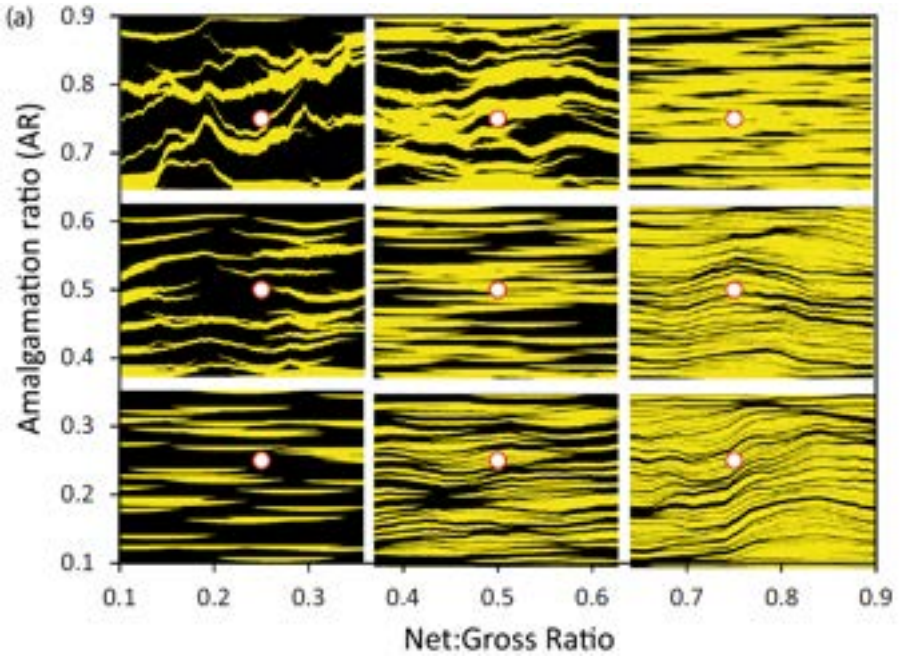

Figure 2.37: *Different CBM models according to NTG and AR. Models in the ascending diagonal are simple boolean models with no deformation and serve as a basis for the other models that are compressed/dilated. White dots show the precise values used to generate each model. Image taken from Manzocchi et al. (2023).*

simulations in the original space employing the chosen method (MPS, OBM). Subsequently, the models undergo compression, following the previously described approach, to derive compressed conditional simulations.

This approach presents a valuable emphasis on connectivity, a factor often neglected in traditional facies modeling. However, a notable drawback of this method lies in its complete erasure of the initial model structure and the underlying geological concepts that guide its construction. Determining the appropriate initial parameters for constructing the prior model, in order to adhere to specified criteria post-deformation, poses a significant challenge. For example, with this method, it is nearly infeasible to reproduce the variogram, although it can be deduced from the data. The HOS are even more difficult to respect.

The difficulty in predefining these initial parameters may limit the applicability of the method and its effectiveness in capturing the desired geological features and spatial statistics. For now, the method has not been widely applied, but this relative simplicity and the fact that it can be used with any facies modeling methods could open the door to a new way of building and thinking models.

2.7.2 Pixel deformation

To alleviate some issues with the choice of the TD for MPS simulations, Straubhaar et al. (2019) have proposed two different operations to edit existing conceptual models (continuous or categorical): painting and wrapping. Although mainly designed to obtain an updated TD for MPS simulations, these operations can also be used with other facies modeling outputs.

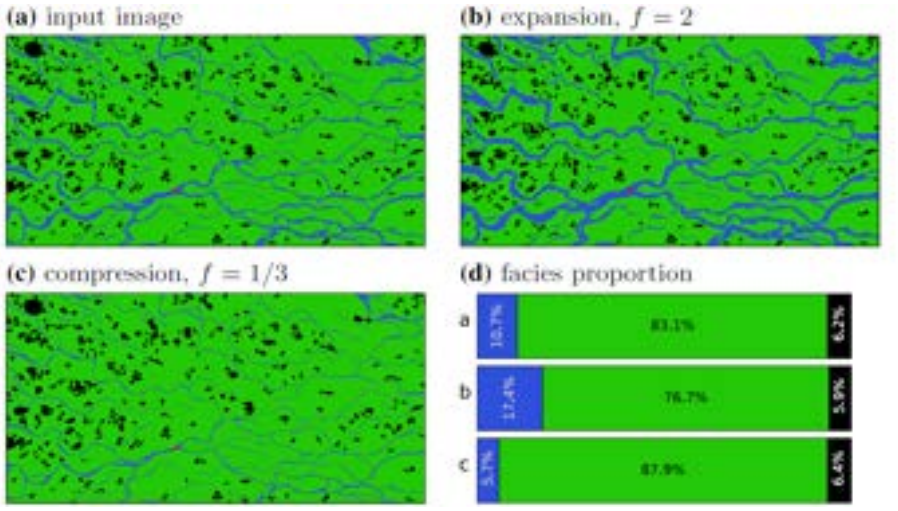

Figure 2.38: *(a) Example of pixel deformation on a initial image of channelized system (b) to which expansion (c) or compression is applied using a specified f value. (d) displays the relative proportions of each facies for each case.*

The method uses the similarity of the model between a given pattern in a certain place of the model and the other locations. The details on how to compute this map are given in Straubhaar et al. (2019).

During the painting operation, pixel values in regions similar to the selected area are directly replaced. A new facies is assigned to the model using the self-similarity map, cut at a user-given threshold to determine the location of the new facies code. The proportions of the properties can then be inflated or eroded, while keeping geological shapes consistent through the transformation.

The warping operation is a little bit more complex and involves a space transformation into zones similar to the chosen area. This involves a deformed grid from which values are moved and subsequently interpolated back onto the original grid. Straubhaar et al. (2019) provides a detailed explanation of how the new grid is constructed, relying on the dissimilarity map. The degree of deformation is controlled by a user input parameter f. In the example shown in Figure 2.38 channel system are expanded (Fig. 2.38b) or compressed (Fig. 2.38c) depending on the f value used. Note how the shape of the channels is preserved through the compression and expansion processes.

More seen as a tool to design and update existing TD for MPS, this approach has other interesting applications that can be considered. It can help with conditioning by locally adapting the models to respect some data or also to adapt the facies proportions. Moreover, it is easy to use and simple to parameterize. From this perspective, interesting applications of this approach are sure to emerge in the years to come.

2.7.3 Summary

Deformation-based methods are a compelling alternative to other techniques. They leverage the generative capabilities of other methods and modify their output models based on specific criteria such as facies probabilities or connectivity. The presented approach, whether CBM or pixel deformation, is flexible and versatile, making it possible to adjust existing models to meet specific needs. Updating a model can correct certain drawbacks in the methods, such as conditioning to soft or hard data or reproducing certain connectivity values. Their scope of application is broad but has not been extensively investigated. Consequently, they will likely receive particular attention in the coming years.

2.8 Machine learning-based

2.8.1 Basic Machine Learning concepts

Machine learning (ML) is, without a doubt, one of the recent techniques that have received most of the attention from the scientific community to easily tackle long-standing problems in various domains. ML algorithms can be broadly categorized into two groups: the "standard" ones, such as Random Forest (RF, Breiman 2001) or Support Vector Machine (SVM, Cortes et al. 1995), which have been in use for decades, and Deep Learning (DL, Ivakhnenko 1971) algorithms, which leverage Artificial Neural Networks with hidden layers to address intricate, nonlinear tasks that traditional ML algorithms struggle with.

The fundamental workflow of most ML algorithms involves considering features as input for each data point. These characteristics can vary widely, including geographical coordinates, clay content, or geophysical measurements for geological applications. The output consists of labels, which in the case of the present study are the facies to be predicted. The idea is to train algorithms using a dataset containing both features and corresponding labels, and then employ the trained algorithms to predict labels based solely on the input features, a process known as supervised learning. It is worth mentioning that it is also possible to use unsupervised learning where labels are unknown to the algorithm.

When it comes to facies modeling, studies mainly focus on DL methods, particularly generative approaches, which have seen significant advancements in recent

years. Generative methods differ somewhat from other algorithms, aiming to directly produce subsurface images resembling a set of training images (TI). This approach bears resemblance to MPS, which, however, does not necessarily require a training phase (i.e. DS, see section 2.5). In addition, MPS methods typically require one or a few TIs, whereas ML-based methods typically require a large number of training data. Among generative methods, Generative Adversarial Networks (GAN) have been the most widely used (Goodfellow et al. 2014) for facies modeling so far.

2.8.2 Artificial neural networks

Some studies have explored direct lithology prediction using nongenerative methods, notable examples include Sahoo et al. (2017), who employed ANN in conjunction with Self-Organizing Maps (SOM) to forecast the spatial distribution of lithofacies. They achieved remarkably high prediction accuracy, reaching up to 90%. Similarly, Hammond et al. (2023) used a comparable approach on a large scale to predict lithologies in a glacial aquifer from more than 13,000 wells. Although these methods show promise in certain scenarios, they lack control over the generated facies shapes, as predictions are made cell by cell. Generative methods prove to be more adept at this task.

2.8.3 Generative methods

As GANs have been widely applied in different areas such as downscaling or the generation of images of human faces, it was logical that they gained great popularity in the field of geosciences to generate intricate and detailed images of the subsurface (Song et al. 2021; Zhan et al. 2023). It is important to note that the intention here is not to provide an exhaustive list of all research utilizing GANs, but rather to highlight notable examples of facies modeling using these techniques and discuss future prospects. While it is impractical and beyond the scope to enumerate all potential applications and methodologies of GANs, readers interested in a comprehensive overview can refer to the review by Zhan et al. (2023), which delves into the various applications of DL for identifying sedimentary structures.

GANs, originally proposed by Goodfellow et al. (2014), involve not one, but two ANNs that are in competition with each other: the generator (G) and the discriminator (D) (Fig. 2.39). The generator takes a latent vector of random values as input and produces an image. Subsequently, either this generated image or an image from a collection of real facies models is fed into the discriminator, which then outputs two scores, one for real and one for fake images. The loss function is computed based on whether the image is real or fake, and is used to update both the generator and the discriminator through backpropagation. Two distinct loss functions are employed: min and max loss. The discriminator strives to maximize the loss function, whereas the generator attempts to

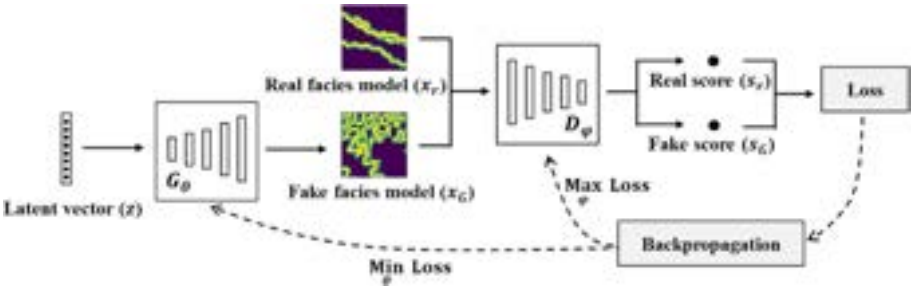

Figure 2.39: *Standard workflow of a GAN where the Generator (G_θ) generate images and the Discriminator (D_ϕ) outputs two scores (one real and one fake) to decide if the image generated by G_θ is a real facies model or not. A Loss is computed according to the scores and used to update both G_θ and D_ϕ. Image taken from Song et al. (2021).*

minimize it. The reason is that these two artificial neural networks are in competition with one another, with the generator seeking to generate images that are the closest of the training datasets and to trick the discriminator, while the discriminator attempts to determine whether an image is a real one or a fake generated.

Initially, at the beginning of training, the generated images are entirely random and easy to distinguish. However, as training progresses, the generated images increasingly resemble those of the training data set. Once trained, G can be used to generate stochastic images nearly instantly by simply changing the input latent vector.

One of the first applications of GANs to facies modeling is attributed to Chan et al. (2017), which divided a large TI river into small images that serves to train a GAN. The final generated images showed a great similarity to the training data set and demonstrated the capability of GAN for facies modeling. Dupont et al. (2018) also proposed a GAN to model 2D conditional images of a fluvial facies. The conditioning is done through constraints applied to the Loss function, which penalizes images that do not respect observed conditioning data. Their GAN was trained on a set of 5000 images generated using FLUVSIM (Deutsch et al. 1996). They also compared their results with the MPS algorithm SNESIM (Fig. 2.40) and they have showed that GAN generated channels are better connected and look more realistic than those generated by SNESIM.

One notable advantage of GANs and other generative methods is their adaptability to inverse problems through adjustments to the latent vector values (e.g., Laloy et al. 2018; Mosser et al. 2019; Jo et al. 2022). For example, Laloy et al. (2018) capitalized on this capability by introducing Spatial GAN (SGAN), which they combined with a MCMC algorithm to solve inversion problems in both 2D and 3D settings. Following the training of SGAN, the MCMC

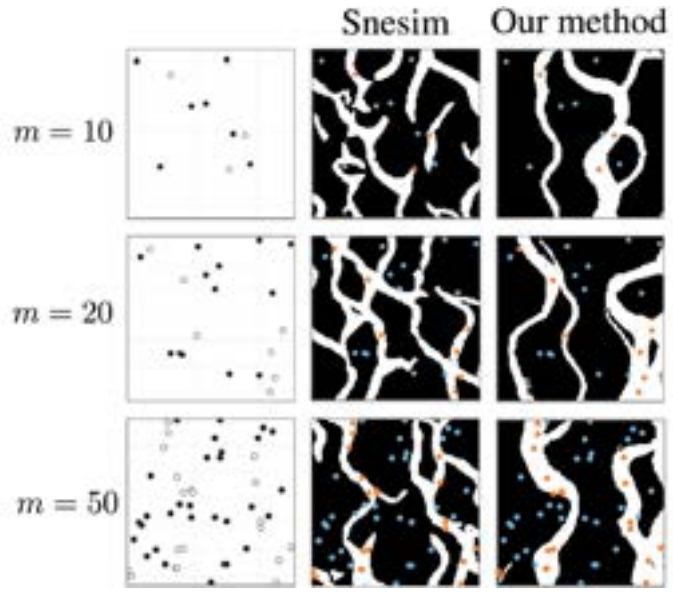

Figure 2.40: *Comparison between the GAN of Dupont et al. (2018) and SNESIM MPS algorithm (Strebelle 2002). Image taken from Dupont et al. (2018).*

procedure enables the sampling of the low-dimensionality latent vector until the generated images closely match the measurements, such as time series of hydraulic heads. However, it is important to note that their method can be highly time-consuming. For example, they reported that it took approximately 12 hours to train the 3D GAN and that an additional day was required for the MCMC algorithm to reach convergence. Recently, Song et al. (2023) combined a GAN with a surrogate Convolutional Neural Network (CNN) flow model to efficiently integrate both geological (facies proportions, channel orientation) and hydrogeological data (water pressure) to generate the facies models. The incorporation of the surrogate, which was trained by integrating physical information, a the groundwater model, helped alleviate the computational burden of the flow simulation and expedited the sampling of latent vector values. This advancement represents a significant step toward more efficient and accurate facies modeling techniques.

GAN architectures for facies modeling have evolved since the first applications to better integrate different kinds of data (soft and hard) directly in the training process such as GANSim (Song et al. 2021), stochastic Pix2Pix (Pan et al. 2021) or spatially adaptive denormalization (Park et al. 2019; Abdellatif et al. 2022) architectures. With these methods, soft information such as local proportions, orientation of channels, width of levees can be considered more easily than with classical architectures.

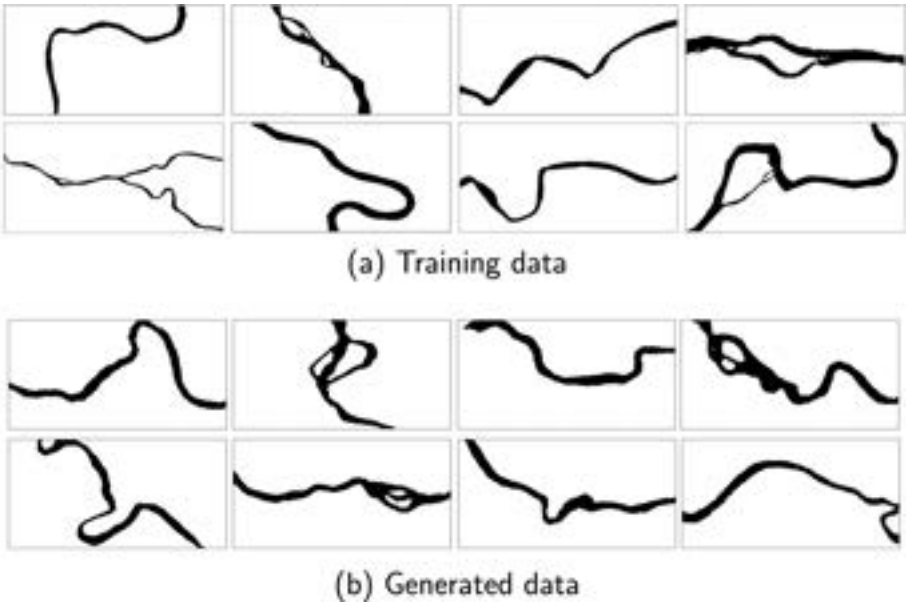

Figure 2.41: *Example of GAN simulations using a multi-scale discriminator with different river style and orientations (b) and the training data for comparison.*

Another important evolution on the GAN architecture concerns the multi-scale discriminator that operates at multiple scales to evaluate the realism of the generated images. It assesses the authenticity of images not only at the final resolution, but also at lower resolutions. The advantage of this is the generation of high-resolution images with better quality and finer details compared to traditional GANs. For example, Hu et al. (2023) employed a multiscale discriminator to simulate highly detailed river segments based on the Yellow River in China (Fig. 2.41). Their model can output rivers in four main directions and choose the river regime (meander vs. braided).

Most of the previously cited researches only consider simple fluvial OBM models, which are quite limited when it comes to producing more detailed and complex geological settings. However, Jo et al. (2020) and Pan et al. (2021) have explored the use of GANs to replicate RBM realizations for lobe models and alluvial models (ALLUVSIM), respectively. The aim was to improve the conditioning of these methods, which has been challenging as previously discussed (see section 2.6.5). Both succeeded in reproducing most of the capabilities and features of the RBM models, such as controlling geometrical parameters (channel and levee widths). However, it is worth noting that the alluvial model presented by Pan et al. (2021) did not consider 3D cases. The GAN lobe model introduced by Jo et al. (2020) offers an intriguing conditioning approach. They achieve conditioning by removing part of an unconditional simulation around the data points. The removed parts are then filled using

semantic image inpainting, a process that involved the generator where the latent vector is optimized with a gradient descent method. The objective is to maintain continuity with the rest of the model while respecting the borehole data, thereby enhancing the realism and coherence of the generated geological representations.

Some researchers have pushed the limits further by trying to reproduce process-based simulations generated with FLUMY software (FLUMY™ 2022). For example, Sun et al. (2023b) introduced the fluvial GAN, which accurately replicates 2D horizontal slices of FLUMY models (Fig. 2.42B), despite the complex shapes and the large number of facies (seven). The Fluvial GAN can consider the avulsion factor to generate a wider variety of alluvial settings. They extended their approach to generate 3D realizations using a sequential method where 2D layers are vertically simulated and conditioned on the previously simulated layers (Sun et al. 2023a). In their approach, the degree of vertical correlation between each subsequent layer is controlled by an avulsion factor. However, direct and soft conditioning was not considered in their method. On the contrary, Bhavsar et al. (2023) proposed 2D and 3D conditional FLUMY models with GAN, which incorporate direct conditioning. However, the resolution of their models is notably limited due to the issues to train 3D generators.

Despite these recent and promising researches, GANs, as for other methods, suffer from several limitations.

One particular issue is the site-specific nature of GANs, which means that models trained on one dataset may not generalize well to other sites or to other resolutions and modeling extents of the same site, necessitating retraining. Furthermore, the effectiveness of GANs often depends heavily on the availability of a large training data set. Most of the studies cited typically use more than 10,000 images. However, creating a high-quality data set and labeling each image is time-consuming and is an inherent part of every ML approach. Some approaches, such as the one proposed by Zhang et al. (2023), which relies on only one training image using a multiscale generator and discriminators, could be areas of future research.

Although the conceptual framework of the GAN training process is straightforward, its practical application is not without challenges. GANs often prove to be difficult to train, leading to the exploration of various approaches to address this issue, such as progressive training (Song et al. 2021), where layers are trained sequentially from shallow to deeper layers.

Moreover, while conditioning (both soft and hard) is feasible, as demonstrated by different studies, it is not straightforward and nearly always involves adapting the structure of the GAN or training the GAN by altering the loss function. This further complicates the training phase, which is already known to be inherently difficult.

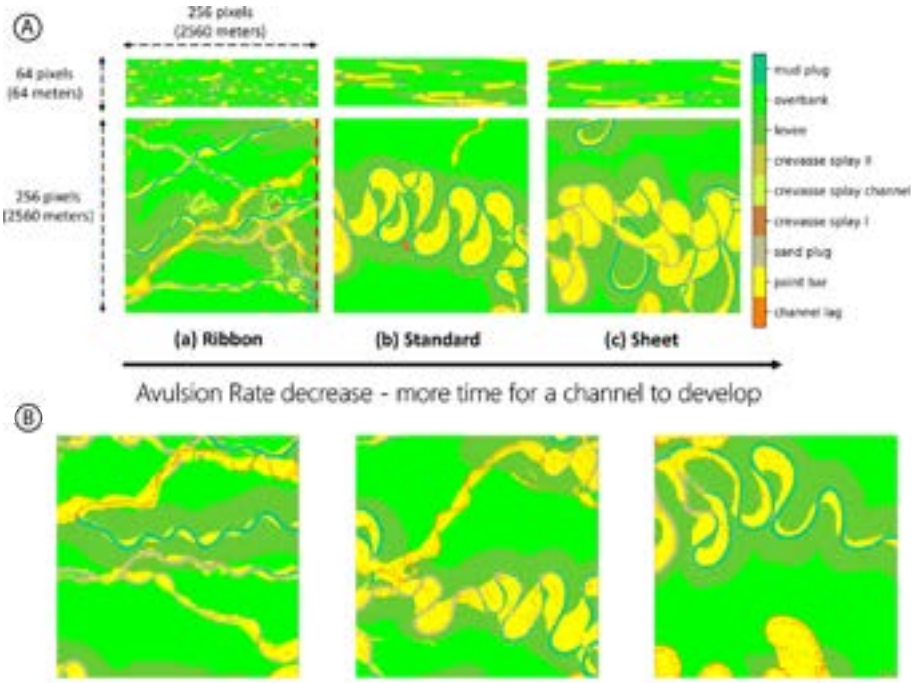

Figure 2.42: ***A****: Examples of flumy models with horizontal and vertical slices. Each model has been generated with a different avulsion factor.* ***B****: Corresponding Fluvial GAN simulations with the similar avulsion factor. Image modified from Sun et al. (2023b).*

Finally, 3D models are important in facies modeling as it is required to correctly simulate 3D flow and transport. However, 3D GANs are known to be extremely computationally and memory-intensive. Indeed, 3D images contain more complex spatial correlations of different facies compared to 2D images, necessitating GANs with more parameters and a higher number of training images. However, memory issues arise as it is not feasible to use more than 10,000 large 3D images, especially if one-hot encoding for categorical variables is employed, which further multiplies memory usage. As for the MPS approach, getting 3D training data is also an issue. It is even worse than for MPS because a large number of images are required. An option to circumvent this problem has been proposed by Coiffier et al. (2020). Only 2D images are used to train the GAN. The generator is constructed to generate 3D images, but the discriminator is working on 2D sections extracted randomly within the 3D simulations (possibly in different directions) and compared to 2D training data using a 2D discriminator.

2.8.4 Summary

The significant advantage of GANs and other generative methods lies in their ability to rapidly generate highly complex images once they are trained. This feature facilitates the use of inverse methods to optimize generated images to align with observed data, including hydraulic heads, geophysical data, and more. GANs can generate really complex and highly detailed features, as demonstrated by the work of Sun et al. (2023b) or Hu et al. (2023), rendering that are nearly impossible to obtain with other methods other than physically-based methods. Despite these advantages, some notable issues persist that currently restrict the widespread applicability of GANs and other generative methods in facies modeling. However, ongoing research and advancements may help overcome these barriers and improve the utility of generative methods in geosciences. For example, ML diffusion models (Sohl-Dickstein et al. 2015) have recently gained popularity because they require fewer parameters and are easier to train than GANs. To date, the use of diffusion models for facies modeling has been poorly explored (Lee et al. 2023) and is still in its infancy. Further research is needed to investigate the advantages and how it compares to GANs.

2.9 Process-based

The last category of facies modeling methods discussed in this overview is the process-based methods (PBM). These methods are known to produce the most realistic and faithful models compared to what can be observed in sedimentological records, although they are also the most challenging to parameterize and constrain to observed data. The defining characteristic of PBM is their reliance on physical processes and related equations, whether simplified or not. For this reason, they are sometimes also referred to as "physically-based methods". "Stratigraphic Forward Model" is also a popular name, particularly in basin and reservoir modeling. This mathematical nature necessitates numerical solution techniques, such as finite-difference, finite-element, or finite-volume methods, along with the definition of initial (IC) and boundary (BC) conditions. In some cases, assumptions are made to derive analytical equations that alleviate this constraint. In all cases, this highly contrasts with other previously seen methods.

Another notable distinction of PBM compared to other methods is that they typically do not output lithological classes, but instead provide proportions of each lithology. Additionally, PBM models contain much more information than standard methods as they store several additional variables. For example, PBM can track the spatial origin of lithologies, paleobathymetries through simulation time, mean sediment age, etc. However, unlike other methods, PBM models do not directly output the geometrical and hydrodynamical shapes commonly used in OBM (such as channels, lobes, etc.). Instead, these shapes and features

emerge naturally from the combination of mathematical expressions, related parameters, and IC and BC conditions.

Several classes of PBM have been developed, each designed to address specific geological contexts and sedimentological processes. Again, it is important to note that this overview aims to provide a snapshot of existing PBM methodologies rather than an exhaustive coverage of all possible approaches. The focus will be on the most widely used and prevalent software and methodologies. In sedimentary modeling, the main PBM include diffusion-based models, hydrodynamic-based models, and channel migration models.

2.9.1 Diffusion-based

Diffusion-based models aim to replicate sediment transport by employing diffusion processes, typically proportional to local slope, water flow, and sediment concentration. A notable diffusion-based model is the Diffusive-Oriented Normal and Inverse Simulation Of Sedimentation (Dionisos) (Granjeon 1996, 2014). Dionisos incorporates two primary processes to model sediment transport: a slow slope-driven and a fast water-driven and slope-driven diffusion transport. In Dionisos, the flow direction is determined based on the slope using a multiple-direction method (Granjeon 2014). The equations controlling these processes are the following (Granjeon 2014):

$$Q_{sc,k} = K_{c,k} c_k S^{m_c} \tag{2.13}$$

$$Q_{w,k} = K_{w,k} c_k Q_w^n S^{m_w} \tag{2.14}$$

where $Q_{sc,k}$ is the slow slope driven flux of sediment k and $Q_{w,k}$ is the fast water and slope-driven flux. Each equation requires its own diffusion coefficient K_k which also depends on the sediment class k. c_k is the surface concentration of the sediment k, S is the local slope and m_c, m_w and n are coefficients between 1 and 2. Finally, Q_w is the local water discharge.

These equations govern the movement of sediments across the model, from sources to sinks. However, it is important to note that these equations represent the local maximum sediment discharge, which may be lower if the local sediment availability does not exceed it. This depends on weathering and incision rates.

Dionisos is a versatile model capable of handling a wide range of sedimentological processes, such as clastic sediments, carbonate sediments, evaporite precipitation, or basement erosion. However, each sediment class in Dionisos requires the definition of diffusion coefficients for both the slow slope-driven and fast water-driven and slope-driven processes. Additionally, BC (e.g., sediment

concentration influx, water influx, eustatic curves), IC, and geometries (paleobathymetries) need to be defined, often at different time steps. This leads to highly parameterized models. Nevertheless, Dionisos offers a simplification of processes by not explicitly solving complex hydrodynamic equations. This simplification enables the model to run relatively quickly, and simulations typically take several minutes to complete (Falivene et al. 2014).

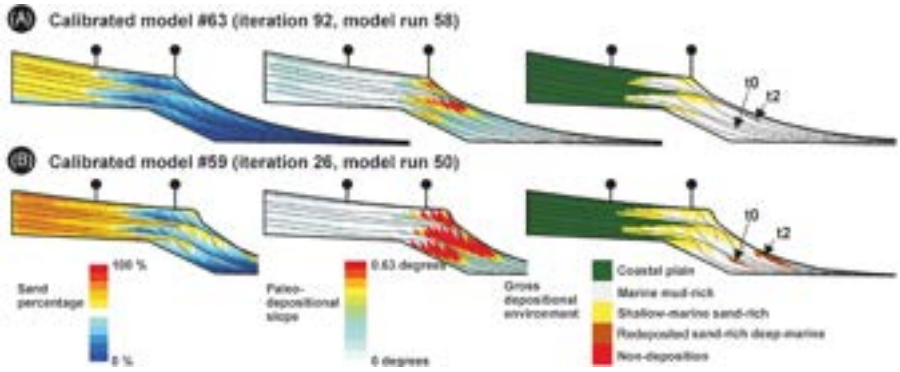

Figure 2.43: *Two calibrated Dionisos models on layer thickness and sand proportions at well locations (indicated by the black dot). The two models have very different input parameter where model 63 has a low input sand percentage and concentration, compared to model 59. Image taken from Falivene et al. (2014).*

However, the direct calibration of such models is not feasible due to the large complexity and the high number of parameters of such problems but there have been several attempts to partially condition Dionisos to soft data (sediment layer thickness or local sand probability). For example, Falivene et al. (2014) utilized a genetic algorithm to sample the posterior probability of a restricted number of parameters (Fig. 2.43). Similarly, Patani et al. (2021) opted for a different approach by employing a surrogate model, specifically a polynomial chaos expansion which maps the Dionisos as entries and outputs some values of interest to match (e.g., sand proportion at well position). This surrogate model helped accelerate the parameter sampling process, making it more computationally efficient while still allowing for the incorporation of soft data into the modeling process.

These conditioning methods are interesting as they employ stochastic approaches. They seek to estimate and optimize the appropriate combinations of input parameters to generate multiple realizations necessary for uncertainty quantification.

Dionisos is generally used to model a large-scale model (basin scale) over a long period of time (millions of years). The reason is that Dionisos proposes averages of sediment transport and that the required BCs are difficult to determine from sedimentological records. Dionisos also do not consider rivers directly, which are simply modeled by adding water and sediment flux BC somewhere

in the simulation domain. For more detailed and smaller-scale models, morpho-hydrodynamic models are generally preferred.

2.9.2 Hydrodynamic-based

Water plays a pivotal role in the transport, deposition, and diagenesis of sediments, making it imperative to understand how and where water flows to accurately replicate complex sedimentological settings. Hydrodynamic models serve as an appropriate solution for this task. Hydrodynamic models represent a more intricate class of models due to their coupling of hydrodynamic equations, the Navier-Stokes equations, with sediment transport equations. These models deal with highly complex processes, as the Navier-Stokes equations are nonlinear partial differential equations known to be, in most cases, impossible to solve in their full form and for 3D cases. Furthermore, sediment transport modifies the properties of the fluid, which in turn affects the flow dynamics. Additionally, sedimentary environments often involve mixed waters with varying salinities, temperatures, and sediment loads, further complicating the determination of fluid density and its impact on flow behavior.

The most widely known and used softwares of this class are the Sedsim program (Tetzlaff et al. 1989) and Delft3D (Lesser et al. 2004). Both models use approximations of the Navier-Stokes equations. For instance, Sedsim simplifies the flow by utilizing isolated fluid elements to represent continuous flow, an approximation that has the drawback of not being able to model rapid changes in fluid flows. Vertical flow is also assumed to be uniform (Tetzlaff et al. 1989). Alternatively, Delft3D relies on the Boussinesq and shallow water approximations which neglect the vertical acceleration in the vertical component of the conservation of the momentum equation. Once the flow is solved, the sediments are transported according to the principle of mass conservation. Both softwares incorporate modules to reproduce different sedimentological environments (e.g., suspended and bedload sediment transport, aeolian transport (for Sedsim), wave effects (for Delft3D)).

As these methods rely on general principles (hydrodynamic, morphodynamic evolution, and sediment transport), they are quite general and can be applied to a large variety of problems. For example, Li et al. (2023b) have used Delft3D to simulate the creation and evolution of the morphology of braided rivers under constant discharge. Also with braided rivers, Nicholas et al. (2013) have used a hydromorphodynamic model (HSTAR) to investigate the effect of vegetation and several other key parameters (water discharge, slope, sediment discharge) on the morphologies of the system (Fig. 2.44).

The features that can be obtained from PBM are unique and very similar to real structures. For this reason, PBM simulation provides very interesting references that can be used as TI with image reproducing algorithms such as

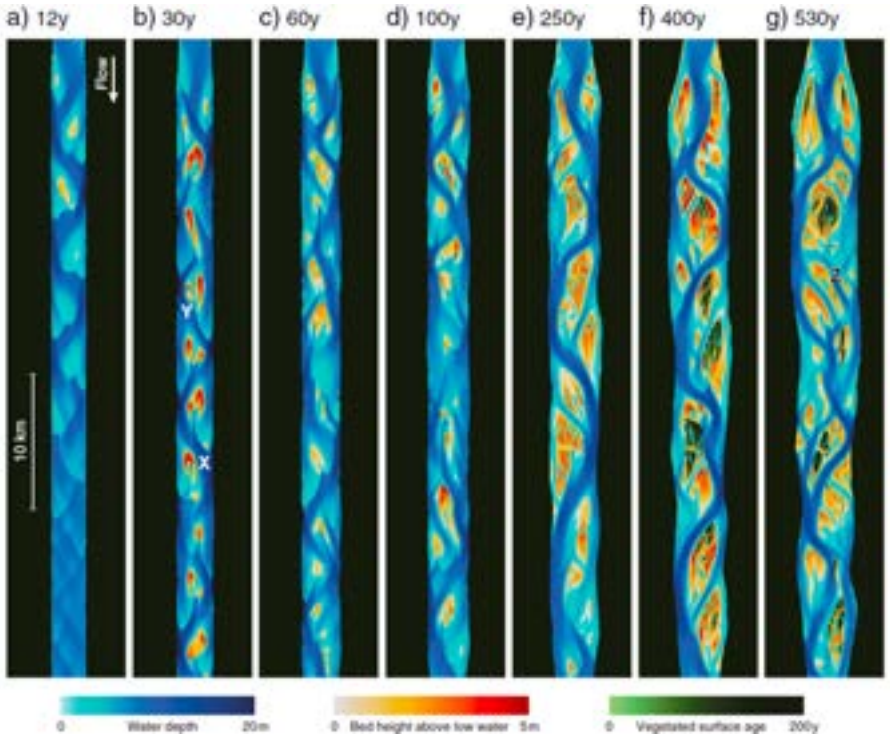

Figure 2.44: *Morphological evolution of a braided river system using the HSTAR model at seven different times. Image taken from Nicholas et al. (2013).*

MPS or GAN. For instance, Aarnes et al. (2019) have used Delft3D to generate 10 different morphological deltas that have been used as TI with the SNESIM algorithm. They were able to reproduce the structures of the simulated channel network and the complex deposits and also showed the benefit of using multiple TIs instead of just one to produce more variability.

However, they are still computationally heavy and for this reason, methodologies have been developed to speed up the simulations (Li et al. 2018). One common approach is to partially decouple the models and speed up the morphological changing by a certain factor (morphological factor). This approach assumes that, for a certain period of deposition/erosion, the hydrodynamic is not changing, which consequently reduces the computational cost by the order of 10 to 1000 (Li et al. 2018). Another approach involves assuming that most sediment transport occurs during specific events, such as large flood events, while smaller daily transports are ignored. Additionally, time compression techniques can be employed, where numerical models emulate the spatial and temporal compression observed in analog models. This compression allows faster simulations by condensing the temporal and spatial scales of sedimentological processes.

Regarding the calibration and conditioning of such models, the examples are very scarce. But some authors have proposed the use of adjoint methods (Clare et al. 2022) that have the advantage of practically not being dependent on the number of parameters, allowing the integration of a large number of parameters, as well as performing more detailed sensitivity analysis. The concept behind adjoint sensitivity analysis involves solving two sets of equations simultaneously: the forward model equations (representing hydrodynamic and sediment transport processes) and the adjoint equations, which describe how a defined cost function changes concerning variations in the system's state variables. In the study by Clare et al. (2022), they successfully calibrated a synthetic river model using adjoint methods. Additionally, they conducted a spatial sensitivity analysis of several parameters, including grain size, bed reference height, and sediment density.

Finally, the interesting use of PBM for glacial environments where subglacial flow and sediment transport models are combined to estimate till formation should be mentioned (Delaney et al. 2019, 2023). The sediments are eroded, based on an equation that depends on the sliding velocity of the glacier, and routed across the glacier bed according to the subglacial flow model. Figure 2.45 shows the thickness evolution of a till using this model in 2D.

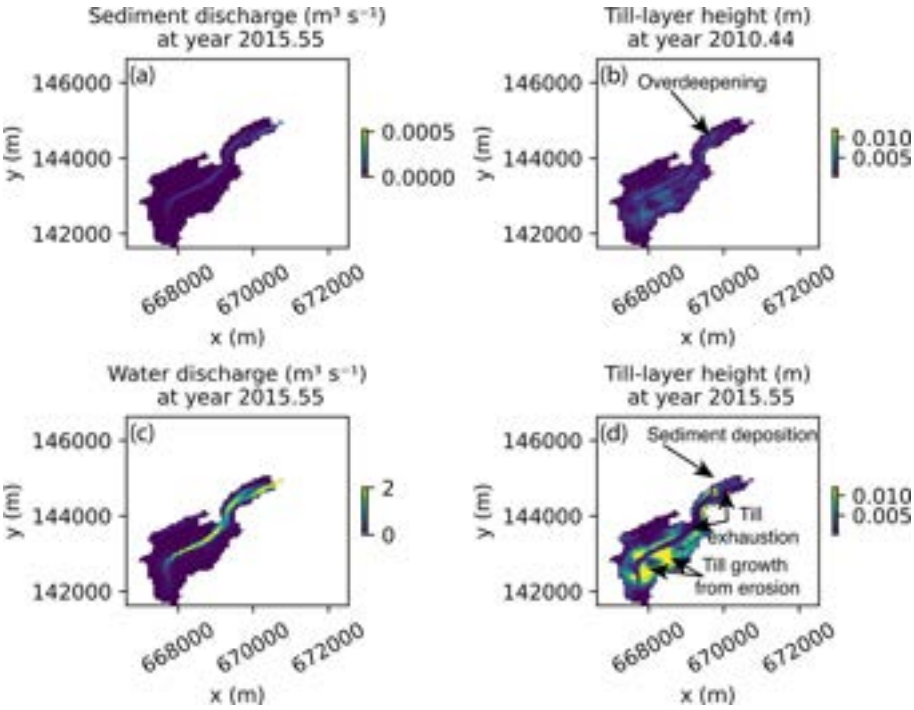

Figure 2.45: *Numerical experiment of the model of Delaney et al. (2023) where the till thickness is shown at two different times as well as the sediment discharge and water discharge. Image taken from Delaney et al. (2023).*

2.9.3 Reduced complexity models

Another approach to address computational challenges is through Reduced Complexity Models (RCM), which aim to achieve outputs comparable to complex PBM but with significantly simplified physical expressions and/or rules. RCM can be seen as a hybrid method that bridges the gap between PBM and RBM. RCM often utilizes cellular automaton techniques to simulate water and sediment transport, as demonstrated by Delta-RCM (Liang et al. 2015). The Delta-RCM approach involves releasing particles (or parcels) of water and sediment at specified input points. These particles are then dispersed throughout the simulation domain via a weighted random walk process that is influenced by the evolving bed topography and hydrology of the system over time (Fig. 2.46). Delta-RCM has also been used to test the effect of sea level rise and input sand fraction on connectivity in a synthetic case (Xu et al. 2021). Quite surprisingly, they have found that the muddier deltas have higher normalized connectivity because the channels stack better.

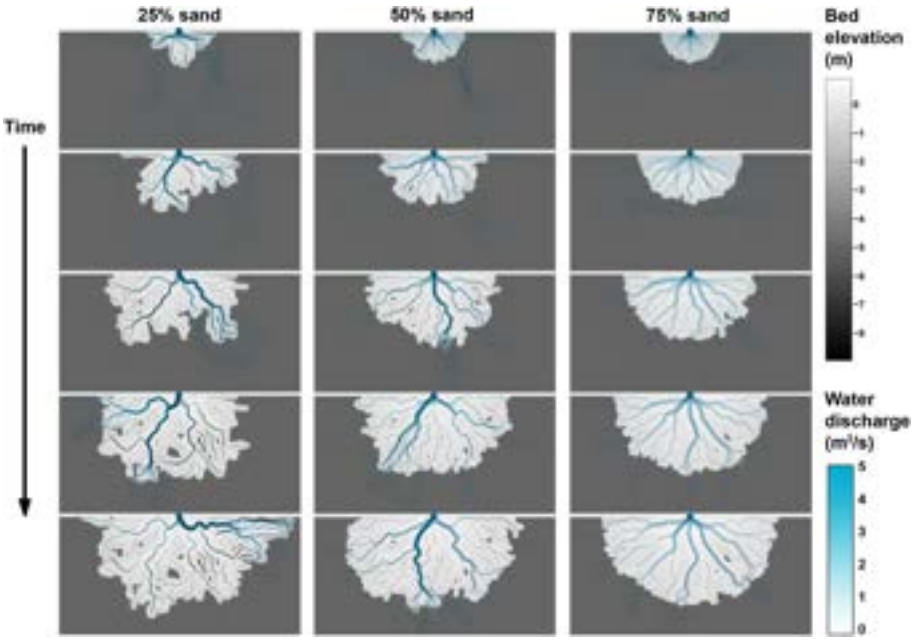

Figure 2.46: *Time snapshots of the evolution of three different scenarios (sand content) using the Delta-RCM model. Image taken from Liang et al. (2015).*

2.9.4 Channel migration-based

Meandering channel-dominated environments represent a distinct sedimentological setting where the spatial distribution of lithologies in the subsurface is largely influenced by the evolution of the channel. Consequently, the availability of information on channel meandering facilitates the determination of

subsurface heterogeneity. In pursuit of this goal, several authors have proposed models that are typically based on certain approximations. For instance, some models assume a river of constant width and posit that channel erosion is directly proportional to the velocity of the flow near the bank (Howard 1996) or the curvature upstream (Howard et al. 1984). In a notable contribution, Sun et al. (1996) derived an equation that establishes a relationship between the hydraulic constant and the curvature of the upstream channel to the flow velocity near the bank.

In particular, this equation has been used to build the more complete FLUMY fluvial model (Lopez 2003; Lopez et al. 2009; FLUMY™ 2022). FLUMY combine physical equations (meandering evolution) and stochastic approach to reproduce the deposits of a typical meandering environment. In FLUMY, the channel deposits primarily coarse sediment along its centerline, while periodic or irregular flood events result in deposits in the levee and overbank. Additionally, FLUMY can simulate chute cutoffs, avulsions, and levee breaching events. By blending physically-based channel migration models with stochastic methodologies, FLUMY can generate all the key elements of fluvial deposits with remarkable fidelity compared to field observations (Fig. 2.42A). Moreover, FLUMY and similar channel meandering models are efficient, as they do not heavily rely on complex physical equations and can rapidly generate large-scale models.

FLUMY does not allow for conditioning to hard data, but is able to reproduce facies proportional trends by playing with the erodibility coefficient which controls the facility (or difficulty) for the channel to erode a particular area (Lopez 2003; Lopez et al. 2009). Erodibility maps are used to constrain the path of the channel in areas where the wells have sand and to avoid boreholes with overbank deposits. An alternative is also to use GAN or MPS, as has already been discussed in the previous section.

FLUMY is not the only existing model of meander channels, and several alternatives have been proposed over the years, such as the integrated landscape development model of the channel-hill slope (CHILD, Tucker et al. 2001) or the python package meanderpy (Fig. 2.47, Sylvester et al. 2019) which is based on the equations of Howard et al. (1984).

The decision to use a particular PBM method is highly context-dependent. If the deposition environment to model is relatively shallow, then hydrodynamic models such as Delft3D may be used. Delft3D has notably demonstrated its use in coastal and deltaic environments. If, on the other hand, large sedimentary basins are involved, then diffusion models (Dionisos) or hydrodynamic models such as Sedsim are more appropriate. In the case of meandering rivers, channel migration algorithms are ideal.

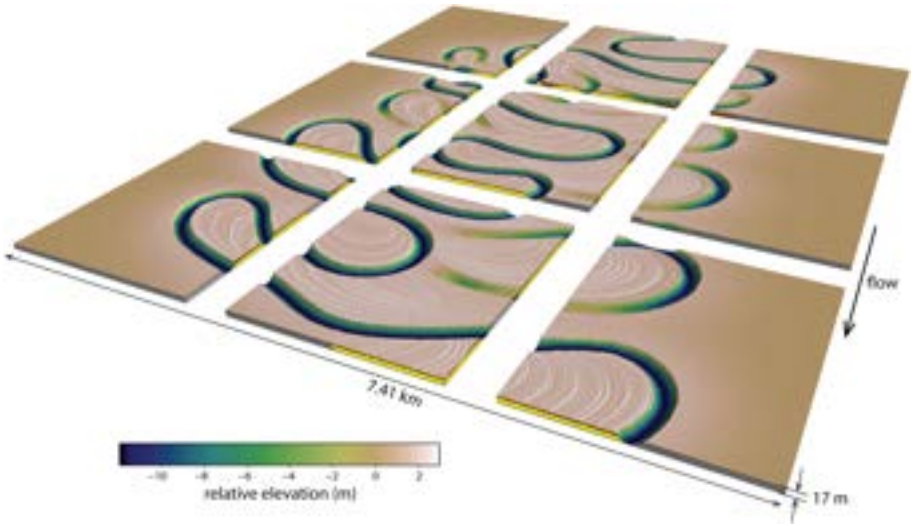

Figure 2.47: *3D diagram of a model made with meanderpy. Image taken from Sylvester et al. (2024).*

2.9.5 Summary

In conclusion, although the physics of sediment transport is universal and can be applied to many different contexts and problems, a large number of parameters need to be defined, as do the boundary conditions, which are generally poorly understood. This makes the use of such methods difficult in concrete, applied cases, all the more so when the modeler is not familiar with the complex physics being modeled. Moreover, the extensive time required for simulations makes calibration difficult, and ensuring effective conditioning becomes even more challenging with an increasing number of conditioning data points. This can be seen as a paradox where PBM (and OBM and RBM) require a certain amount of data to effectively constrain the models and replicate geological structures accurately. However, if too much data is introduced, the task of constraining the models becomes infeasible, prompting the need to resort to simpler and easier-to-condition methods. As a result, the decision to use a PBM for modeling a reservoir depends greatly on the context but, above all, on the availability of the data.

However, PBM are still interesting. They can complement existing training data sets and offer insight into the underlying processes that govern sedimentological structures. As many studies have noted (Miller et al. 2008; Michael et al. 2010; Aarnes et al. 2019), process-based models contain valuable information that can support facies modeling. The notion that "the present is the key to the past," a fundamental principle in sedimentological studies, assumes that past systems are analogs to modern systems. However, the validity of this hypothesis is subject to debate, as geological processes can change over time.

Nevertheless, physical processes and laws remain constant, and PBM can accurately reproduce various processes, providing that past conditions are known, enabling the simulation of a wider range of scenarios than those observable today. Therefore, PBM plays a crucial role in bridging knowledge gaps, statistics, and discrepancies between past records and current observations, thus contributing to a deeper understanding of geological processes and their evolution over time. Furthermore, the possibility of using recently proposed ML techniques, such as physical information neural networks (PINN, Raissi et al. 2017), to overcome some of these limitations may be promising and remains to be investigated.

2.10 Synthesis and classification of the methods

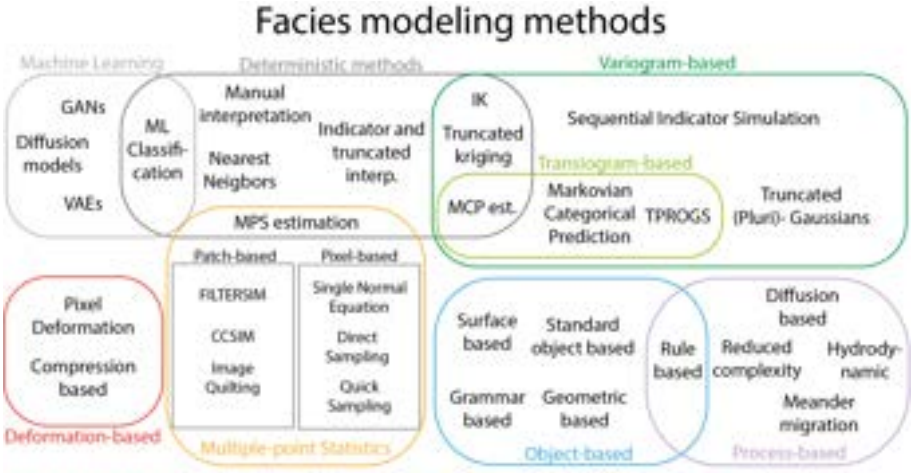

Figure 2.48: *Proposed classification of the existing facies modeling groups and their interrelationships.*

Now that all the methods have been presented, it is time to summarize them and propose some classifications. Figure 2.48 summarizes the different categories of methods and how they are related to each other. Deterministic methods have a special place, as the vast majority of facies methods are stochastic, but can be adapted or used for deterministic models. As such, they are central to almost all methods. Globally, the methods are separated but can be easily linked together as their development and history are intricately linked. For example, the SIS algorithm is the basis of many methods such as some MPS algorithms, MCP or TPROGS. However, the most important separation in methods probably lies between OBM-PBM and other methods. OBM-PBM methods are based on a representation of heterogeneity by delimiting zones or by facies proportions, but always with a reflection on geological processes and geometries. The problem is therefore not only statistical but also geological and sedimentological. Reproductive methods (reproducing patterns of a TD)

Table 2.1: *Requirements and limits in terms of inputs for facies modeling methods. The compared inputs are the ease of integration of soft and hard data, the requirement of a grid, the scale of application, the sedimentological context to which the methods can be applied and the the requirement of an image or training data set.*

Method	Soft data	Hard data	Grid Required	Scale	Sedim. context	Image required
Deterministic Method	yes	yes	no	all	all	no
SIS	yes	yes	yes	all	all	no
IK	yes	yes	no	all	all	no
TPROGS	yes	yes	yes	all	all	no
MCP	yes	yes	no	all	all	no
TPGS	yes	yes	no	all	all	no
TK	yes	yes	no	all	ordering required	no
MPS	yes	yes	yes	all	all	yes
Standard OBM	partly	partly	no	all	objects dependent	no
SBM	no	partly	no	m to km	limited	no
RBM	partly	difficult	no	m to km	method dependent	no
Geometric based	no	no	no	cm to km	alluvial	no
GBM	partly	yes	no	m to km	grammar dependent	no
Deformation based	yes	yes	yes	all	all	yes
ML (GAN)	yes	partly	yes	all	all	yes
Diffusion-based	difficult	no	yes	km	basins, cont. shelves, etc.	no
Hydrodynamic models	yes	no	yes	cm to km	all	no
Meander Migration models	possible	difficult	no	m to km	alluvial, abyssal	no

such as MPS or GANs are at the interface of these methods, trying to bridge the gap between these two worlds. We placed RBM (Rule-Based) between the OBM and PBM categories. The distinction is based on the placement of objects. RBM and RCM (reduced complexity models) are distinguished by the fact that they mimic physics by placing objects in a certain way, while RCM may incorporate simplified physical processes or use them as a basis for rules. RCM are simplified versions of physical models that consider physical concepts, including deposition and transport rules. They do not seek to position objects in space.

Table 2.1 provides a more comprehensive analysis of each method's capabilities, it indicates the constraints and required inputs for each method. Once again, we see the contrast between OBM-PBM and the other methods, particularly concerning the sedimentological context. As these methods are partly based on sedimentological processes, they are often site-dependent in terms of the

objects or physical processes represented. We also clearly observe a gap in terms of conditioning. Statistical methods rely on data and can efficiently integrate them without difficulty, conversely to OBM and PBM.

Concerning the scale of application, many methods can be adapted to all scales. However, some methods require more effort (e.g., OBM, PBM, MPS) whereas some only require adjusting scale parameters (e.g., SIS, TPROGS, MCP). This depends on the generated structures. If the simulated structures are abstract and not geologically realistic, enlarging or shrinking them has little impact on the quality of the simulations. Object methods, on the other hand, produce models at a precise scale, and it is often not possible to change the size of the objects, as this would make no sense geologically. The same applies to PBMs, which reproduce processes at defined scales. If one wants to make a model at a different scale, a complete conceptualization work is necessary.

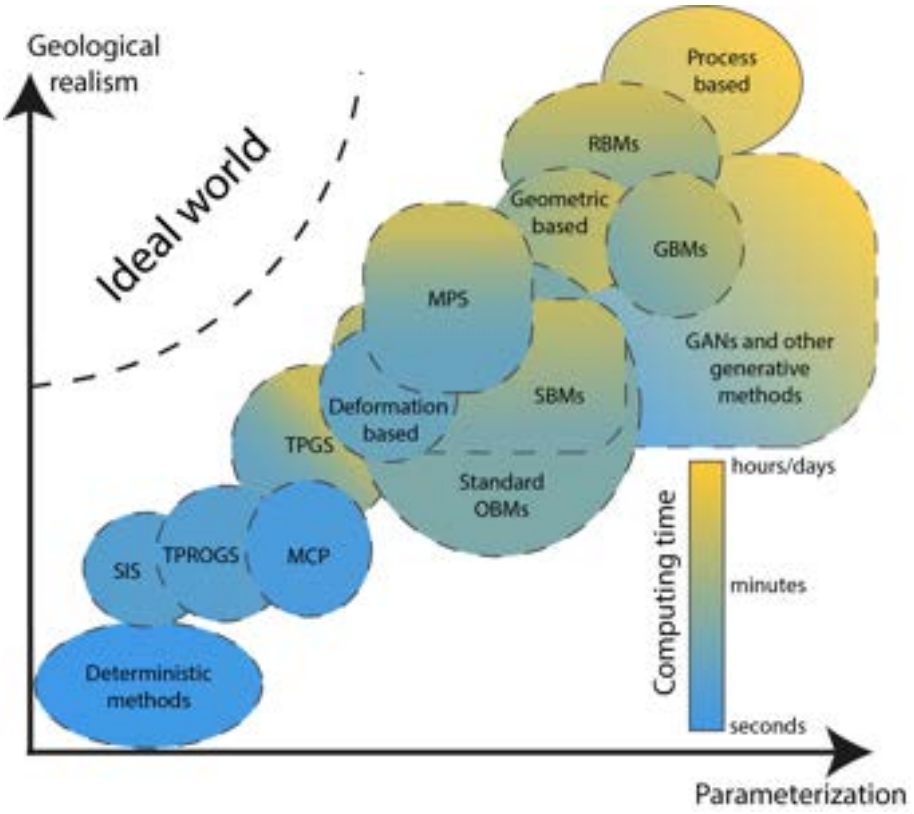

Figure 2.49: *Comparison of the facies modeling methods on three criteria: geological realism, parameterization which represents the efforts and time to put to setup a model and computing time. Computing time represents average values to obtain one realization for typical cases. Note that manual interpretation was not considered in this figure.*

In addition, these methods can be compared using other criteria, as shown in Figure 2.49. This figure illustrates how the methods compare roughly in terms of their ability to produce realistic models as a function of the time required for model parameterization. The parameterization includes several tasks, such as conceptualizing the model, analyzing data or databases to define parameters, training the model on data, and adjusting the parameters of the model. In addition, the general computing time for a standard model of each method is indicated. Note that these values are provided to give a rough idea of the relative computational requirements of each method. A few important points to note: the position of each method also represents a kind of ideal average of the models generated by that method. Also, the limits are arbitrary and can be extended in certain situations and contexts. For this reason the limits are dashed lines.

In general, geological realism increases with parametrization, as more time is spent integrating more and better geological information. No methods are located in the lower right corner, as this would indicate a high parameterization time for poorly realistic models. On the opposite corner are the ideal methods which would require very little parameterization for very realistic models. Unfortunately, such algorithms do not exist (yet) and they are in between these two extremes. Simpler methods such as SIS or TPROGS are located in the lower left corner, while more advanced and realistic methods such as PBM and RBM are located in the upper right corner. The other methods are close to the center, with quite a few differences. It may be noted that the use of objects (standard OBM, SBM, RBM, GBM, Geometric models) often improves the quality of models, but makes them more complicated to set up. Concerning the computing time, it also increases with parameterization but with some exceptions such as GANs and related generative ML techniques that can quickly produce models once the models have been trained. It is important to note that the duration of this training can vary greatly depending on the specific cases and may require several hours or even days. There is also a large difference between PBM and the others as they often need to solve complex systems of equations over large periods of time, resulting in a high computational cost that can lead to simulations exceeding the hour.

This figure emphasizes the significance of taking parametrization into account during the modeling process. It can be a time-consuming process that requires expert advice. This does not mean, however, that we should systematically fall back on the methods that require the least time and effort, as it is important to inject this element of knowledge into the models. This is the only way to improve models. On the contrary, we think it is more important to consider geological realism. It is also expected that the effort involved in parameterization will diminish over time as more and more geological modeling studies and open-source solutions become available.

2.11 The practice of facies modeling

The previous section on facies modeling and synthesis highlights the diversity of methods used, ranging from rigorous mathematical and statistical theories to intricate physical processes. While these methodologies were summarized in the preceding sections, several overarching questions and issues have emerged. The purpose of this section is to discuss these questions and suggest solutions for the future of facies modeling.

2.11.1 How to compare and select?

A natural question arises: how to compare these methods and determine the most suitable one for a given application? And is it useful to compare them? The answer to this last question is obviously yes, because we need to have confidence in the selected methods. After all, the subsurface will always be uncertain and only partially investigated. Indeed, it is imperative to emphasize that without exhaustive subsurface exploration, it remains impossible to ascertain which method will yield the most realistic predictions definitively. Uncovering the truth requires the complete extraction of the subsurface. Unfortunately, such a systematic survey based on meticulously mapped ground truth, fully delineating the internal heterogeneity in unconsolidated and sedimentary environment has never been carried out. The impracticality of such an undertaking requires excavating large volumes of underground materials, which renders it prohibitively costly and politically difficult.

In the literature, several studies have compared different methods (e.g., Falivene et al. 2007a; Dell'Arciprete et al. 2012; Deveugle et al. 2014; Serrano et al. 2014; Marini et al. 2018; Major et al. 2023), but these comparisons typically involve only three or four methods at once. Moreover, comparisons often focus on the same traditional methods (SIS, TPROGS, SNESIM, etc.). Additionally, the cases considered and tested are often limited and may favor certain methods while yielding different results in other settings. The metrics used in these comparisons are also frequently restricted to facies predictions, local proportions, and variograms, without considering flow and transport simulations.

For example, Dell'Arciprete et al. (2012) have compared three pixel-based methods (SIS, TPROGS, MPS) in terms of local proportions but also in terms of connectivity. They show the difficulty for MPS to simulate low-portion facies, but also its ability to generate the complex geometries of dominant facies, compared to SIS and TPROGS. Another interesting study is that of Deveugle et al. (2014) who have compared SIS, MPS, and a standard OBM. They found that no method particularly outperformed the others and that the results were more dependent on the conditioning data and geological concepts underlying the construction of the models. Furthermore, Major et al. (2023) compared TPGS with FLUMY models for a geothermal reservoir and surprisingly found comparable results between the two models. This suggests that in certain cases,

traditional methods may suffice. However, it is important to note that these findings are not universal and that further studies are necessary in different settings with varied parameters to draw general conclusions.

To compare and select a method efficiently, Deutsch et al. (1992) have established a list of criteria which has been further refined by Koltermann et al. (1996): (1) the capacity to generate plausible realizations within a reasonable timeframe, encompassing conceptualization, parameterization, and computation; (2) the ability to incorporate data and expert knowledge into the modeling process; (3) the capability to explore a broad range of uncertainties, not only within facies models but also within physical forward models reliant upon them (e.g., flow, transport); (4) the aptitude to address relevant scales of heterogeneity pertinent to specific flow and transport problems; and finally (5) the ability to generate parameter models that yield plausible forward simulations.

These criteria are well detailed and discussed in Koltermann et al. (1996) and underline the importance of integrating facies models with their intended purpose, that is, combining them with flow and transport models. As stated by Koltermann et al.: "A valid method for map generation is one that accurately reproduces both the spatial patterns of hydraulic properties and the observed subsurface fluid flow and transport behavior" (Koltermann et al. 1996, p. 2652). Therefore, a facies model serves not as an end in itself, but as a means to an end.

However, all of these criteria are not quantitative and can be subjective. For example, what is a "plausible" realization? What is a "reasonable" computing time? What is a broad range of uncertainties? In addition, these criteria depend on a large number of external factors (e.g., algorithms optimization), not directly related to the methods themselves. A way to circumvent this is to rely on quantitative metrics such as cross-validation. In particular, Juda et al. (2023) have proposed a complete cross-validation framework for categorical variables with this aim. However, this type of cross-validation only allows to quantify the quality of the predictions of the methods on a cell-by-cell basis. This means that other features, more difficult to assess, such as feature geometries or geological concepts (e.g., fining-upward sequences) are not tracked. In this way, certain methods that can more easily respect conditioning data (e.g., SIS, TPGS) will have an advantage over others that have less control (standard OBM, SBM, RBM, PBM). However, these methods show more realistic features that respect the geological concepts defined by the modeler.

This raises a crucial question: can a model that is not approved by an expert be considered valid? Or conversely, can a model that does not perfectly respect the data be considered valid?

2.11.2 Issues with data

The level of geological accuracy that a facies method should aim to achieve depends on the particular objectives and needs of the modeling task. Even if the model does not appear to be highly realistic, it can still be useful for its intended purpose if it accurately represents or closely approximates important metrics, such as proportions and connectivity. It is also important to remember that the purpose of facies models is often to be used in flow (and transport) models. In addition, the aim is for the observations in these models to be respected as closely as possible, rather than the underlying geology. But, the data themselves may be uncertain. For instance, soft data is often an interpretation, which can be subjective and depend on the methods and people used to assess them. Uncertainty of hard data must also be considered (e.g., wrong or erroneous descriptions, quality of the boreholes, etc.). If we add to this the effect of support (Chiles et al. 2012) inherent to geostatistical problems, we can legitimately ask whether it is necessary to blindly respect all data and how to integrate at best this source of uncertainty, often neglected.

Moreover, this raises a potential data paradox, mentioned in the section on process-based methods. Usually, the more hard data there is, the better the models are supposed to be for variogram/transiogram-based methods, but it may not be the case for other methods. For example, the more data there is, the more difficult it is to condition the realizations of process-based models. When the number of data is large, the data may become incompatible with each other within a given geological concept, the realizations can become awkward. The conditional realizations then differ significantly from unconditional simulations and no longer completely represent the concept they are intended to model. The attempts to constrain channel migration in FLUMY by adapting locally the erodability is a good example (Lopez 2003). FLUMY realizations aim to respect both hard and soft data by adapting and modifying local physical parameters, such as erodability, to direct the evolution of the river channel. However, the use of this approach is debatable as it may not fully constrain the river migration to follow the natural evolution dictated by the physical equations, since some physical parameters are adjusted on the fly. As a consequence, artifacts of simulations are likely to appear.

However, data is still necessary to constrain these models in various ways, such as choosing parameters, calibration, and boundary conditions. As a result of this paradox, it is possible that modelers prefer variogram/transiogram-based methods without considering other options. While this is not the sole reason, it likely contributes to it. Little can be done about this paradox, except to be aware of it. It should not be a barrier to the use of advanced methods, as they can still prove useful in understanding the processes involved, the geometries produced, the associations of facies, serving as TD for MPS, etc.

2.11.3 Diversity of the methods

The wide variety of facies methods is an interesting point to discuss. Although all these methods aim to categorize a given space with facies, no model, algorithm, or software produces identical results, shapes, or features. The only potential counterexamples are methods that reproduce a TD (MPS, ML), although in this case, the simulations reproduced are not perfect replicas and are not free of artifacts, especially when the TD is complex. Due to the complex and intricate nature of the subsurface, this diversity should be seen as an advantage rather than a drawback. It allows for increasing the number of different realizations and better estimating the uncertainty. The models can then be validated or invalidated by comparing the results of the forward models with observations. It is therefore possible and even recommended to exploit this diversity to increase the reliability and validity of the models by confronting them and combining them.

2.11.4 Accessibility and open solutions

The time dedicated to the model is crucial and, unfortunately, often dictates the choice of the method. It may be tempting to save time by selecting methods that require little or no implementation or reflection. But this would mean neglecting the geological origin of the subsurface and replacing it with a simple geostatistical relationship. The time spent on conceptualization should not be a major obstacle to the use of certain methods. On the contrary, we should be pushing to make these more difficult-to-implement methods (OBM, RBM, SBM, process-based) more accessible and available. It should be noted, however, that a number of commercial software packages already include these methods. However, the high cost of such software may limit its use. To address this issue, it may be beneficial to develop additional open-source alternatives and workflows. This could include the development of open-source or free-to-use geological modeling software (de la Varga et al. 2019), the integration of analogous databases (Colombera et al. 2012), or the creation of a comprehensive TD database for MPS and ML (Pyrcz et al. 2008). The geological processes have this particularity to be both general and site-specific. It is then necessary to combine the knowledge with in-depth analysis to completely understand the geology of a site. The same goes for geological and facies modeling. To facilitate this, we need to develop more free, open-source alternative software.

2.12 Perspectives for further research

This review and synthesis allowed us to identify a list of key potential gaps in facies modeling, which could be addressed in future research.

We think that there is a significant need for more systematic comparisons of facies modeling methods. This is essential for selecting methodology and is

therefore of primal importance. To this aim, researchers could create several reference cases, comprising both digitized examples of real-world subsurface conditions and realistic synthetic models, to rigorously test and compare various techniques.

Moreover, the development of workflows that seamlessly integrate analog databases with facies modeling methods, particularly all OBMs and PBMs, is essential. These workflows can enhance data integration and partially automate the conceptualization process, facilitating model development and reliability. However, to simplify the development of such workflows, more open and accessible tools and databases may be required. Therefore, there is a need to create more open source and freely available alternatives for geological and facies modeling. This is a challenge that we will treat in chapters 3 and 7 of this thesis.

In addition, these workflows must be constructed to integrate at best all possible data. Indeed, by advancing methodologies for incorporating various data types such as well logs, seismic data, and outcrop data, researchers can bolster the accuracy and reliability of facies models. Nevertheless, the substantial diversity of data sources and scales represents a continuing challenge, complicating their use and underlining the need for global solutions for the next years and decades to come.

PBM and RBM are the methods that produce the most realistic models. Although they are often site-specific and time-consuming to construct, they cannot be easily conditioned to data, making them challenging to use in practical situations. Therefore, it is crucial to continue their development to enhance their accessibility and application to other sedimentological contexts, such as glacial environments. One interesting avenue is neural networks, which have received increasing attention over the last ten years, and could prove very useful. Examples include generative methods or physically informed neural networks with PBM.

2.13 Conclusion

This review demonstrates the diversity of facies models and covers a wide range of methods. It includes a state-of-the-art review of the most common facies methods, as well as a classification and comparison of these methods based on various criteria. This synthesis should help users in the complex and often difficult selection of one or more methods to suit their specific needs.

However, the lack of systematic comparative studies makes method selection difficult. This is partly due to the lack of references and standards in facies modeling. There is also a lack of diversity in the sedimentological environments presented in the literature. Most papers consider the same environments, such

as fluvial or abyssal. Other environments, such as glacial, eolian, or volcanic, have been much less modeled. Another issue is the integration of data from a wide variety of sources, such as boreholes, outcrops, analogous geological databases, geophysical, or groundwater data, into the modeling process. The integration of all of these data should improve significantly the reliability of models, as they would be validated by several independent data sources.

To partly solve the issues addressed in this review, several solutions can be considered. First, the community should continue developing methods based on geological processes, such as rule-based or process-based methods. These methods enable geological concepts to be better integrated and can be used as training sets for other methods such as multiple point statistics or machine learning. Facies methods also need to be made more accessible and integrated into open-source workflows. This will not only facilitate their use, but also their combination and data integration. A strong emphasis must also be placed on the conceptualization of models to better define the sedimentological context of each study area and therefore choose the methods best suited to reproduce it.

Facies modeling stands as a pivotal step forward in refining subsurface characterization, acknowledging the profound influence of facies in shaping heterogeneity. The evolution of facies modeling will be driven by the future improvements in modeling techniques, particularly with multiple-point statistics, machine learning, process-based, and rule-based methods. The convergence and synergy among these approaches promise important breakthroughs in the foreseeable future, enriching geological modeling for years and decades to come.

Chapter 3

Automated hierarchical 3D modeling of Quaternary aquifers - the ArchPy approach[1]

[1] This chapter was published as : Ludovic Schorpp, Julien Straubhaar, and Philippe Renard (May 2022). "Automated Hierarchical 3D Modeling of Quaternary Aquifers: The ArchPy Approach". In: *Frontiers in Earth Science* 10. DOI: 10.3389/feart.2022.884075

Abstract

When modeling groundwater systems in Quaternary formations, one of the first steps is to construct a geological and petrophysical model. This is often cumbersome because it requires multiple manual steps which include geophysical interpretation, construction of a structural model, identification of geostatistical model parameters, facies and property simulations. Those steps are often carried out in different software, which makes the automation intractable or very difficult. A non automated approach is time consuming and makes the model updating difficult when new data is available or when some geological interpretations are modified. Furthermore, conducting a cross-validation procedure to assess the overall quality of the models and quantifying the joint structural and parametric uncertainty is tedious. To address these issues, we propose a new approach and a Python module, ArchPy, to automatically generate realistic geological and parameter models. One of its main features is that the modeling operates in a hierarchical manner. The input data consists of a set of borehole data and a stratigraphic pile. The stratigraphic pile describes formally and in a compact manner how the model should be constructed. It contains the list of the different stratigraphic units and their order in the pile, their conformability (eroded or onlap), the surface interpolation method (e.g. kriging, sequential Gaussian simulation (SGS), multiple-point statistics (MPS), etc.), the filling method for the lithologies (e.g. MPS, sequential indicator simulation (SIS), etc.) and the petrophysical properties (e.g. MPS, SGS, etc.). Then, the procedure is automatic. In a first step, the stratigraphic unit boundaries are simulated. Secondly, they are filled with lithologies and finally the petrophysical properties are simulated inside the lithologies. All these steps are straightforward and automated once the stratigraphic pile and its related parameters have been defined. Hence, this approach is extremely flexible. The automation provides a framework to generate end-to-end stochastic models and then the proposed method allows for uncertainty quantification at any level and may be used for fully inversion. In this work, ArchPy is illustrated using data from an alpine Quaternary aquifer in the Upper Aare plain (south-east of Bern, Switzerland).

3.1 Introduction

When constructing a 3D groundwater flow model, one of the first steps is to build a geological model. This includes defining the geometry of the stratigraphic units, filling them with a spatial distribution of litho-facies, and finally filling the litho-facies with petrophysical parameter values. The construction of these models is often complex and involves multiple assumptions and computing tools (Pyrcz et al. 2014; Ringrose et al. 2016; Wellmann et al. 2018). It is necessary not only to evaluate the uncertainties related to the parameters values. Indeed, geological structures of the aquifer or inversion using hydrogeological or geophysical data are also important sources of uncertainty. It is

therefore extremely important to be able to construct all the components of these geological models in a manner that is fully automated, well documented, and repeatable. In this paper, our aim is to introduce a new tool that can be used for this purpose for Quaternary aquifers.

The history of geological modeling techniques is rich and diverse (Matheron 1963; Mallet 1989; Koltermann et al. 1996; Ringrose et al. 2016). However, some geological features such as the Quaternary formations are still difficult to model. These sediments were deposited during various sedimentological events, acting at different scales, both temporally and spatially, leading to complex relations and hierarchical structures. Larger and bigger units are the results of the aggregation of sub-units of smaller hierarchical order, that can themselves be the results of the aggregation of sub-sub-units of even smaller hierarchical order, and so on (Miall 1991; Heinz et al. 2003a; Bridge 2009). The definition of this stratigraphic hierarchy is very important when analyzing field data (Aigner et al. 1996; Ford et al. 2014) but also to develop stochastic modeling techniques.

However, one difficulty is that the concept of hierarchy is used differently depending on the modeling techniques, and the hierarchical modeling does not necessarily match exactly what is meant by stratigraphic hierarchy. For example, Neuman (1990) approaches the question of the hierarchy by showing that it is likely that the hydraulic conductivity of hierarchical sedimentary deposits should have a truncated-power law variogram, Ritzi et al. (2004) used the same type of tools but derive different types of variograms. In these approaches the sedimentological heterogeneity is not represented explicitly but represented by multi-Gaussian fields having specific correlation structures. On the opposite, Scheibe et al. (1995) or Ramanathan et al. (2010b) constructed highly detailed simulations of fluvial deposits using the concept of hierarchical deposits to investigate the effective properties of these types of sediment.

When modeling aquifers, the word *hierarchy* is often used with a slightly different meaning. It generally means that the modeling of the hydraulic conductivity field includes several steps such as the modeling of stratigraphic units with a given technique, followed by the modeling of the litho-facies within the stratigraphic units, and finally followed by the modeling of the hydraulic conductivities within the facies. This hierarchical modeling approach may include only two or all of these steps. It was used in many case studies (Weissmann et al. 1999; Feyen et al. 2006; Comunian et al. 2011a; Bennett et al. 2019). We note that this approach can be refined by using categorical geostatistical modeling methods to define stratigraphic units in which sub-units can be modeled using again categorical simulations tools, and so on to obtain multiple-levels of hierarchy (Zappa et al. 2006; Comunian et al. 2016a). But this last method does not account for the fact that sedimentary units are usually deposited as sub-horizontal layers and that in general their geometry is controlled by a set of stratigraphic rules. Other methods account for that information, such as the implicit interpolation method implemented in the Geomodeller 3D or in

the Gempy software (Calcagno et al. 2008; de la Varga et al. 2019). In this approach, the user defines the order of the stratigraphic units and the relations between them, allowing to model automatically the volumes. This is convenient to build complex models in an efficient manner, but Zuffetti et al. (2020) show that these tools cannot handle properly the concept of sub-units within a stratigraphic unit. These authors propose therefore to formalize the stratigraphic hierarchy and define rules allowing to automatically construct 3D models based on that concept, and they show promising results.

All these observations show that there is still a need for a tool that would facilitate stochastic 3D geological modeling. The tool must allow the user to conduct a complete and proper uncertainty quantification including uncertainty at the level of the units geometry as well as their lithologies and properties. The tool must allow to carry out cross-validation efficiently, meaning that it must be possible to remove any type of data and reconstruct an ensemble of models automatically. The model must also be easy to update when new data are acquired or if the geological interpretation is modified.

The aim of this paper is to present the ArchPy approach. The method includes the two types of hierarchy discussed above. ArchPy defines the stratigraphic units from borehole data while accounting for as many hierarchical levels as needed from a stratigraphic point of view. But the method is also hierarchic in the sense that the same method will include the modeling of the stratigraphic units, and then the modeling of the litho-facies within the units, and finally the modeling of the properties within the litho-facies. ArchPy is a methodology but it is also a Python module allowing the automatic generation of stochastic, reproducible, and hierarchical models from borehole data and a geological concept.

To minimize the user interventions during the simulations, we rely on a formal description of the geological concept that ArchPy uses to construct the hierarchical model. This type of formal description is not new, it was described for example by Renard et al. (1994) for fracture networks, and is at the core of Geomodeller 3D or Gempy in which a geological pile is defined to express the relations between the geological events and must be given explicitly (Calcagno et al. 2008). However, as revealed by Zuffetti et al. (2020), the manner in which the pile is defined and used in these codes does not allow to describe the stratigraphic hierarchy. It is therefore necessary to find more general ways to describe the pile. One approach using a tree was proposed in Zuffetti et al. (2020). Here we adjust this initial data structure, and we extend it to include additional information allowing to encapsulate all the knowledge required to build automatically the 3D model. We call this formal description, the Stratigraphic Pile (SP). The SP contains the description of the interpolation methods for all surfaces bounding the stratigraphic units, as well as the description of the simulation methods and parameters for filling the different units with litho-facies and properties.

It is important to note that the geological data in boreholes or outcrops are not always representing the actual position of the boundary between two units but instead they indicate that this boundary should be lower or above this data. Such situations arise in presence of erosion or hiatus in the deposition sequence, or because a borehole is too shallow and does not reach the base of a given unit. These data are frequent and can be treated as inequalities (Dubrule et al. 1986; Mallet 1989; Freulon et al. 1993a; Straubhaar et al. 2021). The use of such data can increase significantly the quality of the simulations as shown for example by Freulon et al. (1993a). In the ArchPy methodology, we include not only the possibility of interpolating the boundaries between stratigraphic units using such inequalities, but we also propose a method to automatically identify the inequalities in the borehole data to facilitate the automatic updating of models with large borehole data sets.

ArchPy is also an object oriented python package allowing to illustrate the applicability and the benefits of the proposed approach. While describing the methodology, we will also discuss the key objects that are used to implement the concepts underlying the approach. Its python interface and open-source nature facilitate its use for a large number of users.

The main novelty of the proposed approach and this software is to allow fast and reproducible simulations of Quaternary aquifers as well as their related uncertainties to any desired hierarchical level (unit, sub-units, facies and properties).

This paper first describes the different components of the ArchPy approach and then illustrates its main features using a synthetic and a real case example.

3.2 The ArchPy approach

In this section, we first present a brief overview of the main components of the proposed methodology. We then describe in detail the concept of Stratigraphic Pile (SP) as well as the way we deal with the stratigraphic rules (erosion, hiatus). All the simulation steps and modeling guidelines are explained using a synthetic case. In the following, and for the sake of brevity, the word *unit* will refer to the stratigraphic unit as defined in the SP and *lithology* or *facies* will refer to the different litho-facies that can be found inside these units.

3.2.1 General overview

The final aim of ArchPy is to generate an ensemble of petrophysical models (or property models) that describe the spatial distribution of specified properties consistent with the location of the units and facies. To achieve these results, ArchPy proceeds in several steps (Figure 3.1). The input data are a Stratigraphic Pile (SP) and a set of Hard Data (HD). The HD can be either

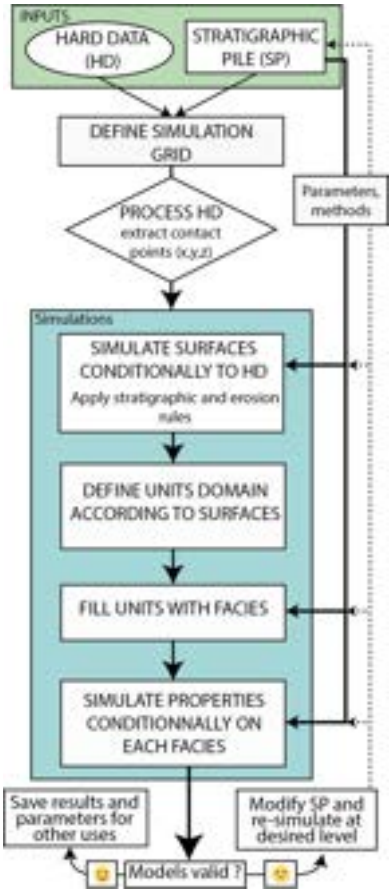

Figure 3.1: *Overview of the ArchPy approach.*

borehole data or punctual information (e.g. from outcrops). First, the HD are processed to extract the contact points (equalities and inequalities). Then, a whole simulation takes place hierarchically in three main steps:

1. simulate the surfaces delimiting the units boundaries and thus allowing to define the stratigraphic units domain;
2. simulate the facies to fill each unit using various geostatistical methods according to prior geological knowledge;
3. simulate the properties inside each facies independently.

All these steps are done conditionally to the HD. In the end, the final models are validated by the user. If they are not satisfying (based on expert knowledge

or on some criterion), the SP can be modified (on the simulation methods for example) and previous steps are re-executed, depending on the modified parameters.

ArchPy can be used in several manners. It can be used to generate one or an ensemble of models to quantify uncertainty. It can be used to facilitate the update of geological models when new data are collected in the field. And it can also be coupled with an inversion technique to express the prior distribution of the geological and petrophysical parameter values.

It is important to note that each step depends on the results of the previous ones. For example, after a first complete simulation, if the only parameters changed are those of the filling step, it will only be required to simulate the facies in the units and subsequently the properties inside them. Similarly, if only one surface has been recomputed and the others have been kept, the only unit domains that will need to be re-simulated (as well as their filling) will be those impacted by a modification of this surface. This flexibility is important for dealing with large inverse problems as the number of unknown parameters can make the problem tedious and difficult (Biegler et al. 2011). It allows to focus on particular units of interest and only simulate parts of the domain at any desired level, without being forced to simulate the whole system each time a modification is decided.

3.2.2 The Stratigraphic Pile

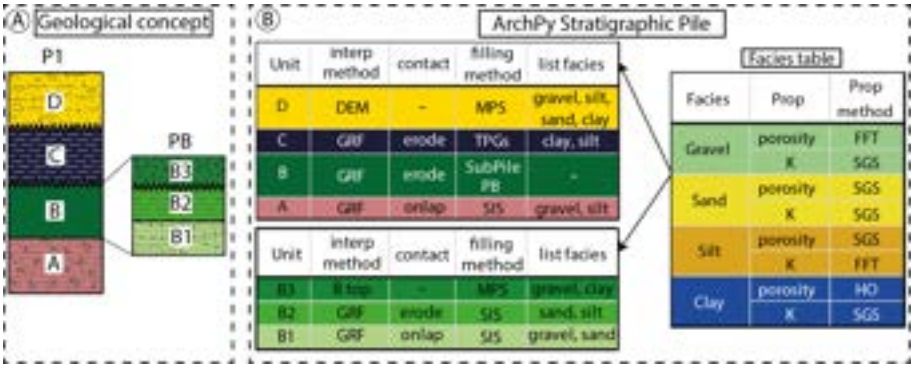

Figure 3.2: *Schematic representation of an ArchPy stratigraphic pile (B) given a geological concept (A): "interp. method" stands for interpolation method, GRF for Gaussian random functions, DEM for Digital Elevation Model, "Prop method" for property simulation method, MPS for Multiple-Points Statistics, SIS for Sequential Indicator Simulation, TPG for Truncated Pluri-Gaussians, HO for homogeneous, K for hydraulic conductivity, FFT for Fast Fourier Transform, SGS for Sequential Gaussian Simulation.*

The concept of Stratigraphic Pile (SP) is the backbone of the ArchPy methodology. Indeed, it contains almost all the information needed for the simulations including the stratigraphic relations between units and the description of the simulation methods of the surfaces, the filling, and the properties as well as the parameters controlling them (Figure 3.2). The SP is made of different components (coded as python objects): units, surfaces, facies, properties and possible other piles. Following an object-oriented programming logic, all these objects have different attributes (name, color, interpolation method, etc.) that define and differentiate them. These object attributes can also be composed of other different objects. A practical example is the unit object which have a *list_lithofacies* attribute, containing the litho-facies objects that populate this unit.

- **Surfaces**. They delimit the top of the units and are defined by an interpolation (or simulation) method and by a contact type to indicate if the surface is conformable (onlap) or erosional (erode). The difference is that an erode surface erodes older units where it is simulated below their top surface while an onlap surface is simply ignored in such locations meaning there is no deposition (see section 3.2.3).

- **Units**. They correspond to stratigraphic units that can be observed in HD or on outcrops. Each unit belongs to a SP, and has a specific order index to determine its position in the pile. A unit also needs a surface object to determine its upper boundary, its lower boundary is defined by the surface at the top of the underlying unit. Finally, the unit contains a description of the filling method and a list of facies objects to simulate inside the unit domain.

- **Facies**. The facies describe the hydro or litho-facies that are contained inside the units. They can be very different depending on the modeling purposes and data available (e.g. stratigraphic facies, lithologies, or USCS codes). A list of facies is given for each unit to indicate which ones to simulate during the facies simulation. Furthermore, each facies can be composed by one or more properties that are simulated inside the facies domain (where a specific facies is present).

- **Properties**. They are independent ArchPy objects that composed the different facies. For each property inside a facies, some parameters can be set such as the mean value of the property (inside a specific facies), the covariance model, the method of simulation, etc.

- **Stratigraphic Pile**. A SP is the combination of all the objects described above that synthesize the geological concept. Note that a SP can be inserted as a filling method within a unit. This allows to construct a stratigraphic hierarchy. For example, in Figure 3.2, the sub-pile PB is used as input for filling unit B.

Thus, the Stratigraphic Pile is an object that can easily be manipulated and modified. Using such an approach, the user can focus more on the conceptual aspects of the modeling (units relations, erosional events, spatial distribution of the lithologies or facies, etc.). In fine, the whole modeling process can be easily reproduced because all the steps are documented in the SP.

3.2.3 Erosion rules

Erosion (stratigraphic) rules (ER) describe how the surfaces influence each other after having been simulated. They are similar to those denominated "geological rules" by Calcagno et al. (2008). The Figure 3.3 shows a simple example of the difference between onlap and erode behaviors. Here two surfaces are simulated: S1 (old) and S2 (young), while the gray surface is simply set to the topography or the Digital Elevation Model (DEM). S1 is defined onlap and S2 has both behaviors. If S2 is specified onlap, the unit 2 (young, in black in the figure) is not deposited where S2 is below S1, whereas if S2 is specified erode, the effective top of unit 1 (young, yellow in the figure) is set to S2. This approach allows incorporating geological time directly by choosing the appropriate truncation operation to remain consistent with the sedimentological history (Wellmann et al. 2018). Another rule is that a surface cannot be above (or below) the DEM (resp. bottom of the domain), if this case arises, the surface will be automatically set to the DEM (resp. bottom). These ER are applied each time a new surface is simulated during the surface simulation.

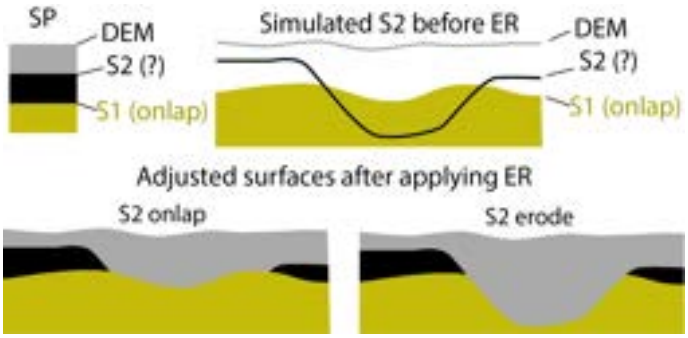

Figure 3.3: *Schematic example of the erosion rules (ER) used in ArchPy. The surfaces are first simulated from oldest to youngest and then adjusted following the ER.*

3.2.4 Synthetic example

To illustrate the ArchPy capabilities, Figure 3.4 shows one stochastic realization of hydraulic conductivity and porosity based on the SP of Figure 3.2. The domain dimensions (x, y, z) are $3 \times 1 \times 0.2$ km^3 with a spatial resolution of $15 \times 15 \times 4$ m^3. The model is purely synthetic but it mimics a valley filled by a series

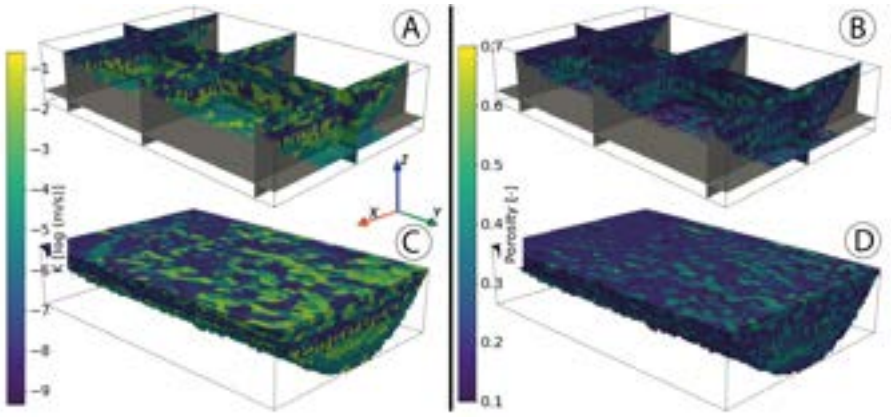

Figure 3.4: *Realizations of two different properties (A: Hydraulic conductivity, B: Porosity) for the synthetic case. C and D are 3D blocs of the A and B realizations respectively. The simulations used respective corresponding facies realization of the figure 3.7 as simulation domains. Vertical exaggeration = 3x.*

sedimentary episodes. For this example, we assume that unit A is a moraine deposit only filled with gravel and silts. The B formation is deposited during three sub-steps (sub-pile PB, 3.2). It represents a fluvio-glacial environment including three stages (B1, B2, B3). On top of that unit C is an important glacio-lacustrine phase where only fine particles are deposited (clay and silt). The unit D ends the process by setting up a fluvial environment that was more active in the southern part of the area (towards -y main axis). The different steps to obtain this result will be explained in detail in the following sections.

3.2.5 Data pre-processing

The main hard data to describe the geology in a Quaternary environment are the borehole information. For each borehole, ArchPy requires: a borehole ID, the depth, and location (x, y and z) of the borehole as well as a stratigraphic unit log and/or a lithology log. Both logs contain the elevation of the top of the interpreted units and lithologies in the simulation grid reference system. These locations will be used as conditioning point for simulations. An important thing to note is that the logs of borehole objects in ArchPy interface only need top elevation for each units/lithologies encountered. To facilitate the geostatistical simulation of the properties, we consider only regular Cartesian grid for the moment in ArchPy (to avoid support effects). The extension and parameters of the grid are provided by the user. The SP and eventual Sub-Piles are also given as input. We then pre-process the borehole data (HD) to check that they are consistent with the SP and to extract the contact points between the units. The difficulty here (which is not intuitive) is that a contact between two units in a borehole does not necessarily correspond to the top of the unit located

below this contact because of possible erosion or sedimentation hiatus. It is therefore necessary to analyze the borehole logs to identify the information that the contacts bring about the possible positions of the surfaces. To code this information, we will define contact points where the position of the surface is perfectly defined (equality contact point) and those which provide only an indirect information (inequality contact point). Formally, an inequality contact point consists of a lower or upper bound for the actual surface.

Figure 3.5 shows how HD are interpreted automatically in the ArchPy pre-processing step given four different examples. We do not fully detail each example for brevity but the main points are covered.

Considering the example showed in Figure 3.5A, three surfaces need to be simulated, blue, green and red tops (yellow top is defined by the DEM). Equality points can be safely attributed in B1 between all contacts as there are no hiatus and no erosion layer in the Pile. However, in B2 and B3 boreholes, as the blue outcrops directly, its top must go above the surface, assuming erosion at the surface. This means that the tops of the borehole B2 and B3 are then lower bounds for the top of the blue unit. Also, the red unit is not encountered by B2 which indicates that it must go below the bottom of the borehole which is a upper bound for the top of the red unit. The Figure 3.5B example adds an erosional event (blue top) that cross-cuts the green and red top layers. This implies that we must add a inequality contact point (lower bound) in B3 for green top and equality contacts along the erosion surface (B2 and B3) for the blue top because of the ER. Indeed, the green top in B3 cannot be considered as the actual green top since the green unit has been eroded. The same event occurs in Figure 3.5C in B3 where the red unit has been eroded by an erosional event (green top).

The more complex example (Figure 3.5D) shows that the number of extracted data can become important, especially when the number of layers increases. Here, additional outcrop information has been added with unit contacts (C1 and C2) that inform about a transition between two units. Yellow goes above as it is the unit reaching the topography. The contact between yellow and blue is an equality for blue (the only erode layer above blue is yellow but it has been deposited and thus can not have eroded blue). The bottom of B2 ends in the blue unit which indicates that all layers below it (dark green and red) must go below the bottom of the borehole. When two units in a borehole are separated by two (or more) erosion surfaces, ArchPy assumes that the contact belongs to the younger erosion surface. This is shown in Figure 3.5D at B4 between the orange and dark green units. In the pile, these two units are separated by two other units (blue and yellow) characterized by their erosional top. As yellow is younger than blue, the equality point is attributed to yellow.

All boreholes are then processed this way, HD are extracted and assigned to respective surfaces. It is relevant to note that this step is completely automated

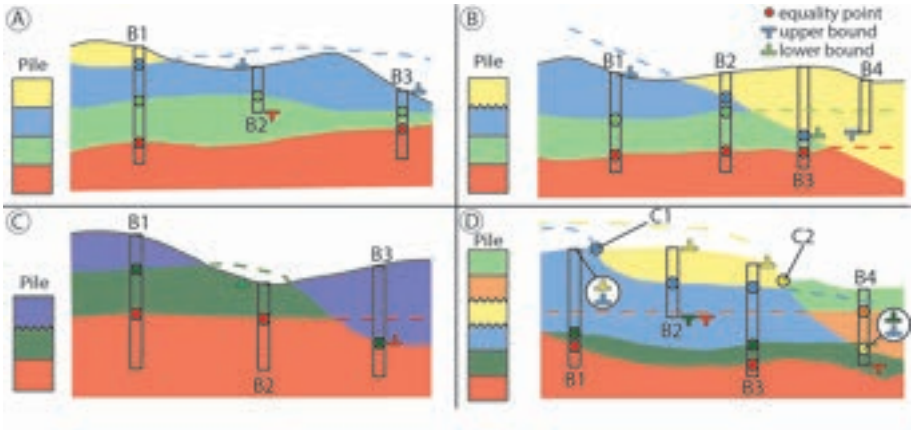

Figure 3.5: *Four examples (A, B, C and D) of how inequalities and equalities are extracted from boreholes and field data. B indicates a borehole information and C a unit contact (observed on the field for example). For each example a Stratigraphic Pile is defined to indicates the relationships between the units and the nature of the surface contact (straight line is onlap and corrugated is erode). Dashed lines represents simulated surfaces before applying erosion rules (see section 3.2.3).*

in ArchPy and the only required inputs are the SP, the boreholes and the simulation grid.

3.2.6 Simulation of the surfaces and units

Using the HD and the information provided by the SP, ArchPy performs a 2D simulation (interpolation) for each surface of the SP over the complete domain. Simulations are generally perform conditionally on HD but unconditional simulations are also possible by defining a mean altitude.

The surfaces are simulated successively from the oldest to the most recent (for a hierarchic level). After having simulated a surface, we apply the ER (see section 3.2.3). The surfaces are also simulated hierarchically, which implies that surfaces of higher order (main units) are simulated before those of lower order (sub-units). For example, in the case of the pile in figure 3.2, ArchPy first computes the surfaces of the top of A, B, and C and only after, the surfaces of the top of B1 and B2 are computed inside the unit B. It means that no surface of the top of these sub-units can go above or under the limits of B unit, even if it is an erode surface. The other lower hierarchical units (if present) are simulated following the same strategy. The top unit surface is not simulated since it must be equal to the Digital Elevation Model (DEM) for consistency, it is then simply sets equal to the DEM. Equivalently, as lower limit of all units are defined by the top of the underlying unit, the bottom last unit must be

defined. In ArchPy, this is done by setting it to the bottom of the simulation domain.

In the SP, the user must indicate for each layer an interpolation method among the following choices: simple and ordinary kriging (SK, OK, resp., Chiles et al. 2012), multi-Gaussian random functions with or without inequalities (GRF, Chiles et al. 2012), basic 2D interpolation methods (linear, nearest neighbors, cubic) using *SciPy* (Virtanen et al. 2020) and finally direct sampling multiple-points statistics algorithm with or without inequalities (MPS, Mariethoz et al. 2010b; Straubhaar et al. 2021). For the multi-Gaussian simulation methods, a normal-score transform, can be applied automatically to the HD if they do not follow a Gaussian distribution. Most of the methods are taken from the python module *Geone* that provides a set of geostatistical and MPS modeling tools. For each method, the user has to provide the set of required parameters. For example, for the kriging or multi-Gaussian simulations a variogram model must be provided. The inference of the parameters can be done manually or automatically if sufficient data are available using the *Geone* toolbox. For the MPS approach, a training image and the relevant parameters also need to be provided. Anisotropy can be easily modeled by choosing appropriate variogram or MPS parameters.

Once all the surfaces of the SP are defined, it is straightforward to define the volumes representing the units (unit domains) knowing for each unit the top and bottom surfaces according to the ER. These volumes are discretized by defining for each (x, y) location which cells are intersected by the surfaces. All the cells lying vertically between these two cells are assigned to the unit domain. Concerning the intersected cells, they belong to the unit domain only if they go above (or below) the middle of the cell for top surface (or bot resp.).

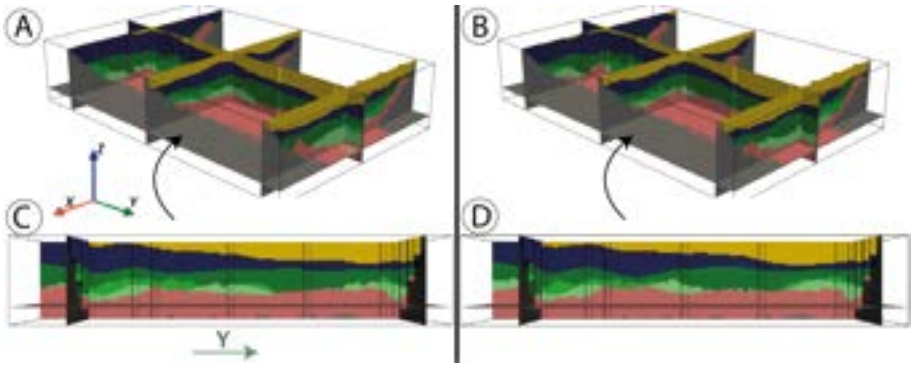

Figure 3.6: *Two realizations (A, B) of the units (1st step of the ArchPy simulations) for the synthetic case. C and D are lateral view of the realizations A and B respectively. The colors of the units are those defined in the Stratigraphic pile of Figure 3.2. They are presented with cross-sections for visualization purposes. Vertical exaggeration = 3x.*

Figure 3.6 shows two realizations of the unit domains. The realizations are conditioned to the borehole data and the stratigraphic pile. The effect of using sub-units is clearly visible: the B2 (middle green) top surface (which is set as erode) does not cross-cut the unit A (as expected) in the front cross-section of both realizations. This approach allows representing the uncertainty of the position and extension of the units. By running a large number of realizations, the uncertainty can be quantified: for example probability maps can be produced for each units by post-processing those results.

3.2.7 Simulation of the facies

Once the stratigraphic unit volumes are defined, it is possible to fill these volumes with different facies or lithologies using different geostatistical methods. The simulation takes place in each unit independently, even if the same facies is present in different units, as in the example in Figure 3.2 where the sand appears in B and D units. This means that only the sand HD located inside the unit D will be taken into account when simulating the facies (sand) inside the unit D. If a certain facies HD, that does not belong to a specific unit, is present inside its domain (e.g. a sand HD in unit C, Figure 3.2), these HD will be ignored. In such cases, warnings are issued by the software. This situation leads to inconsistencies with facies HD that principally reflects a probable mismatch in the HD (false geological interpretation) or in the geological concept.

As facies (resp. property) simulations are dependent of units (resp. facies) simulation results, at least one facies (resp. property) simulation must be done for each unit (resp. facies) realization. It means that if the modeler choose 100 units realizations and 100 facies simulations, a total of 100 x 100 simulations will be generated. The same logic applies for the property simulations.

In the SP, the user must define one simulation method for each unit. The choices available in the current version of the code are: homogeneous (one unique facies for the whole unit), Sequential Indicator Simulations (SIS, Journel 1983a; Journel et al. 1984), Truncated PluriGaussians (TPG, Loc'h et al. 1994; Mariethoz et al. 2009; Armstrong et al. 2011), Multiple-Points Statistics (MPS, Mariethoz et al. 2010b; Straubhaar et al. 2021), and Sub-Pile which indicates that the unit will be populated by another pile containing sub-units (e.g. PB in Figure 3.2).

Thus, multiple facies simulation techniques can be used to assess the uncertainty. Note that it is rather straightforward to switch from one method to another. This capability allows to cover a broad uncertainty space by providing the user with different simulation methods within the same framework. Hence if little geological knowledge is available for the spatial distribution of the facies within a unit, SIS can be used since little user inputs are required, while if there is more detailed geological knowledge available, other methods can be

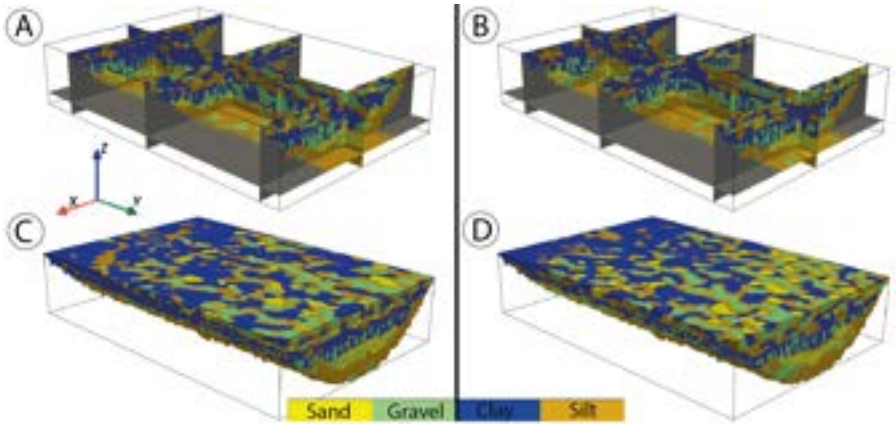

Figure 3.7: *Two realizations (A, B) of the lithofacies (2^{nd} step of the ArchPy simulations) for the synthetic case. C and D are 3D blocs realizations of A and B respectively. The simulations used the respective corresponding units of the figure 3.6 as simulation domains. Vertical exaggeration = 3x.*

used such as TPG or MPS if an analog geological concept can be defined (e.g. Training Image). All the geostatistical methods used for this step are included inside *Geone* except for the TPG that are directly included inside ArchPy with various tools to define the truncated flag or estimate the variogram parameters of the underlying multi-Gaussian random fields.

Figure 3.7 shows two realizations of lithologies according to the unit realizations (Figure 3.6). The spatial variability of the lithologies is significant despite the fact that only four lithologies have been defined. This is mainly due to the combination of structural heterogeneity coming from the stratigraphic units and the lithology distribution within these units. This allows exploring many different plausible realities that are consistent with the HD and the concept. We can also observe the non-stationarity in the unit D where the channels are sparser in the back than in the front (along the y axis). Indeed, it is important to mention that most of the facies simulation methods available in ArchPy can be non-stationary, allowing a much better representation of geological trends and exploration of the uncertainty.

3.2.8 Simulation of the properties

Once the facies are simulated, the simulation of the properties is straightforward and requires little inputs. Indeed, there are only two requirements: define the properties that must be simulated, and define how to simulate them (method and parameters). The available methods for the moment are multi-Gaussian Random Fields (GRF) or homogeneous. If a GRF is used, two methods are possible to generate them: Fast Fourier Transform Moving Average (FFT, Ravalec

et al. 2000) and Sequential Gaussian Simulation (SGS, Deutsch et al. 1992). As the FFT method needs to perform the simulations on an entire grid, it can be less effective than SGS, especially if there are many lithologies and units. It is important to note that properties are simulated, for a given lithofacies, independently and sequentially for each units. For example, if we have a facies which is present in multiple units (consider the sand in Figure 3.2), the properties will be simulated first in the sand occurrences of the top unit and sequentially in the other occurrences in underlying units. This allows to avoid spurious correlations that can arise if we consider the whole sand domains at once. Indeed, if sands of different units are in contact, they should not be considered as part of the same entity and thus should not be simulated together.

Conditional simulations are available with punctual data (x, y, z and property value). As some methods require at most one HD per cell, values that lie in the same cell are averaged if necessary.

3.2.9 Implementation of ArchPy

The ArchPy methodology is coded in an open source python code[2]. The code is designed using an object oriented approach. All the concepts described above are implemented using classes of objects designed to match the concepts and to facilitate their use. Most of the data imports and exports are based on simple text files. The geostatistical kernel of ArchPy is based on the Geone[3] python library. For the visualization, ArchPy integrates some functionalities to produce various figures (e.g. stratigraphic units at a specific hierarchical level, only specified units, cross-sections, etc.). These plots are generated mainly using PyVista[4]. If needed, data can also be exported in a *vtk* format for further use. Post-processing tools are also provided, to estimate for example the probability of encountering a specific unit (facies) or estimate the excepted value of a property over a part of the simulation domain. The structure and the principles underlying the ArchPy code are designed to allow the user scripting in a very flexible manner the construction of the geological model. This also facilitates the coupling of ArchPy with any forward or inverse simulator. Some example python notebooks are given on the online repository of the code.

3.3 A first field application

3.3.1 The Upper Aare Valley

The Upper Aare Valley (Figure 3.8B) is a Quaternary alpine valley located between the cities of Thun and Bern in Switzerland with a complex and rich geological history due to its proximity with the Alps (Kellerhals et al. 1981;

[2]http://www.github.com/randlab/ArchPy
[3]http://www.github.com/randlab/geone
[4]https://www.pyvista.org/

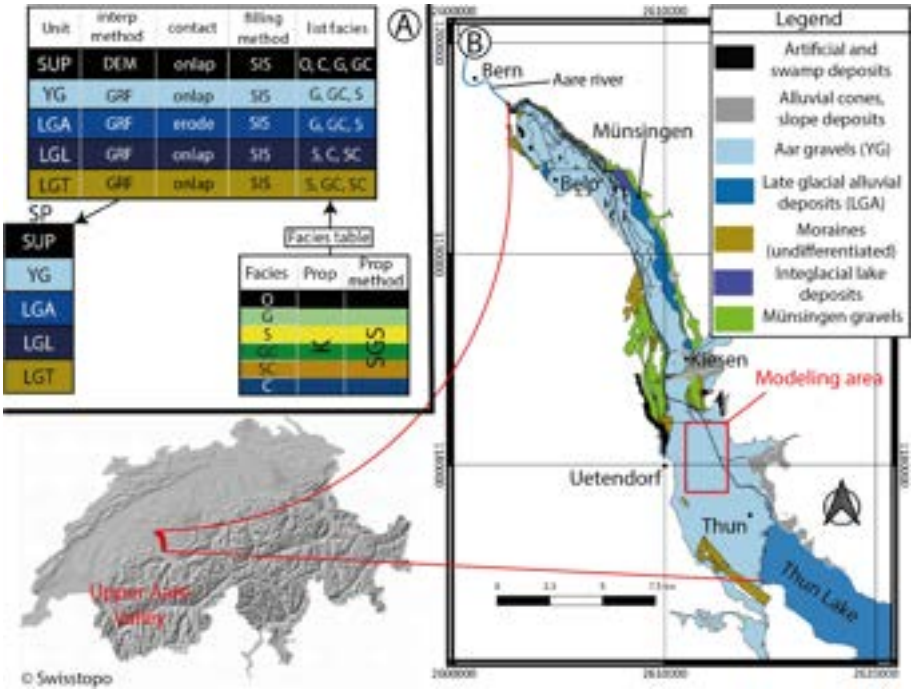

Figure 3.8: ***A****: Schematic stratigraphic pile used for the ArchPy simulations of the local geological models in the Upper Aare Valley. It shows the different units that have been taken into account, their stratigraphic relations (which is above/below (i.e. younger/older) which), the nature of its contact (erode or onlap), the interpolation methods used or still the lithofacies (see Table A.1) and the property to simulate (hydraulic conductivity (K) using Sequential Gaussian Simulations (SGS)). More details in section 3.2.2.* ***B****: Situation and simplified geological map of the Upper Aare Valley. Only unconsolidated deposits that are near the aquifer are shown. The moraines are represented undifferentiated. The coordinates are presented in CH1903+ - LV95 (epsg: 2056). All the data used comes from the Swiss Geological Survey (Swisstopo).*

Haeuselmann et al. 2007). Previous studies on Quaternary deposits, on this particular site (Schlüchter 1989; Preusser et al. 2004), or at a regional scale (Preusser et al. 2011; Graf et al. 2016) have shown the complex relations occurring between multiple depositional and erosional processes (mainly glacial, glacio-fluvial and glacio-lacustrine). This led the valley to be incised and filled with a wide variety of sediments and facies (tills/moraines, fluvial gravels, glacio-lacustrine deposits, lake deposits, alluvial cones, etc.) explaining the great heterogeneity of this type of deposits. Two main aquifers have been identified in the valley: a superficial one which is actively used for drinking water supply, shallow geothermal energy, and some local industries. And a deep one that is poorly known due to its higher depth (only few boreholes have reached it). Figure 3.8B shows that the superficial aquifer is mainly composed of the

Aare gravels, the Late glacial alluvial deposits, alluvial cones and the Münsingen gravels.

A major hydrogeological synthesis of the valley has been undertaken at the end of the 1970s and at the begin of 1980s (Kellerhals et al. 1981). Since then, additional data have been collected (Schlüchter 1989; Preusser et al. 2004) for various projects in different parts of the valley, but no new hydrogeological synthesis has been assembled and published. Among the new data, the Swiss Geological Survey has systematically gathered the borehole data for Quaternary sediments in several pilot sites, and homogenized the data and terminology (Volken et al. 2016). This data set includes around 800 digitized boreholes in the Upper Aare Valley. A geological model of the valley filling has also been produced by the Swiss Geological Survey to illustrate how those data can be used. In addition, a valley scale towed Transient Electromagnetic Survey has been acquired and published in 2021 (Neven et al. 2021) by the University of Neuchâtel to better constrain and characterize the aquifer dimensions and its internal heterogeneity.

3.3.2 Modeling area and borehole dataset

To illustrate the ArchPy approach, we chose an area with a high density of boreholes located in the south of the Valley (fig. 3.8B). The extent of this area is given by its coordinates in the CH1903+ - LV95 system, lower-left corner: 2'611'000 m/1'178'000 m, and upper-right corner: 2'613'000 m/1'182'000 m.

The depth of the boreholes rarely exceeds 50 m; they do not reach the deepest aquifer and stay in the shallow one that is 50-60m thick in this part of the valley (Kellerhals et al. 1981). The data set contains a large part of the boreholes that have been drilled during decades in the area (Volken et al. 2016). Each borehole is described in terms of intervals with information about the granulometry (litho-facies), the units encountered, the quality of the interpretations, etc. However, unit data can be missing, contrary to granulometry data, meaning that for many boreholes, only lithofacies data is available. Granulometry information is described with one, two or up to three different grain sizes, each defined with a USCS classification code (Casagrande 1948). No hydraulic conductivity data have been taken into account.

The boreholes (133 in total) intercept a total of four major stratigraphic units: Aare young gravel (YG, Holocene), Late glacial alluvial deposits (LGA, Holocene), Late glacio-lacustrine deposits (LGL, Holocene) and Late Glacial Till (LGT, late Pleistocene). The LGT appears only on two boreholes on the southern part of this section of the aquifer and will therefore be difficult to model. YG and LGA are the most present units and constitute the largest part of the shallow aquifer in this area while LGL and LGT are more scattered and can be seen as its bottom.

Note that this stratigraphic pile is simplified given that 23 major stratigraphic units can be distinguished on the entire valley (Volken et al. 2016). However, most of these units are absent in the modeled area.

3.3.3 Modeling settings

The extension of the simulation domain is 2 km in the W-E direction and 3.3 km in the N-S direction. The elevation ranges from 520 to 570 m a.s.l and the resolution is $15 \times 15 \times 1$ m which implies a number of cells of $134 \times 220 \times 60$ ($nx \times ny \times nz$). The top of the domain is defined according to the DEM of Switzerland with a resolution of 25×25 m (DHM25, Swisstopo) and the bottom is defined by a raster map of the bedrock elevation (TopFels25, Swisstopo), also with a resolution of 25×25 m, both are freely distributed by the Swiss Federal Office of Topography.

The units were defined mainly on the basis of the HD and the geological knowledge of this area (Kellerhals et al. 1981). Five units were recognized (fig. 3.8A). A superior unit (SUP) was added which includes superficial (soil, peat) and artificial (anthropogenic) deposits. No sub-unit has been defined as such data are not available in this actual dataset. The top surfaces of the units have been modeled with GRF to take the effect of inequalities into account except for SUP top surface which was set to the DEM as it is the most superficial unit. The associated covariance models (variograms) were estimated using an automatic fitting method (least squares optimization) on the HD. The optimized parameters are shown in Table 3.1. Most of the surfaces were defined as *onlap* except the LGA top surface which represents a former terrace of the Aare river, generally deposited at a slightly higher altitude than YG (Kellerhals et al. 1981).

Table 3.1: *Covariance models parameters (C: contribution and r: range) used for the surfaces interpolation of each surface. All models are isotropic, except the LGT one with a orientation N-S for the major axis). No covariance model was fitted for SUP as its surface is defined by the DEM. Subscripts exp and sph indicates exponential and spherical covariance models.*

Units	r_{sph} [m]	C_{sph} [m^2]	r_{exp} [m]	C_{exp} [m^2]	nugget [m^2]
YG	2986	8.9	5000	17.8	0
LGA	2854	24.8	4846	49.5	1.0
LGL	2531	19.0	3942	38.1	1.0
LGT	(2000, 4000)*	200	-	-	-

*(ranges in x and y direction resp.)

In the HD, the litho-facies are described by up to three different grain sizes. We chose to only take the most present one for each layer and we also grouped certain similar USCS codes (Table A.1) to reduce the number of lithofacies to 7: others (O), gravel (G), sand (S), clayey gravel (GC), clayey sand (SC) and

clay (C). The facies others regroups superficial codes such as OH or Pt. Facies were then considered within a unit if their proportions exceed 5% (inside that specific unit).

For the sake of simplicity in that example, all the units were filled using SIS. Prior variography analysis on the lithofacies HD shows significant variability which required the SIS variograms to be fitted manually, the chosen parameters are given in Table A.2. Only the hydraulic conductivity K property has been simulated for that example using the covariance models given in Table A.3. Note, that adding other properties is possible and very simple since only the interpolation method and the covariance models (for each facies) are required.

The ArchPy Aare model was run several times to illustrate its applicability for uncertainty estimation. In that example, we generated 10 simulations of the stratigraphic units. For each stratigraphic unit simulation, we generated 10 facies simulations. And finally, for each combined realization, we generated 1 unconditional simulation for K. This procedure resulted in a total of 100 simulations (10 x 10 x 1). The code allows to proceed in this manner, but it also permits to simulate for each realization all the components successively (units, facies, and properties). These different modes of simulation can be used for quantifying the impact of these different sources of uncertainty on the distribution of the properties but also on their groundwater flow or geophysical responses.

3.3.4 Results

Figures 3.9-3.12 show the results of ArchPy simulations conditioned to the borehole data. The figures illustrate the type of heterogeneity and complexity that can be modeled rather simply using the ArchPy approach. For example, the two units realizations (Figures 3.9A and 3.9B) differ significantly while being consistent and honoring both the borehole data. This variability is important for quantifying the uncertainty. To visualize that part of the uncertainty, ArchPy allows the user to compute the probability of observing a specific unit. Figure 3.10 shows in yellow the locations where it is quite certain that a given unit is present and with which thickness. For example, Figure 3.10A shows that the unit YG is well constrained in the eastern and northern part of the domain due to the important number of boreholes that reach it. The unit LGA seems to be more present in the southern part of the area (Fig. 3.10B), thinner than the unit YG,and almost absent (or very thin) in the north. The unit LGT (Fig. 3.10C) does not display such trends and has a more uncertain distribution, probably mainly due to a lack of data (shallow boreholes).

Litho-facies simulations are shown in Figures 3.9C and 3.11 and are the results of the filling of the simulations shown in Figure 3.9A. These simulations honor both the borehole data and geometry of the stratigraphic units. As for the

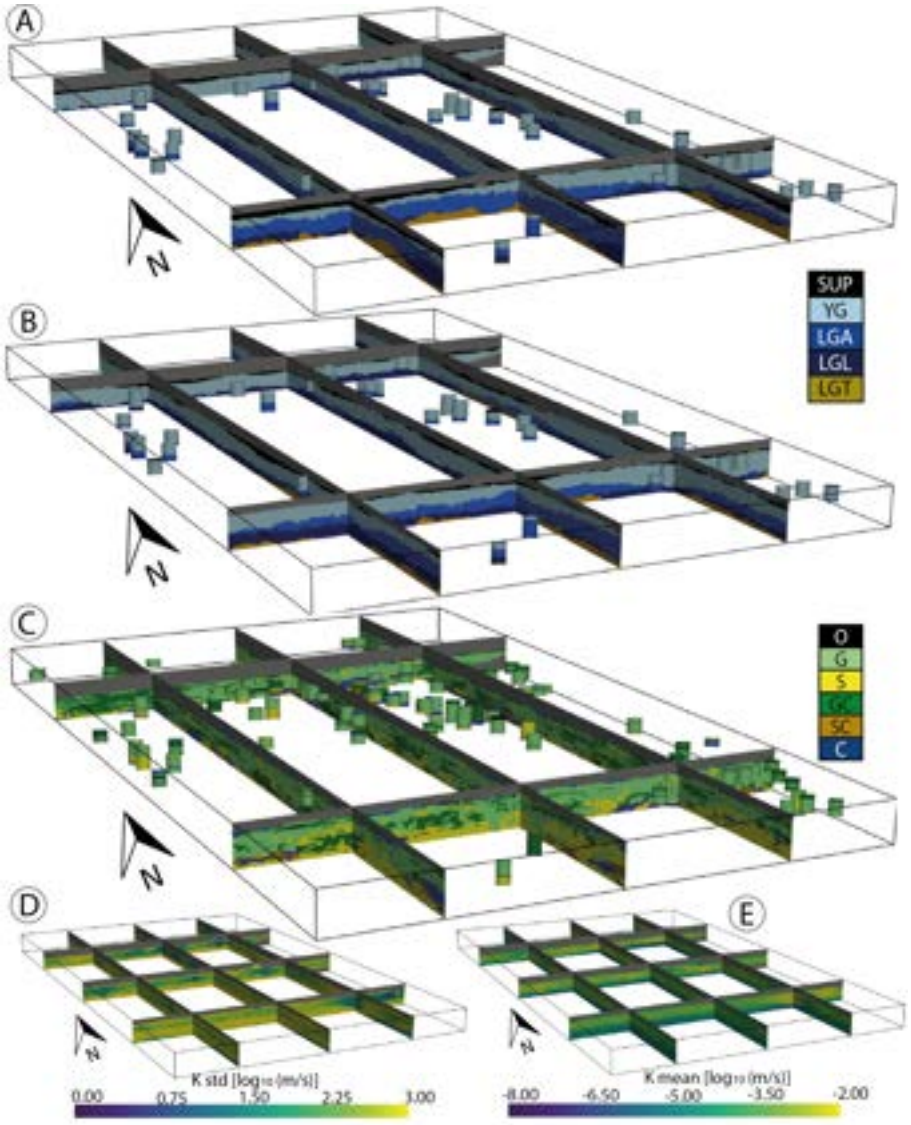

Figure 3.9: *Aare aquifer results obtained for A, B: two unit realizations, C: one facies realization (within model A), D, E: K standard deviation and mean simulated along the 100 models, units are in log10 (m/s). Vertical exaggeration = 3x.*

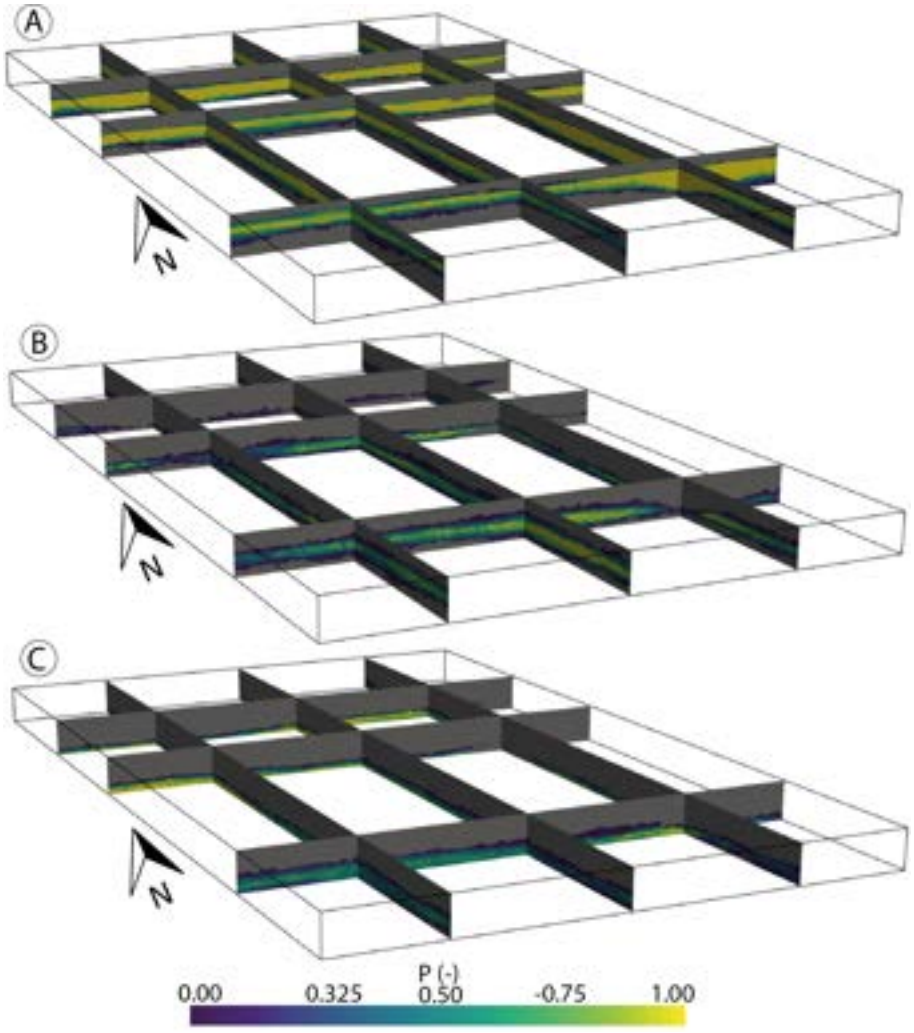

Figure 3.10: *Probability of occurrence along the 100 models for units: YG (A), LGA (B) and LGL (C). Vertical exaggeration = 3x.*

stratigraphic units, it is possible to compute and produce figures showing the probability of occurrence of each facies.

Finally, two simulated hydraulic conductivity fields are shown in Figure 3.12. They display a broad range of values that is expected for this geology and that honor all the borehole data. It also shows the complex relations between the property values, the stratigraphic units, and the litho-facies. The variability between the realizations suggests a strong heterogeneity that would have been extremely difficult to model properly without the hierarchical approach (e.g.

Feyen et al. 2006; Zappa et al. 2006; Zech et al. 2021b). The mean of the logarithm of K (Fig. 3.9E) highlights the location of the aquifer where the values are likely to be especially high. These locations also coincide with those where the standard deviation (Fig. 3.9D) is low, indicating that the property values are better defined inside the aquifer than outside. Elsewhere, the standard deviation values may be quite high, reaching easily 2 $\log_{10}$(m/s) indicating an uncertainty of up to two orders of magnitude. The variance is low around the boreholes as expected.

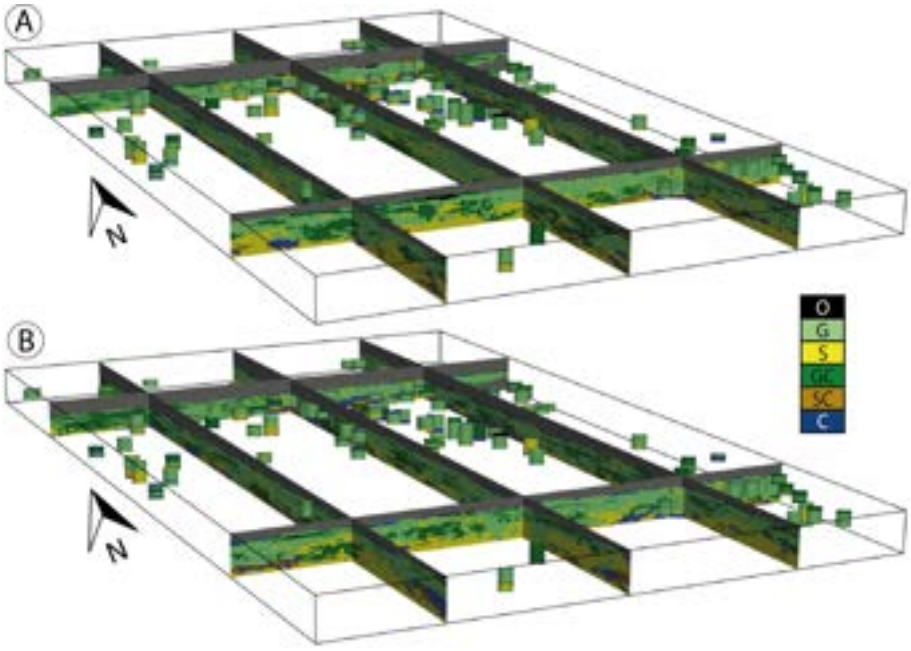

Figure 3.11: *Two facies realizations that are the results of the filling of the unit realization in fig. 3.9A. Boreholes show the spatial distribution of the HD.*

3.4 Discussion

One of the most important novel features of the ArchPy approach is the extended concept of Stratigraphic Pile (SP) as compared to Calcagno et al. (2008) for example. This concept has been shown to be an effective way to formulate all the geological knowledge into one entity (practically, a python object). Thanks to this representation, it is easy to embed multiple SPs inside other SPs and to simulate the units to any level of hierarchy and this without any particular restrictions. By including various interpolation and simulation methods which can be applied independently for each unit, lithofacies and properties, the ArchPy approach offers a high flexibility to the user who can adapt the methods to the quantity of available data and the complexity that he needs

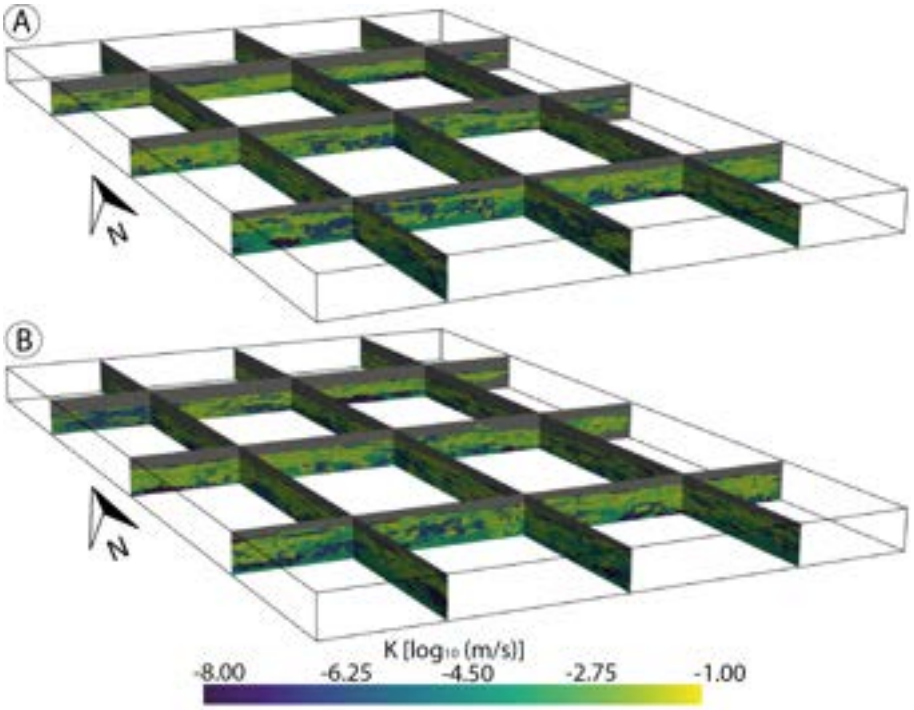

Figure 3.12: *Two property realizations made on the two facies realization in fig. 3.11.*

to represent for a specific site. In addition, the use of inequality data that are automatically derived from the SP and the borehole data allows ArchPy to extract a larger amount of information from boreholes than what is usually done in alternative geo-modeling tools.

The results obtained for the Upper Aare Valley illustrate the type of stochastic models that can be easily and rapidly constructed for Quaternary deposits using the ArchPy approach. Due to the simple assumptions made on the geology and the concepts (simplified SP, use of SIS to fill the units) some aspects of the proposed method could not be illustrated in this example. Several limitations in the data set were also identified. For example, the LGT unit is not well constrained because only a few boreholes reach it. Indeed, most boreholes in this area are drilled for hydrogeological purposes (Kellerhals et al. 1981), and local communities are generally not interested in reaching the LGT unit because of its lower hydraulic conductivity as compared to the YG or LGA unit. A sampling bias is also expected in the litho-facies inside the LGL and LGT units. Indeed, we observe that the simulations of these units tend to have more sand (S code) than expected in glacio-lacustrine or till deposits. This can be due to a sampling bias in the borehole data base because the areas of high

permeability are preferentially drilled while clay and silt areas are generally avoided. Since the simulated proportions of litho-facies are conditioned on the HD, the litho-facies simulations can reflect this bias. It is however possible to correct it by imposing proportions that differ from those of the HD, but further secondary information should then be used to guide the simulations. One possibility to correct that bias could be also to use geophysical data as we will discuss more in detail below.

Another important feature of the ArchPy approach is that it allows quantifying the uncertainty by generating an ensemble of models. The uncertainty can be evaluated at any desired hierarchical level among the units, sub-units, sub-sub-units, etc., lithofacies or properties. The uncertainty on the geological concept and Stratigraphic Pile (SP) itself can also be evaluated. This type of uncertainty was not covered in the example of the upper Aare valley where the concept was simple. But there are situations in which different geological concepts or different geostatistical models for the different components of the SP are plausible. Using the ArchPy approach and its scripting possibilities, it is straightforward to explore automatically all these possibilities and generate an ensemble of models that covers this uncertainty.

Due to its recent existence, ArchPy still lacks some interesting features and has several limitations. First of all, it is only usable through scripts in python which may prevent a certain number of people from using it. However, examples are provided and can easily be edited, therefore it is not necessary to be an expert in python to use ArchPy. This approach has many advantages such as ensuring efficient model update when new data are acquired or documenting accurately the model construction steps. In the future, one could construct a graphical user interface (GUI). The main limitation of ArchPy for the moment is that it assumes that the boundaries of the stratigraphic units can be modeled using functions that can be represented on a 2D grid. Therefore, ArchPy cannot for the moment represent overturned folds. It does not also include faults. We consider that these situations are extremely rare in Quaternary environments, adapting ArchPy to account for these structures would be feasible but is not currently a priority. ArchPy is also limited by the set of geostatistical methods that are proposed. It implies for example that the code may be slow if the number of borehole data and inequalities is important. We will continue to optimize the methods as much as possible. Concerning the simulation of non-Gaussian data, a normal-score transform should always be considered before using any GRF method. But the user must be aware that this kind of transformation is only suitable when the number of data is sufficient (a Cumulative Function Distribution can be built). When data are sparse, it is simply possible to assume that the data follow a normal distribution or the use of other available methods can be considered (MPS). Moreover, GRF simulations, performed on data normally transformed, do not guarantee that the covariance will be preserved in the original data space. The use of more advanced simulation methods such as Direct Sequential Simulation (Soares 2001) could be a solution. A final

note is about the trends in the data (surface elevations or facies proportions). Such behaviors can be modeled but not in a fully automated manner as it requires user-inputs (e.g. local facies proportions over the domain). These must be computed or derived externally. However, implementing such routines in future updates is straightforward.

Because it is simple and easy to run ArchPy automatically, it is straightforward to conduct parameter sensitivity analysis. We even suggest that the parameters should be tested as well as the stratigraphic pile including all its various geostatistical components using cross-validation. This approach should be used to test and compare different alternative SPs. The procedure consists in splitting the borehole data and applying a K-fold cross-validation approach as we discussed in a previous paper (Juda et al. 2020). An ensemble of models is generated to predict the units, lithologies, and properties at the location of a subset of the boreholes (removed from the HD). A score can be then computed to compare the quality of the stochastic predictions with the actual data. We plan to incorporate cross-validation frameworks inside the ArchPy architecture.

To go a step further, ArchPy is already coupled with several geophysical and groundwater flow simulation tools (Cockett et al. 2015; Bakker et al. 2016). Property models generated by ArchPy (e.g. resistivity, gravity, storativity, hydraulic conductivity, etc.) can be passed to forward models. The outputs are retrieved and compared with real field measurements which are then used to adapt the ArchPy models to reduce the misfit between both actual and simulated data. For example, this adaptation could be done in a Monte-Carlo scheme (Tokdar et al. 2010) or with ensemble methods (Chen et al. 2012). This approach opens the way towards geologically constrained joint inversion involving different forward models.

3.5 Conclusion

The ArchPy approach that is proposed in this paper combines many techniques that are well known (geostatistical simulation techniques for continuous or categorical variables). One important novelty is to separate formally the description of the list of tasks that are required to construct the model and the construction of the model itself. This is done by embedding all the geological and geostatistical knowledge in an object called "Stratigraphic Pile". Based on this formalism, a software can be constructed that can automate all the tedious tasks of the model construction. The python module that implements the ArchPy approach allows the fast and reproducible creation of an ensemble of stochastic models respecting both the conditional data and the user inputs (geological concepts). The only inputs required are the digital elevation model, the borehole data, and how to interpolate and simulate the different components of the model (surfaces, lithofacies, properties), the rest is up to ArchPy. The simulations take place during three main phases: simulation of the units, of the lithofacies

and then of the properties. Each step depends on the previous ones. A major novelty is that the stratigraphic pile allows defining a hierarchical stratigraphy and therefore allows modeling automatically consistent sub-units of any hierarchical level within units of higher levels. The code allows quantifying uncertainty using a sound geostatistical model. It also allows updating the model easily when new data are available or embedding the model construction into an inverse procedure. The code is open-source and freely distributed. Due to its open-source nature, the coupling with other software is facilitated. It opens the doors to an easier and more accessible geological modeling of Quaternary aquifers.

Chapter 4

An algorithm for identifying stratigraphic piles from interpreted boreholes

Abstract

The Stratigraphic Pile (SP) is one of the foundation of most geological studies. It represents, in a compact and practical way, a vertical succession of depositional events over geological time. Accurate definition of the SP is crucial for geological modeling, yet challenges arise when relying on borehole data in the absence of clear biostratigraphic indicators or chronostratigraphical data. This manuscript introduces an algorithm designed to automatically determine the SP using borehole unit sequences. The algorithm also addresses the complexities associated with incomplete sedimentological records and subjective geological interpretations. The algorithm was tested on various datasets, taking into account differences in the number of boreholes and available information. The efficiency of the algorithm was demonstrated through real-world applications, providing a basis for a comprehensive discussion of its advantages, limitations, and potential applications. The proposed methodology assumes each borehole vertical and containing at most one occurrence of a given stratigraphic unit, with consideration for possible interpretative errors and inconsistencies. With these considerations, instead of pursuing a single, perfectly consistent SP, the algorithm aims to establish an ensemble of plausible SPs capable of accommodating variations and uncertainties inherent in borehole data. This ensemble of SPs and identified inconsistencies provide valuable insights regarding the geological history and concepts for a specific area. This research contributes to the refinement of geological modeling workflows, offering a valuable tool for automatically refining the choice of the SP.

4.1 Introduction

The stratigraphic pile (SP), also often called parent sequence or stratigraphic sequence, is a major concept in the representation of sedimentary phenomena. It is defined as a vertical stack of distinct depositional events or stages, often called stratigraphic units, that have been deposited one on top of another over geological time. Crucially, the concept of time assumes a central role in defining these stratigraphic units. They are postulated to be bounded by isochronous surfaces (Boggs et al. 2012), underscoring the chronological order within the stratigraphic pile. Consequently, in the absence of tectonic activity, magmatic activity or sediment remobilization, a unit positioned above another is, by definition, younger.

Under normal circumstances, defining the SP is not a problem, as there is already a global geological time scale (Gradstein et al. 2020, GTS). However, its use depends on the success of correctly dating precise units and relating them to the different ages, epoch and era defined in the GTS. In the absence of clear biostratigraphic indicators or radiocarbon data, this task is difficult to achieve. Moreover, the GTS is defined at a coarse time scale where the finest type of unit is the stage, corresponding to periods of time generally lasting 1 million years.

In many cases, it proves more practical to define stratigraphic units with time scales that are tailored to the specific local geological conditions. This approach becomes particularly relevant when dealing with Quaternary deposits. In such geological setting, stratigraphic units are often delineated based on regional glacial stages, a practice well-documented in the literature (Penck et al. 1909; Schlüchter 1989; Graf et al. 2016; Buechi et al. 2018). These stratigraphies are often based on lithological features with a temporal notion (e.g.,Würmian moraines, Last Glacial Maximum retreating fluvioglacial deposits, interglacial between two glacial stages deposits, etc.). However, it is important to note that the identification of these units still involves a degree of subjectivity and is subject to the interpretation of geologists. As a result, there is often a level of uncertainty associated with such classifications. Mistaking two distinct moraines or river deposits with similar lithologies but deposited at different times could lead to inconsistent interpretations that do not align with the SP. This could cause significant issues in the geological modeling of these units.

In the special case where all the events forming the SP are present within a single borehole, the determination of the SP is straightforward. However, it is important to acknowledge that such complete sedimentological records are rarely encountered in practice. This scarcity of complete records primarily arises from the variability of sedimentological processes, including localized depositions and erosional events, which hinder the preservation of a comprehensive stratigraphic sequence, even on a local scale (Boggs et al. 2012).

The SP serves as a fundamental component in numerous geological modeling algorithms (e.g., Calcagno et al. (2008), Allard et al. (2021), and Schorpp et al. (2022)). Geological modeling typically follows a hierarchical workflow, beginning with the delineation of stratigraphical units using explicit or implicit surfaces. These units are then filled with facies using facies modeling algorithms, and finally, continuous values representing subsurface physical properties (e.g., porosity, hydraulic conductivity) are assigned to these facies.

The first step in this hierarchical process, the delineation of stratigraphical units using the SP, is of paramount importance. Inconsistencies in boreholes compared to a given SP must be identified and excluded from the modeling process. This is because geological modeling methods rely on bounding surfaces that assume a certain spatial continuity. When boreholes are inaccurately labeled or when an inappropriate SP is used, it can significantly complicate the generation of these bounding surfaces, resulting in incoherent and unrealistic geological models.

To tackle some of these issues, Allard et al. (2021) have proposed a methodology based on a Markov Chain Monte Carlo (MCMC) algorithm. But, their approach assumes that units having similar lithologies and are indistinguishable, such as multiple events of gravels, sand, etc. Consequently, it becomes challenging to link a particular gravel event in a borehole to another in the SP.

Using an MCMC approach and the likelihood of latent Gaussian fields, they proposed a method that samples plausible borehole configurations. However, it is important to note that this method requires prior knowledge of the SP, a challenge that the authors acknowledge remains unresolved.

If boreholes are in disagreement with the SP, a common solution is to exclude them from the dataset. This assumes that the boreholes have been falsely labeled and/or interpreted. However, it is important to verify the accuracy of the SP, as potentially important boreholes necessary for modeling could be mistakenly removed. It is possible that the interpreted units are actually lithofacies deposited over the same period of time, with potential local variations. Therefore, it may be more appropriate to consider these geological objects in terms of facies modeling rather than unit modeling. Various adapted algorithms, such as Sequential Indicator Simulation (Journel 1989), Multiple-Point Statistics (Mariethoz et al. 2010b), object-based (Wang et al. 2018) or process-based (Granjeon 2014)), exist for this purpose.

Therefore, the aim of this manuscript is to introduce and demonstrate the efficiency of an algorithm for determining the temporal sequence of distinct geological events, often referred to as a stratigraphic pile, using borehole data. The proposed algorithm is designed to determine the stratigraphic pile (SP) within a given area, relying exclusively on borehole data. This SP comprises distinct stratigraphic units. Assuming no tectonic activity, reorganization of deposits and that all boreholes are vertical, each borehole log contains only one or zero occurrence of each unit.

In addition, we acknowledge the possibility of erroneous borehole interpretations and the existence of inconsistencies (e.g., where unit B is situated below unit A, contrary to expectations). In such cases, the pursuit of a single SP that is perfectly consistent with all the borehole data becomes unfeasible. Instead, our objective shifts toward establishing an ensemble of plausible SPs that can account for these variations and inconsistencies.

The paper is structured as follows:

1. Initially, we explain in details the algorithm to retrieve the SP.
2. Subsequently, we test the algorithm on several datasets in order to confront it with different situations (more or less boreholes, more or less information in the boreholes).
3. Finally, we apply the algorithm to real data and we engage in a comprehensive discussion that delves into the advantages, limitations, and perspectives associated with the used methodology and its potential fields of application.

4.2 Methodology

4.2.1 Notations and definitions

Let us first consider a list of distinct deposit events that is called the stratigraphical pile $P = (K_1, K_2, ..., K_k)$, where K_i are the different units and k is the total number of units. Now consider a list of simplified boreholes $\mathbf{B}$, where each borehole B_i is defined as an ordered sequence of distinct units K_i, from younger to older, generally following the order of P. $B_3 = (K_2, K_3, K_5, K_7)$ is an example of borehole with four units and K_2 is the youngest and K_7 is the oldest.

Borehole logs can be incorrectly interpreted or have units that are not properly defined, leading to inaccuracies in the description of the boreholes, as in the case of P. The following algorithm takes these boreholes into consideration. It is important to note that the number of events in each borehole is, by definition, less than or equal to k, which represents the maximum possible number of events.

We also propose an alternative representation of the SP as a matrix M of size $k \times k$ where each row (index i) and column (index j) is attributed to one unit. These can be set in any order but it must be consistent between rows and columns. The entries (m_{ij} based on index or m_{K_i,K_j} based on units) of the matrix are integer numbers that can be either positive, negative or 0. We can read them as "number of times unit in row i is above unit in column j over the analyzed boreholes". A negative number indicates the inverse, i.e. the number of times that the event in row i is below event in column j. A value of 0 indicates that the relative position of these two events (i above j) is not known. Lastly, the diagonal elements ($i = j$) have no entries as it is meaningless to establish the relative position of an event with itself. In the end, the advantages of using a matrix are double: simple logical operations can be easily applied and the number of occurrences of each relative position can be quantified. The latter is particularly interesting when comparing multiple possible output piles.

4.2.2 Algorithm

The algorithm's core concept revolves around a sequential analysis of boreholes, where the entries of a matrix M are adjusted based on the relative positions of geological units within the boreholes. To illustrate this approach, let us consider a four-unit stratigraphic pile denoted as $P = (D, C, B, A)$ for the following examples.

To streamline the borehole analysis, we propose to focus on pairs of adjacent units within each borehole rather than examining the entire borehole at once. Each borehole is divided into $n - 1$ pairs of adjacent units, where n is the number of units observed in the borehole. To ensure all possible relationships

within the borehole are accounted for, including those involving non-adjacent units, we apply three geologically inspired analysis rules to update the pile represented by matrix M for each pair:

1. **Update the Contact:** This rule involves updating the direct contact between the units in the pair. For instance, if unit B is positioned above unit A, the entry m_{BA} is increased by 1, while m_{AB} is decreased by 1 to reflect this relationship.
2. **Propagation Upward:** Under this rule, all known units located above the top unit of the pair are considered to be above the bottom unit of the pair. Consider two pairs of adjacent units, (C, B) and (B, A), when analyzing the second pair, we can deduce that C is also positioned above B and, consequently, above A as well. Corresponding entries are increased (or by symmetry, decreased) by 1.
3. **Propagation Downward:** Similar to rule 2, this rule posits that all known units situated below the bottom unit of the pair are also below the top unit of the pair.

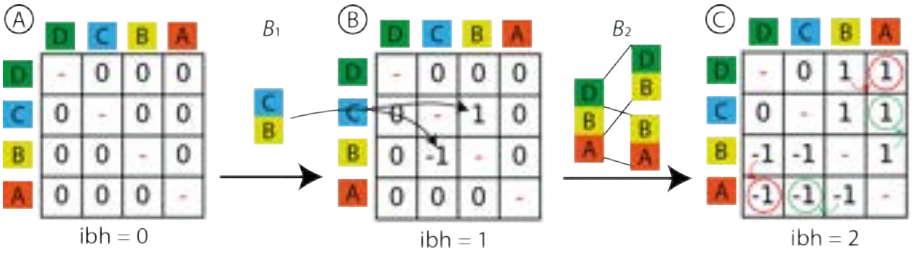

Figure 4.1: *Schematic visualization of the algorithm applied to two boreholes derived from SP of four units. The pile is represented as a matrix of size $k \times k$ where each entry can be read as "the number of times the unit in row i is above the unit in column j". The presence of a 0 indicates that the relative position of these two units is unknown. Black arrows are used to indicate an update of the contact (rule 1). Red arrows indicate a downward propagation (rule 3) while green ones indicate an upward propagation (rule 2). Black arrows are not shown in* $\boldsymbol{C}$ *for the sake of clarity.*

By sequentially applying these rules to pairs of adjacent units within the boreholes, we iteratively refine our understanding of the SP, updating the matrix M to better represent and quantify the relative positions of the geological units.

The Figure 4.1 is a representation how these rules work and how two boreholes are analyzed and integrated. First, an empty matrix of size 4×4 is defined filled with 0 in off-diagonals values (fig. 4.1A), let us call it $M^{(1)}$. A first borehole $B_1 = (C, B)$ is analyzed and by applying rule 1 (update the contact) we can ascertain that C is above B and increment $m^{(1)}_{CB}$ by 1 (and by symmetry, decrement $m^{(1)}_{BC}$ by 1), giving the matrix in Figure 4.1B. Rules 2 and 3 are also applied but as no other information is available (all the others entries are 0), they have no effect. Considering borehole $B_2 = (D, B, A)$, it is initially divided into two pairs, (D, B) and (B, A). These pairs are then analyzed in chronological order, from older (deeper) to younger (shallower). In this case, (B, A) is the first pair to be considered. By applying rule 1, $m^{(1)}_{BA} = 1$ and $m^{(1)}_{AB} = -1$ and by applying rule 2, we know that C is above B (because $m^{(1)}_{CB} > 0$), we add this relation to A as well $m^{(1)}_{AC} = -1$ and $m^{(1)}_{CA} = 1$ (green arrows, fig. 4.1C). Second pair, (D, B) is analysed similarly, first the contact is added $m^{(1)}_{DB} = 1$ and $m^{(1)}_{BD} = -1$. By rule 3, as D is above B, D is also above A ($m^{(1)}_{AD} = -1$ and $m^{(1)}_{DA} = 1$, red arrows fig. 4.1C). After only these two steps, the pile is at this step (ibh = 2, fig. 4.1C) nearly defined. The only contact that is uncertain is the relative of position of C with D which is still 0. An ambiguity that can only be solved if a borehole that contains these two units is analyzed.

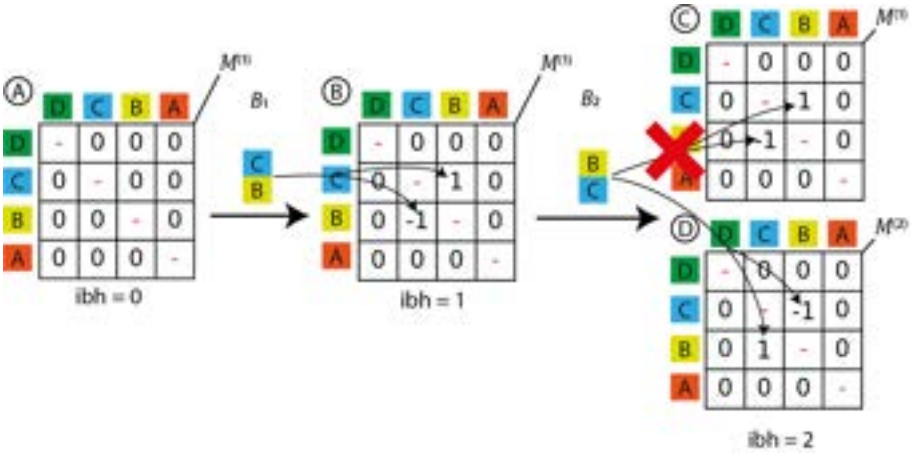

Figure 4.2: *Inconsistent boreholes. In this case, the borehole B_2 is in direct contradiction with the pile $M^{(1)}$ in **B**, which means that it cannot be added to pile $M^{(1)}$ (**C**). In such cases, a new empty pile is created $M^{(2)}$ and problematic borehole added to it (**D**).*

It is important to note that during the update, it is necessary to ensure that a negative number is not increased or that a positive number is not decreased. Such updates would be in direct contradiction with the existing matrix, indicating that the analyzed borehole is inconsistent with the current SP. This is shown in Figure 4.2. In this example, the borehole B_2 cannot be added to

pile $M^{(1)}$ because it would require to increase $m_{BC}^{(1)}$ by 1 and $m_{CB}^{(1)}$ by -1, which eventually would lead to go back to a fully empty matrix. This is an inconsistency. To address such inconsistencies, we propose creating a new and empty matrix $M^{(2)}$ which is equivalent to creating a new pile. This process involves initially analyzing the problematic borehole and then reanalyzing all previously examined boreholes, consistently applying the rules, but this time inconsistent boreholes are ignored. From now on, boreholes are analyzed not on only one matrix but two ($M^{(1)}$ and $M^{(2)}$). This list can be expanded given the encountered boreholes, allowing all boreholes to be reproduced using different SP, taking into account the different spatial configurations of the units.

Ultimately, each SP is assigned a score, calculated based on the percentage of boreholes that align with it. This can be done in several ways, such as retesting all boreholes for all piles once the piles have been determined, or keeping track of the number of boreholes used by each pile during the process.

A summary of all the different steps is given in Algorithm 4.1.

Algorithm 4.1

Require: Parameters
  B : set of boreholes B_i
  k : number of expected units in the pile
Initialize an empty list of matrix l_M
Create a first zero-matrix $M^{(1)}$ of size $k \times k$ and add it to l_M
Set number of piles $n_M = 1$
for $i \leftarrow 1$ to n_{bh} **do** ▷ Loop over the boreholes
  for $o \leftarrow 1$ to n_M **do** ▷ Loop over the piles
    if B_i compatible with $M^{(o)}$ **then**
      Split B_i in pairs and update $M^{(o)}$ given the three rules
    else
      Create a new zero-matrix $M^{(n_M+1)}$ of size $k \times k$
      Split B_i in pairs and update $M^{(n_M+1)}$ given the three rules
      for $j \leftarrow 1$ to $i-1$ **do** ▷ Loop on previous boreholes
        if B_j compatible with $M^{(n_M+1)}$ **then**
          Split B_j in pairs and update $M^{(n_M+1)}$ given the three rules
      add $M^{(n_M+1)}$ to l_M and $n_M = n_M + 1$
Deliver l_M

Once all matrix piles have been estimated, they can be back-transformed into their natural representation. The relationship between the two pile representations is simple. The position of each unit in the pile can be determined by counting the number of positive entries n_p for each column (e.g. for unit at index j, $n_{pj} = \sum_{i=1}^{k} m_{ij} > 0$). Alternatively, the number of negative entries n_m can also be used (e.g. for unit at index j, $n_{mj} = \sum_{i=1}^{k} m_{ij} < 0$). If no

positive entries are found, the unit is at the top of the pile, if one is found, it is at the second position, and so on. This only works for a perfectly defined pile, when there are no zero entries in the matrix. When this is not the case, it is more complicated and units can have several positions. In such cases, it is necessary to determine the possible positions for each of the uncertain units (with 0 entries in their column/row). For example, consider a unit at index j, the possible positions range from $n_{pj} + 1$ to the total number of units minus the number of negative entries found in column j ($k - n_{mj}$).

As an illustration, the back transformation of the matrix shown in Figure 4.1C is made. Units B and A have respectively two and three positive entries which means that they are positioned in three and four positions of the pile. However, units C and D have both 0 positive entry (and two negative entries) which means that several positions are possible. These can be obtained by applying the previously introduced expressions, the possible positions range from $0+1 = 1$ to $4 - 2 = 2$. Final pile is then $P = ((D, C), (D, C), B, A)$.

4.3 Results

4.3.1 Synthetic data application

Synthetic datasets are employed to demonstrate the algorithm theoretical capacity to deduce the SP based on a restricted set of boreholes. We consider two distinct scenarios:

1. **Case 1**: In this scenario, all boreholes originate from the same SP and are in concordance with each other.
2. **Case 2**: This scenario explores a situation where various SPs are employed to generate different sets of boreholes.

The objective is twofold: to demonstrate the algorithm's generability and to identify any anomalies or errors in the dataset. In the context of a SP comprising k distinct units, n_{bh} boreholes are generated assuming a constant probability of occurrence, denoted as p_{occ}, for each unit. As an extreme illustration, if $p_{occ} = 1$, it implies that all boreholes will be identical to the SP because each unit has a probability of 1 to be present (having been deposited and not eroded). For simplicity, we assume this probability to be constant for every unit. Potential issues associated with this simple way of generating boreholes will be discussed later.

Case 1

Figure 4.3 presents two distinct synthetic sets, each comprising $n_{bh} = 20$ boreholes (Fig. 4.3A and Fig. 4.3C), generated using the same pile $P =$

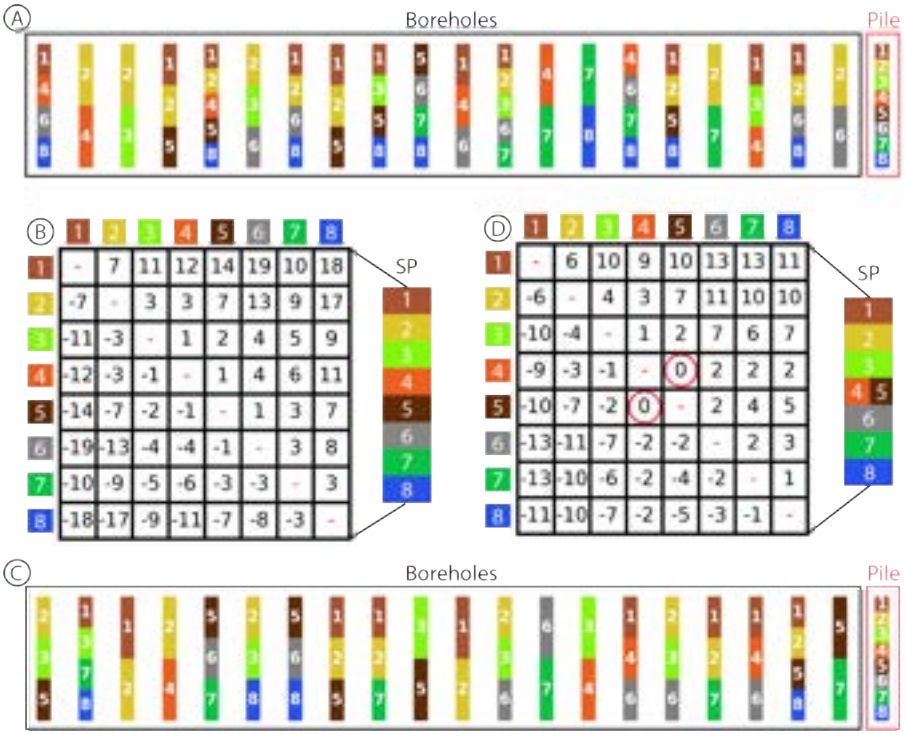

Figure 4.3: *Stratigraphic Pile inference (**B** and **D**) from two synthetic datasets (**A** and **C**, respectively). The inferred piles (**B** and **D**) are shown beside the matrix in standard form. Red circles indicate an uninformed contact (entry equal to 0).*

$(1, 2, 3, 4, 5, 6, 7, 8)$ of size $k = 8$ with a constant $p_{occ} = 0.3$ assigned to each unit.

Considering the first set (Fig. 4.3A), the resulting matrix, as obtained by applying Algorithm 4.1, is depicted in Fig. 4.3B. Note that despite the relatively low number of boreholes (20) and the low probability of occurrence (0.3), the SP is accurately and entirely determined (no 0 entry).

Similar results were obtained with the second dataset (see fig. 4.3C). However, an undefined contact was observed this time (entry m_{54}) due to the absence of an occurrence of unit 4 above 5 among the boreholes. This contact is present in the first borehole set (see fig. 4.3A) and explains why the first pile was completely found. In the second case, the inferred SP is still very close to the reference pile and clearly identifies the missing contact in the dataset. The final choice of SP lies with the user, who can rely on prior geological knowledge to determine the correct SP.

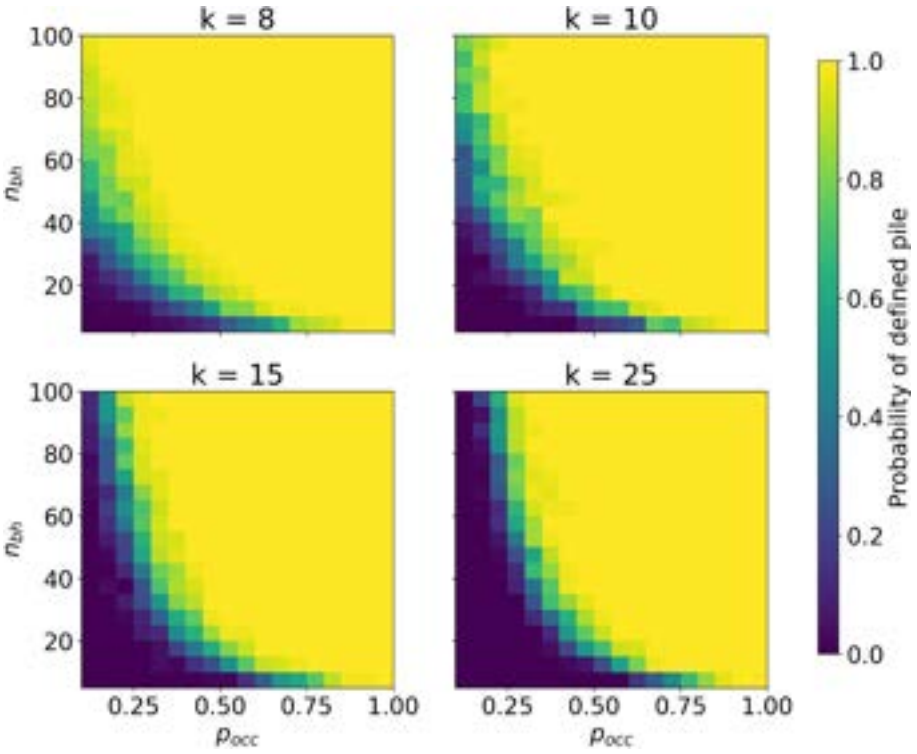

Figure 4.4: *Probabilities of getting a defined pile (no 0 entries) based on number of units in the pile (k), number of boreholes (n_{bh}) and the probability of unit occurrence p_{occ}.*

Based on the previous results, we saw that with the same settings and parameters, two different borehole sets can give different results. We then investigate the effect of p_{occ} and the number of boreholes (n_{bh}) on the chance of retrieving the SP. The results are shown in Figure 4.4 where these probabilities have been computed with different sets of parameters for different number of units in the pile (k).

As expected the chances of identifying the input pile increases with n_{bh}, p_{occ} but decrease with k. We can observe that if $p_{occ} > 0.5$, the SP is always easily defined with a probability nearly always greater than 0.8, even when the there is few boreholes. For lower values of p_{occ}, the required n_{bh} vary between 20 and 50 for getting similar results, except when k is too high. Indeed, k is also important to consider, as the greater the number of units to be determined, the more difficult it is to estimate the SP. This effects is particularly visible for low p_{occ} values where even 100 boreholes are not sufficient to determine a pile with 15 or 25 units. Generally, the fringe between undefined and well defined piles (0 and 1) is asymptotic near x and y axis which makes sense, because

as we approach the x-axis (n_{bh} close to 0), there is no longer enough data to determine the SP, even if p_{occ} is high, and vice versa.

Case 2

This second case investigates the effect of having boreholes that are not completely consistent with each other (i.e. generated using different SP). In fact, data are often inconsistent for a number of reasons such as potential errors in the data, units have been badly defined or the SP is locally varying. With this example, we show how to outline these problems. For this case, we use four different SPs (fig. 4.5A) and generated 80 boreholes, 50 with the first pile using $p_{occ} = 0.5$, 10 with the others using $p_{occ} = 0.3$ for generating less informative boreholes.

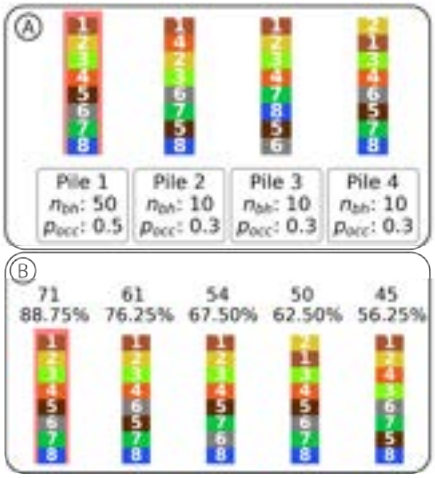

Figure 4.5: *Second synthetic case results.* ***A****: SP and parameters used to generate boreholes. Main pile is surrounded by red. The resulting SPs after the analysis of the 80 boreholes by Algorithm 4.1 are shown in* ***B*** *along with total number and proportions of boreholes in agreement with the pile. Main pile is surrounded by red.*

The algorithm 4.1 found 5 resulting piles (fig. 4.5B), where the most probable one is also the main pile. This demonstrates that in this specific context, it is able to retrieve the main SP from which the boreholes originate. The other piles found are not identical to piles 2, 3 and 4 in Figure 4.5A, probably because there are fewer boreholes generated with these piles and also because they are less informative than the ones from the main pile. However, in these reconstructed piles, we can observe patterns of our own in Piles 2, 3 and 4. For example, in the 2nd most probable pile, unit 6 is above unit 5, a relationship found in Piles 2 and 4. Or in the 4th most likely, unit 2 at the top of the pile is necessarily taken from a borehole in Pile 4.

4.3.2 Real data application

The study site is located in Switzerland, in the Alpine Rhine Valley (fig. 4.6A). It consists of a wide valley of about 230 km^2, carved out by Quaternary glaciers and filled mainly by the Rhine, an essentially fluvial environment. A large number of boreholes (1569) have been drilled, homogenized and digitized in the context of the GeoQuat project (Volken et al. 2016).

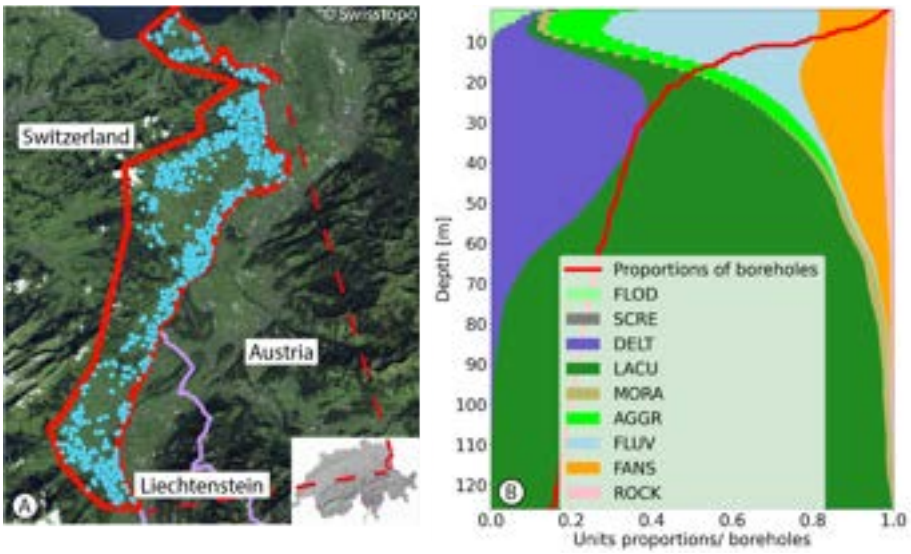

Figure 4.6: ***A****: the red area represents the geographical location of the Rhine Valley, situated at the boundary between Switzerland, Austria, and Liechtenstein. The blue dots on the map indicate the locations of the boreholes that have been collected and digitized by Swisstopo.* ***B****: Evolution of unit proportions and proportions of boreholes reaching a certain depth. Note that data have not been declustered to estimate the proportions. ARTI unit was discarded from the analysis as it is only present on the first meters of depth.*

The geology of this valley is a result of the Rhine river's filling process. The oldest unit found is a moraine (MORA), which is typically associated with the Last Glacial Maximum. It generally follows the bedrock with a thickness of several meters and is generally observed on the sides of the valley. Above it we find lacustrine deposits (LACU) that are themselves below a unit composed of delta sediments (DELT). These two units composed most of the valley infill. Time order of younger sedimentological units is less clear, presuming that some of them were deposited synchronously. Regarding the river deposits, we have direct deposits from the Rhine bed (FLUV) that are mainly composed of gravels and sands, and aggradation deposits (AGGR) that present finer sediments. These river deposits are often covered by flood deposits (FLOD). Aside from the deposits from the Rhine river, we can also observe a significant number of alluvial fans from lateral valleys (FANS) and rock avalanche deposits (ROCK) that are very local and present in few boreholes. Recent scree deposits (SCRE)

are sometimes observed but their proportion in relation to other units remains very low. Finally, soil and artificial deposits (ARTI) generally covers the units.

In total, there are 10 distinct stratigraphical units that have been identified, and their observed proportions in boreholes relative to depth are illustrated in Figure 4.6B. It is clear that the proportions of these units are not equally observed in the boreholes. While some units are quite prominent (LACU, DELT, FLUV), others are barely visible (e.g., MORA), and some are virtually absent, like SCRE, which indicates a poor spatial distribution.

The data were preprocessed and all boreholes that present several occurrences of the same unit were removed from the dataset ensuring that all boreholes can be analyzed with Algorithm 4.1. This reduces the total number of boreholes to 1481 (a reduction of about 5.6%). These multiple occurrences of units are always in pairs, where two units are intertwined. Most common pairs include, by occurrences, (AGGR, FLUV), (AGGR, FANS), (LACU, DELT) and (FLUV, FANS) while others are only observed 1 or 2 times.

The results of Algorithm 4.1 are shown in Figure 4.7A. For consistency not all the piles are shown here and only the five best over eight piles are presented and discussed.

We can note that despite the high number of boreholes, ambiguity still remains in the definition of the piles. Generally due to the relative position of FLOD and SCRE units. This can be explained by the scarcity of the SCRE unit occurrence in the boreholes, implying that these two units have not been observed together. This is not surprising as flood deposits are generally observed near the river (eastern side of the area). Scree deposits on the other hand, are located close to the relief (western side of the area).

All SPs exhibit a high level of agreement with boreholes, ranging from 90% to 96%. While there are notable similarities among the piles (e.g., the presence of DELT, LACU, MORA at the base and ARTI, FLOD at the top), there is also some variability. Specifically, the positions of FANS and AGGR shift in several instances, suggesting that these "units" might actually represent different lithofacies deposited during the same time interval. In certain piles, AGGR is found below FANS and FLUV, while in others, it is above them. FLUV is consistently located just above DELT, except in a few cases (#4 and #5) where AGGR lies in between. Additionally, ROCK consistently appears just above FLUV in all piles.

To quantify these discrepancies, an analysis of boreholes that do not align with a particular pile was conducted. Figure 4.7B displays the three most common unit contacts that conflict with pile #1. Approximately 2.2% of boreholes (32) show FLUV above AGGR, which is the primary source of disagreement with pile #1. The second most common discrepancy is AGGR above FANS, observed in

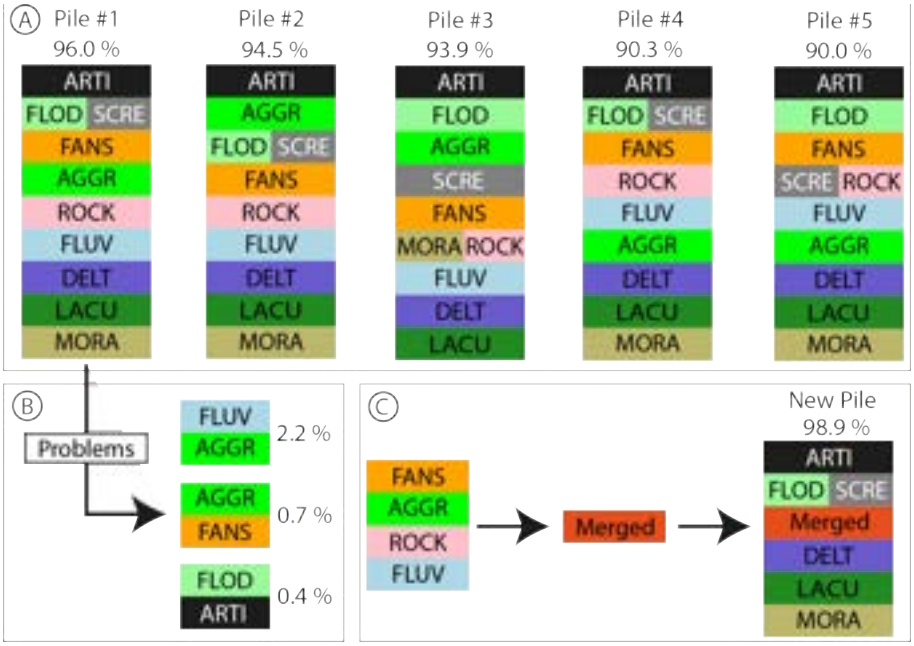

Figure 4.7: ***A****: Five most plausible SP found for the Alpine Rhine Valley using the algorithm. When two units are side by side it means that their relative position is unknown. Percentage indicates the number of consistent boreholes with this pile.* ***B****: Inconsistent unit contacts observed in boreholes that are not in agreement with Pile #1 with proportions of boreholes concerned.* ***C****: Proposition of merging some "units" into one stratigraphical unit to increase the number of boreholes in agreement.*

0.7% of boreholes (11). Interestingly, six boreholes (0.4%) exhibit FLOD above ARTI, which was unexpected. However, this observation should be interpreted cautiously, as more than 100 boreholes show the opposite arrangement (ARTI above FLOD), raising doubts about the authenticity of these six boreholes. The remaining conflicts are only observed in one or two boreholes and were consequently considered as irrelevant.

From these results, it makes sense to consider that the FLUV, FANS and AGGR deposits can be considered part of a single stratigraphic unit. These diverse lithological deposits may be interpreted as lithofacies, encompassing fluvial deposits on one hand and episodically deposited alluvial cones on the other. In between, there are aggradation deposits associated with the river system. Consequently, consolidating these units into a single entity (as depicted in fig. 4.7C) would make sense. This operation raises the overall agreement with boreholes to nearly 99%. Furthermore, by merging these units, many boreholes that previously contained multiple occurrences of the same units would no longer exhibit such redundancy, particularly with respect to the FANS, AGGR, and FLUV units. The inclusion of unit ROCK in the merging was primarily

driven by its consistent occurrence just above FLUV. Given that FLUV was merged, it logically follows that ROCK should be incorporated as well.

Importantly, the decision to merge units should always be driven by a valid geological concept that can elucidate why these three stratigraphic units are, in fact, not distinct. Merging implies that these three formations are heteropic facies (i.e., lithologically different but of the same age), which can have significant implications for their modeling process. Additionally, it is crucial to consider the number of boreholes affected by this merging. In this case, nearly 3 % of the boreholes (45) became consistent with the pile. This number can serve as a justification for such a decision, suggesting that these boreholes may not have been inaccurately labeled.

4.4 Discussion

The presented results, both synthetic and applied, demonstrate the algorithm's ability to efficiently infer the SP or determine problematic contacts if it is not possible. The algorithm's success is highly dependent on the number of boreholes and the probability of occurrence of different units in the boreholes. Determining the absolute position of a rarely observed unit is more challenging. However, the algorithm considers relative positions (through rules 2 and 3) to define their location in relation to a certain number of units. For example, in the applied case of the Rhine Valley, the SCRE unit is rare (present in 2-3% of boreholes), yet it is still possible to identify that it is always located above the majority of the other units.

In addition to its ability to determine the stratigraphic pile, this methodology offers the advantage of automatically identifying and quantifying potential errors in the data or the geological concept itself. Errors can be detected based on the frequency of occurrence. For instance, if unit B is observed above unit A in 100 boreholes, but in just one borehole, unit B is observed below unit A, it raises questions about the accuracy of the latter interpretation. However, if this observation is made in 20 boreholes, it becomes reasonable to question whether these two units are indeed of similar ages, implying that they might not be distinct stratigraphic units.

This brings about several conceptual questions, and it is important to recall that the aim of the present algorithm is to automatically find the sequence of stratigraphic units, units with different ages of deposition. Under normal circumstances, this sequence is known and serves as the basis for the interpretation of the boreholes, interpretation that normally is expected to respect the pile. However, the boundary between units and facies is sometimes blurred, as it is easier (and more natural) to interpret a geological horizon based on its lithology (granulometry, structure, mineralogy, etc.) than its age. As a result, it is entirely possible that some boreholes could be misinterpreted, but also that

the geological concept behind them (the stratigraphic pile) could be wrongly conceived. This is particularly true in the case of the Rhine Valley (Figure 4.6 and Figure 4.7). In this case, many of the so-called stratigraphic units were, in fact, facies deposited over an identical time span. We were able to show that the 4 units FANS, AGGR, ROCK, and FLUV make more sense, stratigraphically, grouped together than separated. Their delineation would require further geological investigations to capture their spatial arrangement and heterogeneities in order to apply adapted facies modeling algorithms.

The choice of this grouping is also reinforced by the presence of a number of boreholes containing multiple occurrences of these same units. Such boreholes actually make no sense if these units are considered different, as an event that is supposed to occur within a single time span cannot be observed more than once. However, by considering them as part of a single unit, these problems disappear. Finally, the methodology used in this article has enabled us to perform an initial stratigraphic analysis of the boreholes, to determine a plausible SP and to provide clues for rethinking the geological concept of certain units.

Results obtained from synthetic examples should be treated with caution. Indeed, the model assumed to generate the boreholes is very simple and based on a simple probability of presence or absence of the unit, largely missing the great complexity of sedimentological systems. Furthermore, some geological units may naturally occur less frequently, resulting in a lower likelihood of being encountered in borehole data. This lower likelihood adds to the algorithm's challenge in accurately determining their positions in the stratigraphic sequence, as demonstrated in the specific case study.

Furthermore, it is essential to consider sampling bias when dealing with real geological data. Boreholes are frequently located near towns or villages and are typically drilled to relatively shallow depths. As a result, certain geological units may not be encountered or be poorly encountered. This sampling bias can introduce limitations and affect the performance of the algorithm, but as it has been demonstrated, this does not prevent to define a coherent SP for the Rhine valley.

This algorithm has direct applications, mainly providing piles for software that require them such as Geomodeller (Calcagno et al. 2008), GemPy (de la Varga et al. 2019), or ArchPy (Schorpp et al. 2022). However, the presented algorithm may pose challenges for Geomodeller and GemPy due to their ability to consider a wide range of geological settings, including folded or faulted environments, which contradict the assumptions made in the algorithm. However, it can still be used if the polarity of the layers in each borehole can be determined. ArchPy is an ideal python module for Quaternary environments where folds or faults are absent. In terms of availability, the present algorithm has already been

integrated into ArchPy's GitHub repository [5], as well as the synthetic examples of this study.

4.5 Conclusion

Using a matrix approach and simple logical rules, the algorithm presented showed that it was capable of retrieving a stratigraphic pile (SP) given a limited set of boreholes. However, this greatly depends on the "completeness" of the boreholes and how a unit is likely to be recorded, as well as the total number of units in the SP. All in all, the algorithm and methodology presented in this research have a number of interesting benefits:

- a way of determining plausible stratigraphic sequence automatically;
- identify potential falsely labeled boreholes;
- quantification of the vertical relations between the units;
- and finally, help to rethink the geological concept of stratigraphical unit of a certain area.

Additionally, the synthetic cases presented help to investigate the limits of the approach. We have notably investigated the effect of several parameters such as the number of boreholes required to estimate a complete pile. We found that this is dependent on the total number of units in the pile, but principally to the probability of a unit to occur in the pile. In some cases, if this probability is too low (< 0.10), even with more than 100 boreholes, the pile can hardly be determined. Conversely, if this probability is high enough (> 0.5), 20 boreholes are sufficient in most cases.

Finally, this tool should not only be seen as a simple tool for determining the stratigraphic pile, but rather as an aid in the pre-processing of geological data and in the construction of the geological conceptual model. Therefore, its applications are wide and diverse.

[5] http://www.github.com/randlab/ArchPy

Chapter 5

Three dimensional geological modeling of the Rhine valley using ArchPy

Abstract

This study presents a three-dimensional geological model of the Rhine Valley near Buchs in the canton of St. Gallen using ArchPy, a free open-source geological modeling software. The hierarchical approach is based on a formal description of a stratigraphic pile that is then used by the code to build the 3D model automatically. It provides a rapid synthesis of the available data, an initial analysis of the data in order to define the stratigraphical pile, and describes the modeling strategy. Various geostatistical approaches have been considered depending on the units: classical Gaussian Random Functions (GRFs) for surfaces and Multiple Point Statistics (MPS) simulations for syndepositional units. The MPS approach required a Training Image (TI) that was built using an object-based model, attempting to reproduce the main features of the geological setting of the units concerned (VERL, BAC, and FLUV). The K-fold cross-validation showed that the model is capable of reproducing the units with an overall precision of the order of 80%. The good results obtained on FLUV, VERL, and BAC units show that the MPS method combined with the object-based TI was efficient in reproducing and simulating these units. Overall, ArchPy's flexibility and robustness enabled us to combine different interpolation methods to better characterize the valley's intricate Quaternary geology.

5.1 Introduction

The geology of the Quaternary Rhine valley, situated near Buchs in the canton of St. Gallen, is intricate and has not yet been modeled using up-to-date tools. Therefore, we propose a geological model using the recently developed (Schorpp et al. 2022). The code is available in open access[6]. It is a hierarchical approach based on a formal description of a stratigraphic pile. Once the pile is defined, the code uses this description to automatically build stochastic 3D realizations of the study site.

In ArchPy, this stratigraphic pile encompasses several hierarchical levels. First, it describes the order in which the sedimentary units have to be modeled, according to their deposition chronology. Second, the pile contains also the description of the modeling methods used for each geological formation that needs to be modeled. ArchPy uses a set of embedded geostatistical methods to interpolate surfaces delimiting vertically the geological units, and the litho-facies and their properties populating the delimited units. Furthermore, ArchPy allows quantifying uncertainty by generating multiple realizations. ArchPy integrates an algorithm that automatically processes borehole data to extract necessary information for surface interpolation while maintaining data integrity. The resulting realizations are compatible with the conceptual model (the pile) and borehole data.

[6]https://github.com/randlab/ArchPy

This chapter presents an application of the ArchPy approach to a real case, including the selection of modeling method and related parameters. It provides a concise summary of the available data, an initial analysis to define the stratigraphic pile, and an explanation of the overall modeling strategy. Additionally, this chapter proposes a model validation using a cross-validation approach. The chapter is structured as follows: Section 2 describes the modeling site and presents the data. Section 3 explains how the stratigraphic pile was defined using the novel algorithm presented in Chapter 4. Section 4 presents the global methodology and modeling parameters. Section 5 depicts the obtained models and their cross-validation. Finally, Sections 6 and 7 conclude this chapter by discussing limits and future perspectives for the present models.

5.2 Site description and data summary

The modeling area is about 228 km^2 and covers the whole Swiss side of the Rhine Valley between the city of Buchs SG and the Bodensee. The simulation area is defined on the basis of the shape file provided by Swisstopo (Fig. 5.1).

The data consists of a set of 1569 boreholes described in terms of stratigraphic units. The data are numerous but not evenly distributed. The largest number of boreholes are located in the northern part of the area. They are also generally deeper there than in other locations. The ArchPy modeling approach considers 3 different hierarchical levels: 1) the stratigraphic unit, 2) the litho-facies and 3) the petrophysical properties. In this study, the aim is to model stratigraphy solely. It means that we are mainly concerned with the first hierarchical level of ArchPy, and we need to establish the stratigraphic pile.

A total of 36 different units are reported, of which 33 need to be modeled. The remaining 3 are neglected as they are artificial deposits and only present locally near the surface. These are the different Bachschutts (BAC, 24 units) that are very local, Bergsturtz formations (BERG, 2 units), Deltasediment (DELT, 1), Fluviatiler schotter Rhein (FLUV, 1), Hangbildungen (HANG, 1), Lackustrisches sediment (LAKU, 1), Moräne (MORA, 1), Überschwemmungssediment (UEBE, 1), Verlandungsbildung detritisch (VERL, 1). For simplicity during the analysis, the 24 Bachschutts have been grouped together, as have the Bergsturtz formations. In the end, nine base units are modeled; the different Bachschutts and Bergsturtz are identified uniquely but only in a second stage.

A certain fraction of the boreholes (5.5%) contain multiple occurrences of the same units along the vertical in their log descriptions. Normally, as a stratigraphic unit corresponds to a given stratigraphic interval (geological age interval), this should not happen. This situation occurs because the stratigraphic codes correspond to deposits occurring simultaneously, but having different natures (slope deposits on one side of the domain, and fluvial deposits in another area for example). These multiple occurrences involve the following pair of

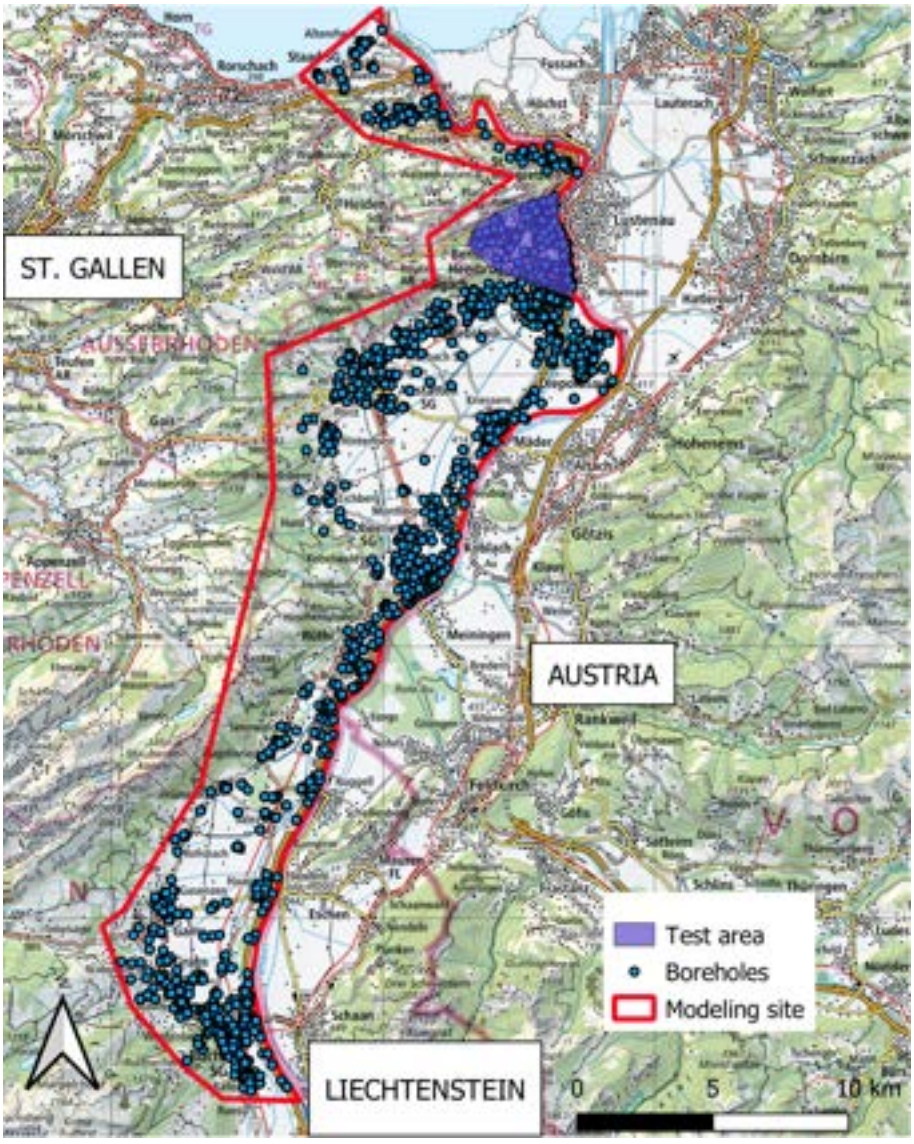

Figure 5.1: *Modeling site whose extent is defined by the red polygon. Blue dots are the available boreholes of the area.*

units: (FLUV, VERL), (BAC, VERL), (FLUV, BAC), in 75% of the concerned boreholes and they involve to a lesser extent (LAKU, DELT). However, compared to the total number of boreholes containing these units, multiple occurrences of (LAKU, DELT) were only found in 3% of the boreholes that contained both units. In contrast, the ratio was almost 20% for the pair (FLUV, VERL). It is suggested that boreholes with multiple occurrences of LAKU and DELT units can be reasonably neglected without significantly affecting the modeling results. However, it is necessary to address the other boreholes with multiple occurrences.

The vertical proportion curves of the different units have been computed from the boreholes and are shown in Figure 5.2. First, it is important to consider this Figure with caution, as those statistics are affected by two sampling biases. The boreholes are not evenly distributed throughout the study area. Some areas are extremely densely sampled, while others are not covered at all by any wells (Fig. 5.1). A second aspect of the bias is related to the depth. The shallow units tend to be over-represented because most of the wells were drilled to reach shallow targets.

Nevertheless, Fig. 5.2 shows significant changes in terms of distribution of units with depth. The most frequent units at shallow depth are FLUV, UEBE and the different Bachschutts. But they tend to disappear with depth. Some older units in the pile (LAKU, DELT) become dominant. The transitions are usually very smooth. It is also interesting to note that all units are represented at shallow depth (< 5m), which implies a great variety of possible environments at this depth. At larger depth (below roughly 90 meters) the data show almost only the presence of lacustrine sediments and very marginally moraines. However, the data are much less scarce and therefore this absence of variability may be simply due to the lack of sufficient data at that depth. However, we observe nearly 20% of the data at these depths which assumes that the number of data is however sufficient.

5.3 Stratigraphic pile identification

A more detailed statistical analysis of the boreholes allows to determine the possible stratigraphic piles for the area (Fig. 5.3). The algorithm presented in chapter 4 was used for this purpose. The Rhine valley was also used as a test case in this chapter, but the major difference with the present chapter is that the superficial and anthropic units have been taken into consideration. This explains the slight differences that can be observed in terms of percentage of match. For the analysis, only the boreholes where there were no multiple occurrences of the same unit have been taken into account. They represent around 95% of the boreholes.

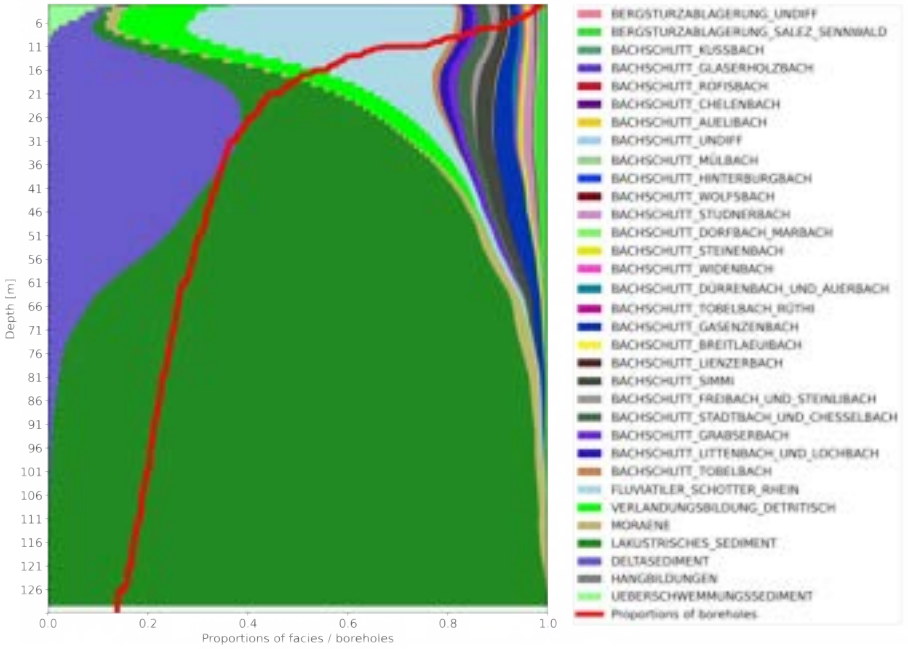

Figure 5.2: *Vertical proportions computed from the boreholes on the modeling site. Red lines indicates the proportions of borehole information that can be found at a specific depth.*

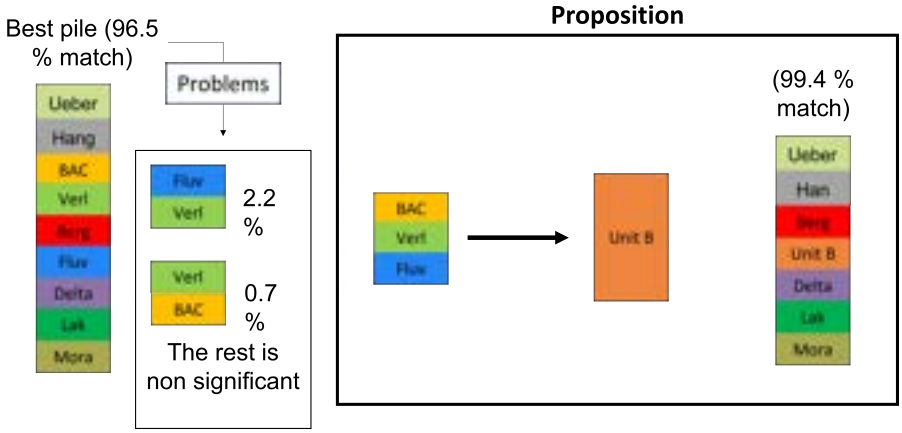

Figure 5.3: *Pile analysis summary. The % of matches correspond to the proportions of boreholes in agreement with the given pile.*

The pile that matches the largest number of boreholes in the area (96.5%) is shown on the left side of Figure 5.3. If we consider the stratigraphic contacts that are in disagreement with this pile, most of the time it concerns a set of 3 units: FLUV, VERL, and BAC. As discussed in the previous section, we think that these units should be treated as syn-depositional and not distinct units. Consequently, they would need to be modeled as a litho-facies, allowing them to be intertwined. To do so, we propose to group these three units into one (called "Unit B") which allows now to have a Pile that matches 99.4% of the boreholes. The proposition of grouping these units is also reinforced by the fact that they often appear several times in a borehole. This stratigraphic unit B represents then a syn-depositional phase, during which the three lithological units (BAC, VERL and FLUV) were deposited simultaneously but inhomogeneously spatially.

5.4 Methodology

5.4.1 Overview

The aim of this application was to produce a stratigraphic unit stochastic model of the Rhine valley. Due to the choice of regrouping some units into one, the public version of ArchPy has been slightly modified to the specific situation encountered in the Rhine valley.

The methodology can be summarized in three main steps: (1) the units simulation, (2) the subunits simulation, and (3) the delimitation of the different Bachschutts. The whole procedure is illustrated in Figure 5.4.

First, we apply the ArchPy approach to simulate the 2D surfaces delimiting the units using the pile defined in the previous section (Fig. 5.3) using Gaussian Random Fields (GRFs). The covariance parameters are inferred directly from the borehole data, except for a few underrepresented layers. In such cases, conceptual knowledge was used to determine a compatible variogram.

Secondly, the subunits that have been grouped together in unit B (the different Bachschutts, VERL, FLUV) are simulated using a 3D categorical geostatistical method: Multiple-point statistics (MPS). The geological concept required for the MPS simulation has been made using an object-based approach.

Then, the different Bachschutts are assigned within the large Bachschutts unit using a nearest-neighbor algorithm. A similar procedure is applied for the Bergsturtz deposits. This step does not change where the Bachschutts are deposited spatially, but just assigns them the specific Bachschutt label observed the closest in the borehole data set.

To test the quality of the models, we performed a K-fold cross-validation analysis. The wells are divided into groups and a simulation is performed intention-

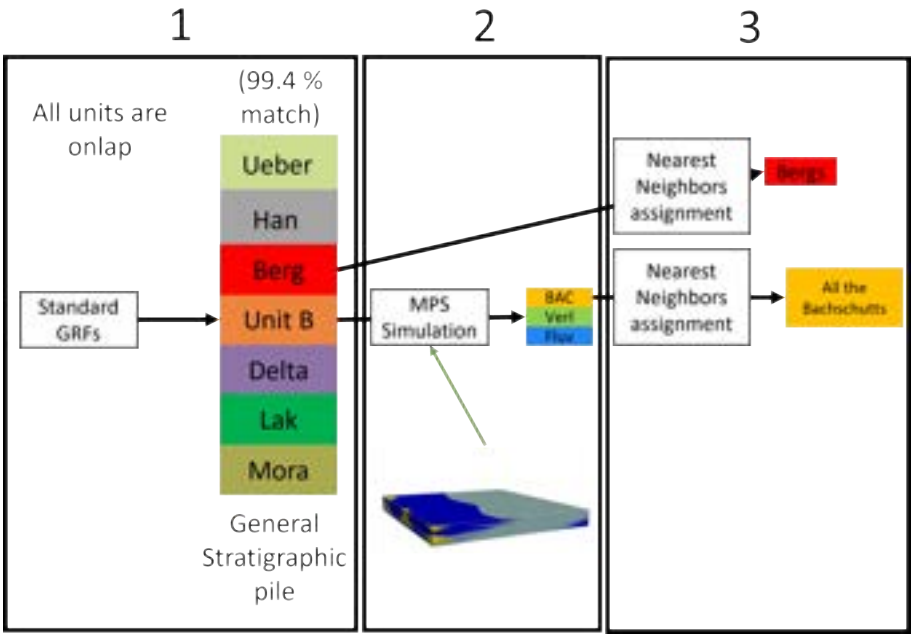

Figure 5.4: *Modeling workflow. It is divided in three steps:* ***1)****: Simulation of the major units that consists of strict stratigraphic units. They are simulated using 2D stochastic surfaces.* ***2)****: Categorical MPS simulation of the Bachschutts, Verlandungsbildung detritisch and Rheinschotter inside the unit B.* ***3)****: Bachschutts and Bergsturtz label assignment using a nearest neighbors algorithm.*

ally omitting one group of boreholes. The resulting model is then compared with the absent data. When constructing the k-fold data sets, we carefully check that these data sets are well balanced in terms of statistical distribution of the wells characteristics. By comparing the model forecast and the omitted boreholes, we can select the best modeling parameters and geological concepts.

Finally, the general philosophy of ArchPy is to generate multiple equiprobable simulations to represent the uncertainty. However, it is sometimes asked in the end to provide one model which is assumed to be the most probable one. Therefore, we explored different approaches to select one single model. One usual approach is to postprocess the simulations to determine which stratigraphical unit is the most likely in any location. However, this approach can incorrectly represents the rare units, therefore we tested three other alternative models and compare their performances using cross-validation. The details of these methods are given in the following sections. To quantify uncertainty, we provided in any location the probability of occurrence of all the lithologies and we summarize this information by providing a 3D grid of Shannon entropy values over the whole simulation domain.

5.4.2 Detailed workflow

This section details each of the modeling step undertaken. The modeling parameters are shown in appendix A.2.

Spatial discretization

The 2D extent of the model was defined by the red polygon shown in Fig. 5.1. The target model has the following characteristics:

- cell size (x, y, z) is $50 \times 50 \times 2$ m^3, in a regular grid
- model dimension in cells is $400 \times 835 \times 251$ ($nx \times ny \times nz$)
- model dimension in meters is $20'000 \times 51'750 \times 502$ m^3 ($Lx \times Ly \times Lz$)
- model origin (lower-left corner) in Swiss CH1903+ / LV95 (EPSG:2056) are

  $2749247.0, 1222618.0, 200$ (ox, oy, oz)

The simulation grid defined above is a regular rectangle. Within the box, the cells outside of the modeling domain are inactivated and not considered for the simulations. In this case, some cells can be above the topography, below the elevation of the bedrock or outside of the polygonal mask provided by Swisstopo. The final model consists of a total of more than 4 millions active cells while 8 millions are inactive. Model top boundary was set according to the Digital Elevation Model (DEM) of the Swiss Geological Survey at a resolution of 25×25 m^2 (DHM25, Swisstopo). The bottom of the model was defined the Swiss model of bedrock elevation (TopFels25, Swisstopo), also at a a resolution of 25×25 m^2.

The lowest altitude of the model was set to 200 meters above sea level (m.a.s.l.), even if bottom of the valley can locally be much deeper. As no boreholes goes beyond this depth, the uncertainty on the exact distribution of units is very high. Indeed, our model will not be able to represent the units at these depths and the associated uncertainties for multiple reasons. First of all, it is possible that unknown units that have never been encountered by drilling exist at these depths. The model will then not be able to simulate something that has not been seen in any of the wells. Second, as ArchPy simulates top surfaces of each unit, it will fill the bottom with the last unit, here Moräne or Lakustrisches sediment. Hence, increasing the depth of the model without more data will simply result in a hundred meters filling by these units. This will be completely non-informative and will add unnecessary computational costs. For all these reasons, we decided to set the lower boundary of the model at 200m above sea level. We think that modeling the deep part of the valley would require acquiring additional data and information from additional sources (geophysics,

analog data from other deep valleys in Switzerland). Based on these data, it should be possible to construct a realistic model with reasonable uncertainty estimates, but this additional work was beyond the scope of this study.

Simulation of the surfaces

This subsection describes how step 1 (Fig. 5.4) was undertaken. Once the stratigraphic pile has been defined through borehole analysis, the units can be defined and separated by 2D surfaces. According to the ArchPy modeling procedure, surfaces can be of two different types: onlap or erode. This impacts how the surfaces interact with each other and represent different sedimentological conditions. For this model, all surfaces were considered as onlap.

The top surfaces of each unit are simulated successively using Gaussian Random Functions models (GRF, Matheron 1963) that were generated using the sequential gaussian simulation (SGS, Alabert 1989; Deutsch et al. 1992) algorithm.

The conditioning points for the simulation can be of two nature: equality points and inequality points. The first type is encountered when a borehole encounters a certain layer. At this stage, an equality "TOP" point is defined, and the altitude of the transition is defined. On the contrary, an inequality point reflects that a borehole has not reached a deeper layer, and that this one should be simulated at a depth unknown, but deeper than the borehole. Additional situations may arise due to the complex interplay of sedimentological processes, such as deposition and erosion. These processes are discussed in the dedicated chapter on ArchPy (see chapter 3).

In addition to the conditioning points, it is necessary to provide a variogram model for each of the surfaces. The variogram model is a function that represents the spatial variability (or correlation) of the surface (Chiles et al. 2012). A variogram model for each surface was automatically fitted to the experimental variogram when enough points were available from the borehole data (Fig. 5.5). The data were insufficient to identify clearly the variograms for the following units: Hangbildungen and Bergsturtz. Consequently, we attributed to them a default variogram, with a range of 7500 m and a sill of 200 m^2. We chose these values based on a visual rough estimate as well as from the expected values of spatial correlations (range) and variability (sill).

The surface delimiting the Moräne is treated differently. We think that the Moräne cannot be modeled properly by just interpolating the available borehole data. Even if this unit is observed in boreholes, we believe that a sampling bias exist. Indeed, it is expected, given the general geological knowledge of the area, that the Moräne should follow, more or less, the bedrock with a variable thickness ranging from 0 (absence of Moräne) up to 30-40 meters according to

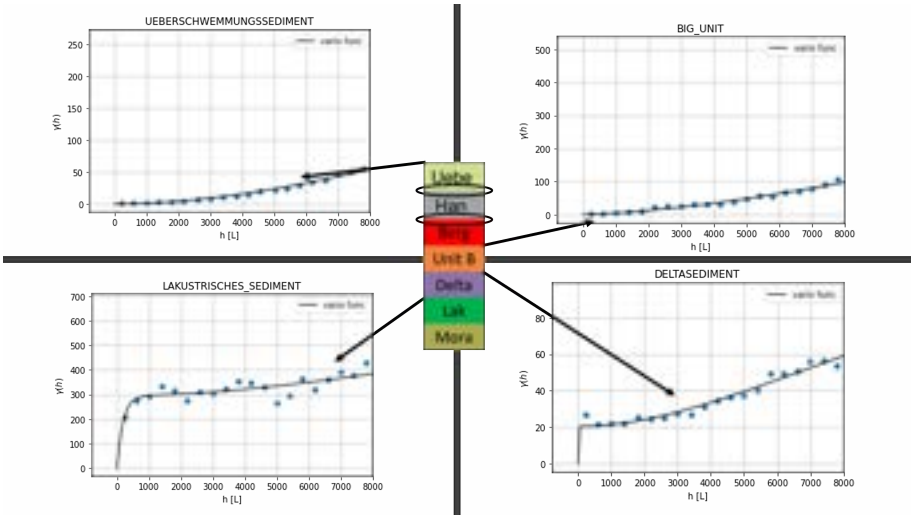

Figure 5.5: *Experimental variograms and the variogram models for Überschwemmungssediment, unit B, Lakustrisches sediment and Deltasediment. Blue dots are measures of the variance based on the boreholes. Interfaces circled in black are surfaces that did not have enough data points to estimate an experimental variogram.*

the boreholes. However, the boreholes that hit the Moräne are almost all on the sides of the valley, where the unit is shallow, and probably do not represent the real spatial variability. In addition, due to the absence of boreholes that contain Moräne in the center of the valley, the model would be totally unconstrained. If we would interpolate directly the observed depth, the risk is the creation of a layer having a very high thicknesses with a Moräne close to the topographical surface, without respecting the concept stated above. To prevent this, we can impose in ArchPy a mean elevation to the top of Moräne that we have set at 15 m above the bedrock depth based on the average thickness of moraine in the boreholes. The variogram was chosen to respect the Moräne thickness distribution.

At the end of this step, the result is an ensemble of unit models, including the grouped unit B. Similarly, all Bergsturtz are grouped in one unit.

Simulation of Rheinschotter, Verlandungsbildung and Bachschutts in unit B

This subsection details how Step 2 (Fig. 5.4) has been undertaken. This step aims to populate the unit B in three litho-stratigraphic units: Rheinschotter, Verlandungsbildung detritisch and the Bachschutts, using DeeSse, a Multiple Points Statistics (MPS) algorithm based on the direct sampling approach (Mariethoz et al. 2010b). MPS is a family of geostatistical techniques that can be used to model complex spatial distribution of a variable. The MPS approach involves building a training image (TI) or training data set, which is often a

simplified representation of the expected geological structure. The training data set is then used and iteratively sampled (Mariethoz et al. 2010b) to generate a set of realizations of the variable of interest at the target locations.

Training image generation

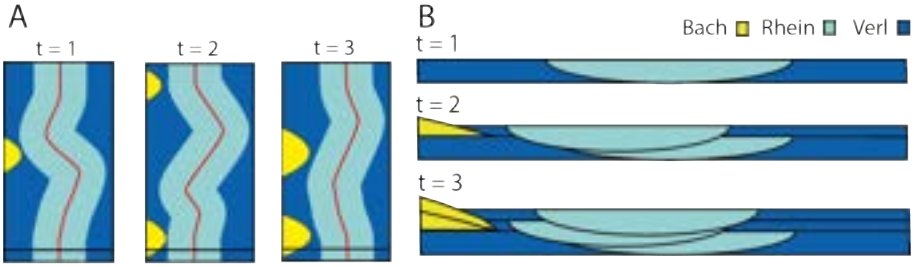

Figure 5.6: *Schematic representation of the object-based approach used to generate the Training Image. Three successive simulation time are shown both in aerial view (**A**) and transversal view (**B**). Transversal views at the position of the black line of aerial views.*

A training image aims to represent the conceptual model of deposition. It represents the expected patterns and spatial statistics.

To generate it for the case of the Rhine valley, we had to code a specific object-based method. These methods (Chiles et al. 2012) allow to control the shapes and sizes of the geological objects, and generate realistic models. But in general they are difficult to condition to borehole data. This is why we use them here to create the training data and then use the MPS approach to condition locally the simulations with the borehole data. Object-based methods rely on predefined geometries representing geological objects that can mimic geological features such as riverbeds, levees, deltas, etc. The objects are positioned stochastically in a simulation domain. An example of a similar approach is FLUVSIM (Deutsch et al. 2002), a relatively common and widely used object-based software to simulate alluvial environments.

The Figure 5.6 summarizes the procedure used. Here, we interpret unit B as a mix between a fluvial environment, from which the Rheinschotter (FLUV) and the Verlandungsbildung (VERL) are deposited, and alluvial fans coming from the side of the valley (Bachschutts, BAC). All these depositions can occur at the same time but at different positions in space. These two sedimentological features are treated as two different independent objects. River objects constrain the position of the Rheinschotter. They are elongated objects whose center position is determined by a 1D stochastic process and their transversal profile is given by their thickness and width which are user inputs. The streams have the ability to remove previous channels and Verlandungsbildung sediments. We also consider that deposits outside of the river channels are considered as the Verlandungsbildung detritisch deposits. Alluvial fans are half-disk objects whose

thickness linearly decreases from their center to their outer limit. Thickness and radius are values drawn randomly in user-given probability distributions each time an event takes place. Instead of having events at each time step, we let them occur with a certain probability. The events stack on the rest of the simulation and can then overlap with the other facies. Three alluvial fan source locations were considered to generate the TI.

The simulation is sequential and can be seen as a progressive filling of the simulation domain (Fig. 5.6) where the surface continuously increases through time. Hence, at each time step, the river object will be set a little higher than the previous one, and a draw is made to determine if a Bachschutt deposition event occurs or not. We can denote the size differences between two different bachschutts events and the incision made by the rivers on previously simulated sediments. The final TI can be seen in Figure 5.7 A.

Auxiliary variables

To better constrain the MPS simulations, we added two auxiliary variables. These variables are not simulation variables in themselves, but they guide the direct sampling algorithm, by adding knowledge. These variables are informed in both the training image and the simulation grid. As mentioned before, the MPS will sample the TI image iteratively to fill the simulation grid. By adding an auxiliary variable, we want to preferentially sample some areas of the TI for some areas in the simulation grid. The assumption is that some features are more represented in some areas of the TI, and that the same behavior is expected in the simulation grid. For example, the Bachschutts must be close to the valley outlets in the TI, and should also be preferentially disposed close to valley outlets in the simulations.

MPS simulations

Within ArchPy, we use the DeeSse algorithm to run the MPS simulations. In addition to the auxiliary variables, the boreholes are added as conditioning points.

The algorithm tries to find not only the pattern that best matches the borehole data, but also the position in the TI that has similar auxiliary variables (Mariethoz et al. 2010b). If no borehole data is available, but the location is near a valley outlet, a Bachschutt is more likely to be simulated. Conversely, river channels are expected to appear far from the valley sides.

Two auxiliary variables are used: the distance from the valley outlets (Figure 5.7 B, C) and the distance from the present river path line (Figure 5.7 D, E). To obtain the distance from the Bachschutts for the real model, the exits of all the lateral valleys leading to the Rhine valley have been identified manually using a DEM.

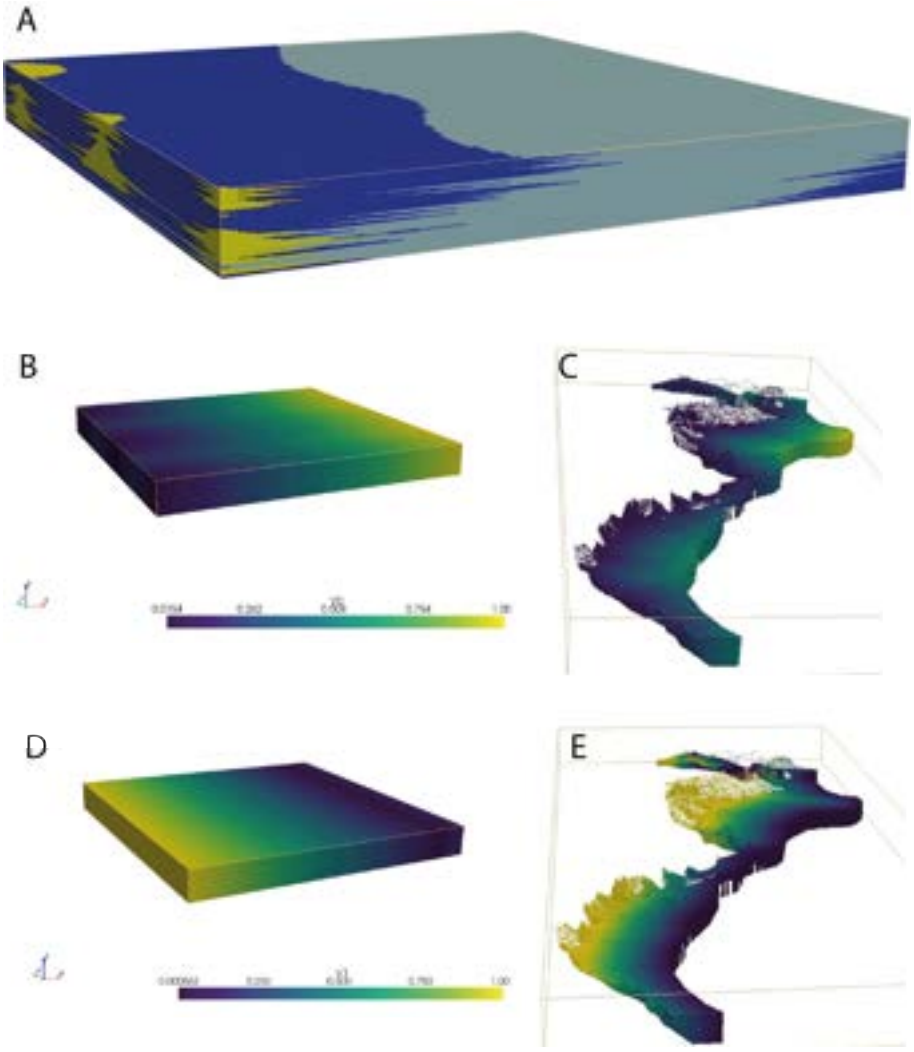

Figure 5.7: *Resulting Training image (**A**) using the object-based approach developed in this research. The associated auxiliary variables: distance from Bachschutts (**B**) and distance from river path line (**D**) are also shown. **C** and **E** show the spatial distribution of these auxiliary variables over the simulation domains.*

At the end of this simulation step, the unit B is divided in 3 distinct subunits: the Rheinschotter, the Verlandungsbildung and the Bachschutts.

Attribution of the Bachschutts and Bergsturtz deposits

As mentioned before, all the different Bachschutts are grouped in one Bachschutt unit. However, they consist of 24 distinct units. Since only the grouped units have been modeled for now, it is necessary to divide it in 24 according to the descriptions of the boreholes. This is done using a Nearest-Neighbors (NN) algorithm. An existing grouped Bachschutt cell will be assigned to the nearest local Bachschutt unit described by the boreholes. Same approach is used to differentiate the Bergusturtz stratigraphic units. The use of MPS and NN in combination is an easy and simple way to model relatively complex distributions such as the Bachschutts. NN is well suited as it is efficient and Bachschutts entities are spatially well distinct.

Final model selection

The ArchPy standard workflow is stochastic. Instead of providing only one model, ArchPy can simulate hundreds of models to quantify uncertainty. The collection of models are all plausible. To select a single model, an appropriate method must be used to identify a model that corresponds to the user's needs. This problem is usually not well defined. For example, one could select the model that is able to provide the highest risk in terms of tunneling if a tunnel would be drilled in the area. This would allow to design a safe tunnel project. But it could also be the model that would predict the worst groundwater production to surface contamination to ensure again the best protection if one consider water supply issues. Most probably, considering the high remaining uncertainty, these two models would be very different.

Since in the framework of this project, we did not have one single and specific objective outside of providing a geological model, we decided to simply illustrate the issue by providing four different unique models based on four different criteria. Aggregating multiple realizations into one is an arbitrary choice and it leads to various results according to the adopted methodology. In this study, we have selected a local area (Fig. 5.1) to illustrate the impact of choosing four different approaches in order to compare each method.

The approaches that we consider here are:

- Method 1: Taking the most probable unit in each cells without any additional constraints.
- Method 2: Progressive assignation based on probability distributions and proportions.

- Method 3: Use of the mean of the ensemble of surfaces to delimit the units.
- Method 4: select one realization that is the closest to the center of the statistical distribution of the ensemble of realizations.

Method 1 is very straightforward. The final unit in a cell is the unit that is simulated most frequently in this cell. If A was simulated 6 times and B 4 times, unit A would be kept. The drawback of that method is that if a unit is rare in the area of interest, it will normally have a low probability in almost all cells, and will not be selected in most of the case. As a consequence, it is likely to almost disappear in the final unique model. At least its global proportion is likely to be smaller in the final model than in the observed data and in any of the simulations.

Method 2 aims at minimizing the issue highlighted above. It begins by computing the proportion of each unit (from 1 to i) in all cells of the domain, through all simulations ($pModel^i_{x,y}$). If a cell is simulated 6 times A and B 4 times, the $pModel^A_{x,y}$ for that cell will be 0.6 and $pModel^B_{x,y}$ will be 0.4. We also calculate p^i_{BH}, which is the proportion of each unit through all the wells. If there are 2 boreholes of same length, one completely described as A, and the other completely described as B, $p^A_{BH} = p^B_{BH}$ and will be 0.5. This is the target proportion of values. We then fill an empty model iteratively, starting from the unit that has the lowest global occurrence using thresholds on the $pModel^i_{x,y}$ values. We determine the probability threshold (τ) between 0 and 1 so that the proportion of cells in $pModel^i_{x,y} \geq \tau$ is the closest to p^i_{BH}. We then assign these cells to unit i in the empty model. We then move to the next unit, still following the order of the occurrence. The cells that have been assigned cannot be updated anymore. We continue iteratively until the whole model is filled. This method has the advantage that the proportion of the different lithologies as observed in the wells is respected by the final unique model.

Method 3 consists in averaging the surface depth. All realizations of the TOP of a surface are averaged. The final model is then constructed. This methodology cannot be applied for units that have been simulated without a surface. The different Bachschutts, Verlandungsbildung, Rheinschotter and the two Bergsturtz were constructed as different facies. For these particular units, we have decided to simply apply Method 1 within Unit B, which regroups them.

Method 4 is different as we do not use an aggregation of models, but select only one within the ensemble. This model is supposed to have a higher probably of occurrence. To estimate the probability of each model, we first need to define a measure of *distance* between each model. Different distance algorithms can be defined depending on the applications. For example, one could use any of the geological model and compute the travel time of a contaminant from a given location (such as a waste disposal) to a target (such as a water production well). The difference in travel time could be our difference between the two geological models. Here, we simply use the number of cells that are different (at the same location) between any two models. The distance is computed between all pairs of models and a distance matrix is constructed (Fig. 5.8 A). The matrix is symmetric around the diagonal. We can denote that in this example, a few models are extremely different from the majority (e.g. index 29). From the distance matrix, we use an algorithm called Multi Dimensional Scaling (MDS), which is a dimension reduction algorithm to obtain a 2D representation of all the models (Fig. 5.8 B). Any point in this 2D map represents one model, the coordinates are abstract scalar values. The distances between the points in this map represent the distances between the 3D geological models that have been computed in the first step. The spread of the cloud of points represents the variability between the models and the uncertainty. If many models are mapped in this graph, it is possible to estimate locally a density of probability and estimate the probability of occurrence of the various 3D geological models (with respect to the selected distance). Here, we decided simply to take the model that would be the closest to the center of gravity of this cloud. The center of gravity of all models is represented by the red cross. The best model is assumed to be the one the closest to the gravity center and is easily identifiable (green dot in Fig. 5.8 B). On the contrary, Model 29 for example is the farthest from the red cross and corresponds to the dot to the extreme left of the point cloud.

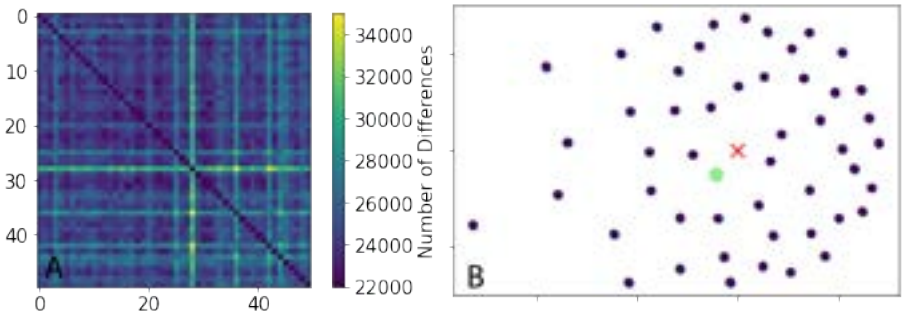

Figure 5.8: *Illustration of the use of the distance method and MDS, to select one among 50 realizations made for the test site.* ***A****: Distance matrix between each of the 50 models.* ***B****: MDS applied on the matrix in* ***A****. Red cross represents the center of gravity of all the points and the green dot is the closest to the center of gravity (i.e. the most "representative" realization).*

Cross-validation

To assess the performance of the model, we have performed a cross-validation procedure. This consists in separating the borehole data set into a predefined number (k) of sets (or folds). One after another, one fold is removed from the data and only used as validation data set, while the others are used as training data. Hence, this procedure is done k times, one for each fold. In our case, we chose a number of five folds ($k = 5$) for the complete model and three folds ($k = 3$) for the unique model comparison. Each of the folds has been determined to respect that they all have the same statistics in terms of unit proportions. This method is robust and allows us to estimate what is the expected error of the model and on which stratigraphical units. It also provides insight into false unit predictions. This makes it possible to know, for example, which units are confused with each other by the model.

Uncertainty representation

The complete uncertainty quantification is given by the set of realizations. This information is summarized in local conditional probability distributions (cpdf) for each of the units. Due to the large number of units, it is difficult to visualize all these cpdfs in the domain. Therefore, the Shannon entropy has also been computed as a measure of the quantity of information to represent the uncertainty in a synthetic manner. The entropy values range from 0 to 1, with higher values indicating greater uncertainty. A value of 0 indicates that the model predicts a unit with total certainty, while a value of 1 indicates that all units have an equal probability of being present. The entropy (H) for each cell of the model is calculated as follows:

$$H(x, y) = -\sum_{i=1}^{n} p^i_{x,y} \log_n(p^i_{x,y}) \tag{5.1}$$

where $p^i_{x,y}$ is the probability of occurrence of the unit i computed over all the models at the cell x, y, and n is the number of different units that can be encountered. If all the different Bachschutts are considered, n is too large which can alter the results of the entropy. We then proposed to compute the entropy at the second level of hierarchy (Fig. 5.4) where there are nine units. Therefore, the uncertainty in prediction of one precise Bachschutts is not assessed.

5.5 Results

This chapter presents the resulting model of the Rhine Valley. First, we compare the four tested methods for the selection of one unique model. Based on these results, one final model is presented in a second time, as well as the stochastic realizations and the measure of the uncertainty using the Shannon entropy.

5.5.1 Unique model comparison

To select one single model (see section 5.4.2), we used a test zone (Fig. 5.1) to compare the different options introduced in the methodology. To do so, we used a k-fold cross-validation procedure. The number of folds was three in this part of the work, and the number of realizations for each one was 100.

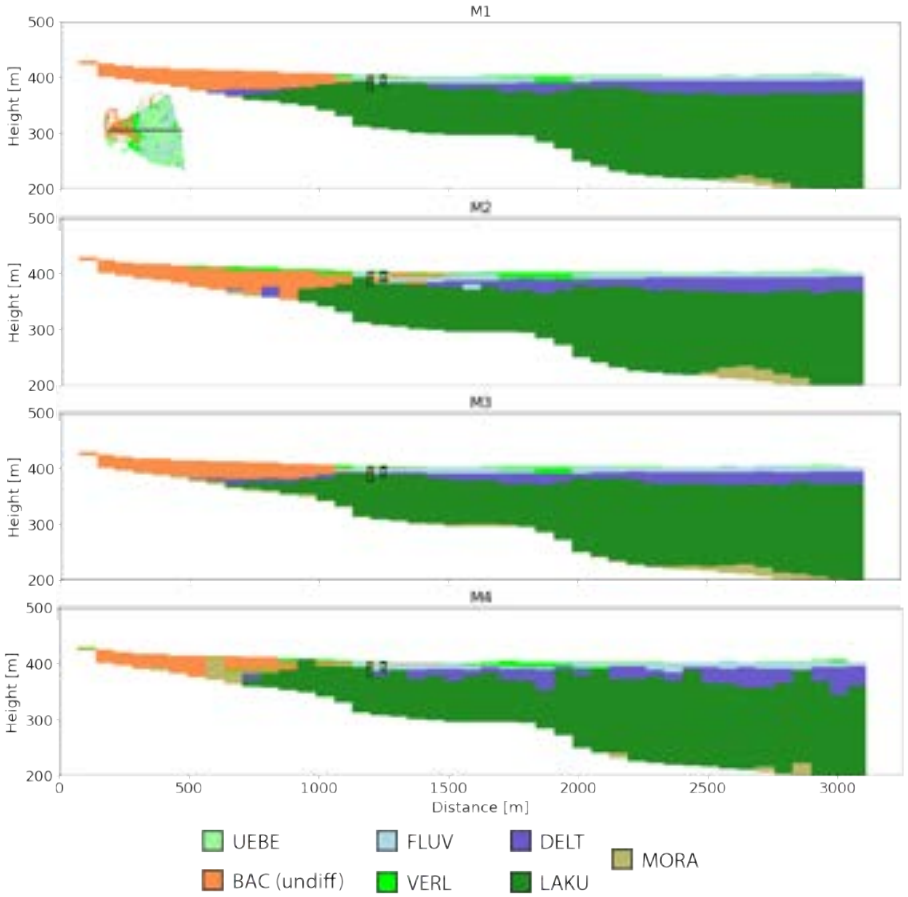

Figure 5.9: *West - East cross-sections at the same place in the model using each of the 4 aggregations methods M1-M4 (Method 1 - Method 4).*

Figure 5.9 shows the geological models obtained along the same cross section using the four methods at the test site. Visually, the four methods give rather similar results, except for M4. This behavior is expected, since the model M4 is one realization chosen within the others, when the other methods involve averaging and, consequently, smoothing. M1 and M3 are very close. M2 shows more complexity, especially at the boundary of multiple units (BAC, DELT, LAKU), for example at a distance of about 600 - 800 m from the left of the

cross-sections. We see also that the moraine are more present in M2 than in M1 and M3.

Table 5.1: *Different scores of the four aggregation methods used. Percentage of correct cells, the sum of the diagonal of the confusion matrix and the number of times the method had the highest score per unit are presented.*

	M1	M2	M3	M4
Percentage correct [%]	73.74	73.65	75.81	74.97
Sum of the diagonal confusion matrix [-]	4.46	4.42	4.56	4.41
Number of best score per unit [n#]	1	0	3	3

The k-fold procedure allows quantifying the performances of the 4 methods in terms of geological predictions. Table 5.1 provides the main statistical scores and show that all 4 methods give pretty decent results with an accuracy ranging from 73 to 76%. These results shows again that the 4 methods are rather close. The best statistics are obtained with the M3 method, while the worst are obtained with M2, which is very close to M1.

We can refine those results by comparing the confusion matrix obtained for each method (Fig. 5.10). Each row represents a predicted category (units), while each column represents what was measured in the borehole. The percentage of correct answers are normalized along the predicted values (row wise). The perfect case would be when the diagonal is filled with "1" and the other cells of the matrix are at "0". This means that the correct unit is predicted correctly each time it is observed. Fig. 5.10 shows that all methods give similar results, at least visually. The differences are rather minor. One thing that can be noted is that method 4 seems to be more uncertain on the simulation of the Moräne than the other methods. And more generally, method 4 has slightly more distributed errors across the different units (less cells close to 0), so it seems less "confident" than the other methods. The sum of the diagonal of the confusion matrix (tab. 5.1) provides a global score where each unit has the same weight. Hence, even rare and sparse units have the same importance as common and spatially distributed ones. These results are given in table 5.1, the best score is again obtained by the method M3 while the worst are obtained by M4 and M2. Finally, the last line in table 5.1 counts the number of times the method was the best to predict a specific unit (i.e. the best score on the diagonal of the confusion matrix for each unit). M3 and M4 are the best, as they both predict three units better than the other methods. M2 is the worst with a score of 0.

Overall, and considering only the scores that were used in this comparison, method 3 (M3) gives the best results. It provides a rather smooth description of the 3D geology of the area. The model M4 gives surprisingly decent results, considering that it is a single realization. It provides a representation with more spatial variability that is probably closer to the reality than model

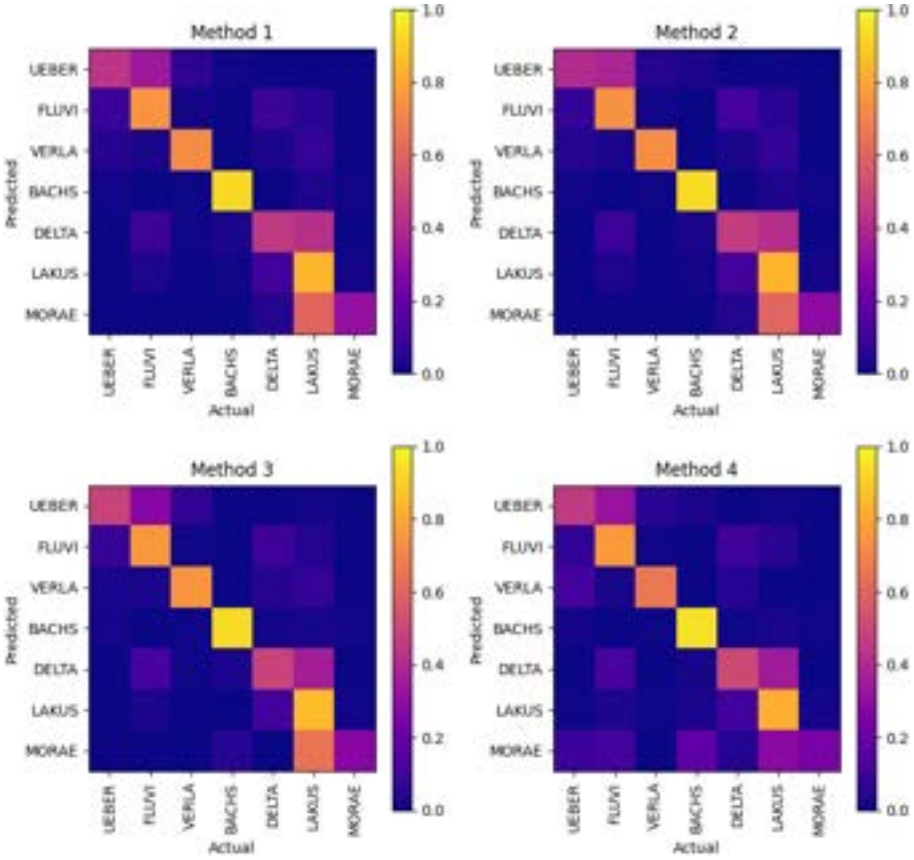

Figure 5.10: *Confusion matrix of the different aggregation methods obtained through the cross-validation performed on the test site. Each row is normalized.*

M3. For example, it shows in this section that the deltaic sediments may not be continuous over the complete section. As a reminder, simulations are constructed specifically to represent properly the expected spatial variability of the unknown reality but their aim is not to be locally accurate. In that example, this specific simulation seems to be slightly more accurate locally than the methods M1 and M2 based on the identification of the most probable units, and this is unexpected.

To conclude that part, without having a specific application and goal for the geological model, we decided to use M3 as our single model for illustration purposes in the following of this chapter.

5.5.2 The regional simulations and unique model

This section details the results obtained at the regional scale. A total of 50 realizations were generated to construct the mean stratigraphic unit model.

Figure 5.11: *Pile and reference for the colors used in the different figures.*

For readability, the legend of the geological units (Fig. 5.11) is not shown in conjunction with each of the figures in the results section.

A 3D view of the final model is shown in Figure 5.12 A and the corresponding Shannon entropy is shown in Figure 5.12 B. As expected, the different units are well spatially distributed, both vertically and laterally. In depth, we mainly observe DELT and LAKU units while the other units share the space near the surface. FLUV deposits are located closer to the river than VERL deposits (Fig. 5.13 and 5.14). BAC units are located near the west side of the valley, at the outside of the lateral valleys. UEBE unit is only presents at shallow depths and near the river.

Inactivated cells are not displayed in the model. The small moräne cells that are going up the hill are areas where the DEM and the Bedrock model are close, but not exactly collocated. Therefore, in these areas, the cells are activated.

The entropy shows, for each location, the amount of information through all 50 realizations. We see that near the boreholes, the entropy is near 0 while it increases until 0.5 at some locations, generally at the interface between multiple units and/or there is no data. In this model, the theoretical maximum entropy is 1. We should be careful in interpreting these results, in particular the one at depth where the entropy is 0, which would imply that there is no uncertainty. Obviously, this is not true, since we have little or no information at these depths. This is due to the fact that LAKU unit is the last one to be simulated (if we exclude MORA which is simulated closer above the bedrock). It will consequently fill the whole model from its top to the Mörane, which better follows the bedrock. But it does not take into account the possible variations of the thicknesses of the units (for example, Moräne unit thicker at the bottom of the valley) or the presence of other unknown units.

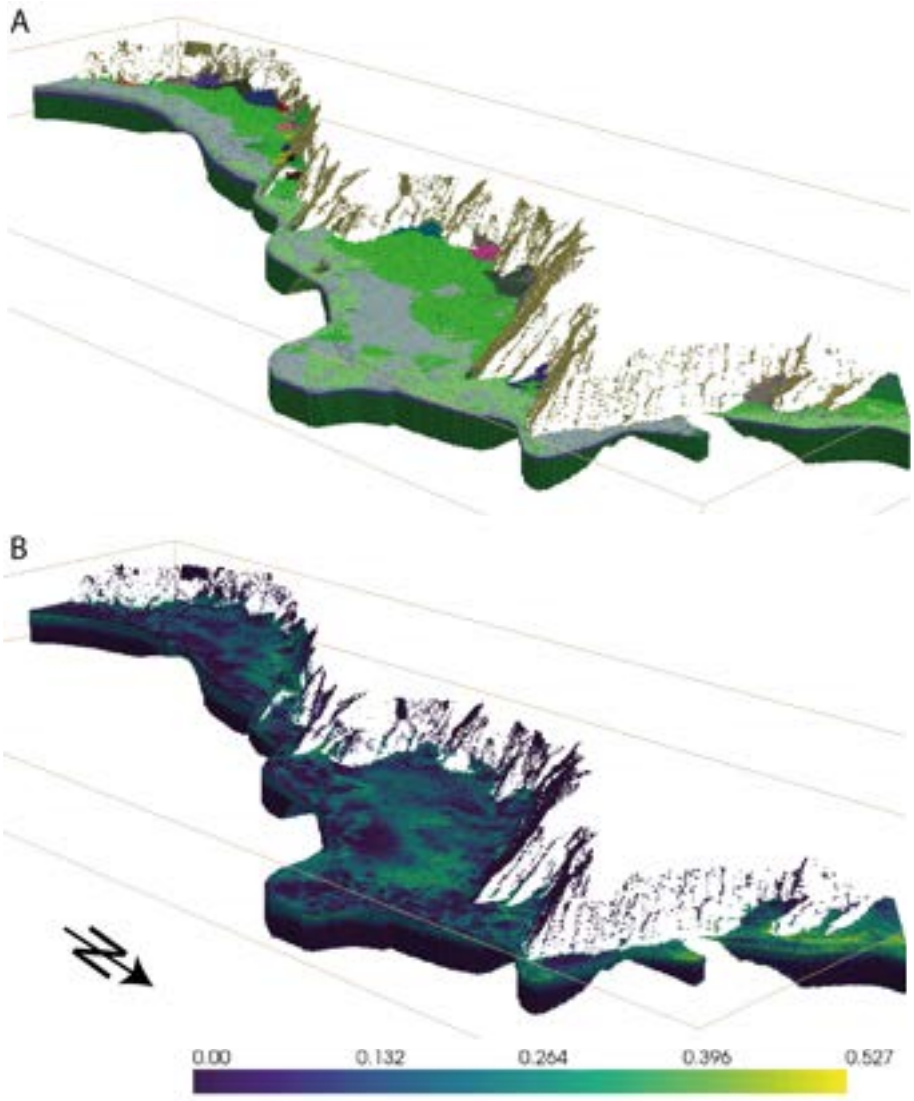

Figure 5.12: ***A****: 3D view of the final model after aggregation of the realizations.* ***B****: Shannon entropy associated to the final model, computed using the 50 realizations.*

Overall, the Shannon entropy should not be seen as a "pure" measure of the uncertainty (it is impossible to obtain), but rather as the uncertainty related to the underlying conceptual model used. If one need to consider or investigate a situation that is not yet included in the conceptual model, one would need to rebuild a model and include these new considerations in the conceptual model. These questions are discussed more in details in section 5.6.

Some cross sections have been drawn to show the internal spatial variability of the units from South to North (Fig. 5.13). We see that LAKU deposits fill the largest part of the model as it is the last unit in the pile (if MORA is not considered). The interfaces between the units are generally smooth and relatively flat. However, the contact between Bachschutts units and VERL or FLUV is very sharp and vertical. This is due to the Method 3 aggregation that, for these three units, takes the most probable one in each cell independently. And, according to the geological concept (TI, Fig. 5.7 A), slope deposits events have a random extent and thickness from the valley outlets. Thus, at the transition zone between BAC and VERL/FLUV, the simulations will produce realistic alternations between these units, simulating the temporal variations. However, when averaged and in the absence of conditioning data, we tend to obtain a vertical contact that no longer represents the geological concept. This phenomenon can be seen on the Figure 5.14 where realizations (Fig. 5.14 A - C, F - G) have a more "natural" contact between Bachschutts and VERL compared to the mean model (Fig. 5.14 D, I).

With respect to the uncertainty of the model, entropy is particularly high at intermediate depth (around 410 m.a.s.l) and to the left of the model (Fig. 5.14 E, K). This is due to the fact that more units are potentially plausible at these locations. Far from the valley sides, we tend to only have UEBE, FLUV, DELT and LAKU that are generally relatively well defined. In contrast, on the left close to the valley sides, practically all the units can be present and cause a high uncertainty in the prediction. Again and as mentioned before, we can notice the entropy of 0 at great depth, more than 100 - 150 m, because only LAKU deposits are simulated at these depths. Therefore, the results should be interpreted with care.

The longitudinal profiles (Fig. 5.15) shows the possible trends of the units. FLUV deposits seem to be thicker in the south than in the north. On the contrary, the thickness of the DELT deposits seems constant. The difference between the realizations (Fig. 5.15 A-C) and the average model (Fig. 5.15 D) can be clearly seen.

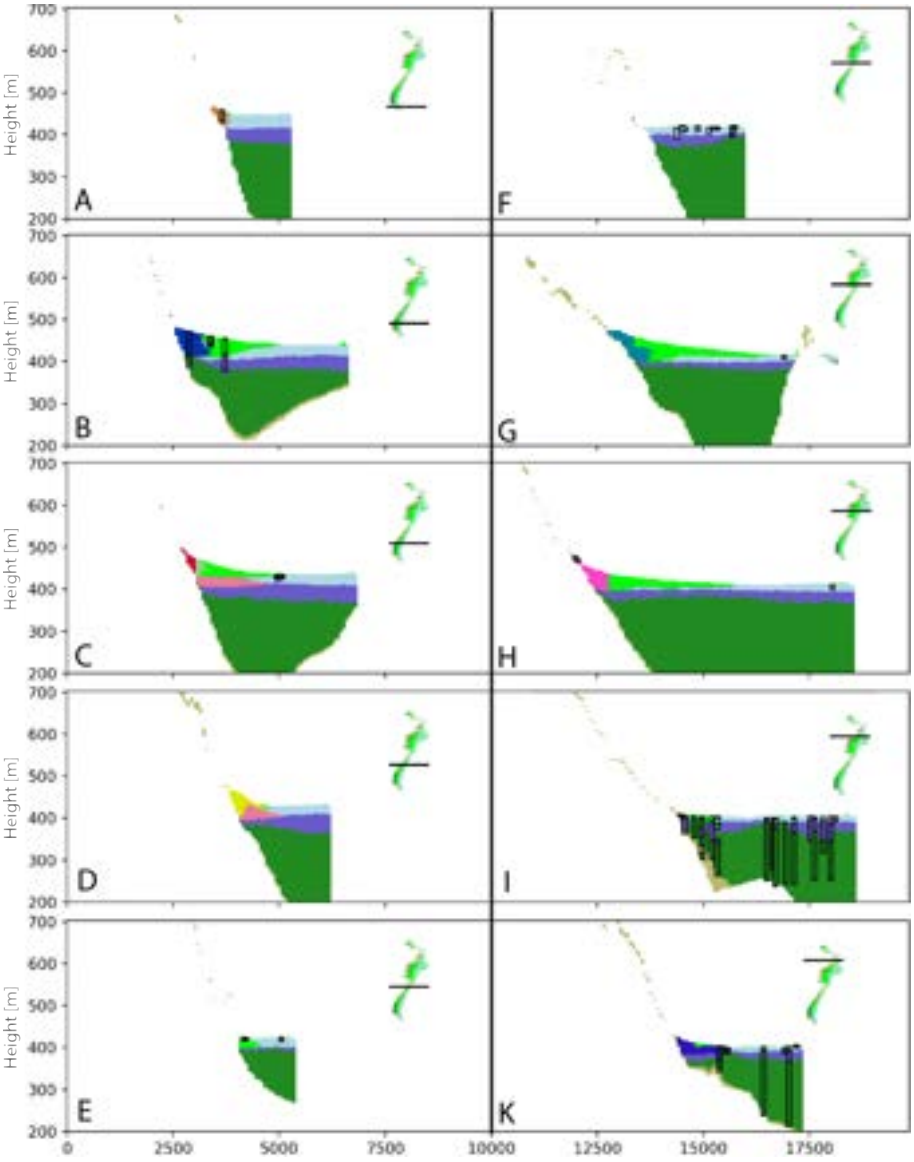

Figure 5.13: *Set of cross-sections made on the final model from south (A) to north (K). The colors correspond to the units in Fig. 5.11. The boreholes that are displayed are those located at a distance of less than 100 m from the cross-section.*

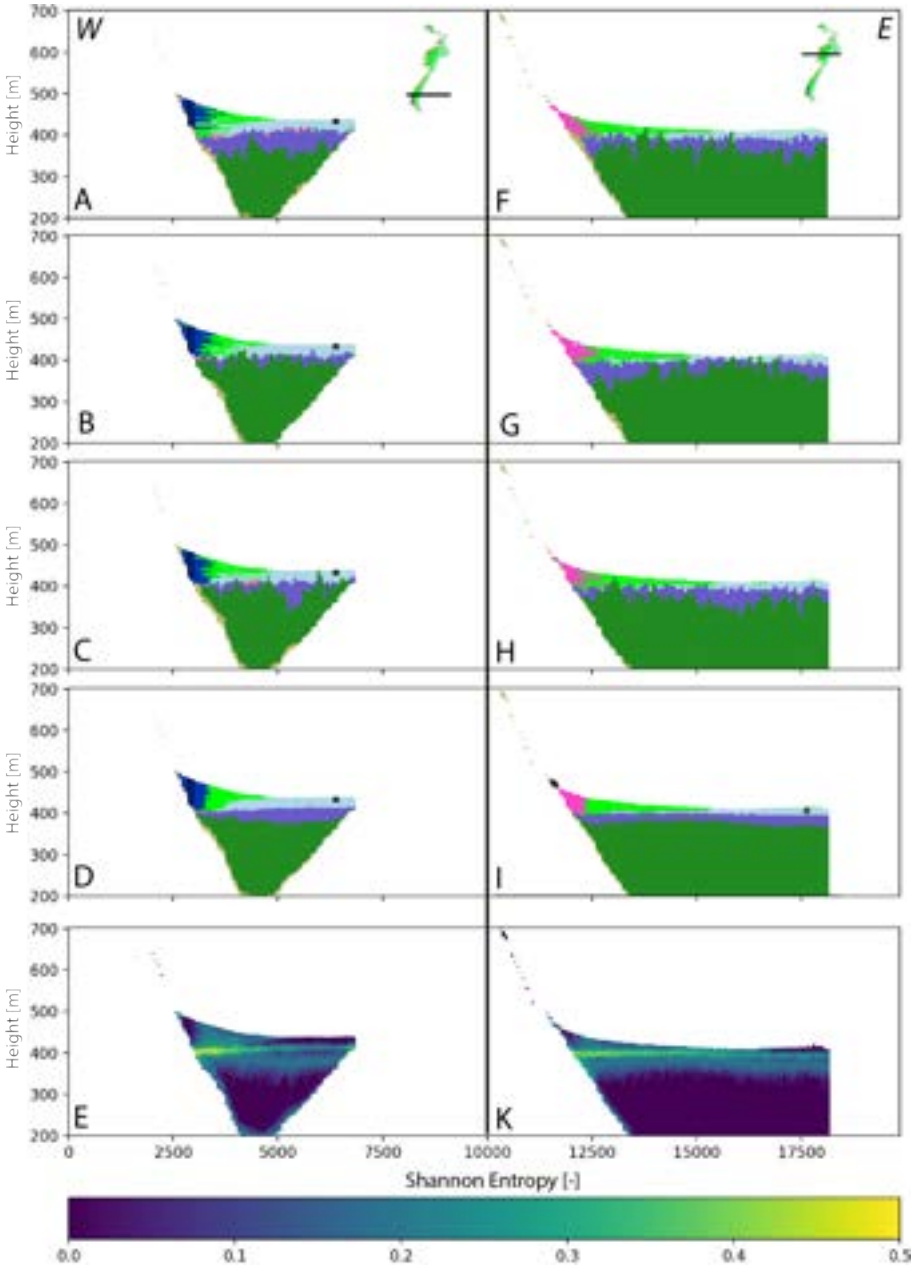

Figure 5.14: *Cross sections made at two different locations. For location 1:* ***A*** *-* ***C*** *are three different realizations,* ***D*** *is the mean model and* ***E*** *is the entropy. For location 2:* ***F*** *-* ***H*** *are three different realizations,* ***I*** *is the mean model and* ***K*** *is the entropy.*

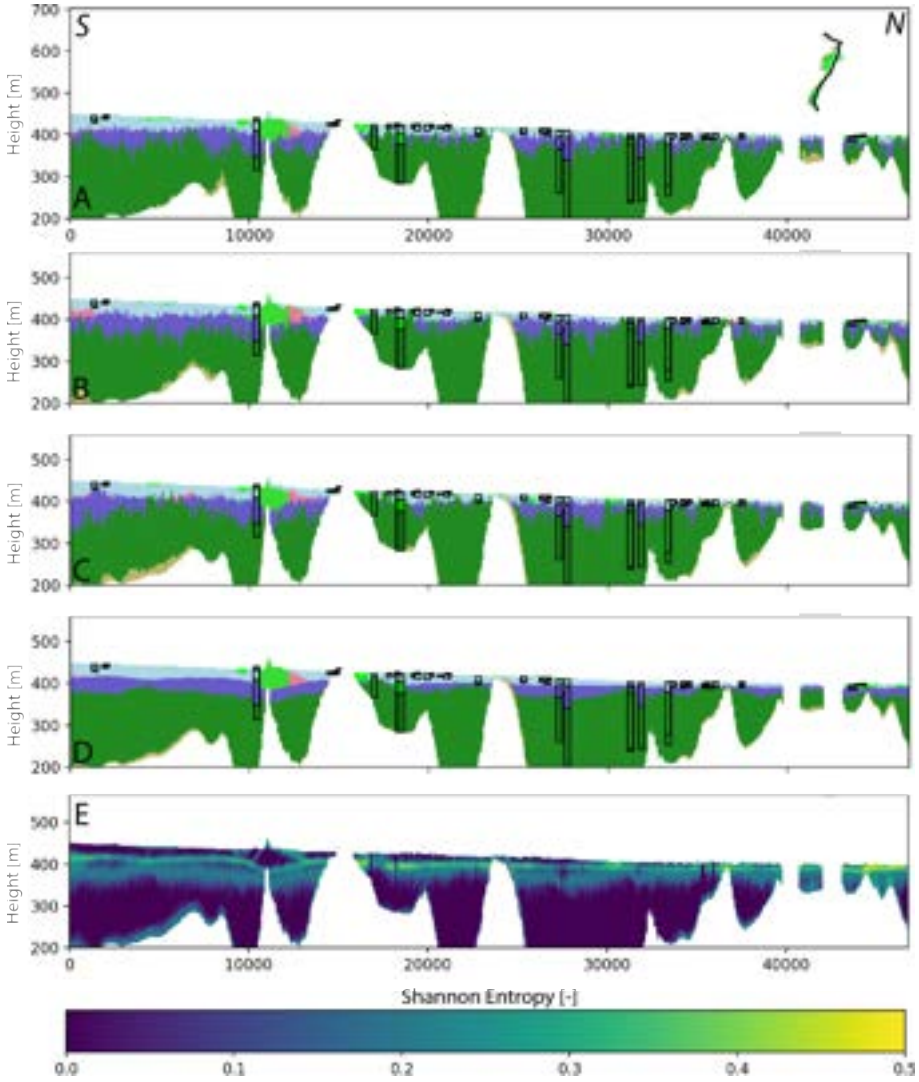

Figure 5.15: *Cross sections going from south to North.* ***A*** *-* ***C*** *are three different realizations,* ***D*** *is the mean model and* ***E*** *is the entropy.*

5.5.3 Cross-validation

Cross-validation was performed using a 5-fold procedure with a total of 50 realizations for each fold. Realizations were then aggregated using the method 3 and the resulting "mean" model was used for comparison with the data. Boreholes were randomly selected for each fold. For the sake of simplicity, the different BAC and BERG units have been merged for this section.

The results (Fig. 5.16, tab. 5.2) show drastic differences in results between units. Some units are well predicted (e.g. FLUV, VERL, BAC, LAKU, $> 80\%$ correct predictions). These are mainly very common layers. However, the results are relatively poor for other units (e.g. UEBE, DELT, MORA, HANG $< 56\%$)). It can be noted that most of these layers are relatively sparse or thin units. Consequently, the probability of it being correctly simulated is much smaller. For example, the HANG layer is present only in 2.5% of the boreholes. An exception must be denoted with the DELT deposits. DELT has a score of about 55%, but is quite a common layer. Most of the time, DELT is confused with LAKU deposits (Fig. 5.16, "DELT" row). It indicates that the major problem is the determination of the limit between these two units. The use of a "near-nugget" variogram (Fig. 5.5, Lak) is probably the origin of this. The nugget effect in a variogram can usually be explained by noise in the data. Two neighboring wells show important differences in terms of the depth of transition between DELT and LAKU. The variogram was fitted on the data and reflects this important noise. The good results obtained on FLUV, VERL and BAC units show that the MPS approach seems appropriate to simulate these units. The BERG unit also has satisfactory results by reaching almost 75%. Finally, the overall accuracy of the model reaches 82%, demonstrating the rather good overall capabilities of the modeling strategy presented here.

Table 5.2: *Percentage of correct predictions per unit. Bachschutts and Bergsturtz deposits have been aggregated (BAC and BERG, respectively). "Overall" indicates the overall proportions of correctly simulated cells.*

Units	Correct prediction [%]	Number of Boreholes with the Layer	Percentage of total number of Boreholes [%]
UEBE	39.10	539	34.35
BERG	74.40	29	1.85
FLUV	85.45	911	58.06
VERL	82.05	381	24.28
BAC	88.97	304	18.24
HANG	0.0	38	2.42
DELT	55.34	446	28.43
LAKU	89.93	543	34.61
MORA	48.83	203	12.94
Overall	82.42	1569	100

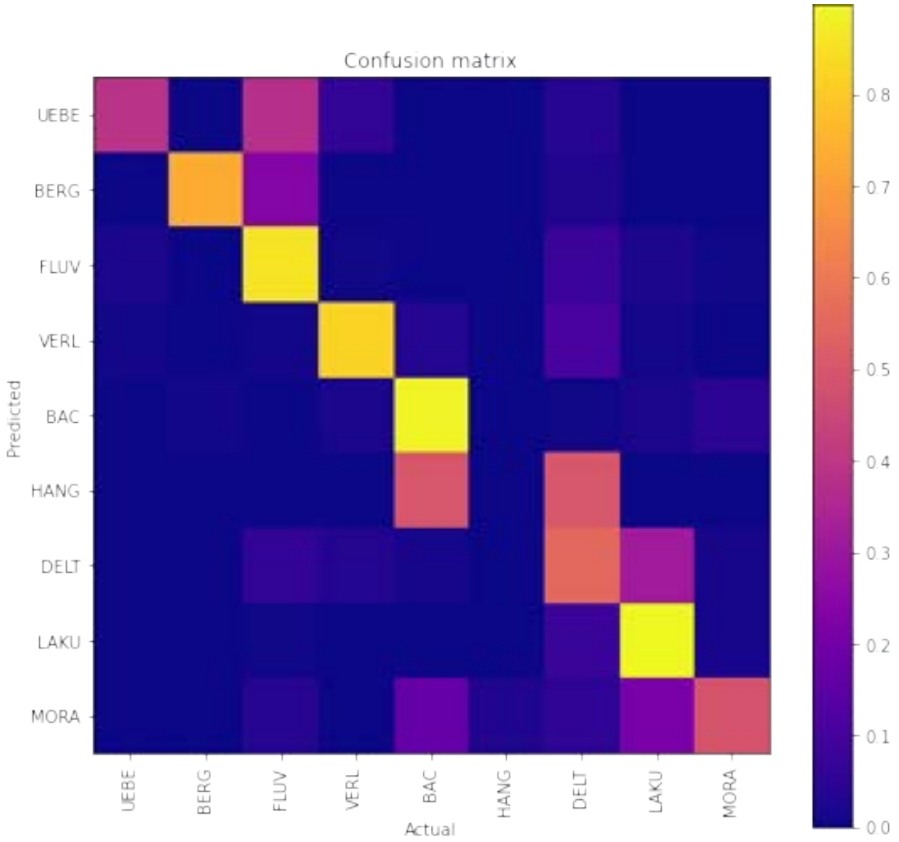

Figure 5.16: *Results of the cross-validation performed on the full model (Fig. 5.12).*

5.6 Limits and perspectives

5.6.1 Unique model selection

Regarding the results obtained through the model selection section (Section 5.5.1), it may seem clear that M3 or M4 are the best choices, but it is necessary to clarify some points.

Method 2 could certainly be improved as it is subject to a sampling bias problem. The wells are not equally distributed spatially, both laterally and vertically. This unequal distribution of the data generally leads to an over-representation in certain areas and consequently of units in the data. A declustering technique (e.g. Olea 2007) could be applied to correct for this spatial bias. Weighting the data using such a method could be a possible solution to mitigate the issue identified and probably improve the performance of the method 2.

It is important to note that all these methods require a large number of realizations to provide good results. But concerning method 4, it is very likely that it requires even more realizations than the other methods. Indeed, the model space should be sufficiently covered. The question is how many simulations are needed if the model is large and complex as in this case. For the test case, we have used 100 realizations on a small area, with limited variability, which gave very good results (tab. 5.1, M4). But concerning the whole model, only 50 realizations have been made, and it is difficult to know if it is enough to really get the most representative model. But the question remains whether 100 or even 200 simulations would have had a significant impact on the final model.

Method 4 also has the problem of defining an appropriate distance between the models (sec. 5.5.1). In the present chapter, the distance was set as being the total number of cells in disagreement between two simulations. This measure of distance should be fine in many situations, but one can imagine, for example, distances based on the proportions of the units or the connectivity of the units, or even more specialized quantities related to some specific applications. The choice should be a function of the final purpose of the model. We believe that if the models were used later as a tool to forecast groundwater, for example, it would be more appropriate to run the hydraulic simulation on the ensemble of model (in this case 50) and then integrate the results. We can then obtain the predicted heads, with a uncertainty reflecting the uncertainty on the geology.

In the end, what needs to be remembered is that no aggregation method is perfect and general. Keeping this point in mind is important, even if our results show that the global accuracies are very similar (between 73.5 - 76%) for the 4 methods, and hence the choice of aggregating the realizations into one final model is quite arbitrary. Further research and investigations on all these aspects could be undertaken to clarify the impact of one or the other methods on practical decisions taken on the base of this unique 3D geological model.

5.6.2 Model quality and confidence

Even if the results are good on the overall, the accuracy can vary drastically between the units. The worse results are obtained for sparse or thin units (UEBE and HANG). Concerning HANG deposits, whose accuracy result is 0%, it is important to note that this unit is rare and scattered in the data set (present in 38 boreholes). In ArchPy, some boreholes were also discarded because they fall in the same cell. If multiple wells are present, the deepest well is kept, since it is assumed to provide more information. Then some wells containing HANG deposits are likely to have been discarded. In addition to that, during the cross-validation process, 20% of the wells are removed for each fold, and it is possible that the HANG deposits are almost not represented. UEBE for example does not have this problem as it is present in one third

of the boreholes. However, it is particularly thin, making its simulation more difficult.

Stochastic models allow quantifying uncertainty. Here we summarized these results using the Shannon entropy. The entropy map shows some reasonable results. For example, it can accurately identify where the model is the most uncertain (generally at intermediate depth (20 - 50 m) and to the left of the model). But this map does not highlight well the places where the uncertainty concerns only two different units such as UEBE vs FLUV. In addition, it does not show at all the large uncertainty existing at large depth ($>$ 100 m), the entropy becomes 0 because the only outcome of the realizations is LAKU deposits. Obviously, at these depths, the uncertainty should be greater because of the lack of conditioning data. The issue is not related to the use of the entropy measure but it relates to the fact that the ArchPy model relies on the stratigraphic pile reflecting a given conceptual geological model. If some unknown aspects of the geology at these depths are not considered in the original geological concept, they cannot be simulated and the uncertainty cannot be quantified. Hence, the Shannon entropy of 0 at these locations does not mean that there is no uncertainty.

To overcome this limitation requires further research. One approach could be to consider multiple conceptual models of equal (or not) prior probabilities. The realization of multiple realizations with different conceptual models would then infuse uncertainty. For example, the presence of a deeper unknown layer or variations in the Moräne concept could be added. The question will then be to define a strategy and acquire data to construct and test these various conceptual models.

Another approach to quantify the uncertainty could be to consider a measure of the distance from the conditioning points. Cells at a distance greater than a given range would be considered highly uncertain. To link the distance with the uncertainty, one could rely on classical geostatistical techniques and infer 3D variograms. Based on this type of models, it would be possible to apply kriging and define an indicator of uncertainty across the entire simulation domain. The difficulty will then be to combine this measure with the results of ArchPy. Also, it should be recalled that the Shannon entropy is a measure that assumes that any unit can be found anywhere. But geologically speaking in this case, we know that it becomes increasingly difficult to find, for example, Bachschutts (BAC) or floodplain (UEBE) units with depth. To take account of this bias in the measure of uncertainty, it could be beneficial to spatially estimate the maximum number of units we expect to find. Some numerical experiments should be conducted to test the feasibility of these ideas and adjust the methodology in order to obtain meaningful results.

5.6.3 Moräne simulation

MORA is simulated differently from the other units. We have constrained the top of the moräne to be simulated, on average, 15 meters above the bedrock elevation. The purpose of this constraint is to respect a particular geological concept. The results of this modeling choice are not very good, given that one out of two cells predicted as "MORA" is wrong. MORA is often mispredicted by LAKU and BAC units (Fig. 5.16) in the majority of cases. This can be the result of an inappropriate covariance model or an incorrect modeling strategy. MORA being the last unit in the pile, it is rarely completely sampled by boreholes. And when it is, it is usually on the side of the valley, where the Moräne thickness is probably affected. Consequently, the MORA thickness that was inferred from the boreholes and used to estimate its position above the bedrock is very likely to be underestimated. This inevitably leads to incorrect data integration in the modeling process. It would be interesting to test different geological concepts and variograms in order to determine which ones give the best results for this challenging layer.

There is also an issue regarding the simulation of the Moräne in the center of the valley. Boreholes only reach the MORA on the west-side of the valley. There is no information on the depth or thicknesses distributions of the moräne at other locations. This does not influence the results of the cross-validation (as no data are available), but it is important to take this into account because there is a high uncertainty at great depth on the spatial distribution of the MORA unit. More data should be collected and more investigation should be carried out. For example, information on the distribution of moraines in similar Alpine valleys could be sought. Geophysical data (such as seismic) could be useful if the contrast between moraine, bedrock, and LAKU deposits is expected to be strong enough. Ideally, the best thing to do would be to drill a couple of boreholes over the valley to reach the Moräne in order to get real in-situ information.

5.6.4 Other issues and perspectives

The lateral alluvial fans or slope deposits (BAC, BERG) are currently identified using the nearest neighbor algorithm. This results in sharp vertical boundaries between these units. These boundaries are not geologically realistic since two fans are expected to be intertwined along their boundary. Improving this feature of the model is feasible but would require to develop a novel manner to model the boundary between these types of objects. In the present model, we decided to consider that this was not necessary since the type of lithologies that one can find in each of these fans are rather similar.

One technical issue that we faced during this work was that the grid was very large and contained a majority of inactive cells. This lead to some memory and visualization issues especially when handling a large number of stochastic

simulations. One perspective is therefore to work on the data structure to make it more efficient when the lateral extension of the model domain is not rectangular.

5.7 Conclusion

This study presents a stochastic geological model of the Rhine Valley near Buchs, SG. The model was constructed using the ArchPy approach and module. Various geostatistical approaches have been considered depending on the units: classical Gaussian Random functions (GRF) for surfaces, and Multiple Point Statistics (MPS) simulations for syndepositional layers. We estimated the GRF parameters using an automatic approach available in ArchPy that analyzes the boreholes, extracts the data points and infers the covariance functions (variograms). The MPS approach required a Training Image (TI) that was built using an object-based model, attempting to reproduce the main features of the geological setting of the concerned units (VERL, BAC and FLUV). Finally, all of the different Bachschutts deposits were differentiated using a Nearest-Neighbor algorithm. A total of 50 realizations have been made to quantify the uncertainty that was estimated through the Shannon entropy and a 5-fold cross-validation procedure.

k-fold cross-validation showed that the model is capable of reproducing the units with an overall accuracy on the order of 80%. There are, however, a lot of differences between the units. Some are rather easy to forecast and therefore well simulated (FLUV, VERL, BAC, LAKU) while others are more difficult to simulate properly (UEBE, HANG, DELT, MORA). The good results obtained on FLUV, VERL and BAC units show that the MPS approach combined with the object-based TI was efficient in reproducing and simulating these units.

In general, this study has demonstrated how ArchPy, a free Open-Source software, performed on a real large case of Quaternary modeling. It also identified some of its limitations and how it could be improved to make it more robust and general-purpose. In addition, key issues in stochastic geological modeling were raised, such as the determination of a single model among a set of stochastic realizations, or the representation of uncertainty. These are issues that will certainly require further study in order to be fully understood.

Chapter 6

From lithological descriptions to geological models: an example from the Upper Aare Valley

Abstract

Geological models form a crucial foundation for hydrogeological models, significantly influencing the spatial distribution of key hydraulic parameters such as permeability, transmissivity, and porosity. The conventional modeling workflow involves a hierarchical approach that simulates three levels: stratigraphical units, lithologies, and finally properties. Although lithological descriptions are often available in the data (boreholes), the same is not true for unit descriptions, leading to potential inconsistencies in the modeling process. This limitation not only hinders the delineation of unit boundaries but also uses existing data, given that the information is present in an alternative form, lithological descriptions. To address this challenge, a geostatistical learning approach is presented, which aims to predict stratigraphical units at boreholes where this information is lacking, primarily using lithological logs as input. Various standard machine learning algorithms have been compared and evaluated to identify the most effective ones. The outputs of these algorithms are processed and utilized to simulate consistently the stratigraphy in boreholes having only lithological information. Subsequently, these boreholes contribute to the construction of stochastic geological models, which are then compared with models generated without the inclusion of these supplementary boreholes. This method is instrumental in reducing uncertainty in specific locations and mitigating inconsistencies between units and lithologies. It not only improves the accuracy of stratigraphical unit predictions, it also maximizes the use of available data, contributing to more robust hydrogeological models.

6.1 Introduction

The preceding chapters have demonstrated the usefulness of the ArchPy approach in various geological contexts. However, it has some important limitations that could restrict its application. This chapter focuses on a specific issue with the ArchPy approach (see Chapter 3), which concerns the need for a significant amount of geological data, primarily obtained from boreholes, to generate accurate and reliable models. Boreholes can provide information on units (stratigraphic logs), facies (lithological logs), and properties (e.g. pump test values). Although lithological logs are usually easier to obtain, determining stratigraphic units can be a challenging task, often resulting in the absence of stratigraphic logs. The problem is that inconsistencies can arise when units and facies are modeled sequentially.

Even though there may be no simple relationship between units and lithologies, the definition of stratigraphic units often adheres to a logic that tends to separate geological time periods with different climatic and sedimentological settings, resulting in the deposition of different types of sediments (Teles et al. 2001). As a consequence, some units can be mainly composed of coarse sediments (gravels, sand) or, conversely, fine sediments (clay, silt). In cases where

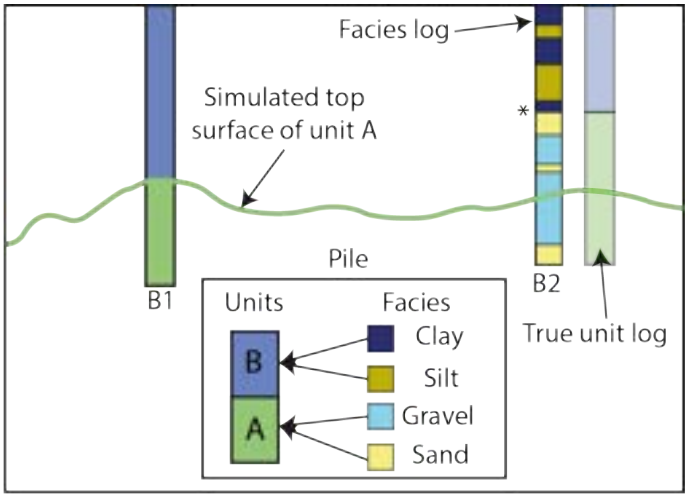

Figure 6.1: *Illustrative example demonstrating a possible consequence of the absence of the unit log. Borehole B2 is excluded from the simulation of the surface (green line), leading to inconsistent results. The surface must pass at the interface between unit B and A, corresponding to the interface between the facies clay, silt vs gravel, sand (indicated by the asterisk).*

stratigraphic logs are missing, simulations may yield inconsistent facies models compared to unit models, as illustrated in Figure 6.1. In this simple example, the absence of the unit log for borehole B2 leads to an inaccurate representation of the interface between A and B. Subsequently, the simulated facies will be partially erroneous, and a portion of the facies log for B2 will not be respected. Note that while this is a simplified illustration, determining the true unit log is not challenging in this case. In reality, more complex relations emerge, where dozens of units and facies can be combined.

Recently, Machine Learning (ML) algorithms have emerged as an interesting alternative to traditional geostatistical methods. For example, Aliouane et al. (2013) evaluated the performance of various ML algorithms for the prediction of lithology. Similarly, Hammond et al. (2023) employed Artificial Neural Networks in conjunction with Self-Organizing Maps to predict the spatial distribution of lithofacies in a large and intricate glacial aquifer, using a substantial database of more than 13,000 boreholes. Another notable example is the work of Sahoo et al. (2017), who applied a similar approach on a smaller scale, achieving highly accurate prediction results with precisions reaching 90%. Furthermore, Zhou et al. (2019) suggested the application of a recurrent neural network, a form of Deep Learning network, to directly model sequences of geological units (i.e., boreholes) based on geographical coordinates.

However, it is crucial to note that these methodologies were developed to model specific geological entities (such as units or facies) in isolation, without an ex-

plicit consideration of the interdependence between them. Addressing this limitation, Li et al. (2023a) have introduced a sequential approach in which a stratigraphic ML model is initially trained on spatial coordinates only. Subsequently, the results of this model are used to constrain a facies ML model, ensuring coherence between stratigraphic and facies representations and avoiding the challenges depicted in Figure 6.1.

To fill this gap, our study introduces a novel approach for inferring stratigraphical units using lithological descriptions and geographical coordinates. This methodology is applied to the Upper Aare Valley. A stochastic geological model is generated and compared with a similar model that integrates these new sources of information. The paper is organized as follows. Section 2 provides an overview of the study area and the available data, while Section 3 elaborates on the construction of the geological model. In Section 4, we dive into the machine learning methodology used to infer stratigraphy. Finally, Sections 5 and 6 present and discuss the results, along with an exploration of potential limitations and avenues for improvement within the current workflow.

6.2 Study Area

6.2.1 Geological context

The test area selected for this methodology is the Upper Aare Valley, which is a Quaternary Alpine Valley situated between the cities of Thun and Bern in Switzerland (Fig. 6.2). This valley has undergone a complex geological history primarily influenced by glacial and river processes (Kellerhals et al. 1981; Haeuselmann et al. 2007). The main river in the valley is the Aare, which flows from south to north. Previous investigations focused on Quaternary deposits, regionally (Schlüchter 1989; Preusser et al. 2004), as well as locally (Preusser et al. 2011; Graf et al. 2016), have revealed complex relationships among various depositional and erosional processes, including fluvial, glacial, glacio-fluvial, and glacio-lacustrine. Consequently, the geology of the valley is diverse and exhibits a wide range of sediments and facies, such as tills/moraines, fluvial gravels, glacio-lacustrine deposits, lake deposits, and alluvial cones, contributing to the notable heterogeneity of these deposits. From a hydrogeological point of view, two primary aquifers have been identified: a shallow aquifer actively utilized for drinking water supply, shallow geothermal energy and local industries, and a deeper aquifer, which remains poorly understood due to its greater depth (with only a limited number of boreholes reaching it). The thickness of the shallow aquifer exhibits variation, ranging from 0-5 meters in the north, where a local absence of the aquifer can be observed, to 50-80 meters in the south.

A brief summary of the geological history is presented, but a more complete geological review can be found in Kellerhals et al. (1981). It begins in the Pleistocene, where the erosion of the Swiss Molasse (bedrock) by the glaciers

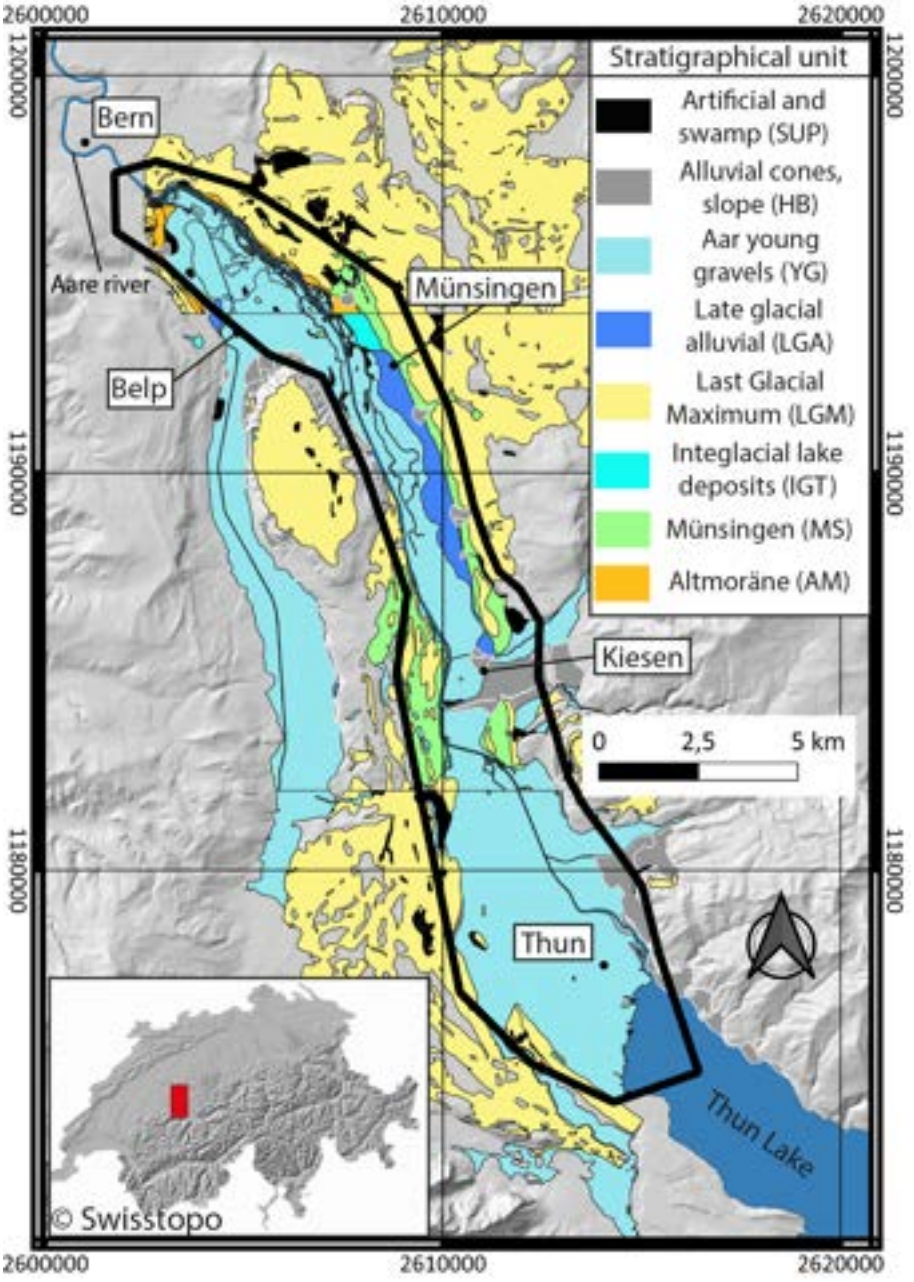

Figure 6.2: *Geographical situation and simplified geological map of the Upper Aare Valley. Only unconsolidated deposits are shown. The coordinates are presented in CH1903+ - LV95 (epsg: 2056). All data used come from the Swiss Geological Survey (Swisstopo) and are freely accessible. The black polygon delimits the modeling area for the study.*

has shaped the valleys that can be observed today. The earliest Quaternary sediments, locally denominated as "Alte Seetone" (AT), are old lacustrine deposits that make up the valley's predominant geological volume, presuming the presence of a large lake at that time. Locally, these deposits are overlain by Oppligen sands (OS), a unit mainly composed of sand ($> 70\%$), compared to the others. Ascenting further, the Uttigen-Bümberg-Steghalde gravels (UBS), a fluvial deposit, rest atop AT and OS. This particular formation is known to be a major constituent of the deep aquifer. AT, OS, and UBS do not outcrop (Fig. 6.2), and are shallower in the southern and lateral parts of the valley. Following these events, one or more glacial episodes were recorded, attributed to the previously named Riss glaciation. These episodes entailed the erosion of existing deposits and the deposition of new ones, specifically glaciolacustrine deposits (GL), "Altmoräne" (AM, Old Moraine, probably from Riss glaciation), and retreat fluviogravels, following a typical glacial sequence. The retreat gravels have practically all been eroded. This sequence is followed by an interglacial lacustrine clay (IGT). Outcrops and borehole observations of GL, AM, and IGT are limited, predominantly located on the northern sides of the valley.

Following the interglacial stage, a major gravel deposition event, Münsingen gravels (MS) can still be found across the whole valley. This occurs right before the last glacial maximum (LGM), during which large moraines have been deposited. After LGM, phases of late glaciation followed, with localized and anecdotal deposits of gravel and moraine. The conclusion of these late glacial phases is marked by post- to late-glacial lacustrine deposits (LGL). In addition to the LGLs, postglacial to lateglacial gravels (LGA) were also deposited. Subsequently, the Aare River contributed to the deposition of gravel (YG), forming a significant component of the upper aquifer. These gravels are occasionally overlain by slope deposits and lateral alluvial fans (HB), as well as swamp and artificial deposits (SUP). LGL, LGA, YG and HB are located in the center of the main and lateral valleys and are surrounded by the bedrock and the other units.

6.2.2 Available data

The Swiss Geological Survey has compiled and standardized a significant borehole database (Volken et al. 2016), resulting in a substantial data set that comprises 791 boreholes for the designated area. The distribution of the depths of the boreholes is highly uneven. The vast majority ($> 95\%$) of the depths of the boreholes range between a few and 50 meters deep, while some outliers can reach up to 200 m. Each borehole is characterized by intervals containing information on granulometry (lithologies), stratigraphical units, and details regarding the quality and reliability of the interpretations. The rich geological history has contributed to the identification of many interpreted stratigraphical units (24 in total). However, it should be noted that only one third of the wells includes a unit description (266 out of 791 boreholes, see Fig. 6.3), and

certain units are absent within the modeling area. Granulometry information is described with one, two, or up to three distinct grain sizes, each defined following the USCS system (Casagrande 1948).

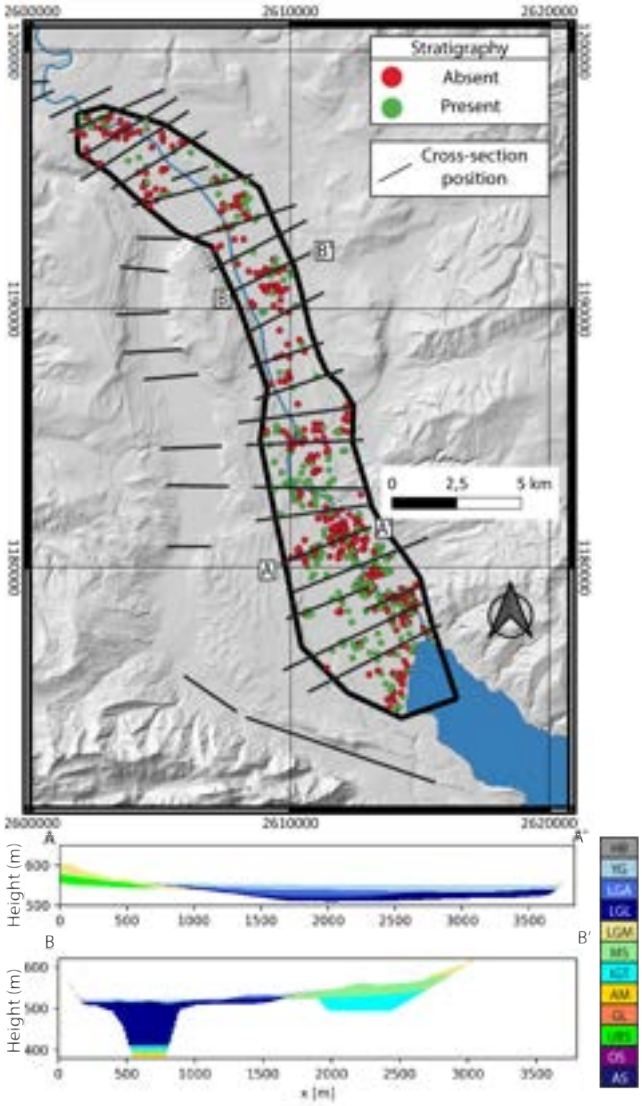

Figure 6.3: *Borehole and cross-section positions over the modeling area. Boreholes with stratigraphic unit descriptions are colored in green while those without are colored in red. Two cross-sections, whose positions are marked by A-A' and B-B', are also shown. The colors used in the cross-sections to represent the units are described Figure 6.4.*

In addition to boreholes, a set of geological cross sections has been drawn by Kellerhals et al. (1981) (Fig. 6.3), complemented by a geological map (Fig. 6.2), derived from the GeoCover dataset of the Swiss Geological Survey. The cross sections do not reach the bottom of the valley and provide limited information about deep geology, but still provide constraints at shallow depths (< 50 m).

6.3 Geological model

Recently, several studies have tested different approaches to model the heterogeneity of the valley (Volken et al. 2016; Neven et al. 2022a; Schorpp et al. 2022; Neven et al. 2023), supported by recent geophysical data acquisition, nearly over the entire valley (Neven et al. 2021). Neven et al. (2022a) proposed a clay fraction model that combined boreholes and geophysical data in a stochastic workflow. However, a limitation of their approach was the lack of geological consistency in the final model. This issue was addressed to some extent in a subsequent work, where ArchPy was integrated with a joint inversion workflow utilizing an Ensemble Smoother with Multiple Data Assimilation (Neven et al. 2023). However, the geological model used in this refinement remained restricted (complete stratigraphy not considered, lacking a facies modeling step), leaving room for further enhancements. In response to these considerations, a comprehensive and stochastic geological model of the Upper Aare Valley is presented, drawing on available geological data.

The model is constructed using the ArchPy geological modeling package (Schorpp et al. 2022), which is based on the Geone [7] geostatistical library. ArchPy workflow is hierarchical and relies on three major steps: units, facies (lithologies), and properties. In the unit simulation, 2D surfaces are simulated to delineate the upper and lower boundaries of each unit. Subsequently, facies simulation employs 3D categorical methods (facies methods) to fill the previously simulated units with facies. Finally, independent continuous simulations are performed within each facies to obtain the property models.

6.3.1 ArchPy Pile

The main ingredient of an ArchPy model is the definition of the Stratigraphic Pile (SP). The SP does not solely consist in defining the order of deposition of the units but also the interpolation (and related parameters) to use to delimit their lateral extent, the type of contact of their top surface, the lithologies that compose these units, etc. Alternatively, the SP can be viewed as the geological concept translated into a format comprehensible by the modeling package, in this case ArchPy. The SP for the present study is shown in Figure 6.4.

[7] http://www.github.com/randlab/geone

The simulation of all unit surfaces (interp method column, Fig. 6.4 A) uses Gaussian Random Functions (GRF) (Chiles et al. 2012), except for the SUP unit, where its top surface is simply set at the elevation of the Digital Elevation Model (DEM). Two surfaces, MS and UBS, are treated as erosive. This decision is based on the assumption that, at the conclusion of these units, a significant glaciation event occurred, suggesting a corresponding major erosive episode. To keep things simple, Sequential Indicator Simulation (Journel et al. 1990, SIS) is used to model the distribution of the lithology.

Unit name	Unit	Interp method	Top contact	Filling method	List facies (A)
Swamp and artificial deposits	SUP	DEM	onlap	SIS	O, C, G, GC
Lateral alluvial fans	HB	GRF	onlap	SIS	CG, G, C
Aare River deposits	YG	GRF	onlap	SIS	G, GC, S
Lateglacial river deposits	LGA	GRF	onlap	SIS	G, GC, S
Lateglacial lacustrine deposits	LGL	GRF	onlap	SIS	S, C, SC
Last glacial maximum	LGM	GRF	onlap	SIS	CG, C, SC, S, G
Münsingen gravels	MS	GRF	erode	SIS	CG, C, SC, S, G
Interglacial lacustrine clay	IGT	GRF	onlap	SIS	C
Old Moraine (prob. Riss glacial)	AM	GRF	onlap	SIS	CG, C, SC, S, G
Glacio-lacustrine deposits	GL	GRF	onlap	SIS	G, C, S, CG
Uttigen-Bümberg-Steghalde gravels	UBS	GRF	erode	SIS	CG, C, SC, S, G
Oppligen Sands	OS	GRF	onlap	SIS	S, G, SC
Alte Seetone (old lacustrine clays)	AS	GRF	onlap	SIS	C, SC, S, O

	Litho.	Prop	Prop method	USCS Codes (B)
Organic	O	K	SGS	OH, OL, PT
Gravels	G	K	SGS	G, G-GM, GW-GM, GP-GM, GP, GW, GP-GC, G-GC
Sands	S	K	SGS	S-SM, S, SP-SM, SP, SW, S-SC, SP-SC, SW-SM
Clayey gravels	GC	K	SGS	GM, GC, GC-GM
Clayey sands	SC	K	SGS	SM, SC, SC-SM
Clay and silts	C	K	SGS	ML, CL-ML, CL

Figure 6.4: *ArchPy Stratigraphic Pile for the Aar model.* ***A****: Details about the stratigraphic unit such as interpolation method (GRF: Gaussian Random Function), contact of top surface, filling method for the facies step and the list of facies to model inside this unit.* ***B****: Facies table containing details about the facies such as the property to simulate (K: hydraulic conductivity), Interpolation method (SGS: Sequential Gaussian Simulation) and USCS codes that correspond to the facies.*

Lithologies are categorized into six groups according to the main grain size, expressed in terms of USCS codes. The corresponding codes for each category

are provided in Figure 6.4B. Sequential Gaussian simulation (SGS) (Deutsch et al. 1992) is used to simulate the hydraulic conductivity (K), the unique property considered in this study, but others can be easily and quickly integrated.

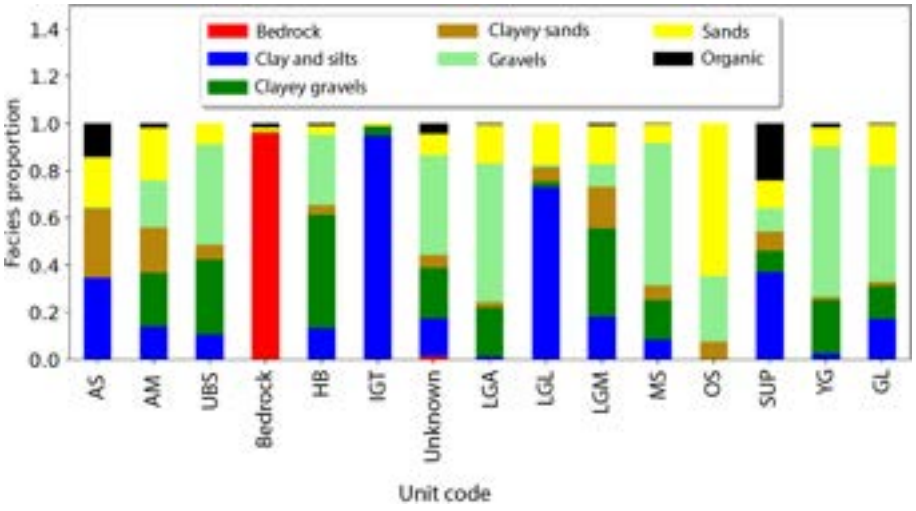

Figure 6.5: *Lithologies group proportions in each of the stratigraphic units. In addition, proportions are also given for the bedrock unit and when the unit is unknown.*

The facies proportion in each unit are shown in Figure 6.5. The assignment of facies to units is determined by their relative proportions. If a facies constitutes less than 5%, it is supposed to be absent from the unit. The facies associations for each unit allows to clearly identify the lithological nature of these units. For instance, LGM and AM, both moraines, encompass nearly all categories, aligning with the expectation that moraines exhibit very poor sorting. However, we can observe that the aquifer formations (YG, LGA, MS, UBS, and OS) mainly contain the most permeable categories (G, S, and GC). However, MS and UBS also include clay (C) and clayey sand (SC), which shows that the relationship between facies and units is not so straightforward.

6.3.2 Data and modeling grid

Input data are the boreholes described in the previous section as well as the geological map (Fig. 6.2) and the cross sections (Fig. 6.3). To be used with ArchPy and take advantage of its automated processing step, these two data (map and cross-sections) are converted into fake boreholes.

The extent of the modeling considers the polygon shown in Figure 6.2, with a spatial resolution set at $25 \times 25 \times 2$ meters ($sx \times sy \times sz$). The origin of the z direction is established at 350 m above sea level, with the maximum elevation reaching 590 m above sea level. This configuration results in a grid size of $548 \times 958 \times 120$ cells ($nx \times ny \times nz$). The top of the domain is defined by the

Swiss DEM with a resolution of 25×25 meters (DHM25, Swisstopo). At the same time, the bottom is determined by a raster map of the elevation of the bedrock (TopFels25, Swisstopo), which also has a resolution of 25×25 meters. Both datasets are accessible through the Swiss Federal Office of Topography. Only cells in the domain delimited by the polygon, top and bottom are actives.

6.3.3 Modeling parameters

Once the SP, a grid, and the data are defined, ArchPy processes the boreholes which are analyzed and necessary data are extracted. This step automatically determines the equality data (data points through which a surface must pass) and inequality data (data indicating that the surface must go above or below this point) for surface interpolation. The result is a list of coordinates for the equality and inequality data for each unit. More details on this procedure can be found in chapter 3.

In order to use GRF, covariance models (variograms) must be specified for each top surface. For YG, LGA, and LGL, where no discernible anisotropy is apparent, isotropic models were automatically fitted (through least-square optimization) to their equality points. However, for the remaining units, a clear anisotropy is observed, aligned with the main axis of the valley. Unfortunately, the number of points is insufficient to estimate a reliable 2D variogram. Consequently, a default anisotropic variogram model was estimated using the elevation surface of the bedrock (TopFels25) as a surrogate, which is known and assumed to represent the general shape of the unit surfaces. The total variance for each unit was adjusted on the basis of the observed variance in the data. Additionally, this model incorporates a locally variable anisotropy through a rotation map that accounts for the orientation of the axis of the valley.

The facies modeling stage using SIS also necessitates variograms, one for each facies within each unit. These variograms were manually adjusted, assuming that there was no horizontal anisotropy (i.e., the variogram range in the x-direction equals the range in the y-direction) whenever the number of data points was sufficient. In cases where the data points were insufficient, variograms for the same facies in another unit were considered.

For the simulation of hydraulic conductivity (K), no available data were used to estimate the variograms. Instead, they were defined on the basis of previous research in the area (Schorpp et al. 2022; Neven et al. 2023) and the scientific literature related to similar lithologies (Das et al. 1990; Fogg et al. 1998).

Complete details of the variograms for each unit, facies, and property, as well as the anisotropic map, are shown in Appendix A.3.

6.4 Borehole units inference

This section outlines the methodology used to predict stratigraphic unit information in boreholes where it is absent, relying on lithological and spatial information. The approach is divided into two distinct steps: first, a machine learning (ML) step where algorithms are trained and applied to derive probabilities of unit occurrences along the boreholes; and second, the utilization of these probabilities in a simulation step to generate plausible boreholes. The data considered for this analysis are boreholes from the GeoQuat database, simplified according to the ArchPy Pile (Fig. 6.4), resulting in 13 units for six lithofacies. Two more classes, not used in the geological model, have been considered in the ML process, which are Bedrock and Unknown. Unknown represents a gap in the unit log interpretation.

6.4.1 Machine learning step

Initially, the boreholes are divided into two datasets, a training set and a test set, for the validation of the present methodology. Of the 791 existing boreholes, only 266 contain stratigraphic information (Fig. 6.3), forming the total data set. From these 266 boreholes, a training set is generated, consisting of 75% (200) of the boreholes, while the test set comprises the remaining 25% (66) of the boreholes. This partition is achieved through iterative stratified sampling, ensuring a similar unit proportion distribution in both sets. It is important to note that some units, such as AM or IGT, are very rare and are present in only a few boreholes. This rarity posed challenges for stratified sampling, resulting in a less straightforward and imperfect process. However, efforts were made to restrict the disparity in class distribution between the two sets to within 2%, relative to the total proportion.

To integrate borehole information into the ML process, it is essential to transform training and test sets into data structures consisting of features (inputs) and labels (outputs). ML algorithms, operating on each data point characterized by multiple features, generate predictions for a single label or assign probabilities to each potential label. Obviously, algorithms are trained to give the best possible predictions. Features can take a variety of forms, including continuous or categorical values, but each data point must consistently have the same number of features. Figure 6.6 illustrates how a training borehole is transformed into a collection of multiple data points, each with its list of features and the resulting labels.

Boreholes are initially segmented into intervals of uniform thickness (e), and for each interval, a data point is constructed using a list of lithological and spatial features that vary along the boreholes. The spatial features consist of four elements: the x, y, and z coordinates of the interval (X_{bh}, Y_{bh}, and Z_i), along with its depth relative to the top of the borehole (D_i). Regarding lithological features, they encompass the lithology observed within the interval (red square

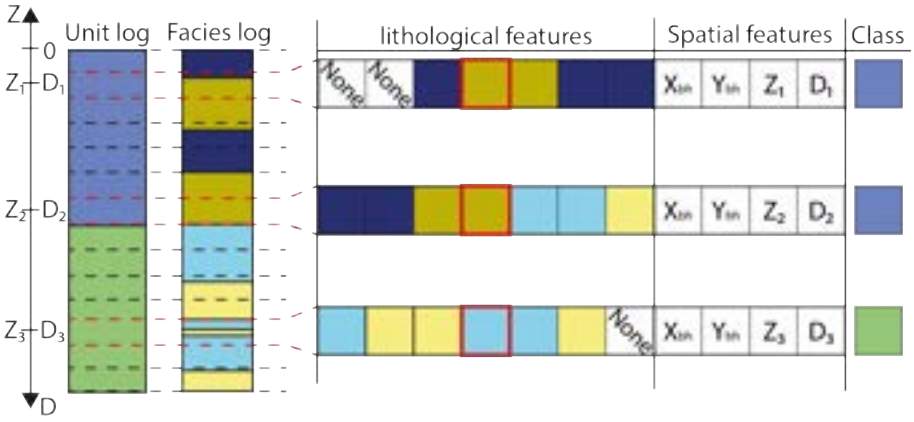

Figure 6.6: *Schematic representation of the features and label creation of training borehole for the machine learning algorithm. For the sake of clarity, only three data are shown, but each interval in the borehole, separated by the dashed lines, is transformed. For each interval i, there is a datum defined by seven categorical lithological features that correspond to the three lithologies above and below the interval, as well as the lithology in the interval (surrounded in red). If no lithology data are available above or below, the feature is set as "none". Furthermore, four additional numerical features are considered, which are: the x and y coordinates of the borehole (X_{bh} and Y_{bh}, respectively), the elevation (Z_i) and depth (D_i) of the interval.*

in Figure 6.6), as well as a specified number of lithologies above (n_a) and below (n_b). In Figure 6.6, three intervals are considered above and below ($n_a = n_b = 3$). If multiple lithologies are observed within a single interval, the most dominant one is considered (see Figure 6.6).

The inclusion of lithologies both above and below a given interval serves a crucial purpose in mitigating potential errors in predictions arising from the presence of rare or inconsistent lithology/unit associations.To illustrate this, consider a scenario involving an aquifer unit primarily composed of gravel and sands. In the presence of thin sporadic clay layers (with a thickness of e), relying solely on the lithology within the specific interval can lead to inaccuracies in ML predictions, such as incorrectly predicting that these intervals belong to another unit, possibly one that is more clay rich. However, if we integrate a larger picture of the situation by considering the lithologies above and below, this effect can be mitigated.

e, n_a and n_b are user inputs of the methodology that need to be defined. e should be low enough to capture vertical variability in terms of lithologies in the modeling area. On the contrary, n_a and n_b should be high enough to encompass a sufficient number of lithological variations above and below each interval. Conceptually, these parameters act as a viewing window through which the algorithm can gain insight into the prediction problem. For this study, the

selected parameters are $e = 20$ cm, $n_a = n_b = 10$, indicating the consideration of a 2 meter span above and below each interval with a resolution of 20 cm. This roughly corresponds to the finest level of detail that can be obtained from the geological description of this area.

Different standard ML algorithms have been tested in order to select the one that gives the best predictions; these include: Random Forest (RF, Breiman 2001), adaptive boost (Adaboost, Freund et al. 1995), gradient boost (Gboost, Friedman 2001), multilayer perceptron (MLP, Haykin 1998) and finally support vector classifier (SVC, Cortes et al. 1995). These algorithms were implemented and used through the Pedregosa et al. (2011) python package. They are compared based on metrics including precision, recall, F-score, and Brier score for each class (unit). Given our focus on probability predictions, conventional machine learning metrics such as precision, recall, and F-score might not provide the nuanced insights we require. For these reasons, we also rely on the Brier score, which is a metric commonly used for evaluating the accuracy of probabilistic predictions, particularly for classification problems.

Brier score (Brier 1950) was recently proposed as a metric to validate categorical models in geosciences (Juda et al. 2020). It is defined as:

$$BS = \frac{1}{N} \sum_{i=1}^{N} \sum_{j=1}^{M} (P_{ij} - O_{ij})^2 \tag{6.1}$$

where BS is the Brier Score, N is the number of data points, M is the number of classes, P_{ij} is the predicted probability for the j-th class of the i-th data point, and O_{ij} is an indicator variable (0 or 1) that represents whether the j-th class is the true class for the i-th data point. A lower Brier score indicates better performance, 0 being a perfect score, which means that the model predicts with precision 100%. On the contrary, a score of 1 indicates the worst performance, where the predicted probabilities are completely inaccurate, implying a prediction of 100% in any other class. Brier score is useful because it has the ability to evaluate both the correctness of the predicted class and the confidence in that prediction. It strongly penalizes overconfident predictions that are incorrect, in contrast to predictions that are wrong but marked by uncertainty. This feature underlines the importance of conservative forecasts and provides a more reliable quantification of uncertainty.

Each ML algorithm is tuned by a set of hyperparameters (HP). Their choice is important because an improper combination of HP can lead to imprecise predictions and overfitting. For the five algorithms tested (RF, SVC, MLP, Adaboost, Gboost), various sets of hyperparameters have been adjusted using a 5-fold cross-validation using the RandomizedSearchCV function from the scikit-learn Python package (Pedregosa et al. 2011). It is also this package that has

been used to manipulate, train, and test the algorithms. The optimized HP are given in the appendix A.3.

6.4.2 Borehole simulation step

With the inputs outlined in the previous subsection, the algorithms predict the unit for each interval independently, rather than considering the entire borehole as a whole. This approach can result in predictions that do not adhere to the expected stratigraphy, which should ideally remain consistent throughout the borehole. To address this issue, the borehole simulation step introduces a stochastic method to alleviate these inconsistencies.

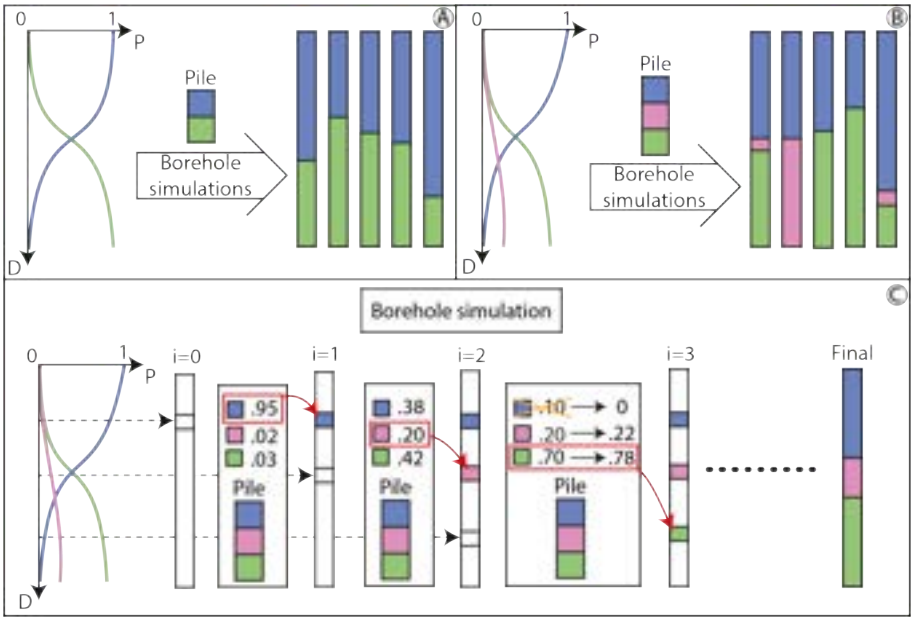

Figure 6.7: ***A*** *and* ***B****: Illustrated are examples of borehole simulation under two distinct settings. The curves depict the ML outputs, representing probabilities for each class as a function of depth. It is important to note that simulated boreholes are purely for illustrative purposes and do not reflect equiprobable simulations from the given curves.* ***C****: Schematic representation of the workflow. The methodology iteratively identifies vacant intervals within the borehole and simulates the corresponding unit based on probabilities derived from ML. Notably, probabilities are adjusted in accordance with the existing stratigraphy, ensuring that units deemed impossible are assigned a probability of 0 (blue unit at iteration 2).*

Many ML algorithms are able to predict not only one class per data, but they can also propose probabilities for each class. Taking advantage of this, the idea is then to use this information to simulate boreholes that are consistent with the stratigraphy. Figures 6.7A and 6.7B show two examples of this procedure,

where five plausible boreholes are shown. The procedure is illustrated in Figure 6.7C, and now we detail its different steps.

The adopted methodology follows the sequential algorithm proposed by Journel et al. (1990), using ML for probability predictions. The process starts with an empty borehole, segmented into intervals identical to those in the facies log (refer to Fig. 6.6). Subsequently, a random empty interval is chosen, and the trained ML algorithm is employed to obtain the predicted probabilities. On the basis of these probabilities, a unit is randomly drawn and assigned to the interval. This sequence is repeated iteratively, with additional intervals selected and filled until the entire borehole is populated. The particularity here is that probabilities are adapted according to the stratigraphic pile. This means that impossible to simulated units have a probability set to 0, while the others are rescaled. This step is shown in Figure 6.7C, iteration 2 where the only possible units are pink and green due to the previously simulated units (blue cannot be located below pink).

Note that, this simulation procedure might encounter a deadlock when all probabilities are reduced to 0. In such instances, the simulation is stopped and a new empty borehole is generated. To avoid being stuck, if the number of these errors exceeds a specified value (n_e, user defined), the borehole is deemed impractical to simulate.

Furthermore, ML predictions can exhibit significant noise, especially when dealing with a large number of units, resulting in numerous small probabilities assigned to a vast array of units. This noise can adversely affect the performance of the simulation algorithm, leading to artifacts characterized by numerous occurrences of units with small thickness. To address this issue, a filtering mechanism is implemented to remove probabilities below a certain threshold (τ, user-defined). This threshold should be set high enough to reduce noise, but a too large value reduces the variations in the simulated boreholes and can even lead to impossible simulations. After some trial and error, a value of 0.15 was identified as a suitable compromise for the boreholes within the study area.

6.5 Results

6.5.1 Machine learning

In Figure 6.8A, the mean metric values for different algorithms are compared. Overall, all models exhibit reasonable performance, except Adaboost, which demonstrates notably low precision (20%) and a high Brier score (0.9). The remaining models show precision, recall, F-score, and Brier score values in the range of 0.5-0.6. In particular, MLP is marginally less accurate compared to others, exhibiting a higher Brier score that exceeds 0.6, while RF, SVC, and Gboost maintain scores below 0.55. This indicates that predictions made with MLP are overconfident, compared to the others. Figures 6.8B to 6.8D provide

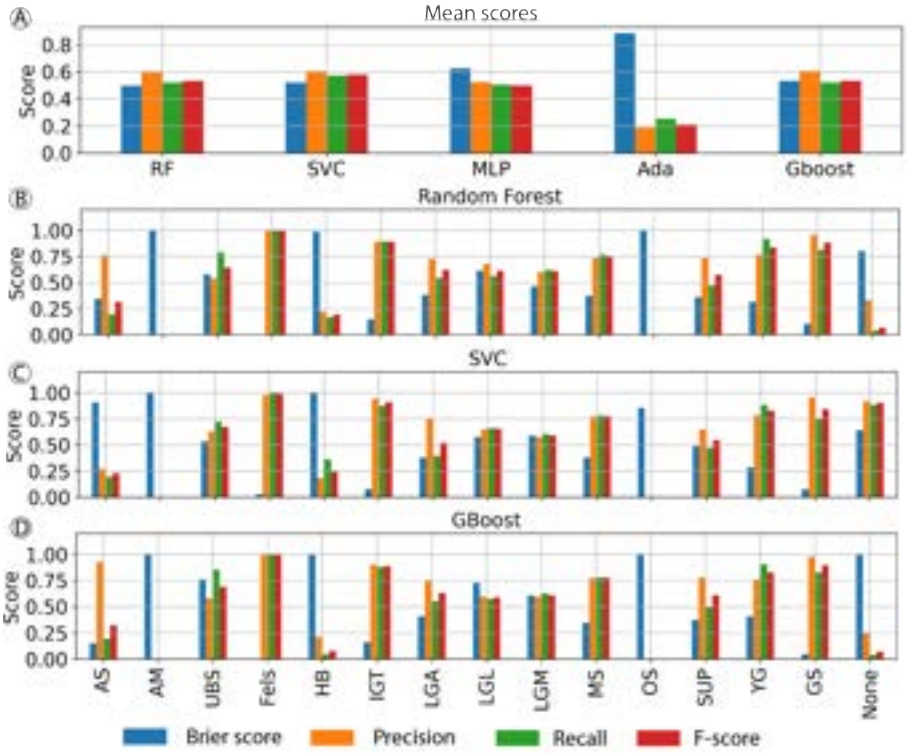

Figure 6.8: ***A****: mean scores for all models. Each class was assigned the same weight.* ***B****,* ***C****,* ***D*** *detailed scores for each class for the RF, SVC and Gboost algorithms.*

a detailed summary of the scores for each class for RF, SVC, and Gboost. It is blatant that certain classes, such as AM, OS, AS, or HB, are not accurately modeled. This discrepancy can be attributed to the low number of boreholes in the test set that contain these units, making the validation step less reliable. A similar situation is observed for IGT, which, despite having very good results, is represented by only one borehole in the test set. Consequently, assessing the reliability of the predictions for these units is not feasible. Fels unit, which represents the bedrock, has a perfect prediction for the only reason that this unit is characterized by a single and unique "lithology", not integrated in the geological model, as it defines the bottom of the geological model. The other units exhibit decent results with precisions around 0.6 and 0.8. The Brier score is a bit more variable and can be near 0 (for GS) but can reach 0.75 (for UBS, Fig. 6.8D).

To go further into depth and control that the borehole simulations produce reasonable results, Figure 6.9 shows the simulations for one borehole. 20 boreholes were simulated in each case and can be compared with the reference unit and facies logs. Predictions are close to the reference and three out of four methods

are able to predict the reference borehole correctly. Only MLP predicts the SUP unit base too deep as compared to the reference. However, all methods were able to determine the transition between the aquifer and the aquiclude (YG and LGL) which is clear on the facies log. Note how the method is able to consider that there is a certain variety of lithologies in the YG aquifer unit where we find sands, clayey sands, gravels, and clayey gravels.

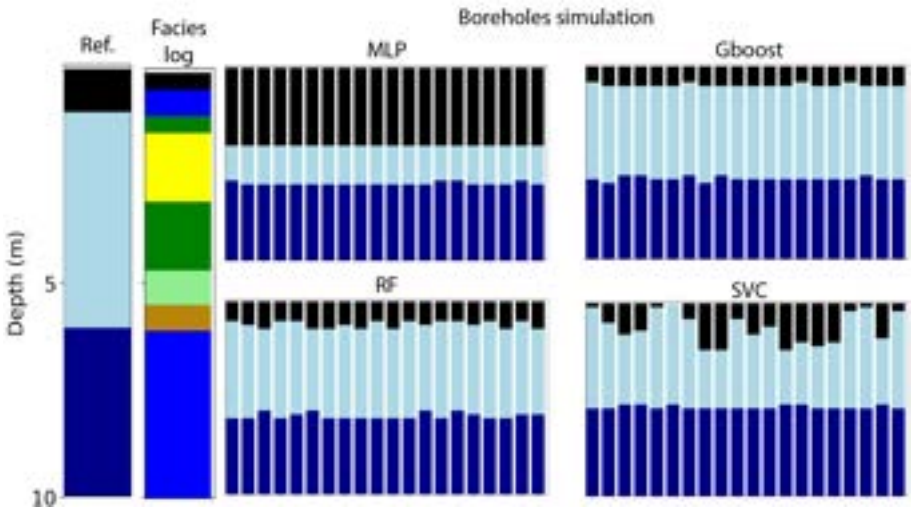

Figure 6.9: *Borehole simulations for a 10 m depth borehole. Reference and facies log are shown to the left while simulations are shown to the right, each distinct bar corresponds to one simulation. The threshold used was set at 0.15, but if simulations were not feasible with this value, it was decreased until simulations were feasible. See Figure 6.4 for corresponding colors for unit and facies.*

Figure 6.10 shows less satisfactory results from another borehole. The observations reveal that MLP and Gboost offer minimal variations, with outputs exhibiting near-deterministic behavior, in contrast to RF or SVC predictions. None of the methods predict the reference borehole in any simulation, but they provide reasonable results if we look at the lithology log. All methods predict the SUP unit from the surface to a depth of 5-7 meters, similar to the reference. The lithologies, shown in the facies log, significantly influence the prediction of this unit, with clay, sand, and clayey sand, which is a common assemblage of lithologies for this unit. All models predict the main aquifer unit, young Aar gravels (YG), and a transition to late lacustrine deposits (LGL) around 17 meters in depth. RF and SVC additionally forecast a thin layer of the LGA unit, albeit deeper than indicated by the reference borehole. Although the predictions do not align with the reference borehole, they make sense based on the lithological log that shows a clear transition between sand and clay lithologies around 17 meters in depth.

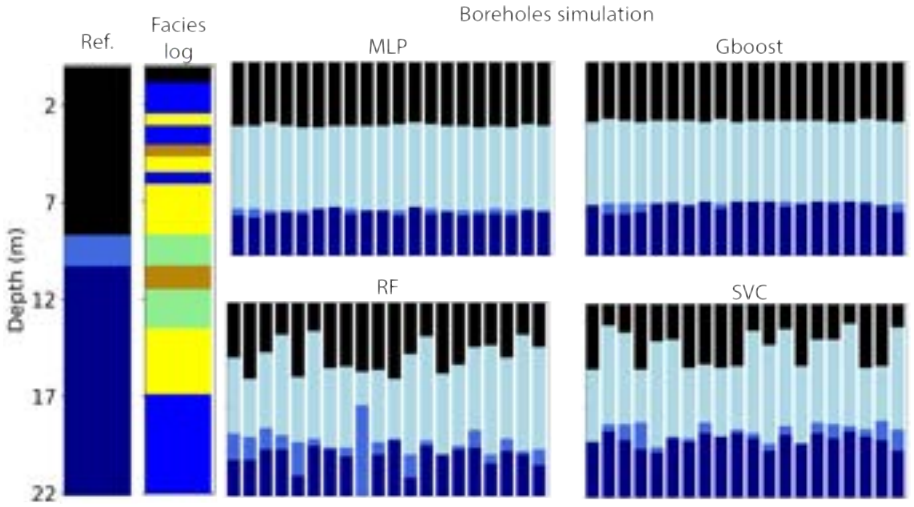

Figure 6.10: *Simulations of another borehole. See Figure 6.4 for corresponding colors for unit and facies.*

For the sake of brevity, only simulations for two boreholes are shown, but several others can be found in the Appendix A.3. For example, Figures A.3 and A.4 show that algorithms can give very different results that are completely different from each other. In the former case, algorithms predict two distinct units for the clay-rich layer at 7 meters, where Gboost and RF suggest IGT while SVC proposes LGL (which is ultimately correct). Just above, Gboost and RF also suggest a blend of YG and MS with occasional LGA, while SVC predicts solely YG (which is also correct). In the case of Figure A.4, MLP and SVC anticipate a sequence of HB and LGL, while Gboost and RF foresee a sequence of YG and LGL (which aligns with the correct succession, as per the interpreted log).

In certain cases, the facies log provides limited information, as shown in Figure A.5, where the predominance of gravels complicates the differentiation between units. The models anticipate a succession of MS and UBS, both predominantly composed of gravels, with SVC even indicating some LGA at the top. Distinguishing between these units based on lithologies proves impractical, prompting models to depend on spatial features constrained by other boreholes. The UBS predictions in all models are likely attributed to one or more other boreholes containing a similar succession of units and facies.

Simulations in Figures A.6 and A.7 show that the algorithm is also able to predict the correct units (YG, LGA) even when the facies log provides limited information. Determining the transition between these two units is not straightforward as they both globally have the same proportions of facies (Fig. 6.5). In such cases, the predictions are probably dictated by other boreholes that help to find the transition between two similar units such as YG and LGA.

Despite the adoption of a flexible approach for simulating boreholes based on probabilities, there is no guarantee that a borehole can be successfully simulated if the predictions lack consistency. In particular, with RF models, only one borehole from the test set encountered this situation. In contrast, other models exhibited less favorable outcomes, with three failed simulations for SVC, six for Gboost, and a more substantial 15 for MLP. The root cause of these failures can be traced to overconfident predictions that restrict the necessary flexibility required for successful simulation.

Taking these findings into account, it appears that there are no large differences between SVC, Gboost, and RF in terms of standard metrics. However, RF shows a slightly lower Brier score than the others (0.49 vs. 0.53), while SVC excels in precision, recall, and F-score. Furthermore, visual inspection of the simulated boreholes seems to allow us to show that RF proposes better predictions with greater variability, compared to MLP and Gboost. RF also seems to propose more accurate simulations than SVC.

Based on these results, the preference is to continue with the RF algorithm over SVC, despite its lower recall and F-score. This choice aligns with the priority of favoring models that are not overly confident and retain a degree of uncertainty in their predictions. Since probability predictions are the focus rather than the most probable ones, it is deemed more appropriate to continue with models that demonstrate superior performance in terms of the Brier score.

6.5.2 Geological Models

Comparison

In this section, we present the geological models obtained with and without the newly added ML boreholes, and compare the models using the test set boreholes. Moreover, the number of inconsistencies between facies data and simulated stratigraphic units are also compared. Two models are developed following the specifications detailed in Section 6.3: a basis model (ArchPy-BAS) that relies solely on boreholes from the training set, complemented by geological maps and cross-sections; and an ML-augmented model (ArchPy-ML) that is enhanced through the integration of ML-generated boreholes utilizing the tuned RF model described in the previous section.

It is important to note that the SUP unit may unintentionally fill the simulation grid near the surface, depending on the surface simulations. This is due to how ArchPy defines the unit domains, which depend on the top and bottom surfaces of each unit. For the SUP unit, the top surface is set at DEM to prevent unsimulated cells. However, this can result in a significant exaggeration of the SUP unit's thickness, depending on how the older unit surfaces (HG, YG, etc.) have been simulated. For consistency reasons, the final geological models

excluded this unit as it was deemed irrelevant. In such cases the SUP unit simulated cells were assigned the unit of the nearest non-SUP unit cell.

The confusion matrix between the two models is shown in Figure 6.11A. Most of the units are relatively well simulated, except for AM, OS, and SUP. The main reason is the same as for ML algorithms validation, as the poor number of boreholes in the test set containing these units, particularly for AM and OS. Another reason is also the scarcity of the deposits which are only located in some part of the simulation domain. ArchPy-BAS model is slightly better than ArchPy-ML in terms of global predictions (66% vs. 64%), primarily due to BAS's better accuracy in reproducing the YG unit, while ArchPy-ML is better with LGL, LGA, and SUP units. However, ArchPy-BAS exhibits a worse Brier score (0.56 vs. 0.50), suggesting that the ML-enriched model offers less confident simulations and enhances uncertainty quantification.

ArchPy-ML models also decrease the number of "errors" (or inconsistencies) between facies data and simulated units as shown in the Figure 6.1. Inconsistencies can arise when a stratigraphic unit is missing from borehole logs. These errors can be quantified by comparing the number of cells where facies data are found within inconsistent, simulated stratigraphic units, as shown in SP (Fig. 6.4). This is shown in Figures 6.11C and 6.11D. In total, the number of discrepancies decreases from 536 for the ArchPy-BAS model to 374 for the ArchPy-ML model. However, errors remain after the integration of ML boreholes. This is because the SP was constructed with the assumption that lithologies present in less than 5% proportion were absent from a unit. This can lead to errors, as a lithology present in small proportions may cause these errors. This is clearly visible for the YG unit, which has low proportions of C and SC lithologies. These lithologies have not been considered as part of the unit, but their exclusion results in a high number of errors (Fig. 6.11C and 6.11D), even with ML model. Therefore, these errors are included in the data and cannot be eliminated with the current approach. Possible causes of these occurrences include rare lithology inclusions in specific units or misinterpretation of either lithologies or units.

Final models

The previous results show that ML techniques can enhance geological modeling. To optimize the model's performance, the RF model was retrained, but using all the existing borehole data and utilized to simulate the boreholes. This subsection presents the models (ArchPy-BAS and ArchPy-ML) integrated with all available borehole data. A total of 50 realizations were made for each model, for each realization, one different ML borehole simulation is made.

Figure 6.12 provides information on the internal structures of the unit for the two models. In some cases, the boreholes shown on the cross sections do not

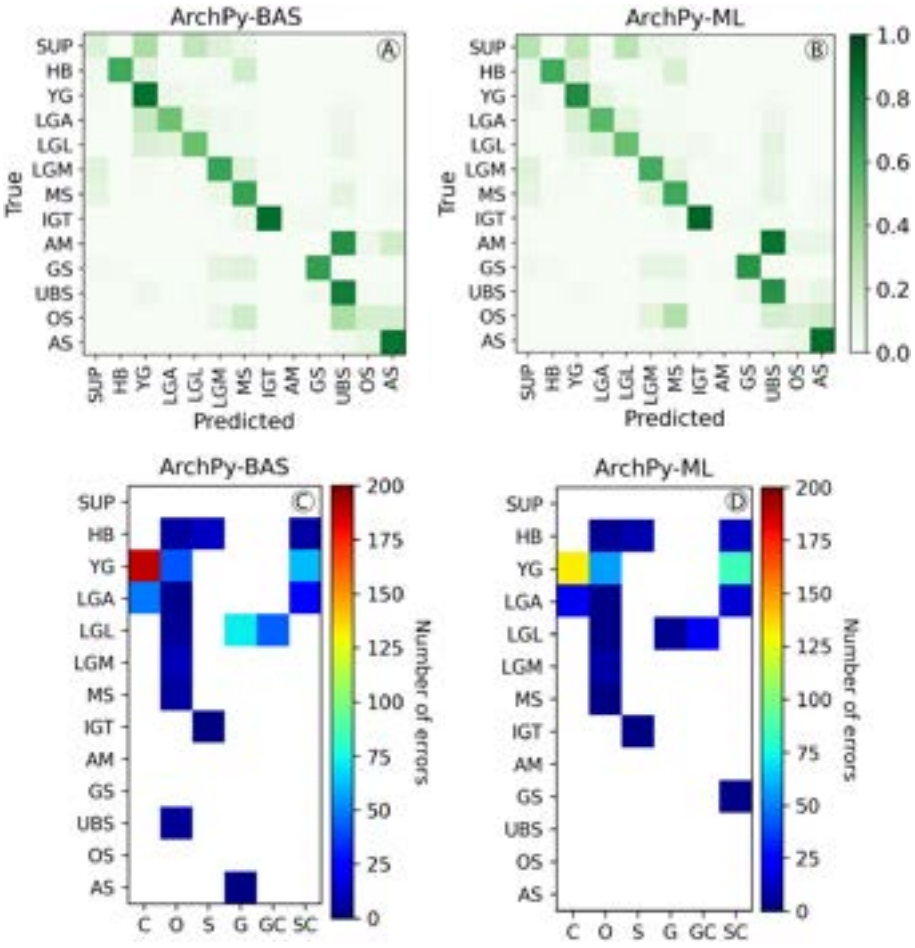

Figure 6.11: *Comparisons metrics between ArchPy-BAS and ArchPy-ML Aar geological models. Figures* ***A*** *and* ***B*** *show the normalized confusion matrix of the predicted classes against true (observed) classes in the test set for ArchPy-BAS and ArchPy-ML, respectively. Figures* ***C*** *and* ***D*** *depict the frequency of inconsistencies found in terms of lithological data within each unit domain.*

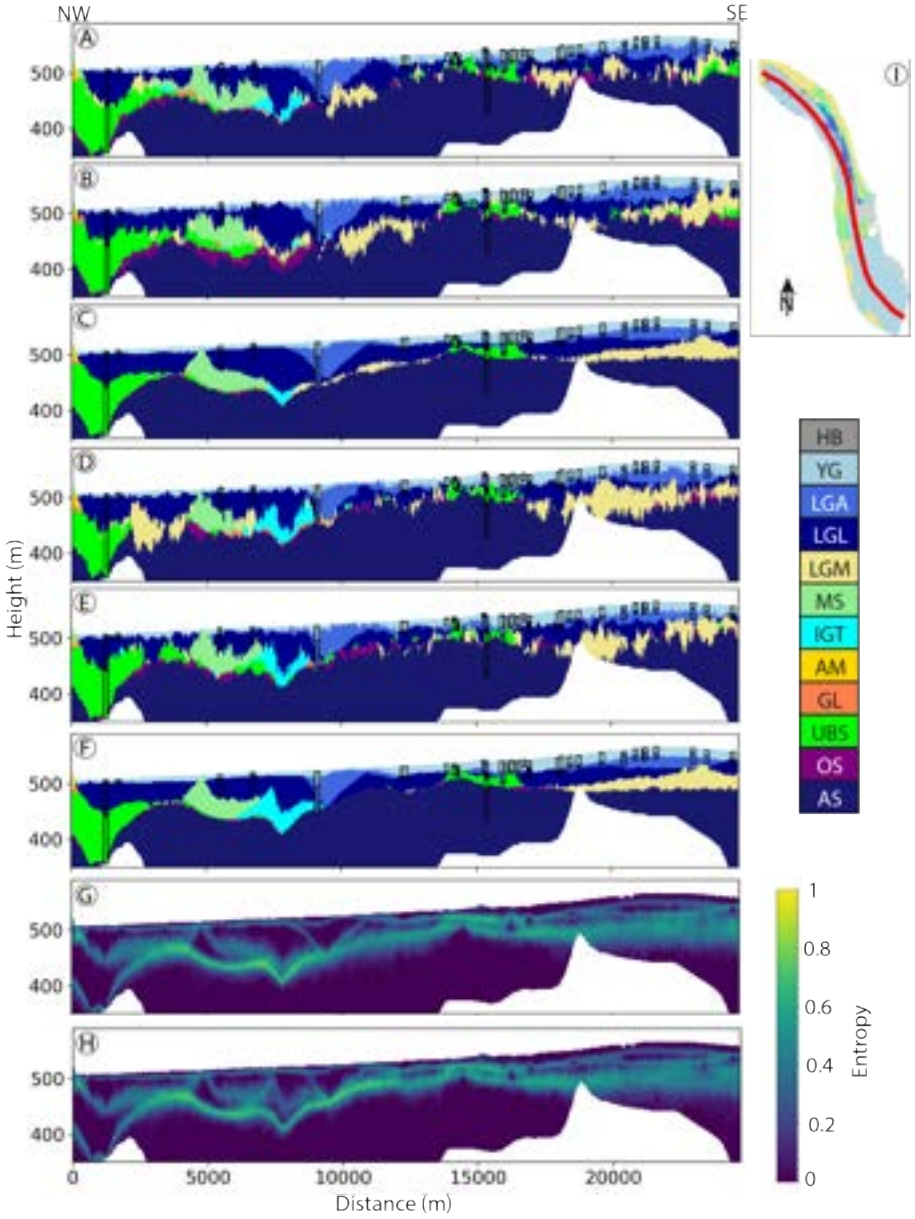

Figure 6.12: *Longitudinal cross-section across two realizations of the ArchPy-BAS (**A** and **B**) and ArchPy-ML model (**D** and **E**). Cross-sections of highest indicator facies value for both models are also shown (**C** for ArchPy-BAS and **F** for ArchPy-ML). Closest boreholes of the cross-section are displayed. The Shannon entropy is also shown for both models (**G** and **H** for ArchPy-BAS and ArchPy-ML, respectively). Location of the cross-section is illustrated in **I**.*

exactly match the simulated values. This is because the boreholes shown are not exactly on the section, but at a maximum distance of 100 m from the section. In general, both models exhibit similar geological structures at shallower depths and greater depths. The shallow aquifer appears closer to the surface in the northern regions (approximately 5-10 m) and gradually deepens towards the south (up to 50 m, locally reaching 100 m). Southern areas show low variability in geology, with a shallow aquifer overlaying LGM deposits, which in turn rest on older clay deposits (AS), indicating the absence of a deep aquifer in the south. On the contrary, the northern regions display more intricate stratigraphic sequences, suggesting the presence of aquifer formations (UBS, OS, MS) at intermediate depths, beneath the shallow aquifer (YG, LGA). Intermediate layers typically comprise LGL and IGT units. MS is not necessarily in contact with UBS, suggesting that the deep heterogeneity in this area is more complex than just a two-layered aquifer.

Although the two models share common features, discrepancies emerge particularly in the intermediate depths in the northern part of the area. ArchPy-ML simulations indicate a thicker presence of IGT compared to ArchPy-ML simulations in this region. This is more clear when observing the "most probable" models (Figs. 6.12C and 6.12F for ArchPy-BAS and ArchPy-ML, respectively) that show the most probable unit in each cell according to the realizations. We see that the mean models are very close except around 7'500 m of distance, where the IGT layer is clearly thicker and present in ArchPy-BAS than in ArchPy-BAS model. Locally, we can note differences for the transition between YG-LGA-LGL units, but these are relatively rare.

Entropy values appear visually similar (Fig. 6.12G and 6.12H); they do not indicate any significant reduction or increase in uncertainty. The only noticeable difference is that the ArchPy-ML model entropy is higher at intermediate depth between a distance of 10'000 and 13'000 m, suggesting a wider diversity in terms of units.

Transverse cross-sections (Fig. A.9A - A.9I and 6.13A - 6.13I) offer more detailed insights. Similarly to previous observations (Fig. 6.12, the ArchPy-ML model consistently depicts the IGT as thicker and more extensive in the northern part, compared to the ArchPy-BAS model (Fig. 6.13D vs Fig. A.9D). Furthermore, small and very thin occurrences of certain units, particularly at the interface between two thick units (e.g., IGT vs. AS in Figure 6.13C), are more common in the ArchPy-BAS simulations compared to the ArchPy-ML model. Although only one simulation is presented per model here, these trends are observable across other realizations as well. Both models clearly show that the north appears to be more complex than the south, which is mainly represented by a succession of YG-LGA-LGL-LGM and AS, with some local deposits of OS and UBS. On the contrary, in the north, all units can be present, according to the models.

The two models exhibit minimal disparity in terms of lithologies and properties, with the primary distinction being the incorporation of unit logs. In particular, it is difficult to visually discern between the two facies models (see Figures A.10 and 6.14). The 3D views (Figure A.10K vs Figure 6.14K) suggest that clay facies (C) are more present at depth in ArchPy-ML than in ArchPy-BAS model. Although, despite employing a relatively straightforward facies modeling technique such as SIS, complex, intricate, and constrained facies and property simulations can be obtained.

Property models (see Figures A.11 and 6.15) offer valuable information on the potential distribution of hydrogeological characteristics (aquifers and aquitards). The average hydraulic conductivity within the valley is approximately $10^{-5}[\frac{m}{s}]$, but it greatly varies in space, both vertically and horizontally. The shallow aquifer is discernible near the surface with a conductivity of more than $10^{-3}[\frac{m}{s}]$, particularly in the southern region, where it exhibits a greater thickness (over 50 m). The presence of an impermeable layer between the superficial aquifer and the potential deep aquifer is clearly visible in the north and seems to have disappeared almost completely in the south. Although some deeper conductive lenses are observable (e.g., Figure 6.15F or Figure 6.15C), conclusive evidence of a deep aquifer over the entire valley is lacking. In the south, the models suggest the presence of only one shallow and thick (50 m) aquifer. The geology in the north seems more complex, and possible vertical interactions between shallow and deep water reservoirs can be considered. It is essential to note that these models represent only averages and do not capture the complete heterogeneity of the subsurface. They provide information on areas that are likely to be more conductive to groundwater flow than others.

Between the two models, ArchPy-ML models exhibit a larger contrast, mainly due to the conductivity of the AS unit, which is lower than for ArchPy-BAS models. The reason is the proportion of the lithologies that are different between the two models. The integration of new unit ML generated logs has changed the proportions of the facies for each units. For rare units, such as AS, this was sufficient to provoke a reduction of the mean hydraulic conductivity by nearly one order of magnitude.

We can also compare models based on their "mean" unit and facies models (Figures A.12 - A.15). In these figures, the unit (or facies) that is shown in each cell is the one that has the most probability to appear according to the 50 realizations.

Unit models are very similar and only differ in some specific locations, particularly in the Northern part where the first cross-section with ArchPy-ML (Fig. A.13A) shows a thicker GL unit than with BAS model (Fig. A.12A). IGT unit is also thicker and widespread in ML model (Fig. A.13D) than in BAS model (Fig. A.12D).

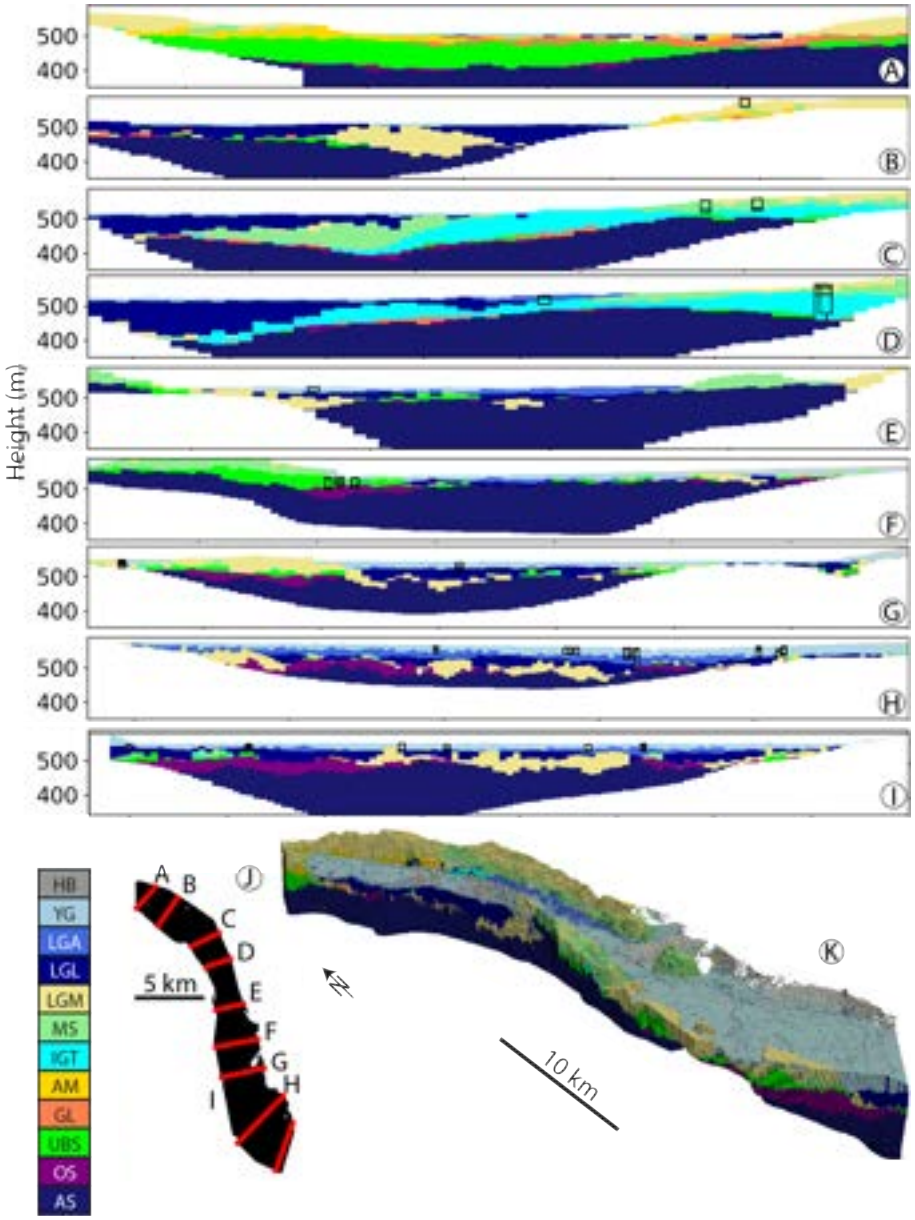

Figure 6.13: ***A*-*I***: *transversal cross-sections in one realization of the ArchPy-ML unit model. Corresponding locations are shown in* ***J***. ***K***: *3D visualisation of the realization. Corresponding color for units are given in Figure 6.4.*

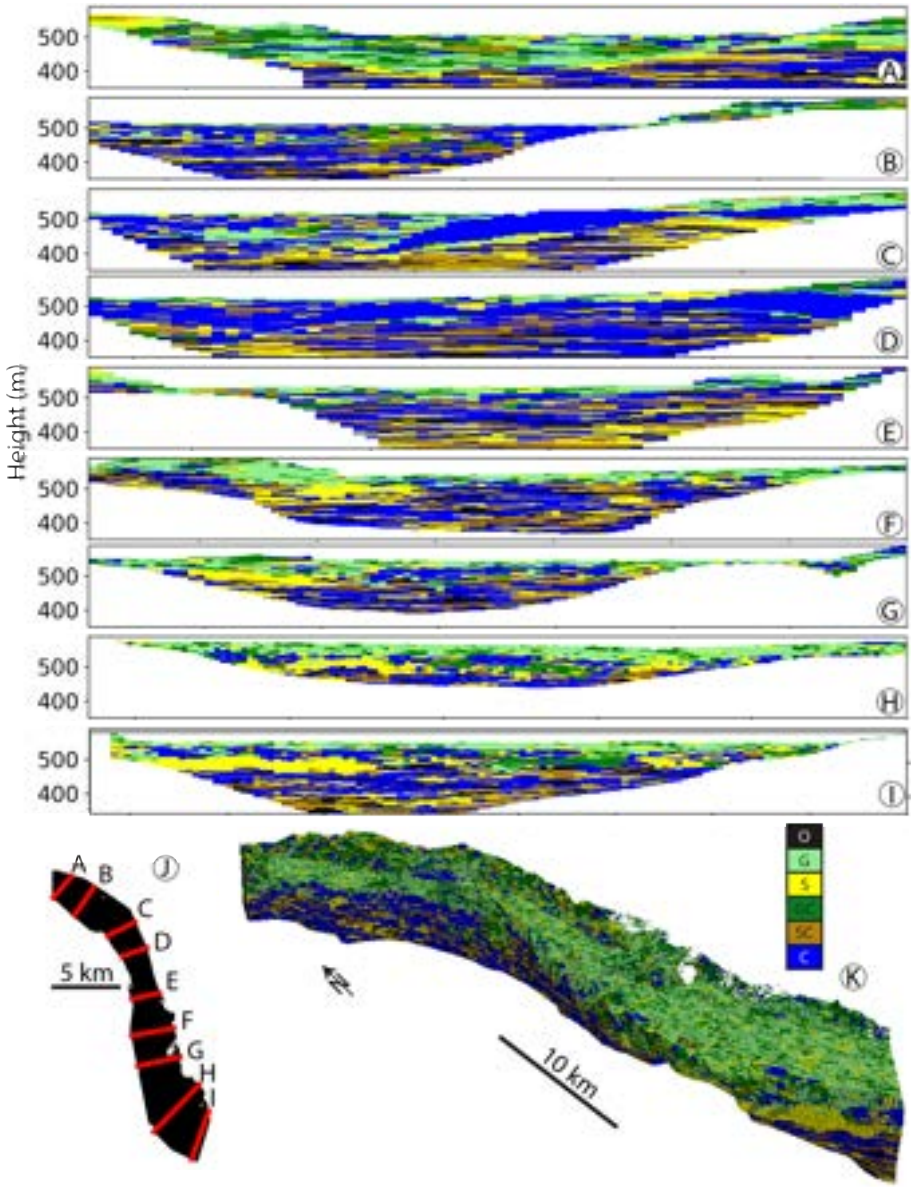

Figure 6.14: ***A*-*I***: *transversal cross-sections in one realization of the ArchPy-ML facies model. Corresponding locations are shown in* ***J***. ***K***: *3D visualisation of the realization. Corresponding color for facies are given in Figure 6.4.*

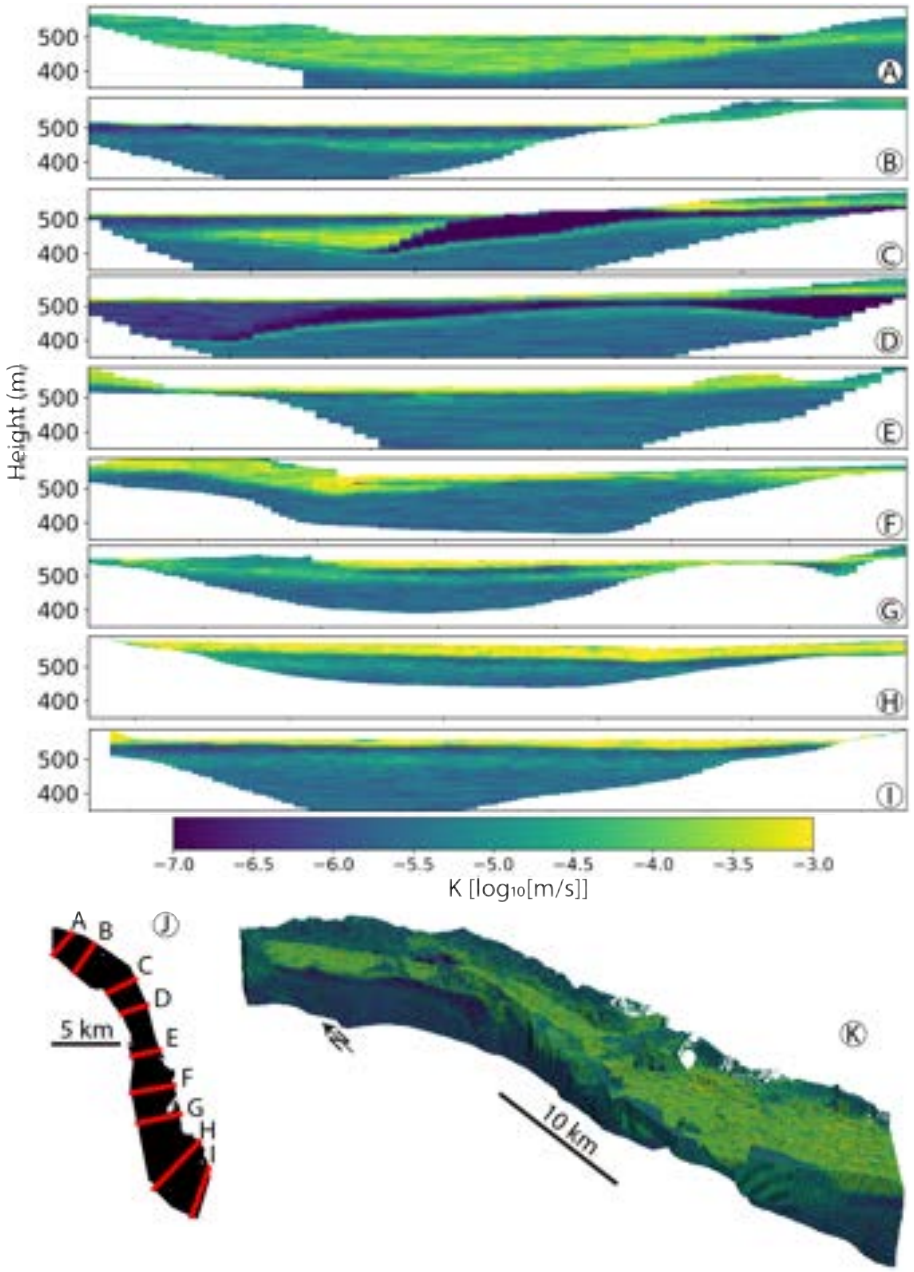

Figure 6.15: ***A*-*I***: *transversal cross-sections in mean of all property realizations of ArchPy-ML. Corresponding locations are shown in* ***J***. ***K***: *3D visualization.*

Mean facies models (Fig. A.14 and A.15) are really useful as facies with highest proportions in each unit are presented which shows the difficulty to obtain a mean facies model and the risk to aggregate realizations using the "most probable" method. Nevertheless, aquifer, aquitards and aquicludes are clearly discernible which can help to identify zones with higher groundwater potential. Overall, the gravel facies is present close to the surface, with clay and silts at depth. There are no notable differences between the ML and BAS models.

6.6 Discussion

6.6.1 Geostatistical methodology

The methodology used to infer geological units was able to simulate reasonable stratigraphic units based on lithology information. Despite the complexity of the task, ML algorithms yield relatively decent results. In particular, the use of probabilistic ML outputs rather than deterministic predictions allowed us to introduce a level of uncertainty and preserve it through the modeling process.

Integration of a larger number of boreholes has improved the geological model, allowing better capture the spatial statistics of the surfaces that bound these units. Another interest of this methodology is that it can help detect or correct potentially erroneously interpreted wells, thereby improving the accuracy of geological models.

However, there are several challenges and areas of improvement remaining. In particular, the limited dataset size poses challenges in performing comprehensive cross-validation to assess the method's viability accurately. If the number of boreholes is consequent (791 in total and 266 labeled), they are not equally distributed over the modeling area and rarely exceed 50 m depth. This eventually reduces the quality of ML predictions for deep boreholes and also increases the uncertainty of geological models at intermediate and high depths. Grouping of lithologies and units also requires careful consideration to mitigate potential biases. It is possible that grouping all lithologies into six groups could remove patterns useful for predicting units. It is also important to mention that the definition of the facies and their grouping have to be done according to the modeling facies methods. Here we used SIS which is flexible and makes no supposition on deposit conditions, but if more advanced methods would have been employed such as Object-based or Rule-based methods, it is clear that a more detailed description of the data would be required.

In fact, the quality and homogenization of the data is another critical consideration. It is evident that improperly homogenized lithological logs can misguide ML algorithms. Specifically, the level of detail in descriptions varies widely because they originate from different companies, individuals, times, and purposes, complicating the homogenization process. In the case of the upper Aare Valley, these discrepancies exist and were not filtered or corrected prior to algorithm

training, likely influencing the predictions. It is crucial to bear this in mind when interpreting the results.

Another clear limitation is that, overall, the simulation on the boreholes does not provide satisfactory results in all cases, which points to some limitations of the current approach. The roots of this problem can be partly attributed to the ML predictions that are on average quite low (around 50-60 %), with a high variability between the predicted classes. The reason for this are multiple. The lithologies were aggregated into six groups, which may have impacted the ML predictions, making them more difficult to estimate. Additionally, the approach involves a scanning window that provides lithological information 2 meters above and below each elevation. Although this approach has the advantage of neglecting small facies occurrences, it also provides unnecessary information that makes it difficult to determine the transition between two units. Finally, the borehole simulation approach is not very robust and has limited global applicability. It requires the selection of a parameter (τ) and may generate artifacts in cases where multiple thin layers are simulated based on ML predictions.

However, it should also be noted that the prediction problem in this case is difficult where the relations between the 13 units with the lithologies and spatial coordinates are hard to make. It would be interesting to use this approach or an improved version on simpler synthetic cases to see in which situations the methodology works best, or on the contrary when it does not and how it can be improved. Overall, the problem addressed in this chapter is of primal importance and the results obtained, despite unsatisfactory, are encouraging.

To address these issues, several improvements can be explored. Alternative feature strategies, such as integrating more lithologies above and below the target layers, adjusting layer thicknesses of each feature, and incorporating additional features (e.g., distance from the center of the valley, geophysical data, predicted units at borehole location using ArchPy), could enhance model performance. Data augmentation, such as generating synthetic boreholes with ArchPy, could also be an option to adhere to stratigraphic rules and improve machine learning predictions. Furthermore, instead of predicting units layer by layer, a direct prediction of surface elevation could provide a more efficient approach when coupled with the ArchPy borehole preprocessing algorithm (Schorpp et al. 2022). To enhance the robustness of the borehole simulation step, a more robust and general approach should be taken. For instance, instead of using a random path, a deterministic path, going from the top to the bottom of the boreholes could be used. In a similar way, a Markov process could be employed, where transition probabilities are determined by the machine learning predictions. Alternatively, directly predicting the elevation of each unit's surfaces would eliminate the need for this step.

However, it is worth noting that, in most cases, algorithms can generate reasonable predictions. For example, in the borehole depicted in Figure A.2, the transition between YG and LGL at a depth of 10 meters is characterized by the appearance of a sand layer. However, since clays dominate the LGL, algorithms do not predict the transition at this depth. The same comment can be made in Figure A.3 where the transition between YG and LGL is predicted some meters below the reference (approximately 10 m depth) because the lithological log shows a transition between sandy deposits to clayey deposits around 10 m depth. In such instances, the relevance of the data itself comes into question, prompting discussions of whether it is reasonable to pinpoint the transition at this precise depth or whether it would be more consistent to provide a range.

6.6.2 Geological models

The geological models show an intermediate uncertainty but that greatly varies in space. It is particularly high at intermediate depths (between 30 and 100 m), as shown by the entropy values (Fig. 6.12G and 6.12H). This is logical because at shallow depth, geology is well known thanks to the numerous boreholes. On the opposite, in the deepest part, there is only one dominant unit, the AS. In between, the other units have a certain probability of appearing, depending on the boreholes and their covariance model. Although this uncertainty may seem high, it should be remembered that the geological complexity of the study area (13 units). Moreover, models provide stochastic simulations that consider this uncertainty and allow to propagate it through the subsequent modeling steps.

Indeed, it is important to emphasize that the prediction of geological units should not be viewed as an end in itself, but rather as a means to understanding the larger geological context. Imperfections in unit modeling are acceptable as long as they do not compromise the accuracy of the facies model (lithologies), which exert significant control over the distribution of properties in the subsurface. Therefore, it becomes imperative to dive deeper into this aspect to propose facies models that more accurately reflect the geological setting.

In this study, only the SIS method was considered for facies modeling. However, it should be noted that the inferring of variograms, particularly in the horizontal direction, posed significant challenges. Variogram parameters were determined primarily by trial and error, supplemented with expert knowledge of lithologies in the area. Unfortunately, such knowledge remains critically lacking for many units, leaving uncertainties that are difficult to address comprehensively.

As a result, the facies models can seem very uncertain, but it should be recalled that the resolution of the model is 25 m by 25 m, and it is very likely that the lithology heterogeneity displays a spatial range of heterogeneity below this value. Additionally, the SIS simulations were constrained in terms of facies proportions in each unit based on borehole data, but there is a high probability

that these proportions are wrong due to a sampling bias. Drillers and local companies generally look for areas that have a high conductivity to better extract the water, as a consequence, the borehole generally stops when they reach large and thick clay and silty lithologies. Therefore, the proportions of sand and gravel in low permeable units are more likely to be overestimated.

The existence of a deep aquifer has been suggested and used as a working basis in several studies in the area (Kellerhals et al. 1981; Neven et al. 2023). From the results obtained in this study (Figure 6.12 and Figures 6.13 to 6.15), it is difficult to assess the existence of a deep aquifer throughout the valley. However, we can clearly see that in the northern part of the area some conductive units (MS, UBS) seem to be present locally. YG and LGA, which are part of the shallow aquifer, are separated from these deeper units by LGL and IGT, suggesting that there are little to no exchanges between these two. These units seem to vanish as soon as the cross section in Figure A.11D. Some other deep conductive lenses (50-70 m) can be observed, such as the one in Figure A.11F but they are not widespread and are not observed in the other cross sections. All of this suggests that a second aquifer is likely to exist beneath the shallow one, but its extent is limited to the northern area. Its hydraulic conductivity is also expected to be lower as a result of the presence of more clayey deposits (SC, GC) compared to those of YG or LGA. To further characterize this lower aquifer, thresholds could be applied to hydraulic conductivity models to identify permeable areas. Probabilities of exceeding these thresholds could then be calculated. Or a numerical flow model could be used to study regional three-dimensional flows using these geological models.

In comparison of the ArchPy-BAS and ArchPy-ML models, both exhibit similar geological features. However, a notable difference emerges, particularly evident in property models (Figures A.11 and 6.15): variable hydraulic conductivity for identical units. This discrepancy arises from the addition of ML-generated boreholes, which altered the lithological proportions within each unit. Consequently, certain units, such as AS, display a nearly one-order-of-magnitude difference in the simulated properties.

Hence, there is a great deal of room for improvement regarding geological models, mostly on the facies modeling part. Apart from other more complex methods (Multiple Point Statistics (e.g., Mariethoz et al. 2010b), Surface-based (e.g., Schorpp et al. submited)) that can be employed, we can also imagine defining a more solid and complete geological conceptual model of the area, use of analogs for each unit, consider locally varying lithology proportions, etc. However, all of these steps would require an important amount of work that is beyond the scope of this research.

6.7 Conclusion

We presented a novel methodology for inferring stratigraphical unit logs based on lithological data using Machine Learning (ML). Several algorithms were tested, and it turned out that the Random Forest (RF) and Support Vector Machine (SVC) gave the best results in terms of accuracy and Brier score. The RF model was used to simulate consistent boreholes in areas where local stratigraphy data were missing. These simulated boreholes were then integrated into a geological model (ArchPy-BAS), resulting in an enhanced version (ArchPy-ML). The geological model operates on three hierarchical levels: stratigraphical units, lithologies (facies), and hydraulic conductivity properties. Although ArchPy-BAS exhibits marginally better accuracy than ArchPy-ML, the latter demonstrates superior performance in quantifying uncertainty, as indicated by its improved Brier score.

Visually, both models yield similar results, albeit with ArchPy-ML showing a greater presence of certain units, notably IGT. Analysis of these results enabled the determination of the lateral and vertical extent of potential deep aquifers. Our models suggest that their lateral spatial extent is limited and that there are uncertain connections between them. Furthermore, their hydraulic conductivity appears to be lower than that of the shallow aquifer, particularly in the south, where the aquifer is thicker. Exploiting these potential aquifers requires further investigation to obtain accurate estimates of their petrophysical properties.

This work also shows that there is room for further improvements. Identifying consistent stratigraphic data from lithological logs could be improved by involving probabilistic information or by using more advanced statistical learning techniques. It was also not possible during the timeframe of the research to integrate completely the geophysical data acquired by Neven et al. (2021) in a large part of the valley. However, our approach still offers valuable information on the integration of ML with traditional geostatistical methods to improve the reliability of geological models. Ultimately, these advances contribute to improving the quality of groundwater models and understanding subsurface heterogeneity.

Chapter 7

EROSim: A novel surface-based approach to represent aquifer heterogeneity in sedimentary formations[8]

[8]This chapter has been submitted for publication to journal Water Resources Research.

Abstract

Sedimentary formations that compose most aquifers are difficult to model as a result of the nature of their deposition. Their formation generally involves multiple processes (alluvial, glacial, lacustrine, etc.) that contribute to the complex organization of these deposits. Representative models can be obtained using process-based or rule-based methods. However, such methods have several drawbacks: complicated parametrization, a large computing time, and challenging, if not impossible, conditioning. To address these problems, we propose a new hierarchical surface-based algorithm, named EROSim. First, a predefined number of stochastic surfaces are simulated in a given order (from older to younger). These surfaces are simulated independently but interact with each other through erosion-deposition rules. Each surface is an erosive or a deposition surface. The deposition surfaces represent the boundaries of the depositional events, whereas the erosive surfaces can remove parts of the previously simulated deposits. Finally, these surfaces delimit sedimentary regions that are filled with facies. The approach is quite simple, general, flexible, and can be conditioned to borehole data. The applicability of the method is illustrated using data from fluvioglacial sedimentary deposits observed in the Bümberg quarry in Switzerland.

7.1 Introduction

Groundwater flow and solute transport processes including dispersion, mixing, or chemical reactions are heavily influenced by geological heterogeneity that occurs on multiple scales (Chiogna et al. 2015; Kitanidis 2015; Bennett et al. 2017; Soltanian et al. 2020; Wallace et al. 2021). To investigate the impact of geological heterogeneity on these processes, multi-Gaussian random functions are often used (Dagan 1989; Rubin 2003; Chiles et al. 2012; Geng et al. 2020; Zech et al. 2021a) because they provide a parsimonious but flexible mathematical framework. To incorporate more geological concepts and knowledge into these analyzes and to account for different types of connectivity, alternative models (from process-based to structure-imitating approaches) have also been developed for a wide range of geological environments (Koltermann et al. 1996; De Marsily et al. 2005).

In this paper, we propose a new model to represent the geological heterogeneity produced by sedimentary processes in unconsolidated fluvioglacial environments. We focus on this geological setting because it contains the most heavily exploited groundwater resources in Switzerland (and many other countries) for drinking water and shallow geothermal supply. Being close to the surface, these aquifers are also prone to anthropogenic contamination, and describing their internal heterogeneity is important for the analysis of contaminant transport. These formations are the result of a rich and complex sedimentological history (Miall 1996). Outcrop observations and geostatistical analysis show that

fluvioglacial sediments are structured hierarchically (Miall 1991; Heinz et al. 2003b; Ritzi et al. 2004; Bayer et al. 2011). Therefore, modeling approaches aiming at studying the impact of this type of heterogeneity should also include these hierarchical relationships. One way to achieve this goal is to directly construct a hierarchical multi-Gaussian model (Neuman et al. 2008). To integrate more geological concepts, Scheibe et al. (1995) and Ramanathan et al. (2010b), use sophisticated object-based methods where sedimentary structures are created hierarchically following sedimentological rules. Webb (1994) or Pirot et al. (2015) also proposed a hierarchical approach, in which multiple geomorphological surfaces are stochastically generated and stacked together to define the major units. These units are then filled with facies using a deformation process (Pirot et al. 2015) or based on an estimate of the Froude number (Webb 1994). Although these methods provide models that exhibit realistic geological features, they are difficult to constrain to field data and borehole observations. Comunian et al. (2011b) or Bennett et al. (2017) decompose the problem and model a set of surfaces that delimit volumes that can then be filled with other facies simulation techniques. Zuffetti et al. (2020) describe in detail the limitations of most of the previous methods and show that they do not fully account for the stratigraphical hierarchy. Following these observations, Zuffetti et al. (2020) introduced a generic framework to overcome these limitations by defining how sub-units should be modeled into larger units at multiple scales. Based on these concepts, Schorpp et al. (2022) proposed the ArchPy approach that is capable of handling the hierarchical relations when constructing a 3D geological model. This approach has been coupled with geophysical and hydrogeological inversion and applied successfully to synthetic data (Neven et al. 2022b) and to characterize the northern area of the upper Aare fluvio-glacial aquifer in Switzerland (Neven et al. 2023).

In this paper, we propose to go a step further and develop the EROSim method that allows filling the stratigraphic units with detailed facies models while ensuring conditioning. The proposed method belongs to the family of surface-based methods (SBM) that emerged in the early 2000s (Pyrcz et al. 2014) with the pioneering work of Xie et al. (1999) and Xie et al. (2001). SBMs consider that the different geological features (layers, architectural elements, facies, etc.) can be separated by surfaces (Pyrcz et al. 2015; Jo et al. 2020; Titus et al. 2021). These methods also integrate the notion of time during which geological objects are deposited. The different surfaces are stacked on top of each other and delimit the geological units or sediment types. The surfaces can either be deterministic or stochastic. Compared to pixel-based methods, SBM can maintain complex geometries throughout the modeling process.

The general idea of the proposed approach consists of generating multiple stochastic surfaces and combining them to delimit the different rock types or lithofacies. This strategy is highly flexible and allows performing conditional simulations even with a complex and realistic sedimentary structure. We show

in the paper how this model is capable of simulating and extending detailed sedimentary structures that are directly observable in outcrops.

The paper is organized as follows. We first introduce the proposed simulation methodology in section 2. Section 3 illustrates the sensitivity of the method to its parameters and shows how it compares to other facies simulation techniques in simple cases. Then, we illustrate how this model can be used to represent and extend detailed information collected on outcrops in a gravel pit in the upper Aare Valley in Switzerland. The relevance of the results and the different advantages and limitations of the method are discussed in section 4.

7.2 A surface-based approach to represent aquifer heterogeneity

This section describes the EROSim approach and its implementation. First, the general workflow is introduced, we then present the notations and definitions that are used in the following to describe precisely each step of the method.

7.2.1 General principle

The principle of the method is to decompose the simulation domain into multiple regions (or volumes) using stochastic surfaces. Each region for each simulation corresponds to a single categorical value representing a lithology, a facies, or a unit, in a finite 2D or 3D domain. The three main steps of the method are therefore the following.

1. *Surface simulation.* A set of surfaces are stochastically simulated and modified according to erosion rules. These surfaces represent sedimentological events (deposition or erosion).
2. *Region delimitation.* The ensemble of surfaces simulated in step 1 forms a tessellation of the simulation domain, where each tile is individualized as a region. A graph of the spatial relationships between the regions is constructed.
3. *Facies assignment.* During this step, a facies is assigned to each of the regions defined in step 2 while accounting for the spatial continuity of the facies.

7.2.2 Notations and definitions

The simulation domain is denoted $\Omega \subset \mathbb{R}^n$ where $n = 2$ or 3 is its spatial dimension. We then consider a finite set of lithofacies $\mathbf{K} = \{K_1, K_2, ..., K_k\}$, where k is the number of facies to simulate. The goal is to obtain a stochastic process f that can map any location to a certain facies such that $f : \Omega \to \mathbf{K}$.

We also consider a number of ordered stochastic surfaces S_t that delimit different regions V_i stored in a set $\mathbf{V}$. Each volume can only take one value in $\mathbf{K}$, i.e. f is constant on each volume V_i. The subscript $t \in \mathbb{N}$ in S_t represents the simulation time step and can be seen as analogous to geological time. These surfaces are stochastic processes of dimension $n-1$, which means, for example, that if the simulation domain is in 3D ($n = 3$), S_t are 2D stochastic surfaces. The regions V_i are objects of dimension n each corresponding to a single connected component, they do not intersect each other. Furthermore, the ensemble of all the V_i fills Ω. We can also refer to the V_i as areas if $n = 2$ or volumes if $n = 3$. The boundaries S_t are ordered by age (from younger to older) in a list $\mathbf{S}$. The order of the surfaces is important because it represents the sedimentological history of the simulation domain and has consequences on the interactions that can exist between the surfaces through erosion rules.

An important aspect of stochastic geological models is their ability to be conditioned by borehole data. In this study, each borehole is assumed to be 1D and vertical. The list of boreholes is denoted $\mathbf{B}$. A borehole contains a sequence of contiguous intervals. For a simulation in 2D (resp. 3D), a borehole is located by a position $\mathbf{x} = (x)$ (resp. $\mathbf{x} = (x, y)$). The facies encountered along the borehole are defined with a sequence of elevations $z_1 < \cdots < z_m$ and a sequence of facies $k_1, \ldots k_{m-1} \in \mathbf{K}$. The i-th interval between the bottom and top elevations z_i and z_{i+1}, is filled with the facies k_i, i.e. $f(\mathbf{x}, z) = k_i$ if $z_i \leq z < z_{i+1}$ (and $(\mathbf{x}, z) \in \Omega$), for $i = 1, \ldots, m$. Hence, a borehole B is expressed as $B = (\mathbf{x}, \{z_1, \ldots, z_m\}, \{k_1, \ldots, k_{m-1}\})$ or as $B = (\mathbf{x}, ([z_1, z_2[, k_1), \ldots, ([z_{m-1}, z_m[, k_{m-1}))$.

7.2.3 Unconditional simulation

The unconditional simulation algorithm is summarized in algorithm 7.1. The steps are described in detail below.

Surface ordering

Assuming that the parameters are defined, and before generating the surfaces, the first step (line 1) consists of checking the input parameters and ordering the surfaces by their mean elevation (from low to high).

Algorithm 7.1 Unconditional algorithm

Require: Parameters

N : integer - number of simulated depositional surfaces
$\gamma_0, \ldots, \gamma_{N-1}$: covariance (or variogram) models for each surface
$\mu_0, \ldots, \mu_{N-1}$: mean elevations for each surface
ξ : in $[0, 1]$ - proportion of eroding surfaces
p_{global} : target proportions of the facies, over the whole domain
α : in $[0, 1]$ - clustering parameter

1: Order all the surfaces in **S** by their means (μ_i)
2: Set surface index $t = 0$
3: **while** $t < N$ **do**
4: Determine if S_t is erode or onlap, given ξ
5: Unconditional simulation
6: **if** S_t is *onlap* **then**
7: $t = t + 1$
8: Apply erosion-deposition Rules (EDR, Eq. 7.3 - 7.4)
9: Define regions V_i as described in section 7.2.3
10: Assign facies to V_i using Algorithm 7.2 (depending on p_{global}, α)

This sorting is used to represent the evolution of geological time, with each event (a surface) occurring one after the other. Proceeding that way, we assume that the geological processes gradually increase upward due to the gradual accumulation of the sediments in the system.

Surface simulation

The second step consists of simulating N depositional surfaces through the domain Ω. Each time a new surface is simulated, from oldest to youngest, erosion-deposition rules (EDR) are applied. We consider here only the depositional surfaces because the erosion events are assumed to deposit no sediments, as explained below.

Let S_t be the simulated surface at time t, before applying the EDR. In the following examples, S_t is modeled as a Gaussian Random Field (GRF) following a specified mean μ_t and a specified covariance (or variogram) model γ_t. But, the mathematical model used to simulate the surfaces could be different. We use GRFs for convenience and simplicity. GRFs are easy to simulate (Chiles et al. 2012) and to constrain (useful for the conditional case). They are also flexible as they can handle non-stationary mean or covariance parameters. To generate our GRFs, we used the Geone[9] python library that provides a set of common geostatistical, Multiple Point Statistics modeling and image analysis tools. In the following, for illustration purposes, we generally consider that all

[9] http://www.github.com/randlab/geone

the surfaces follow the same covariance model (all γ_i are identical) but differ from each other by their mean. Moreover, the stochastic processes are assumed stationary, i.e. the mean and covariance are constant spatially.

Every surface S_t can be expressed as a function $S_t = S_t(\mathbf{x})$, defined for spatial locations $\mathbf{x} \in \mathbb{R}^{n-1}$. Let us then denote by S_t^* the surface at time t modified by the application of the EDR.

At time $t = 0$, the surface S_0^* is initialized as

$$S_0^*(\mathbf{x}) \longleftarrow S_0(\mathbf{x}). \tag{7.1}$$

For the following time steps ($t > 0$), we first determine if the event is an erosional event or a depositional event. The decision is randomized based on the probability ξ given by the user. This probability represents the fraction of erosive events among all the geological events (deposition and erosion) that are simulated. Then we generate a new surface.

$$S_t = \mathrm{GRF}(\mu_t, \gamma_t). \tag{7.2}$$

If the event is depositional, we apply the depositional rule:

$$S_t^*(\mathbf{x}) \longleftarrow \max(S_t(\mathbf{x}),\ S_{t-1}^*(\mathbf{x})). \tag{7.3}$$

and increment the value of t for the next iteration. For depositional events (Eq. 7.3), if the simulated surface is below a part of a previously simulated surface, there is no deposition and the elevation at that location is equal to the latter.

Otherwise, if the event is erosive, the computed surface S_t erodes the previously deposited formations.

$$S_k^*(\mathbf{x}) \longleftarrow \min(S_t(\mathbf{x}),\ S_k^*(\mathbf{x})), \quad \text{for } k = 0, \ldots, t-1 \tag{7.4}$$

All previously simulated surfaces that are above the simulated erosional surfaces are updated (Eq. 7.4). The time t is not incremented in that situation.

A schematic representation of these rules is shown in Figure 7.1A-B. In this example, the first three surfaces are depositional and the last (S_3) is erosive. The surfaces S_0, S_1, and S_2 are first simulated and adjusted according to the first two equations (Eqs. 7.1 and 7.3), and the surface S_3 erodes them where S_3 is simulated below the others (Eq. 7.4).

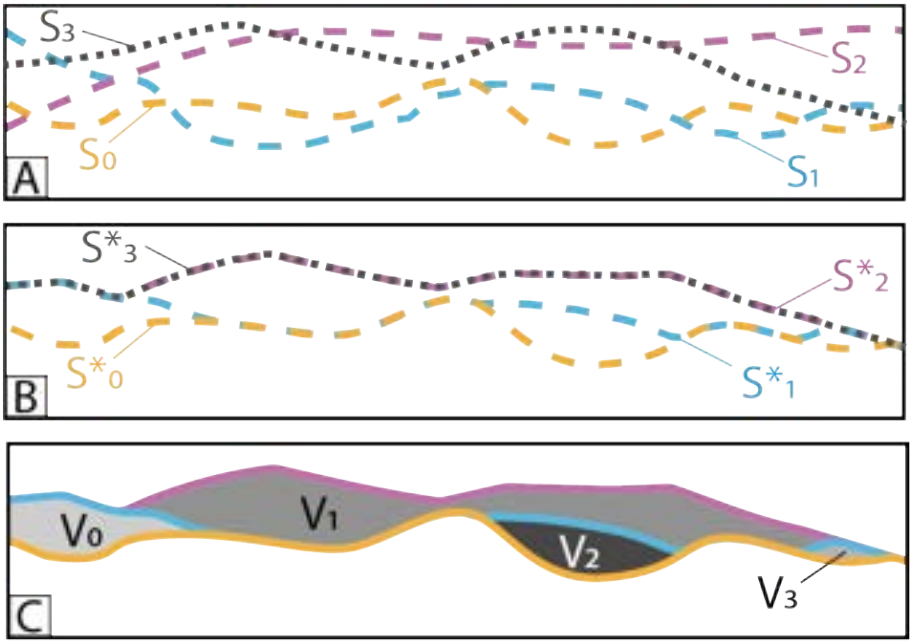

Figure 7.1: *Schematic representation of the delimitation procedure for the regions.* ***A****: four surfaces have been simulated: yellow, blue, pink, and grey. The last one (grey) is eroding while the others are onlap.* ***B****: Situation after the application of the deposition and erosion rules.* ***C****: distinct regions are differentiated.*

Region delimitation

Once the surfaces have been simulated and the EDR applied (Algorithm 7.1, lines 1 to 10), the simulation domain Ω is divided into distinct regions. All of these regions V_i are defined by exactly two successive (in simulation time) onlap surfaces (two depositional events), one delimiting its top and the other its base. A region can only exist where its top surface is strictly above its bottom surface. It does not exist where the two surfaces are exactly at the same elevation. This implies that regions are delimited on the sides when the top and bottom surfaces meet. If multiple distinct regions occur between two surfaces, they will be treated as completely different and independent regions. This means that later in the simulation different facies may be assigned to these regions, even if they are defined by the same surfaces. This is in contrast to previous studies, where each simulated surface delimits one sedimentological entity (Webb 1994; Pyrcz et al. 2005; Pirot et al. 2015). In practice, the individual regions are identified as the connected components of the sets $\{(\mathbf{x}, z) \in \Omega \ : \ S_t^*(\mathbf{x}) \leq z < S_{t+1}^*(\mathbf{x})\}$, $t = 0, \ldots, N-1$, where N is the total number of onlap surfaces simulated. Finally, two supplementary regions, made up of all points of Ω respectively below the surface S_0^* and above the last surface S_{N-1}^*, are added, to cover the entire simulation domain. Alternatively, Ω can be reduced to the domain between S_0^*

and S^*_{N-1}. An example of region delimitation in 2D is illustrated in Figure 7.1C.

Facies attribution

The aim is to assign a facies to each of the regions V_i determined in the previous step. To do so, we propose a simple algorithm that is summarized in Algorithm 7.2.

Algorithm 7.2 Graph-based indicator simulation

Require: Parameters
p_{global} : global proportions of the facies, over the whole domain
α : in $[0, 1]$ - clustering parameter
$\mathbf{V}$: set of regions covering the whole domain
G : a spatial graph G representing the connections of the regions

1: $V_i \leftarrow$ select a random region in $\mathbf{V}$
2: $p_{target} \leftarrow$ compute target proportions using Eq. 7.6
3: **if** $\alpha < 1$ **then**
4: $\quad \mathbf{V}_{\mathcal{J}} \leftarrow$ get the neighbours of V_i using G
5: $\quad p_{neig} \leftarrow$ compute the local proportions using Eq. 7.7
6: **else**
7: $\quad p_{neig} = 0$ (unused)
8: $p_{V_i} \leftarrow$ compute facies probabilities for V_i using Eq. 7.8
9: Draw a facies in K according to p_{V_i} and assign it to V_i
10: Update the global current proportions p_{cur}
11: Go to 1 until all regions are filled

We are assuming that based on borehole or outcrop data, the user can provide an estimate of the target global facies proportions p_{global} in the study area, e.g. 50% of sand, 20% of gravel, and 30% of clay. In addition, we want to provide a simple parametrization allowing the user to control the spatial continuity of the facies. For this, we introduce a clustering parameter α that the user can adjust.

The attribution then follows a simple method with adaptive target proportions to respect as well as possible the global facies proportions and spatial continuity. The idea is to sequentially populate the regions with random facies according to a probability distribution adapted for each region. At each step, the target facies probabilities are first computed accounting for the global target proportions p_{global}, the current proportions p_{cur} over the already simulated regions, and also the local proportions derived from the surrounding regions.

First, target proportions p_{target} are calculated such that

$$\phi p_{cur} + (1 - \phi) p_{target} = p_{global}, \tag{7.5}$$

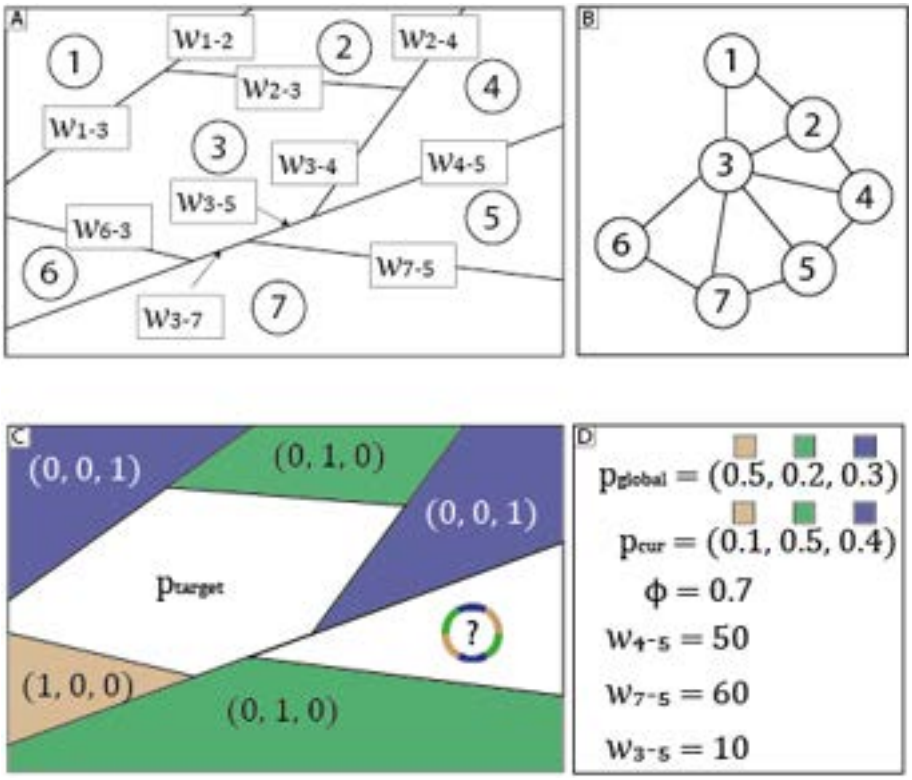

Figure 7.2: *Conceptual representation of a 2D simulation domain separated in seven regions (**A**) and its associated spatial graph (**B**). The w_{i-j} correspond to the length of contact between V_i and V_j, they are used as weights for the edges in the graph. **C** represents a situation during the attribution of the facies (three in total) for volume 5. The facies proportions are written in each region (note that region 3 is not defined at this point of the simulation and the modified global proportion p_{target} is used). **D** details the variables required to compute the probability mass used to draw a facies in region 5 (see text for details).*

where ϕ is the ratio of the total volume of the already simulated regions over the volume of Ω. Equation (7.5) means that if the entire non-simulated volume was filled with proportions p_{target}, the final proportion over Ω would be p_{global}. The target proportions are explicitly expressed as

$$p_{target} = \frac{p_{global} - \phi p_{cur}}{(1 - \phi)} \tag{7.6}$$

If p_{target} for a certain facies becomes negative, it is set to 0 and the proportions for the other facies are rescaled so that the sum of p_{target} is equal to 1. This situation can occur when a current proportion is too high ($\phi p_{cur}(i)$ exceeds $p_{global}(i)$ for some component i). It is important to understand that p_{target} is

computed before the facies attribution of each region, and then it can vary since it depends on p_{cur} and ϕ. Therefore, the global target proportions for the unsimulated part of the domain are continuously corrected until the simulation is finished.

Secondly, to introduce some spatial continuity, the local proportions p_{neigh} are computed from the regions around the simulated one. This is done by using a spatial graph G describing the regions and their contacts. Each vertex in G refers to a region, and an edge links two vertices if the two corresponding regions are in contact (adjacent). The size of the contact (length if $n = 2$ or area if $n = 3$) is the weight attached to the edge. An example in 2D is shown in Figure 7.2A-B. Note that the graph is constructed prior to the facies assignment procedure.

We consider V_i the region in which a facies has to be attributed (currently simulated region) and $\mathcal{J}$ the set of indices j of the regions adjacent to V_i, i.e. $j \in \mathcal{J}$ when the vertices corresponding to V_i and V_j are linked in G by an edge, of weight w_{ij}. Then, the local facies probabilities p_{neig} for V_i are defined based on the neighbors V_j as follows:

$$p_{neig} = \frac{\sum_{j \in \mathcal{J}} w_{ij} \cdot p_{V_j}}{\sum_{j \in \mathcal{J}} w_{ij}} \tag{7.7}$$

where p_{V_j} is the proportions of facies in the neighbor region V_j. The vector p_{V_j} is of length k where k is the number of facies and it is defined as follows. If a facies K_l has already been assigned in V_j, then all the components of p_{V_j} are set to 0 except the l-th component that is set to 1. If V_j is a region not yet simulated (with no assigned facies), then p_{V_j} is set to the target proportions p_{target} computed above.

Finally, the probability distribution, p_{V_i}, used to draw a facies in the region V_i is obtained by combining probabilities p_{target} and p_{neigh} (see equations 7.5 and 7.6) via a log-linear pooling operator (Allard et al. 2012b):

$$p_{V_i} = (p_{target})^{\alpha} (p_{neig})^{1-\alpha} \tag{7.8}$$

where α is a user-defined parameter ranging from 0 to 1 that controls the clustering of the regions of identical facies. If $\alpha = 0$, the same facies are more likely to be adjacent and, in contrast, if $\alpha = 1$, the facies are drawn only according to p_{target} (p_{neigh} is ignored).

The main advantage of this method is that it is simple and requires only the global target proportion p_{global} and the parameter α as input. Note that the graph-based approach presented here is applied to a domain divided into tiles and then is independent of the first part of the EROSim methodology. More complex methods could be considered, such as those using rules to guide the position of the facies (for example, by constraining some facies to appear more frequently in small regions).

To illustrate the procedure, let us consider the 2D case shown in Figure 7.2C, based on the domain delimitation in Figure 7.2A. Here the facies in V_5 have to be drawn from p_{V_5} using the equation 7.8. First, we need to calculate p_{target} which depends on p_{cur} and ϕ (Eq. 7.6). We obtain $p_{target} = (\frac{43}{30}, -\frac{1}{2}, \frac{1}{15})$ which after setting the second probability to 0 and rescaling becomes: $p_{target} = (\frac{43}{45}, 0, \frac{2}{45}) \approx (0.96, 0, 0.04)$. Then we need to compute p_{neig}, which depends on the facies in the regions surrounding V_5, which are V_3, V_4, V_7 according to the graph. Applying Eq. 7.7 with values in Figure 7.2 gives: $p_{neig} = (0.08, 0.50, 0.42)$ which is very different from p_{target}. We see that the most probable facies according to neighbors are, in fact, the green and blue facies, as they share the longest contact length with V_5. We can also note that since the facies proportion is undefined in region 3, p_{target} is taken for that region. Finally, we can apply Eq. 7.8 and obtain p_{V_5} that can range from p_{neig} to p_{target}, depending on the α parameter chosen. In this particular case, α has a strong impact as if it is close to 0, priority is given to the neighbors, and the beige facies has poor chances of being drawn. In contrast, if α is close to 1, priority is given to the adjusted global proportions, which gives a great chance for the beige facies to be drawn. This is due to the over-representation of green and blue facies in Figure 7.2C compared to the global target proportions p^0_{global}.

7.2.4 Conditional algorithm

We now consider the problem of conditioning the simulations. The conditioning data are facies intervals in boreholes as defined in Section 7.2.2. Considering any borehole,

$$B_i = (\mathbf{x}_i, \{z_1, \ldots, z_m\}, \{k_1, \ldots, k_{m-1}\}), \tag{7.9}$$

conditioning consists of ensuring that at least one surface must pass through each of the geological interfaces $(\mathbf{x}_i; z_j)$ observed in each borehole. Then, to condition the regions V_i with the proper facies, it is sufficient to ensure that no region covers two intervals having different facies.

The method that we propose to ensure the conditioning is described in detail in Algorithm 7.3. The method is direct and requires no iteration, but it requires checking at each step that it does not create situations that will lead to a violation of the conditioning data. This is the reason why the algorithm is complex. In the following, we explain the main principles of the algorithm.

The surfaces are simulated from the bottom to the top. Surfaces can be onlap deposits or erosive as for the unconditional algorithms and they define regions. Because of their erosional capabilities, they can remove or cut parts of the regions that have been defined by previous depositions. The general aim of the algorithm is to ensure that in the end, no region covers two intervals having different facies in the boreholes.

Algorithm 7.3 Conditional algorithm

Require: Same parameters as the Algorithm 7.1
Require: List of boreholes **B**
Order all the surfaces in **S** by their means
$d_s \leftarrow$ attribute a surface to each borehole facies transition and store it
Set surface index $t = 0$
$LB \leftarrow$ initialize lists for lower bounds conditioning
while $t < N$ **do** ▷ loop over the surfaces
  if S_t in d_s **then** ▷ If the surface is attributed
    $EP, UB \leftarrow$ Initialize lists for conditioning points (equality points and upper bounds)
    $B_i \leftarrow$ get borehole(s) and facies interval(s) associated with S_t
    Check situation at B_i according to Figure 7.3
    if Situation 1 **then**
      Set S_t to *onlap*
      $EP \leftarrow$ set an equality point to top of facies interval(s)
      $UB \leftarrow$ set upper bounds at other near boreholes locations to prevent connecting nonidentical facies (given Figure 7.3A)
    else if Situation 2 **then**
      Set S_t to *erode*
      $EP \leftarrow$ set an equality point to top of facies interval
    Compute one conditional surface with conditioning points EP, UB and LB
    Add EP to list of LB
    Remove facies interval of d_s
  else
    Determine if S_t is *erode* or *onlap*, given ξ
    if S_t is *onlap* **then**
      Set LB and UB to prevent connecting two different facies as shown in Figure 7.3C
      Conditional simulation with LB and UB
    else
      Conditional simulation with only LB
  if S_t is *onlap* **then**
    $t = t + 1$ ▷ Increment time of deposition
  Apply Erosion Rules (Eq. 7.3 - 7.4)
Define regions V_i as described in section 7.2.3
Assign facies to V_i using Algorithm 7.2

This problem can happen in two situations: if the newly simulated region covers two (or more) intervals with different facies within the *same borehole*, or if the new region covers two (or more) intervals in *different boreholes*.

The first situation is avoided by forcing at least one surface to pass through each of the facies interface in each borehole as indicated above.

The second situation is more complex. It requires analyzing the position of the regions and intervals encountered in the different boreholes. As some surfaces have the potential to remove older ones by erosion, some situations that are compatible with the conditioning data at a certain time step may become incompatible with the data later on. The inverse is also possible. To solve this problem, the conditioning algorithm proceeds by generating the surfaces sequentially from oldest to youngest and uses inequality data (upper or lower bounds) to constrain the simulation. Three rules are defined and implemented in the algorithm:

R1 For each interface point along each borehole with a facies transition, attribute a surface in $\mathbf{S}$ that has to go through that point; store this information in a data structure (a python dictionary) referred to as d_s. Note that one surface $\mathbf{S}$ can be attributed to one or several interfaces (in one or several boreholes).

R2 When a facies interval is constrained (attributed to a region), we consider it untouchable and no *future* changes can alter it. This is done by imposing lower bounds (LB) along the borehole when simulating future erosive surfaces.

R3 Onlap surfaces have to avoid creating (temporary) regions overlapping two different facies intervals to prevent the apparition of conditioning errors in the following steps.

To start, we generate N values within a uniform distribution between the minimum and maximum altitudes of the zone of interest. These values are ranked (step 1, in Algo. 7.3) from minimum to maximum and will correspond to the mean altitudes of the N surfaces delimiting the regions.

Following rule R1, one surface is attributed to each interface (step 2, in Algo. 7.3): for a given interface at elevation z, a surface S_t in $\mathbf{S}$ is chosen randomly according to a probability computed with a Gaussian distribution $\varphi_{\mu_t,\sigma_t^2}(z)$ of mean μ_t and variance σ_t^2, with μ_t being the prescribed mean elevation of S_t and σ_t^2 the prescribed variance of S_t. $\varphi_{\mu_t,\sigma_t^2}(z)$ is the probability that the surface S_t takes the value z at any location. Using this approach ensures that there is a reasonable chance that these transitions will be represented by a surface that is likely to be present at that depth. In addition, surface allocation

ensures that surfaces associated with intervals in a borehole are of increasing index. This is to avoid the unrealistic situation where a younger interval is constrained before an older one. To do this, surface indices are randomly drawn, as described above until they are higher than the index previously drawn for the lower interval. At the end of the process, only a subset of the surfaces S_t are attributed to the interfaces observed in the boreholes. A surface can be assigned to several intervals of identical facies (below the interface). This is forbidden if the facies are different because there is a high risk of creating a region that would connect them.

The surfaces are then simulated successively.

If the current surface is attributed to an interface, several situations can arise. Figure 7.3 shows some of these situations. In the figure, the surfaces that have been simulated previously are represented in black and the intervals of the borehole data that have already been constrained by the conditioning algorithm and that should therefore not be perturbed anymore are highlighted with a red rectangle (rule R2). The new surface to be simulated is represented in green. In situations 1 and 2, the green rectangle highlights the current interval with a given facies that needs to be constrained during that iteration.

In situation 1 (Fig. 7.3A), an onlap surface has to be considered. The current simulation elevation (last surface elevation, in black) at the well location (left well) is below the attributed interface. The green circle represents the position of the interface attributed to that surface (during step 2). It is a conditioning data, or equality point (EP) for the GRF simulation of this surface (step 12, in Algo. 7.3). But the facies located above the already constrained interval in the second well (right well) is blue and therefore different from the facies in the left well (brown). To avoid creating a region that would connect these different facies, we impose in the right well an inequality (upper bound or UB) for the simulation of this surface (step 13, in Algo. 7.3). We then use a Gibbs sampler (Freulon et al. 1993b) to constrain the conditional GRF simulation (step 17). After applying the erosion-deposition rules (step 29), the new region will cover only the brown interval in the left well in that case.

In situation 2 (Fig. 7.3B), the current simulation elevation at the left well location is above the attributed interface. In this situation, an erosive surface has to be considered to ensure the removal of the previously simulated deposits. We add an EP at the interface (step 16). Then, to avoid breaking an interval that has already been constrained in other wells, we impose an LB constraint on the top of the intervals that were previously constrained (see right well with red rectangle in Fig. 7.3B). We then use the GRF simulation technique with these new constraints to generate the conditional simulation and apply the erosion-deposition rules as described above (steps 17 and 29).

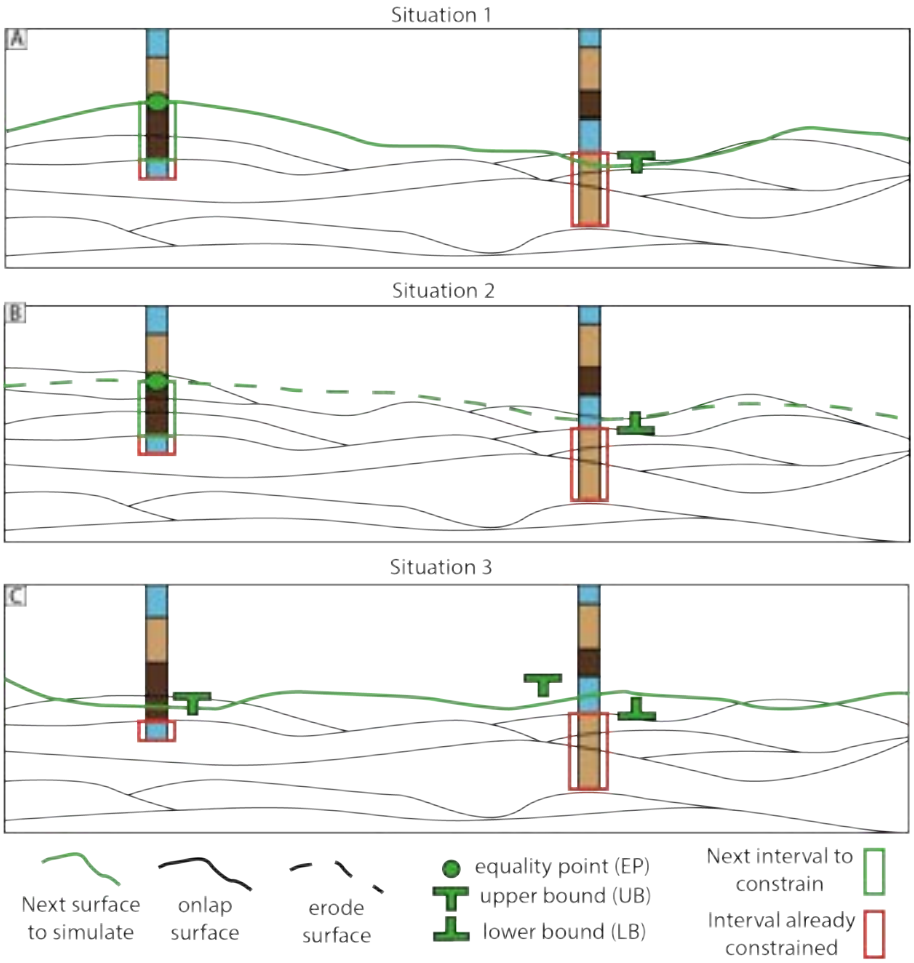

Figure 7.3: *Three different situations can arise during the simulations of the surfaces. Situations 1 and 2 (**A** and **B**) concern a case where an interval has to be constrained while situation 3 (**C**) concerns onlap surfaces not constrained by an interface. See text for details. The horizontal bar of the "T" of the upper and lower bounds (UB and LB) is positioned at the altitude where the bound is applied. Note that these symbols are slightly offset to the left or right for better visibility. But they still apply to the borehole position.*

The interval being now constrained, we can add the EP data to LB to prevent them being eroded by subsequent erosive surfaces (step 18) and interface is no longer attributed (step 19).

If the current surface is not attributed to an interface, We decide with a probability ξ if it is onlap or erosive (Step 21 in Algo. 7.3). To prevent to connect different facies intervals, we add several constraints to onlap surface, as illustrated in situation 3 (Fig. 7.3C). In this example the surface is forced to pass in the blue interval in the right borehole while avoiding the brown interval in the left borehole. The rest of the procedure is the same as before. Practically, this is done by randomly choosing a facies interval among the next to be constrained in each borehole and forcing the surface to pass through it using UB and LB, while avoiding other nonidentical facies intervals by applying UB. This prevents the connection of different facies.

The remaining steps (volume definition and facies assignment) are almost identical to the unconditional case. Before applying Algorithm 7.2, we simply attribute the facies from the boreholes to the regions that intersect them.

7.2.5 Hierarchical workflow

Hierarchical structures are very common in Quaternary deposits (Miall 1991; Miall 2013). To model these features, one can apply EROSim within a hierarchical workflow. The hierarchical levels can be seen as the results of sedimentological processes at different spatial and temporal scales (or levels).

We consider these levels as sets of surfaces that separate not only lithofacies but also distinct sedimentological units. The basic principle is that a surface of a specific hierarchical level can only affect surfaces that have an equal or lower hierarchical level. For example, a specific sedimentological body delimited by surfaces of a higher rank, cannot be eroded by a surface of a lower rank. From a computational point of view, this implies that we can simulate these deposits sequentially by hierarchical level from higher to lower levels.

For example, let us consider a case with two hierarchical ranks: one defined by surfaces having a large extent and delimiting large sedimentological units (or regions), and another one defined on a smaller scale with numerous surfaces frequently intersecting each other and producing regions of smaller sizes. To model this system, it is possible to decompose the simulation in two steps: first, high-order surfaces are simulated to delimit the boundaries of the different sedimentary units. In the second step, EROSim simulations are performed inside these units. Practically, this implies constraining the upper and lower boundaries of the simulation domain of EROSim with the simulated surfaces of the first. This can be extended to as many hierarchical levels as needed.

Using such a hierarchical approach, it is also possible to include more constraints in the model by setting different simulation parameters (α, ξ, N, surfaces interpolation parameters) for each unit or hierarchical level. But it also implies inferring a large number of parameters.

The usefulness of the hierarchical approach is presented in section 7.4.

7.3 Parameter sensitivity

This section illustrates the EROSim capability to simulate a wide variety of sedimentary structures. We first present some unconditional 2D examples, as well as the effect of the different parameters (α, ξ, etc.) on the simulations (e.g. shape and size of the regions). We then demonstrate that the algorithm can be conditioned to well-data. Some 3D simulations are presented in section 7.4 with a case study.

7.3.1 Unconditional simulations

For most of the examples shown in this section, we consider a 2D vertical slice (x, z) of dimension 60×30 m^2 and with a spatial resolution of 0.33×0.15 m^2. We simulate a total of four facies ($k = 4$) in equal proportions. To keep things simple, we used the same covariance for all surfaces in a single EROSim simulation. However, there is no difficulty in using different covariance models. For example, erosive surfaces could be assimilated to more energetic events and therefore could have smoother surfaces. In all simulations, the surface means are drawn from a uniform law between the top and bottom of the simulation domain. This allows distributing the surfaces uniformly over the domain and obtaining stationary simulations, but this is not a fixed feature of the algorithm.

Figure 7.4 shows one unconditional simulation with a stationary cubic covariance with a range of 45 m and a total variance of 5 m^2. The simulation parameters are $N = 100$ surfaces, 10% of erosive surfaces ($\xi = 0.1$), and the facies simulation being only driven by the marginal target probability ($\alpha = 1$).

Figure 7.5 illustrates the effects of the different simulation parameters. As expected the range of the covariance controls the geometry of the surfaces. A shorter range leads to rougher surfaces. But it also controls the size of the regions. A shorter range creates more intersections between the surfaces and leads to smaller regions (Figs. 7.5A to 7.5C). Logically, the number of regions also increases with the range. The proportion of erosional surfaces (ξ) does not modify significantly the size of the regions, but it changes rather their shapes (Figs 7.5D - 7.5F). When there is no erosion ($\xi = 0$) the boundaries of the regions are mostly concave, but as ξ increases, more and more convex boundaries appear. This is the effect of erosion, which removes some parts of the regions that are filled later. As expected, the number of surfaces (N) influences

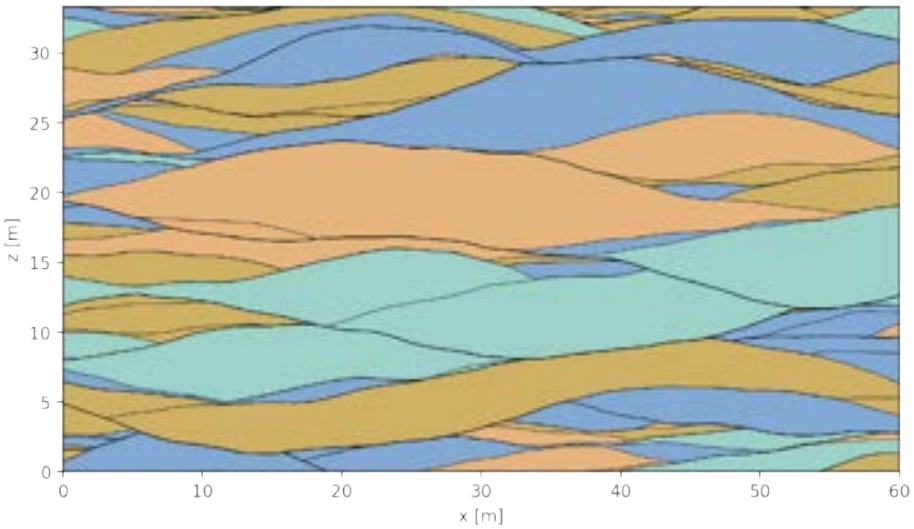

Figure 7.4: *Example of an EROSim unconditional simulation with 100 surfaces. The four different colors represent four different facies. The black lines delimit the regions.*

the thickness of the regions (Figs. 7.5G to 7.5I), and their numbers. This is mainly due to our choice of drawing the surface means in a uniform law. The influence of the α parameter is also clearly visible (Figs. 7.5J to 7.5L). When α is equal to 0 (Fig. 7.5J), the regions of the same facies tend to be clustered through the whole simulation domain, while when α is equal to 1, they are evenly distributed.

Different covariance models can also affect the shape of the regions. For example, Fig. 7.6B shows a simulation with a spherical covariance model with a small range. The boundary between the regions are rough, and they are more individual regions than with a larger range.

Figures 7.6A, 7.6C, and 7.6D illustrate the possibility of using non-stationary means or variograms through the simulation domain. In Fig. 7.6A, the means are following a sinusoidal trend. In Fig. 7.6C the means follow linear trends with varying slopes. And finally, in Fig. 7.6D the sill and range of the variograms are progressively increasing to the right. These examples, even if they are a bit theoretical, show that if some information is known about the non-stationarity of the sedimentary structure, EROSim is capable of handling this information.

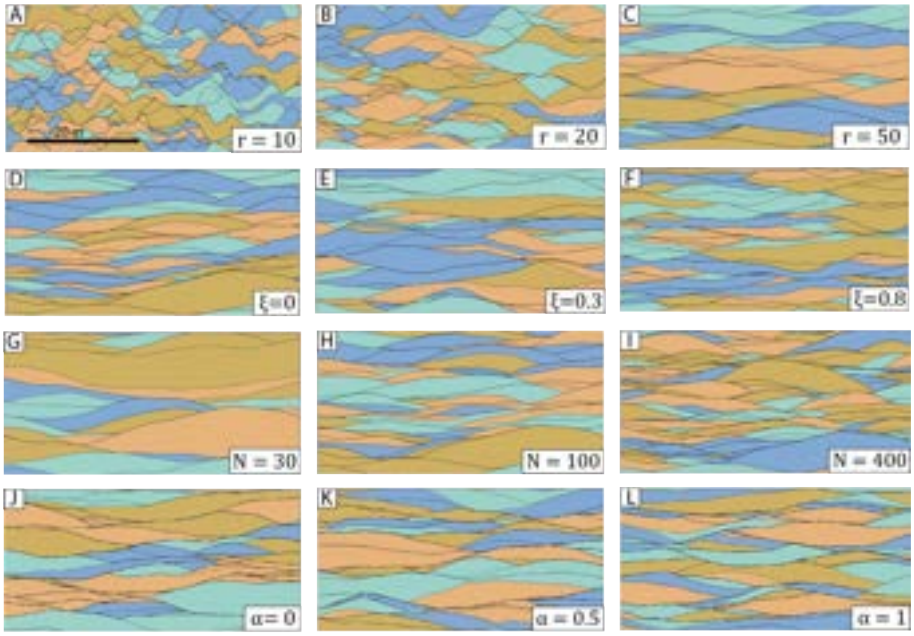

Figure 7.5: *Different EROSim simulations where one parameter has been changed on each.* ***A*** *-* ***C****: Simulations where the variogram range increases from 10 to 20 and then to 50.* ***D*** *-* ***F****: Simulations where the ratio of erosive layer (ξ) increases from 0 to 30% and then to 80%.* ***G*** *-* ***I****: Simulations where the number of surfaces (N) is modified, from 30 to 100 and then to 400.* ***J*** *-* ***L****: Simulations where the α has been modified, from 0 to 0.5 and then to 1.*

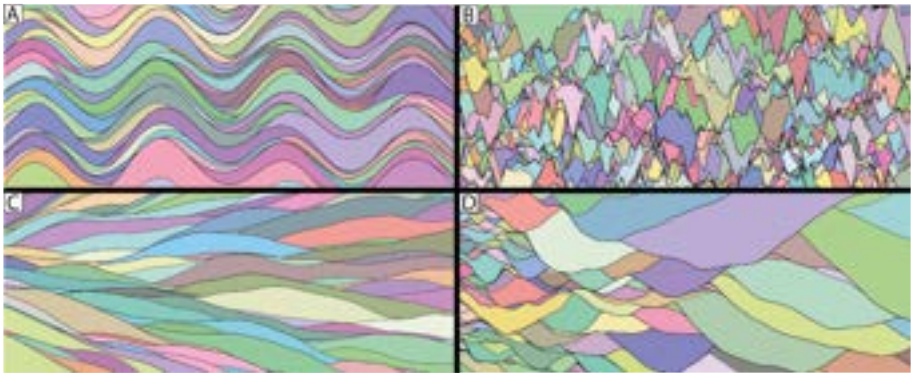

Figure 7.6: *Realizations showing the capabilities of EROSim by varying different modeling parameters such as the mean (****A****,* ***C****), the variance (****D****) or the covariance model (****B****, spherical). The different colors of the regions do not represent anything in particular and are just used to distinguish them.*

7.3.2 Conditional simulations

In this section, we illustrate the capabilities of EROSim to produce conditional simulations based on borehole data. The number of facies is reduced to three in equal proportions. For all the examples, we used the same simulation parameters ($N = 100$, $\xi = 0.1$, and $\alpha = 0.5$). The surface means were randomly drawn from a uniform distribution between the minimal and maximal elevations. All surfaces are simulated with the same cubic covariance model with a sill of 5 m^2 and a range of 15 m or 55 m.

Figure 7.7 shows different conditional EROSim simulations using a range of 15 m (Fig. 7.7A, B) or a range of 55 m (Fig. 7.7C, D). The borehole intervals are correctly respected without any apparent deformation of the regions. Note that despite using the same value for the clustering parameter α (=0.5) for both cases, the facies regions are distributed differently. Realizations obtained with a variogram range of 15 m display more variability in the types of contact between the regions than the ones made with a variogram range of 55 m, since using the lower range results in a larger number of regions.

We used Sequential Indicator Simulations (SIS, Journel 1983a) to compare EROSim capabilities over one of the most standard facies modeling tools. Indicator variograms were estimated using EROSim simulations and used to produce SIS realizations. Four of those simulations are shown in Figure 7.8. SIS respects the conditioning data, proportions, and input variograms but does not succeed in reproducing some of the patterns (sharp contacts) proposed by EROSim. SIS produces more noisy and pixelized simulations with irregular facies boundaries.

If we compare the probability maps obtained by averaging 100 realizations (Fig. 7.9), we observe strong similarities between the two methods. Indeed, facies probabilities seem practically identical. But if we compare Shannon's Entropy (Shannon 1948), we see that SIS results are generally more uncertain (higher entropy) between the boreholes than EROSim. This is visible between the second and third boreholes (between $x = 25$ m and $x = 55$ m) which have nearly identical facies logs, implying a possible connection between the two. While EROSim is almost certain that a continuous connection exists between the two blue facies, SIS is not. The same comment can be made for the orange facies but the difference is not blatant.

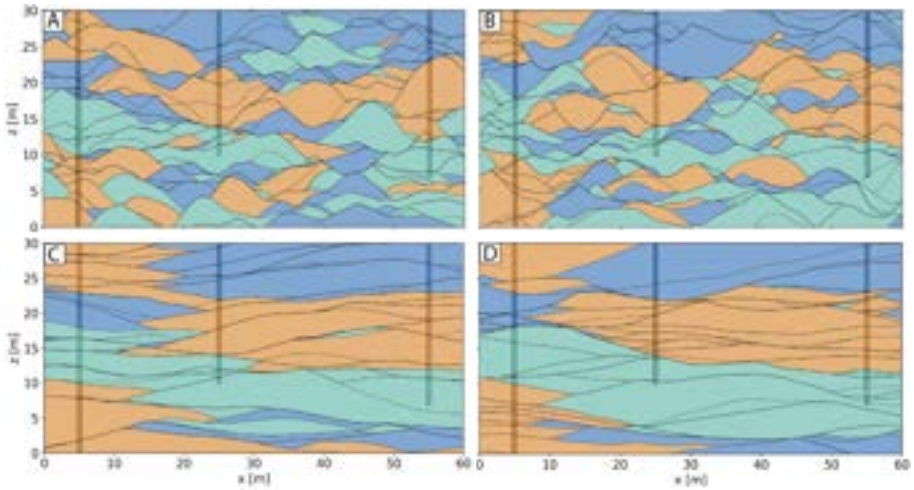

Figure 7.7: *EROSim conditional simulations based on borehole data.* ***A*** *and* ***B*** *are two equiprobable realizations using a cubic covariance model with a range of 15 m and* ***C*** *and* ***D*** *were made with a cubic covariance with a range of 55 m.*

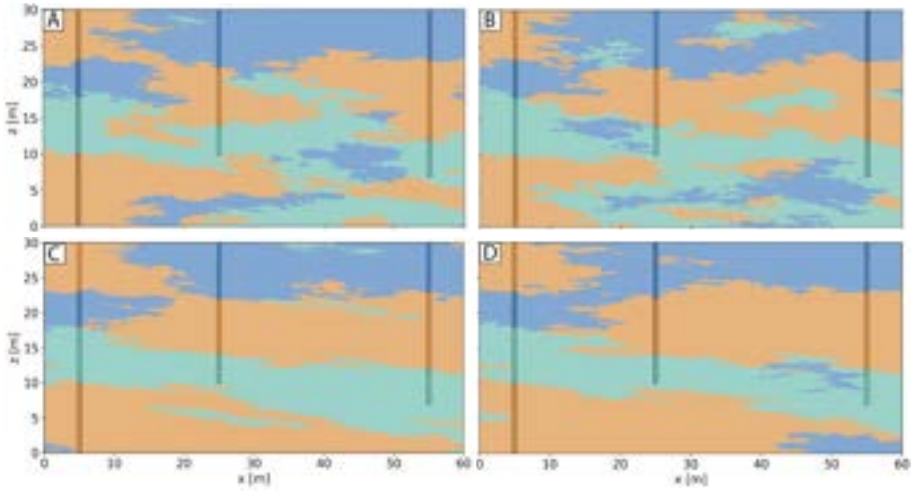

Figure 7.8: *SIS simulations where each indicator variogram has been inferred from the corresponding EROSim simulations. Indicator variograms used to generate* ***A*** *and* ***B*** *were inferred on EROSim simulations with a range of 15 m (fig. 7.7 A, B). Identical procedure was applied to generate* ***C*** *and* ***D*** *but on EROSim simulations with a range of 55 m (fig. 7.7 C, D).*

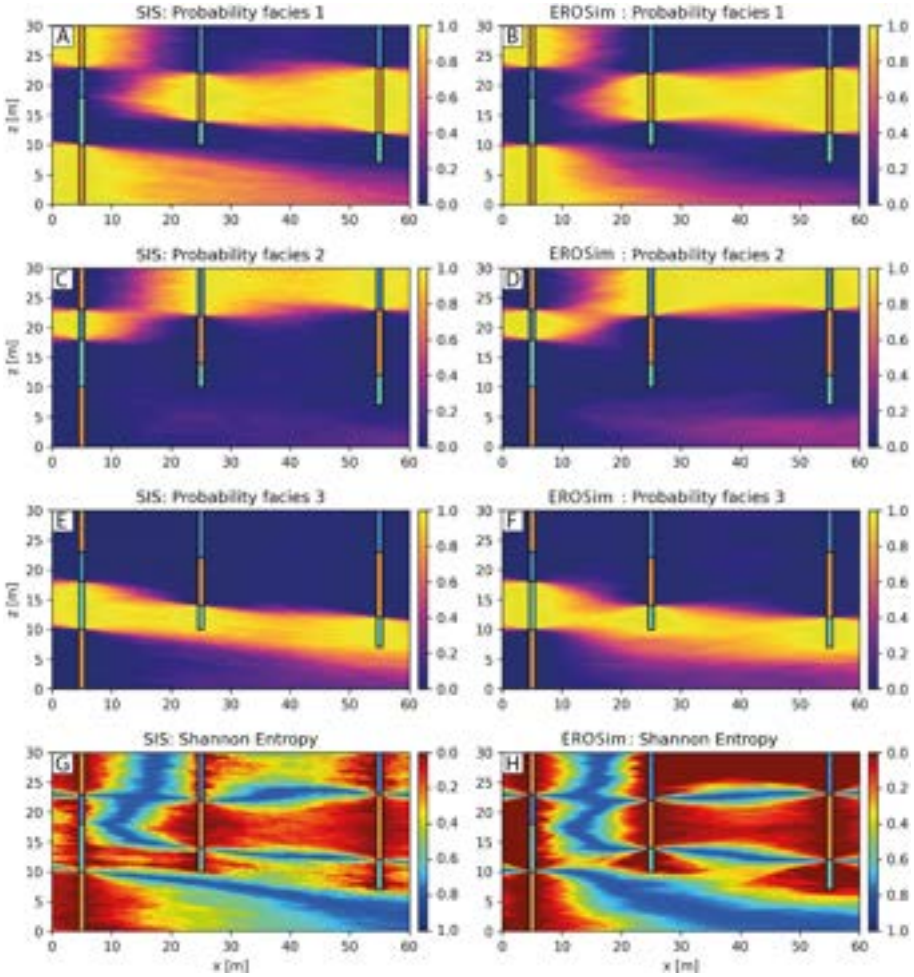

Figure 7.9: *Probability of occurrence for each facies (computed over* 100 *realizations) considering a variogram range of 55 for EROSim simulations (fig. 7.7C, D) and SIS simulations made with variograms inferred on EROS simulations (fig. 7.8C, D).* ***A****,* ***C****,* ***E*** *are the probability maps for facies 1 to 3 for SIS method and* ***B****,* ***D****,* ***F*** *are the probability maps for facies 1 to 3 for EROSim method.* ***G*** *and* ***H*** *are the related Shannon entropies to probability maps for SIS and EROSim, respectively.*

7.4 Application to the upper Aare valley

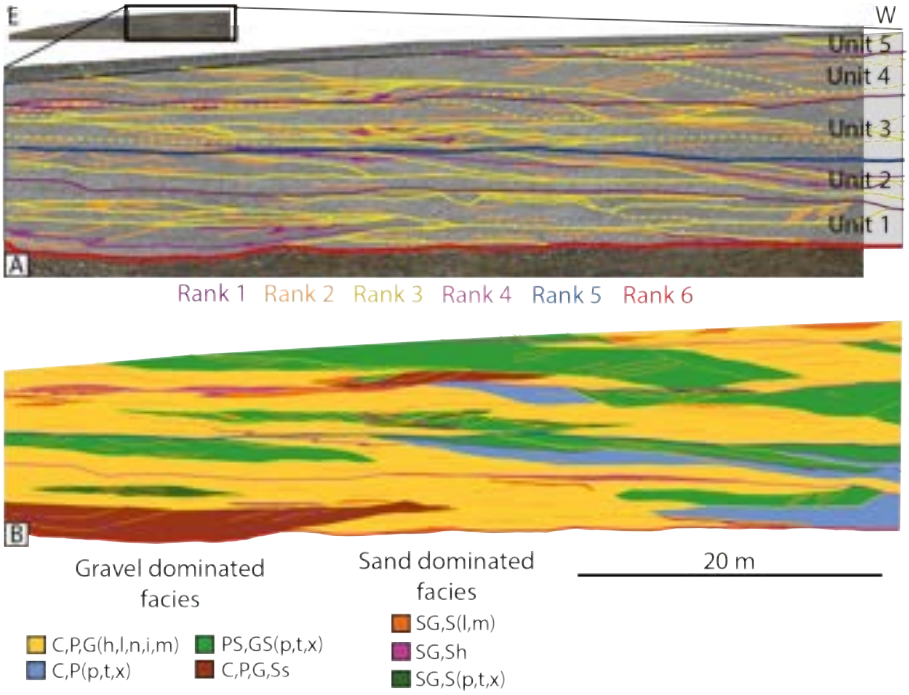

Figure 7.10: *Interpretation of a part of the East-West wall of the Bümberg quarry realized by Menga (2021).* ***A*** *is the reconstructed image of the wall acquired by the drone as well as the sedimentological surfaces that separate the subfacies bodies. The hierarchical rank of each surface is given by its color. The five stratigraphical units, delimited by surfaces of rank 4 or higher are also shown.* ***B*** *shows the corresponding colorized facies groups interpretation. For readability and clarity, only half of the wall is shown. Figures and data are taken and modified from Menga (2021)).*

In this last section, we illustrate the ability of EROSim to simulate structures similar to the ones observed in the field.

7.4.1 Study site and field data

The study site is located in the Bümberg quarry, in the canton of Bern, in Switzerland. The quarry walls show fluvio-glacial Quaternary sediments made up of different sand and gravel facies that show complex relationships. This type of sedimentary architecture can be observed in many other queries in Switzerland and abroad. The Bümberg quarry has been identified as a suitable sedimentological analog for the Upper Aare Valley aquifer. To characterize its heterogeneity, the sedimentological structures, hierarchical levels, and deposits of the quarry walls were manually interpreted based on a field survey and a high-resolution photogrammetric UAV survey to obtain 3D ortho-normal images (Menga 2021). This enabled the digitization of the delimitation and the

characterization of the different stratigraphic boundaries and unit extents. In this quarry, Menga (2021) analyzed two walls, one oriented North-South (180 m long and 13 m high) and one oriented East-West (115 m long and 12 m high) to characterize the possible anisotropy of the sedimentological structures.

Several different lithofacies have been identified and described according to the classification proposed in Miall (2013) that takes into account the grain size and the sedimentological structures of the deposits. The different grain sizes are described by a capital letter: C (cobbles), P (pebbles), G (gravels), S (sands), and L (silts). The arrangement and/or the structure of the sediments are described by a lowercase letter: o (open framework), i (imbricated), h (horizontal stratification), n (normally graded), r (reverse graded), l (low angle stratification), p (planar-cross stratification), t (trough-cross stratification), s (draping troughs), x (cross-stratification), m (massive).

Menga (2021) regrouped them into seven facies groups and for each group a sedimentological origin interpretation has been proposed. These groups and interpretations are shown in Table 7.1 and Figure 7.10B shows the spatial organization of these facies on the East-West wall of the quarry. Gravel-dominated facies are the predominant groups of facies, whereas sand-dominated facies are quite dispersed and only present locally. Gravel facies are distinguished into four groups: bedload sheet aggradation (yellow), transverse bar migration (blue), scour fills (brown), and gravelly dunes (green), for a more comprehensive understanding of these sedimentological formations, please refer to Miall (1996).

Table 7.1: *Facies code and their interpretation in the Bümberg quarry. The colors used to represent them are also given.*

Facies code	Interpretation	Facies color
C,P,G(h,l,n,i,m)	Bedload sheet aggradation	Yellow
C,P(p,t,x)	Transverse bar migration	Blue
C,P,G,Ss	Scour fill	Brown
PS,GS(p,t,x)	Gravelly dunes	Green
SG,S(p,t,x)	Sandy-gravelly dunes	Dark Green
SG,Sh	Sandy wedges	Pink
SH,S(l,m)	High flow regime sandy levels	Orange

In addition, six levels of sedimentological hierarchies have also been recognized, and named *Rank 1* (lowest rank) to *Rank 6* (highest rank). Figure 7.10A shows the interpreted surfaces on the wall of the Bümberg quarry. The surfaces of *Rank 1* to *Rank 2* are likely the result of very local processes ($\sim$ 1 - 5 m) while *Rank 3* surfaces have a larger extent ($\sim$ 5 - 60 m). Higher-order surfaces (*Rank 4* - *Rank 6*) exceed the size of the domain and can be treated equally in this situation. There are a total of six of these surfaces on the two walls,

which delimit five sedimentological bodies (Units in Figure 7.10A) that differ in terms of facies proportions and structures.

7.4.2 Model setup and parameters

To account for the hierarchical relations observed on the study site, we consider the hierarchical approach proposed in section 7.2.5. At the lowest rank, the regions are filled with facies while surfaces of higher ranks are simulated independently to delimit stratigraphic units. For the upper Aare valley, the aim is to produce a model of lithofacies. Based on the field observations, we consider that it is reasonable to set the lowest rank to *Rank 3* surfaces (Fig. 7.10A, yellow lines) and to fill the delimited regions with the facies that are mostly differentiated by these surfaces. Figure 7.10B shows that these are gravel-dominated facies. The sand facies (dark green, pink, and orange) are more dispersed and often delimited by surfaces of *Rank 1* or *2*. Therefore, we must consider as well the hierarchical levels above *Rank 3* (pink, blue and red surfaces). Furthermore, the regions delimited by these higher rank surfaces have different characteristics in terms of sedimentary body sizes and facies proportions. Finally, we only simulate the four dominating facies (mainly gravels). Orange and pink facies have been regrouped into the yellow facies, while dark green facies has been regrouped with green facies.

As explained in section 7.2.5, the approach is decomposed in two steps. First, the geostatistical parameters of the higher-rank surfaces are required to define the extent of each unit. From base to top in this quarry, Menga (2021) recognized a first unit bounded by a surface of *Rank 6* and *Rank 4*, a second unit bounded at the top by a *Rank 5* surface, a third, fourth and fifth units, bounded at the top by *Rank 4* surfaces (fig. 7.10A). Consequently, it is required to simulate three *Rank 4* surfaces and one *Rank 5* surface. Therefore, for each wall, the variograms for *Rank 4* and *Rank 5* were estimated on the available surfaces as well as the mean altitudes of each of the surfaces. The parameters to model those surfaces are provided in tables A.10-A.11 in the appendix. *Rank 6* surface was not modeled and was simply considered to be the bottom of the simulations.

In this phase, we undertake the simulation of *Rank 3* surfaces within each distinct unit. EROSim requires that we infer the following parameters: the number of surfaces (N), a distribution for the mean altitudes of the surfaces, the variogram models of the surfaces (μ_i and γ_i), the proportion of erosive surfaces (ξ), the proportions of the facies (p_{global}), and lastly, the clustering parameter (α).

The γ_i were estimated using the interpreted surfaces, drawn by Menga (2021), by computing the experimental variogram on each independent line (or surfaces) and by adjusting a variogram model on them. Note that we only consid-

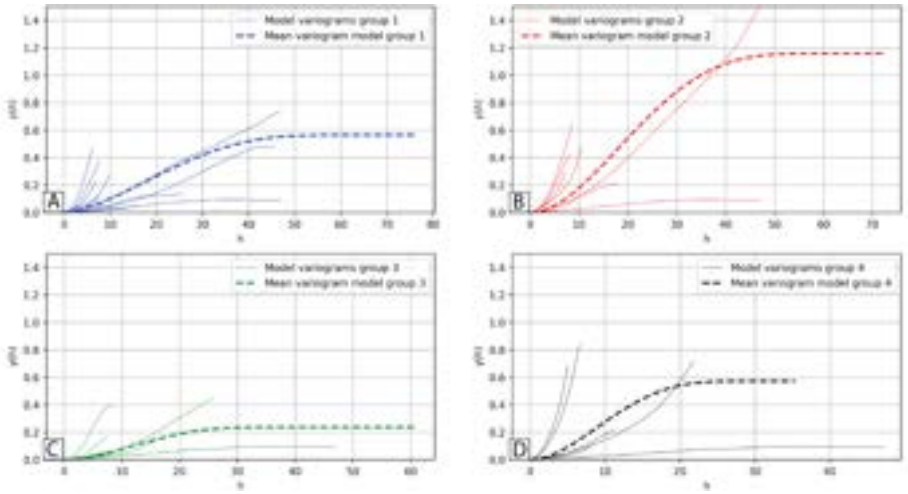

Figure 7.11: *Experimental and fitted model variograms realized on the EW wall of the Bümberg quarry for each different unit.*

ered lines with a minimal length of 5 m to obtain representative statistics. The spatial statistics of these surfaces for the EW Bümberg wall are summarized in Fig. 7.11 for each unit. Unit 5 is not represented, as there was not enough surfaces to infer proper variogram models. In this case, we used the mean values of the parameters, averaged on all the variogram models. Finally, for each unit, the inferred parameters of the variogram models were averaged to keep only one set of parameters.

The other parameters (N, ξ, p_{global}, α) were estimated by trial and error and are given in Table A.12 in the Appendix.

7.4.3 Results

We first compare 2D simulations with actual observations on the quarry walls and then present results from simulated 3D blocks.

2D cross-sections

Figures 7.12 and 7.13 show EROSim simulations of the quarry walls and the observed geology for the same locations. In these figures, the lines delimiting the regions are not shown for clarity. Generally, the simulations reproduce rather well the shapes of the regions as compared to the reference. A more quantitative analysis of the results has been conducted on an ensemble of 100 realizations for the two sections. It shows that the indicator variograms computed for each facies for each EROSim simulation are well distributed around the reference indicator variograms, as illustrated in Figures 7.14A to 7.14C for N-S wall. The

proportions are also well respected (Fig. 7.14D). Similar results are obtained with the E-W wall.

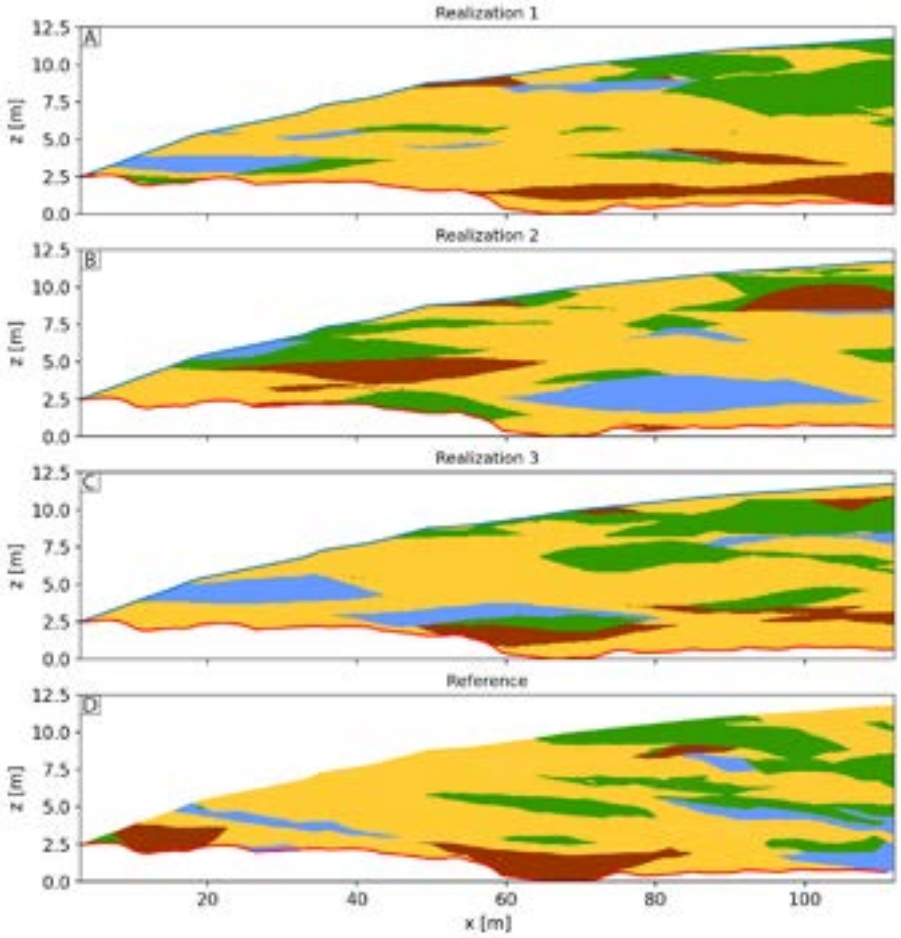

Figure 7.12: *Three EROSim simulations of the East-West wall of the Bümberg quarry (**A - C**) and the interpreted wall made by Menga (2021) considered as the reference (**D**). The sedimentological lines that separate the regions are not shown.*

3D models

EROSim can also be used in 3D. Figure 7.15 shows 3D simulations using the sedimentological statistics inferred on both walls of the Bümberg quarry. Standard parameters (tab. A.12) have been averaged between the two walls, as well as the altitudes of the surfaces of the higher ranks. The 1D variograms were also combined to obtain 2D variograms for the surface simulations. This was done assuming that the spatial statistics inferred on the walls represent the statistics on the major and minor axes of anisotropy of the 2D variogram. The

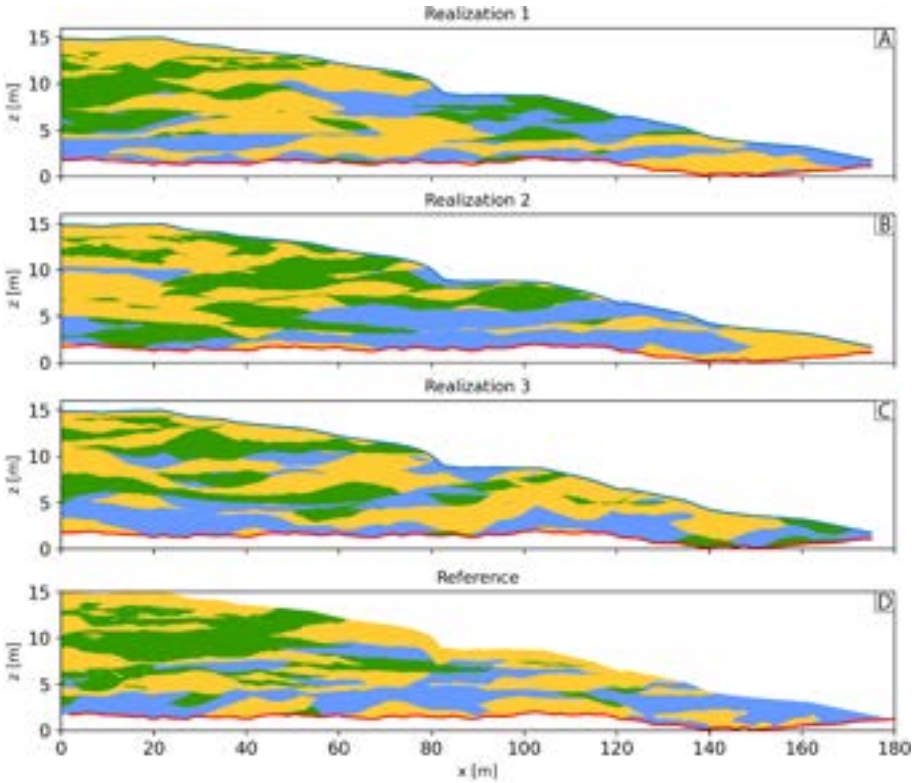

Figure 7.13: *Three EROSim simulations of the North-South wall of the Bümberg quarry (**A** - **C**) and the interpreted wall made by Menga (2021) considered as the reference (**D**). The sedimentological lines that separate the regions are not shown.*

variogram ranges on the NS wall were assigned to the range on the Y axis of the 2D variograms, and the variogram ranges on the EW wall were assigned to the range on the X axis. Sills were averaged. The grid used for the visualization has a cell size of $0.85 \times 0.85 \times 0.14$ m^3 and contains $100 \times 100 \times 100$ cells.

Figure 7.15 shows significant variability between the realizations because of the absence of conditioning. It also shows that EROSim can reproduce the expected shapes of the sedimentological structures while exploring a broad variety of plausible configurations. The sedimentological lines bounding the regions are not shown here for the sake of visibility, but it is important to remember that this additional information is available. Regions can be individualized and treated differently in successive modeling steps (e.g. simulation of physical properties).

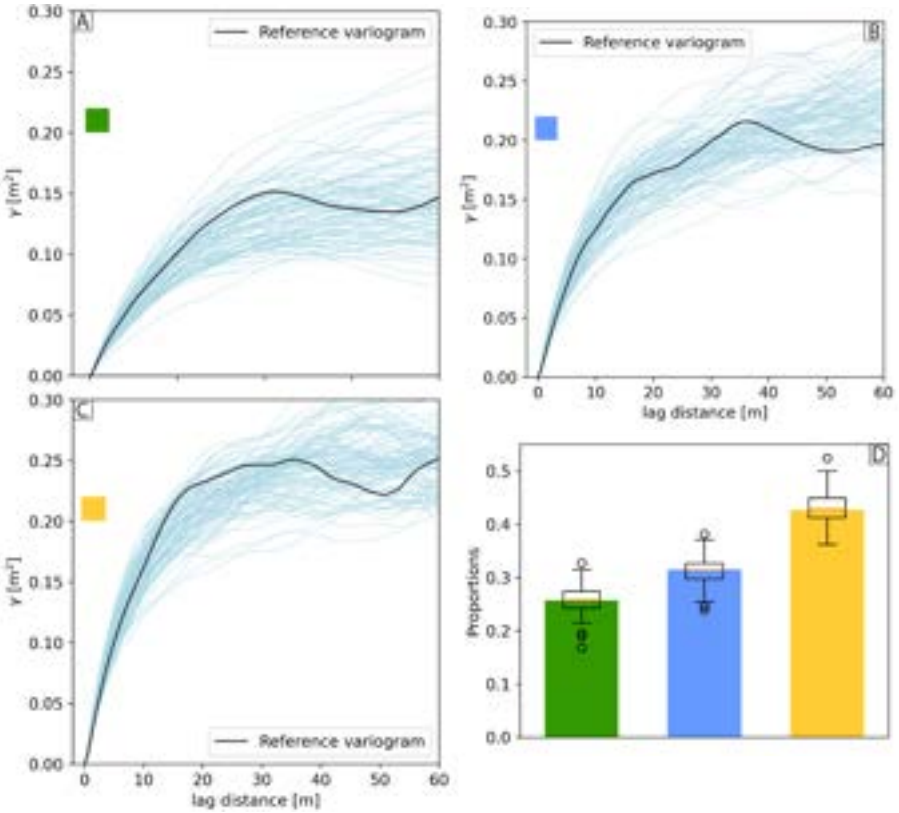

Figure 7.14: *Comparison of proportions (**D**) and indicator variograms (**A**-**C**) for each facies between the references and 100 realizations of the N-S wall.*

7.5 Discussion

In this paper, we presented EROSim, a novel surface-based simulation method and a conditioning algorithm that can model sedimentological heterogeneity that is frequently observed in fluvio-glacial systems.

The application of this method with the data from the Bümberg quarry site shows that the results obtained with this method represent well the main sedimentological features observed on the quarry walls. Slight visual differences remain in both the shape of the regions and the distribution of the facies. This is most probably due to using one unique variogram to model all the internal surfaces. Indeed, Figure 7.11 shows a large spectrum of estimated variogram models from the field data, regardless of the unit in which we are. The same thing is also observed on the NS wall. Therefore, the use of a single variogram model cannot capture this variability. However, the observed variability is related to the estimation of variograms on very short lines which may create artifacts, whereas EROSim uses these variograms to simulate surfaces over

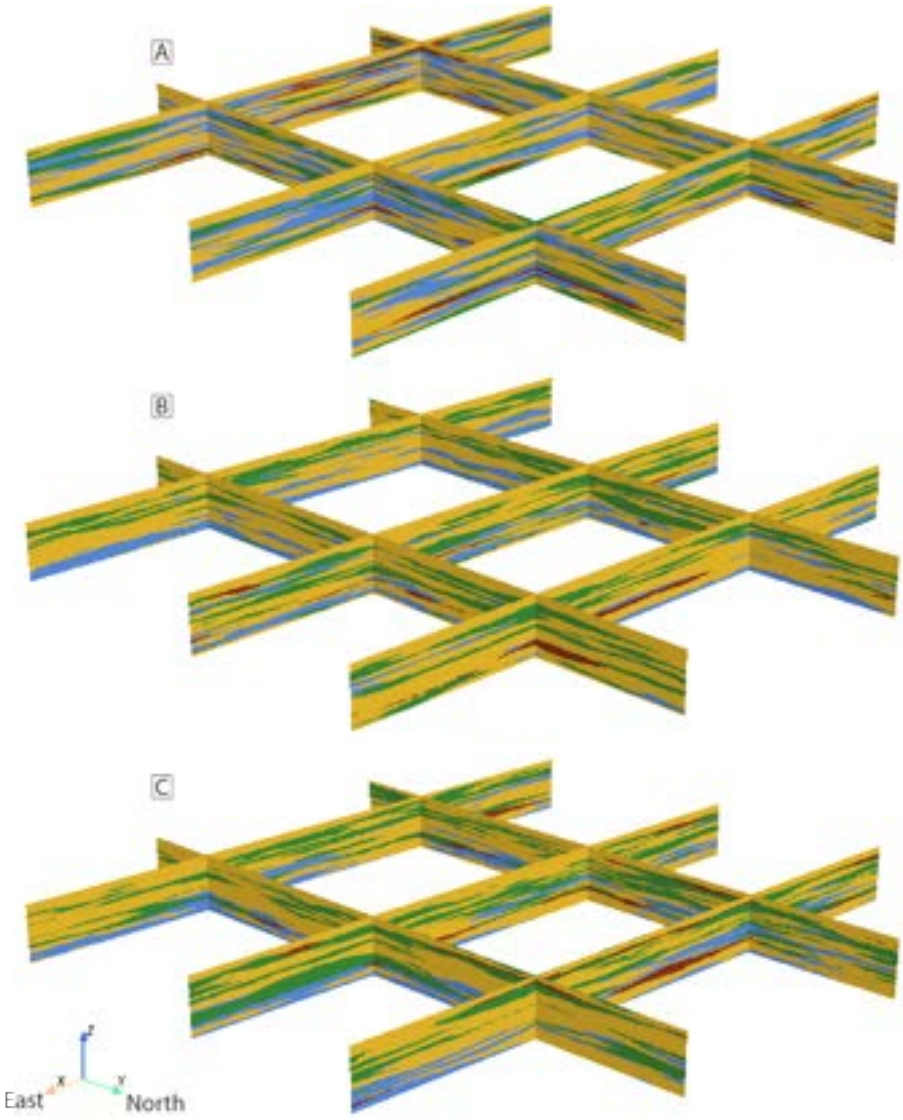

Figure 7.15: *Three different realizations (**A** - **C**) of EROSim 3D simulations of the Bumberg quarry. The model dimensions are 170 m x 170 m x 14 m, there is no vertical exaggeration.*

the whole simulation domain. It is also important to remember that erosion processes influence the shape of these lines, which necessarily influences the spatial statistics of these objects. Modeling the interfaces with different variograms would be possible but it would make the parametrization of EROSim much more complex and we argue that it would not necessarily be useful or critical for groundwater applications.

As compared to other variogram-based facies simulation methods EROSim provides more control over the geometry of the geological interfaces for the user. The simulated models include a representation of internal structures within single facies such as orientations of the deposition patterns, and a hierarchical structure. The orientation of the local patterns, given by the simulated surfaces, can be used to orient the local anisotropy of permeability. The definition of these surfaces permits as well defining thin and continuous structures such as clay plugs which may have an important influence on flow and transport and which are difficult to simulate with other variogram-based approaches.

Compared to object-based methods (OBM) or Multiple Point Statistics (MPS), EROSim is not designed to generate specific geological shapes, such as meanders, deep-water lobes, etc. However, EROSim does not require sophisticated inputs, such as a training dataset (TD) for MPS or the definition of geological objects and their spatial relations for OBM. Determining the parameters of EROSim from outcrop data is simpler than determining all the input required for MPS or OBM. In addition, more complexity could be added in EROSim relatively easily by including for example some non-stationarity as shown in Figure 7.6 or by having a more complex parametrization. While we presented a brief comparison with SIS in terms of conditioning in this paper, a more comprehensive comparison involving other methods and including the impact of the sedimentary structures on flow and transport has still to be done. It will be the topic of future research.

A few limitations and possible extensions of the proposed approach can be identified. The conditional algorithm requires imposing rules on the simulation of surfaces. This is permitted thanks to the use of inequality data when modeling Gaussian Random Fields, and this is one of the main novel contributions of this paper. In most cases, the conditioning does not perturb the shape of the regions but it may distort them if the conditioning data are very dense (high number of borehole data). Input parameters must be compatible with the data. If too few surfaces are defined, the algorithm may not be able to respect all the interfaces within the boreholes. But this limitation is not specific to EROSim and applies to all geostatistical methods in general.

There is also room for improvement to integrate other kinds of conditioning data (seismic data, locally varying facies proportions, etc.). For the simulation of the facies, we decided to keep the parametrization extremely simple. This is a potential limitation and more sophisticated rules involving transition proba-

bilities between each facies, similar to what is done in TPROGS (Carle 2007), could be accounted for. We could also account for the volume or shape of the region when estimating the probability of affecting a facies to a certain region. However, once again, we argue that the simplicity of the proposed model is probably sufficient for many applications and we leave this possible extensions to future works. In the Bümberg case study, we identified the parameters by computing individual variograms and averaging them. The other parameters were mainly identified by trial and error. Further research should be devoted to developing a more automated technique to infer the parameters.

7.6 Conclusion

In this paper, we presented a new approach, EROSim, to model geological heterogeneity by simulating litho-facies models. The method is designed to represent sedimentary structures typically present in fluvio-glacial Quaternary deposits which are the most frequently used aquifers in Switzerland. EROSim offers a new perspective in the field of facies modeling by initially creating regions and subsequently populating them with facies. Moreover, it seamlessly integrates geological principles via erosion-deposition rules, introducing a significant degree of flexibility into its realizations and rendering it suitable for diverse sedimentological contexts. The litho-facies are assigned to the regions using a graph-based approach accounting for global proportions over the entire domain and for local proportions derived from adjacent regions. The conditioning algorithm employs inequality data derived from the borehole observations and the sedimentological rules.

The capacity of this model to represent different geometries and sedimentary patterns has been illustrated with several unconditional and conditional examples. Through these examples, we show the influence of the model parameters (e.g., α, ξ, etc.) on the resulting simulations. Furthermore, EROSim is applied to a real field site from a gravel quarry, where the spatial statistics of the sedimentological surfaces are inferred and used to parameterize the simulations. The resulting simulations show spatial patterns closely similar to those observed on the quarry walls. A numerical comparison of the proportions of the facies and the indicator variograms of the facies confirms this similarity.

The main advantages of this approach are: its simplicity for the parameterization, its capacity to generate realistic 3D simulations from data acquired in 2D, its hierarchical structures, the possibility to condition the simulations by borehole data, and finally the availability of the code.

Further research is still needed to analyze the impact of the structures generated by EROSim on flow and solute transport and to compare the performances of this model with other facies modeling techniques.

Chapter 8

Conclusion

This thesis proposed novel approaches and tools for modeling Quaternary deposits and applied them to different study sites such as the Upper Aare and the Rhine Valleys, in Switzerland. It was shown that the hierarchical approach (units, facies, properties) is able to offer the flexibility and complexity needed to model this kind of environment. The various aspects and limitations of this workflow were then investigated, particularly with regard to facies modeling and the difficulty of having boreholes with stratigraphic interpretations. The integration of conceptual and expert data and the choice of a single model from a set of stochastic realizations were also discussed. Overall, the proposed methods provide interesting results and lay the foundations for a possible future of more accurate, automated, and simpler geological modeling.

This chapter presents the main contributions of this research as well as the main limitations of the proposed methods. Some ideas, proposals, and recommendations are discussed to help solve these remaining issues and to go beyond the scope of this thesis.

8.1 Main contributions and limitations

To illustrate the methodological contributions of this thesis, the different stages in the construction and creation of a geological model are presented.

Every geological study starts with data collection, including in situ data such as outcrops, boreholes, and geophysics, as well as conceptual data like expert opinions, previous studies, and drilling logs. The purpose of this data collection is to compile all available information on the subject and create a summary of its quantity, quality, and diversity. These data also need to be homogenized. On this basis, a conceptual model can begin to take shape. Following a hierarchical approach, the concept can be defined in terms of stratigraphic units, facies, and properties. The properties to be modeled depend mainly on the objectives of the study and are generally not the most difficult part of the conceptualization. The other two, on the other hand, are more problematic. They are covered and discussed in the chapters of this thesis.

8.1.1 Automatic Stratigraphic Pile

We start with the first hierarchical level, the stratigraphic units, which represent geological time units, generally reflecting different climatic and geological conditions. Borehole logs frequently contain this information, indicating which units are present (or absent) in what thickness. As the complete sequence of units is assumed to be the same across the entire domain, the concept should be a faithful representation of the complete succession of these units, the stratigraphic pile. However, due to conflicting data and difficulties in accurately identifying a stratigraphic unit in a borehole, determining the most consistent pile is not always obvious. To this end, an algorithm for the automatic determi-

nation of unit succession has been proposed in chapter 4. Using the boreholes, already interpreted in terms of units, the algorithm proposes several plausible piles, giving each one a score according to the rate of boreholes in agreement with it. Then it is possible to select the more appropriate pile given its score or expert knowledge.

The algorithm can also refine the conceptual model by identifying erroneous or disagreeing stratigraphic contacts attributed to each proposed pile. If these errors are infrequent and varied, they can be assumed to be simple errors of interpretation. However, if a contact is frequently incorrect, it may indicate an error in the concept itself. It is then possible to test different strategies and concepts, for example by merging units, to see if it is possible to improve the pile's score. This was used to determine the stratigraphic pile for the Rhine Valley model, described in Chapters 4 and 5. We found that by merging three units, initially considered independent, it was possible to find a pile that matched 99% of the boreholes (compared to 96% before merging). These three units were in fact facies that, while very different geologically, were deposited synchronously, leading to interfingering. It was therefore necessary to adapt the concept to reproduce the spatial distribution of these facies within a single stratigraphic unit. In this case, we used an MPS approach. Therefore, the algorithm allowed one to refine an initial geological concept which globally improved the reliability of the model and was more consistent with the sedimentological history.

The aim here is not to replace the conceptualization phase, but rather to automate what can be automated. The algorithm can propose plausible piles, list noncompatible boreholes and divergent stratigraphic contacts for each pile. With this algorithm, these elements can be obtained in a matter of seconds, much less than if this had been done manually. In the end, the task of selecting a particular pile or grouping certain units remains with the user, but is greatly simplified.

8.1.2 Automated stratigraphic unit interpretation using machine learning

Once the succession of stratigraphic units was established, another issue remained: the lack of stratigraphic logs in the data. This problem, which is addressed in chapter 6, arises from the fact that it is more challenging to assign an age (unit) to a deposit than to describe it geologically (facies). As a consequence, unit models are less accurate and can even lead to inconsistencies between the model and facies data. The proposed solution in chapter 6 was a Machine Learning (ML) approach combined with a borehole simulation step. Several ML algorithms were tested to determine if there were any significant differences between them. The algorithms were trained on a limited number of interpreted boreholes to predict the stratigraphic units interval by interval based on lithological descriptions (facies) and geometrical coordinates. To

maximize the effectiveness of the ML algorithms and account for uncertainties, probabilities were used instead of direct predictions. These probabilities were then used as the basis for the borehole simulation step. The outcome consists of a series of random simulations of stratigraphic records for each uninterpreted borehole.

Overall, this approach has yielded reasonable results. In some cases, clear links have been established between lithologies (facies) and units, while in others, the links are less clear, making predictions more hazardous or even incorrect. However, in some of these cases, manual interpretation would also fail to provide satisfactory results. Moreover, the total number of inconsistencies between facies and units at the borehole locations has decreased. We have demonstrated the importance of comparing different methods, as some have shown very poor predictions (such as Adaboost) or overconfident predictions (such as Multi-Layer Perceptron).

However, this automatic stratigraphic simulation of boreholes has one notable important limitation which is, for now, the difficulty of correctly predicting the reference stratigraphic logs in some cases, as shown in Figure 6.9 and Figures A.2-A.4. This means that potentially incorrect information is fed to the geological model. The main reason for this lies probably in the second step of the method, the borehole simulation. The first step, ML predictions, can, of course, be improved by adding or modifying features according to the situation, but on the whole the predictions seem reasonable. On the other hand, borehole simulation is more hazardous and involves the threshold τ, the minimum probability value to be considered, which is not readily determinable. Ideally, a threshold should be set automatically for each borehole, but the question remains as to how this should be done. The method for simulating boreholes is straightforward. Other methods, such as SIS, which consider spatial correlation, could be taken into account. Integrating constraints on thickness would likely be beneficial. One could also consider using a Markov process, where transition probabilities are derived from the ML predictions. Other strategies could be considered, such as directly estimating the upper altitude of each unit surface instead of predicting the probability of occurrence of each unit layer by layer.

In the end, the method is not perfect and there is room for improvement. For now, it is unclear if it should be used as the advantages are outweighed by potential errors. Statistically, the method reduces the number of inconsistencies and the Brier score, but with the risk of adding incorrect boreholes in the modeling process. Finally, it should be recalled that the Upper Aare Valley exhibits a complex geology with 13 units. The method would likely perform better in a simpler area.

8.1.3 Choice of facies modeling method

The last two subsections concerned the conceptualization and data about the unit model. Once this is done, we can move to the definition of the conceptual facies models for each unit. This step consists in choosing a method to represent the internal heterogeneity of a unit on the basis that it is characterized by the spatial distribution of facies (e.g., lithologies, lithofacies, and hydrofacies). The world of facies methods is vast and diverse, and choosing one in particular is no simple matter. This problem is extensively covered and discussed in chapter 2.

This chapter summarizes and discusses the advantages, disadvantages, and applicability of each method. More than 15 different groups of methods are discussed, ranging from simple ones such as Nearest-Neighbor or Sequential Indicator Simulation to more complex methods such as rule-based and process-based methods. Several recommendations and research gaps are also identified. For example, it is suggested that the choice of one method over another should be dictated primarily by the sedimentological context and conceptual model, rather than solely by the data. In fact, the sedimentary structures generated depend directly on the method used (and its parameters), so the sedimentological and geological context is of paramount importance in understanding the spatial distribution of facies in the subsurface. It was also suggested that the most advanced and realistic methods are underutilized and can be used in many situations to account for more available data, constrain the geometries of the geological features to be simulated, and refine the conceptual model. The review also points out the lack of comparative studies between methods in the literature and the lack of reference models to allow more standardized and systematic comparisons.

Another major issue with facies modeling methods is their accessibility, which is largely uneven between methods. Although some are widely used and available through many open and private software packages, others are proprietary and not freely available. This severely limits the development and improvement of facies methods and partly explains the problems mentioned above and in Chapter 2. A possible solution to this problem is to develop and propose more options, software and open source packages to make these methods more accessible and easier to use. In this direction, EROSim and ArchPy are presented in chapters 7 and 3 of this thesis.

8.1.4 Usefulness of surface-based methods for Quaternary modeling

Chapter 7 presented and examined a surface-based approach, called EROSim, for modeling Quaternary deposits and other sedimentary structures. Quaternary formations are known to be complex due to the interaction of various processes and can present intricate patterns. EROSim proposes to divide the modeling into two steps: tessellation of the domain into distinct regions and as-

signment of a facies to each region. The first step is accomplished by combining stochastic surfaces with depositional and erosional rules, taking into account that the surfaces can be the result of either a depositional or an erosional event. The geometry of the regions (or volumes) created by these surfaces depends on several parameters, such as the spatial statistics of these surfaces (mean and covariance) and the frequency of erosive surfaces. In the second step, a simple graph-based approach is proposed, taking into account the overall proportions and neighboring regions.

EROSim introduces a new approach to facies modeling by dividing the domain into multiple zones and assigning a categorical value (facies) to each zone. This method is easy to set up and does not require the creation of a training data set (e.g., as for MPS or GANs) or the determination of the geometry of the objects to be generated (e.g., as for standard OBM or RBM). Additionally, EROSim can be conditioned to borehole data and can be further developed to account for non-stationarity. The application case of a quarry wall in the Aare Valley showed the effectiveness of the method in parameterizing using an interpreted outcrop and in reproducing the expected geological shapes. Finally, it is the first time that such a surface-based approach has been applied to this kind of Quaternary deposits. However, it is essential to acknowledge certain limitations; EROSim is not specifically tailored to replicate intricate shapes, such as channels, a task better suited to alternative OBM methods. The features generated by EROSim are contingent upon the surfaces utilized, typically manifesting as concave or convex half-lens with varying elongation and thickness. Additionally, another limitation arises in the simplicity of the second step, which offers ease of parameterization but provides limited control over facies placement within regions. This limitation prompts consideration of alternative approaches, such as considering the transition probabilities matrix or constraining facies distribution based on region sizes or geometries. Finally, the links between the nature of the stochastic surfaces and the generated tessellated domain are still unclear and remain to be investigated.

We insist on this part of the workflow as it is probably the one with the greatest impact but also the most uncertain. It is also for this reason that a good part of the thesis is devoted to it. Although not all aspects have been covered, these two chapters (chapters 2 and 7) do give some hints and insights into the conceptualization and choice of facies methods.

8.1.5 ArchPy approach

Once the conceptual model has been defined for units and facies, all that remains is to determine the petrophysical properties to be simulated. These can be very varied, depending on the forward models to be used, but include hydraulic conductivity, porosity, electrical conductivity, and so on. They can be integrated into the model in a number of ways, either by assigning a single

value per facies (assuming homogeneous facies) or by geostatistical simulations to reproduce a scale of heterogeneity smaller than that of the facies. Having done this, we now need to create the various models (units, facies, and properties) in a hierarchical fashion, which can quickly prove complicated given the vast amount of information that needs to be integrated and pre-processed. Fortunately, the ArchPy package makes this task simple and semi-automatic.

The core of the thesis is the ArchPy approach, presented in chapter 3. This methodology proposes to group all the conceptual knowledge of a geological model into one entity, the Stratigraphic Pile. The ArchPy simulation workflow is hierarchical and decomposed in three steps: units, facies, and properties. Units are delineated using 2D surfaces which are interpolated from the borehole data. They are combined by considering sedimentary rules to represent basic sedimentological processes of erosion and deposition. At this step, several additional levels of hierarchy can be considered by integrating smaller subunits inside other larger units, as is commonly represented in sedimentological studies. Note that it is a feature that is generally absent from other geological modeling software and packages. The unit models are then populated with facies using categorical methods (facies modeling methods), which are themselves filled with continuous values to represent the petrophysical properties.

ArchPy places great emphasis on workflow automation, integrating an algorithm for the automatic extraction of conditional data from boreholes for the surface interpolation. This means that once the pile is defined and borehole data imported, the simulations can be easily generated. Other innovations and features of ArchPy include the use of inequalities to simulate stratigraphic surfaces, allowing any sedimentary succession to be reproduced automatically and easily at borehole locations. The use of the stratigraphic pile as a repository for conceptual information also makes it easy to nest different piles and, therefore, consider different levels of stratigraphic hierarchy. With ArchPy, the focus of modeling is on conceptualization and pile construction, rather than on data processing. The automation and use of scripts also implies that existing models can be updated quickly and easily as new data is added. The pile can be modified and adjusted at any time and whenever necessary, as new data or information justifies a change in concept. The pile is flexible, allowing users to create their own "tailor-made" concept. Each unit, facies, and property can be simulated using the methods, parameters, and sedimentological rules of user choice. These choices can be based on previous research, analysis of the data, or expert knowledge, as explained in the previous subsections. This flexibility allows for easy updates to the concept and facilitates the comparison of different concepts (i.e., different piles). Additionally, the utilization of stochastic methods allows for easy quantification of uncertainty at various levels (e.g., unit, subunit, facies, properties). These methods can generate a set of prior models for use in data assimilation (Emerick et al. 2013) or inversion methods (Delottier et al. 2023). ArchPy has been used in two different studies in a joint inversion scheme (Neven et al. 2022b, 2023). In these studies, Ensemble

Smoother with Multiple Data Assimilation (ESMDA) was used in combination with ArchPy unit and property models to integrate both geophysical and hydrogeological measurements. ESMDA has proved to be a very efficient algorithm for determining unit models and integrating different data in an inversion process at a reasonable computational cost.

However, the ArchPy approach presented in this thesis has some limitations. Specifically, the delineation of units is made using 2D explicit interpolation, which prevents the representation of important geological structures such as faults, folding, or intrusions. But it should be remembered that the subject of this thesis concerns Quaternary deposits, and geological features of this kind are rare in such formations. Moreover, it would not be too difficult to integrate more sophisticated surface interpolation methods, such as the implicit potential method (Calcagno et al. 2008). However, integrating inequality data with this method remains challenging. Although it is theoretically possible, automatically determining inequalities (and equalities) in boreholes from a given pile becomes much more difficult when faults or folds must be considered. For each borehole, it is necessary to determine the polarity of the stratigraphic layers, which is not impossible but adds to the difficulty. Finally, ArchPy is also in its infancy, and the number of modeling methods and automated routines integrated is still limited.

To summarize the workflow, the first step is to define the stratigraphic order of the units and establish an initial conceptual model. This includes defining the order of units and subunits, as well as the nature of surface contact (erosion or onlap). Tools such as the automatic pile (Chapter 4) can be useful for making automatic suggestions. If there is a significant shortage of stratigraphic logs in the data, the geostatistical learning approach (Chapter 6) can be helpful. It is then necessary to choose facies and facies methods (Chapters 2 and 7), which may be different for each unit and are mainly determined by modeling objectives and geological context. Once the overall conceptual model is established, the interpolation methods and associated parameters should be selected for each unit, facies, and property. These selections must consider the data, geological context, and expert knowledge. The information is then integrated and synthesized into a stratigraphic pile and integrated into ArchPy to produce the desired number of realizations (Chapters 3, 5, and 6).

8.1.6 Upper Aare geological model

In addition to its methodological contributions, this thesis offers practical applications of these methodologies through case studies conducted in the Upper Aare and Rhine Valleys. Notably, Chapter 6 presents a novel geological model developed for the Upper Aare Valley, which incorporates 13 distinct geological units and 6 facies, focusing primarily on hydraulic conductivity as a property of interest. Two models were devised, depending on the consideration of strati-

graphic logs obtained through machine learning techniques. These models offer valuable information on the shallow and deep geological formations within the Upper Aare Valley, providing a comprehensive understanding of the regional geology. The models suggest the existence of a deep aquifer, which was previously hypothesized. However, it is likely limited to the northern region of the area. The models also indicate minimal connectivity between the shallow and deep aquifers, which could be investigated further with a groundwater flow model.

Models can be improved, especially in the facies modeling step. It is important to consider and compare other approaches and methods. When creating a regional-scale model, it may not be necessary to provide extensive detail on facies methods as the flow is primarily controlled by large, extended structures such as stratigraphic units. However, if the goal is to propose local transport models, adjustments and refinements will likely be required.

8.2 Perspectives and future of geological modeling

The previous section presented an ideal geological modeling workflow. Each step can be adapted to suit the situation and the problems to be solved. Although this thesis has covered many aspects of geological modeling, there is still room for improvement and future research.

First, and perhaps most important, are the data. No matter how well the algorithms and methods are developed, and no matter how many elements and features are taken into account to produce the most robust and reliable models possible, if the data used are not properly prepared, the models will not be accurate. Therefore, significant effort is required to retrieve subsurface data, including geological, geotechnical, hydrogeological, and geophysical information. This data must be homogenized and standardized to align with the regional geological context. Finally, it should be centralized and made available to both private and public stakeholders who require access. Although this aspect of the work may not fall within the academic field, it is still crucial and should be carefully considered, taking into account the opinions and positions of various stakeholders, including the public, private, and academic sectors. For example, in the context of this thesis and the overall *Phenix* project, the data harmonization work carried out by the *Geoquat* project was essential. However, the available data could have been more extensive, but this was complicated by several challenges and issues. The complexity of Swiss federal legislation, which involves multiple levels of public authority (communes, cantons, and national), private companies, and offices, each with its own databases, made this task notably challenging. Additionally, legislation differs from one canton to another, posing a number of problems for water and subsurface management across borders. To solve partly some of these issues, it would be more logical to move toward more centralized and standardized data management.

Although adding to the workload, providing access to an up-to-date and complete database would benefit everyone. The advantages include more reliable geological studies, fewer geotechnical and geological incidents, and lower costs due to reduced data acquisition. This should be a top priority for subsurface management in the coming years.

The second aspect considers the improvement and development of the presented methodologies. The ArchPy approach presented in this thesis could be improved on this aspect in several ways. For instance, the hierarchy could be extended to integrate more levels. Similarly to what is done with units and subunits, multiple hierarchical facies levels can be considered (Bennett et al. 2019). However, this poses a number of problems in terms of data, particularly borehole data. It is indeed difficult to characterize several levels of facies hierarchies in boreholes, which complicates the generation of conditioned models. It may be possible to automatically identify facies hierarchical levels by analyzing lithological successions and having knowledge of the depositional environment. However, further research is required to better integrate this knowledge into hierarchical geological models. Furthermore, surface simulation is still limited (2D interpolation) and improved approaches such as implicit methods (Lajaunie et al. 1997; Calcagno et al. 2008; de la Varga et al. 2019) could be considered. In addition, many additional facies modeling methods could be added to ArchPy to reproduce different and more specific sedimentological settings.

Another important aspect to further develop is to strengthen the bonds and links with physical forward models such as groundwater (e.g., MODFLOW and flopy interface, Bakker et al. 2016; Langevin et al. 2017), geophysical or geotechnical models. This would simplify the modeling process and facilitate the creation of links and synergies. For example, inverse workflows can be set up, as demonstrated by Neven et al. (2022b, 2023). In the context of climate change, more pressure is put on the hydrological and economic world, and optimization strategies in hydro-economic models could be more easily addressed using integrated and open-source resources. Significant improvements can be made toward this path.

ArchPy is expected to undergo significant changes in the coming years due to its increasing use in various sedimentological environments and for different purposes. The goal is to create an integrated and comprehensive geological modeling toolbox that can be easily combined with other open-source packages and resources. The toolbox will include the latest and most up-to-date methods and algorithms, making them accessible to everyone.

Apart from ArchPy and geological modeling methods, this thesis has not investigated groundwater modeling and they merit further investigation. Specifically, the impact of geological model heterogeneity on flow and transport patterns has not been covered. It would be interesting to test the effect of sedimentary structures generated by EROSim and complex ArchPy models on trans-

port simulations. These results could then be compared with experiments on laboratory-scale analog models to assess their reliability.

Another point, which may seem anecdotal at first sight, is the choice or determination of a single deterministic "best" (or mean) model from a set of stochastic realizations. A practice that we refer to as realization aggregation. While it may seem preferable to use the stochastic realizations directly, it is common to use only one final deterministic model in the end. In Chapter 5, a subsection (see Section 5.4.2) briefly discussed an experiment involving four different methods tested on the Rhine Valley aquifer but this experiment was not comprehensive. A poor method of realization aggregation can lead to problems where certain criteria are no longer respected, such as the proportion of facies or their spatial correlation. Hence, it would be beneficial to test these methods in other contexts and with different objectives. For example, realizations could be aggregated to produce a model that best reflects hydrogeological measurements, such as groundwater heads or tracer concentrations. This will surely influence the determination of the "best" model and should be investigated.

Finally, perspectives on automation in geological modeling are discussed. This thesis proposed several improvements toward more automation in different steps of geological modeling. In particular, the flexible framework of ArchPy can be combined with joint inversion procedures to automatically integrate different types of data (Neven et al. 2023). Additionally, the preprocessing of the borehole data has been automated. However, it is important to note that there are limits to automation in geological modeling. For instance, parameterization of facies models remains challenging and requires manual effort to determine the facies to models, the size of the objects to place, and the rules to apply. Although analog model databases can partially automate this process, they are still rare and not always freely accessible. Therefore, exploring this avenue could improve the automation of geological models.

Automating conceptualization is a challenging task. However, it is worth considering whether complete automation is necessary for every task. Conceptualization involves integrating geological context and knowledge of geological processes with expert knowledge while considering available data and computational constraints. It is important to note that this process requires significant manual effort. The result is a concept that can be applied numerically within a reasonable time frame. Due to the complexity of the task, it is unlikely that the complete conceptualization of geological models will be fully automated soon. However, this should not be viewed as a disadvantage, but rather an opportunity for modelers and experts to collaborate and generate the best possible models.

Although this thesis has extensively talked about uncertainty and how to quantify it, there is at least one thing that is certain, geological modeling cannot be covered exhaustively in a single thesis. As a consequence, many other im-

portant topics were left out or only briefly discussed. However, in addition to the perspectives discussed above, this leaves the door open to a wide range of future ideas and research.

Specifically, the future of geological modeling lies in making it as accessible as possible, and this means considering a number of objectives for models and methods: **A**ccurate, **C**ollaborative, **C**omprehensive, **E**fficient, **S**calable, **S**uccessful, **I**nteroperable, **B**rowsable, **L**ightweight, **E**mbeddable. Models and methods need to be more accurate and successful to improve the reliability and quality of predictions. They need to be collaborative so that techniques and knowledge can be shared with as many people as possible. It is also important not to forget to make them comprehensive so that they can be more easily grasped by as many people as possible. Efficient and scalable models are necessary to be able to generalize them and apply them to a large variety of geological contexts while coupling them with other models and approaches. Interoperability and embeddability are perhaps the most central items on this list, as they require approaches to be built with the aim of combining and synergizing them. Taking advantage of some methods to fill in the gaps of others. Finally, accessibility also means methods that are available and easily obtainable (browsable), and that they are simple to use (lightweight). Open-source solutions, good code practices, and documentation are essential to achieving these goals. With these objectives in mind, it is more than certain that geological modeling will continue to progress in the right direction. This thesis followed this philosophy by proposing several open-source modeling algorithms and approaches for modeling Quaternary formations. However, the amount of work is still very large, and many more years and decades of further research will be needed to reach its culmination.

Appendix A

Appendix

A.1 Chapter 3

Table A.1: *Grouped USCS codes. It indicates in which group code the classical USCS groups are rearranged.*

Grouped Code	USCS classical groups
O	(OH, OL, Pt)
G	(G, G-GM, GW-GM, GP-GM, GP, GW, GP-GC, G-GC)
S	(S-SM, S, SP-SM, SP, SW, S-SC, SP-SC, SW-SM)
GC	(GM, GC, GC-GM)
SC	(SM, SC, SC-SM)
C	(ML, CL-ML, CL, CM, CH)

Table A.2: *Covariance models parameters (C: contribution and r: ranges in x, y and z direction) manually adjusted and used for the SIS of each units. For units where the number of data points was too low (LGL and LGT), a default model was taken ("Default" row). The ranges are given in the three main axis directions without any rotation (x axis goes toward E, y axis toward N). Subscripts exp and sph indicate exponential and spherical covariance models.*

Unit (Litho-facies)	r_{sph} [m]	C_{sph} [m^2]	r_{exp} [m]	C_{exp} [m^2]	nugget [m^2]
SUP (O)	(200, 400, 5)	0.15	-	-	0.1
SUP (C)	(200, 200, 5)	0.11	-	-	0
SUP (G)	(200, 200, 5)	0.25	-	-	0
SUP (GC)	(300, 100, 4)	0.20	-	-	0
YG (G)	-	-	(50, 50, 15)	0.22	0
YG (GC)	(200, 200, 1)	0.06	(300, 200, 6)	0.09	0
YG (S)	(200, 200, 15)	0.03	(200, 200, 1)	0.03	0
LGA (G)	(100, 200, 8)	0.12	(100, 200, 20)	0.12	0
LGA (GC)	(100, 150, 15)	0.10	(100, 150, 15)	0.11	0
LGA (S)	(50, 100, 15)	0.13	-	-	0.01
Default	(100, 100, 10)	variable*	-	-	0

* variance was adjusted according to lithofacies proportions.

Table A.3: *Covariance models parameters (C : contribution and r : ranges in x, y and z direction) used for the property simulations. Subscript exp indicates an exponential covariance model.*

Lithofacies	r_{exp} [m]	C_{exp} [m^2]
O	(50, 50, 2)	0.1
G	(50, 50, 2)	0.25
S	(50, 50, 2)	0.16
GC	(50, 50, 2)	0.2
SC	(50, 50, 2)	0.2
C	(50, 50, 2)	0.2

A.2 Chapter 5

A.2.1 Modeling parameters

Covariance models

The table A.5 show the covariance models used for the generation of the top surfaces of the units. The others units

Table A.4: *Covariance models parameters (C: contribution (i.e. sill) and r: range) used for the surfaces interpolation of each top surface of the units. All models are isotropic. Subscripts exp, sph and cub indicates exponential, spherical and cubic models which are different family of covariances models.*

Units	r_{cub} [m]	C_{cub} [m^2]	r_{sph} [m]	C_{sph} [m^2]	r_{exp} [m]	C_{exp} [m^2]
UEBE	38500	245	-	-	-	-
UNIT B	31933	296	92586	34	-	-
DELT	21718	74	-	-	34	20
LAKU	35737	382	-	-	559	290
MORA	-	-	-	-	3000	200
other units	-	-	7500	200	-	-

MPS parameters

The table A.5 shows the MPS parameters used to fill the unit B.

Table A.5: *Used MPS parameters to simulate FLUV, BAC and VERL units in Unit B. Some parameters required to be defined for all the variables (the two auxiliary variables and the variable of interest (facies code)). This is the case for the number of neihboring nodes or the dsitance threshold.*

MPS parameters	values
Homothety Usage	1
Homothety XRatio	1
Homothety YRatio	1
Homothety ZRatio	0.3
Nneighboring Node	(1, 1, 15)
Distance Threshold	(0.1, 0.1, 0.05)
Max Scan Fraction	0.05

A.3 Chapter 6

ML models hyperparameters

Table A.6: *Machine learning hyperparameters chosen for each algorithm. RF: Random Forest, SVC: Supper Vector Machines, MLP: Multilayer Perceptron, Adaboost: Adaptive boosting, Gboost: Gradient boosting.*

ML algorithm	Hyperparameter	value
RF	mean depth	15
	mean features	45
	n estimators	164
SVC	γ	0.014
	C	6.32
MLP	Learning rate	0.084
	Layers	(277, 17, 264, 160)
Adaboost	n estimators	414
	learning rate	0.001
Gboost	n estimators	266
	learning rate	0.0186
	max depth	24
	max features	26

Geological model parameters

The Table A.7 gives the variogram parameters for the interpolation of the top surface of each unit. Direction of the ranges of the covariances models change spatially according to the rotation map (Fig. A.1) that indicates for each location the rotation of the range axis of the covariances.

The table A.9 shows the SIS variogram parameters for each facies in each unit. For AM, UBS, OS and AS units, variogram models were taken from other units as the number of points were not sufficient to estimate a variogram. AM considered the same variograms as for LGM, UBS those from MS, OS from LGM, AS from LGM and SUP. Contribution of the variograms were rescaled according to the relative proportions of the facies in the unit.

Table A.7: *Covariance models parameters (C: contribution and r: range in relative x and y direction) used for the surfaces interpolation of each surface. Ranges are expressed using two numbers. No covariance model was fitted for SUP as its surface is defined by the DEM. Subscripts exp, cub and nug indicates exponential, cubical and nugget covariance models.*

Units	r_{cub} [m]	C_{cub} [m^2]	r_{exp} [m]	C_{exp} [m^2]	C_{nug} [m^2]
HB	-	-	(5000, 5000)	150	-
YG	(8000, 8000)	100	-	-	3
LGA	(6100, 6100)	160	-	-	10
LGL	-	-	(5000, 5000)	135	-
LGM	-	-	(2000, 5000)	800	-
MS	-	-	(2000, 5000)	1000	-
IGT	-	-	(2000, 5000)	200	-
AM	-	-	(2000, 5000)	1000	-
GL	-	-	(2000, 5000)	200	-
UBS	-	-	(2000, 5000)	150	-
OS	-	-	(2000, 5000)	150	-
AS	-	-	(2000, 5000)	300	-

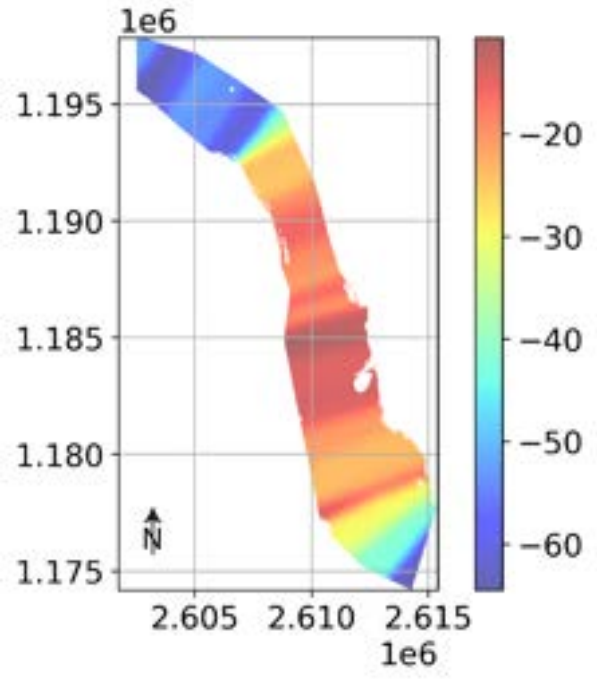

Figure A.1: *Rotation map used for the orientation of the anisotropic variograms*

Table A.8: *Covariance models parameters (C : contribution and r : ranges in x, y and z direction) used for the property simulations. Subscript exp indicates an exponential covariance model.*

Lithofacies	r_{exp} [m]	C_{exp} [m^2]	mean [$\log[\frac{m}{s}]$]
O	(50, 50, 2)	0.1	-5
G	(50, 50, 2)	0.25	-2
S	(50, 50, 2)	0.16	-3.5
GC	(50, 50, 2)	0.2	-6
SC	(50, 50, 2)	0.2	-5.5
C	(50, 50, 2)	0.2	-8

Table A.9: *Covariance models parameters (C: contribution and r: ranges in x, y and z direction) used for the SIS of each units. The ranges are given in the relative directions according to the main directions (x towards E and y towards N). The relative x and y directions are locally obtained by applying the rotation map (see Fig. A.1). No other rotations were considered which means that only x and y axis rotate and the z axis is always directed upwards. Subscripts exp and sph indicate exponential and spherical covariance models.*

Unit (Litho-facies)	r_{exp} [m]	C_{exp} [m^2]
SUP (O)	(200, 400, 5)	0.15
SUP (C)	(200, 200, 5)	0.11
SUP (G)	(200, 200, 5)	0.25
SUP (GC)	(300, 100, 4)	0.20
HB (GC)	(400, 400, 10)	0.25
HB (C)	(200, 200, 10)	0.16
HB (G)	(200, 200, 10)	0.20
YG (G)	(100, 200, 12)	0.23
YG (GC)	(100, 300, 15)	0.20
YG (S)	(100, 300, 6)	0.08
LGA (G)	(100, 200, 10)	0.25
LGA (GC)	(100, 300, 15)	0.20
LGA (S)	(100, 300, 6)	0.08
LGL (C)	(150, 300, 10)	0.18
LGL (S)	(100, 200, 10)	0.15
LGL (SC)	(200, 300, 20)	0.06
LGM (GC)	(150, 300, 20)	0.24
LGM (C)	(300, 500, 15)	0.15
LGM (SC)	(300, 500, 10)	0.10
LGM (S)	(300, 500, 10)	0.13
LGM (G)	(400, 400, 15)	0.13
MS (G)	(200, 200, 10)	0.25
MS (GC)	(100, 200, 15)	0.14
MS (C)	(400, 600, 20)	0.10
MS (S)	(400, 600, 20)	0.09
MS (SC)	(250, 250, 15)	0.06
GL (G)	(150, 300, 25)	0.25
GL (C)	(150, 300, 10)	0.13
GL (S)	(150, 300, 20)	0.16
GL (GC)	(150, 300, 25)	0.15

Borehole simulations

We show here few more examples of borehole simulations with the methodology of the present study. All simulations where realized with a threshold of 0.15 ($\tau = 0.15$) if possible, if not it was decreased until simulations could be obtained. For some boreholes and algorithms (Figures A.3, A.5), There are situations where it was impossible to generate a simulation. For corresponding colors for unit and facies, see Figure 6.4.

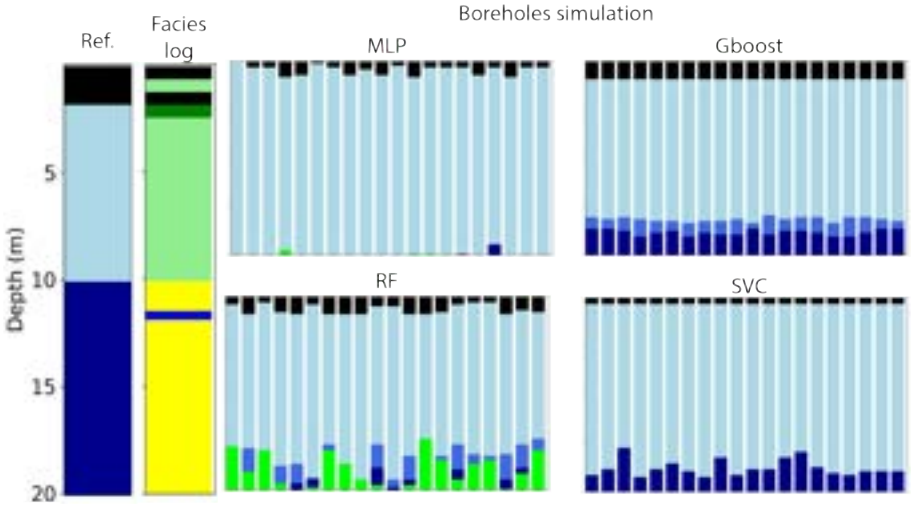

Figure A.2

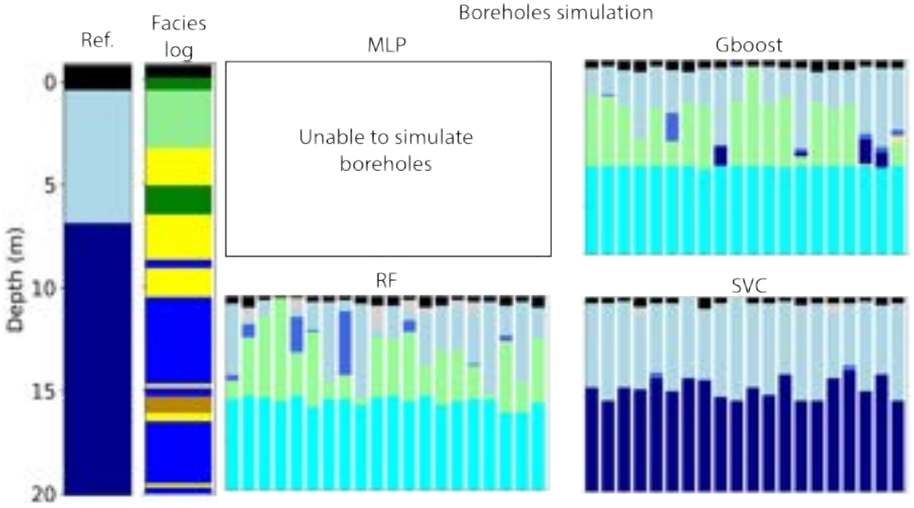

Figure A.3

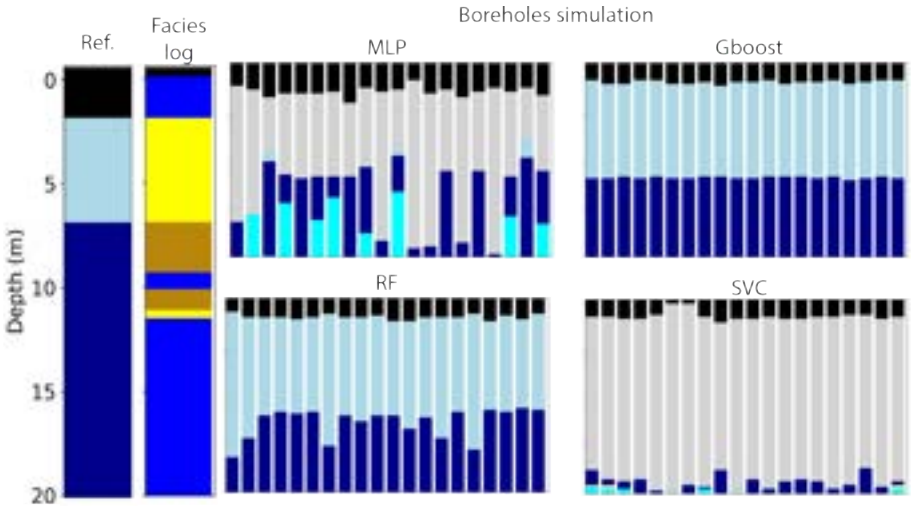

Figure A.4

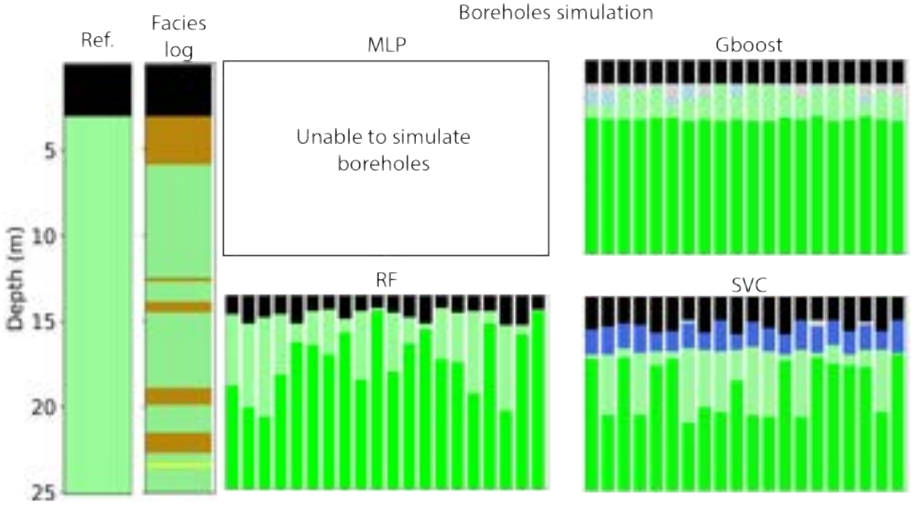

Figure A.5

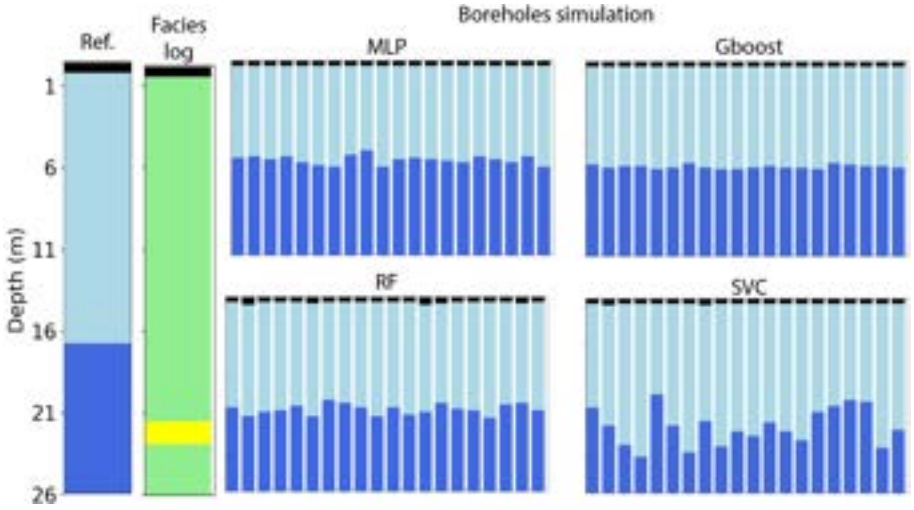

Figure A.6

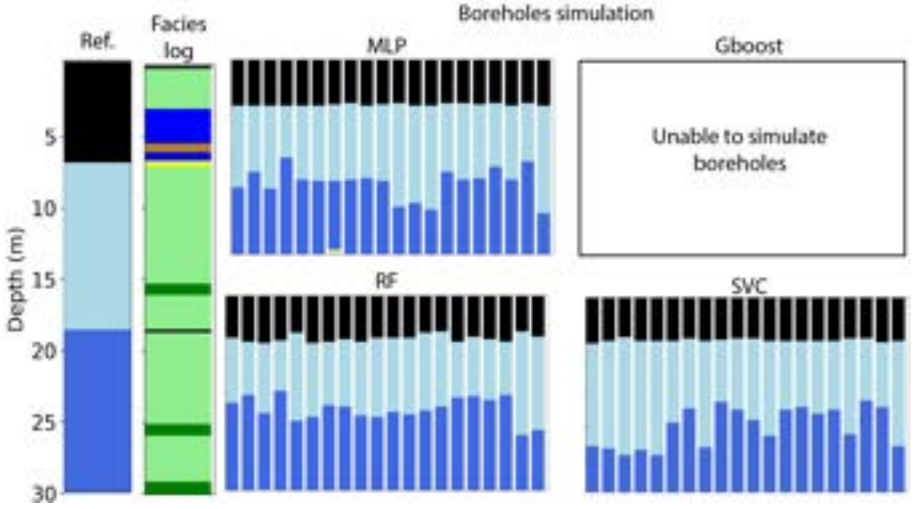

Figure A.7

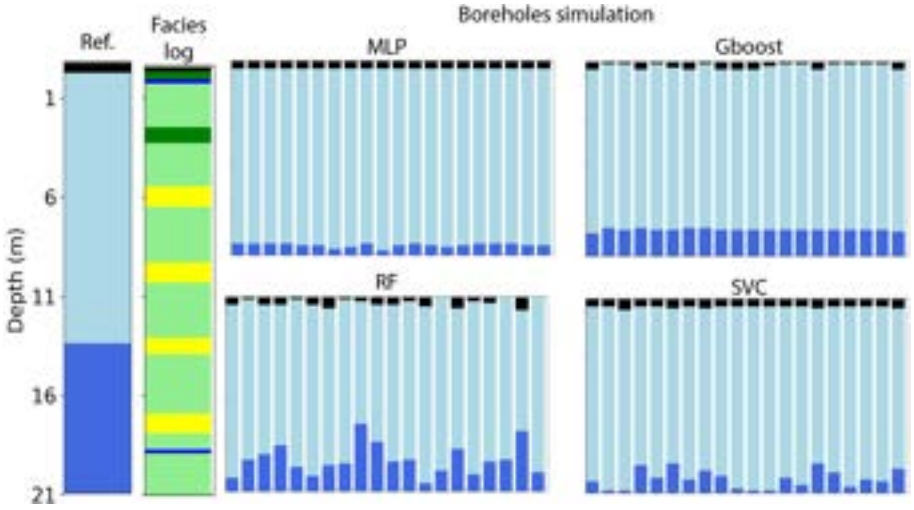
Boreholes simulation
Ref.
Facies log
MLP
Gboost
RF
SVC
Depth (m)
1
6
11
16
21

Figure A.8

Geological models

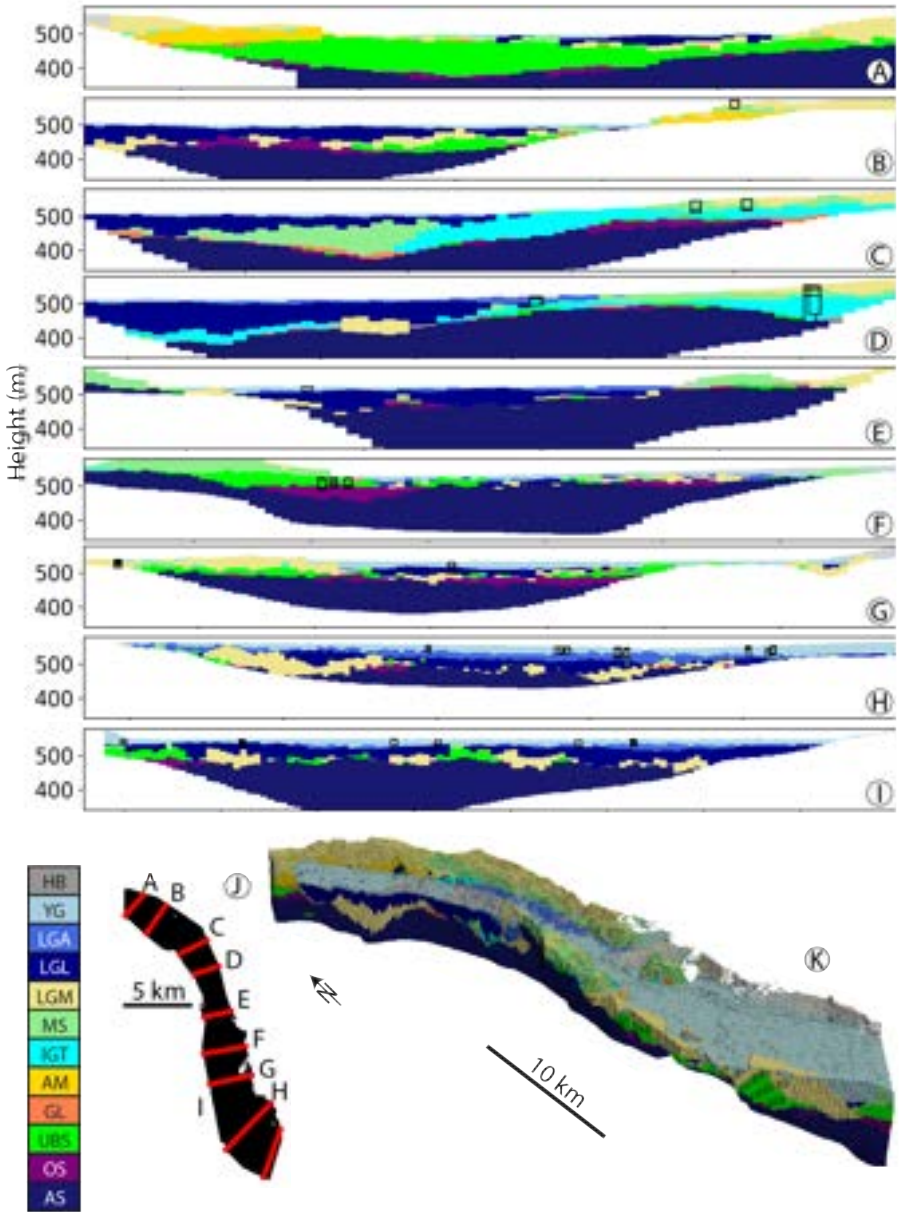

Figure A.9: ***A*-*I***: *transversal cross-sections in one realization of the ArchPy-BAS unit model. Corresponding locations are shown in* ***J***. ***K***: *3D visualisation of the realization. Corresponding color for units are given in Figure 6.4.*

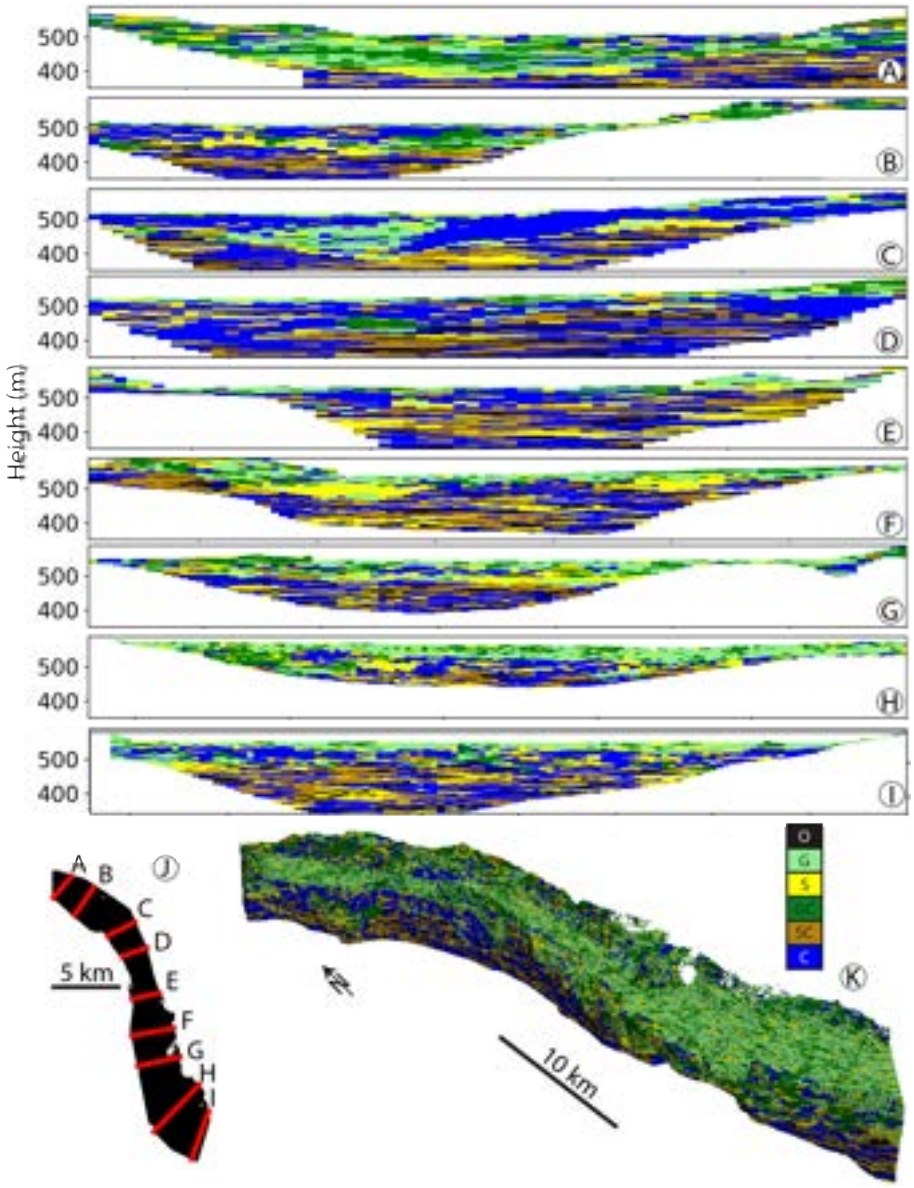

Figure A.10: ***A*-*I***: *transversal cross-sections in one realization of the ArchPy-BAS facies model. Corresponding locations are shown in* ***J***. ***K***: *3D visualisation of the realization. Corresponding color for facies are given in Figure 6.4.*

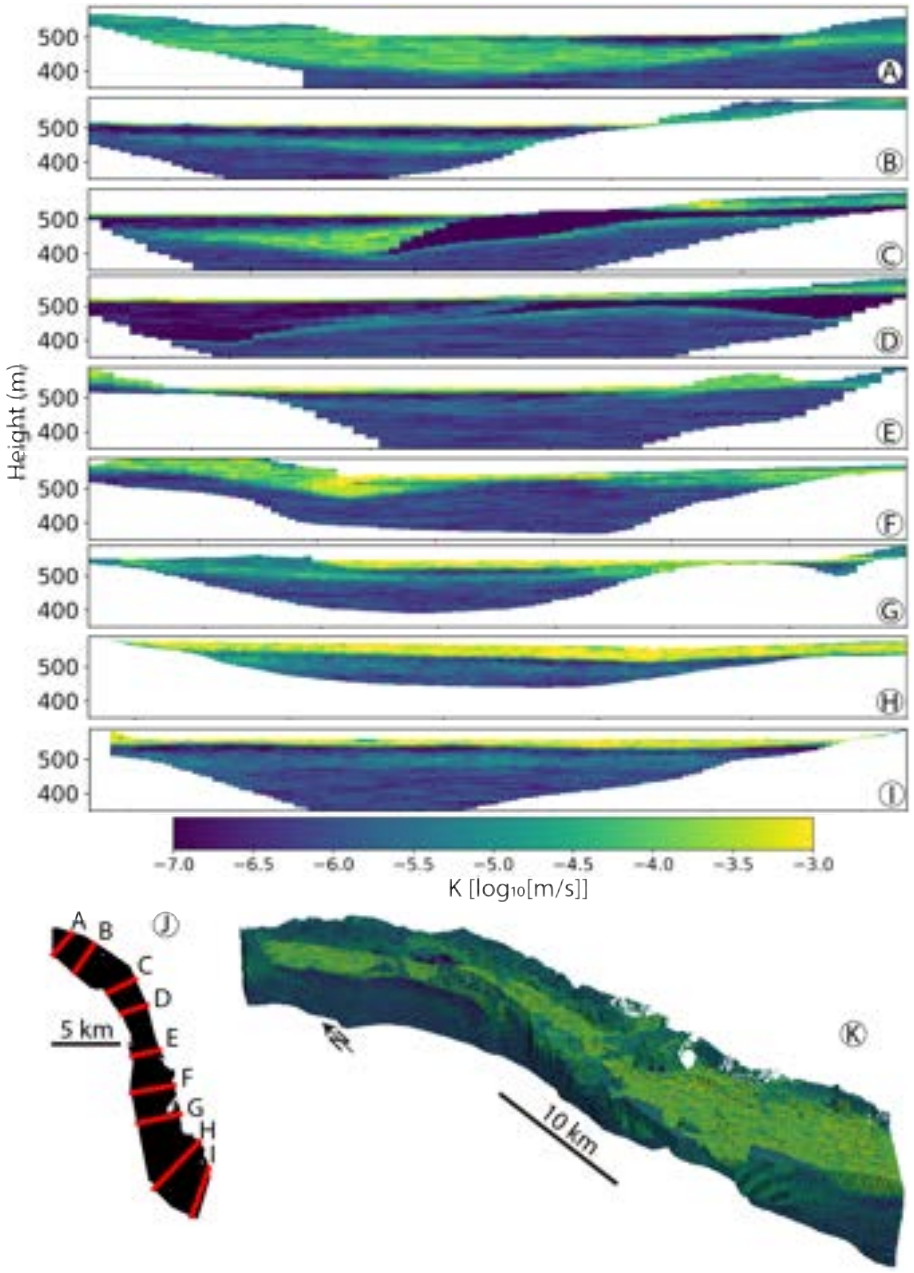

Figure A.11: ***A*-*I***: *transversal cross-sections in mean of all property realization of ArchPy-BAS. Corresponding locations are shown in* ***J***. ***K***: *3D visualisation of the realization.*

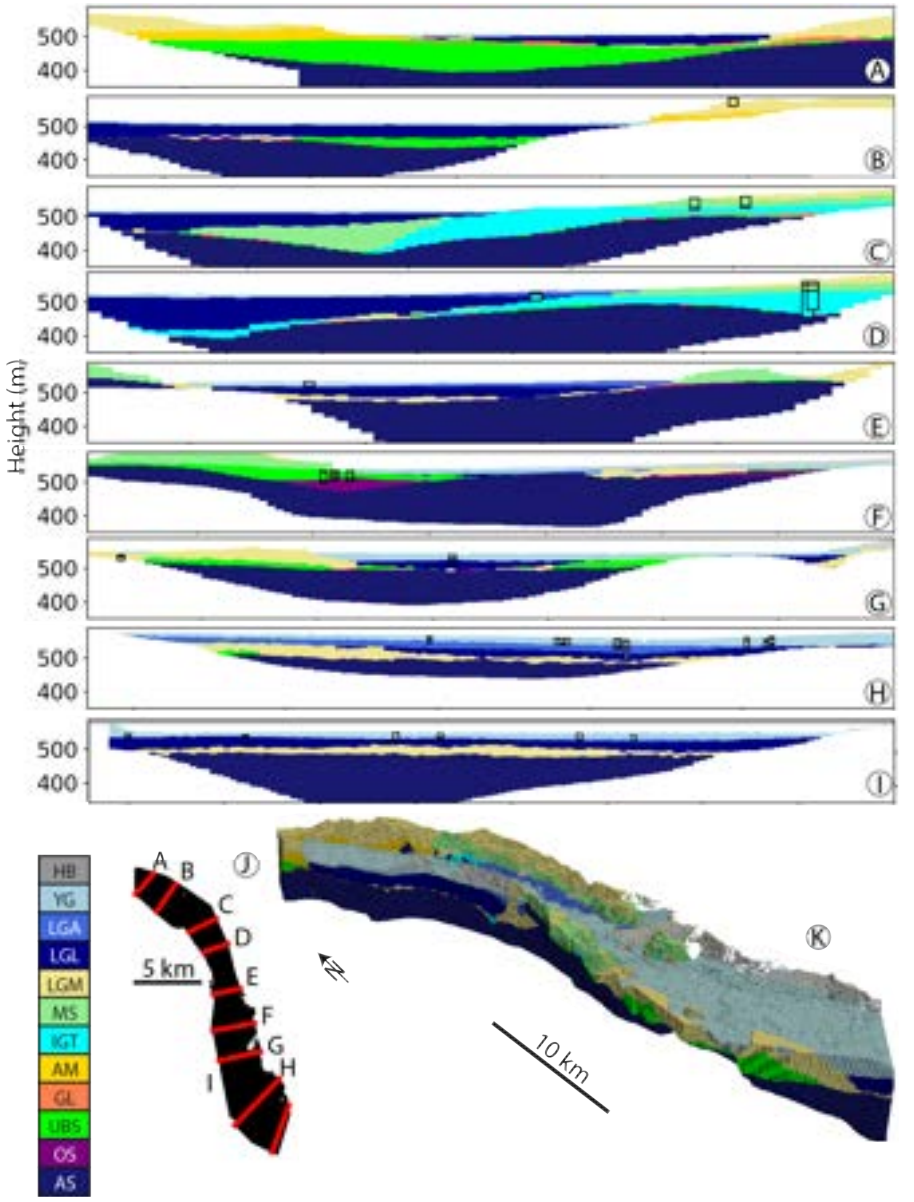

Figure A.12: ***A*-*I***: *transversal cross-sections in mean of all unit realizations of ArchPy-BAS. Corresponding locations are shown in* ***J***. ***K***: *3D visualisation of the realization.*

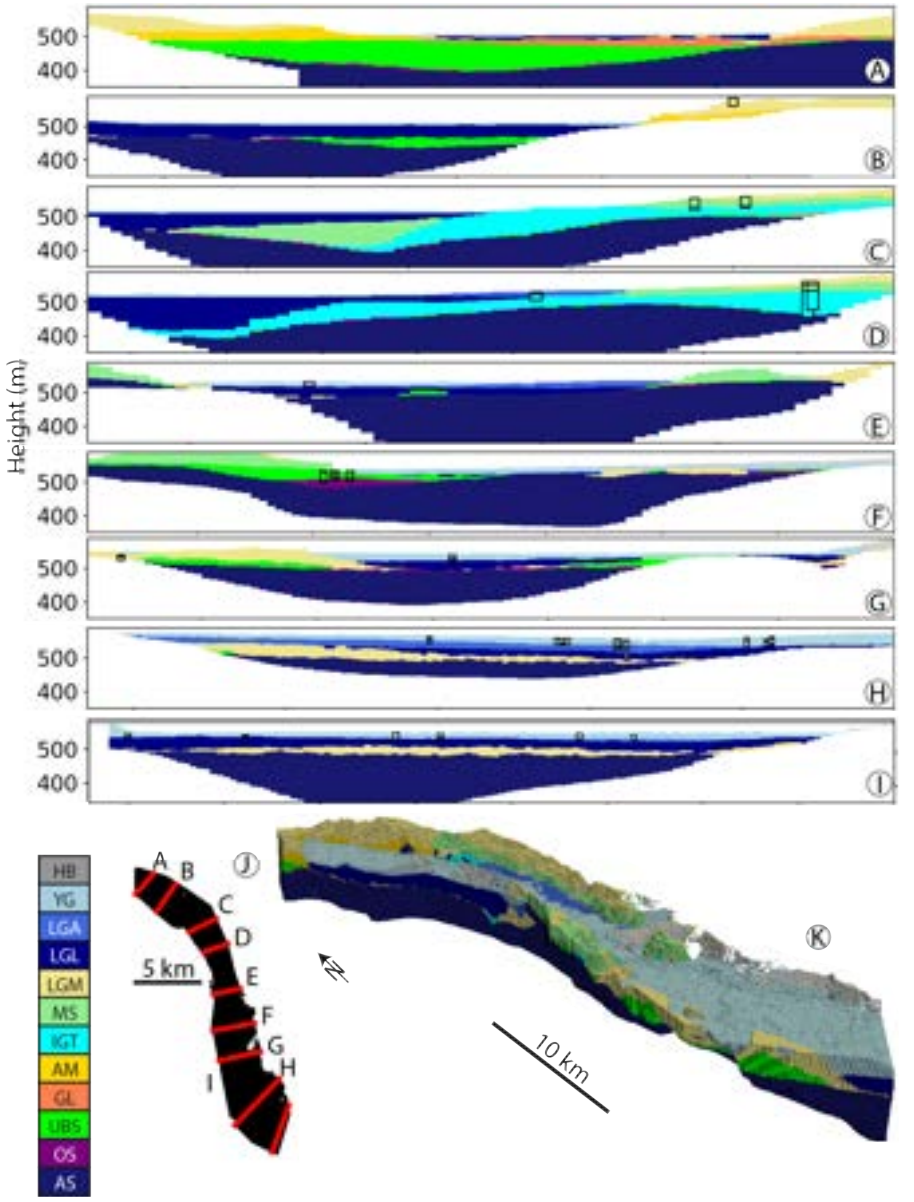

Figure A.13: ***A*-*I***: *transversal cross-sections in mean of all unit realizations of ArchPy-ML. Corresponding locations are shown in* ***J***. ***K***: *3D visualisation of the realization.*

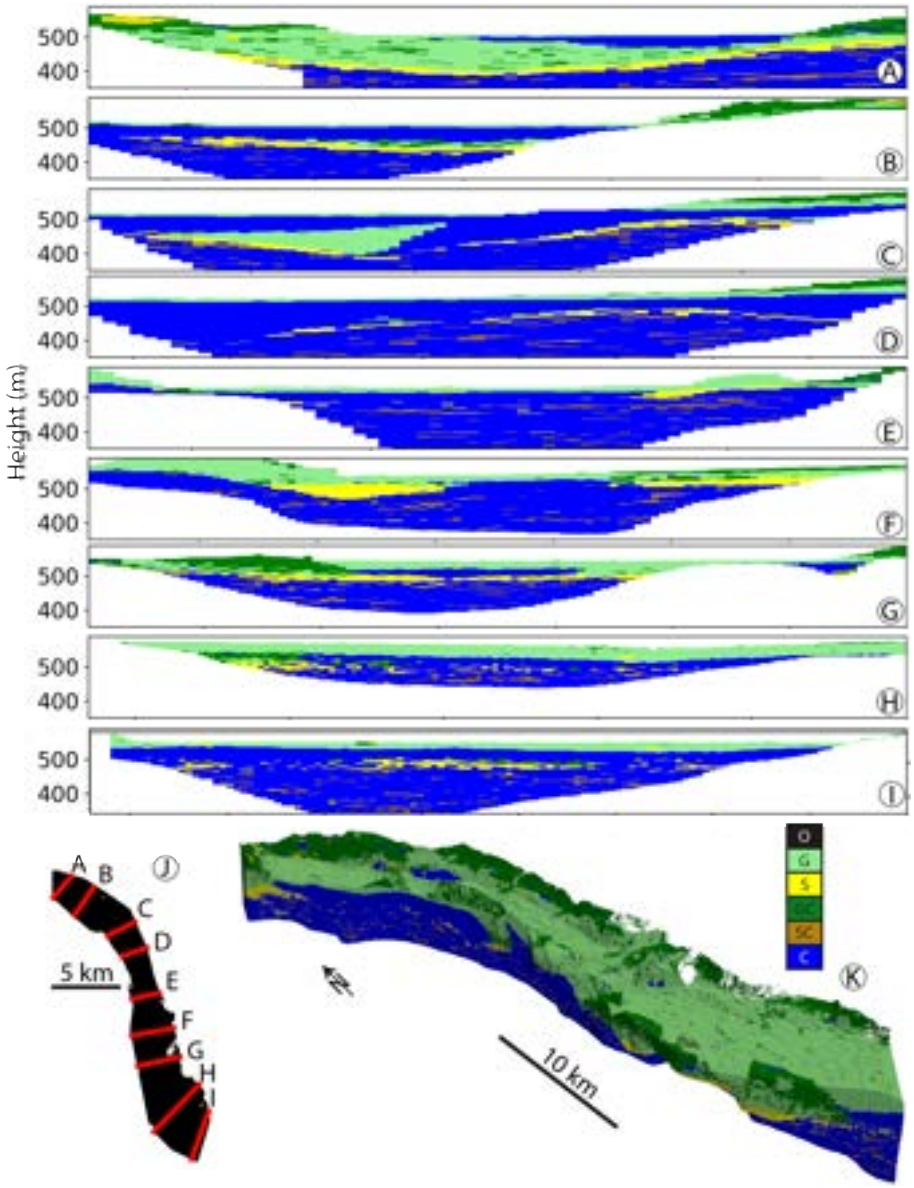

Figure A.14: ***A-I****: transversal cross-sections in mean facies model (most probable facies according to all facies realizations) of ArchPy-BAS. Corresponding locations are shown in* ***J****.* ***K****: 3D visualisation of the realization.*

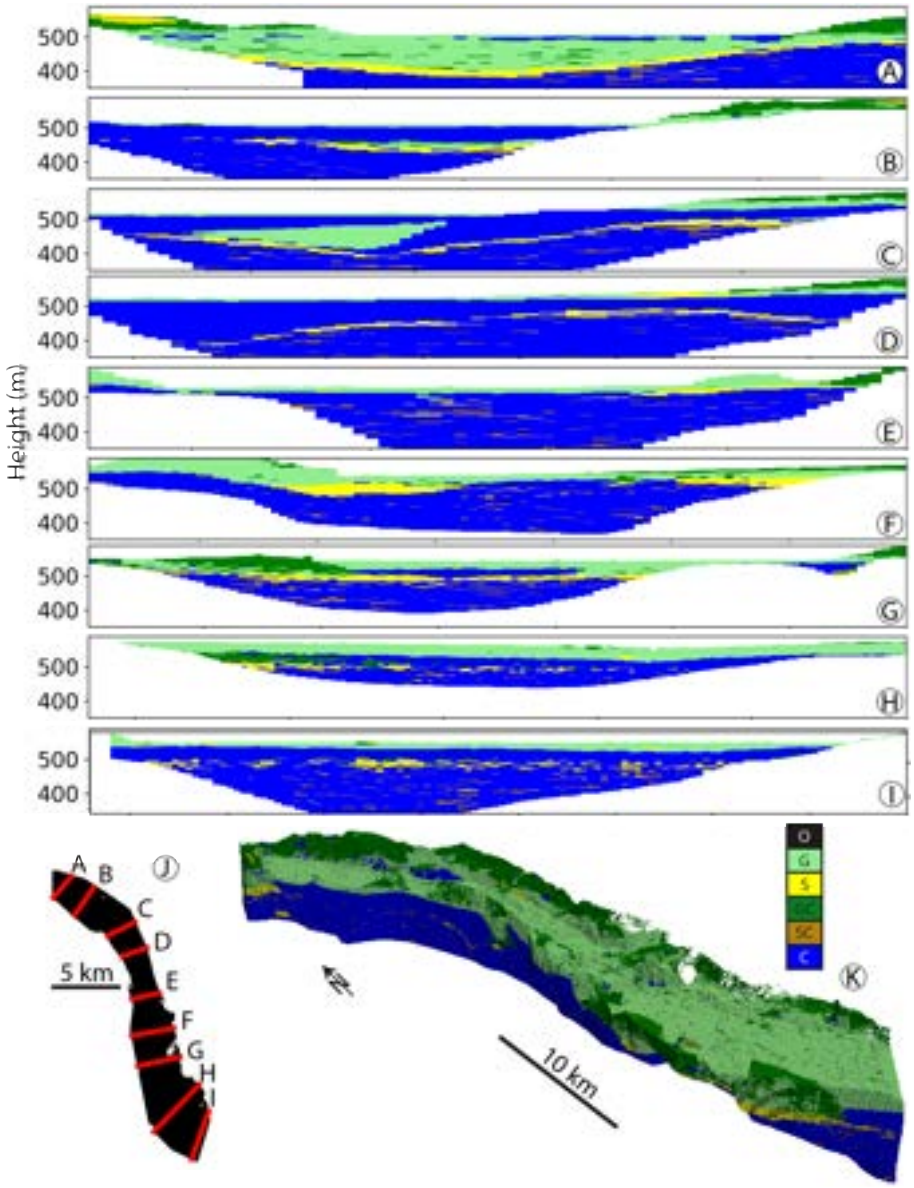

Figure A.15: ***A-I****: transversal cross-sections in mean facies model (most probable facies according to all facies realizations) of ArchPy-ML. Corresponding locations are shown in* ***J****.* ***K****: 3D visualisation of the realization.*

A.4 Chapter 7

Simulation parameters

Table A.10: *Covariance models parameters (C: contribution (sill) and r: range). Subscripts cub1 and cub2 indicate two different cubic covariance models. Contributions that were lower than 0.01 were discarded.*

Quarry wall	Rank surfaces	r_{cub1} [m]	C_{cub1} [m^2]	r_{cub2} [m]	C_{cub2} [m^2]
NS	3 in unit 5	-	-	32	0.35
	3 in unit 4	15	0.27	30	0.39
	3 in unit 3	-	-	25	0.64
	3 in unit 2	-	-	35	1.06
	3 in unit 1	28	0.41	23	0.38
	4	-	-	90	0.26
	5	68	0.65	30	0.1
EW	3 in unit 5	-	-	44	0.44
	3 in unit 4	-	-	29	0.77
	3 in unit 3	-	-	35	0.55
	3 in unit 2	-	-	60	1.35
	3 in unit 1	70	0.51	45	0.29
	4	-	-	90	0.25
	5	25	0.12	60	0.15

Table A.11: *List of high-order surfaces with their rank and mean altitude used for the simulations.*

Quarry wall	Surface ID	Rank	Mean altitude [m]	Bottom of ...	Top of ...
NS	1	4	13.68	unit 5	unit 4
	2	4	10.99	unit 4	unit 3
	3	5	7.22	unit 3	unit 2
	4	4	4.43	unit 2	unit 1
EW	1	4	10.59	unit 5	unit 4
	2	4	8.23	unit 4	unit 3
	3	5	5.75	unit 3	unit 2
	4	4	3.90	unit 2	unit 1

Table A.12: *EROSim parameters used for the simulation of the quarry walls.*

Quarry wall	Unit group	α	N	ξ	p_{global} (blue, brown, green, yellow)
NS	unit 1	0.8	10	0.2	(0.5, 0, 0.1, 0.4)
	unit 2	0.8	15	0.2	(0.32, 0, 0.31, 0.37)
	unit 3	0.5	10	0.2	(0.20, 0, 0.35, 0.45)
	unit 4	0.9	20	0.2	(0, 0, 0.50, 0.50)
	unit 5	0.9	3	0.2	(0, 0, 0, 1)
EW	unit 1	1	20	0.2	(0.10, 0.15, 0.10, 0.70)
	unit 2	1	15	0.2	(0.08, 0, 0.12, 0.8)
	unit 3	1	10	0.2	(0.05, 0, 0.22, 0.73)
	unit 4	0.9	10	0.2	(0, 0.10, 0.50, 0.40)
	unit 5	0.9	3	0.2	(0, 0, 0.10, 0.90)

Bibliography

Aarnes, Ingrid, Helena van der Vegt, Ragnar Hauge, Bjørn Fjellvoll, and Kjetil Nordahl (2019). "Utilizing sedimentary process-based models as training images for multipoint facies simulations". In: *Bulletin of Canadian Petroleum Geology* 67.4, pp. 217–230. DOI: 10.35767/gscpgbull.67.4.217.

Abdellatif, Alhasan, Ahmed H Elsheikh, Daniel Busby, and Philippe Berthet (2022). "Generation of non-stationary stochastic fields using Generative Adversarial Networks". In: *arXiv preprint arXiv:2205.05469*. DOI: 10.48550/arXiv.2205.05469.

Aigner, T, U Asprion, J Hornung, W-D Junghans, and R Kostrewa (1996). "Integrated outcrop analogue studies for Triassic alluvial reservoirs: examples from southern Germany". In: *Journal of Petroleum Geology* 19.4, pp. 393–406.

Alabert, FG (1989). "Constraining description of randomly heterogeneous reservoirs to pressure test data: a Monte Carlo study". In: *SPE Annual Technical Conference and Exhibition*. SPE, SPE–19600. DOI: 10.2118/19600-MS.

Alabert, FG and GJ Massonnat (1990). "Heterogeneity in a complex turbiditic reservoir: stochastic modelling of facies and petrophysical variability". In: *SPE Annual Technical Conference and Exhibition*. SPE, SPE–20604. DOI: 10.2118/20604-MS.

Aliouane, Leila, Sid-Ali Ouadfeul, Noureddine Djarfour, and Amar Boudella (2013). "Lithofacies prediction from well logs data using different neural network models". In: *Special Session on Pattern Recognition in Geosciences: Theory and Applications*. Vol. 2. SCITEPRESS, pp. 702–706. DOI: 10.5220/0004380707020706.

Allaire, Grégoire, François Jouve, and Anca-Maria Toader (2002). "A level-set method for shape optimization". In: *Comptes rendus. Mathématique* 334.12, pp. 1125–1130. DOI: 10.1016/S1631-073X(02)02412-3.

Allard, D, D D'Or, and R Froidevaux (2011). "An efficient maximum entropy approach for categorical variable prediction". In: *European Journal of Soil Science* 62.3, pp. 381–393. DOI: 10.1111/j.1365-2389.2011.01362.x.

Allard, D, D D'Or, P Biver, and R Froidevaux (2012a). "Non-parametric diagrams for plurigaussian simulations of lithologies". In: *9th international geostatistical congress, Oslo, Norway*. Vol. 1115.

Allard, Denis, Alessandro Comunian, and Philippe Renard (2012b). "Probability aggregation methods in geoscience". In: *Mathematical Geosciences* 44, pp. 545–581. DOI: 10.1007/s11004-012-9396-3.

Allard, Denis, Paolo Fabbri, and Carlo Gaetan (2021). "Modeling and simulating depositional sequences using latent Gaussian random fields". In: *Mathematical Geosciences* 53, pp. 469–497. DOI: 10.1007/s11004-020-09875-0.

Allen, JRL (1978). "Studies in fluviatile sedimentation: an exploratory quantitative model for the architecture of avulsion-controlled alluvial suites". In: *Sedimentary Geology* 21.2, pp. 129–147. DOI: 10.1016/0037-0738(78)90002-7.

Alpak, Faruk O and Guangri Xue (2022). "Effects of fine-scale turbidite lobe stratigraphic architecture on dynamic reservoir performance". In: *Marine and Petroleum Geology* 139, p. 105540. DOI: 10.1016/j.marpetgeo.2022.105540.

Anderson, Mary P (1989). "Hydrogeologic facies models to delineate large-scale spatial trends in glacial and glaciofluvial sediments". In: *Geological Society of America Bulletin* 101.4, pp. 501–511. DOI: 10.1130/0016-7606(1989)101<0501:HFMTDL>2.3.CO;2.

Anderson, Mary P, JS Aiken, EK Webb, and DM Mickelson (1999). "Sedimentology and hydrogeology of two braided stream deposits". In: *Sedimentary Geology* 129.3-4, pp. 187–199. DOI: 10.1016/S0037-0738(99)00015-9.

Anderson, Mary P, William W Woessner, and Randall J Hunt (2015). *Applied groundwater modeling: simulation of flow and advective transport*. Academic press. DOI: 10.1016/C2009-0-21563-7.

Armstrong, Margaret, Alain Galli, Hélène Beucher, Gaelle Loc'h, Didier Renard, Brigitte Doligez, Rémi Eschard, and Francois Geffroy (2011). *Plurigaussian simulations in geosciences*. Springer Science & Business Media. DOI: 10.1007/978-3-642-19607-2.

Astrakova, Alina and Dean S Oliver (2015). "Conditioning truncated pluri-Gaussian models to facies observations in ensemble-Kalman-based data assimilation". In: *Mathematical Geosciences* 47, pp. 345–367. DOI: 10.1007/s11004-014-9532-3.

Babak, Olena (2014). "Inverse distance interpolation for facies modeling". In: *Stochastic environmental research and risk assessment* 28, pp. 1373–1382. DOI: 10.1007/s00477-013-0833-8.

Bakker, Mark, V.+ Post, Christian D Langevin, Joseph D Hughes, Jeremy T White, JJ Starn, and Michael N Fienen (2016). "Scripting MODFLOW model development using Python and FloPy". In: *Groundwater* 54.5, pp. 733–739.

Bastante, FG, C Ordóñez, J Taboada, and JM Matías (2008). "Comparison of indicator kriging, conditional indicator simulation and multiple-point statistics used to model slate deposits". In: *Engineering Geology* 98.1-2, pp. 50–59. DOI: 10.1016/j.enggeo.2008.01.006.

Bayer, P, P Huggenberger, Philippe Renard, and Alessandro Comunian (2011). "Three-dimensional high resolution fluvio-glacial aquifer analog: Part 1: Field study". In: *Journal of Hydrology* 405.1-2, pp. 1–9. DOI: 10.1016/j.jhydrol.2011.03.038.

Begg, SH and PR King (1985). "Modelling the effects of shales on reservoir performance: calculation of effective vertical permeability". In: *SPE Reservoir Simulation Conference*. SPE, SPE–13529. DOI: 10.2118/13529-MS.

Bennett, Jeremy P, Claus P Haslauer, and Olaf A Cirpka (2017). "The impact of sedimentary anisotropy on solute mixing in stacked scour-pool structures". In: *Water Resources Research* 53.4, pp. 2813–2832. DOI: 10.1002/2016WR019665.

Bennett, Jeremy P, Claus P Haslauer, Martin Ross, and Olaf A Cirpka (2019). "An open, object-based framework for generating anisotropy in sedimentary subsurface models". In: *Groundwater* 57.3, pp. 420–429. DOI: 10.1111/gwat.12803.

Benoit, Nicolas, Denis Marcotte, Alexandre Boucher, Dimitri D'Or, Andy Bajc, and Hassan Rezaee (2018). "Directional hydrostratigraphic units simulation using MCP algorithm". In: *Stochastic Environmental Research and Risk Assessment* 32, pp. 1435–1455. DOI: 10.1007/s00477-017-1506-9.

Bertoncello, Antoine, Tao Sun, Hongmei Li, Gregoire Mariethoz, and Jef Caers (2013). "Conditioning surface-based geological models to well and thickness data". In: *Mathematical Geosciences* 45, pp. 873–893. DOI: 10.1007/s11004-013-9455-4.

Beucher, Hélène and Didier Renard (2016). "Truncated Gaussian and derived methods". In: *Comptes Rendus Geoscience* 348.7, pp. 510–519. DOI: 10.1016/j.crte.2015.10.004.

Bhavsar, Ferdinand, Nicolas Desassis, Fabien Ors, and Thomas Romary (2023). "A principled deep learning approach for geological facies generation". In: *arXiv preprint arXiv:2305.13318*. DOI: 10.48550/arXiv.2305.13318.

Bianchi, Marco, Timothy Kearsey, and Andrew Kingdon (2015). "Integrating deterministic lithostratigraphic models in stochastic realizations of subsurface heterogeneity. Impact on predictions of lithology, hydraulic heads and groundwater fluxes". In: *Journal of Hydrology* 531, pp. 557–573. DOI: 10.1016/j.jhydrol.2015.10.072.

Biegler, Lorenz, George Biros, Omar Ghattas, Matthias Heinkenschloss, David Keyes, Bani Mallick, Luis Tenorio, Bart van Bloemen Waanders, Karen Willcox, and Youssef Marzouk (June 2011). *Large-Scale Inverse Problems and Quantification of Uncertainty*. John Wiley & Sons. ISBN: 978-1-119-95758-4.

Biver, PYA, D Allard, F Pivot, and P Ruelland (2015). "Recent advances for facies modelling in pluri-Gaussian formalism". In: *Petroleum Geostatistics 2015*, cp–456. DOI: 10.3997/2214-4609.201413615.

Bogaert, Patrick (2002). "Spatial prediction of categorical variables: the Bayesian maximum entropy approach". In: *Stochastic Environmental Research and Risk Assessment* 16.6, pp. 425–448. DOI: 10.1007/s00477-002-0114-4.

Boggs, Sam et al. (2012). *Principles of sedimentology and stratigraphy*. Fourth. Biblioteca Hernán Malo González. ISBN: 0131547283.

Boisvert, Jeff B and Michael J Pyrcz (2014). "Conditioning 3D object based models to a large number of wells: a channel example". In: *Mathematics of Planet Earth: Proceedings of the 15th Annual Conference of the International Association for Mathematical Geosciences*. Springer, pp. 575–579. DOI: 10.1007/978-3-642-32408-6_126.

Bosch, JH Aleid, Marcel AJ Bakker, Jan L Gunnink, and Bob F Paap (2009). "Airborne electromagnetic measurements as basis for a 3D geological model of an Elsterian incision". In: *Zeitschrift der Deutschen Gesellschaft fur Geowissenschaften* 160.3, p. 249. DOI: 10.1127/1860-1804/2009/0160-0258.

Boucher, Alexandre, Rahul Gupta, Jef Caers, and Addy Satija (2010). "Tetris: a training image generator for SGeMS". In: *Stanford Center for Reservoir Forecasting*.

Bouma, Arnold H (1962). "Sedimentology of some flysch deposits". In: *Agraphic approach to facies interpretation* 168.

Bowling, Jerry C, Antonio B Rodriguez, Dennis L Harry, and Chunmiao Zheng (2005). "Delineating alluvial aquifer heterogeneity using resistivity and GPR data". In: *Groundwater* 43.6, pp. 890–903. DOI: 10.1111/j.1745-6584.2005.00103.x.

Breiman, Leo (2001). "Random forests". In: *Machine learning* 45, pp. 5–32. DOI: 10.1023/a:1010933404324.

Bridge, John S and Michael R Leeder (1979). "A simulation model of alluvial stratigraphy". In: *Sedimentology* 26.5, pp. 617–644. DOI: 10.1111/j.1365-3091.1979.tb00935.x.

Bridge, John S and Ian A Lunt (2006). *Depositional models of braided rivers*. Vol. 36. International Association of Sedimentologists Special Publication 36.

Bridge, John S. (Apr. 2009). *Rivers and Floodplains: Forms, Processes, and Sedimentary Record*. John Wiley & Sons. ISBN: 978-1-4443-1126-6.

Bridge, JS and SD Mackey (1993). "A revised alluvial stratigraphy model". In: *Alluvial sedimentation*, pp. 317–336. DOI: 10.1002/9781444303995.ch22.

Brier, Glenn W (1950). "Verification of forecasts expressed in terms of probability". In: *Monthly weather review* 78.1, pp. 1–3.

Bruna, Pierre-Olivier, Julien Straubhaar, Rahul Prabhakaran, Giovanni Bertotti, Kevin Bisdom, Grégoire Mariethoz, and Marco Meda (2019). "A new methodology to train fracture network simulation using multiple-point statistics". In: *Solid Earth* 10.2, pp. 537–559. DOI: 10.5194/se-10-537-2019.

Buechi, Marius W, Hans Rudolf Graf, Peter Haldimann, Sally E Lowick, and Flavio S Anselmetti (2018). "Multiple Quaternary erosion and infill cycles in overdeepened basins of the northern Alpine foreland". In: *Swiss Journal of Geosciences* 111.1, pp. 133–167. DOI: 10.1007/s00015-017-0289-9.

Caers, J, C Scheidt, Z Yin, L Wang, T Mukerji, and K House (2022). "Efficacy of information in mineral exploration drilling". In: *Natural Resources Research* 31.3, pp. 1157–1173. DOI: 10.1007/s11053-022-10030-1.

Caers, Jef and Tuanfeng Zhang (2004). "Multiple-point geostatistics: a quantitative vehicle for integrating geologic analogs into multiple reservoir models". In: DOI: 10.1306/M80924C18.

Calcagno, Philippe, Jean-Paul Chilès, Gabriel Courrioux, and Antonio Guillen (2008). "Geological modelling from field data and geological knowledge: Part I. Modelling method coupling 3D potential-field interpolation and geological rules". In: *Physics of the Earth and Planetary Interiors* 171.1-4, pp. 147–157. DOI: 10.1016/j.pepi.2008.06.013.

Cardiff, M and PK Kitanidis (2009). "Bayesian inversion for facies detection: An extensible level set framework". In: *Water Resources Research* 45.10. DOI: 10.1029/2008WR007675.

Carle, Steven F (1997). "Implementation schemes for avoiding artifact discontinuities in simulated annealing". In: *Mathematical Geology* 29, pp. 231–244. DOI: 10.1007/BF02769630.

— (2007). "T-PROGS: transition probability geostatistical software, version 2.1". In: *Department of Land, Air and Water Resources, University of California, Davis*.

Carle, Steven F and Graham E Fogg (1996). "Transition probability-based indicator geostatistics". In: *Mathematical geology* 28, pp. 453–476. DOI: 10.1007/BF02083656.

— (1997). "Modeling spatial variability with one and multidimensional continuous-lag Markov chains". In: *Mathematical Geology* 29, pp. 891–918. DOI: 10.1023/A:1022303706942.

Carle, STEVEN F, ERIC M Labolle, GARY S Weissmann, DAVID Van Brocklin, and Graham E Fogg (1998). "Conditional simulation of hydrofacies architecture: a transition probability/Markov approach". In: *Hydrogeologic models of sedimentary aquifers, concepts in hydrogeology and environmental geology* 1.1, pp. 147–170. DOI: 10.2110/sepmcheg.01.147.

Casagrande, Arthur (Jan. 1948). "Classification and Identification of Soils". In: *Transactions of the American Society of Civil Engineers* 113.1, pp. 901–930. DOI: 10.1061/TACEAT.0006109.

Cazanacli, Dan (2021). "Probabilistic, Rule-Based Modeling of Deltaic Networks and Stratigraphy". PhD thesis. University of Minnesota. DOI: https://hdl.handle.net/11299/225121.

Chan, Shing and Ahmed H Elsheikh (2017). "Parametrization and generation of geological models with generative adversarial networks". In: *arXiv preprint arXiv:1708.01810*. DOI: 10.48550/arXiv.1708.01810.

Chen, Yan and Dean S. Oliver (Jan. 2012). "Ensemble Randomized Maximum Likelihood Method as an Iterative Ensemble Smoother". In: *Mathematical Geosciences* 44.1, pp. 1–26. ISSN: 1874-8953. DOI: 10.1007/s11004-011-9376-z.

Cherubini, Claudia, CONCETTA I Giasi, FAUSTA Musci, and Nicola Pastore (2009). "Application of truncated plurigaussian method for the reactive transport modeling of a contaminated aquifer". In: *Proceedings of the 4th IASME/WSEAS International Conference on Water Resources, Hydraulics & Hydrology*, pp. 119–124.

Chiles, Jean-Paul and Pierre Delfiner (2012). *Geostatistics: modeling spatial uncertainty*. Vol. 713. John Wiley & Sons. DOI: 10.1002/9781118136188.

Chiogna, Gabriele, Olaf A Cirpka, Massimo Rolle, and Alberto Bellin (2015). "Helical flow in three-dimensional nonstationary anisotropic heterogeneous porous media". In: *Water Resources Research* 51.1, pp. 261–280. DOI: 10.1002/2014WR015330.

Christakos, George (1990). "A Bayesian/maximum-entropy view to the spatial estimation problem". In: *Mathematical Geology* 22, pp. 763–777. DOI: 10.1007/BF00890661.

Clare, Mariana CA, Stephan C Kramer, Colin J Cotter, and Matthew D Piggott (2022). "Calibration, inversion and sensitivity analysis for hydro-morphodynamic models through the application of adjoint methods". In: *Computers & Geosciences* 163, p. 105104. DOI: 10.1016/j.cageo.2022.105104.

Clemetsen, Rolf, AR Hurst, Ragnar Knarud, and Henning Omre (1990). "A computer program for evaluation of fluvial reservoirs". In: *North Sea Oil and Gas Reservoirs—II: Proceedings of the 2nd North Sea Oil and Gas Reservoirs Conference organized and hosted by the Norwegian Institute of Technology (NTH), Trondheim, Norway, May 8–11, 1989*. Springer, pp. 373–385. DOI: 10.1007/978-94-009-0791-1_32.

Cockett, Rowan, Seogi Kang, Lindsey J Heagy, Adam Pidlisecky, and Douglas W Oldenburg (2015). "SimPEG: An open source framework for simulation and gradient based parameter estimation in geophysical applications". In: *Computers & Geosciences*.

Coiffier, Guillaume, Philippe Renard, and Sylvain Lefebvre (2020). "3d geological image synthesis from 2d examples using generative adversarial networks". In: *Frontiers in Water* 2, p. 560598. DOI: 10.3389/frwa.2020.560598/full.

Colombera, Luca, Nigel P Mountney, and William D McCaffrey (2012). "A relational database for the digitization of fluvial architecture: concepts and example applications". In: *Petroleum Geoscience* 18.1, pp. 129–140. DOI: 10.1144/1354-079311-021.

Colombera, Luca, Nigel P Mountney, Giacomo Medici, and L Jared West (2019). "The geometry of fluvial channel bodies: Empirical characterization and implications for object-based models of the subsurface". In: *AAPG bulletin* 103.4, pp. 905–929. DOI: 10.1306/10031817417.

Comunian, A., P. Renard, J. Straubhaar, and P. Bayer (July 2011a). "Three-Dimensional High Resolution Fluvio-Glacial Aquifer Analog – Part 2: Geostatistical Modeling". In: *Journal of Hydrology* 405.1, pp. 10–23. ISSN: 0022-1694. DOI: 10.1016/j.jhydrol.2011.03.037.

Comunian, Alessandro, Leonardo De Micheli, Claudio Lazzati, Fabrizio Felletti, Francesca Giacobbo, Mauro Giudici, and Riccardo Bersezio (2016a). "Hierar-

chical simulation of aquifer heterogeneity: implications of different simulation settings on solute-transport modeling". In: *Hydrogeology journal* 24.2, pp. 319–334.

Comunian, Alessandro, Leonardo De Micheli, Claudio Lazzati, Fabrizio Felletti, FRANCESCA CELSA Giacobbo, Mauro Giudici, Riccardo Bersezio, et al. (2016b). "Hierarchical simulation of aquifer heterogeneity: implications of different simulation settings on solute-transport modeling". In: *Hydrogeology journal* 24.2, pp. 319–334. DOI: 10.1007/s10040-015-1343-1.

Comunian, Alessandro, Philippe Renard, Julien Straubhaar, and Peter Bayer (2011b). "Three-dimensional high resolution fluvio-glacial aquifer analog–Part 2: Geostatistical modeling". In: *Journal of hydrology* 405.1-2, pp. 10–23. DOI: 10.1016/j.jhydrol.2011.03.037.

Cortes, Corinna and Vladimir Vapnik (1995). "Support-vector networks". In: *Machine learning* 20, pp. 273–297. DOI: 10.1007/Bf00994018.

Cowan, EJ, RK Beatson, WR Fright, TJ McLennan, and TJ Mitchell (2002). "Rapid geological modelling". In: *Applied structural geology for mineral exploration and mining, international symposium*, pp. 23–25.

D'Or, Dimitri and Patrick Bogaert (2004). "Spatial prediction of categorical variables with the Bayesian Maximum Entropy approach: the Ooypolder case study". In: *European Journal of Soil Science* 55.4, pp. 763–775. DOI: 10.1111/j.1365-2389.2004.00628.x.

Dagan, Gedeon (1989). *Flow and transport in porous formations*. Springer Science & Business Media. DOI: 10.1007/978-3-642-75015-1.

Daley, Daryl J, David Vere-Jones, et al. (2003). *An introduction to the theory of point processes: volume I: elementary theory and methods*. Springer. DOI: 10.1007/b97277.

Dall'Alba, Valentin, Philippe Renard, Julien Straubhaar, Benoit Issautier, Cédric Duvail, and Yvan Caballero (2020). "3D multiple-point statistics simulations of the Roussillon Continental Pliocene aquifer using DeeSse". In: *Hydrology and Earth System Sciences* 24.10, pp. 4997–5013. DOI: 10.5194/hess-24-4997-2020.

Damsleth, Elvind, Charlotte B Tjolsen, Henning Omre, and Helge H Haldorsen (1992). "A two-stage stochastic model applied to a North Sea reservoir". In: *Journal of Petroleum Technology* 44.04, pp. 402–486. DOI: 10.2118/20605-PA.

Das, Braja M and Khaled Sobhan (1990). "Principles of geotechnical engineering". In.

de la Varga, Miguel, Alexander Schaaf, and Florian Wellmann (Jan. 2019). "GemPy 1.0: Open-Source Stochastic Geological Modeling and Inversion". In: *Geoscientific Model Development* 12.1, pp. 1–32. ISSN: 1991-959X. DOI: 10.5194/gmd-12-1-2019.

De Marsily, G, F Delay, V Teles, and MT Schafmeister (1998). "Some current methods to represent the heterogeneity of natural media in hydrogeology". In: *Hydrogeology Journal* 6, pp. 115–130. DOI: 10.1007/s100400050138.

De Marsily, Gh, Frédéric Delay, Julio Gonçalvès, Ph Renard, Vanessa Teles, and Sophie Violette (2005). "Dealing with spatial heterogeneity". In: *Hydrogeology Journal* 13, pp. 161–183. DOI: 10.1007/s10040-004-0432-3.

Delaney, Ian, Leif Anderson, and Frédéric Herman (2023). "Modeling the spatially distributed nature of subglacial sediment transport and erosion". In: *Earth Surface Dynamics* 11.4, pp. 663–680. DOI: 10.5194/esurf-11-663-2023.

Delaney, Ian, Mauro A Werder, and Daniel Farinotti (2019). "A numerical model for fluvial transport of subglacial sediment". In: *Journal of Geophysical Research: Earth Surface* 124.8, pp. 2197–2223. DOI: 10.1029/2019JF005004.

Delhomme, AK and JF Giannesini (1979). *New reservoir description techniques improve simulation results in Hassi-Messaoud field-Algeria*. Tech. rep.

Dell'Arciprete, Diana, Riccardo Bersezio, Fabrizio Felletti, Mauro Giudici, Alessandro Comunian, and Philippe Renard (2012). "Comparison of three geostatistical methods for hydrofacies simulation: a test on alluvial sediments". In: *Hydrogeology Journal* 20.2, p. 299. DOI: 10.1007/s10040-011-0808-0.

Delottier, Hugo, John Doherty, and Philip Brunner (2023). "Data space inversion for efficient uncertainty quantification using an integrated surface and subsurface hydrologic model". In: *Geoscientific Model Development Discussions* 2023, pp. 1–30. DOI: 10.5194/gmd-16-4213-2023.

Dervieux, Alain and François Thomasset (2006). "A finite element method for the simulation of a Rayleigh-Taylor instability". In: *Approximation Methods for Navier-Stokes Problems: Proceedings of the Symposium Held by the International Union of Theoretical and Applied Mechanics (IUTAM) at the University of Paderborn, Germany, September 9–15, 1979*. Springer, pp. 145–158. DOI: 10.1007/BFb0086904.

Deutsch, Clayton V (1998). "A short note on cross validation of facies simulation methods". In: *Centre for Computational Geostatistics Annual Report, Report* 1, p. 109.

— (2006). "A sequential indicator simulation program for categorical variables with point and block data: BlockSIS". In: *Computers & Geosciences* 32.10, pp. 1669–1681. DOI: 10.1016/j.cageo.2006.03.005.

Deutsch, Clayton V and Perry W Cockerham (1994). "Practical considerations in the application of simulated annealing to stochastic simulation". In: *Mathematical Geology* 26, pp. 67–82. DOI: 10.1007/BF02065876.

Deutsch, Clayton V, Andre G Journel, et al. (1992). *Geostatistical software library and user's guide*. First. Vol. 119. 147, p. 578.

Deutsch, Clayton V and Libing Wang (1996). "Hierarchical object-based stochastic modeling of fluvial reservoirs". In: *Mathematical geology* 28, pp. 857–880. DOI: 10.1007/BF02066005.

Deutsch, CV and TT Tran (2002). "FLUVSIM: a program for object-based stochastic modeling of fluvial depositional systems". In: *Computers & Geosciences* 28.4, pp. 525–535. DOI: 10.1016/S0098-3004(01)00075-9a.

Deveugle, Peter EK, Matthew D Jackson, Gary J Hampson, Jonathan Stewart, Martyn D Clough, Thaddeus Ehighebolo, Michael E Farrell, Craig S Calvert, and James K Miller (2014). "A comparative study of reservoir modeling techniques and their impact on predicted performance of fluvial-dominated deltaic reservoirs". In: *AAPG bulletin* 98.4, pp. 729–763. DOI: 10.1306/01081817409.

Donovan, Mitchell, Patrick Belmont, and Zoltán Sylvester (2021). "Evaluating the relationship between meander-bend curvature, sediment supply, and migration rates". In: *Journal of Geophysical Research: Earth Surface* 126.3, e2020JF006058. DOI: 10.1029/2020JF006058.

Doyen, PM, DE Psaila, and S Strandenes (1994). "Bayesian sequential indicator simulation of channel sands from 3-D seismic data in the Oseberg field, Norwegian North Sea". In: *SPE Annual Technical Conference and Exhibition*. SPE, SPE–28382. DOI: 10.2118/28382-MS.

Duan, Xianqian, Yinger Deng, Xuewei Chu, Xin Peng, Hu Su, and Hongkun Yang (2022). "Identification of hydraulic conductivity field of a karst aquifer by using transition probability geostatistics and discrete cosine transform with an ensemble method". In: *Hydrological Processes* 36.11, e14755. DOI: 10.1002/hyp.14755.

Dubrule, Olivier and Clement Kostov (Jan. 1986). "An Interpolation Method Taking into Account Inequality Constraints: I. Methodology". In: *Mathematical Geology* 18.1, pp. 33–51. ISSN: 1573-8868. DOI: 10.1007/BF00897654.

Dupont, Emilien, Tuanfeng Zhang, Peter Tilke, Lin Liang, and William Bailey (2018). "Generating realistic geology conditioned on physical measurements with generative adversarial networks". In: *arXiv preprint arXiv:1802.03065*. DOI: 10.48550/arXiv.1802.03065.

Emerick, Alexandre A and Albert C Reynolds (2013). "Ensemble smoother with multiple data assimilation". In: *Computers & Geosciences* 55, pp. 3–15. DOI: 10.1016/j.cageo.2012.03.011.

Emery, Xavier (2004). "Properties and limitations of sequential indicator simulation". In: *Stochastic Environmental Research and Risk Assessment* 18, pp. 414–424. DOI: 10.1007/s00477-004-0213-5.

— (2007). "Simulation of geological domains using the plurigaussian model: new developments and computer programs". In: *Computers & geosciences* 33.9, pp. 1189–1201. DOI: 10.1016/j.cageo.2007.01.006.

Erharter, Georg H, Franz Tschuchnigg, and Gerhard Poscher (2021). "Stochastic 3D modelling of discrete sediment bodies for geotechnical applications". In: *Applied Computing and Geosciences* 11, p. 100066. DOI: 10.1016/j.acags.2021.100066.

Ershadnia, Reza, Sassan Hajirezaie, Amin Amooie, Corey D Wallace, Naum I Gershenzon, Seyyed Abolfazl Hosseini, Daniel Murray Sturmer, Robert W Ritzi, and Mohamad Reza Soltanian (2021). "CO2 geological sequestration in multiscale heterogeneous aquifers: Effects of heterogeneity, connectivity, impurity, and hysteresis". In: *Advances in Water Resources* 151, p. 103895. DOI: 10.1016/j.advwatres.2021.103895.

Fabbri, Paolo, Carlo Gaetan, Luca Sartore, and Nico Dalla Libera (2020). "Subsoil reconstruction in geostatistics beyond kriging: A case study in Veneto (NE Italy)". In: *Hydrology* 7.1, p. 15. DOI: 10.3390/hydrology7010015.

Falivene, O, A Frascati, S Gesbert, J Pickens, Y Hsu, and A Rovira (2014). "Automatic calibration of stratigraphic forward models for predicting reservoir presence in exploration". In: *AAPG Bulletin* 98.9, pp. 1811–1835. DOI: 10.1306/02271413028.

Falivene, Oriol, Lluís Cabrera, JA Muñoz, Pau Arbués, O Fernández, and Alberto Sáez (2007a). "Statistical grid-based facies reconstruction and modelling for sedimentary bodies. Alluvial-palustrine and turbiditic examples". In: *Geologica Acta: an international earth science journal* 5.3, pp. 199–230. DOI: 10.1344/105.000000295.

Falivene, Oriol, Lluís Cabrera, and Alberto Sáez (2007b). "Optimum and robust 3D facies interpolation strategies in a heterogeneous coal zone (Tertiary As Pontes basin, NW Spain)". In: *International Journal of Coal Geology* 71.2-3, pp. 185–208. DOI: 10.1016/j.coal.2006.08.008.

Ferguson, RI (1976). "Disturbed periodic model for river meanders". In: *Earth Surface Processes* 1.4, pp. 337–347. DOI: 10.1002/esp.3290010403.

Feyen, Luc and Jef Caers (June 2006). "Quantifying Geological Uncertainty for Flow and Transport Modeling in Multi-Modal Heterogeneous Formations". In: *Advances in Water Resources* 29.6, pp. 912–929. ISSN: 0309-1708. DOI: 10.1016/j.advwatres.2005.08.002.

FLUMY™ (2022). Process-based channelized reservoir models Copyright © MINES PARIS PSL / ARMINES.

Fogg, Graham E, Charles D Noyes, and Steven F Carle (1998). "Geologically based model of heterogeneous hydraulic conductivity in an alluvial setting". In: *Hydrogeology Journal* 6, pp. 131–143. DOI: 10.1007/s100400050139.

Ford, Grace L. and David R. Pyles (July 2014). "A Hierarchical Approach for Evaluating Fluvial Systems: Architectural Analysis and Sequential Evolution of the High Net-Sand Content, Middle Wasatch Formation, Uinta Basin, Utah". In: *AAPG Bulletin* 98.7, pp. 1273–1304. ISSN: 0149-1423. DOI: 10.1306/12171313052.

Freulon, Xavier and Chantal de Fouquet (1993a). "Conditioning a Gaussian Model with Inequalities". In: *Geostatistics Tróia '92: Volume 1*. Ed. by Amilcar Soares. Quantitative Geology and Geostatistics. Dordrecht: Springer Netherlands, pp. 201–212. ISBN: 978-94-011-1739-5. DOI: 10.1007/978-94-011-1739-5_17.

Freulon, Xavier and Chantal de Fouquet (1993b). "Conditioning a Gaussian model with inequalities". In: *Geostatistics Tróia'92: Volume 1*, pp. 201–212. DOI: 10.1007/978-94-011-1739-5_17.

Freund, Yoav and Robert E Schapire (1995). "A desicion-theoretic generalization of on-line learning and an application to boosting". In: *European conference on computational learning theory*. Springer, pp. 23–37. DOI: 10.1007/3-540-59119-2_166.

Friedman, Jerome H (2001). "Greedy function approximation: a gradient boosting machine". In: *Annals of statistics*, pp. 1189–1232. DOI: 10.1214/aos/1013203451.

Galli, A, H Beucher, G Le Loc'h, B Doligez, and Heresim Group (1994). "The pros and cons of the truncated Gaussian method". In: *Geostatistical Simulations: Proceedings of the Geostatistical Simulation Workshop, Fontainebleau, France, 27–28 May 1993*. Springer, pp. 217–233. DOI: 10.1007/978-94-015-8267-4_18.

Gelfand, Alan E and Adrian FM Smith (1990). "Sampling-based approaches to calculating marginal densities". In: *Journal of the American statistical association* 85.410, pp. 398–409. DOI: 10.1080/01621459.1990.10476213.

Geman, Stuart and Donald Geman (1984). "Stochastic relaxation, Gibbs distributions, and the Bayesian restoration of images". In: *IEEE Transactions on pattern analysis and machine intelligence* 6, pp. 721–741. DOI: 10.1109/TPAMI.1984.4767596.

Geng, Xiaolong, Holly A Michael, Michel C Boufadel, Fred J Molz, Firas Gerges, and Kenneth Lee (2020). "Heterogeneity affects intertidal flow topology in coastal beach aquifers". In: *Geophysical Research Letters* 47.17, e2020GL089612. DOI: 10.1029/2020GL089612.

Gershenzon, Naum I, Mohamad Reza Soltanian, Robert W Ritzi Jr, David F Dominic, Don Keefer, Eric Shaffer, and Brynne Storsved (2015). "How does the connectivity of open-framework conglomerates within multi-scale hierarchical fluvial architecture affect oil-sweep efficiency in waterflooding?" In: *Geosphere* 11.6, pp. 2049–2066. DOI: 10.1130/GES01115.1.

Gómez-Hernández, J Jaime and R Mohan Srivastava (2021). "One step at a time: The origins of sequential simulation and beyond". In: *Mathematical Geosciences* 53.2, pp. 193–209. DOI: 10.1007/s11004-021-09926-0.

Gómez-Hernández, J Jaime and Xian-Huan Wen (1998). "To be or not to be multi-Gaussian? A reflection on stochastic hydrogeology". In: *Advances in Water Resources* 21.1, pp. 47–61. DOI: 10.1016/S0309-1708(96)00031-0.

Goodfellow, Ian, Jean Pouget-Abadie, Mehdi Mirza, Bing Xu, David Warde-Farley, Sherjil Ozair, Aaron Courville, and Yoshua Bengio (2014). "Generative adversarial nets". In: *Advances in neural information processing systems* 27. DOI: 10.1145/3422622.

Gradstein, Felix M, James G Ogg, Mark D Schmitz, and Gabi M Ogg (2020). *Geologic time scale 2020*. Elsevier.

Graf, Hans Rudolf and Reto Burkhalter (Sept. 2016). "Quaternary Deposits: Concept for a Stratigraphic Classification and Nomenclature—an Example from Northern Switzerland". In: *Swiss Journal of Geosciences* 109.2, pp. 137–147. ISSN: 1661-8734. DOI: 10.1007/s00015-016-0222-7.

Granjeon, Didier (1996). "Modélisation stratigraphique déterministe: conception et applications d'un modèle diffusif 3D multilithologique". PhD thesis. Rennes 1. DOI: https://theses.hal.science/tel-00648827.

— (2014). "3D forward modelling of the impact of sediment transport and base level cycles on continental margins and incised valleys". In: *From depositional systems to sedimentary successions on the norwegian continental margin*, pp. 453–472. DOI: 10.1002/9781118920435.ch16.

Green, Christopher T, Yong Zhang, Bryant C Jurgens, J Jeffrey Starn, and Matthew K Landon (2014). "Accuracy of travel time distribution (TTD) models as affected by TTD complexity, observation errors, and model and tracer selection". In: *Water Resources Research* 50.7, pp. 6191–6213. DOI: 10.1002/2014WR015625.

Guadagnini, Laura, Alberto Guadagnini, and Daniel M Tartakovsky (2004). "Probabilistic reconstruction of geologic facies". In: *Journal of Hydrology* 294.1-3, pp. 57–67. DOI: 10.1016/j.jhydrol.2004.02.007.

Guardiano, Felipe B and R Mohan Srivastava (1993). "Multivariate geostatistics: beyond bivariate moments". In: *Geostatistics Tróia'92: Volume 1*. Springer, pp. 133–144. DOI: 10.1007/978-94-011-1739-5_12.

Guin, Arijit, Ramya Ramanathan, Robert W Ritzi Jr, David F Dominic, Ian A Lunt, Timothy D Scheibe, and Vicky L Freedman (2010). "Simulating the heterogeneity in braided channel belt deposits: 2. Examples of results and comparison to natural deposits". In: *Water Resources Research* 46.4. DOI: 10.1029/2009WR008112.

Gundesø, R and O Egeland (1990). "SESIMIRA—A new geological tool for 3D modelling of heterogeneous reservoirs". In: *North Sea Oil and Gas Reservoirs—II: Proceedings of the 2nd North Sea Oil and Gas Reservoirs Conference organized and hosted by the Norwegian Institute of Technology (NTH), Trondheim, Norway, May 8–11, 1989*. Springer, pp. 363–371. DOI: 10.1007/978-94-009-0791-1_31.

Guo, Zhilin, Graham E Fogg, Mark L Brusseau, Eric M LaBolle, and Jose Lopez (2019). "Modeling groundwater contaminant transport in the presence of large heterogeneity: a case study comparing MT3D and RWhet". In: *Hydrogeology journal* 27.4, p. 1363. DOI: 10.1007/s10040-019-01938-9.

Haeuselmann, Philipp, Darryl E. Granger, Pierre-Yves Jeannin, and Stein-Erik Lauritzen (Feb. 2007). "Abrupt Glacial Valley Incision at 0.8 Ma Dated from Cave Deposits in Switzerland". In: *Geology* 35.2, pp. 143–146. ISSN: 0091-7613. DOI: 10.1130/G23094A.

Haldorsen, Helge H and David M Chang (1986). "Notes on stochastic shales; from outcrop to simulation model". In: *Reservoir characterization*. Elsevier, pp. 445–485. DOI: 10.1016/B978-0-12-434065-7.50020-4.

Haldorsen, Helge H and Larry W Lake (1984). "A new approach to shale management in field-scale models". In: *Society of Petroleum Engineers Journal* 24.04, pp. 447–457. DOI: 10.2118/10976-PA.

Hammond, Zidra and Diana M Allen (2023). "Evaluating the feasibility of using artificial neural networks to predict lithofacies in complex glacial deposits". In: *Hydrogeology Journal*, pp. 1–18. DOI: 10.1007/s10040-023-02726-2.

Hassanpour, Mehran M, Michael J Pyrcz, and Clayton V Deutsch (2013). "Improved geostatistical models of inclined heterolithic strata for McMurray Formation, Alberta, Canada". In: *AAPG bulletin* 97.7, pp. 1209–1224. DOI: 10.1306/01021312054.

Hastie, Trevor, Robert Tibshirani, Jerome H Friedman, and Jerome H Friedman (2009). *The elements of statistical learning: data mining, inference, and prediction*. Vol. 2. Springer. DOI: 10.1007/978-0-387-21606-5.

Hatloy, Andres S (1994). "Numerical facies modeling combining deterministic and stochastic methods". In: *Stochastic Modeling and Geostatistics*. Ed. by J. M. Yarus and R.L. (Eds.) Chambers. AAPG Special Volumes, pp. 109–120. DOI: 10.5194/hess-25-1-2021.

Hauge, Ragnar, Maria Vigsnes, Bjørn Fjellvoll, Markus Lund Vevle, and Arne Skorstad (2017). "Object-Based Modeling with Dense Well Data". In: *Geostatistics Valencia 2016*, pp. 557–572. DOI: 10.1007/978-3-319-46819-8_37.

Haykin, Simon (1998). *Neural networks: a comprehensive foundation*. Prentice Hall PTR. DOI: 10.5555/521706.

He, Xin, Anker Lajer Højberg, Flemming Jørgensen, and Jens Christian Refsgaard (2015). "Assessing hydrological model predictive uncertainty using stochastically generated geological models". In: *Hydrological Processes* 29.19, pp. 4293–4311. DOI: 10.1002/hyp.10488.

He, Xin, Julian Koch, Torben O Sonnenborg, Flemming Jørgensen, Cyril Schamper, and Jens Christian Refsgaard (2014). "Transition probability-based stochastic geological modeling using airborne geophysical data and borehole data". In: *Water Resources Research* 50.4, pp. 3147–3169. DOI: 10.1002/2013WR014593.

He, Y de, KL Hu, DL Chen, HC Suter, Y Li, BG Li, XY Yuan, and YF Huang (2010). "Three dimensional spatial distribution modeling of soil texture under agricultural systems using a sequence indicator simulation algorithm". In: *Computers and Electronics in Agriculture* 71, S24–S31. DOI: 10.1016/j.compag.2009.06.012.

Heinz, Jürgen and Thomas Aigner (Dec. 2003a). "Hierarchical Dynamic Stratigraphy in Various Quaternary Gravel Deposits, Rhine Glacier Area (SW Germany): Implications for Hydrostratigraphy". In: *International Journal of Earth Sciences* 92.6, pp. 923–938. ISSN: 1437-3262. DOI: 10.1007/s00531-003-0359-2.

Heinz, Jürgen, Sybille Kleineidam, Georg Teutsch, and Thomas Aigner (2003b). "Heterogeneity patterns of Quaternary glaciofluvial gravel bodies (SW-Germany): application to hydrogeology". In: *Sedimentary geology* 158.1-2, pp. 1–23. DOI: 10.1016/S0037-0738(02)00239-7.

Henrion, Vincent, Guillaume Caumon, and Nicolas Cherpeau (2010). "ODSIM: an object-distance simulation method for conditioning complex natural structures". In: *Mathematical Geosciences* 42, pp. 911–924. DOI: 10.1007/s11004-010-9299-0.

Henriquez, Adolfo, Kelly J Tyler, and Andrew Hurst (1990). "Characterization of fluvial sedimentology for reservoir simulation modeling". In: *SPE Formation Evaluation* 5.03, pp. 211–216. DOI: 10.2118/18323-PA.

Hill, E June and Cedric Griffiths (2007). "Simulating sedimentary successions using syntactic pattern recognition techniques". In: *Mathematical geology* 39.2, pp. 141–157. DOI: 10.1007/s11004-006-9074-4.

Hill, EJ and CM Griffiths (2008). "Formal description of sedimentary architecture of analogue models for use in 2D reservoir simulation". In: *Marine and petroleum geology* 25.2, pp. 131–141. DOI: 10.1016/j.marpetgeo.2007.05.001.

Hill, EJ and CM Griffiths (2009). "Describing and generating facies models for reservoir characterisation: 2D map view". In: *Marine and petroleum geology* 26.8, pp. 1554–1563. DOI: 10.1016/j.marpetgeo.2008.09.004.

Hill, June (2009). *The GeoSyntax Project 2003-2009: A New Concept for Generating Stochastic Facies Models of Petroleum Reservoirs*. CSIRO. DOI: 10.13140/2.1.1653.1209.

Hoffimann, Júlio, Céline Scheidt, Adrian Barfod, and Jef Caers (2017). "Stochastic simulation by image quilting of process-based geological models". In: *Computers & Geosciences* 106, pp. 18–32. DOI: 10.1016/j.cageo.2017.05.012.

Holden, Lars, Ragnar Hauge, Øivind Skare, and Arne Skorstad (1998). "Modeling of fluvial reservoirs with object models". In: *Mathematical Geology* 30, pp. 473–496. DOI: 10.1023/A:1021769526425.

Houlding, Simon W and Simon W Houlding (1994). "Geological interpretation and modeling". In: *3D Geoscience Modeling: Computer Techniques for Geological Characterization*, pp. 113–129. DOI: 10.1007/978-3-642-79012-6_7.

Howard, Alan D (1996). "Modeling channel evolution and floodplain morphology". In: *Floodplain processes*, pp. 15–62.

Howard, Alan D and Thomas R Knutson (1984). "Sufficient conditions for river meandering: A simulation approach". In: *Water Resources Research* 20.11, pp. 1659–1667. DOI: 10.1029/WR020i011p01659.

Hu, Fei, Chunlei Wu, Jiangwei Shang, Yiming Yan, Leiquan Wang, and Huan Zhang (2023). "Multi-condition controlled sedimentary facies modeling based on generative adversarial network". In: *Computers & Geosciences* 171, p. 105290. DOI: 10.1016/j.cageo.2022.105290.

Huggenberger, Peter and Christian Regli (2006). "A sedimentological model to characterize braided river deposits for hydrogeological applications". In: *Braided rivers: process, deposits, ecology and management*, pp. 51–74.

Huysmans, Marijke and Alain Dassargues (2009). "Application of multiple-point geostatistics on modelling groundwater flow and transport in a cross-bedded aquifer". In: *Hydrogeology Journal* 17.8. DOI: 10.1007/s10040-009-0495-2.

Imbeaux, Ed (1930). "Essai d'hydrogéologie: recherche, étude et captage des eaux souterraines". In: *(No Title)*.

Ivakhnenko, Alexey Grigorevich (1971). "Polynomial theory of complex systems". In: *IEEE transactions on Systems, Man, and Cybernetics* 4, pp. 364–378.

Jacquemyn, Carl, Matthew D Jackson, and Gary J Hampson (2019). "Surface-based geological reservoir modelling using grid-free NURBS curves and surfaces". In: *Mathematical Geosciences* 51, pp. 1–28. DOI: 10.1007/s11004-018-9764-8.

Jaynes, Edwin T (1957). "Information theory and statistical mechanics". In: *Physical review* 106.4, p. 620. DOI: 10.1103/PhysRev.106.620.

Jo, Honggeun, Javier E Santos, and Michael J Pyrcz (2020). "Conditioning well data to rule-based lobe model by machine learning with a generative adversarial network". In: *Energy Exploration & Exploitation* 38.6, pp. 2558–2578. DOI: 10.1177/0144598720937524.

Jo, Suryeom, Seongin Ahn, Changhyup Park, and Jaejun Kim (2022). "Generative geomodeling based on flow responses in latent space". In: *Journal of Petroleum Science and Engineering* 211, p. 110177. DOI: 10.1016/j.petrol.2022.110177.

Jóhannsson, Óli D and Thomas Mejer Hansen (2021). "Estimation using multiple-point statistics". In: *Computers & Geosciences* 156, p. 104894. DOI: 10.1016/j.cageo.2021.104894.

Jørgensen, Flemming, Anne-Sophie Høyer, Peter BE Sandersen, Xiulan He, and Nikolaj Foged (2015). "Combining 3D geological modelling techniques to address variations in geology, data type and density–An example from Southern Denmark". In: *Computers & geosciences* 81, pp. 53–63. DOI: 10.1016/j.cageo.2015.04.010.

Jorreto-Zaguirre, S, PA Dowd, E Pardo-Igúzquiza, A Pulido-Bosch, and F Sánchez-Martos (2020). "Stochastic simulation of the spatial heterogeneity of deltaic hydrofacies accounting for the uncertainty of facies proportions". In: *Frontiers in Earth Science* 8, p. 563122. DOI: 10.3389/feart.2020.563122/full.

Journel, A. G. (June 1983a). "Nonparametric Estimation of Spatial Distributions". In: *Journal of the International Association for Mathematical Geology* 15.3, pp. 445–468. ISSN: 0020-5958, 1573-8868. DOI: 10.1007/BF01031292.

Journel, A. G. and E. H. Isaaks (Oct. 1984). "Conditional Indicator Simulation: Application to a Saskatchewan Uranium Deposit". In: *Journal of the International Association for Mathematical Geology* 16.7, pp. 685–718. ISSN: 1573-8868. DOI: 10.1007/BF01033030.

Journel, AG, R Gundeso, E Gringarten, and T Yao (1998). "Stochastic modelling of a fluvial reservoir: a comparative review of algorithms". In: *Journal of Petroleum Science and Engineering* 21.1-2, pp. 95–121. DOI: 10.1016/S0920-4105(98)00044-8.

Journel, André G (1983b). "Nonparametric estimation of spatial distributions". In: *Journal of the International Association for Mathematical Geology* 15, pp. 445–468. DOI: 10.1007/BF01031292.

Journel, Andre G (1989). *Fundamentals of geostatistics in five lessons*. Vol. 8. American Geophysical Union Washington, DC. ISBN: 0-87590-708-3.

Journel, Andre G and Francois G Alabert (1990). "New method for reservoir mapping". In: *Journal of Petroleum technology* 42.02, pp. 212–218. DOI: 10.2118/18324-PA.

Journel, Andre G and J Jaime Gómez-Hernández (1993). "Stochastic imaging of the Wilmington clastic sequence". In: *SPE formation Evaluation* 8.01, pp. 33–40. DOI: 10.2118/19857-PA.

Juda, Przemysław, Philippe Renard, and Julien Straubhaar (2020). "A Framework for the Cross-Validation of Categorical Geostatistical Simulations". In: *Earth and Space Science* 7.8, e2020EA001152. ISSN: 2333-5084. DOI: 10.1029/2020EA001152.

Juda, Przemysław, Julien Straubhaar, and Philippe Renard (2023). "Comparison of three recent discrete stochastic inversion methods and influence of the prior choice". In: *Comptes Rendus. Géoscience* 355.S1, pp. 1–26. DOI: 10.5802/crgeos.160.

Jussel, Peter, Fritz Stauffer, and Themistocles Dracos (1994). "Transport modeling in heterogeneous aquifers: 1. Statistical description and numerical generation of gravel deposits". In: *Water Resources Research* 30.6, pp. 1803–1817. DOI: 10.1029/94WR00162.

Kawo, Nafyad Serre, Jesse Korus, and Mats Lundh Gulbrandsen (2023). "Multiple-point statistical modeling of three-dimensional glacial aquifer heterogeneity for improved groundwater management". In: *Hydrogeology Journal* 31.6, pp. 1525–1546. DOI: 10.1007/s10040-023-02658-x.

Kellerhals, P., Ch. Haefeli, and B. Tröhler (1981). *Grundlagen für Schutz und Bewirtschaftung der Grundwasser des Kantons Bern Hydrogeologie Aaretal, zwischen Thun und Bern*. Tech. rep. Bern: Wasser- u. Energiewirtschaftsamt des Kantons Bern, p. 144.

Kitanidis, Peter K (2015). "Persistent questions of heterogeneity, uncertainty, and scale in subsurface flow and transport". In: *Water Resources Research* 51.8, pp. 5888–5904. DOI: 10.1002/2015WR017639.

Klingbeil, Ralf, Sybille Kleineidam, Ulrich Asprion, Thomas Aigner, and Georg Teutsch (1999). "Relating lithofacies to hydrofacies: outcrop-based hydrogeological characterisation of Quaternary gravel deposits". In: *Sedimentary Geology* 129.3-4, pp. 299–310. DOI: 10.1016/S0037-0738(99)00067-6.

Koltermann, Christine E and Steven M Gorelick (1996). "Heterogeneity in sedimentary deposits: A review of structure-imitating, process-imitating, and descriptive approaches". In: *Water Resources Research* 32.9, pp. 2617–2658. DOI: 10.1029/96WR00025.

Koneshloo, Mohammad, Pieter Kreyns, and Holly A Michael (2018). "Combining process-based and surface-based models to simulate subsurface heterogeneity in volcanic aquifers". In: *Stochastic Environmental Research and Risk Assessment* 32, pp. 2565–2583. DOI: 10.1007/s00477-018-1511-7.

Krige, Daniel G (1951). "A statistical approach to some basic mine valuation problems on the Witwatersrand". In: *Journal of the Southern African Institute of Mining and Metallurgy* 52.6, pp. 119–139. DOI: 10.10520/AJA0038223X_4792.

Lajaunie, Christian, Gabriel Courrioux, and Laurent Manuel (1997). "Foliation fields and 3D cartography in geology: principles of a method based on potential interpolation". In: *Mathematical Geology* 29, pp. 571–584. DOI: 10.1007/BF02775087.

Laloy, Eric, Romain Hérault, Diederik Jacques, and Niklas Linde (2018). "Training-image based geostatistical inversion using a spatial generative adversarial neural network". In: *Water Resources Research* 54.1, pp. 381–406. DOI: 10.1002/2017WR022148.

Lam, Dan-Thuy, Jaouher Kerrou, Philippe Renard, Hakim Benabderrahmane, and Pierre Perrochet (2020). "Conditioning Multi-Gaussian Groundwater Flow Parameters to Transient Hydraulic Head and Flowrate Data With Iterative Ensemble Smoothers: A Synthetic Case Study". In: *Frontiers in Earth Science* 8, p. 202. DOI: 10.3389/feart.2020.00202.

Langevin, Christian D, Joseph D Hughes, Edward R Banta, Richard G Niswonger, Sorab Panday, and Alden M Provost (2017). *Documentation for the MODFLOW 6 groundwater flow model*. Tech. rep. US Geological Survey. DOI: 10.3133/tm6A55.

Langousis, Andreas, Vassilios Kaleris, Angeliki Kokosi, and George Mamounakis (2018). "Markov based transition probability geostatistics in groundwater applications: assumptions and limitations". In: *Stochastic Environmental Research and Risk Assessment* 32, pp. 2129–2146. DOI: 10.1007/s00477-017-1504-y.

Lantuéjoul, Christian (2001). *Geostatistical simulation: models and algorithms*. 1139. Springer Science & Business Media. DOI: 10.1007/978-3-662-04808-5.

Lauzon, Dany and Denis Marcotte (2020a). "Calibration of random fields by a sequential spectral turning bands method". In: *Computers & Geosciences* 135, p. 104390. DOI: 10.1016/j.cageo.2019.104390.

— (2020b). "The sequential spectral turning band simulator as an alternative to Gibbs sampler in large truncated-or pluri-Gaussian simulations". In: *Stochastic Environmental Research and Risk Assessment* 34, pp. 1939–1951. DOI: 10.1007/s00477-020-01850-9.

— (2023). "Joint hydrofacies-hydraulic conductivity modeling based on a constructive spectral algorithm constrained by transient head data". In: *Hydrogeology Journal*, pp. 1–18. DOI: 10.1007/s10040-023-02638-1.

Le Blévec, Thomas, Olivier Dubrule, Cédric M John, and Gary J Hampson (2018). "Geostatistical modelling of cyclic and rhythmic facies architectures". In: *Mathematical Geosciences* 50, pp. 609–637. DOI: 10.1007/s11004-018-9737-y.

— (2020). "Geostatistical Earth modeling of cyclic depositional facies and diagenesis". In: *AAPG Bulletin* 104.3, pp. 711–734. DOI: 10.1306/05091918122.

Le Loc'h, G and A Galli (1997). "Truncated plurigaussian method: theoretical and practical points of view". In: *Geostatistics wollongong* 96.1, pp. 211–222.

Lee, Daesoo, Oscar Ovanger, Jo Eidsvik, Erlend Aune, Jacob Skauvold, and Ragnar Hauge (2023). "Latent Diffusion Model for Conditional Reservoir Facies Generation". In: *arXiv preprint arXiv:2311.01968*. DOI: 10.48550/arXiv.2311.01968.

Lesser, Giles R, JA v Roelvink, JA Th M van Kester, and GS Stelling (2004). "Development and validation of a three-dimensional morphological model". In: *Coastal engineering* 51.8-9, pp. 883–915. DOI: 10.1016/j.coastaleng.2004.07.014.

Li, Hong, Bo Wan, Deping Chu, Run Wang, Guoxi Ma, Jinming Fu, and Zhuocheng Xiao (2023a). "Progressive Geological Modeling and Uncertainty Analysis Using Machine Learning". In: *ISPRS International Journal of Geo-Information* 12.3, p. 97. DOI: 10.3390/ijgi12030097.

Li, L, JEA Storms, and DJR Walstra (2018). "On the upscaling of process-based models in deltaic applications". In: *Geomorphology* 304, pp. 201–213. DOI: 10.1016/j.geomorph.2017.10.015.

Li, Wei, Luca Colombera, Dali Yue, and Nigel P Mountney (2023b). "Controls on the morphology of braided rivers and braid bars: An empirical characterization of numerical models". In: *Sedimentology* 70.1, pp. 259–279. DOI: 10.1111/sed.13040.

Liang, Man, VR Voller, and Chris Paola (2015). "A reduced-complexity model for river delta formation–Part 1: Modeling deltas with channel dynamics". In: *Earth Surface Dynamics* 3.1, pp. 67–86. DOI: 10.5194/esurf-3-67-2015.

Liu, Ning and Dean S Oliver (2004). "Automatic history matching of geologic facies". In: *Spe Journal* 9.04, pp. 429–436. DOI: 10.2118/84594-PA.

Loc'h, G. Le, H. Beucher, A. Galli, and B. Doligez (June 1994). "Improvement In The Truncated Gaussian Method: Combining Several Gaussian Functions". In: *ECMOR IV - 4th European Conference on the Mathematics of Oil Recovery*. European Association of Geoscientists & Engineers, cp. ISBN: 978-82-91505-00-8. DOI: 10.3997/2214-4609.201411149.

Lopez, Simon (2003). "Modélisation de réservoirs chenalisés méandriformes: une approche génétique et stochastique". PhD thesis. École Nationale Supérieure des Mines de Paris.

Lopez, Simon, Isabelle Cojan, Jacques Rivoirard, and Alain Galli (2009). "Process-based stochastic modelling: meandering channelized reservoirs". In: *Analogue and Numerical Modelling of Sedimentary Systems: From Understanding to Prediction, Wiley, Oxford, UK*, pp. 139–144. DOI: 10.1002/9781444303131.ch5.

Mackey, Scudder D and John S Bridge (1995). "Three-dimensional model of alluvial stratigraphy; theory and applications". In: *Journal of Sedimentary Research* 65.1b, pp. 7–31. DOI: 10.1306/D42681D5-2B26-11D7-8648000102C1865D.

Madani, Nasser, Bijan Biranvand, Asghar Naderi, and Nasser Keshavarz (2019). "Lithofacies uncertainty modeling in a siliciclastic reservoir setting by incorporating geological contacts and seismic information". In: *Journal of Petroleum Exploration and Production Technology* 9, pp. 1–16. DOI: 10.1007/s13202-018-0531-7.

Madani, Nasser and Xavier Emery (2015). "Simulation of geo-domains accounting for chronology and contact relationships: application to the Río Blanco copper

deposit". In: *Stochastic environmental research and risk assessment* 29, pp. 2173–2191. DOI: 10.1007/s00477-014-0997-x.

Maharaja, Amisha (2008). "TiGenerator: Object-based training image generator". In: *Computers & Geosciences* 34.12, pp. 1753–1761. DOI: 10.1016/j.cageo.2007.08.012.

Major, Márton, Alexandros Daniilidis, Thomas Mejer Hansen, Mark Khait, and Denis Voskov (2023). "Influence of process-based, stochastic and deterministic methods for representing heterogeneity in fluvial geothermal systems". In: *Geothermics* 109, p. 102651. DOI: 10.1016/j.geothermics.2023.102651.

Mallet, Jean-Laurent (1989). "Discrete smooth interpolation". In: *ACM Transactions on Graphics (TOG)* 8.2, pp. 121–144.

Manzocchi, Tom, Deirdre A Walsh, Marcus Carneiro, and Javier López-Cabrera (2023). "Compression-based facies modelling". In: *Mathematical Geosciences*, pp. 1–20. DOI: 10.1007/s11004-023-10048-y.

Manzocchi, Tom, John J Walsh, Mark Tomasso, Julian Strand, Conrad Childs, and Peter DW Haughton (2007). "Static and dynamic connectivity in bed-scale models of faulted and unfaulted turbidites". In: *Geological Society, London, Special Publications* 292.1, pp. 309–336. DOI: 10.1144/SP292.18.

Mariethoz, Gregoire and Jef Caers (2014). *Multiple-point geostatistics: stochastic modeling with training images*. John Wiley & Sons. DOI: 10.1002/9781118662953.

Mariethoz, Gregoire, Matthew F McCabe, and Philippe Renard (2012). "Spatiotemporal reconstruction of gaps in multivariate fields using the direct sampling approach". In: *Water Resources Research* 48.10. DOI: 10.1029/2012WR012115.

Mariethoz, Gregoire, Philippe Renard, and Julien Straubhaar (2010a). "The Direct Sampling Method to Perform Multiple-Point Geostatistical Simulations". In: *Water Resources Research* 46.11. ISSN: 1944-7973. DOI: 10.1029/2008WR007621.

— (2010b). "The direct sampling method to perform multiple-point geostatistical simulations". In: *Water Resources Research* 46.11. DOI: 10.1029/2008WR007621.

Mariethoz, Grégoire, Philippe Renard, Fabien Cornaton, and Olivier Jaquet (2009). "Truncated plurigaussian simulations to characterize aquifer heterogeneity". In: *Groundwater* 47.1, pp. 13–24. DOI: 10.1111/j.1745-6584.2008.00489.x.

Marini, Mattia, Fabrizio Felletti, Giovanni Pietro Beretta, and Jacopo Terrenghi (2018). "Three Geostatistical methods for hydrofacies simulation ranked using a large borehole lithology dataset from the Venice Hinterland (NE Italy)". In: *Water* 10.7, p. 844. DOI: 10.3390/w10070844.

Martín-Martín, Manuel, Manuel Bullejos, David Cabezas, and Francisco Javier Alcalá (2023). "Using Python libraries and k-Nearest neighbors algorithms to delineate syn-sedimentary faults in sedimentary porous media". In: *Marine and Petroleum Geology* 153, p. 106283. DOI: 10.1016/j.marpetgeo.2023.106283.

Matheron, Georges (1963). "Principles of geostatistics". In: *Economic geology* 58.8, pp. 1246–1266. DOI: 10.2113/gsecongeo.58.8.1246.

— (1967). "Eléments pour une théorie des milieux poreux". In: *(No Title)*.

— (1972). "Random sets theory and its applications to stereology". In: *Journal of Microscopy* 95.1, pp. 15–23. DOI: 10.1111/j.1365-2818.1972.tb03708.x.

Matheron, Georges, Hélène Beucher, Chantal de Fouquet, A Galli, Dominique Guérillot, and Ch Ravenne (1987). "Conditional simulation of the geometry of fluvio-deltaic reservoirs". In: *SPE Annual Technical Conference and Exhibition*. Spe, SPE–16753. DOI: 10.2118/16753-MS.

McHargue, Tim, Michael J Pyrcz, Morgan D Sullivan, JD Clark, Andrea Fildani, BW Romans, JA Covault, Marjorie Levy, HW Posamentier, and NJ Drinkwater

(2011). "Architecture of turbidite channel systems on the continental slope: patterns and predictions". In: *Marine and petroleum geology* 28.3, pp. 728–743. DOI: 10.1016/j.marpetgeo.2010.07.008.

Menga, Ilaria (2021). "Analysis of late Pleistocene Aquifer Analogues to characterize heterogeneity of the post glacial aquifers of the Aare Valley (Switzerland)". MA thesis. Via Luigi Mangiagalli, 34, 20133 Milano MI, Italy: Universita' degli studi di Milano, facoltà di Scienze e Tecnologie.

Miall, A.D. (1991). "Hierarchies of Architectural Units in Terrigenous Clastic Rocks and Their Relationship to Sedimentation Rate." In: *The Three-Dimensional Facies Architecture of Terrigenous Clastic Sediments, and Its Implications for Hydrocarbon Discovery and Recovery*. A.D. Miall and N. Tyler. Tulsa, Oklahoma: Society for Sedimentary Geology.

— (1996). *The geology of fluvial deposits. Sedimentary facies, basin analysis, and petroleum geology*. Springer. DOI: 10.1007/978-3-662-03237-4.

Miall, Andrew D (2013). *The geology of fluvial deposits: sedimentary facies, basin analysis, and petroleum geology*. Springer. DOI: 10.1007/978-3-662-03237-4.

— (2014). *Fluvial depositional systems*. Vol. 14. Springer. DOI: 10.1007/978-3-319-00666-6.

Michael, HA, H Li, A Boucher, T Sun, J Caers, and SM Gorelick (2010). "Combining geologic-process models and geostatistics for conditional simulation of 3-D subsurface heterogeneity". In: *Water Resources Research* 46.5. DOI: 10.1029/2009WR008414.

Miller, James Keith, Tao Sun, Hongmei Li, Jonathon Stewart, Coralie Genty, Dachang Li, and Colin Lyttle (2008). "Direct modeling of reservoirs through forward process-based models: Can we get there?" In: *International petroleum technology conference*. OnePetro. DOI: 10.2523/IPTC-12729-MS.

Miller, Russell B, James W Castle, and Tom J Temples (2000). "Deterministic and stochastic modeling of aquifer stratigraphy, South Carolina". In: *Groundwater* 38.2, pp. 284–295. DOI: 10.1111/j.1745-6584.2000.tb00339.x.

Modis, K and D Sideri (2013). "Geostatistical simulation of hydrofacies heterogeneity of the West Thessaly aquifer systems in Greece". In: *Natural Resources Research* 22, pp. 123–138. DOI: 10.1007/s11053-013-9200-1.

Montero, Jose M, Luca Colombera, Na Yan, and Nigel P Mountney (2021). "A workflow for modelling fluvial meander-belt successions: Combining forward stratigraphic modelling and multi-point geostatistics". In: *Journal of Petroleum Science and Engineering* 201, p. 108411. DOI: 10.1016/j.petrol.2021.108411.

Moreno, Ziv and Amir Paster (2017). "Prediction of remediation of a heterogeneous aquifer: A case study". In: *Groundwater* 55.3, pp. 428–439. DOI: 10.1111/gwat.12493.

Mosser, Lukas, Olivier Dubrule, and Martin J Blunt (2019). "Deepflow: history matching in the space of deep generative models". In: *arXiv preprint arXiv:1905.05749*. DOI: 10.48550/arXiv.1905.05749.

Moulaeifard, Mohammad, Florian Wellmann, Simon Bernard, Miguel de la Varga, and David Bommes (2023). "Subdivide and Conquer: Adapting Non-Manifold Subdivision Surfaces to Surface-Based Representation and Reconstruction of Complex Geological Structures". In: *Mathematical Geosciences* 55.1, pp. 81–111. DOI: 10.1007/s11004-022-10017-x.

Neuman, Shlomo P (1990). "Universal scaling of hydraulic conductivities and dispersivities in geologic media". In: *Water resources research* 26.8, pp. 1749–1758.

Neuman, Shlomo P, Monica Riva, and Alberto Guadagnini (2008). "On the geostatistical characterization of hierarchical media". In: *Water Resources Research* 44.2. DOI: 10.1029/2007WR006228.

Neven, Alexis, Anders Vest Christiansen, and Philippe Renard (2022a). "Automatic stochastic 3D clay fraction model from tTEM survey and borehole data". In: *Scientific Reports* 12.1, p. 17112. DOI: s41598-022-21555-z.

Neven, Alexis, Pradip Kumar Maurya, Anders Vest Christiansen, and Philippe Renard (June 2021). "tTEM20AAR: A Benchmark Geophysical Data Set for Unconsolidated Fluvioglacial Sediments". In: *Earth System Science Data* 13.6, pp. 2743–2752. ISSN: 1866-3508. DOI: 10.5194/essd-13-2743-2021.

Neven, Alexis and Philippe Renard (2023). "A novel methodology for the stochastic integration of geophysical and hydrogeological data in geologically consistent models". In: *Water Resources Research* 59.7, e2023WR034992. DOI: 10.1029/2023WR034992.

Neven, Alexis, Ludovic Schorpp, and Philippe Renard (2022b). "Stochastic multifidelity joint hydrogeophysical inversion of consistent geological models". In: *Frontiers in Water* 4, p. 989440. DOI: 10.3389/frwa.2022.989440.

Nicholas, AP, PJ Ashworth, GH Sambrook Smith, and SD Sandbach (2013). "Numerical simulation of bar and island morphodynamics in anabranching megarivers". In: *Journal of Geophysical Research: Earth Surface* 118.4, pp. 2019–2044. DOI: 10.1002/jgrf.20132.

Niu, Bo, Zhidong Bao, Dengfei Yu, Chi Zhang, Ming Long, Jinchang Su, Xingjun Gao, Li Zhang, Dongsheng Zang, Min Li, et al. (2021). "Hierarchical modeling method based on multilevel architecture surface restriction and its application in point-bar internal architecture of a complex meandering river". In: *Journal of Petroleum Science and Engineering* 205, p. 108808. DOI: 10.1016/j.petrol.2021.108808.

Nordahl, Kjetil and Philip S Ringrose (2008). "Identifying the representative elementary volume for permeability in heterolithic deposits using numerical rock models". In: *Mathematical geosciences* 40.7, pp. 753–771. DOI: 10.1007/s11004-008-9182-4.

Olea, Ricardo A (2007). "Declustering of clustered preferential sampling for histogram and semivariogram inference". In: *Mathematical Geology* 39, pp. 453–467. DOI: 10.1007/s11004-007-9108-6.

Oliver, Dean S and Yan Chen (2018). "Data assimilation in truncated plurigaussian models: impact of the truncation map". In: *Mathematical Geosciences* 50.8, pp. 867–893. DOI: 10.1007/s11004-018-9753-y.

Oriani, Fabio, Julien Straubhaar, Philippe Renard, and Grégoire Mariethoz (2014). "Simulation of rainfall time series from different climatic regions using the direct sampling technique". In: *Hydrology and Earth System Sciences* 18.8, pp. 3015–3031. DOI: 10.5194/hess-18-3015-2014.

Osher, Stanley and James A Sethian (1988). "Fronts propagating with curvature-dependent speed: Algorithms based on Hamilton-Jacobi formulations". In: *Journal of computational physics* 79.1, pp. 12–49. DOI: 10.1016/0021-9991(88)90002-2.

Pan, Wen, Carlos Torres-Verdín, and Michael J Pyrcz (2021). "Stochastic Pix2pix: a new machine learning method for geophysical and well conditioning of rule-based channel reservoir models". In: *Natural Resources Research* 30, pp. 1319–1345. DOI: 10.1007/s11053-020-09778-1.

Park, Taesung, Ming-Yu Liu, Ting-Chun Wang, and Jun-Yan Zhu (2019). "Semantic image synthesis with spatially-adaptive normalization". In: *Proceedings of the*

IEEE/CVF conference on computer vision and pattern recognition, pp. 2337–2346. DOI: 10.48550/arXiv.1903.07291.

Parquer, Marion, Na Yan, Luca Colombera, Nigel P Mountney, Pauline Collon, and Guillaume Caumon (2020). "Combined inverse and forward numerical modelling for reconstruction of channel evolution and facies distributions in fluvial meander-belt deposits". In: *Marine and Petroleum Geology* 117, p. 104409. DOI: 10.1016/j.marpetgeo.2020.104409.

Parquer, Marion N, Pauline Collon, and Guillaume Caumon (2017). "Reconstruction of channelized systems through a conditioned reverse migration method". In: *Mathematical Geosciences* 49.8, pp. 965–994. DOI: 10.1007/s11004-017-9700-3.

Patani, SE, GM Porta, V Caronni, P Ruffo, and A Guadagnini (2021). "Stochastic inverse modeling and parametric uncertainty of sediment deposition processes across geologic time scales". In: *Mathematical Geosciences* 53, pp. 1101–1124. DOI: 10.1007/s11004-020-09911-z.

Pedregosa, F., G. Varoquaux, A. Gramfort, V. Michel, B. Thirion, O. Grisel, M. Blondel, P. Prettenhofer, R. Weiss, V. Dubourg, J. Vanderplas, A. Passos, D. Cournapeau, M. Brucher, M. Perrot, and E. Duchesnay (2011). "Scikit-learn: Machine Learning in Python". In: *Journal of Machine Learning Research* 12, pp. 2825–2830.

Penck, Albrecht and Eduard Brückner (1909). *Die alpen im Eiszeitalter*. Vol. 3. Tauchnitz.

Pescimoro, Eugenio, Matteo Icardi, Giovanni Porta, and Marco Bianchi (2022). "Emergence of non-Fickian transport in truncated pluri-Gaussian permeability fields". In: *GEM-International Journal on Geomathematics* 13.1, p. 17. DOI: 10.1007/s13137-022-00207-4.

Pirot, Guillaume, Julien Straubhaar, and Philippe Renard (2015). "A pseudo genetic model of coarse braided-river deposits". In: *Water Resources Research* 51.12, pp. 9595–9611. DOI: 10.1002/2015WR017078.

Preusser, Frank, Hans Rudolf Graf, Oskar Keller, Edgar Krayss, and Christian Schlüchter (July 2011). "Quaternary Glaciation History of Northern Switzerland". In: *E&G Quaternary Science Journal* 60.2/3, pp. 282–305. ISSN: 0424-7116. DOI: 10.3285/eg.60.2-3.06.

Preusser, Frank and Christian Schlüchter (Aug. 2004). "Dates from an Important Early Late Pleistocene Ice Advance in the Aare Valley, Switzerland". In: *Eclogae Geologicae Helvetiae* 97.2, pp. 245–253. ISSN: 1420-9128. DOI: 10.1007/s00015-004-1119-4.

Prusinkiewicz, Przemyslaw, Mark Hammel, Jim Hanan, and Radomir Mech (1996). "L-systems: from the theory to visual models of plants". In: *Proceedings of the 2nd CSIRO Symposium on Computational Challenges in Life Sciences*. Vol. 3. Citeseer, pp. 1–32.

Pyrcz, Michael J, Jeff B Boisvert, and Clayton V Deutsch (2008). "A library of training images for fluvial and deepwater reservoirs and associated code". In: *Computers & Geosciences* 34.5, pp. 542–560. DOI: 10.1016/j.cageo.2007.05.015.

— (2009). "ALLUVSIM: A program for event-based stochastic modeling of fluvial depositional systems". In: *Computers & Geosciences* 35.8, pp. 1671–1685. DOI: 10.1016/j.cageo.2008.09.012.

Pyrcz, Michael J, Octavian Catuneanu, and Clayton V Deutsch (2005). "Stochastic surface-based modeling of turbidite lobes". In: *AAPG bulletin* 89.2, pp. 177–191. DOI: 10.1306/09220403112.

Pyrcz, Michael J and Clayton V Deutsch (2014). *Geostatistical reservoir modeling*. Oxford University Press, USA.

Pyrcz, Michael J, Richard P Sech, Jacob A Covault, Brian J Willis, Zoltan Sylvester, and Tao Sun (2015). "Stratigraphic rule-based reservoir modeling". In: *Bulletin of Canadian Petroleum Geology* 63.4, pp. 287–303. DOI: 10.2113/gscpgbull.63.4.287.

Quental, Paulo, José António Almeida, and Manuela Simões (2012). "Construction of high-resolution stochastic geological models and optimal upscaling to a simplified layer-type hydrogeological model". In: *Advances in Water Resources* 39, pp. 18–32. DOI: 10.1016/j.advwatres.2012.01.001.

Raissi, Maziar, Paris Perdikaris, and George Em Karniadakis (2017). "Physics informed deep learning (part i): Data-driven solutions of nonlinear partial differential equations". In: *arXiv preprint arXiv:1711.10561*. DOI: 10.48550/arXiv.1711.10561.

Ramanathan, Ramya, Arijit Guin, Robert W Ritzi Jr, David F Dominic, Vicky L Freedman, Timothy D Scheibe, and Ian A Lunt (2010a). "Simulating the heterogeneity in braided channel belt deposits: 1. A geometric-based methodology and code". In: *Water Resources Research* 46.4. DOI: 10.1029/2009WR008111.

— (2010b). "Simulating the heterogeneity in braided channel belt deposits: 1. A geometric-based methodology and code". In: *Water Resources Research* 46.4.

Rauber, Martin, Fritz Stauffer, Peter Huggenberger, and Themistocles Dracos (1998). "A numerical three-dimensional conditioned/unconditioned stochastic facies type model applied to a remediation well system". In: *Water Resources Research* 34.9, pp. 2225–2233. DOI: 10.1029/98WR01378.

Ravalec, Mickaële Le, Benoît Noetinger, and Lin Y. Hu (Aug. 2000). "The FFT Moving Average (FFT-MA) Generator: An Efficient Numerical Method for Generating and Conditioning Gaussian Simulations". In: *Mathematical Geology* 32.6, pp. 701–723. ISSN: 1573-8868. DOI: 10.1023/A:1007542406333.

Renard, Philippe and Denis Allard (2013). "Connectivity metrics for subsurface flow and transport". In: *Advances in Water Resources* 51, pp. 168–196. DOI: 10.1016/j.advwatres.2011.12.001.

Renard, Philippe and Gabriel Courrioux (1994). "Three-dimensional geometric modeling of a faulted domain: The Soultz Horst example (Alsace, France)". In: *Computers & Geosciences* 20.9, pp. 1379–1390.

Ringrose, Philip and Mark Bentley (2016). *Reservoir model design*. Vol. 467. Springer. DOI: 10.1007/978-94-007-5497-3.

Ritzi, Robert W, Zhenxue Dai, David F Dominic, and Yoram N Rubin (2004). "Spatial correlation of permeability in cross-stratified sediment with hierarchical architecture". In: *Water Resources Research* 40.3.

Ritzi Jr, Robert W (2000). "Behavior of indicator variograms and transition probabilities in relation to the variance in lengths of hydrofacies". In: *Water resources research* 36.11, pp. 3375–3381. DOI: 10.1029/2000WR900139.

Ritzi Jr, Robert W, Dale F Jayne, Arthur J Zahradnik Jr, Adrian A Field, and Graham E Fogg (1994). "Geostatistical modeling of heterogeneity in glaciofluvial, buried-valley aquifers". In: *Groundwater* 32.4, pp. 666–674. DOI: 10.1111/j.1745-6584.1994.tb00903.x.

Rongier, Guillaume, Pauline Collon, and Philippe Renard (2017). "Stochastic simulation of channelized sedimentary bodies using a constrained L-system". In: *Computers & Geosciences* 105, pp. 158–168. DOI: 10.1016/j.cageo.2017.05.006.

Rubin, Yoram (2003). *Applied stochastic hydrogeology*. Oxford University Press. ISBN: 9780197561676. DOI: 10.1093/oso/9780195138047.001.0001.

Ruiu, Jeremy, Guillaume Caumon, and Sophie Viseur (2016). "Modeling channel forms and related sedimentary objects using a boundary representation based on non-uniform rational B-splines". In: *Mathematical Geosciences* 48, pp. 259–284. DOI: 10.1007/s11004-015-9629-3.

Sahoo, Sasmita and Madan K Jha (2017). "Pattern recognition in lithology classification: modeling using neural networks, self-organizing maps and genetic algorithms". In: *Hydrogeology journal* 25.2, p. 311. DOI: 10.1007/s10040-016-1478-8.

Salsabili, Mohammad, Ali Saeidi, Alain Rouleau, and Miroslav Nastev (2021). "3D probabilistic modelling and uncertainty analysis of glacial and post-glacial deposits of the city of Saguenay, Canada". In: *Geosciences* 11.5, p. 204. DOI: 10.3390/geosciences11050204.

Sartore, Luca, Paolo Fabbri, and Carlo Gaetan (2016). "spMC: an R-package for 3D lithological reconstructions based on spatial Markov chains". In: *Computers & Geosciences* 94, pp. 40–47. DOI: 10.1016/j.cageo.2016.06.001.

Scheibe, Timothy D and David L Freyberg (1995). "Use of sedimentological information for geometric simulation of natural porous media structure". In: *Water Resources Research* 31.12, pp. 3259–3270. DOI: 10.1029/95WR02570.

Schlüchter, Christian (Jan. 1989). "The Most Complete Quaternary Record of the Swiss Alpine Foreland". In: *Palaeogeography, Palaeoclimatology, Palaeoecology*. XIIth INQUA Congress 72, pp. 141–146. ISSN: 0031-0182. DOI: 10.1016/0031-0182(89)90138-7.

Schorpp, Ludovic, Julien Straubhaar, and Philippe Renard (May 2022). "Automated Hierarchical 3D Modeling of Quaternary Aquifers: The ArchPy Approach". In: *Frontiers in Earth Science* 10. DOI: 10.3389/feart.2022.884075.

— (submited). "A novel surface-based approach to represent aquifer heterogeneity in sedimentary formations". In: *Water resources research*.

Sebacher, Bogdan, Remus Hanea, and Andreas S Stordal (2017). "An adaptive pluri-Gaussian simulation model for geological uncertainty quantification". In: *Journal of Petroleum Science and Engineering* 158, pp. 494–508. DOI: 10.1016/j.petrol.2017.08.038.

Sech, Richard P, Matthew D Jackson, and Gary J Hampson (2009). "Three-dimensional modeling of a shoreface-shelf parasequence reservoir analog: Part 1. Surface-based modeling to capture high-resolution facies architecture". In: *AAPG bulletin* 93.9, pp. 1155–1181. DOI: 10.1306/05110908144.

Serra, J (1981). "The Boolean model and random sets". In: *Image modeling*. Elsevier, pp. 343–370. DOI: 10.1016/B978-0-12-597320-5.50025-5.

Serrano, Raul Perulero, Laura Guadagnini, Monica Riva, Mauro Giudici, and Alberto Guadagnini (2014). "Impact of two geostatistical hydro-facies simulation strategies on head statistics under non-uniform groundwater flow". In: *Journal of Hydrology* 508, pp. 343–355. DOI: 10.1016/j.jhydrol.2013.11.009.

Severino, Gerardo, Carmine Fallico, and Guglielmo Federico Antonio Brunetti (2024). "Correlation Structure of Steady Well-Type Flows Through Heterogeneous Porous Media: Results and Application". In: *Water Resources Research* 60.2. e2023WR036279 2023WR036279, e2023WR036279. DOI: 10.1029/2023WR036279. eprint: https://agupubs.onlinelibrary.wiley.com/doi/pdf/10.1029/2023WR036279.

Shannon, Claude Elwood (1948). "A mathematical theory of communication". In: *The Bell system technical journal* 27.3, pp. 379–423.

Shepard, Donald (1968). "A two-dimensional interpolation function for irregularly-spaced data". In: *Proceedings of the 1968 23rd ACM national conference*, pp. 517–524. DOI: 10.1145/800186.810616.

Shmaryan, LE and CV Deutsch (1999). "Object-based modeling of fluvial/deepwater reservoirs with fast data conditioning: methodology and case studies". In: *SPE Annual Technical Conference and Exhibition*. SPE, SPE–56821. DOI: 10.2118/56821-MS.

Silva, Diogo and Clayton Deutsch (2019). "Multivariate categorical modeling with hierarchical truncated pluri-gaussian simulation". In: *Mathematical Geosciences* 51.5, pp. 527–552. DOI: 10.1007/s11004-018-09782-5.

Slatt, Roger M and Graham L Hopkins (1990). "Scaling geologic reservoir description to engineering needs". In: *Journal of Petroleum Technology* 42.02, pp. 202–210. DOI: 10.2118/18136-PA.

Smirnoff, Alex, Eric Boisvert, and Serge J Paradis (2008). "Support vector machine for 3D modelling from sparse geological information of various origins". In: *Computers & Geosciences* 34.2, pp. 127–143. DOI: 10.1016/j.cageo.2006.12.008.

Soares, Amilcar (2001). "Direct sequential simulation and cosimulation". In: *Mathematical geology* 33.8, pp. 911–926.

Sohl-Dickstein, Jascha, Eric Weiss, Niru Maheswaranathan, and Surya Ganguli (2015). "Deep unsupervised learning using nonequilibrium thermodynamics". In: *International conference on machine learning*. PMLR, pp. 2256–2265. DOI: 10.48550/arXiv.1503.03585.

Soltanian, Mohamad Reza, Faranak Behzadi, and Felipe PJ de Barros (2020). "Dilution enhancement in hierarchical and multiscale heterogeneous sediments". In: *Journal of Hydrology* 587, p. 125025. DOI: 10.1016/j.jhydrol.2020.125025.

Song, Suihong, Tapan Mukerji, and Jiagen Hou (2021). "GANSim: Conditional facies simulation using an improved progressive growing of generative adversarial networks (GANs)". In: *Mathematical Geosciences*, pp. 1–32. DOI: 10.1007/s11004-021-09934-0.

Song, Suihong, Dongxiao Zhang, Tapan Mukerji, and Nanzhe Wang (2023). "GANSim-surrogate: An integrated framework for stochastic conditional geomodelling". In: *Journal of Hydrology* 620, p. 129493. DOI: 10.1016/j.jhydrol.2023.129493.

Srivastava, R Mohan (2018). "The origins of the multiple-point statistics (MPS) algorithm". In: *Handbook of Mathematical Geosciences*, p. 655. DOI: 10.1007/978-3-319-78999-6_32.

Straubhaar, J (2019). "DeeSse user's guide". In: *The Centre for Hydrogeology and Geothermics (CHYN), University of Neuchatel, Neuchâtel, Switzerland*.

Straubhaar, Julien and Philippe Renard (2021). "Conditioning Multiple-Point Statistics Simulation to Inequality Data". In: *Earth and Space Science* 8.5. e2020EA001515 2020EA001515, e2020EA001515. ISSN: 2333-5084. DOI: 10.1029/2020EA001515.

— (2024). "Exploring substitution random functions composed of stationary multi-Gaussian processes". In: *Stochastic Environmental Research and Risk Assessment*, pp. 1–16. DOI: 10.1007/s00477-024-02662-x.

Straubhaar, Julien, Philippe Renard, Grégoire Mariethoz, Tatiana Chugunova, and Pierre Biver (2019). "Fast and interactive editing tools for spatial models". In: *Mathematical Geosciences* 51, pp. 109–125. DOI: 10.1111/j.1365-2389.2011.01362.x.

Straubhaar, Julien, Philippe Renard, Grégoire Mariethoz, Roland Froidevaux, and Olivier Besson (2011). "An improved parallel multiple-point algorithm using a list

approach". In: *Mathematical Geosciences* 43, pp. 305–328. DOI: 10.1007/s11004-011-9328-7.

Strebelle, Sebastien (2002). "Conditional simulation of complex geological structures using multiple-point statistics". In: *Mathematical geology* 34, pp. 1–21. DOI: 10.1023/A:1014009426274.

Strebelle, Sebastien and Claude Cavelius (2014). "Solving speed and memory issues in multiple-point statistics simulation program SNESIM". In: *Mathematical Geosciences* 46, pp. 171–186. DOI: 10.1007/s11004-013-9489-7.

Strebelle, Sebastien and Tuanfeng Zhang (2004). "Non-stationary multiple-point geostatistical models". In: *Geostatistics Banff 2004*. Springer, pp. 235–244. DOI: 10.1007/978-1-4020-3610-1_24.

Strebelle, Sebastien Bruno (2000). *Sequential simulation drawing structures from training images*. Stanford University.

Sun, Chao, Vasily Demyanov, and Daniel Arnold (2023a). "A conditional GAN-based approach to build 3D facies models sequentially upwards". In: *Computers & Geosciences* 181, p. 105460. DOI: 10.1016/j.cageo.2023.105460.

— (2023b). "Geological realism in Fluvial facies modelling with GAN under variable depositional conditions". In: *Computational Geosciences* 27.2, pp. 203–221. DOI: 10.1007/s10596-023-10190-w.

Sun, Tao, Paul Meakin, Torstein Jøssang, and Klaus Schwarz (1996). "A simulation model for meandering rivers". In: *Water resources research* 32.9, pp. 2937–2954. DOI: 10.1029/96WR00998.

Sylvester, Zoltán, Paul Durkin, and Jacob A Covault (2019). "High curvatures drive river meandering". In: *Geology* 47.3, pp. 263–266. DOI: 10.1130/G45608.1.

Sylvester, Zoltán, Carlos Pirmez, and Alessandro Cantelli (2011). "A model of submarine channel-levee evolution based on channel trajectories: Implications for stratigraphic architecture". In: *Marine and Petroleum Geology* 28.3, pp. 716–727. DOI: 10.1016/j.marpetgeo.2010.05.012.

Sylvester, Zoltán, Kyle M Straub, and Jacob A Covault (2024). "Stratigraphy in space and time: A reproducible approach to analysis and visualization". In: *Earth-Science Reviews*, p. 104706. DOI: 10.1016/j.earscirev.2024.104706.

Tahmasebi, Pejman (2018). "Multiple point statistics: a review". In: *Handbook of mathematical geosciences: Fifty years of IAMG*, pp. 613–643. DOI: 10.1007/978-3-319-78999-6_30.

Tahmasebi, Pejman, Ardeshir Hezarkhani, and Muhammad Sahimi (2012). "Multiple-point geostatistical modeling based on the cross-correlation functions". In: *Computational Geosciences* 16, pp. 779–797. DOI: 10.1007/s10596-012-9287-1.

Tartakovsky, Daniel M, Brendt Wohlberg, and Alberto Guadagnini (2007). "Nearest-neighbor classification for facies delineation". In: *Water resources research* 43.7. DOI: 10.1029/2007WR005968.

Tartakovsky, Daniel M and Brendt E Wohlberg (2004). "Delineation of geologic facies with statistical learning theory". In: *Geophysical research letters* 31.18. DOI: 10.1029/2004GL020864.

Teles, V, JP Bravard, G De Marsily, and Edith Perrier (2001). "Modelling of the construction of the Rhône alluvial plain since 15 000 years BP". In: *Sedimentology* 48.6, pp. 1209–1224. DOI: 10.1046/j.1365-3091.2001.00419.x.

Teles, V, F Delay, and G De Marsily (2004). "Comparison of genesis and geostatistical methods for characterizing the heterogeneity of alluvial media: Groundwater flow and transport simulations". In: *Journal of hydrology* 294.1-3, pp. 103–121. DOI: 10.1016/j.jhydrol.2003.11.041.

Teles, V, F Delay, and G de Marsily (2006). "Comparison of transport simulations and equivalent dispersion coefficients in heterogeneous media generated by different numerical methods: A genesis model and a simple geostatistical sequential Gaussian simulator". In: *Geosphere* 2.5, pp. 275–286. DOI: 10.1130/GES00034.1.

Tetzlaff, Daniel M, John Warvelle Harbaugh, et al. (1989). *Simulating clastic sedimentation*. Vol. 1110. Springer. ISBN: 978-1-4757-0694-9.

Thomas, AT, S Reiche, M Riedel, and C Clauser (2019). "The fate of submarine fresh groundwater reservoirs at the New Jersey shelf, USA". In: *Hydrogeology Journal* 27.7, pp. 2673–2694. DOI: 10.1007/s10040-019-01997-y.

Titus, Zainab, Claire Heaney, Carl Jacquemyn, Pablo Salinas, MD Jackson, and Christopher Pain (2021). "Conditioning surface-based geological models to well data using artificial neural networks". In: *Computational Geosciences*, pp. 1–24. DOI: 10.1007/s10596-021-10088-5.

Todaro, Valeria, Marco D'Oria, Andrea Zanini, J Jaime Gómez-Hernández, and Maria Giovanna Tanda (2023). "Experimental sandbox tracer tests to characterize a two-facies aquifer via an ensemble smoother". In: *Hydrogeology Journal*, pp. 1–14. DOI: 10.1007/s10040-023-02662-1.

Tokdar, Surya T. and Robert E. Kass (2010). "Importance Sampling: A Review". In: *WIREs Computational Statistics* 2.1, pp. 54–60. ISSN: 1939-0068. DOI: 10.1002/wics.56.

Tucker, Gregory, Stephen Lancaster, Nicole Gasparini, and Rafael Bras (2001). "The channel-hillslope integrated landscape development model (CHILD)". In: *Landscape erosion and evolution modeling*, pp. 349–388. DOI: 10.1007/978-1-4615-0575-4_12.

Tye, Robert S (2004). "Geomorphology: An approach to determining subsurface reservoir dimensions". In: *AAPG bulletin* 88.8, pp. 1123–1147. DOI: 10.1306/02090403100.

Tyler, Kelly and A Henriquez (1992). "A program for 3-D modelling of heterogeneities in a fluvial reservoir". In: *ECMOR III-3rd European Conference on the Mathematics of Oil Recovery*. European Association of Geoscientists & Engineers, cp–232. DOI: 10.3997/2214-4609.201411061.

Vaswani, Ashish, Noam Shazeer, Niki Parmar, Jakob Uszkoreit, Llion Jones, Aidan N Gomez, Łukasz Kaiser, and Illia Polosukhin (2017). "Attention is all you need". In: *Advances in neural information processing systems* 30.

Velasquez Sanchez, Harold G (2023). "Truncation Trees in Hierarchical Truncated PluriGaussian Simulation". MA thesis. University of Alberta. DOI: 10.7939/r3-phth-qt71.

Villamizar, Carlos A, Gary J Hampson, Yvette S Flood, and Peter JR Fitch (2015). "Object-based modelling of avulsion-generated sandbody distributions and connectivity in a fluvial reservoir analogue of low to moderate net-to-gross ratio". In: DOI: 10.1144/petgeo2015-004.

Virtanen, Pauli et al. (Mar. 2020). "SciPy 1.0: Fundamental Algorithms for Scientific Computing in Python". In: *Nature Methods* 17.3, pp. 261–272. ISSN: 1548-7091, 1548-7105. DOI: 10.1038/s41592-019-0686-2.

Viseur, Sophie, Arben Shtuka, and Jean-Laurent Mallet (1998). "New Fast, Stochastic, Boolean Simulation of Fluvial Deposits." In: *SPE Annual Technical Conference and Exhibition*. SPE, SPE–49281. DOI: 10.2118/49281-MS.

Volken, Stefan, Giona Preisig, and Michael Gaehwiler (Oct. 2016). "GeoQuat: Developing a system for the sustainable management, 3D modelling and application of

Quaternary deposit data". In: *Swiss Bulletin for Applied Geology* 21, pp. 3–16. DOI: 10.5169/seals-658182.

Wallace, Corey D, Daniele Tonina, Jeffrey T McGarr, Felipe PJ de Barros, and Mohamad Reza Soltanian (2021). "Spatiotemporal dynamics of nitrous oxide emission hotspots in heterogeneous riparian sediments". In: *Water Resources Research* 57.12, e2021WR030496. DOI: 10.1029/2021WR030496.

Walsh, DA and T Manzocchi (2021a). "Connectivity in pixel-based facies models". In: *Mathematical Geosciences* 53.3, pp. 415–435. DOI: 10.1007/s11004-021-09931-3.

Walsh, Deirdre A and Tom Manzocchi (2021b). "A method for generating geomodels conditioned to well data with high net: gross ratios but low connectivity". In: *Marine and Petroleum Geology* 129, p. 105104. DOI: 10.1016/j.marpetgeo.2021.105104.

Wang, Yimin C, Michael J Pyrcz, Octavian Catuneanu, and Jeff B Boisvert (2018). "Conditioning 3D object-based models to dense well data". In: *Computers & Geosciences* 115, pp. 1–11. DOI: 10.1016/j.cageo.2018.02.006.

Webb, Erik K (1994). "Simulating the three-dimensional distribution of sediment units in braided-stream deposits". In: *Journal of Sedimentary Research* 64.2b, pp. 219–231. DOI: 10.1306/D4267F96-2B26-11D7-8648000102C1865D.

Weber, Dennis and Evan Englund (1992). "Evaluation and comparison of spatial interpolators". In: *Mathematical Geology* 24, pp. 381–391. DOI: 10.1007/bf00891270.

Weissmann, Gary S and Graham E Fogg (1999). "Multi-scale alluvial fan heterogeneity modeled with transition probability geostatistics in a sequence stratigraphic framework". In: *Journal of Hydrology* 226.1-2, pp. 48–65. DOI: 10.1016/S0022-1694(99)00160-2.

Weissmann, Gary S, Yong Zhang, Eric M LaBolle, and Graham E Fogg (2002). "Dispersion of groundwater age in an alluvial aquifer system". In: *Water Resources Research* 38.10, pp. 16–1. DOI: 10.1029/2001WR000907.

Wellmann, Florian and Guillaume Caumon (2018). "3-D Structural geological models: Concepts, methods, and uncertainties". In: *Advances in geophysics*. Vol. 59. Elsevier, pp. 1–121. DOI: 10.1016/bs.agph.2018.09.001.

Wen, Renjun, Allard W Martinius, Arve Næss, Philip Ringrose, A Buccianti, G Nardi, and R Potenza (1998). "Three-dimensional simulation of small-scale heterogeneity in tidal deposits–a process-based stochastic simulation method". In.

Wilkinson, GN, SR Eckert, TW Hancock, and O Mayo (1983). "Nearest neighbour (NN) analysis of field experiments". In: *Journal of the Royal Statistical Society: Series B (Methodological)* 45.2, pp. 151–178. DOI: 10.1111/j.2517-6161.1983.tb01240.x.

Wingate, David, Jonathan Kane, Matt Wolinsky, and Zoltán Sylvester (2016). "A new approach for conditioning process-based geologic models to well data". In: *Mathematical Geosciences* 48, pp. 371–397. DOI: 10.1007/s11004-015-9596-8.

Wohlberg, Brendt, Daniel M Tartakovsky, and Alberto Guadagnini (2005). "Subsurface characterization with support vector machines". In: *IEEE transactions on geoscience and remote sensing* 44.1, pp. 47–57. DOI: 10.1109/TGRS.2005.859953.

Wu, Jianbing, Alexandre Boucher, and Tuanfeng Zhang (2008). "A SGeMS code for pattern simulation of continuous and categorical variables: FILTERSIM". In: *Computers & Geosciences* 34.12, pp. 1863–1876. DOI: 10.1016/j.cageo.2007.08.008.

Xie, Y, Clayton V Deutsch, and AS Cullick (1999). "A Short Note on Surface-Based Modelling for Integration of Stratigraphic Data in Geostatistical Reservoir Models". In: *CCG Annual Report One, Edmonton: University of Alberta*.

Xie, YuLong, A Stan Cullick, and Clayton V Deutsch (2000). "Surface-geometry and trend modeling for integration of stratigraphic data in reservoir models". In: *GEOSTATS 2000. W.J. Kleingeld and D.G. Krige (eds.). Proceedings of the 6th International Geostatistics Congress, Cape Town, South Africa*.

— (2001). "Surface-geometry and trend modeling for integration of stratigraphic data in reservoir models". In: *SPE western regional meeting*. OnePetro. DOI: 10.2118/68817-MS.

Xu, Zhongyuan, Jayaram Hariharan, Paola Passalacqua, Elisabeth Steel, Chris Paola, and Holly A Michael (2021). "Linking the surface and subsurface in river deltas—part 2: relating subsurface geometry to groundwater flow behavior". In: *Water Resources Research* 57.8, e2020WR029281. DOI: 10.1029/2020WR029281.

Xue, Peipei, Zhang Wen, Eungyu Park, Hamza Jakada, Dejun Zhao, and Xing Liang (2022). "Geostatistical analysis and hydrofacies simulation for estimating the spatial variability of hydraulic conductivity in the Jianghan Plain, central China". In: *Hydrogeology Journal* 30.4, pp. 1135–1155. DOI: 10.1007/s10040-022-02495-4.

Yan, Na, Luca Colombera, Grace IE Cosgrove, and Nigel P Mountney (2024). "A 3D forward stratigraphic model of aeolian dune evolution for prediction of lithofacies heterogeneity". In: *Computers & Geosciences*, p. 105594. DOI: 10.1016/j.cageo.2024.105594.

Yan, Na, Nigel P Mountney, Luca Colombera, and Robert M Dorrell (2017). "A 3D forward stratigraphic model of fluvial meander-bend evolution for prediction of point-bar lithofacies architecture". In: *Computers & Geosciences* 105, pp. 65–80. DOI: 10.1016/j.cageo.2017.04.012.

Zappa, G, R Bersezio, F Felletti, and M Giudici (2006). "Modeling heterogeneity of gravel-sand, braided stream, alluvial aquifers at the facies scale". In: *Journal of Hydrology* 325.1-4, pp. 134–153. DOI: 10.1016/j.jhydrol.2005.10.016.

Zech, Alraune, Sabine Attinger, Alberto Bellin, Vladimir Cvetkovic, Gedeon Dagan, Marco Dentz, Peter Dietrich, Aldo Fiori, and Georg Teutsch (2021a). "A comparison of six transport models of the MADE-1 experiment implemented with different types of hydraulic data". In: *Water resources research* 57.5, e2020WR028672. DOI: 10.1029/2020WR028672.

Zech, Alraune, Peter Dietrich, Sabine Attinger, and Georg Teutsch (Jan. 2021b). "A Field Evidence Model: How to Predict Transport in Heterogeneous Aquifers at Low Investigation Level". In: *Hydrology and Earth System Sciences* 25.1, pp. 1–15. ISSN: 1027-5606. DOI: 10.5194/hess-25-1-2021.

Zhan, Chuanjun, Zhenxue Dai, Zhijie Yang, Xiaoying Zhang, Ziqi Ma, Hung Vo Thanh, and Mohamad Reza Soltanian (2023). "Subsurface sedimentary structure identification using deep learning: A review". In: *Earth-Science Reviews*, p. 104370. DOI: 10.1016/j.earscirev.2023.104370.

Zhang, Ting, Yue Dong, Hualin Bai, and Yuan Peng (2023). "Stochastic reconstruction of shale combining multi-scale generators and discriminators with attention mechanisms". In: *Computational Geosciences*, pp. 1–25. DOI: 10.1007/s10596-023-10249-8.

Zhang, Tuanfeng (2006). *Filter-based training pattern classification for spatial pattern simulation*. Stanford University. DOI: 10.1007/s11004-005-9004-x.

Zhang, X, Michael J Pyrcz, and Clayton V Deutsch (2009). "Stochastic surface modeling of deepwater depositional systems for improved reservoir models". In: *Journal of Petroleum Science and Engineering* 68.1-2, pp. 118–134. DOI: 10.1016/j.petrol.2009.06.019.

Zhou, Cuiying, Jinwu Ouyang, Weihua Ming, Guohao Zhang, Zichun Du, and Zhen Liu (2019). "A stratigraphic prediction method based on machine learning". In: *Applied Sciences* 9.17, p. 3553. DOI: 10.3390/app9173553.

Zhou, Dan, Ye Zhang, Guillaume Gianni, Peter Lichtner, and Irina Engelhardt (2018). "Numerical modelling of stream–aquifer interaction: Quantifying the impact of transient streambed permeability and aquifer heterogeneity". In: *Hydrological Processes* 32.14, pp. 2279–2292. DOI: 10.1002/hyp.13169.

Zuffetti, Chiara, Alessandro Comunian, Riccardo Bersezio, and Philippe Renard (2020). "A new perspective to model subsurface stratigraphy in alluvial hydrogeological basins, introducing geological hierarchy and relative chronology". In: *Computers & Geosciences* 140, p. 104506. DOI: 10.1016/j.cageo.2020.104506.